

43406

National Library of Canada

Bibliothèque nationale du Canada

CANADIAN THESES ON MICROFICHE

THÈSES CANADIENNES SUR MICROFICHE

NAME OF AUTHOR/NOM DE L'AUTEUR

NORMAN GEE

TITLE OF THESIS/TITRE DE LA THÈSE

ELECTRON AND ION TRANSPORT IN HYDROCARBON FLUIDS

UNIVERSITY/UNIVERSITÉ

UNIVERSITY OF ALTA

DEGREE FOR WHICH THESIS WAS PRESENTED/ GRADE POUR LEQUEL CETTE THÈSE FUT PRÉSENTÉE

PH.D.

YEAR THIS DEGREE CONFERRED/ANNÉE D'OBTENTION DE CE GRADE

1979

NAME OF SUPERVISOR/NOM DU DIRECTEUR DE THÈSE

GORDON R. FREEMAN

Permission is hereby granted to the NATIONAL LIBRARY OF CANADA to microfilm this thesis and to lend or sell copies of the film.

L'autorisation est, par la présente, accordée à la BIBLIOTHÈQUE NATIONALE DU CANADA de microfilmer cette thèse et de prêter ou de vendre des exemplaires du film.

The author reserves other publication rights, and neither the thesis nor extensive extracts from it may be printed or otherwise reproduced without the author's written permission.

L'auteur se réserve les autres droits de publication; ni la thèse ni de longs extraits de celle-ci ne doivent être imprimés ou autrement reproduits sans l'autorisation écrite de l'auteur.

DATED/DATE

July 10/79

SIGNED/SIGNÉ

Norman Gee

PERMANENT ADDRESS/RÉSIDENCE FIXE

9116-156 ST

EDMONTON ALTA

T5R 1Y8



National Library of Canada

Cataloguing Branch
Canadian Theses Division

Ottawa, Canada
K1A 0N4

Bibliothèque nationale du Canada

Direction du catalogage
Division des thèses canadiennes

NOTICE

AVIS

The quality of this microfiche is heavily dependent upon the quality of the original thesis submitted for microfilming. Every effort has been made to ensure the highest quality of reproduction possible.

La qualité de cette microfiche dépend grandement de la qualité de la thèse soumise au microfilmage. Nous avons tout fait pour assurer une qualité supérieure de reproduction.

If pages are missing, contact the university which granted the degree.

S'il manque des pages, veuillez communiquer avec l'université qui a conféré le grade.

Some pages may have indistinct print especially if the original pages were typed with a poor typewriter ribbon or if the university sent us a poor photocopy.

La qualité d'impression de certaines pages peut laisser à désirer, surtout si les pages originales ont été dactylographiées à l'aide d'un ruban usé ou si l'université nous a fait parvenir une photocopie de mauvaise qualité.

Previously copyrighted materials (journal articles, published tests, etc.) are not filmed.

Les documents qui font déjà l'objet d'un droit d'auteur (articles de revue, examens publiés, etc.) ne sont pas microfilmés.

Reproduction in full or in part of this film is governed by the Canadian Copyright Act, R.S.C. 1970, c. C-30. Please read the authorization forms which accompany this thesis.

La reproduction, même partielle, de ce microfilm est soumise à la Loi canadienne sur le droit d'auteur, SRC 1970, c. C-30. Veuillez prendre connaissance des formules d'autorisation qui accompagnent cette thèse.

**THIS DISSERTATION
HAS BEEN MICROFILMED
EXACTLY AS RECEIVED**

**LA THÈSE A ÉTÉ
MICROFILMÉE TELLE QUE
NOUS L'AVONS REÇUE**

THE UNIVERSITY OF ALBERTA

ELECTRON AND ION TRANSPORT IN HYDROCARBON FLUIDS

BY

©

NORMAN GEE

A THESIS

SUBMITTED TO THE FACULTY OF GRADUATE STUDIES AND RESEARCH
IN PARTIAL FULFILMENT OF THE REQUIREMENTS FOR THE DEGREE
OF

DOCTOR OF PHILOSOPHY

DEPARTMENT OF CHEMISTRY

EDMONTON, ALBERTA

FALL, 1979

THE UNIVERSITY OF ALBERTA
FACULTY OF GRADUATE STUDIES AND RESEARCH

The undersigned certify that they have read, and
recommend to the Faculty of Graduate Studies and
Research for acceptance, a thesis entitled

"ELECTRON AND ION TRANSPORT IN HYDROCARBON FLUIDS"

submitted by NORMAN GEE in partial fulfilment of the
requirements for the degree of Doctor of Philosophy.

J.P. Newman
.....
Supervisor

John E. Butler
.....

R.S. Brown
.....

Gary Hordley
.....

B. Paramee
.....

Eric O. Potts
.....
External Examiner

July 6, 1979
.....
Date

DEDICATION

I would like to dedicate this thesis to my proofreader, my typist and to the Minnesota Mining and Manufacturing Co.

A B S T R A C T

A pulse radiolysis conductance method has been used to measure electron mobilities, ion mobilities, and free ion yields in the $C_1 - C_4$ alkanes and alkenes, with the exception of the butenes. Measurements were made as functions of electric field strength E , along the co-existence curve from the densities of the normal vapors and liquids to that of the supercritical fluid. Measurements were also made in the gas phase along a number of isochores.

The low field density-normalized electron mobility, μ_{en} , decreased in the low density gas with increasing molecular size, permanent dipole moment, or degree of sphericity. At constant density the mobility had a non-negative temperature coefficient. At high electric field strengths the electron mobility in the low density gases, increased with E , except in ethene, cyclopropane and *n*-butane. At higher densities, the mobility decreased at high field strengths in all the compounds. With the exception of isobutane, the μ_{en} values decreased at higher densities. These values tended to increase again as the critical density was approached. At high liquid phase densities, the μ_{en} values decreased once more. The electron mobility was affected more by the temperature than by the density in the liquid phase.

The ion mobility was independent of electric field strength up to the highest fields used, which was 40 ± 10 kV/cm in the liquid and 3 ± 2 kV/cm in the dilute gas. The

density-normalized ion mobility, $\mu_+ n$, was affected in the dilute gas largely by the molecular size. The temperature coefficient of the ion mobility at constant density was positive in all cases, and tended to be larger than that of the electron mobility at the same density. Along the co-existence curve at temperatures away from the critical region, the vapor phase temperature coefficient of the ion mobility was similar to ΔH_{vap} , the heat of vaporization of the liquid at its normal boiling point, since μ_+ varied as n^{-1} . The liquid phase coefficient correlated with the activation energy of the viscosity.

Assumption of a modified gaussian distribution of electron thermalization lengths allowed application of a model based on Onsager's equation to extract electron thermalization ranges from the experimental free ion yields. In the low density gas, the density-normalized thermalization range bd was found to decrease with increasing molecular size, unsaturation of the carbon-carbon bonds and permanent dipole moment. In the liquid near the critical point the bd values were strongly affected by the stability of the localized electron state. Addition of SF_6 to isobutane decreased the bd values and removed the temperature variation.

A C K N O W L E D G E M E N T S

I would like to thank the many persons associated with me during the thesis work including the staff of the Radiation Research Center and the support departments of the Chemistry Department.

I am grateful for the help I received from Prof. J.-P. Dodelet (University of Quebec a Trois Rivières) when I started graduate school.

Thanks are due to Larry Coulson who developed the plotting package for the figures in this thesis, John Toonen who developed the technique of working with cm. thick glass, Mary Waters and Moira Day who produced this thesis, and Luigi Ghidina who maintained the physical condition of the laboratory.

Special thanks are due to Professor G. R. Freeman for the direction I received in the course of this work.

TABLE OF CONTENTS

	<u>PAGE</u>
I. INTRODUCTION.....	1
A. General.....	1
1. The Ionization Process.....	1
2. Terminology.....	3
B. Historical.....	4
1. Origins of Conductivity Studies.....	4
2. Gas Phase Experiments.....	7
a. Ramsauer Type Experiments.....	7
b. Swarm Experiments.....	8
i) Description of Methods.....	8
ii) Townsend's Work.....	9
iii) Application of Townsend's Method to Hydrocarbons.....	11
iv) Electrical Shutter Methods.....	12
(a) Application of Electrical Shutters to Ion Studies.....	12
(b) Application of Electrical Shutters to Electron Studies..	13
3. Electron Mobilities in Hydrocarbon Vapors..	15
a. Methane.....	15
i) Low Pressure.....	15
ii) High Pressure.....	20
iii) Application.....	21
b. Methane-d ₄	21
c. Silane and Silane-d ₄	22

	<u>PAGE</u>
d. <u>n</u> -Alkanes.....	23
1) Ethane and Propane.....	23
ii) Other <u>n</u> -Alkanes.....	26
e. Branched Alkanes.....	29
f. Ethene, Propene and Cyclopropane.....	32
4. Liquid Phase Mobilities.....	33
a. Ion Mobilities.....	33
i) Adamczewski.....	33
ii) Photo Injection.....	35
iii) Free Ion Yield Related Measurements	37
iv) Other Results.....	38
b. Electron Mobilities in Liquid Hydro- carbons.....	39
i) Background.....	39
ii) Low Pressure Observations.....	40
iii) High Pressure Observations.....	41
5. Free Ion Yields.....	42
a. Older Results.....	43
b. Conductance.....	44
c. Clearing Field (Charge Clearing).....	45
i) Schmidt and Allen.....	46
ii) Freeman and Co-workers.....	47
d. Scavenging Experiments.....	48
e. Gas Phase Total Ion Yields.....	50

	<u>PAGE</u>
C. Theory	53
1. Mobility in Gases.....	53
a. Ion Mobility.....	53
b. Electron Mobility.....	55
i) Temperature Dependence.....	55
ii) Field Strength Dependence of Mobility and of (D/μ)	57
2. Electron Mobility in Liquids.....	57
a. Quasifree Electrons.....	57
b. Localized Electrons.....	59
i) Nature of Localized Electrons.....	59
ii) Bubble Model.....	61
iii) Ether Model.....	62
iv) Percolation.....	63
c. Field Effect.....	63
i) Positive Dependence.....	63
ii) Negative Dependence.....	64
3. Free Ion Yields.....	65
a. High LET.....	65
b. Low LET.....	66
4. Correlations.....	67
D. Present Study.....	69
II. EXPERIMENTAL	70
A. Materials.....	70
B. Apparatus and Procedures.....	70
1. The Vacuum System.....	70

	<u>PAGE</u>
2. Sample Purification.....	73
3. Sample Cells.....	74
4. Filling the Cell.....	79
5. Temperature Control.....	80
6. Van de Graaf Accelerator.....	81
7. Gold Target.....	83
8. Charge Clearing Measurement.....	83
9. Mobility Measurements.....	85
C. Physical Properties.....	90
III. RESULTS	93
A. Electron Mobilities.....	93
1. Methane.....	93
2. Ethane.....	118
3. Propane.....	134
4. <u>n</u> -Butane.....	146
5. Isobutane.....	161
6. Ethene.....	175
7. Propene.....	185
8. Cyclopropane.....	198
B. Ion Mobility.....	208
1. Methane.....	209
2. Ethane.....	218
3. Propane.....	227

	<u>PAGE</u>
4. <u>n</u> -Butane.....	241
5. Isobutane.....	255
6. Ethene.....	268
7. Propene.....	276
8. Cyclopropane.....	287
C. Free Ion Yields.....	296
1. Methane.....	297
2. Ethane.....	310
3. Propane.....	318
4. <u>n</u> -Butane.....	331
5. Isobutane.....	345
6. Ethene.....	361
7. Propene.....	374
8. Cyclopropane.....	386
9. Isobutane + SF ₆	398
IV. DISCUSSION.....	406
A. Electron Mobility.....	406
1. Methane.....	406
a. Electric Field Effect.....	406
i) Low Density.....	406
ii) Effect of Density.....	408
b. Temperature Effect.....	413
i) Low Density Gas.....	413
ii) Effect of Density.....	416

2.	n-Alkanes	422
a.	Electric Field Effect.....	422
i)	Low Field Strengths.....	422
ii)	Threshold Field Strengths.....	422
b.	Temperature Effect.....	426
i)	Gas Phase.....	426
ii)	Liquid Phase.....	432
3.	Ethene, Propene and Cyclopropane.....	437
a.	Electric Field Effect.....	437
b.	Density-normalized Mobility.....	439
c.	Temperature Effect.....	445
i)	Gas Phase.....	445
ii)	Liquid Phase.....	450
4.	Isobutane.....	456
a.	Electric Field Effect.....	456
b.	Density-normalized Electron Mobility...	457
c.	Temperature Effect.....	458
5.	Liquid Phase Model Parameters.....	460
B.	Ion Mobility.....	462
1.	Electric Field Strength.....	462
2.	Density-normalized Mobility.....	462
a.	Low Density.....	462
b.	Effect of Density.....	465
3.	Temperature Dependence.....	466

PAGE

a. Low Density.....	466
b. Effect of Density.....	474
C. Free Ion Yields.....	479
1. General.....	479
2. Low Density.....	480
3. Effect of Density.....	481
4. Effect of Scavenger.....	485
D. Summary.....	487
1. Electron Mobility.....	487
2. Ion Mobility.....	488
3. Electron Thermalization Range.....	489
REFERENCES.....	490
APPENDIX	507

L I S T O F T A B L E S

		<u>Page</u>
Table I-1	Total Ion Yields in the Dilute Gases	52
Tables III-1 to III-8	Summary of Electron Mobility Results	
1.	Methane	115
2.	Ethane	132
3.	Propane	144
4.	<u>n</u> -Butane	159
5.	Isobutane	173
6.	Ethene	183
7.	Propene	196
8.	Cyclopropane	206
Tables III-9 to III-16	Summary of Ion Mobility Results	
9.	Methane	217
10.	Ethane	226
11.	Propane	239
12.	<u>n</u> -Butane	253
13.	Isobutane	266
14.	Ethene	275
15.	Propene	285
16.	Cyclopropane	295
Tables III-17 to III-25	Summary of Free Ion Yield Results	
17.	Methane	308
18.	Ethane	317.

		<u>Page</u>
19.	Propane	329
20.	<u>n</u> -Butane	343
21.	Isobutane	359
22.	Ethene	372
23.	Propene	384
24.	Cyclopropane	396
25.	Isobutane + SF ₆	405
Table IV-1	Temperature Coefficients of Thermal Electron Mobilities in Methane Gas at Different Densities	420
Table IV-2	Thermal Parameters of the <u>n</u> -Alkane Gases	431
Table IV-3	Liquid Phase Mobility Model Parameters	435
Table IV-4	Molecular Properties for the C ₃ Hydrocarbons and Ethene	442
Table IV-5	Mobilities and Dipole Moments for C ₄ Hydrocarbons at 296K	454
Table IV-6	Parameters for Ion Scattering Cross-sections	475
Table IV-7	Temperature Coefficients of Ion Mobilities	477
Table A-1	Mobility Errors	508
Table A-2	Free Ion Yield Errors	510

L I S T O F F I G U R E S

<u>FIGURE</u>		<u>PAGE</u>
II-1	Main Vacuum Manifold	71
II-2	System for Na-K Treatment and Filling Cells	72
II-3	Low Pressure Liquid Phase Cell	75
II-4	High Pressure Liquid Phase Cell	76
II-5	High Pressure Gas Phase Cell	77
II-6	Circuit to Measure Cell Constant	78
II-7	High Temperature Apparatus	82
II-8	System for Charge Clearing Measurements	84
II-9	System for Mobility Measurements	86
II-10	Amplifier #8	87
III-1 - III-4	Electron Mobilities, in Liquid Methane, Plotted against E/n at Different Temperatures	
1	181 to 189K	94
2	172 and 178K	96
3	122 to 176K	97
4	91 to 180K	98
III-5	Electron Mobilities, in Supercritical Methane Plotted against E/n at 192 to 196K	100
III-6 - III-17	Electron Mobilities, in Gaseous Methane, Plotted against E/n at Different Temperatures (K) and Densities (molec/cm ³).	
6	Co-existence vapor at 173 to 190K	101
7	Co-existence vapor at 168 to 185K	102
8	$n = 3.09 \times 10^{21}$ at 188 to 196K	103
9	Co-existence vapor at 154 to 169K	105

FIGUREPAGE

10	$n = 1.48 \times 10^{21}$ at 174 to 187K	106
11	Co-existence vapor at 145 to 153K	107
12	$n = 6.57 \times 10^{20}$ at 159 to 208K	108
13	Co-existence vapor at 120 to 134K	109
14	$n = 3.28 \times 10^{20}$ at 181 to 297K	110
15	$n = 7.13 \times 10^{19}$ at 117 to 297K	112
16	Co-existence vapor at 108 and 112K	113
17	Co-existence vapor at 97 to 117K	114
III-18	Electron Mobilities, in Liquid Ethane, Plotted as Functions of E/n at 148 to 241K	119
III-19	Electron Mobilities Plotted against E/n in Liquid Ethane at 281 to 304K and in the Supercritical Fluid at 306 to 310K	120
III-20	Electron Mobilities Plotted against E/n in Supercritical Ethane at 306 to 308K and in the Co-existence Gas at 296 and 302K	121
III-21- III-26	Electron Mobilities Plotted against E/n in Gaseous Ethane at Different Temperatures (K) and Densities (molec/cm ³)	
21	Co-existence vapor at 286 and 292K, and $n = 2.02 \times 10^{21}$ at 298 to 308K	123
22	$n = 1.02 \times 10^{21}$ at 276 to 309K	124
23	Co-existence vapor at 256 to 274K	126
24	Co-existence vapor at 236 to 254K	127
25	$n = 5.31 \times 10^{20}$ at 255 to 325K	128
26	Co-existence Vapor at 193 and 197K	129
27	$n = 6.77 \times 10^{19}$ at 203 to 326K	130
III-28	Electron Mobilities, in Liquid Propane, Plotted against E/n at 169 to 328K	135

<u>FIGURE</u>		<u>PAGE</u>
III-29	Electron Mobilities Plotted against E/n in Liquid Propane at 340 to 370K and in Supercritical Propane at 371 to 383K	136
III-30- III-34	Electron Mobilities, in Gaseous Propane, as Functions of E/n at Different Temperatures (K) and Densities (molec/cm ³)	
30	Co-existence Vapor at 369K and Supercritical Fluid at 370 to 377K	137
31	Co-existence Vapor at 328 to 360K and n = 1.50 x 10 ²¹ at 372 and 385K	138
32	Co-existence Vapor at 317K and n = 7.50 x 10 ²⁰ at 338 to 383K	140
33	Co-existence Vapor at 297 and 303K and n = 3.41 x 10 ²⁰ at 306 to 436K	141
34	Co-existence Vapor at 245K and n = 6.69 x 10 ¹⁹ at 253 to 394K	142
III-35- III-37	Electron Mobilities, in Liquid n-Butane, Plotted against E/n at Different Temperatures	
35	154 to 203K	147
36	222 to 298K	148
37	305 to 400K	149
III-38	Electron Mobilities Plotted against E/n in Liquid n-Butane at 414 and 421K, and in the Supercritical Fluid at 425 and 430K	150
III-39	Electron Mobilities Plotted against E/n in Gaseous n-Butane at 365 to 424.8K and in the Supercritical Fluid at 425 to 430K	151
III-40- III-44	Electron Mobilities in Gaseous n-Butane as Functions of E/n at Different Temperatures (K) and Densities (molec/cm ³)	
40	n = 1.18 x 10 ²¹ at 419 to 440K	152
41	n = 5.99 x 10 ²⁰ at 391 to 444K	154
42	Co-existence Vapor at 333K and n = 2.42 x 10 ²⁰ at 355 to 458K	155

<u>FIGURE</u>		<u>PAGE</u>
43	Co-existence Vapor at 296 to 304K	156
44	$n = 7.56 \times 10^{19}$ at 308 to 424K	157
III-45- III-46	Electron Mobilities Plotted against E/n in Liquid Isobutane at Different Temperatures (K)	
45	140 to 270K	162
46	298 to 406.7K	163
III-47	Electron Mobilities Plotted against E/h in Liquid Isobutane at 407.4K and in the Super- critical Fluid at 408 to 423K	164
III-48	Electron Mobilities Plotted against E/n in Gaseous Isobutane at 398 and 406K and in the Supercritical Fluid at 408 to 421K	165
III-49- III-53	Electron Mobilities, in Gaseous Isobutane, Plotted against E/n at Different Temperatures (K) and Densities (molec/cm ³)	
49	Co-existence vapor at 391K and $n = 1.15 \times 10^{21}$ at 400 to 425K	166
50	$n = 5.91 \times 10^{20}$ at 377 to 430K	168
51	Co-existence vapor at 297K to 371K	169
52	$n = 2.59 \times 10^{20}$ at 365 to 430K and $n =$ 5.91×10^{19} at 295 to 435K	170
53	Co-existence Vapor at 270 to 340K	172
III-54	Electron Mobilities Plotted against E/n in Liquid Ethene at 225 to 282.7K, and in Supercritical Ethene at 283 and 284.1K	176
III-55- III-58	Electron mobilities Plotted against E/n in Gaseous Ethene at Different Temperatures (K) and Densities (molec/cm ³)	
55	Co-existence Vapor at 274.4 to 281.6K	177
56	Co-existence Vapor at 256 and 265K, and $n = 1.64 \times 10^{21}$ at 268 to 294K	179

<u>FIGURE</u>		<u>PAGE</u>
57	Co-existence Vapor at 227 and 241K, and $n = 7.95 \times 10^{20}$ at 245 to 296K	180
58	Co-existence Vapor at 166 and 196K and $n = 1.89 \times 10^{20}$ at 203 to 298K	181
III-59	Electron Mobilities, in Liquid Propene, Plotted against E/n at 231 to 318K	186
III-60	Electron Mobilities Plotted against E/n in Liquid Propene at 350 and 365K, and in the Supercritical Fluid at 265.7 to 370K	187
III-61	Electron Mobilities Plotted against E/n in Supercritical Propene at 365.4 and 368K, and in the Co-existence Vapor at 362 and 364K	188
III-62- III-66	Electron Mobilities, in Gaseous Propene, Plotted against E/n at Different Temperatures (K) and Densities (molec/cm ³)	
62	$n = 1.66 \times 10^{21}$ at 358 to 368K	190
63	$n = 8.23 \times 10^{20}$ at 323 to 389K	191
64	Co-existence Vapor at 296K and $n = 4.15 \times$ 10^{20} at 305 to 382K	192
65	$n = 6.61 \times 10^{19}$ at 252 to 393K	193
66	Co-existence Vapor at 233 to 247K	194
III-67	Electron Mobilities, in Liquid Cyclopropane, Plotted against E/n at 254 to 367K	199
III-68	Electron Mobilities Plotted against E/n in Liquid Cyclopropane at 393K and in the Supercritical Fluid at 397.8K and 398.7K	200
III-69	Electron Mobilities Plotted against E/n in Supercritical Cyclopropane at 397.8 and 398.4K, in the Co-existence Vapor at 385 to 397K, and for $n = 1.64 \times 10^{21}$ at 387 and 399K	201
III-70- III-71	Electron Mobilities, in Gaseous Cyclopropane, Plotted against E/n at Different Temperatures (K) and Densities (molec/cm ³)	

FIGURE		PAGE
70	Co-existence Vapor at 358K and $n = 8.74 \times 10^{20}$ at 360 to 405K	203
71	Co-existence Vapor at 296K and $n = 3.51 \times 10^{20}$ at 322 to 406K	204
III-72	Ion Mobilities, in Liquid Methane, Plotted against E/n at 122 to 180K	210
III-73	Ion Mobilities, in Liquid Methane at 91 to 189K, and in Supercritical Methane at 195K, Plotted against E/n	211
III-74	Ion Mobilities Plotted against E/n in Supercritical Methane at 192, and 195K, and in the Co-existence Vapor at 173 to 190K	212
III-75- III-77	Ion Mobilities, in Gaseous Methane, Plotted against E/n at Different Temperatures (K) and Densities (molec/cm ³)	
75	Co-existence Vapors at 133 to 158K	213
76	$n = 7.13 \times 10^{19}$ at 117 to 297K	214
77	Co-existence Vapors at 108 and 112K	216
III-78	Ion Mobilities, in Liquid Ethane, Plotted against E/n at 166 to 281K	219
III-79	Ion Mobilities Plotted against E/n in Liquid Ethane at 224 and 298K, and in Supercritical Ethane at 306 and 309K	220
III-80	Ion Mobilities Plotted against E/n in Supercritical Ethane at 306 and 308K, and in the Co-existence Vapor at 296K	221
III-81- III-83	Ion Mobilities, in Gaseous Ethane, Plotted against E/n at Different Temperatures (K) and Densities (molec/cm ³)	
81	Co-existence Vapor at 256K to 286K	222
82	$n = 6.77 \times 10^{19}$ at 203 to 326K	224
83	$n = 6.77 \times 10^{19}$ at 197K and Co-existence Vapor at 193K	225

FIGURE		PAGE
III-84- III-85	Ion Mobilities, in Liquid and Supercritical Propane, Plotted against E/n at Different Temperatures	
84	169 to 371K	228
85	298 to 373K	229
III-86	Ion Mobilities Plotted against E/n in Supercritical Propane at 370 to 377K, and in the Co-existence Vapor at 369K	230
III-87- III-93	Ion Mobilities, in Gaseous Propane, Plotted against E/n at Different Temperatures (K) and Densities (molec/cm ³).	
87	Co-existence Vapor at 328 to 360K	232
88	$n = 1.50 \times 10^{21}$ at 372 and 385K	233
89	Co-existence Vapor at 317K, and $n = 7.51 \times 10^{20}$ at 338 to 383K	234
90	$n = 3.41 \times 10^{20}$ at 306 to 426K	235
91	Co-existence Vapor at 297 and 303K	236
92	$n = 6.69 \times 10^{19}$ at 257 to 394K	237
93	Co-existence Vapor at 245K, and $n = 6.69 \times 10^{19}$ at 253K	238
III-94	Fast Ion Mobility, in Liquid n-Butane; Plotted against E/n at 208 to 298K	242
III-95	Ion Mobility, in Liquid n-Butane, Plotted against E/n at 208 to 298K	243
III-96	Ion Mobility Plotted against E/n in Liquid n-Butane at 365K and Supercritical n-Butane at 427 to 443K	244
III-97	Ion Mobility Plotted against E/n, in Supercritical n-Butane and Co-existence Vapors, at 365 to 430K	246
III-98- III-102	Ion Mobilities, in Gaseous n-Butane at Different Temperatures (K) and Densities (molec/cm ³), Plotted against E/n	

<u>FIGURE</u>		<u>PAGE</u>
98	$n = 1.18 \times 10^{21}$ at 419 to 440K	247
99	Co-existence Vapor at 333K, and $n = 5.99 \times 10^{20}$ at 391 to 444K	248
100	$n = 2.42 \times 10^{20}$ at 355 to 458K	249
101	$n = 7.56 \times 10^{19}$ at 304 to 424K	250
102	Co-existence Vapor at 296 and 300K	251
III-103- III-104	Ion Mobilities, in Liquid Isobutane, Plotted against E/n, at Different Temperatures	
103	140 to 270K	256
104	298 to 403K	257
III-105	Ion Mobilities Plotted against E/n, in Liquid Isobutane at 393K and in Supercritical Isobutane at 408 to 423K	258
III-106	Ion Mobilities Plotted against E/n in Supercritical Isobutane at 408 to 421K	259
III-107- III-111	Ion Mobilities, in Gaseous Isobutane, Plotted against E/n, at Different Temperatures (K) and Densities (molec/cm ³)	
107	Co-existence Vapor at 352 to 406K	260
108	Co-existence Vapor at 391K, and $n = 1.15 \times 10^{21}$ at 400 to 425K	261
109	$n = 5.91 \times 10^{20}$ at 377 to 430K	262
110	$n = 5.91 \times 10^{19}$ at 283 to 435K	263
111	Co-existence Vapors at 270 to 297K	265
III-112	Ion Mobilities, in Liquid and Supercritical Ethene at 173 to 284K, Plotted against E/n	269
III-113	Ion Mobilities Plotted against E/n, in Supercritical Ethene at 253 and 285K, and in Co-existence Vapor at 275 and 281K	270
III-114- III-116	Ion Mobilities Plotted against E/n, in Gaseous Ethene at Different Temperatures (K) and Densities (molec/cm ³)	

FIGURE		PAGE
114	$n = 7.95 \times 10^{20}$ at 245 to 296K, and $n = 1.64 \times 10^{21}$ at 268 to 294K	271
115	Co-existence Vapor at 227 to 265K	272
116	Co-existence Vapor at 166 and 196K, and $n = 1.89 \times 10^{20}$ at 203 to 298K	273
III-117	Ion Mobilities, in Liquid Propene, Plotted against E/n at 231 to 370K	277
III-118	Ion Mobilities Plotted against E/n in Supercritical Propene at 365.4 and 368K, and in Co-existence Vapor at 362 and 364.2K	278
III-119- III-123	Ion Mobilities, in Gaseous Propene, Plotted against E/n, at Different Temperatures (K) and Densities (molec/cm ³)	
119	$n = 1.66 \times 10^{21}$ at 358 to 368K	279
120	$n = 8.23 \times 10^{20}$ at 349 to 389K	280
121	Co-existence Vapor at 296K and $n = 4.15 \times 10^{20}$ at 305 to 382K	281
122	$n = 6.61 \times 10^{19}$ at 247 to 393K	282
123	Co-existence Vapor at 233 and 240K	284
III-124	Ion Mobilities, in Liquid Cyclopropane at 254 to 393K, Plotted against E/n	288
III-125	Ion Mobilities, in Supercritical Cyclopropane at 397.8 and 398.7K, Plotted against E/n	289
III-126	Ion Mobilities, in Supercritical Cyclopropane at 397.8K and 398.4K, and in Co-existence Vapor at 395 and 397K, Plotted against E/n	290
III-127- III-129	Ion Mobilities, in Gaseous Cyclopropane Plotted against E/n, at Different Temperatures (K) and Densities (molec/cm ³)	
127	Co-existence Vapor at 385K and $n = 1.64 \times 10^{21}$ at 387 to 399K	291
128	Co-existence Vapor at 358K and $n = 8.74 \times 10^{20}$ at 360 to 405K	292

<u>FIGURE</u>		<u>PAGE</u>
129	Co-existence Vapor at 296K and $n = 3.51 \times 10^{20}$ at 322 to 406K	293
III-130- III-133	Free Ion Yields Plotted against E in Liquid Methane at Different Temperatures (K)	
130	91 and 118K	298
131	153 and 170K	299
132	173 and 179K	300
133	180 and 188K	301
III-134	Free Ion Yields, in Supercritical Methane at 192 and 194K, Plotted against E	303
III-135- III-137	Free Ion Yields, in Methane Plotted against E in Co-existence Vapor	
135	183 and 190K	304
136	158 and 173K	305
137	123 to 144K	306
III-138	Free Ion Yields, in Liquid Ethane at 166 to 298K, Plotted against E	311
III-139	Free Ion Yields, in Supercritical Ethane at 306 to 310K, Plotted against E	312
III-140	Free Ion Yields in Supercritical Ethane at 306 and 308K, and in the Co-existence Vapor at 296K, Plotted against E	314
III-141- III-142	Free Ion Yields, in Ethane in Co-existence Vapor, Plotted against E	
141	256 and 286K	315
142	273 and 276K	316
III-143- III-144	Free Ion Yields, in Liquid Propane at Different Temperatures, Plotted against E	
143	149 to 276K	320
144	297 to 365K	321

FIGURE

PAGE

III-145- III-146	Free Ion Yields, in Supercritical Propane at Different Temperatures, Plotted against E	
145	370 and 371K	322
146	370 to 374K	323
III-147- III-151	Free Ion Yields, in Gaseous Propane at Different Temperatures (K) and Densities (gm/cm^3), Plotted against E	
147	Co-existence Vapor at 369K, and $d = 0.110$ at 372 and 385K	324
148	Co-existence Vapor at 328 to 354K	325
149	$d = 0.0557$ at 338 to 383K	326
150	Co-existence Vapor at 317K, and $d = 0.025$ at 306 to 436K	327
151	Co-existence Vapor at 297 and 303K	328
III-152- III-153	Free Ion Yields, in Liquid <u>n</u> -Butane at Different Temperatures, Plotted against E.	
152	154 to 298K	332
153	299 to 421K	333
III-154- III-155	Free Ion Yields, in Supercritical <u>n</u> -Butane at Different Temperatures, Plotted against E	
154	425 to 441K	334
155	425 and 430K	335
III-156- III-161	Free Ion Yields Plotted against E in Gaseous <u>n</u> -Butane at Different Temperatures (K) and Densities (gm/cm^3)	
156	Co-existence Vapor at 384 to 423K	336
157	$d = 0.114$ at 420 to 441K	337
158	$d = 0.0575$ at 407 to 444K	338
159	Co-existence Vapor at 365 to 391K	339
160	$d = 0.0234$ at 354 to 458K	340

FIGUREPAGE

161	Co-existence Vapor at 295K	341
III-162- III-164	Free Ion Yields Plotted against E, in Liquid Isobutane at Different Temperatures (K)	
162	140 to 181K	346
163	214 to 270K	347
164	293 to 403K	348
III-165- III-166	Free Ion Yields Plotted against E, in Supercritical Isobutane at Different Tem- peratures (K)	
165	408 to 423K	350
166	408 to 420K	351
III-167- III-172	Free Ion Yields Plotted against E, in Gaseous Isobutane at Different Temperatures (K) and Densities (gm/cm ³)	
167	Co-existence Vapor at 398 and 10	352
168	d = 0.111 at 404 to 424K	353
169	Co-existence Vapor at 391K and d = 0.111 at 399K	354
170	d = 0.0565 at 376 to 428K	355
171	Co-existence Vapor at 352 and 371K	356
172	Co-existence Vapor at 297K	357
III-173	Free Ion Yields Plotted against E, in Liquid Ethene at 173 to 281K	362
III-174	Free Ion Yields, in Supercritical Ethene at 283 to 285K, Plotted against E	363
III-175- III-181	Free Ion Yields Plotted against E, in Gaseous Ethene at Different Temperatures (K) and Densities (gm/cm ³)	
175	Co-existence Vapor at 275 and 282K	364
176	d = 0.0762 at 268 to 294K	365

<u>FIGURE</u>		<u>PAGE</u>
177	Co-existence Vapor at 256 and 265K	366
178	$d = 0.037$ at 244 to 295K	367
179	Co-existence Vapor at 226 and 241K	368
180	$d = 0.0088$ at 206 to 297K	369
181	Co-existence Vapor at 195K, and $d = 0.0088$ at 203K	370
III-182- III-183	Free Ion Yields, in Liquid Propene at Different Temperatures, Plotted against E	
182	231 to 296K	375
183	296 to 364.5K	376
III-184	Free Ion Yields Plotted against E, in Supercritical Propene at 365 to 370K	377
III-185- III-189	Free Ion Yields, in Gaseous Propene at Different Temperatures Plotted against E	
185	Co-existence Vapor at 361 and 364K	378
186	$d = 0.116$ at 358 to 368K	379
187	$d = 0.0575$ at 348 to 388K	380
188	$d = 0.029$ at 305 to 381K	381
189	Co-existence Vapor at 296K	383
III-190	Free Ion Yields, in Cyclopropane at 254 to 332K, Plotted against E	387
III-191	Free Ion Yields Plotted against E, in Liquid Cyclopropane at 367 to 393K, and in Supercritical Cyclopropane at 398 and 399K	388
III-192	Free Ion Yields, in Supercritical Cyclopropane at 398 and 399K, plotted against E	390
III-193- III-197	Free Ion Yields, in Gaseous Cyclopropane at Different Temperatures, Plotted against E	
193	Co-existence Vapor at 396 and 397.7K	391

<u>FIGURE</u>		<u>PAGE</u>
194	Co-existence Vapor at 385K, and $d = 0.115$ at 387 to 398K	392
195	$d = 0.0611$ at 360 to 404K	393
196	Co-existence Vapor at 296 and 358K	394
197	$d = 0.0245$ at 321 to 406K	395
III-198- III-201	Free Ion Yields, in Liquid Phase Mixtures of Isobutane + SF ₆ at Different Temperatures, Plotted against E	
198	0.15 mol % of SF ₆	401
199	1.2 mol % of SF ₆	402
200	4.9 mol % of SF ₆	403
201	9.5 mol % of SF ₆	404
IV-1	Electron Drift Velocities in Methane Plotted against E/n	407
IV-2	(E/n) _{threshold} and (v _d) _{threshold} in Methane Plotted against n.	409
IV-3	(v _d) _{threshold} /c ₀ in Methane Plotted against n	410
IV-4	Density-normalized Electron Mobilities in Methane and Xenon Plotted against n	411
IV-5	Arrhenius Plot of Thermal Electron Mobilities in Gaseous Methane	414
IV-6	σ_v and f(v) for Low Density Methane Gas Plotted against Electron Energy	415
IV-7	Arrhenius Plot of Thermal Electron Mobilities in Methane in the Co-existent Liquid and Gas Phases	417
IV-8	Density-normalized Electron Mobilities <u>versus</u> n for Ethane, Propane and n-Butane	423
IV-9	(E/n) _{threshold} <u>versus</u> n for Ethane, Propane and n-Butane	424

<u>FIGURE</u>		<u>PAGE</u>
IV-10- IV-13	Electron Mobility <u>versus</u> T^{-1} .	
10	Gaseous Ethane	427
11	Gaseous Propane	428
12	Gaseous <u>n</u> -Butane	429
13	Liquid Ethane, Propane and <u>n</u> -Butane	434
IV-14	$(E/n)_{\text{threshold}}$ <u>versus</u> n for Ethene, Propene and Cyclopropane	438
IV-15- IV-16	Density-normalized Electron Mobilities <u>versus</u> n	
15	Propane, Propene and Cyclopropane	440
16	Ethene and Isobutane	441
IV-17- IV-22	Thermal Electron Mobilities <u>versus</u> T^{-1}	
17	Gaseous Ethene	446
18	Gaseous Propene	447
19	Gaseous Cyclopropane	448
20	Liquid C_3 Hydrocarbons	45T
21	Liquid Ethene and Liquid Isobutane	452
22	Gaseous Isobutane	459
IV-23- IV-24	Density-normalized Ion Mobilities <u>versus</u> n	
23	Methane and C_2 to C_4 <u>n</u> -Alkanes	463
24	Ethene, Propene, Cyclopropane and Isobutane	464
IV-25- IV-31	Ion Mobility <u>versus</u> T^{-1}	
25	Methane and Ethane	467
26	Propane	468
27	<u>n</u> -Butane	469
28	Ethene	470
29	Propene	471

<u>FIGURE</u>		<u>PAGE</u>
30	Cyclopropane	472
31	Isobutane	473
IV-32- IV-34	Density-normalized Electron Thermalization Ranges <u>versus</u> n	
32	Methane and Ethane	482
33	Ethene, <u>n</u> -Butane and Isobutane	483
34	C ₃ Hydrocarbons	484
IV-35	Density-normalized Electron Thermalization Range <u>versus</u> T for Liquid Phase Mixtures of Isobutane + SF ₆	486

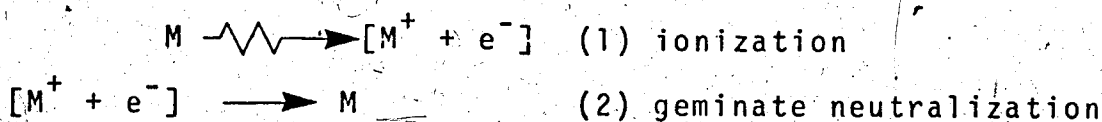
I N T R O D U C T I O N

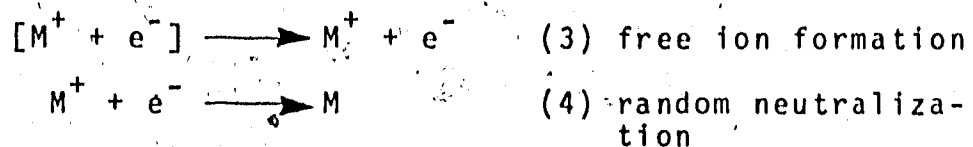
A. General

1. The Ionization Process

High energy radiation travelling through a medium interacts with the molecules in its path. These molecules absorb energy and dissociate into a high energy electron and an ion (1,2). In turn, the electron can cause further dissociations until its kinetic energy is reduced below the ionization potential of the molecules (~10 eV). The electron will continue to lose energy in electronic excitation of molecules until its kinetic energy drops below the electronic excitation threshold (~4 eV). Further losses of energy can occur by intramolecular vibrational excitation (~0.1 eV). The electron loses the final part of its energy (0.1 > energy > thermal energy) by rotational excitation of the molecules and to intermolecular modes. When the electron reaches thermal energy, there can still be appreciable electrostatic attraction towards the ion. The ion-electron pair can recombine (geminate neutralization) or drift apart (free ion formation). If the latter occurs, the electron and ion will diffuse randomly through the fluid until eventually recombining with other free ions (random neutralization).

These processes can be represented by:





where M is a molecule and e^- an electron. The squiggly arrow indicates the absorption of energy. The square brackets indicate the existence of electrostatic attraction that is appreciable compared to thermal energy.

Free ions are so named because there is a negligible interaction between them, so they diffuse separately in the bulk fluid. On the other hand, a group of ion pairs can be created close to each other. The ionization probability of a molecule by a 10 to 50 eV electron is near 1. As a result, if a molecule ionizes, ejecting a 30 eV electron, that electron will ionize the first molecule it encounters, which in a liquid or dense gas will be within a molecular diameter or two of the ionized molecule. The second molecule will also eject an electron and if its energy is ~10 eV, will also ionize a nearest neighbour. After their energies decrease below the ionization potential the electrons will move away from the molecules an average thermalization distance (in a hydrocarbon liquid) of about 10^{-6} cm (3). The ions will have moved very little during this time. There is appreciable electrostatic repulsion between the ions and attraction between ions and the electrons. In any group of ion-electron pairs where this is true there is a significant

ability that they will react with each other before diffusing into the bulk medium. These groups are said to be in a "spur".

If a liquid is irradiated by high energy electrons or photons about half of the ionizations occur as isolated events, forming single pair spurs. The other half of the ionizations occur in clusters of two or more, forming multipair spurs (3). Kinetic treatment of multipair spurs has only been accomplished with gross assumptions. However, multipair spurs rapidly decay to single pair spurs through the geminate neutralization of the innermost electrons. As a result, about two thirds of the ionizations in the liquid can be treated by a single pair spur model. Almost all estimates of electron thermalization distances reported to date are based on the single pair spur model (4-6).

2. Terminology

A charged particle in an electric field E is accelerated by the electric force eE and gains energy (7). In a fluid, the particle will undergo collisions and lose energy. A constant average velocity called the drift velocity is reached. If the energy gained between collisions is lost at a collision, then the drift velocity depends linearly on E . The proportionality constant between the drift velocity and the electric field strength is called the mobility. The maximum velocity attained between collisions (and hence the drift velocity) depends

on the length of time that the particle is accelerated by the field, that is the time between collisions. The time between collisions in a low density gas is inversely proportional to the number of molecules per unit volume, n . As a result, the drift velocity depends on (E/n) . This ratio will be used in discussions of mobility in subsequent sections.

If a beam of electrons is passed through a gas sample, the beam will be attenuated by collisions of the electrons with the molecules. If the sample is sufficiently thin, that is an electron once scattered from the beam is unlikely to undergo a second collision that scatters it back into the beam, the intensity of the beam is given by

$$I = I_0 \exp(-n\sigma x) \quad (5)$$

where I_0 is the intensity when $n = 0$, x is the distance that the beam travels through the sample (8), and σ is the scattering cross-section of a molecule.

B. Historical

1. Origins of Conductivity Studies

The effect of high energy radiation on the conductivity of insulators has been known since the turn of the century. Thomson found that X-rays increased the conductivity not only of gases (air), but also of liquids (vaseline oil) and solids (glass) (9). Similar findings

In the gas (10-12), liquid (13) and solid (14) phases were reported during the same period. Townsend determined that electrons accelerated by an electric field E can lead to further ionizations of air (11). Furthermore he found that at low values of E , the radiation induced current increased linearly with an increase in E (12). At intermediate fields, the current levelled off to attain a saturation plateau. At high field strengths, the current increased sharply for fairly small increases in E . This was understood to mean that at low values of E , not all the ions being generated were collected. The saturation current indicated that the fields used were large enough to collect all the ions. When the current increased sharply once more, the field strength reached was so large that the ions were accelerated enough to cause further ionizations in their collisions with the molecules.

Curie conducted an extensive investigation of the effects of electric field strength, molecular structure, temperature and phase on the radiation induced conductivities in liquids (13). The induced conductivity was found to increase with field strength, but to a much lesser extent than in the air. No levelling off was observed. The range of field strength used was $0 < E < 450$ V/cm. Curie also found that the size of the currents was independent of whether the radiation source was radium salts or a cathode tube. Curie found that the conduct-

ivity decreased in the liquids in the order carbon disulfide > petroleum ether > pentene > carbon tetrachloride > benzene > liquid air > vaseline oil. The high conductivity current in carbon disulfide was the first recorded occurrence of its anomalous behavior towards electrons (15). It is an efficient scavenger of electrons when present as a dilute solution in water but possesses a long thermalization distance in the neat liquid. A long thermalization distance meant that the compound would have a larger conductivity current, which was Curie's observation. The difference between petroleum ether and vaseline oil was attributed to the difference in volatility of the two compounds. It is now attributed mainly to the difference in liquid fluidities. In both petroleum ether and in pentene Curie found that the conductivity current at -170°C was only one tenth of its value at 10°C . Finally Curie made measurements in liquid air. This was the first determination of the induced conductivity of a cryogenic fluid. The current was found to possess the same characteristics as in the other dielectric liquids. The current in liquid air was more than a hundred times smaller than that in the gas at the same field strength.

2. Gas Phase Experiments

Two types of experiments were done in the gas phase. There was the direct determination of the collision cross-sections (Ramsauer type method) and there was the calculation of the cross-sections from swarm type experiments.

a. Ramsauer type experiments

The Ramsauer experiment was developed to allow the direct determination of electron-molecule total scattering cross sections (16-23). The method involved passing photoelectrically produced electrons through a magnetic field and collimating slits to select a particular energy. The final chamber contained the sample gas. The scattering cross-section was obtainable from the extent of attenuation of the electron beam by the gas (equation 5).

Ramsauer found that the cross-section depended upon the electron energy (16). As the electron energy was decreased towards 1 eV the cross-sections for the heavy rare gases decreased sharply. Extension of this work to energies lower than 1 eV led to the discovery that the cross-sections for these gases passed through a minimum and then increased once more (17). The same shape of curve was also found for methane (18).

Measurements were made in other molecular systems (19-22). In the n-alkane series, increasing the carbon chain length increased the cross-section. The qualitative features of the series methane through to n-pentane were

the same for electron energies greater than 1 eV. Branching of the hydrocarbon structure yielded a difference at low energies. The cross-sections of isobutane and *n*-butane (20) and neopentane and *n*-pentane (21) showed no difference at higher energies, but at lower values the cross-section of the more branched compound decreased much more rapidly than the other paraffin. The cross-sections for nitrogen- or oxygen-containing compounds and of unsaturated carbon bonds formed complex shapes. There was no simple pattern.

This method required pressures < 1 Pa, so could not be used to determine cross-sections at high densities. Furthermore, most of these studies could not be extended to near thermal energies (23). These difficulties could be circumvented by swarm measurements.

b. Swarm Experiments

i) Description of Methods

Swarm experiments involved the determination of a flight time or the determination of the amount of diffusion of a pulse of charged particles travelling a known distance (24,25). From the flight time, the drift velocity could be determined. From the diffusion across an electric field the ratio of the lateral diffusion coefficient D_L to the mobility μ , which depended on the characteristic energy, could be determined.

ii) Townsend's Work

Even in the earliest swarm measurements, pressures attained were hundreds to thousands times larger than those attainable in Ramsauer type experiments (26-34). Townsend measured two quantities, the drift velocity and the ratio of the mean kinetic energy of the electrons to that of the gas molecules (26,30). This ratio, which he designated k , was equal to the characteristic energy (eD_L/μ) divided by $k_B T$ where e was the electronic charge and k_B Boltzmann's constant and T the temperature. Townsend measured the lateral diffusion of the electron swarm across a known distance to get k . Next, by applying a magnetic field H at the same time, perpendicular to E , he obtained the drift velocity. An inherent problem was that while the calculated drift velocity depended proportionally on E , it depended inversely on H . The size of the magnetic field needed increased with pressure. With the fields available of a couple of thousand oersted, Townsend was limited to pressures less than 10^4 Pa (100 torr). Resolution of the method was also poor (24). At the lowest values of E/n used, Townsend found that k was greater than unity. This lower field was in the order of 10^{-17} V cm²/molec. For argon (29), the field was extended to 3×10^{-18} V cm²/molec. To obtain the mean velocity of the electrons, the mean velocity of the molecules was multiplied by the square root of k . The mean free path λ was calculated from a modification of Langevin's work for ions (see Section C).

Although the values for λ were likely incorrect, qualitatively the features were important. Although the bands obtained were broad rather than the sharper bands of the Ramsauer method, the calculated λ 's showed, as early as 1922, that the mean free path for argon was ten times larger than that in nitrogen or oxygen at the same pressure in the low field region. At higher values of E/n the mean free path of argon decreased by an order of magnitude. Townsend also found that there was no mean free path maximum in hydrogen (29) or helium (30), that is, no Ramsauer minimum in the scattering cross-section. Furthermore, the mean free paths stayed low and relatively constant. Indeed in He, the mean free path was constant in the range of $5 \times 10^7 < u < 10 \times 10^7$ cm/s ($0.5 < \epsilon < 2$ eV) where u was the mean agitation velocity of the electrons and ϵ was their energy. Over the same energy range, the mean free path in argon decreased by a factor of 6. It was not until six years later that this difference in behavior was confirmed by direct measurements of the scattering cross-sections. The large mean free path in argon corresponded to the small scattering cross-section of the Ramsauer type experiments. The relative transparency of the heavy rare gases to electrons of a certain energy near 1 eV is called the Ramsauer-Townsend effect.

iii) Application of Townsend's Method to Hydrocarbons

Swarm experiments were also used to determine mean free paths in ethene (31) and pentane (32). The curve in ethene closely paralleled that in oxygen though 60% of size of the oxygen curve. Both curves reached a maximum at $u = 4.5 \times 10^7$ cm/s (~ 0.4 eV). Oxygen, however, showed a distinct minimum at $u = 9.7 \times 10^7$ cm/s (~ 1.8 eV) while the ethene curve did not. The ethene curve appeared to be still levelling off. In pentane, the mean free path was measured in the range $2 \times 10^7 < u < 10 \times 10^7$ ($0.08 < \epsilon < 2$ eV). A sharp maximum was found at $u = 2.46 \times 10^7$ (~ 0.11 eV). This was the first indication that a minimum in the electron molecule scattering cross-section could occur in organic molecules other than methane.

The experiments of Schmeider (21) were limited to $\epsilon > 1$ eV so that the validity of McGee and Jaegers' finding could not be confirmed with a direct measurement. A degree of doubt could be attached since the maximum occurs near the lower energy limit of McGee and Jaegers' measurements. This was a clear demonstration of the other great advantage of swarm techniques. Values of u near 10^7 cm/s were routinely available, which corresponded to $\epsilon \sim 0.02$. Ramsauer measurements were at best done at $\epsilon > 0.1$ eV, and works on hydrocarbons at $\epsilon > 1$ eV.

iv) Electrical Shutter Methods

Townsend's method of determining characteristic energies has survived, with minor variations, to the present day. His cross fields method of measuring drift velocities was soon replaced by the more direct method of electrical shutters (24,25,33,34). This technique employed electrical shutters, both to form the groups of charged particles as well as to determine the drift times.

(a) Application of Electrical Shutters to Ion Studies.

Applications of this method to the determination of ion mobilities are described in references 24 and 25. Tyndall measured in gases the mobilities of ions of the same species as well as the mobilities of foreign ions. The major portion dealt with rare gases and inorganic molecular gases. A fair portion of his studies involved the application of Langevin's mobility equation (see section C) to studies of cluster sizes about ions. Tyndall pointed out that available data to date (1938) indicated that the ions were in two states. They could be moving through the gas unattached to other molecules, or they could be in clusters of varying sizes. The mobility measured depended upon the ratio of unattached to attached ions. Another detail noted was that (wP/E) over the investigated range of E/n was constant irrespective of the nature of the ionizing agent (w was the ion drift velocity, P was

the pressure of the gas and E was the electric field strength). (wP/E) reflected the ion-molecule collision cross-section. Its invariance indicated that the ions quickly reached the same state no matter what the initial conditions since the cross-section depended upon the reduced mass of the colliding pair, and that the ions were in thermal equilibrium with the gas. Normalized to 18°C and 760 mm of Hg (1.01×10^5 Pa) the mobilities were in the range of 1 to $10 \text{ cm}^2/\text{Vs}$.

In the subsequent years nearly all work in ion transport has involved studies of inorganic systems. Little work has been done to date on organic vapors. Ion work up to 1973 is summarized in reference 38. The remainder of this section will deal with electron studies.

(b) Application of Electrical Shutters to Electron Studies

Bradbury and Nielson adapted the electrical shutter method for electron mobilities (24,33,34,39). The wires making up the shutter were insulated from each other by mica, glass or ceramic plates. Electrons were generated photoelectrically. Absolute values of electron mobilities were determined in hydrogen (33) as well as oxygen, air, nitrous oxide and ammonia (34). Pressures up to 10^3 Pa and field strengths up to $6 \times 10^{-16} \text{ V cm}^2/\text{molec}$ were used. The drift velocity curve for hydrogen rose up steeply at low energies. Between $0 < E/n <$

2.4×10^{-16} v cm²/molec, the curve was concave towards the field strength axis. As the field strength increased the curve bent upwards, then at about $E/n \sim 4 \times 10^{-16}$, bent towards the E/n axis once more. Oxygen possessed the same dipping shape. The drift velocity over the entire field strength range used was almost twice that of the curve in hydrogen. There was a bump in the curve at $E/n \sim 6 \times 10^{-17}$, an upward shift at 1×10^{-16} and the curve bent towards the E/n axis at $E/n \sim 3.3 \times 10^{-16}$ and again at $E/n \sim 5.6 \times 10^{-16}$. In air a sole curve concave towards the E/n axis was obtained. The curve was intermediate between that of oxygen and that of hydrogen. In ammonia the curve increased linearly with E/n up to 7×10^{-17} v cm²/molec, sloped upwards until $E/n = 2 \times 10^{-16}$, where it sharply increased up to $E/n = 4 \times 10^{-16}$, then bent towards the E/n curve again. At $E/n < 2.4 \times 10^{-16}$, the drift velocity in ammonia was much less than in the other systems. By $E/n \sim 5 \times 10^{-16}$, the drift velocity had risen above that in air. Nitrous oxide results were given for $E/n < 1.2 \times 10^{-16}$. The curve was concave towards the E/n axis. Increasing the field led to a large increase of drift velocity. At $E/n \sim 6 \times 10^{-17}$, the drift velocity was four times that in air though at $E/n \sim 6 \times 10^{-18}$, the velocities were nearly the same.

Three other early works are important since they represent an extension of the gas pressure region to near

10^5 Pa (35-37). Mobilities were determined in nitrogen at 80 kPa, hydrogen at 85 kPa and carbon monoxide at 96 kPa. Over the voltage range $4.5 < V < 48$ V/cm, Wahlin found that the mean free path was independent of E. This was one of the first recorded determinations in the thermal electron region in a gas, that is, where the energy gained from the field by the electron is being lost at a collision.

3. Electron Mobilities in Hydrocarbon Vapors

From about 1940, the amount of swarm measurements in the gas phase has mushroomed (7,39-43). Of particular interest to the present work are the measurements performed on hydrocarbon systems especially small hydrocarbons such as alkanes from methane through to *n*-butane, and compounds such as ethene, propene, cyclopropane and isobutane (2-methylpropane). Available information on these systems will be considered in turn.

a. Methane

i) Low Pressure

Methane has been studied extensively (44-60). Early studies were concerned with methane because of its use in ionization chambers. Methane was approached from two directions. It was considered to be an extension of studies progressing from the monatomic rare gases to diatomic molecules to polyatomic molecules (i.e. methane). Alternatively, methane was approached as the

simplest alkane, as an extension from hexane to pentane and so on down the series to ethane and methane.

English and Hanna (44) exemplified the first approach, as did Bortner, Hurst and Stone (45). English and Hanna measured drift velocities in the rare gases, in methane and carbon dioxide and in mixtures of the rare gases with the molecular gases. Between $2 \times 10^{-18} < E/n < 2 \times 10^{-17}$ V cm²/molec, the drift velocity was found to increase super-linearly with E/n , with a bump being reached, followed by a levelling towards the E/n axis. Addition of methane to the rare gases was found to increase the value of E/n where the super-linearity sharply increased, as well as increasing the saturation drift velocity. Bortner, Hurst and Stone measured drift velocities in pure methane as well as mixtures. Addition of nitrogen to argon increased the saturation drift velocity in the same manner as English and Hanna reported for the addition of methane to argon. Bortner also found that the addition of oxygen or carbon dioxide to methane lowered the saturation drift velocity in the methane. The saturation drift velocity in the mixture fell between those of the pure components.

Devins and Crowe (46) investigated methane as part of the alkane series. Sparking potentials were measured as functions of pressure and gap separations. It was found that the sparking potential decreased linearly with the carbon number, but was almost independent of branching.

No structure effect could be noted in the hexane isomers. This was also true for the pentanes and the butanes at low values of Pd where P was the pressure and d was the gap separation. At higher values of Pd , the more branched isomers have larger sparking potentials than the n-alkanes (branching was beginning to increase the electric strength).

Attempts were also made to determine drift velocities at high field strengths. Frommhold measured drift velocities and diffusion coefficients at fields of $9 \times 10^{-16} < E/n < 1.8 \times 10^{-15} \text{ V cm}^2/\text{molec}$ (47). Pressures used were in the order of $5 \times 10^4 \text{ Pa}$ ($50 < Pd < 1500 \text{ cm torr}$, $d = 2, 3, \text{ or } 6 \text{ cm}$). The current due to the electrons (number of electrons) was found to increase exponentially with time. In the range of $0.38 < \epsilon < 0.76 \text{ eV}$ ($30 < E/P < 60 \text{ V/cm torr}$) the drift velocity could be approximated by $w = 2.36 \times 10^5 (E/P) - 4 \times 10^5$, where w was the drift velocity. In about the same region, Thall measured drift velocities in pure nitrogen, pure methane and a mixture of 390 torr of nitrogen (52 kPa) with 10 torr of methane (1.3 kPa). The measurements in nitrogen were made at 200 and at 400 torr. The measurements in methane were made at 275 and 400 torr. No pressure effect was observed. The methane results at $30 < E/P < 35 \text{ V/cm torr}$ ($9 \times 10^{-16} < E/n < 1.1 \times 10^{-15} \text{ V cm}^2/\text{molec}$) could be fitted to $w = 1.6 \times 10^6 (E/P) - 1.94 \times 10^6 \text{ cm/s}$. The addition of methane to nitrogen

increased the slope of the curve sharply to 3.44×10^5 (compared to 2.56×10^5 in pure nitrogen).. Schlumbohm achieved even higher field strengths (49). The drift velocity was measured at $120 < E/P < 1000$ V/cm torr ($3.6 \times 10^{-15} < E/n < 3.0 \times 10^{-14}$ V cm²/molec). The electron velocity was fitted to the expression $w = 5.8 \times 10^3 (E/P)^{0.758}$. Schlumbohm also measured positive ion mobilities in methane for $50 < E/P < 5000$ ($1.5 \times 10^{-15} < E/n < 1.5 \times 10^{-14}$). The curve had a fairly clear break at about $E/P = 300$, although it was already bending over at lower fields. The data was fitted to $w_+ = 2.1 \times 10^3 (E/P)$ for $50 < E/P < 200$, and $w_+ = 3.2 \times 10^4 (E/P)^{3/2}$ for $300 < E/P < 5000$.

Most of the more recent works attempted to extract the electron-molecule momentum transfer cross-section from measurements of the drift velocity and of the ratio of the diffusion coefficient to the mobility (D/μ). An account of some of the calculations is given in Section C.

Cottrell⁹ and Walker (50), Wagner, Davis and Hurst (51), Bowman and Gordon (52), and Pollock (53) all measured drift velocities. Field strengths were fairly high, usually in the range of $3 \times 10^{-18} < E/n < 9 \times 10^{-17}$ V cm²/molec. Only the 298K data of ref. 52 reached as low as 6×10^{-19} . Even though in the lower portions of these measurements, the drift velocities were roughly proportional to E/n , they were increasing with field strength

as $(E/n)^r$ with $r > 1$. The electrons were not in thermal equilibrium with the gas at these field strengths. The pressures used were less than 10^5 Pa. Although scatter between and within data sets was appreciable, the general features were constant. The curve possessed a maximum at $E/n \sim 3 \times 10^{-17}$ and decreased to a minimum 4×10^{-16} . At higher fields, the velocity would be expected to increase once more (47-49).

If the drift velocity depended on $(E/n)^r$ with $r = 1$, the cross-section could be extracted by a simple temperature variation of the low field mobility (see Section C). Unfortunately as noted above, this condition did not hold at $E/n > 6 \times 10^{-19}$. Extraction of the cross-section required the separate determination of the Townsend k factor or of the diffusion coefficient. Cottrell and Walker (54) determined the k factor and Nelson and Davis determined the diffusion coefficient (55). Duncan and Walker determined the ratio of the diffusion coefficient to the mobility (56). Nelson and Davis did not determine the absolute cross-sections but merely the product of DP , which varied inversely to the scattering cross-section. The methane curve rose sharply at $0.15 < E/n < 0.9$ which meant in this range the cross-section should be decreasing. The cross-sections calculated by Duncan and Walker in the range $0.02 < \epsilon < 4$ eV showed a minimum at 0.25 eV with a value of $1 \times 10^{-16} \text{ cm}^2$.

ii) High Pressures

Measurements have been made in compressed methane. Cookson measured the drift velocity at $9 \times 10^{-16} < E/n < 1.8 \times 10^{-15} \text{ V cm}^2/\text{molec}$ and at $P = 1.3 \text{ MPa}$ (57). The result was found to be the same as in the dilute gases. More interesting high pressure results were found in a study made by Lehning at $6 \times 10^{-19} < E/n < 2 \times 10^{-17}$ (58). The quantity measured was the ratio of the drift velocity at the pressure of the measurement to the drift velocity at 500 torr. Lehning labelled this quantity q . Plotting q as a function of E/n showed that q increased with E/n up to 3×10^{-18} , decreased between 3×10^{-18} and 3×10^{-17} , and was roughly constant at higher fields. Furthermore, the amount of increase from 3×10^{-19} to 3×10^{-18} depended on the pressure. The greater the pressure, the larger was the increase in q . Above 3×10^{-17} , q was constant, independent of the pressure. This explained why Cookson found no pressure effect. A plot of q^{-1} vs P for a fixed E/n , showed a linear dependence with a negative slope. The slope increased as E/n decreased from 3×10^{-17} to 3×10^{-18} .

The mobility was measured in methane as a function of density at temperature between 196K and 295K (59). In all cases, the electron mobility varied as n^{-1} at low densities, achieved a minimum at about $3.6 \times 10^{21} \text{ molec/cm}^3$ and then increased, passing through a maximum at about $10 \times 10^{21} \text{ molec/cm}^3$. The mobility was higher

for a higher temperature. Although not commented upon, the mobilities for the 196K curve at $n = 8.5 \times 10^{20}$ and at 1.2×10^{21} were higher than the line extrapolated from the higher densities (Figure 1 of ref. 55).

iii) Application

An indication of the general acceptance of drift velocities in methane can be seen from the recent application to drift chambers (60). The methane results were used to calibrate the chamber for studies on rare gas mixtures.

b. Methane-d₄

Methane is a good starting point for investigations of structural effects on drift velocities or cross-sections. The simplest change, which maintains methane in the same structural symmetry, would be to replace all the hydrogen atoms with deuterium atoms (50,53).

At field strengths up to $E/P = 0.5$ V/cm torr ($\sim 1.5 \times 10^{-17}$ V cm²/molec) the CH₄ and CD₄ curves were the same. At higher fields, the CD₄ curve was lower than that of CH₄. These observations were taken to mean that at the lower energies the energy loss was elastic and that the size of CH₄ and CD₄ were sufficiently similar that no difference could be observed. At higher energies, the vibrational excitation became more important. Vibrational quanta were smaller in the deuterio compound so that the fractional energy loss to CD₄ would be smaller, and

hence its cooling ability towards the electrons was less than that of CH_4 .

Measurements of the Townsend k factor (54) showed that at low fields, the electron energy was the same in CD_4 as in CH_4 . At higher fields, the electron energy was larger in CD_4 than in CH_4 . At $E/P = 2 \text{ V/cm torr}$, the CD_4 curve was 45% higher than that of CH_4 .

Cottrell and Walker combined k factors (54) and drift velocities (50) to estimate the fractional energy loss per collision (λ) and the momentum transfer cross-section (Q_D). λ depended on the square of the drift velocity, w^2 , and inversely on k . At high fields, electrons in CD_4 possessed both a smaller drift velocity, and a larger Townsend coefficient, k , so that λ was much smaller in CD_4 than in CH_4 . Q_D depended inversely on the product of w and k . The differences were in inverse directions. The decrease in w was cancelled by the increase in k so that Q_D was found to be the same in CD_4 as in CH_4 .

c. Silane and Silane- d_4

An additional comparison could be done by replacing the carbon atom of methane with a silicon atom (50,53,54). The drift velocity attained near the maximum and the general shape of the drift velocity curve were the same in silane as in methane. The curve for silane was shifted along the E/n curve by a factor of 6. The frac-

tional energy loss per collision between CH_4 and SiH_4 near the maximum was larger in SiH_4 by 13%. Q_D was also larger in SiH_4 than in CH_4 by a factor of 6. The energy of the Q_D minimum was about the same in both compounds.

The deuterium isotope effect was the same in silane as in methane. The k factor rose more quickly in SiD_4 at high fields than in SiH_4 . The λ values on the low energy side of the maximum were much more similar than those between CH_4 and CD_4 .

d. n-Alkanes

i) Ethane and Propane

Methane although an alkane has properties unlike those of higher n-alkanes. For example, the inverse of boiling points of the n-alkanes can be related to the carbon number of the alkanes raised to the two-thirds power. All the normal boiling points agree with this correlation to within two degrees, except that of methane (61). The simplest compound which possesses properties similar to the other n-alkanes is ethane.

Drift velocities in low density ethane and propane gases have been measured by Cottrell and co-workers (50,62) and Christophorou and co-workers (63,64). Bowman and Gordon made measurements in low pressure ethane (52). Huber determined drift velocities in ethane (65,66) and in propane (66) from low pressures (0.06 MPa) to high pressures (4.5 MPa for ethane and 1 MPa for propane). In

order to obtain electron scattering cross-sections, measurements were made of the Townsend k factor in the low density gas (54), of (D/μ) where D is the diffusion coefficient and μ is the mobility (67), and of the temperature dependence of the drift velocity (52,64).

The drift velocity curve as a function of E/n for both compounds had the same shape. At pressures $0.1 < P < 10^2$ kPa, w was independent of pressure. At 298K, the propane curve lay below that of ethane, for all values of E/n up to 1.2×10^{-16} V cm²/molec. The lowest field strengths were attained by Huber (66) and Christophorou (64). As the field strength was increased, the drift velocity rose gradually, then increased sharply, and then curved over towards a saturation velocity of about 5×10^6 cm/s. The same was true for propane but the field strength where the drift velocity became superlinear with respect to E/n was larger. The saturation drift velocity was also about 5×10^6 cm/s. The low density results of all four research groups where they overlapped agreed to within 15%.

Huber had also studied the effect of pressure on the drift velocity in these two compounds (65,66). In both cases, an increase in pressure led to a decrease in drift velocity. The ratio $q = w(P)/w(450 \text{ torr})$ plotted against E/n showed a minimum in ethane at 6.5×10^{-18} V cm²/molec. The minimum deepened as the pressure was increased from 0.6 MPa to 4.5 MPa. A plot of q^{-1} vs P showed that a

linear relationship existed at constant E/n . Addition of 2, 3 and 5% CO_2 did not change the shape of the q vs E/n plot (for $n = 1.5 \times 10^{20}$ molec/cm³). The position of the minimum was shifted to high field strengths.

Similar results were found in propane. The drift velocity decreased with pressure. However, no minimum was found in the q vs E/n plot. At $E/n \leq 5 \times 10^{-18}$ V cm²/molec, the curve was constant. At larger E/n , the curve increased. At about 4×10^{-16} , the pressure difference disappeared. The pressure effect was largest at $E/n \leq 5 \times 10^{-18}$ and decreased as the pressure was increased towards 1 MPa.

The temperature dependences of the drift velocities of the two compounds have been measured. In ethane (52,64), the low field drift velocity increased between 225K up to 373K, stayed constant until 573K and then decreased. The high field results merged into a single curve at about 9×10^{-18} V cm²/molec. In propane, the merge occurred near 4×10^{-18} V cm²/molec (64). The drift velocity increased between 297K and 373K. Change between 373K and 473K was slight. Further increases to 573K and 673K led to a decrease in the drift velocity. The curves at 573 and 673 did not seem to show a superlinear increase of w before levelling off towards the saturation drift velocity. The saturation velocity was the same for all temperatures and was about 5×10^6 .

ii) Other n-Alkanes

Data are available for all the n-alkanes from butane through to octane. Most results were measured at room temperature. Pressures used by Christophorou and co-workers were not stated. Results were normalized to 1 torr (63), 100 torr (64) or by multiplying the measured (wP/E) by the ratio of (n_G/n_L) where n_G is the density of the gas in molec/cm³ at the specified gas temperature and n_L is the density of the liquid at the same temperature, also in molec/cm³ (68). Roznerski and Gazda used pressures between $0.6 < P < 6\text{kPa}$ (69). György and Freeman (70) and Huang and Freeman (71) made measurements along the co-existence curve at the vapor pressure of the liquid.

Christophorou and his collaborators have made extensive measurements over the past twenty years of drift velocities in the dilute gases. Work prior to 1970 is collected in ref. 72. Measurements for the series n-butane, n-pentane and n-hexane revealed that normalizing the (drift velocity x pressure) by n_G/n_L leads to similar values, but that the values still decrease in the order n-butane > n-pentane > n-hexane (68). Field strengths up to $E/n \sim 3 \times 10^{-18} \text{ V cm}^2/\text{molec}$ were used. Subsequent extension of measurements to cover all the alkanes from ethane through to n-decane showed that the mobility (normalized to 1 torr) decreased continuously as the

carbon number increased (62). There appeared to be a roughly linear correlation between the momentum transfer cross-section and the static polarizability α . Christophorou actually used a cubic equation to fit the data since the methane cross-section calculated from a gas phase mobility supplied by Davis and Nelson as a private communication, was slightly greater than that of ethane. However, the μ vs α plot (Figure 2 of ref. 3) also showed that methane did not fall on the same curve as the other alkanes.

Christophorou determined the effect of the temperature on the drift velocity in n-butane (64). At 299K, there was a slight superlinearity to the drift velocity increase as E/n was increased. The extent of the superlinearity was not beyond the experimental scatter. At 373K there was no superlinearity. Increasing the temperature further to 473K did not change the low field drift velocity but it decreased slightly in the range $2 \times 10^{-18} < E/n < 2 \times 10^{-17}$ V cm²/molec and increased above the 373K curve at $E/n > 4.5 \times 10^{-17}$. The 573K was below that of 473K, and the 673K curve was below that of 573K except for the two highest field strengths. For all temperatures, the drift velocity seemed to increase linearly with E/n up to 1×10^{-17} V cm²/molec. At $E/n > 4.5 \times 10^{-17}$ the difference between w curves at different temperatures may have been due to scatter. The saturation drift velocity

was about 4.2×10^6 cm/s.

Roznerski and Gaza (69) measured the drift velocities at 296K for n-hexane, n-heptane and n-octane. Hexane measurements were made in the range $1.8 \times 10^{-18} \leq E/n \leq 9.2 \times 10^{-17}$ V cm²/molec. Results at $1.8 \times 10^{-18} \leq E/n \leq 3.8 \times 10^{-18}$ were lower than those in ref. 67 by 5%. Above 1×10^{-17} V cm²/molec, the results were up to 30% higher. As the carbon number increased, the initial slope of the drift velocity vs E/n plot, and the saturation drift velocity both decreased.

György and Freeman (70) studied n-pentane along the entire co-existence curve as well as along isochores. Mobilities were independent of applied field strength up to $E/n = 2 \times 10^{-17}$ V cm²/molec. Increasing the temperature at constant density caused an increase in mobility. The amount of increase was larger if n/n_c was larger (n was the gas density, and n_c was the critical density). At higher temperatures, the mobility along the $n/n_c = 1, 0.8, 0.6, 0.4$ and 0.15 isochores tended towards a leveling off. A plot of the mobility vs n along the co-existence curve showed that the mobility varied as n^{-1} for $n \leq 1 \times 10^{20}$ molec/cm³. A plot of μn vs n revealed this as a constant μn up to 1×10^{20} molec/cm³. At higher densities multibody scattering became more important, leading to a decrease in μn , which reached a minimum at about 1.7×10^{21} molec/cm³. For the low density

vapor in the vicinity of 400K, the electron scattering cross-section varied as the electron velocity raised to a power of -1.1.

Huang and Freeman (71) made similar measurements in n-hexane. Measurements were made along the co-existence curve for $T \geq 296\text{K}$ and for the isochores where $n/n_c = 1.0, 0.80, 0.51, 0.25, 0.10$ and 0.021 . Within experimental scatter, the mobility was independent of E/n up to $1 \times 10^{-17} \text{ V cm}^2/\text{molec}$. A temperature increase increased the mobility for all the isochores. The temperature coefficient decreased as n/n_c decreased. A plot of μn vs n along the co-existence curve showed that μn was independent of n for $n \leq 4 \times 10^{19} \text{ molec/cm}^3$. At higher n , the μn curve decreased to a minimum at $n = 1.3 \times 10^{21}$, and then increased as the critical point was approached. (This was attributed to an increase in multibody effects). An average cross-section of $1.6 \times 10^{-15} \text{ cm}^2$ was estimated at 500K from the temperature variation of the $n/n_c = 0.021$ curve. The cross-section was found to vary as the electron velocity raised to a power of -0.9.

e. Branched Alkanes

Christophorou and co-workers have measured the drift velocity in isobutane at room temperature (68) and in neopentane, both at room temperature (68) and as a function of temperature at 100 torr and as a function of pressure at 373K (64). Freeman and co-workers have measured elect-

ron mobilities in neopentane along the co-existence curve and at fixed densities as functions of temperature from the dilute gas up to the supercritical fluid (70,71):

Christophorou (68) found that the drift velocity in isobutane was independent of field strength up to $E/n = 2.5 \times 10^{-18} \text{ V cm}^2/\text{molec}$. The mobility, normalized by n_G/n_L , was found to be a factor of 2 smaller than that of n-butane. In neopentane this value was about a factor of 3 smaller than that of n-pentane. Christophorou also found that from 298K to 673K, w increased with temperature. Increasing the pressure from 10 to 100 torr led to no change. However, when the pressure was raised to 1000 torr and then to 8230 torr, the drift velocity decreased.

Electron mobilities, measured in neopentane increased at high field strengths for all densities from the dilute gas to the critical fluid (70,71). The threshold field decreased as the density approached the critical value. A plot of μn vs n was constant up to about $1 \times 10^{20} \text{ molec/cm}^3$. Further increases in density led to a continuous increase up to the critical point.

Increasing the temperature along isochores led to a sharp increase in mobility even at $n/n_c = 0.038$. The temperature coefficient of mobility was 0.044 eV at that density. The $n/n_c = 0.11$ curve had almost the same temperature coefficient, but as n/n_c continued to increase, the temperature coefficient increased as well.

The curves for $n/n_c = 0.79, 0.86, 0.95$ and 1.0 nearly coincided. At temperatures above 446K , all four curves merged into that of the $n/n_c = 0.53$ curve. This meant that the mobility vs n plot would have roughly the shape measured in methane (59). This was found to be true. A minimum occurred at about 1.7×10^{21} . Little variation was found between $n/n_c = 0.7$ and $n/n_c = 1.0$.

Huang made measurements of electron mobilities in neopentane in a cell constructed so that the liquid level rose up to the center of the electrodes as the critical region was approached (73). As a result, two distinct signals were observed, one corresponding to each phase. The critical point was reached when the two signals merged into a single signal. Huang found that the mobility at the critical point was higher than those at $0.5 \leq n < n_c$, which the experimental scatter in György's work could not confirm. The smooth transition of the mobility curve through the critical region showed that the large density fluctuations that characterize the critical fluid have diameters that are too great to hinder electron migration. The prediction (74) that such scattering would occur was earlier shown to be untrue for electron mobilities in critical xenon (75). Huang also found that at 2.42×10^{21} molec/cm³, the electric field effect changed sign. At lower densities the mobility at high field strengths increased with E/n . At higher densities, the mobility

decreased as E/n increased. It was suggested that a Ramsauer-Townsend minimum occurred at thermal energy at that density.

f. Ethene, Propene and Cyclopropane

Drift velocities have been measured in ethene (45,50, 51,52,62,76), propene (52,67) and cyclopropane (45). Diffusion coefficients were also measured. Data for ethene are in ref. 55, 77 and 78, for propene in ref. 67 and for cyclopropane in ref. 77 and 78.

In ethene and in propene, there was no superlinear increase in drift velocity with E/n . The curves varied linearly with E/n up to about 5×10^{-18} V cm²/molec in ethene, and up to about 3×10^{-17} V cm²/molec in propene. From the temperature variation of w , Bowman and Gordon determined that the cross-section in both compounds decreased with energy between $0.02 < \epsilon < 0.06$ eV (52). However, using the (D/μ) as well as the drift velocities, Duncan and Walker determined that the momentum transfer cross-section was constant up to 0.05 eV and thereafter rose in a s-curve with a bump at about 0.1 eV (78). The propene cross-section was also constant at $\epsilon < 0.07$ but dipped to a minimum at 0.2 eV before increasing again (67). These results placed doubt on the drift velocity measurements of ref. 52. If the results of Duncan and Walker were correct, the drift velocity should have had a negligible temperature coefficient. As well, the drift velocity in

propene should be seen to increase superlinearly with electric field strength at the higher values.

In cyclopropane, the drift velocity was not linear in the low field region (45). From (D/μ) measurements Duncan and Walker calculated that the cross-section was constant at $\epsilon < 0.04$ eV and increased at higher energies (67). The drift velocity should have no superlinear dependence. The drift velocity data of ref. 45 at $E/n < 1 \times 10^{-17}$ V cm²/molec can be fitted to a straight line with scatter of less than 15%.

The saturation drift velocities in these three compounds decreased in the order ethene > propene > cyclopropane. The values were (in the same order of compound) 4.8×10^6 , 4.5×10^6 and 3.6×10^6 cm/s.

In ethene a study had been conducted on the effect of pressure on the drift velocity (76). As the pressure at $\epsilon < 0.05$ eV increased from 39 kPa to pressure of 320, 610, and 810 kPa, the drift velocity continued to decrease. As the energy increased, the pressure effect got smaller. At $0.15 < \epsilon < 0.2$ eV, no pressure effect was observed.

4. Liquid Phase Mobilities

a. Ion Mobilities

i) Adamczewski

One of the first extensive investigations of ion mobilities in liquid hydrocarbons was conducted by

Adamczewski in the 1930's (61,79): The series of n-alkanes, n-pentane to n-decane, was used since properties such as boiling point, density and viscosity decreased systematically as the carbon number increased. 7

By Walden's rule, the product of the mobility and the viscosity, η , was approximately constant. Alternatively, by Stoke's rule, the mobility varied as $(nr)^{-1}$, where r is the radius of the ion. Adamczewski found that the room temperature mobilities in the alkane series varied as $\eta^{-3/2}$. A possible explanation offered was that r varied as $\eta^{-1/2}$. He also noted that since η depended on $\exp(c/T)$ where c is a constant and T the temperature, the mobility μ should be related to the temperature by

$$\mu \sim \exp[-3c/2T] \quad (6)$$

In order to see if the mobility always varied as $\eta^{-3/2}$ Adamczewski measured the mobility as a function of temperature in paraffin oil (80). Walden's rule was found to hold. The activation energy obtained from plotting the logarithm of the mobility against $1/T$ was equal to the activation energy for the viscosity. It should be noted that the viscosity of the paraffin oil was also thousands of times larger than that in the smaller hydrocarbons.

References to earlier ion studies (before 1937) are in ref. 79.

ii) Photo Injection

Electrons can be injected into a liquid by flashing light at a metal electrode. Should the liquid be insufficiently pure, the electrons would quickly be attached to impurities such as oxygen to form negative ions.

LeBlanc used this method to study charge transport in liquid n-hexane (81). He found that the mobility appeared to be fitted to the equation,

$$\mu = \mu_0 \exp(-\Delta\epsilon/kT) \quad (7)$$

where he defined μ as the mobility, μ_0 the mobility at infinite temperature and $\Delta\epsilon$ as the average trapping energy. The charged particle was considered to be either trapped or untrapped, and the mobility depended upon the fraction of the time that was spent in each state. The idea of a two state transport mechanism had been earlier proposed by Tyndall for ion transport in gases (25) and by Crowe for liquid hydrocarbons (82). At about the same time as LeBlanc, a definite ion cluster transport mechanism in liquid He^4 had been reported by Atkins (83).

Other temperature studies on alkanes were being performed in Poland using the same method as LeBlanc. Terlecki found that the negative ion mobilities in n-hexane, n-octane and n-decane, which equalled 9.8×10^{-4} , 7.0×10^{-4} , and $3.0 \times 10^{-4} \text{ cm}^2/\text{Vs}$ respectively, were all independent of electric field strength up to 300

kV/cm (84). Gzowski determined ion mobilities in n-hexane, n-heptane, n-octane and n-decane as well as in mixtures of n-hexane plus n-octane and n-hexane plus n-decane at temperatures of $281 < T < 323\text{K}$ (85). He found that in all cases, the negative ion mobility varied as n^{-1} . The positive ion mobility on the other hand varied as $n^{-3/2}$, which was what Adamczewski had found in the 1930's.

In Japan, Chong and Inuishi also measured the mobility in n-hexane (86). The mobility of the negative ion was found to be independent of electric field strength up to 510 kV/cm. The mobility was independent of drift distance. Addition of 1% of ethanol decreased the mobility by a factor of 2.3.

All the above workers had thought that the negative ion mobility corresponded to the actual electron mobility. Samuel and co-workers found evidence that even at low field strengths ($750 < E < 7500 \text{ V/cm}$), the mean free path of electrons in liquid hydrocarbons may be larger than previously thought (87). The method was the same as that used to detect quasifree electrons in liquid argon (88). Conductance pulses of 10^{-5} s duration were detected in liquid hydrocarbons subjected to steady-state, low intensity (8 rad/hr) γ radiation. While a satisfactory mechanism for the generation of the pulses has not been proposed, Samuel suggested at the time that their presence implied that the electron mobility in n-hexane may be as large

as $20 \text{ cm}^2/\text{Vs}$ rather than the 10^{-3} previously reported.

iii) Free Ion Yield Related Measurements

A fair amount of work was done on ion mobilities to determine free ion yields, which depend directly on the ion-neutralization rate constant, and as the square of the quotient of the induced specific conductance divided by the mobilities (positive plus negative). Ion mobilities need to be estimated (89,90) or measured (91-94).

Freeman and Fayadh suggested that the electron may be trapped in cavities in the liquid structure (90). Hummel, Allen and Watson found that addition of oxygen at 1 atmosphere pressure decreased the positive ion mobility by 20%, but did not affect that of the negative ion (92). It was suggested that the ion mobility was that of an oxygen ion formed by the addition of the electron to minute traces of oxygen not removed by the degassing or chemical purification.

Tewari and Freeman noted that the ion mobility and the free ion yield appeared to increase as the molecule became more spherical (93). Purification procedures had improved so that an initial sharp peak was found on the current vs time trace obtained when neohexane or neopentane was exposed to a pulse of X-rays (94). Addition of oxygen or SF_6 eliminated the "overshoot" (as the initial spike was called) and decreased the free ion

yield. Although not confirmed until the next year (95), this overshoot was the first recorded observation of a true thermal electron signal in a liquid hydrocarbon.

iv) Other Results

Schmidt and co-workers have measured ion mobilities in methane (96) and ethane (97). The mobilities were of the same order of magnitude and were independent of applied electric field up to the highest fields used (60 kV/cm for methane and 160 kV/cm for ethane). Walden's rule held for both liquids at $T < 137\text{K}$ for methane and $T < 216\text{K}$ for ethane. Application of Stoke's Law using a hard core radius of 0.19 nm for methane and 0.219 nm for ethane led to calculated mobilities larger than those actually observed, by a factor of 1.4 in methane and 3.0 in ethane. The explanation was offered that the lower observed mobility in methane was due to the polarization interaction between the ion and the molecules, while that in ethane was due to the dragging by the ion of a solvation shell of nearest neighbours.

Recently, even more extensively purified hydrocarbons such as n-hexane have been examined (98,99). Earlier workers had found a single negative charge carrier but often several positive charge carriers. The more recent results confirmed that the negative ions were more mobile than the positive, but there was only one major charge carrier of each sign.

b. Electron Mobilities in Liquid Hydrocarbons

i) Background

Electron mobilities had been measured in liquified rare gases since 1951 (100). However, sufficient purification to allow the observations of a signal that could definitely be attributed to electrons was not accomplished in liquid hydrocarbons until 1968 (94). Confirmation by several research groups followed quickly afterwards (95, 101-103) and measurements were made in a wide number of systems (104-106). These experimenters used glass conductance cells that could only withstand gas pressures up to about 0.4 MPa, which placed a practical limitation on the temperature range over which measurements could be made.

Despite the limited temperature range a great amount of data was collected, especially after 1972 (96,97,107-122). Higher pressures had been used in work with liquified rare gases (123,124). This design has recently been adopted for use with hydrocarbons (125-129). Freeman and co-workers developed a glass cell with walls 1 cm thick (in contrast with previous cells of 0.2 cm) which could stand pressures up to 6.5 MPa. Measurements could be made over a continuous density range from the dense liquid to the critical fluid and into the dilute gas (70,71, 73, 130-132). It should be noted that the pressure that a cylindrical glass cell could withstand depended on the

ratio of the inner diameter of the cell to the thickness of the cell wall. Cipollini and Allen used the normal low pressure cell wall (~0.2 cm) but decreased the inner diameter to 0.1 cm (133). The cell was able to withstand the critical pressure of tetramethylsilane which was 2.8 MPa (134).

ii) Low Pressure Observations

From the low pressure studies a number of generalizations were made. The most noticeable change was in the n-alkane series as the length of the carbon chain was increased from that of methane to that of n-butane (96,97, 109,120). Over the entire temperature range from near the triple point to above the boiling point, the mobility of electrons in methane was greater than $300 \text{ cm}^2/\text{Vs}$. The Arrhenius activation energy was negative. In ethane, the mobility was more than two orders of magnitude less, and the activation energy was about 3 kcal/mol. From ethane to propane to n-butane, the mobility, at the same reduced temperature $T_r = T/T_c$ where T_c is the critical temperature, would continue to decrease but to a much less extent than for the methane to ethane transition. The activation energy continued to increase.

Branching of the carbon skeleton increased the mobility. It was noted that the mobility increased as the degree of sphericity increased (107). For alkanes this appeared to be related to the anisotropy of the polariz-

ability. The mobility in isobutane was therefore much higher than that of n-butane, and its activation energy near the boiling point lesser (109,114). Neopentane possessed a much larger mobility than n-pentane or isopentane (104,105,107,108). It was also found that the branching effect only extended to about two C-C bonds in series (107).

In general, the introduction of a carbon-carbon double bond decreased the mobility from that of the corresponding alkane. The mobility in ethene was much less than that in ethane, and the mobility in propene much less than that in propane (132). An anomaly was found in the case of the butenes which were analogous to n-butane, i.e. cis- and trans-butene-2. Electrons in both trans-butene-2 and butene-1 (108) had lower mobilities than in n-butane (109). The electrons in cis-butene-2 had a mobility an order of magnitude larger than that in n-butane. The reason for the difference in behavior between cis-butene-2 and that of trans-butene-2 has yet to be satisfactorily explained.

iii) High Pressure Observations

As measurements were extended into the critical region, it was found that all the mobility curves increased as the temperature was raised above the boiling point of the compound. Mobility maxima were found in methane (126, 127), ethane (128), cis-butene-2 (131), cyclopentane, neopentane and neohexane (130), cyclohexane (71), and 2,3-dimethylbutane, 3,3-dimethylpentane, 2,2,4-trimethylpentane, and 2,2,4,4-tetramethylpentane (132). For

the larger alkanes the size of the maximum and the difference ($T-T_c$) where T was the temperature where the maximum occurred tended to increase as the molecules became more sphere-like. The presence of trimethyl groups seemed especially important. The size of the maximum decreased drastically as the carbon chain increased from that of methane to that of ethane.

A recent work of electron mobilities μ in dense methane gas deserves special mention at this time (59). Measurements of μ as functions of number density along isotherms showed that the shape of the mobility curve and the existence of a mobility maximum were independent of temperature. The position of the maximum was also independent of temperature. This work had shown that the existence and position of the maximum in methane were independent of phase, since the position of the maximum agreed with that found in the liquid (126,127). The high pressure cells allowed measurements through the critical region which showed that the electron did not change its behavior drastically right at the critical point.

5. Free Ion Yields

The number of ion pairs that escape into the bulk medium per 100 eV of absorbed dose can be determined in three ways. A substance can be added that reacts with the electron to form a measureable product. Alternatively,

the specific conductance of the system can be measured. If the mobilities of the ions are known, the number of ions formed can be calculated. Finally, the free ions can be swept from the fluid by an electric field, collected at electrodes, and their charge measured. Each method, as well as some older works, will be discussed in turn.

a. Older Results

Initial workers measured the ionization currents i which were proportional to the free ion yields. Mohler and Taylor determined the ionization current created in liquid carbon disulfide by X rays at field strengths up to 60 kV/cm (135). At higher fields the ionization current tended towards saturation. Using Jaffé's theory (see section C), a plot of i^{-1} vs E^{-1} was made. Extrapolation of the curve to infinite field strength led to a W value for the liquid of 26 eV, which was taken to be the same as the gas phase result of 24 eV (within their estimated error). It should be noted that Jaffé's theory was developed for columnar recombination in the high linear energy transfer (LET) tracks of alpha particles. As such, application of this model was really inappropriate to measurements where the ionization was caused by low LET radiations such as X rays or γ rays.

Gerritsen and Kolhaas made measurements in liquid nitrogen and in liquid helium I and helium II (136)

irradiated with X rays. The curves were similar but the field strength where the current vs E plot bent downwards was higher in nitrogen than in the helium. At about the same time Pao measured ionization currents induced by γ rays in oxygen and in iso-octane (137). Pao also made plots of i^{-1} against E^{-1} . He found that for $191 < T < 313\text{K}$, the curves all have the same value at $E^{-1} = 0$ in isooctane.

Extensive study of the field effect was conducted by Ullmaier (138). Measurements were made using soft X rays and field strengths up to 50 kV/cm . Ullmaier noted that increased branching of the carbon skeleton led to a large ionization current. Furthermore, the more spherical the compound, the smaller was the field strength at which the curve bent over (began to approach saturation). The W values determined from application of Jaffé's theory were higher than those of the gas. For the n-alkanes, W increased with chain length.

b. Conductance

As previously noted in the section on ion mobilities, the free ion yield could be calculated from the conductance of the system if the mobility of the ions were known. The earliest works using this method had to estimate the mobilities (89,90), but in later works, the mobilities were directly measured (91-94).

Freeman and Fayadh found that free ion yields increased with the static dielectric constant of the liquid

(90). The samples were irradiated with γ rays from a ^{60}Co source. On the basis of their results, it was proposed that the electron may be trapped in liquid cavities. Furthermore, the trapping process required that the electron lost energy to the molecules in such a manner that it cannot be considered to be quasifree as proposed in an earlier model (139).

Hummel, Allen and Watson found that an Arrhenius plot of the free ion yields for n-hexane gave a good straight line in agreement with the idea that the escape probability varied as an exponential of $1/T$ (92). X rays (1.5 MeV) from an electrostatic generator were used. It was noted that the range of the electrons was greater in n-hexane than can be expected from extrapolation of high energy ranges. It was also suggested that temporary negative ion formation with accompanying energy transfer to vibrational modes may occur, and that this formation be more important for solvents with electronegative atoms than for hydrocarbons.

It was noted that range type calculations refer to the average distance that the electrons travelled to be moderated to the sub-excitation region, and that a significant additional distance must be travelled before the electrons are thermalized.

c. Clearing Field (Charge Clearing)

The clearing field method involved the collection

of all free ions before appreciable random recombination could occur (140,141). In order to accomplish this, the total absorbed dose was kept low and the field strength high. The G_{fi}^0 was obtained by extrapolation of the high field yields to zero field strength. The method has been used to collect a large amount of data on hydrocarbon systems (107,109-114, 118, 141-149). Radiation was supplied by electrostatic generators except in ref. 142 which used a ^{60}Co source. Data were fitted with models (3,6,107, 141) based on Onsager's theory, and the thermalization length of the electron b_d extracted (see section C). Comparison between different hydrocarbon systems was usually effected by use of the density normalized thermalization length bd .

i) Schmidt and Allen

Schmidt and Allen noted in their works that the bd should be the most important parameter characterizing the energy loss process of the electron to the liquid medium (141). The parameter bd was much increased in compounds with a quaternary C atom, and decreased by introduction of double bonds or the introduction of oxygen atoms for a CH_2 group in a molecule. Neopentane was found to have an exceptionally high G_{fi}^0 in agreement with the result of Tewari and Freeman (94). Extension of the work (143) led to the discovery that bd at room temperature was almost constant for all the n-alkanes

from n-butane to n-decane plus n-tetradecane. This indicated the similarity of the energy loss process in these compounds. Comparison of olefins to ethers showed that the oxygen atom was better at thermalizing the electrons than the double bond.

ii) Freeman and Co-workers

The bulk of free ion yield measurements after 1970 have been done by Freeman and co-workers (107, 109-114, 144-149). Systems were examined to separate out the effects caused by increasing the length of the carbon skeleton, by unsaturated carbon-carbon bonds, by aromaticity, by cyclicization, by branching, by replacing a CH₂ group with an oxygen, and by temperature variations. The effect of the position of substitution was also examined. For example it was found that from propene, the introduction of a methyl group to form cis-butene-2 or isobutene led to an increase in bd but that if trans-butene-2 was formed bd decreased (149). It was noted at the time that the range of the energy loss interaction only extended over two C-C bonds in series. Conjugation of double bonds did not appear to have a special effect. Oddly enough while alkyne-1's de-energize electrons much more efficiently than alkanes, an internal triple bond has a larger bd than the alkane. This was taken to mean that the electrons may interfere with the polar C-H in the alkyne-1 rather than with the

triple bond. The greater range in cis-alkene-2's compared to that of the trans-alkene-2's has not been satisfactorily explained. It was suggested that for hydrocarbons the rates of energy loss correlated to the anisotropy of polarizability of the molecules.

d. Scavenging Experiments

A serious problem in the extraction of the most probable thermalization length b from charge clearing experiments was that the distribution of thermalization distances must be known. As well, fitting of the data required that the total ion yield G_{tot} also be known. The total ion yield can be assumed to equal the gas phase value or it can be used as a fitting parameter. Measurements for a series of alkanes over the entire liquid range showed that assumption of an exponential distribution required an assumed G_{tot} of 7.5 ± 1 while assumption of a Gaussian type distribution required an assumed G_{tot} of 4 ± 1 in order to fit the data (6). The fit of the calculated curve was just as good in each case to the experimental points.

Scavenging effects on the γ -radiolysis of organic compounds can yield either the free ion yield at zero electric field, G_{fi}^0 , or the total ion yield (151). For a wide range of organic compounds, the total ion yield was 4.7 ± 0.5 (152-155) which lent support to the usage of a Gaussian type distribution function. The

free ion yield can also be used to check the values obtained from electrical methods. The free ion yield in neopentane determined by Tewari and Freeman (94) of 0.86 was much larger than that of n-pentane ($G_{fi}^0 = 0.12$). A scavenging experiment determined that $G_{fi}^0 = 0.9$, a value within 10% of that of the electrical method (153). This agreement lent credence to the accuracy of the clearing field method.

Nishikawa and co-workers used scavenging experiments to examine thermalization lengths in the supercritical fluid of C_2-C_4 alkanes and alkenes (156-159). Nitrogen yields released by the nitrous oxide electron scavenger were measured and plotted against the square root of the concentration of N_2O . The nitrogen yield at $[N_2O]$ extrapolated to zero was taken to equal G_{fi}^0 . It was found that at a fixed temperature, the value of G_{fi}^0 in all the compounds increased as the gas density decreased. Variation of the density at $0.2 \leq d \leq 0.45 \text{ g/cm}^3$ changed the value of bd by less than 10% (where comparison was possible). Variation of the density at $0.1 < d < 0.2 \text{ g/cm}^3$ can increase bd by as much as a factor of 2. The sudden increase in bd at these lower densities was taken to indicate that the degeneration of clusters in the fluid was occurring over a fairly narrow density range (157, 158).

e. Gas Phase Total Ion Yields

Gas phase dosimetry using ionization chambers required a knowledge of W , the average energy expended in formation of an ion pair. If a strong enough field was applied so that all the ions were collected, and if the total energy absorption needed to generate these ion pairs could be measured, then W could be calculated.

The W value was usually determined relative to a standard. Meisels (160), Adler and Bothe (161), LeBlanc and Herman (162) used the ionization current in air, Cooper and Mooring (163) used six gases (H_2 , He, air, N_2 , Ar and C_2H_2) and Stoneham, Ethridge and Meisels (164) used nitrogen. Meisels (160) noted that there appeared to be a systematic decrease in W with chain length within the alkane and alkene series. No clear differentiation could be made between structural isomers. Adler and Bothe noted that within a homologous series the rates of (W/I) was roughly constant, where I was the ionization potential (161). LeBlanc and Herman presented an empirical formula based on the number of atoms of each type in the compound (162). Calculated values were within 5% of the experimental values. Cooper and Mooring (163) also attempted to correlate W values to ionization currents. The product of (WJ^*/Z) was fitted as a function of $\log I$, where J^* was the ion current per mole, Z was the atomic number of the material and I was the average ionization potential

of electrons in the material. Stoneheim and co-workers made measurements at temperatures of $298\text{K} < T < 473\text{K}$ and at pressures between $53\text{ kPa} < P < 360\text{ kPa}$. No variation of W with T or P was found (164).

The usual quantity used in conductivity experiments is the ion yield (the number of ion pairs produced per 100 eV of absorbed energy). The relationship between G_{tot} , the total number of ions produced per 100 eV absorbed dose and W is given by:

$$G_{\text{tot}} = 100/W \quad (8)$$

Total ion yields in hydrocarbons with a carbon number of 4 or less, excluding the butenes, are contained in Table I-1. Air and nitrogen values are also given (165,166).

TABLE I-1

Total Ion Yields in the Dilute Gases^a

Compound	G _{tot}	Ref.	Compound	G _{tot}	Ref.
CH ₄	3.7	160	i-C ₄ H ₁₀	4.3	160
	3.6	161		4.3	162
	3.6	162		4.1	163
	3.7	164		4.2	164
	3.7	*		4.2	*
C ₂ H ₆	3.9	160	C ₂ H ₄	3.9	160
	3.8	161		3.8	161
	3.9	162		3.9	162
	3.9	163		4.0	163
	4.1	164		3.9	*
	4.0	*			
C ₃ H ₈	4.3	160	C ₃ H ₆	4.0	160
	4.1	161		4.0	162
	4.3	162		4.0	*
	4.1	163	c-C ₃ H ₆	4.2	162
	4.2	164		4.2	*
	4.2	*			
n-C ₄ H ₁₀	4.4	160	air	2.96	165
	4.2	161	N ₂	2.89	166
	4.4	162			
	4.1	163			
	4.3	164			
	4.3	*			

C₂H₄ is ethene, C₃H₆ is propene and c-C₃H₆ is cyclopropane.
 (*) indicates the preferred value.

a. For β -rays.

C. Theory

In this section an outline will be given of a number of models commonly used in the treatment of experimental data.

1. Mobility in Gases

a. Ion Mobility

Langevin had treated the problem of diffusion and applied it to the gas phase mobility (167). The molecules were assumed to be elastic spheres. The spheres were taken to be polarizable in the field of the ions. The force of attraction f between the ion and the molecule was

$$f = \frac{2\bar{m}e}{r^3} \quad (9)$$

where \bar{m} was an average effective moment induced on the molecule by the ion, e was the electronic charge and r was the distance between the ion and the molecule. The effective moment was given by

$$\bar{m} = \frac{\gamma e}{r^2} \quad (10)$$

where γ was the total effective molecular polarizability, and was given by

$$\gamma = \frac{\epsilon - 1}{4\pi n} \quad (11)$$

where n was the number density of molecules and ϵ was the dielectric constant. This led to the force of attraction being set equal to

$$f = \frac{(\epsilon-1)e^2}{2\pi nr^5} \quad (12)$$

corresponding to a potential energy of

$$V = \frac{-(\epsilon-1)e^2}{8\pi nr^4} \quad (13)$$

Assuming as well that the random thermal velocities of the ions followed a Maxwellian distribution, Langevin obtained

$$\mu = A \left(\frac{1 + m/M}{n(\epsilon-1)} \right)^{1/2} \quad (14)$$

where μ was the mobility, m the mass of the molecule, M the mass of the ion and A a function of a quantity, λ which is a measure of the relative importance of the size of the particles and the polarization forces in determining the path of the ion. A small λ meant that the attractive force due to polarization was much more important than direct collisions. Conversely, a large λ meant that the attractive forces were weak and that direct collisions were mainly responsible for scattering of the ions. A equalled 0.505 when $\lambda = 0$, increased to a maximum of 0.58 at $\lambda = 0.6$, then decreased as λ increased further.

The product λA approached 0.75 when λ was large. Since

$$\lambda = \frac{\sigma^2}{e} \left(\frac{8\pi P}{\epsilon-1} \right)^{1/2} \quad (15)$$

where σ was the sum of the radius of the molecule and ion, and P was the pressure, elimination of

(ε-1) from equation (14) led to

$$\begin{aligned}\mu &= \frac{(\lambda A)e}{\sigma^2} \left(\frac{1+m/M}{8\pi P n} \right)^{\frac{1}{2}} \\ &= \frac{0.75e}{\sigma^2} \left(\frac{1+m/M}{8\pi P n} \right)^{\frac{1}{2}}\end{aligned}\quad (16)$$

which was the formula used by Tyndall and co-workers in their investigations on ion sizes (25). As P depended upon n, equation (16) also indicated that the mobility should decrease with n, which was the same conclusion reached in section A.

b. Electron Mobility

A fair amount of work has been done by J. L. Pack and A. V. Phelps in developing simple models that could be used in extracting electron-molecule scattering cross-sections from transport measurements (168). The earlier model obtained cross-sections from the variation of the low field mobility as a function of temperature. The latter used the variation of mobility and the variation of (D/μ) as a function of electric field strength. Both were solutions to the drift velocity equation given in ref. 169.

1) Temperature Dependence

The drift velocity w of electrons in a dc electric field E was taken to be

$$w = \frac{4}{3} \pi \frac{e}{m} \left(\frac{E}{n} \right) \int_0^{\infty} f_0 \frac{d}{dv} \left(\frac{v^2}{\sigma} \right) dv \quad (17)$$

where f_0 was the spherically symmetrical term of the electron velocity distribution, v the electron velocity and σ the momentum transfer cross-section (170). For low E/n , the electrons are in thermal equilibrium with the gas and the Maxwellian distribution could be used, f_0 was then given by

$$f_0 = \left(\frac{m_e}{2\pi kT} \right)^{3/2} \exp \left(\frac{-m_e v^2}{2kT} \right) \quad (18)$$

Assuming that

$$\sigma = \sum_j b_j v^{-j} \quad (19)$$

combination of equations (17), (18) and (19) led to

$$\begin{aligned} \mu n = \frac{w}{E} &= \frac{e}{m_e} \sum_j \frac{(3/2 - j/2)!}{(3/2)!} b_j \left(\frac{2kT}{m_e} \right)^{-j/2} \\ &= \sum_j B_j \left(\frac{2kT}{m_e} \right)^{-j/2} \end{aligned} \quad (20)$$

This is equation (3) of ref. 170. The temperature variation of the mobility could be used to obtain j and B_j values. The cross-section σ was given by

$$\sigma^{-1} = \frac{m_e}{e} \sum_j \frac{(3/2)!}{(3/2 - j/2)!} B_j v^{1-j} \quad (21)$$

This method and an equivalent formulation by Viehland

and Mason for ions (171,172) have been widely used (52,64, 70,71,73,173,174).

ii) Field Strength Dependence of Mobility
and of (D/μ)

Pack and Phelps also led the way in solution of the drift velocity equation without having to assume a Maxwellian distribution or the assumption of the power law dependence of σ on v (175). Values, however, had to be assumed for the various elastic and inelastic scattering processes as well as the form of the distribution function in the energy range used. Values of w and of D/μ were calculated and compared with the experimental numbers. Adjustments were made to the cross-sections until the calculated transport coefficients were in agreement with the experimental values. This method has been used in a wide number of systems (53,56,67,78,175,177).

2. Electron Mobility in Liquids

a. Quasifree Electrons

Lekner calculated quasifree electron drift velocities in liquid argon using a model that introduced the structure factor $S(o)$ into the drift velocity expression (178). For the weak field region the electrons were assumed to have a Maxwellian distribution of velocities and the momentum transfer cross-section equalled $[4\pi a^2 S(o)]$, where a was the scattering length. The

drift velocity was then given by

$$w = \frac{2}{3} \left(\frac{2}{\pi m_e k_B T} \right) \frac{eE}{n 4\pi a^2 S(0)} \quad (22)$$

where m_e was the electronic mass and k_B was Boltzmann's constant. Calculated values had the correct shape and agreed well with the data of ref. 179 up to 10^4 V/cm. The model curve decreased at higher fields while the experimental points still increased. The model leading up to this expression was actually developed in ref. 180 and is referred to as the Cohen-Lekner model.

Schnyders and co-workers had observed that in liquid argon and krypton, the mobility as a function of temperature went through a minimum and then increased (123).

Lekner noted that the scattering length was positive in liquid argon near the triple point and negative in the gas phase. He proposed that the scattering length go through a zero point at an intermediate density and that the mobility was increasing towards a maximum (181).

This maximum was subsequently found in liquid argon near the critical region (124). Lekner and Bishop also examined the effect of critical fluctuations as the temperature was raised towards the critical temperature for noble liquids (74). It was predicted that scattering of the electrons by long wavelength density fluctuations would be increased, decreasing the electron mobility.

Near the critical point, the electrons would be localized

within the fluctuations and the mobility would be decreased by about four orders of magnitude. More recent experimental work had found discrepancies between the predicted mobility values and those measured (75,185).

The Cohen-Lekner model has been used to calculate the mobility of quasifree electrons in hydrocarbons (182-184).

b. Localized electrons

i) Nature of Localized Electrons

In liquid hydrocarbons, electron mobilities were found to be orders of magnitude larger than those of the ions. However, they were orders of magnitude smaller than those found in the liquified rare gases in which the electrons were quasifree. The inclusion of the incoherent scattering by the polyatomic molecules was insufficient to explain the difference (182). Models were developed which estimated the effects of a temporary negative-ion being formed or of the effects of trapping. Both types of model had the same requirement. There had to be two states of the electron, one corresponding to the quasifree electron and one to a slower mobility state. The two state idea had been proposed by Thomson for electron transport in gases (186), by Tyndall for ion transport in gases (25), and by Crowe (82) and LeBlanc (81) for electron transport in liquid hydrocarbons.

Minday, Schmidt and Davis conducted a series of

experiments in 1971-1972 that led to the acceptance of the trapping model of electronic transport in liquid hydrocarbons (105,106). The most convincing set of measurements were done on a series of neopentane-n-hexane mixture (106). Assumption of a short lived negative ion, or some other form of single molecule process, would have required that the mobility of the mixture depended inversely upon the mole fraction of n-hexane (106). The activation energy should have been constant. Instead it was found that the activation energy of the mixture depended upon the mole fraction of n-hexane. This required a multi-molecular trapping process. For the mixture, the activation energy was of the form

$$E = E_1 X_1 + E_2 X_2 \quad (23)$$

where E_i was the activation energy of component i and X_i was the mole fraction. This equation was in accordance to a statement that the mobility depended on the time that the electron spent in the high mobility state compared to the time in the low mobility. The problem then laid in the calculation of the probability that the electron would be in the free state. The existence of a localized state has been shown by the detection of absorption signals from electrons solvated in liquid hydrocarbons (187-191).

ii) Bubble Model

Schiller in analogy to bubble states in liquid He developed a two state model in which the localized electron state was a bubble (192-194). The medium was considered to be divided into a number of small equal-sized subsystems. The energy content of the subsystems was described by the probability distribution

$$p(E)dE = (2\pi\sigma^2)^{-\frac{1}{2}} \exp\left[-\frac{(E-\langle E \rangle)^2}{2\sigma^2}\right] dE \quad (24)$$

where $p(E)dE$ was the likelihood of finding a cell with energy between E and dE , $\langle E \rangle$ was the average energy of the system and σ was the dispersion parameter for the distribution. The dispersion parameter was given by:

$$\sigma^2 = kT^2 C_V + \left(\frac{\partial E}{\partial N}\right)_{T,V}^2 (\langle N \rangle - \langle N \rangle^2) \quad (25)$$

where C_V was the heat capacity at constant volume for the system, V the volume and N was the number of molecules in the cell (93). Schiller used the case where N was small so that equation (24) converged to $(kT^2 C_V)$. Localization occurred if $E - \langle E \rangle < V_0 - E_t$ where E_t was the energy of the localized state and V_0 was the energy of the extended state. Integration of $p(E)dE$ between $-\infty$ and $(V_0 - E_t)$ gave the probability of localization. The mobility in the liquid depended solely upon the fraction of electrons in the extended state.

111) Ether Model

A similar type of model was developed by Freeman from observations of electron mobility and optical absorption energy in ethers (112,195), and applied to liquid hydrocarbons (70,71,114,130-132). The medium was taken to be homogeneous towards charge transport and a distribution for localization probability was assumed. The final equations appeared to be similar to those of Schiller's. The basis of the model was considerably different. Schiller had assumed that a bubble could form in liquid hydrocarbons as in helium (196), positronium studies (197,198), or alcohols (199,200). Freeman's model made no assumption as to the nature of the traps but was based on the observation that the low temperature electron mobility was about double those of the anions and that at high temperatures, it was orders of magnitude larger than that of the anions. It was also noted that the low temperature (ion-like) mechanism was unlikely to have involved the migration of the nearest neighbour solvation shell along with the electron. The mobility μ_e at any temperature was taken to be

$$\mu_e = (1-x)\mu_{il}^0 \exp(-E_{il}/RT) + x\mu_h^0 \quad (26)$$

where μ_{il}^0 was the pre-exponential factor of the ion-like mobility, E_{il} the activation of the ion-like mobility, μ_h^0 the mobility in the extended state and x the fraction of electrons in the conduction band.

iv) Percolation

Freeman and Schiller assumed that the medium was homogeneous towards charge transport and that the difference in mobility states was due to the existence of two modes of charge transport. Kestner and Jortner developed a model which assumed that there was only one transport mechanism (201). The proposal was made that since electron mobility depended upon local rotational fluctuations (103,104), the medium should be described in terms of regions that were "transparent" or were "almost opaque" towards electrons. The fraction of transparent regions c determined the mobility. The relationship between the mobility and the energy of the extended state was calculated in terms of c .

c. Field Effect

i) Positive Dependence

Bagley developed a model for transport of localized electrons (202). The transport involved an activated process of motion from one site to another across an average distance of λ and over an average energy barrier of ΔG . At constant temperature and pressure, the exchange frequency in the absence of an electric field E was

$$k = \gamma \exp\left(\frac{-\Delta G}{k_B T}\right) \quad (27)$$

where γ was the attempted frequency and k_B the Boltzmann constant. With an applied field, the net jump frequency

was

$$f_+ - f_- = k \left[\exp\left(\frac{\lambda e E}{2kT}\right) - \exp\left(-\frac{\lambda e E}{2kT}\right) \right] \\ = 2k \sinh\left(\frac{\lambda e E}{2kT}\right) \quad (28)$$

where f_+ and f_- were the jump frequencies with and against the electric field. The mobility was then given by

$$\mu = \lambda f / E \\ = \left(\frac{\lambda}{E}\right) 2k \exp\left[\frac{-\Delta G}{kT}\right] \sinh\left(\frac{\lambda e E}{2kT}\right) \quad (29)$$

Note that at small x , $\sinh x = x$ so that at small E a field independent mobility was recovered. This model has been applied to liquid paraffins. Jump distances in ethane and propane were estimated to be about 30 \AA which correspond to eight molecular diameters (120). Allowance for variable barrier energies leads to a more reasonable estimate of 7.5 \AA in propane (203). Application of two barrier heights to drift velocities in mixtures of methane and ethane leads to an estimated average jump distance of 10 \AA in pure ethane (204).

(ii) Negative Dependence

In liquid methane, neopentane, neohexane and tetramethylsilane, the mobilities were found to decrease at high electric field strengths (96,130,205). That a transition from a positive to a negative field dependence could occur in the liquid was evident from liquid ethane results (119,129). At $T < 216\text{K}$ a positive dependence was observed. At 294K , a negative dependence was

observed. It has been noted that the decreasing threshold field for the field effect as the temperature was increased appeared related to the ratio of the drift velocity w to the speed of sound in the liquid (130).

w varied with E^x with x being less than one and possibly as low as zero. There was no simple dependence of w with E . Variation of x from 1 was attributed to a heating of the electron distribution.

3. Free Ion Yields

a. High LET

Jaffé developed a theory of ionization in liquids irradiated by α -particles (206). The ions were known to be grouped along the track of the ionizing radiation rather than being uniformly distributed throughout the liquid (207). The larger the linear energy transfer (LET) the more dense became the grouping of the ions in the track. An important part of Jaffé's solution was that α -particles created dense cylindrical tracks. A relationship between the measured charge and the saturation charge was obtained, which was the same as the ratio of the measured current to that of the saturation current. The relationship was of the form

$$\frac{1}{i} = \frac{1}{i_s} + cf(E) \quad (30)$$

where i was the measured current, i_s the saturation current, c' was a constant quantity and $f(E)$ was a function of E that equalled c'/E at high field strengths (c' was another constant). Hence a plot of i^{-1} vs E^{-1} for large

values of E allowed the determination of i_s and hence W . Use of this theory to interpret results where the ionization source was X rays or γ rays, is incorrect since ion columns are unlikely to exist.

b. Low LET

Results involving low LET radiation such as cosmic rays, electrons or γ rays are currently interpreted by various models based on Onsager's model which was developed for single pair spurs (208). In the absence of an electric field, the probability of escape depended solely upon the Coulomb attraction between the ion and the electron and equalled the reciprocal of the Boltzmann factor,

$\exp[V/kT]$ where V was the Coulomb potential. If a field was applied, V would also have contained a contribution from the electric field. Solution for the yield of ions also required a guess of the distribution of the initial ion-electron separation distances.

This model had been adopted for liquid hydrocarbons (1-6, 89, 209-212). The free ion yield at a field strength E , G_{fi}^E was usually calculated from

$$G_{fi}^E = G_{tot} \int_0^{\infty} F(y) \phi(y, E) dy \quad (31)$$

where G_{tot} was the total ion yield, $F(y)$ the initial distribution of ion-electron separations and $\phi(y, E)$ the probability that an ion pair with a separation of y would

form a free ion pair at field strength E . $\phi(y, E)$ was taken from Onsager's solution. The exact form of $F(y)$ could not be obtained from experimental data and had to be estimated. A gaussian type distribution was often used. Another popular choice was an exponential function. It should be noted that the ratio G_{fi}^E / G_{tot} was the average probability of escape for the distribution $F(y)$. The distributions were picked so as to fit the data. For the same free ion yield G_{fi}^E if the standard deviations were the same for both the exponential and the gaussian curves, equally good fit of the calculated and experimental points could be obtained (213). The difference in the use of the two different distributions was that the exponential form required large G_{tot} 's to be assumed and resulted in smaller thermalization yields (130, 214). As mentioned in section B.5.d, scavenging experiments supported the use of gaussian type distribution functions.

4. Correlations

The common parameters measured in conductance experiments were the mobility μ , free ion yield G_{fi}^0 , and the extended state energy V_0 . These parameters appeared to be related to common properties of the fluid.

Since 1968 a correlation between the sphericity of the molecules and a large electron signal as well as a large G_{fi}^0 had been noted (94). The larger the G_{fi}^0

became, the larger was the thermalization length b . In general, compounds with a large electron mobility would also have a large b (107,114,130 and ref. therein). The density normalized thermalization range was also frequently used. It has been found that μ and bd seemed related to each other over the entire liquid range for the pentanes and that a maximum in μ , if it existed would appear at about the same density as a maximum in bd (130). Attempts had been made to relate the mobility and the free ion yield data through energy loss parameters (215, 216).

The energy of the extended state for electron transport V_0 , was usually measured by a photoemission method (217). It was noted that μ increased as V_0 became more negative. It was understood that a more negative V_0 (lower energy level) meant that the electron trap depths were correspondingly smaller. Correlations between μ and V_0 have been examined (201,215,218,219). It has been noted that μ and V_0 appeared correlated over the entire liquid range (59,219) and that a minimum in V_0 occurred at about the same density as the maximum in μ . This correlation has been used to predict the density at which electron localization transitions may occur (220,221).

D. the Present Study

The purpose of the present work was to extend the study of electron and ion transport in fluid hydrocarbons with different molecular structures. Mobilities of electrons and of positive ions were measured in C₁ to C₄ alkanes and alkenes, excluding butenes, over wide ranges of density, temperature and electric field strength. Electron thermalization ranges in these fluids were also estimated.

II. EXPERIMENTAL

A. Materials

The following gases were supplied by Phillips Petroleum Co.: ethane (99.99%), ethene (99.97%), propane (99.99%), propene (99.94%), *n*-butane (99.97%) and isobutane (99.90%). Methane (99.99%) was obtained from Matheson of Canada Ltd. and the Linde Division of Union Carbide Corp. Cyclopropane (99.0%) was also supplied by Linde. All of these gases were further purified with Molecular Sieves and either sodium-potassium alloy or potassium mirrors. The procedure is more extensively described below. Potassium metal was obtained from BDH Chemicals and sodium metal (Certified), from Fisher Scientific Co.. Davison 3A and 4A Molecular Sieves were obtained from Fisher Scientific Co. Potassium hydroxide pellets were obtained from BDH Chemicals.

B. Apparatus and Procedures

1. The Vacuum System

The main manifold is similar to that shown schematically in Fig. II-1. A vacuum of $\leq 10^{-4}$ Pa ($\leq 10^{-6}$ torr) was achieved using a Welsh duo-seal vacuum pump in series with a mercury diffusion pump and cold traps at liquid nitrogen temperature (traps T_1 and T_2 in Figure II-1). The pressure was measured with a Bendix Corp. GPH-320 Penning gauge. The gauge head was connected to the vacuum mani-

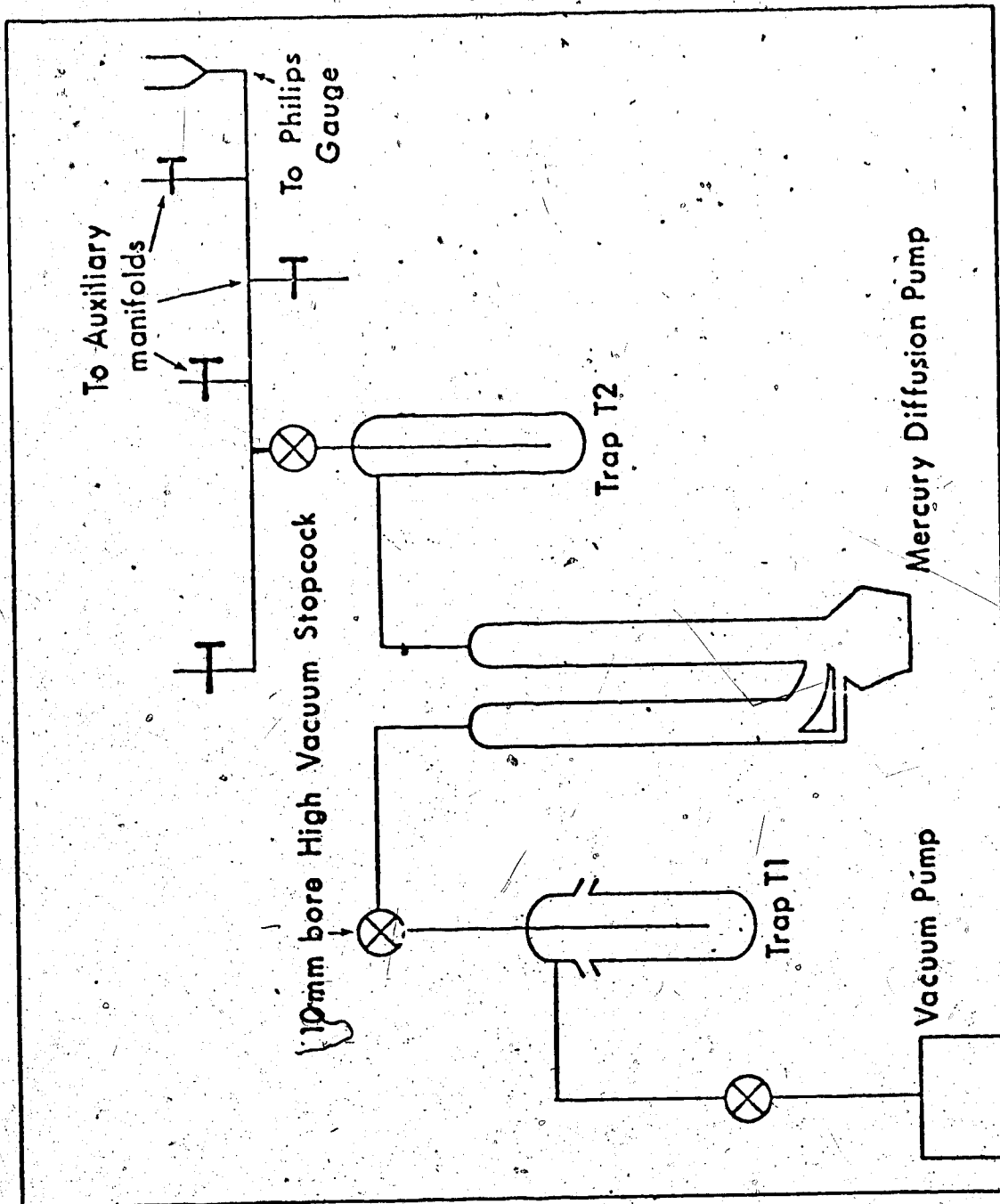


Figure II-1 Main Vacuum Manifold

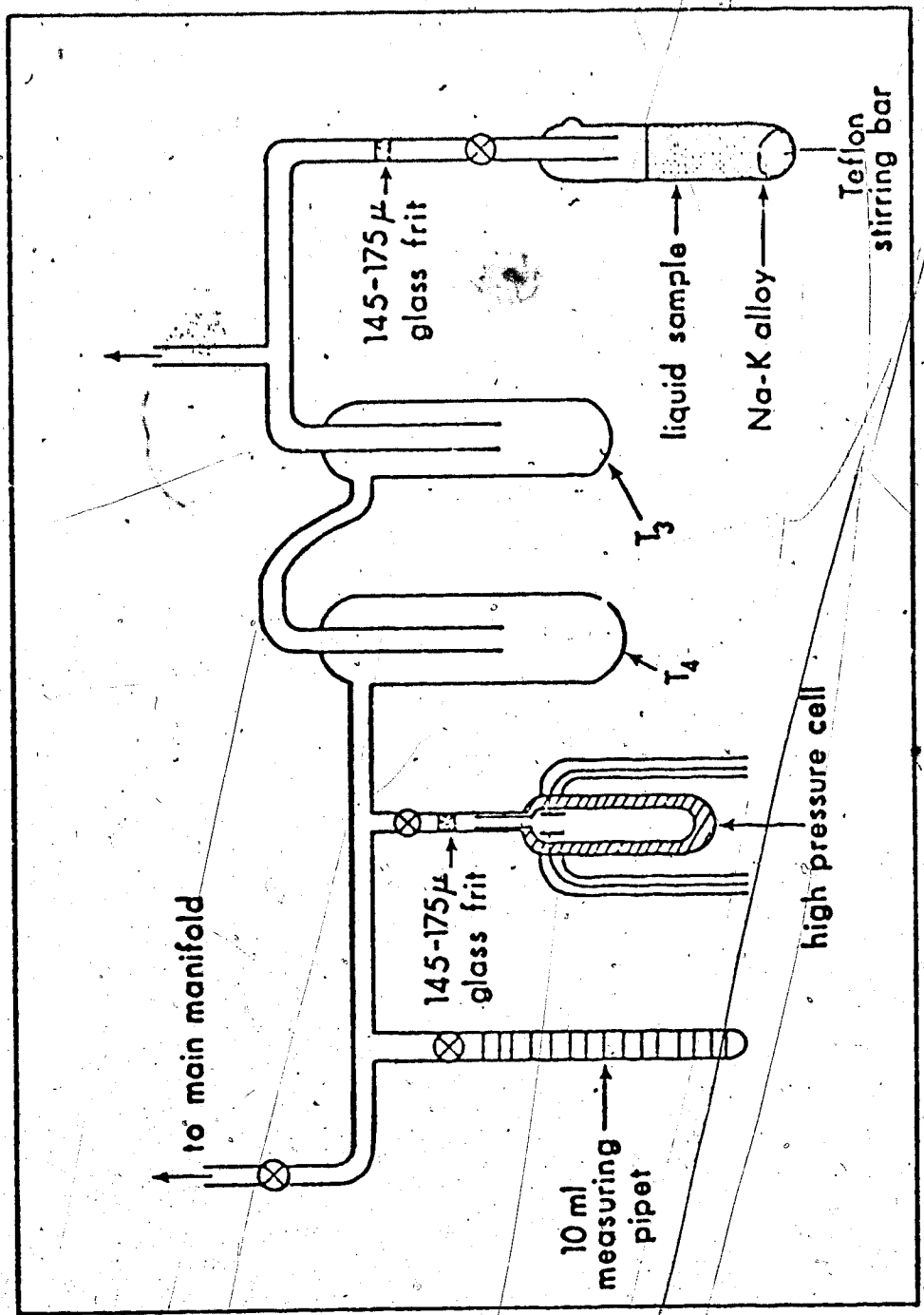


Figure II -2 System for Na-K treatment and filling cells

fold by a Kovar seal. All stopcocks on the upstream side of the mercury diffusion pump were grease free, metal-Teflon valves supplied by Hoke Inc. (model 4251N6Y) or by Nupro Co. (model 5S-5BK-SW), or glass-Teflon valves supplied by Ace Glass Inc. The latter valves used Viton A O-rings to effect the vacuum seal. Two auxiliary manifolds were attached to the main vacuum line. Traps containing the Molecular Sieves, the sodium-potassium alloys, the potassium mirrors, and traps used in degassing the samples were attached directly to the auxiliary lines. The measuring pipettes and the conductivity cells were also directly attached to the auxiliary lines. A possible layout is shown in Figure II-2.

2. Sample Purification

The gas cylinders were connected directly to the vacuum line through flexible stainless steel tubing welded to a Kovar seal. After thorough evacuation, about 50 ml of liquid sample was introduced into the line, degassed by distillation while pumping from trap T_3 to T_4 , and then held on Molecular Sieve overnight. The exceptions to this procedure were methane, which was only flowed through Davison 3A Molecular Sieve at -78°C , and ethene, which was held overnight on KOH pellets at -78°C instead of on the Sieve. The next step was to degas the sample once more, and then to treat it with a

series of 5 or more freshly activated potassium mirrors. To better effect purification the samples were held as liquids on the mirrors, using an acetone/Dry Ice slush bath. For methane, an isopentane slush was used instead. For cyclopropane, n-butane and isobutane, the sample was stirred on a sodium-potassium alloy instead of the potassium mirror. Cyclopropane had to be cooled to $\sim -5^{\circ}\text{C}$ by a Thermoelectrics Unlimited Inc. Stir Kool SK-14 refrigerator unit, using n-hexanol (Aldrich Chem. Co.) as the coolant. n-Butane and isobutane were purified at room temperature. Cyclopropane was stirred for 7 days prior to use; n-butane and isobutane, for 2 days. The sample was held on the alloy until use.

3. Sample Cells

There were two types of cells used, one for high pressures and one for low. The low pressure cell used for liquid phase measurements is shown in Figure II-3, and the high pressure cell for liquid phase measurements, in Figure II-4. Cells for gas phase measurements were similar except that the side arms point up instead of down (Figure II-5). The electrode areas were measured directly. The cell constant for the cell was determined by a conductance method involving standard potassium chloride solutions. The conductance bridge used is shown schematically in Figure II-6. The circuit maintained

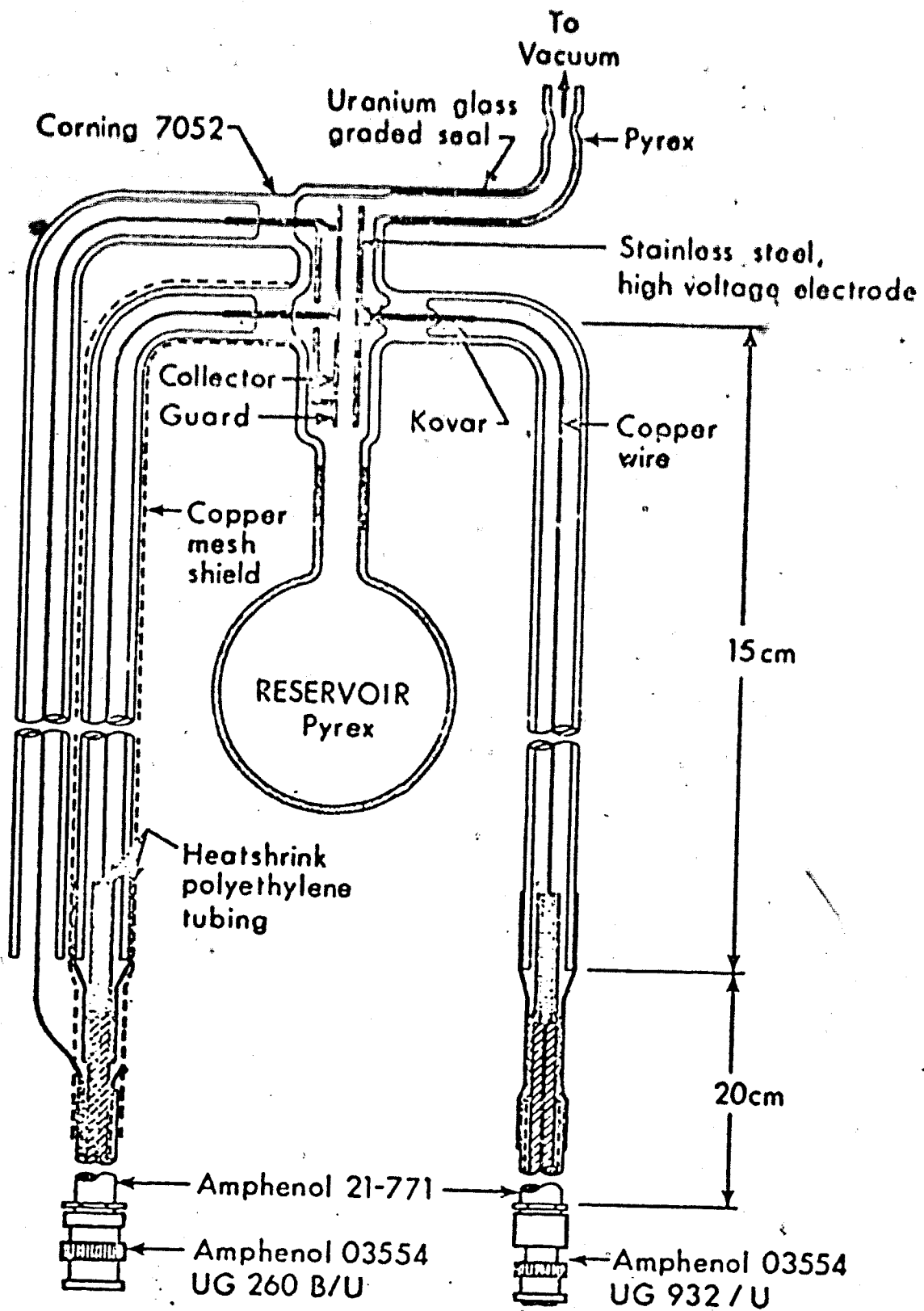


FIGURE II-3. Low Pressure Liquid Phase Cell

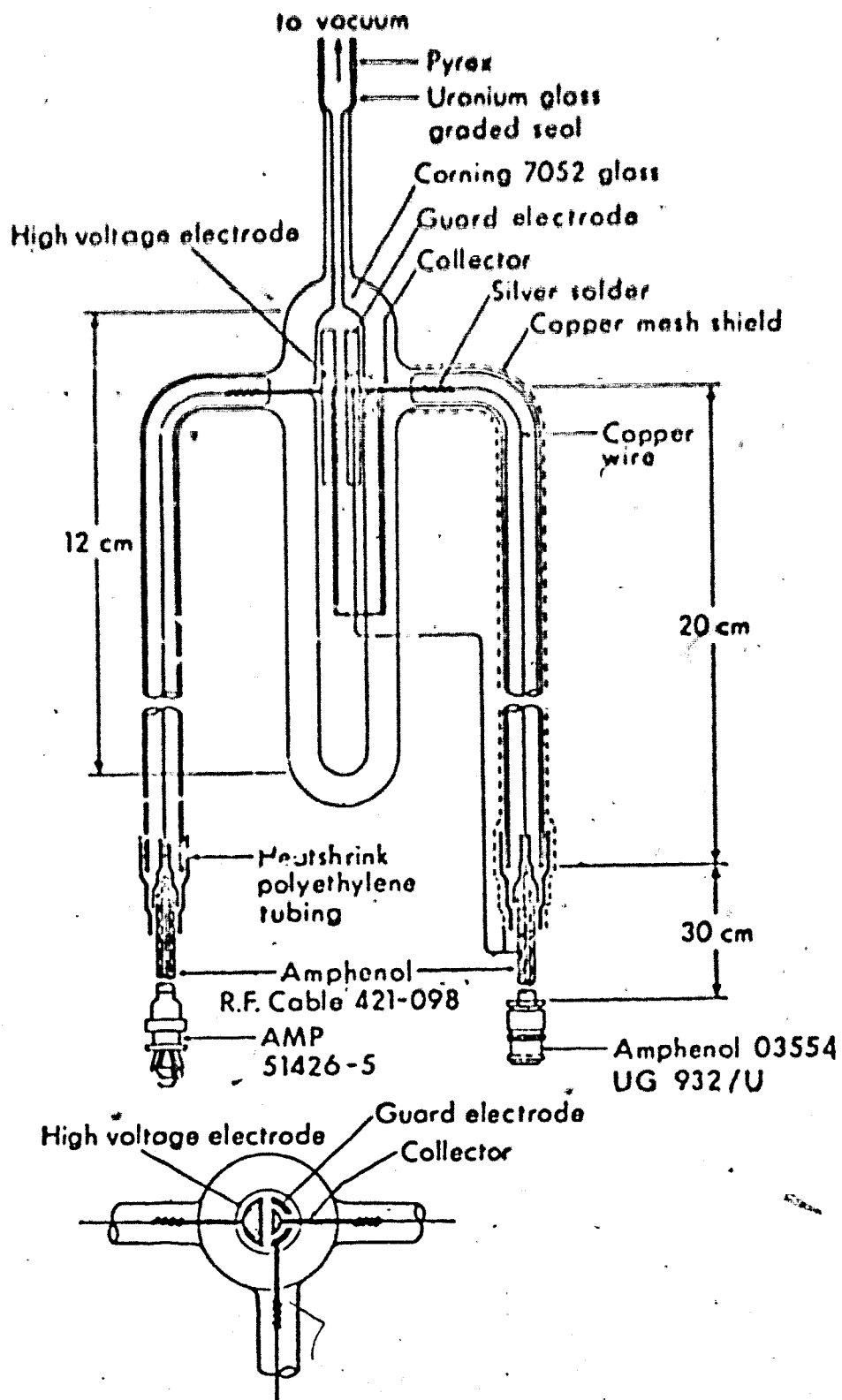


FIGURE II-4. High Pressure Liquid Phase Cell

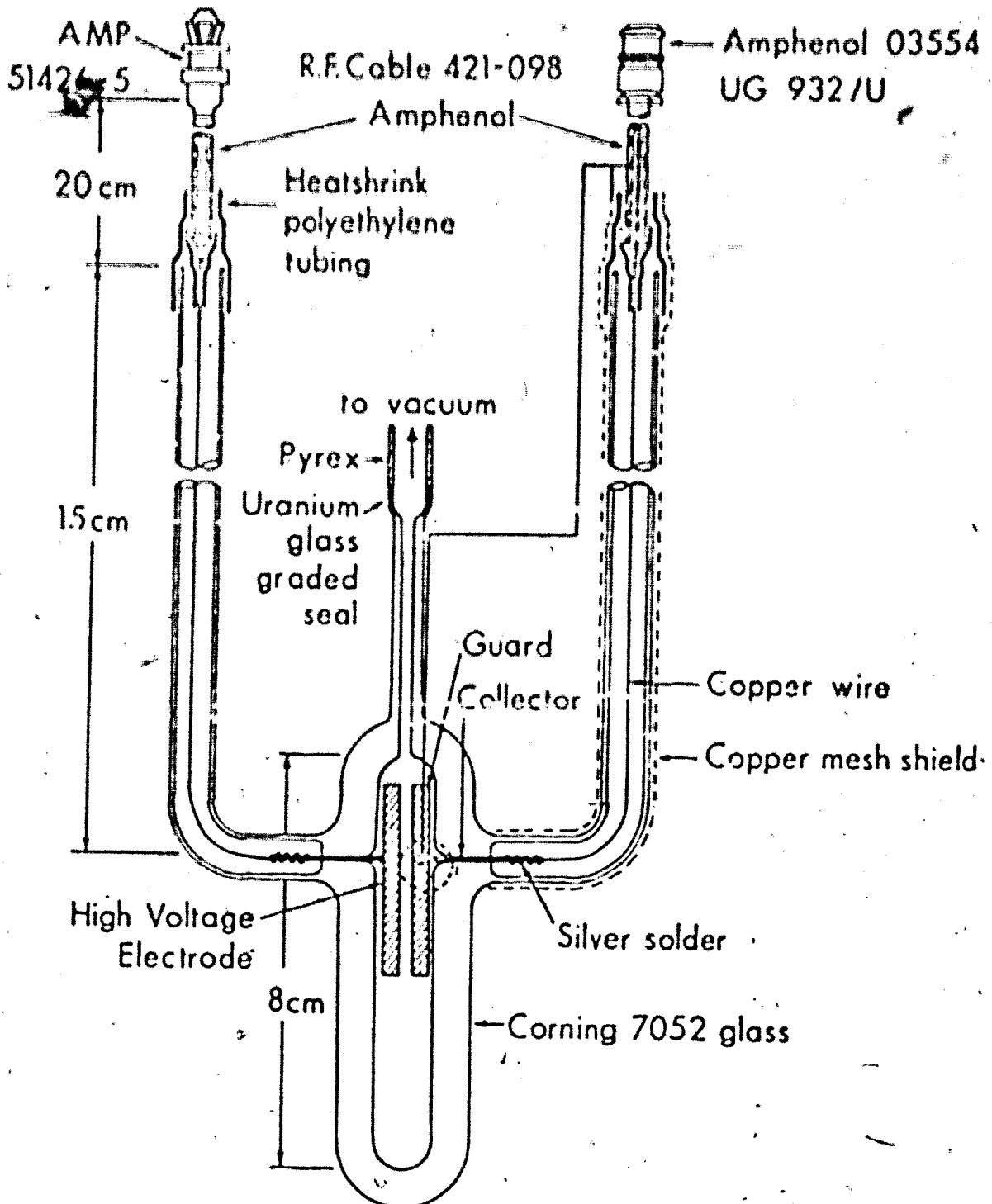


FIGURE II-5 High Pressure Gas Phase Cell

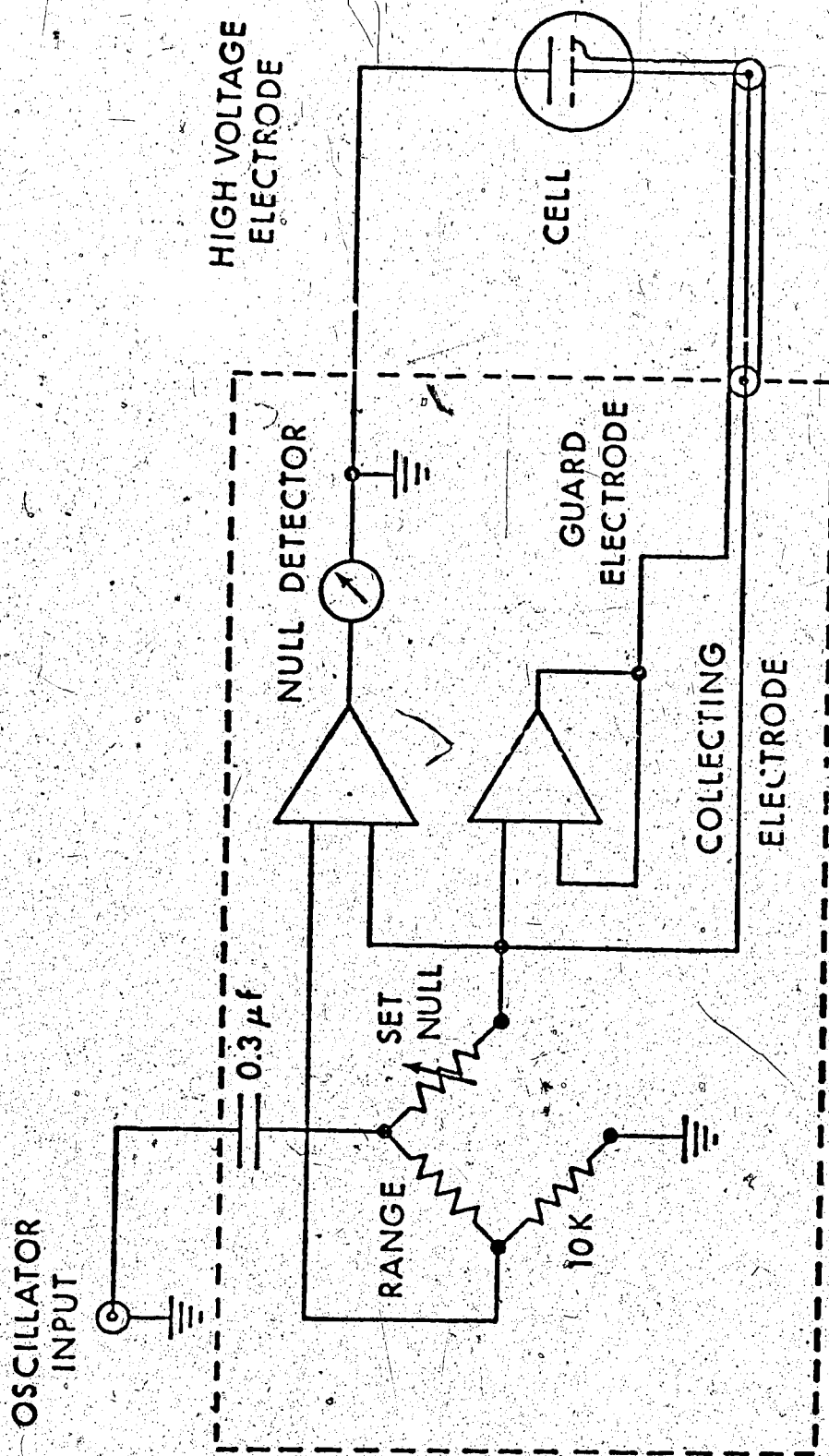


FIGURE IV-6. Circuit to Measure Cell Constant

the guard and collector electrodes at the same A.C. potential. The cell constant was independent of frequency over the range of 1 to 3K Hz. The product of the cell constant and the area of the collecting electrode gave the separation between the high voltage electrode and the collecting electrode.

4. Filling the Cell

The cells were heated to 100°K above the highest temperature that was to be used in the experiment, or to 150°C, whichever was higher. The outer surface of the cell was covered with Aqua Dag (G. C. Electronics T.V. tube coat), which was grounded to the copper braid that shielded the lead connected to the collecting electrode. With the exceptions of methane and ethene, a window was left in the coating at the front and back so that the disappearance of the liquid could be observed. The windows were also omitted if the temperature where the liquid disappeared was less than room temperature, because there was no window in the styrofoam cooling box. The glass side arm over the high voltage lead was also not coated, as it was found that the coating caused the glass to break more readily. The high voltage side arm was wrapped with Teflon tape for the first 5 cm from the cell wall. This decreased the background conductance during charge clearing measurements.

During heating preliminary to filling, the cell was

pumped on until a pressure of 10^{-5} Pa was achieved. The cell was left in this state overnight and cooled slowly before filling. The necessary amount of sample was taken from the reservoir and degassed three times. A first portion was then pumped away and the middle portion was transferred to the measuring pipet. The amount to give the needed density was then transferred to the cell, which was then sealed off with a torch.

5. Temperature Control

A box made of polystyrene foam was used to achieve low temperatures. A stream of cold nitrogen from a 50 l Dewar of liquid nitrogen was introduced through a port at the bottom of the box. The stream passed through channels up the wall of the box and entered the cell compartment through narrow slit openings near the top. The gas exited from the chamber through a tube which extended from 3 cm above the floor of the chamber, up through the lid. The rate of flow of the nitrogen gas was controlled by varying the current passing through a 1 kW resistor immersed in the liquid nitrogen. The temperature of the cell was monitored by three thermocouples, one at the top of the cell, one at the electrode area and one at the bottom of the cell. A fourth thermocouple acted as the monitor for the temperature controller. The entire box was inside a brass Faraday cage.

The set-up for heating measurements is shown in Figure II-7. The cell was positioned on asbestos supports glued to the wall of the clear walled Dewar. The heat gun (Master Appliance Corp. model AH0751) was fitted to a glass tube. The heating coil in the gun was connected to an LFE Corp. model 226-A21 temperature controller and the heat gun fan was powered from a normal 60 cycle outlet. The heated air entered the Dewar at about 1/3 of the way down the cell body. The Faraday cage was constructed of aluminum or brass. Copper screens in holes in the front and back walls allowed the observation of the disappearance of the liquid as the temperature was raised.

6. Van de Graaff Accelerator

A 2.0 MeV van de Graaff accelerator (High Voltage Engineering Corp.) was the source of the high energy electrons. The accelerator was operated at 1.7 MeV for this work, and pulse lengths of 30 ns, 100 ns, and 1.0 μ s were used. The vacuum inside the accelerator tube was of the order of 10^{-7} torr. The beam was focussed with the aid of a piece of phosphorescent paper placed at the end of the accelerator tube. Each pulse of electrons hitting the paper produced a visible glow which could be seen on closed circuit television. Steering and focussing of the beam was achieved by controlling current to electro magnets.

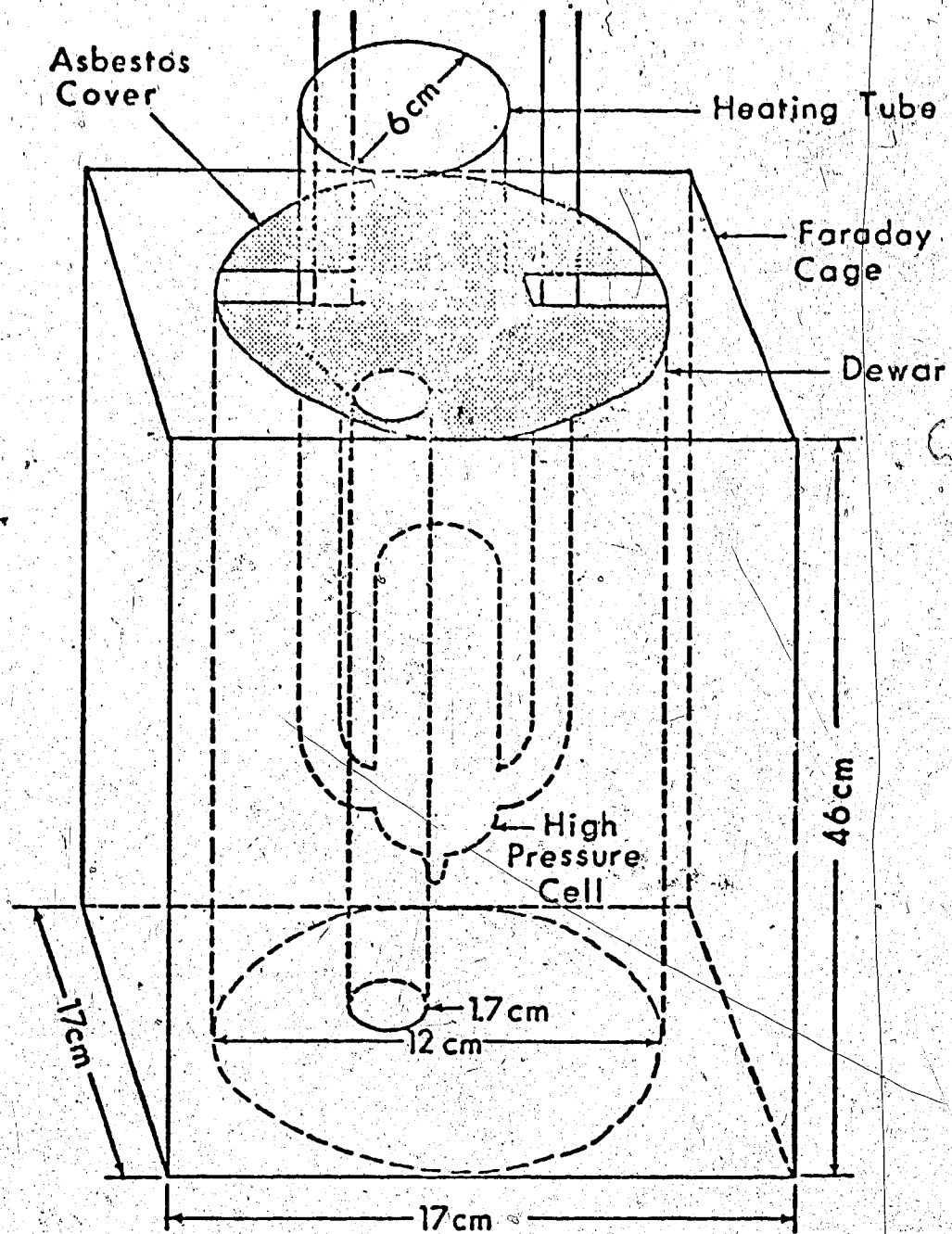


Figure II - 7 High Temperature Apparatus

7. Gold Target

The gold target was used to produce X rays to irradiate the sample. The target was placed at the end of the beam pipe and was insulated from ground so that the beam of 1.7 MeV electrons could cause the build up of a charge for measurement of the pulse dose. The charge created was measured by an Ortec model 439 current digitizer. A TSI model 1535 counter was used to display the signal as picocoulombs of charge. S

8. Charge Clearing Measurement

The method used for the charge clearing experiment was the Schmidt adaptation of the Hudson method (140,141). The ions generated between two parallel plates were collected by application of an electric field. The transient current produced was integrated and the collected charge measured. The layout is shown in Figure II-8. The P.A.R. amplifier had an adjustable gain which was set to an appropriate value depending on the size of the signal. The signal was monitored on the scope at the same time that it was fed into a Fabritek signal averager. For a noisy signal, a greater number of signals was averaged.

The free ion yield is calculated from the charge collected after the radiation pulse and with the dose absorbed from the pulse. The calculation can be written as

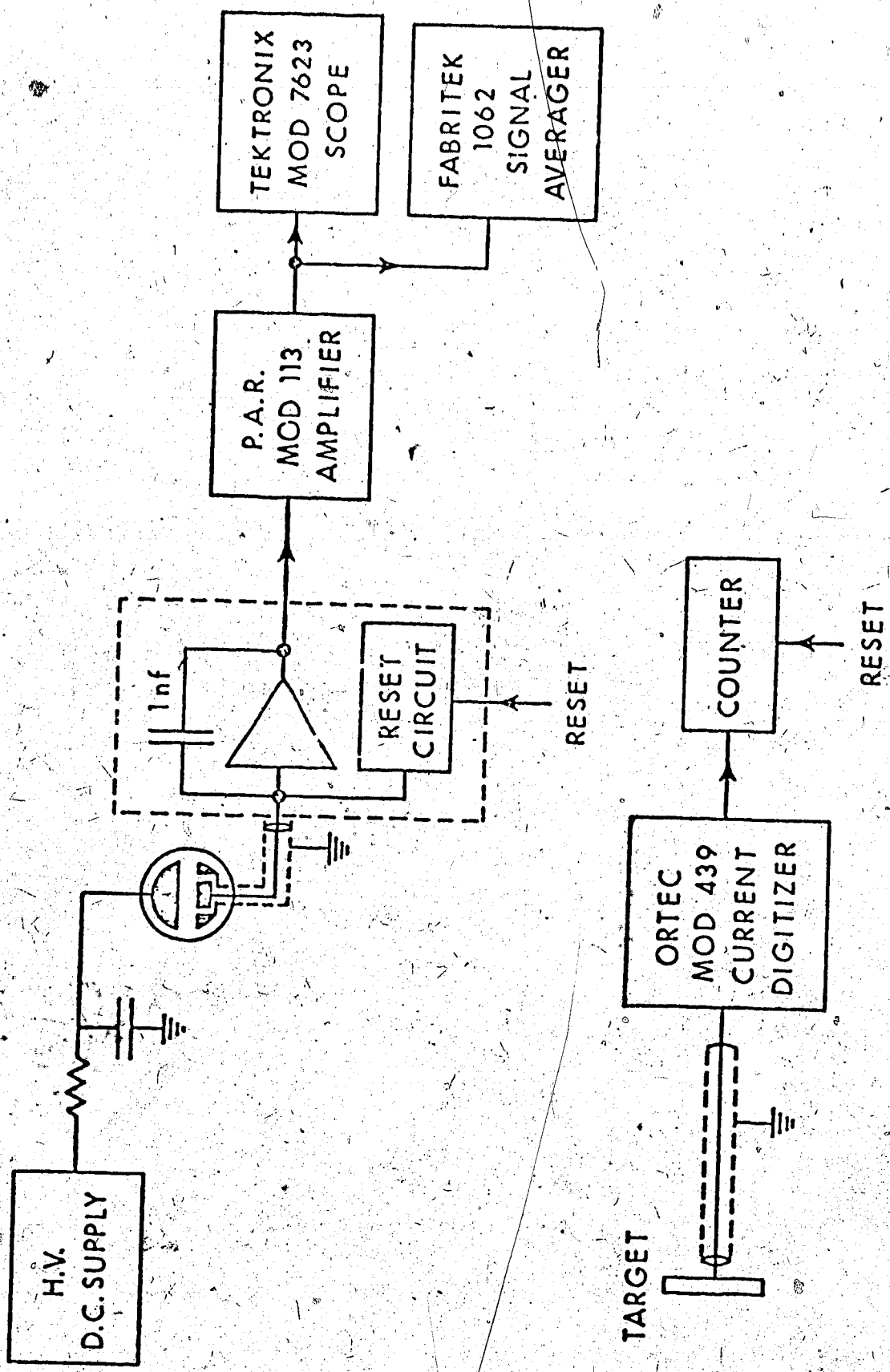


FIGURE II-8 System for Charge Clearing Measurements

$$G_{fi}^E = \frac{Q \times 6.24 \times 10^{20}}{DV} \quad (1)$$

where G_{fi}^E is the free ion yield per 100 eV at field strength E , Q is the charge collected in coulombs, V is the collection volume in cm^3 , D is the absorbed dose in eV/cm^3 by the sample between the electrodes from the pulse, and 6.24×10^{20} is the product of the electron charge in coulombs per electron and 100, because of the definition of G_{fi}^E . Thermoluminescence dosimetry, using LiF crystals calibrated with a standard ^{60}Co source, was used to obtain the dose.

9. Mobility Measurements

The circuit used to measure ion conductance signals is shown in Figure II-9. The signal was carried from the target room to the control room on a low noise cable. The response time and gain of the circuit were varied by the gain setting on the P.A.R. amplifier, and the resistor value. For electron signals, the amplifier (109) was moved to the cell end of the low noise cable. For liquid phase measurements on n-butane, i-butane, propane and ethane, the amplifier had a gain of 100 k and a response time of about 150 ns. For the rest of the work, amplifier #8, Figure II-10, which has a gain of 50 k and a response time of about 50 ns, was used. The low noise cable was replaced by 1 meter of Heliax cable.

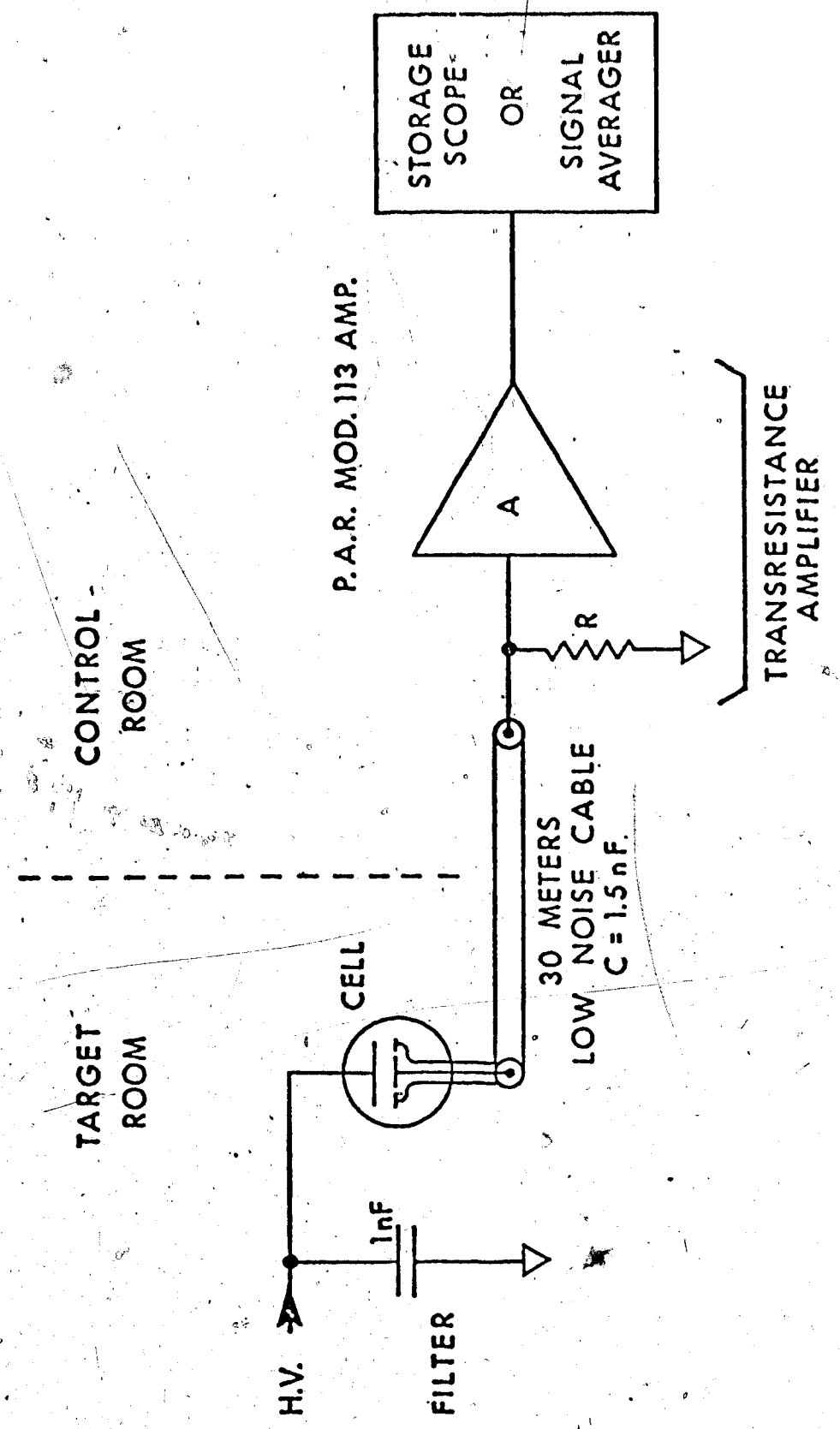


FIGURE II-9 System for Mobility Measurements

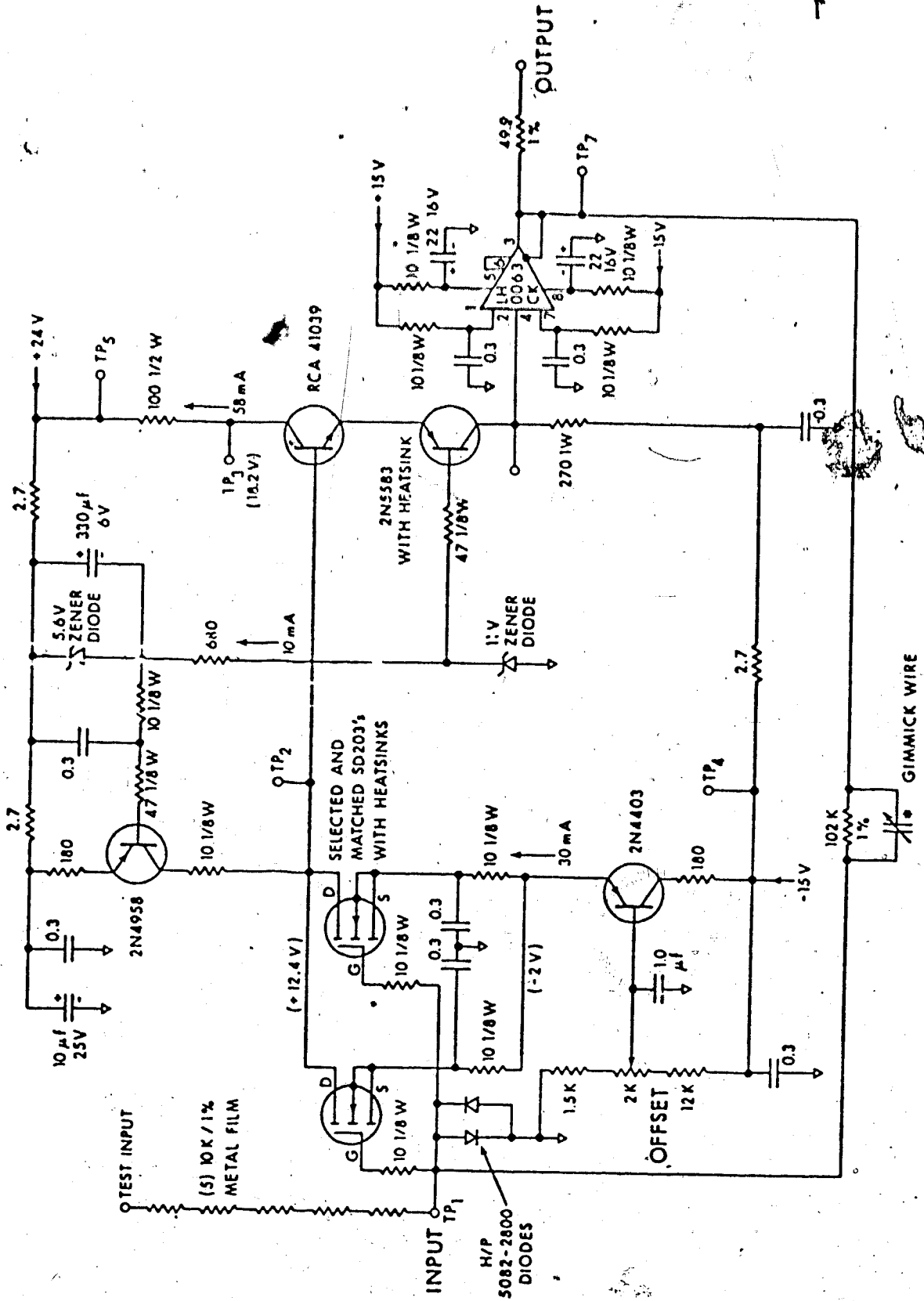


FIGURE II-10 Amplifier #8

The electron mobilities were obtained by a time of flight measurement for all the gas phase results, for all the liquid phase results in methane, and at the high temperatures of the other liquids. In this method, all the electrons are collected before they can be scavenged and converted into negative ions. Electrons are formed uniformly between two electrodes of separation L . The electrons closest to the collecting electrodes are collected first, and the farthest, last. The time of collection is the time τ needed for the electrons to drift across the separation. The average drift velocity is then

$$v_d = L/\tau \quad (2)$$

where v_d is the drift velocity in cm/sec. The electron mobility, which is defined as the drift velocity per unit field strength is then

$$\mu_e = \frac{L}{\tau E} = \frac{L^2}{\tau V} \quad (3)$$

where E is the electric field strength in volts/cm and V is the voltage applied across the plates. Measurements were made with positive and negative voltages. The two different polarities gave results agreeing to within 15%. The average of the positive and negative results were used.

When only a fraction of the electrons was collected before scavenging by impurities occurred, an electron

conductance method was used (107). The main disadvantage of the latter method is that independent determinations of the free ion yield and the total dose absorbed during the pulse are needed. The measurement of the free ion yields is described in section (h). When electron loss during the pulse is negligible, the current at the end of the pulse is given by

$$i_0 = v_d A C_0 \quad (4)$$

where i_0 is the current in amps, C_0 is the concentration of electrons at the end of the pulse (in coulombs/cm³), and A is the area of the collecting electrode in cm².

Normally, the current was corrected for decay during the pulse. Corrections were usually 10-15%. The electron concentration at the end of the pulse can be related to the free ion yield and the dose absorbed from the pulse by

$$C_0 = \frac{10^{-2} D G_{fi}^E}{6.24 \times 10^{18}} \quad (5)$$

where G_{fi}^E is the number of ion pairs generated per 100 eV of absorbed dose, D is the absorbed dose in eV/cm³, and 6.24×10^{18} is the number of electrons per coulomb. Combining (4) and (5) gives

$$i_0 = \frac{D G_{fi}^E v_d A}{6.24 \times 10^{20}} \quad (5)$$

or

$$v_d = \frac{i_0 \times 6.24 \times 10^{20}}{DG_{fi}^E A} \quad (7)$$

and finally, to get μ_e

$$\mu_e = v_d / E = \frac{i_0 \times 6.24 \times 10^{20}}{DG_{fi}^E AE} \quad (8)$$

For the ion mobilities, the time of flight measurement was used in all cases. For ions, τ is taken to be the time needed to collect all the slow charge carriers. In all cases except liquid n-butane, τ was obtained from the charge clearing measurement. For n-butane, an independent measurement of the time of flight was made.

C. Physical Properties

The compounds in the present study are the C_1 to C_4 alkanes and alkenes, excluding the butenes. The densities of the liquids were obtained from reference 222. Gas densities were obtained from reference 223 except for cyclopropane. The density of gaseous cyclopropane was calculated from the Van der Waal equation (224) up to 0.03 g/cm^3 and from the rectilinear diameters for $>0.11 \text{ g/cm}^3$ (using the low density gas and the critical fluid as anchor points). Densities between 0.03 and 0.11 g/cm^3 were obtained by smooth interpolation. Extensive tables are available for

methane (225) and for ethane (226).

The dielectric constants (except for liquid propene) were calculated from the Onsager equation (227) using refractive indices from reference 224 and dipole moments from 228. The refractive index for methane was unavailable. It was calculated from the liquid phase dielectric constant at six different temperatures (229), and used in the Onsager equation to calculate other dielectric constants. The dielectric constants of propene over most of the liquid range were obtained from reference 230. The value at the lowest temperature 230K was estimated from the Onsager equation. Values between 230K and 293K were obtained by linear interpolation between the measured (293K) and the calculated (230K) values.

Critical temperatures, pressures and densities were obtained from references 222, 223, 225, 226 and 231. Reference 223 has no data on cyclopropane, reference 225 has data on just methane and 226 on just ethane. Agreement between the different sources is within a degree for the critical temperatures and within 5% for the critical pressures and densities. The preferred critical parameters are listed in Table II-1.

TABLE II-1

Critical Properties

	T_c	P_c	n_c (10^{21} molec/cm 3)	ϵ_c	D (debye)
CH $_4$	191	4.5	6.1	1.23	0
C $_2$ H $_6$	306	4.8	4.06	1.25	0
C $_2$ H $_4$	283	5.0	4.66	1.27	0
C $_3$ H $_8$	370	4.3	3.00	1.26	0.084
c-C $_3$ H $_6$	398	5.5	3.55	1.27	0.00
C $_3$ H $_6$ -1	365	4.6	3.32	1.33	0.366
n-C $_4$ H $_{10}$	425	3.8	2.36	1.26	0.05 \leq
i-C $_4$ H $_{10}$	408	3.6	2.3	1.26	0.132

III RESULTS

Measurements have been made of the electron mobilities, of the ion mobilities and of the free ion yields as functions of the electric field strength for methane, ethane, propane, *n*-butane, isobutane, (2-methylpropane), ethene, propene and cyclopropane over a temperature range spanning from the normal vapors and liquids to the supercritical fluid. Section A will contain the electron mobilities, section B the ion mobilities and section C the free ion yields. In each section the order of presentation will be the same as above, that is, the results for methane will appear first, followed by ethane and the rest. Cyclopropane will be the last.

All of the curves in the figures of Chapters III and IV were drawn empirically unless otherwise specified.

A discussion of errors is given in the appendix.

A. Electron Mobilities

In this section all the mobilities are plotted as functions of the density normalized electric field strength E/n . For each compound, the liquid phase results will be given first. The gas phase results will be given in order of decreasing density.

(i) Methane

Figures III-1 to III-17 give the electron mobilities in methane as functions of E/n . Figure III-1 shows the liquid near the critical point. The mobility is field

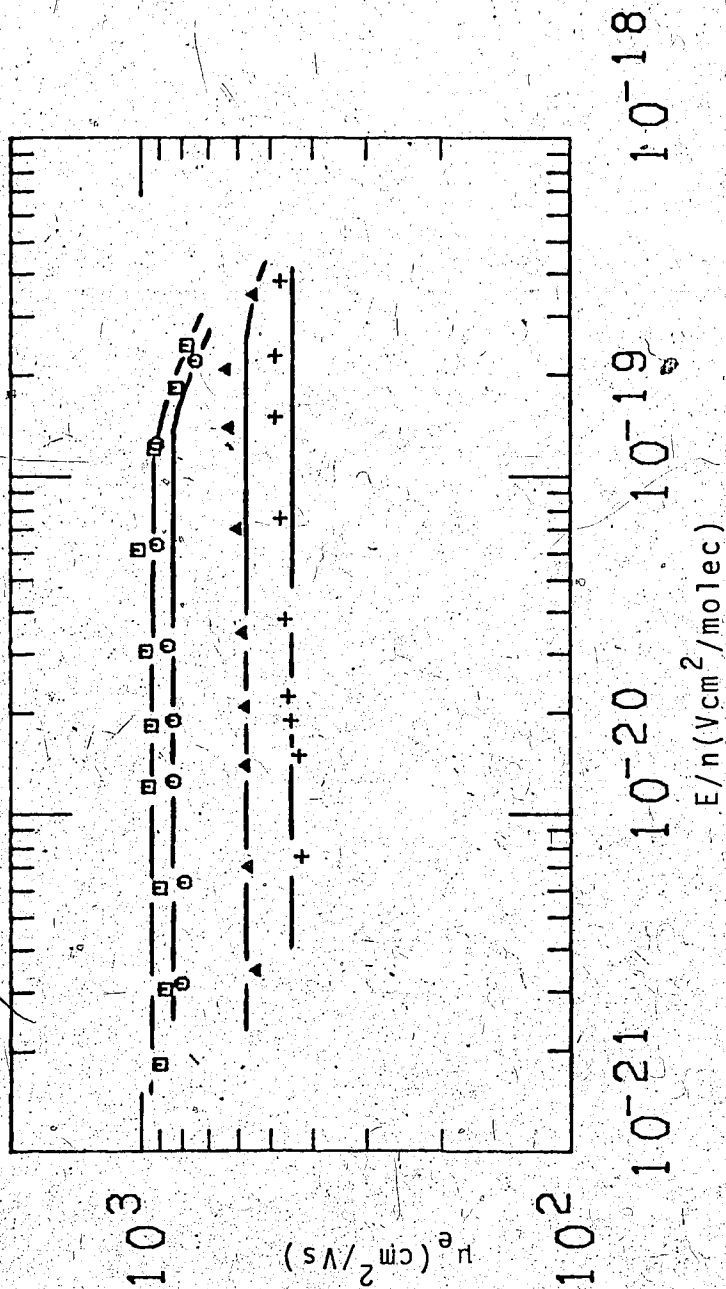


FIGURE III-1 Electron mobilities μ_e in liquid methane plotted against

the density normalized electric field strength E/n .

Densities and temperatures ($n/10^{21}$ molec/ cm^3 , T):

\square (10.2, 181K), \circ (9.87, 183K), Δ (8.93, 187K),
 + (8.26, 189K).

independent up to a value of $E/n \geq 1 \times 10^{-19} \text{ Vcm}^2/\text{molec}$. The slight positive slope at low field strengths is due to diffusive broadening of the electron swarm during the drift time. Correction for the broadening would raise the square at $E/n = 1 \times 10^{-21} \text{ Vcm}^2/\text{molec}$ by 10% and that at 1×10^{-19} by 1%. At higher fields, the mobility decreases. Decreasing the density leads to an increase in the threshold field strength. Over this same range, decreasing the density also leads to a decrease of the low field mobility. Figure III-2 shows results at slightly higher densities. These have been plotted separately from Figure III-1 to avoid overcrowding.

The points for 178K in Figure III-2 are only slightly different from those for 181K in Figure III-1. The threshold fields for the two are both about $E/n = 1.3 \times 10^{-19} \text{ Vcm}^2/\text{molec}$. As the density increases from $10.7 \times 10^{21} \text{ molec/cm}^3$ at 178K to $11.5 \times 10^{21} \text{ molec/cm}^3$ at 172K, the threshold field and the low field mobilities decrease (Figure III-2). Figure III-3 shows the effect of a further increase in density. The low field mobilities continue to decrease, but the threshold fields slightly increase. Electron mobilities near the triple point (91K) and at a few temperatures near the mobility maximum are given in Figure III-4. The increase in density from $15.5 \times 10^{21} \text{ molec/cm}^3$ in Figure III-3 to $17.0 \times 10^{21} \text{ molec/cm}^3$ in Figure III-4 causes an increase in the low field mobilities, though the threshold field seems the same.

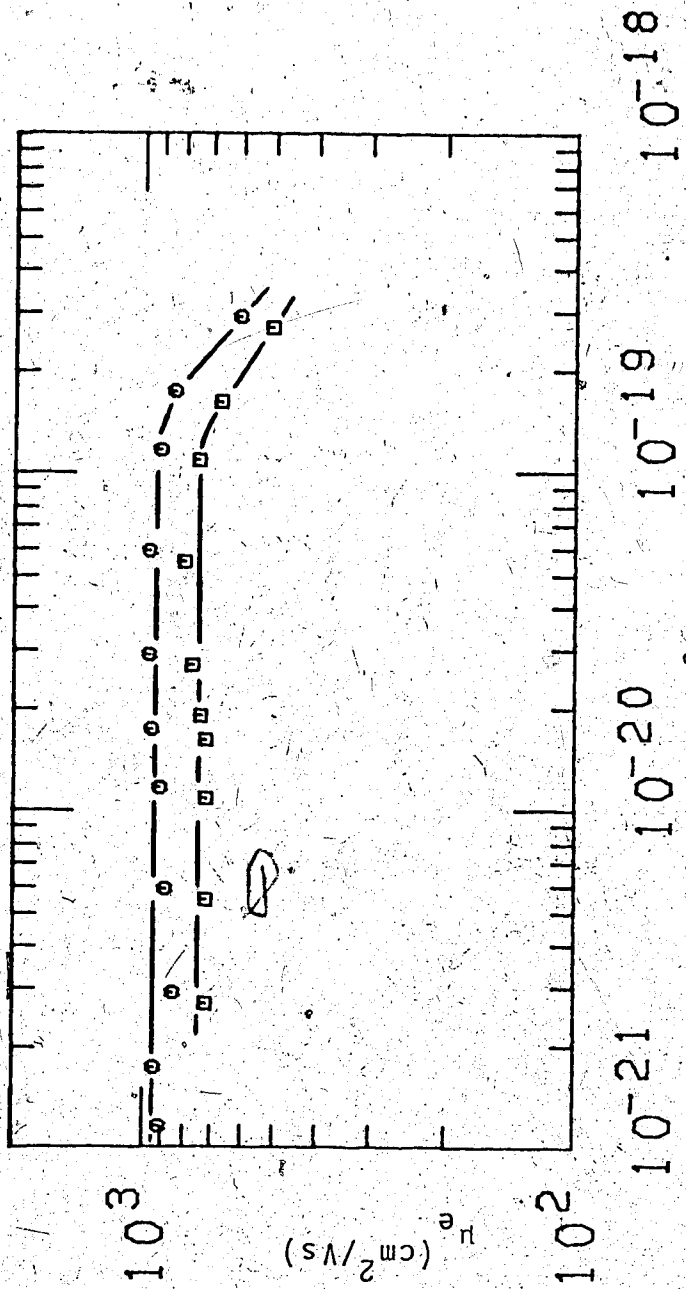


FIGURE III-2 Electron mobilities μ_e in liquid methane plotted against the density normalized electric field strength E/n .
 Densities and temperatures ($n/10^{21}$ molec/ cm^3 , T):
 □(11.5, 172K), O(10.7, 178K)

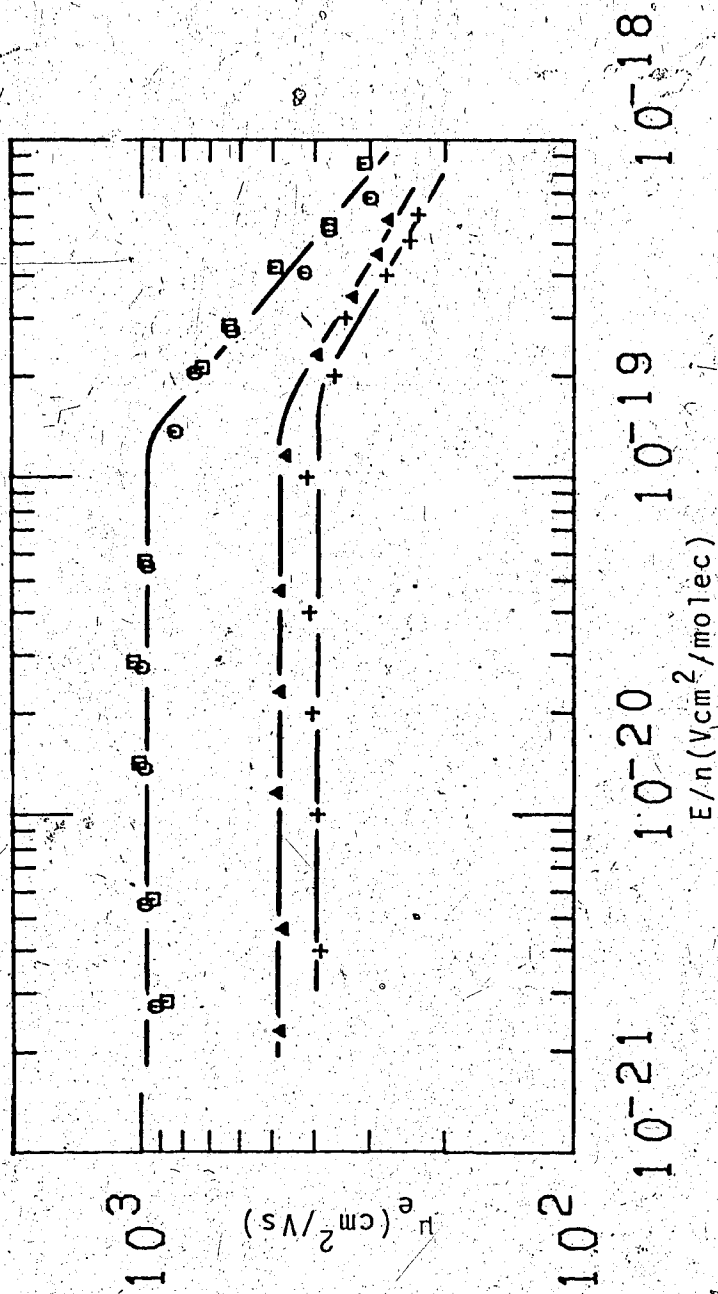


FIGURE III-3 Electron mobilities μ_e in liquid methane plotted against the density normalized electric field strength E/n .

Densities and temperatures ($n/10^{21}$, T): \square (11.0, 176K), \circ (11.4, 173K), Δ (13.4, 153K), + (15.5, 122K).

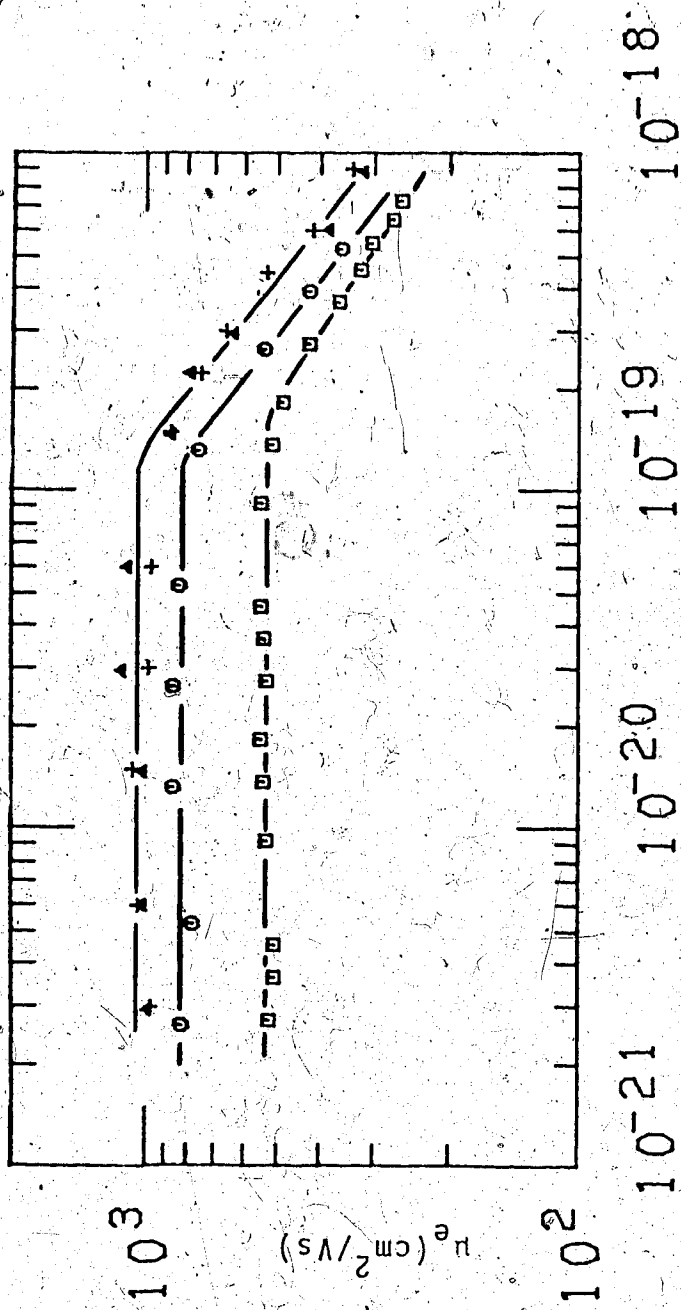
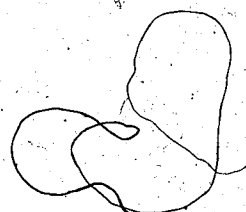


FIGURE III-4 Electron mobilities μ_e in liquid methane plotted against the density normalized electric field strength E/n .
 Densities and temperatures ($n/10^{21}$, T): \square (17.0, 91K), \circ (11.8, 170K), Δ (10.5, 179K), + (10.4, 180K).

Figure III-5 shows the effect of field and temperature on the electron mobility in the supercritical fluid. An increase in temperature leads to an increase in the low field mobility, and to a decrease in the threshold field. A reversal in the direction of the field effect also occurs. Unlike the liquid phase, high electric field strengths lead to an increase of the mobility. The low field mobility is an order of magnitude lower than in the liquid phase. The threshold field is also larger than in the nearest liquid phase density (8.26×10^{21} molec/cm³ in Figure III-1). The solid symbols in Figure III-5 represent results obtained in liquid type conductance cells (Figure II-4). The stick symbols represent results obtained using gas type cells.

In Figure III-6, the density decreases from that of the critical fluid. The decrease of density increases the low field mobility and decreases the threshold field. The same tendencies are observable in Figure III-7.

The effect of increasing the temperature at $n = 3.09 \times 10^{21}$ molec/cm³ is shown in Figure III-8. A lower temperature at the same density is given in Figure III-7. The temperature increase raises the mobility at all field strengths, but to a lesser extent at the higher fields. The different mobility curves approach each other as the field strength increases.



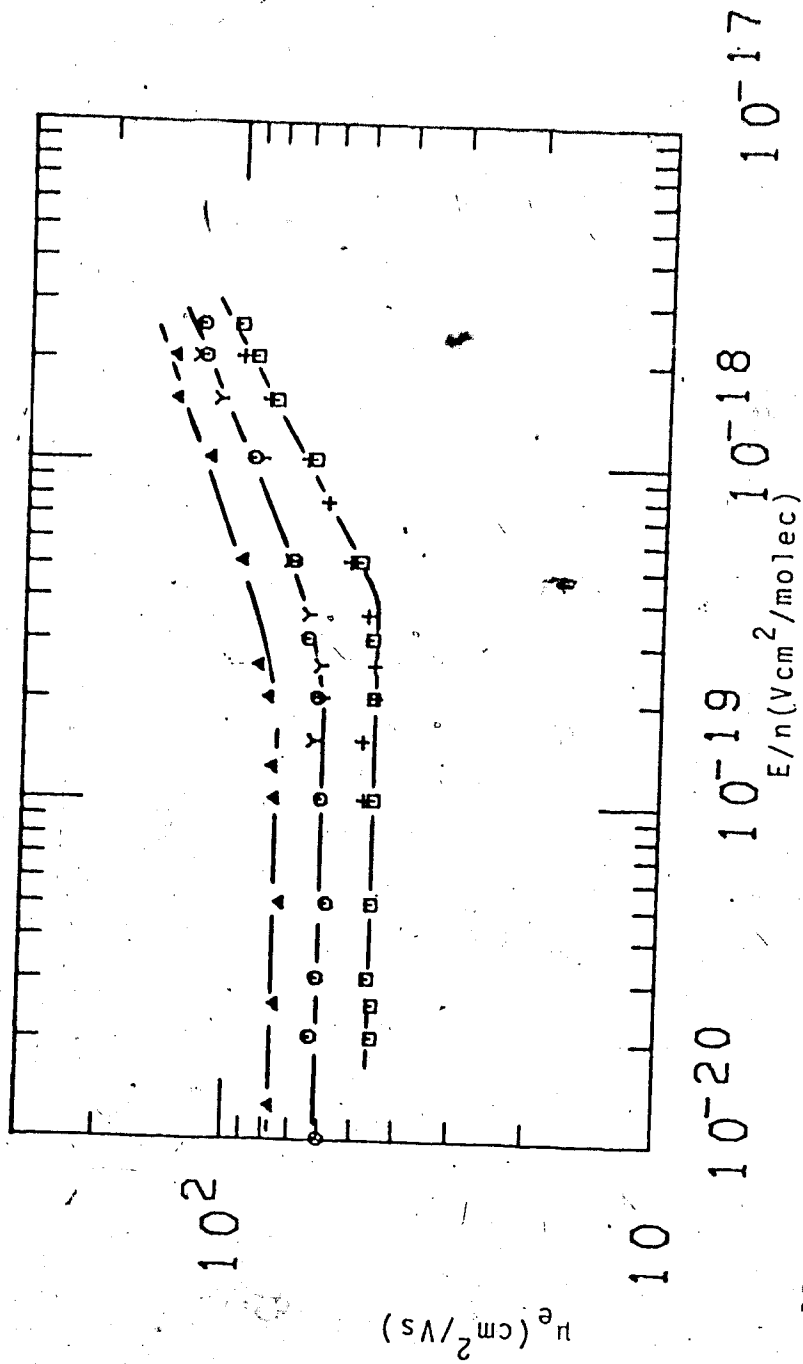


Figure III-5. Electron mobilities μ_e in supercritical methane plotted against the density normalized electric field strength E/n . All samples are at $n = 6.1 \times 10^{21}$ molec/cm³. Temperatures (T): \square (193K), \circ (195K), Δ (196K), $+$ (192K), γ (195K).

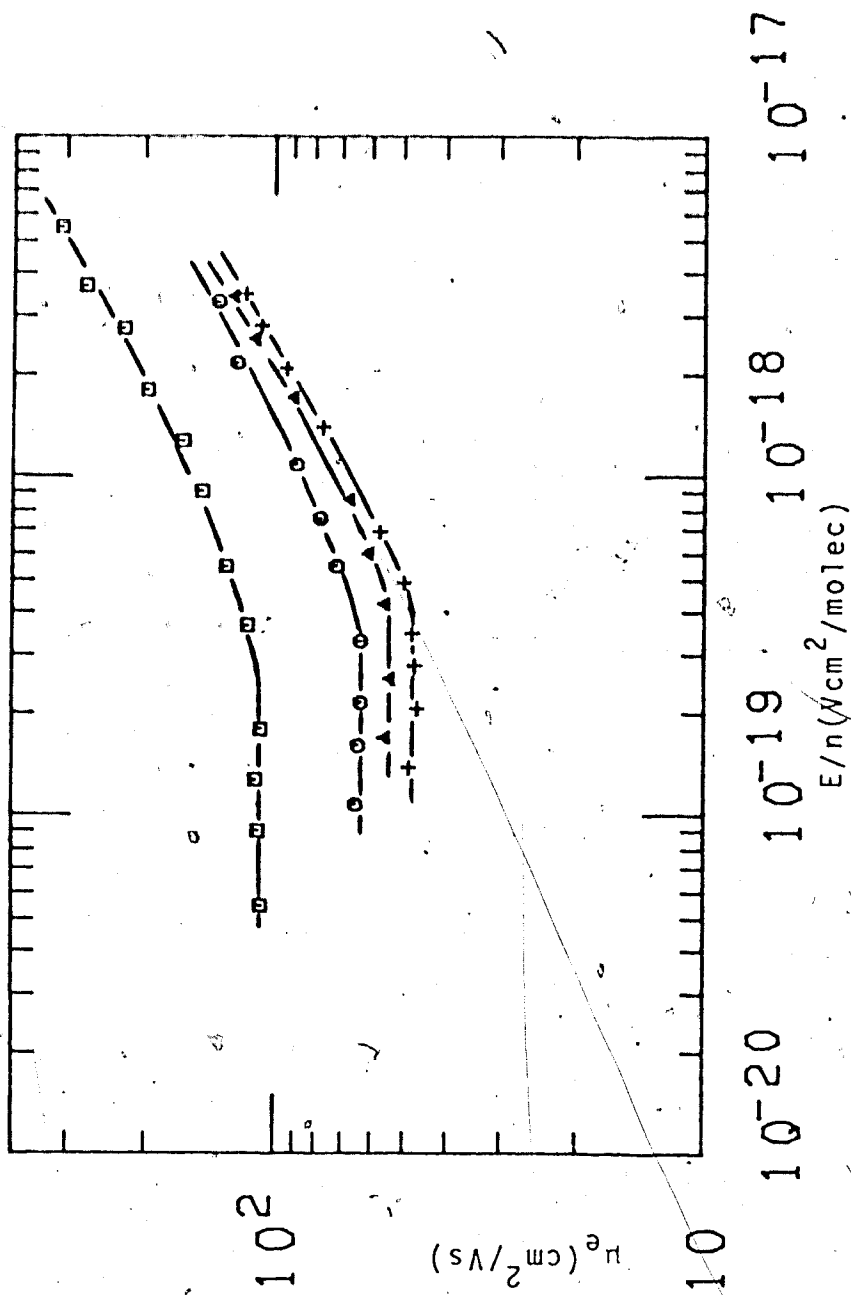


FIGURE III-6. Electron mobilities in gaseous methane plotted against the density normalized electric field strength E/n . Densities and temperatures ($n/10^{21}$, T): \square (1.71, 173K), \circ (2.87, 184K), Δ (3.66, 188K), $+$ (4.47, 190K).

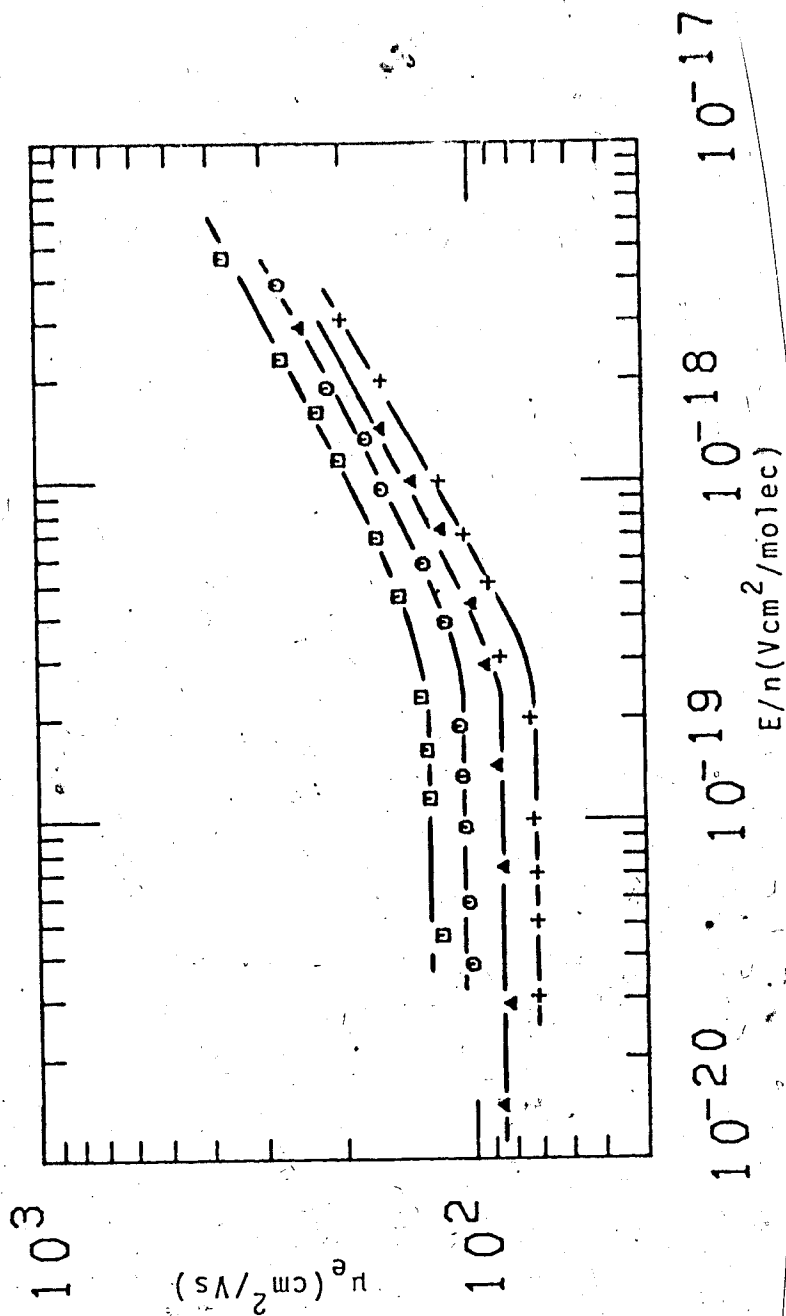


FIGURE III-7. Electron mobilities as functions of E/n in gaseous methane.

Densities and temperatures ($n/10^{21}$, T): \square (1.35, 168K)

\circ (1.63, 172K), \triangle (2.15, 178K), $+$ (3.09, 185K).

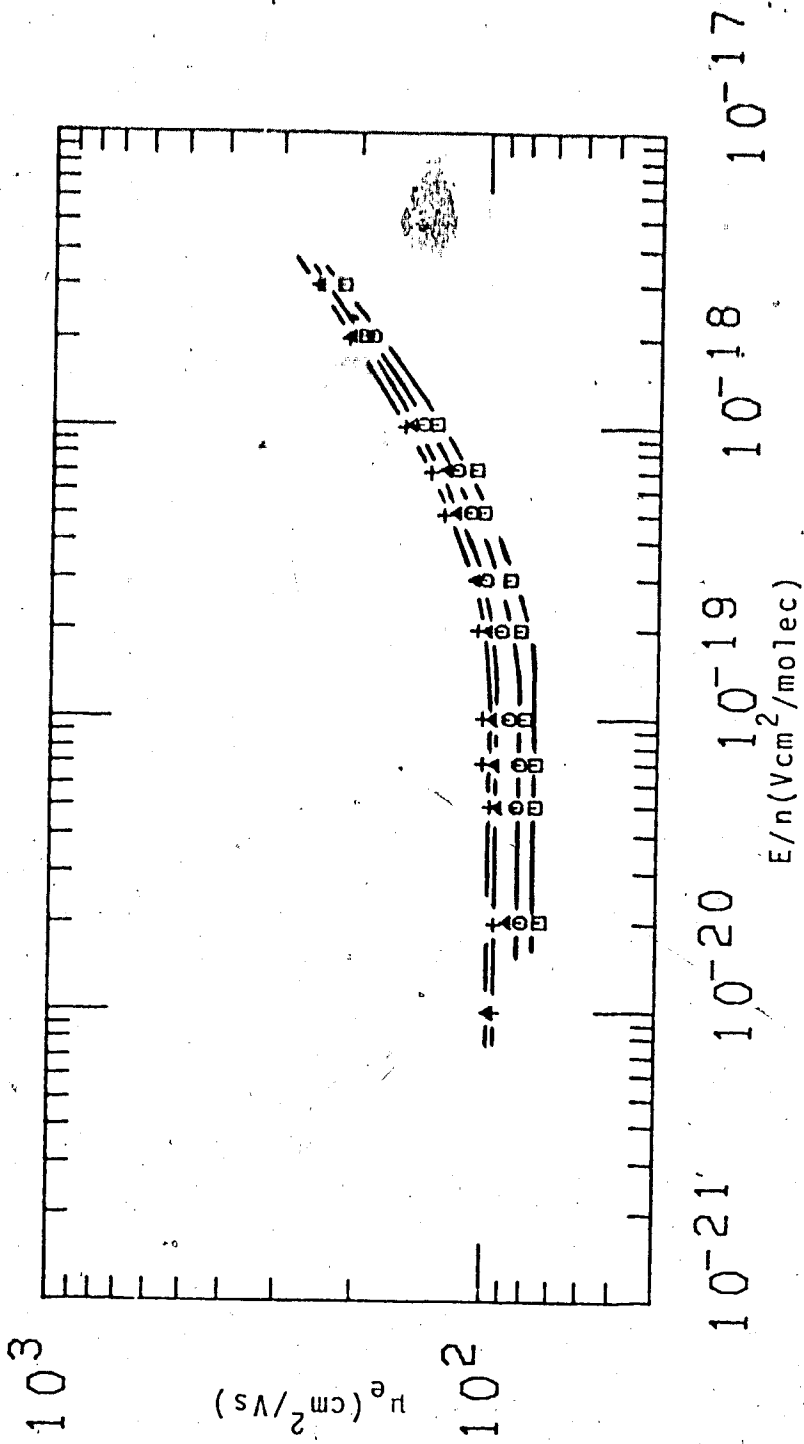


FIGURE III-8. Electron mobilities as functions of E/n in gaseous methane
 $n = 3.09 \times 10^{21}$ molec/ cm^3 . Temperatures: \square (188K), \circ (191K),
 Δ (194K), $+$ (196K).

The effect of a further decrease in density is shown in Figure III-9. The low field mobility increases by almost the inverse ratio of the density change. Variation in the size of the threshold fields is slight. The same trends can be seen in Figure III-10, where the temperature effect at $n = 1.5 \times 10^{21}$ molec/cm³ is shown. At high fields, the mobility curves approach each other.

Figure III-11 shows a difference of density of an order of magnitude from that of Figure III-7. While the low field mobilities increase roughly as the inverse ratio of the densities, the threshold field varies by less than a factor of 2. The effect of temperature at $n = 6.57 \times 10^{20}$ molec/cm³ is shown in Figure III-12. As for Figure III-8 and III-10, the mobility differences at the various temperatures decrease as the field strength increases. Variation of the threshold field is slight (about 15%). Further decreases in density lead to a further increase in low field mobility and little variation in threshold field (Figure III-13). At 1.58×10^{20} molec/cm³, measurements extend to a high enough field to observe a bending of the mobility curve. Temperature increase at (Figure III-14) at $n = 3.28 \times 10^{20}$ molec/cm³ clearly shows the merging of the mobility curves at high field strengths. The temperature increase leads again to an increase of the low field mobilities and little variation in the threshold fields. Increases in temperature at $n = 7.13 \times 10^{19}$ molec/cm³

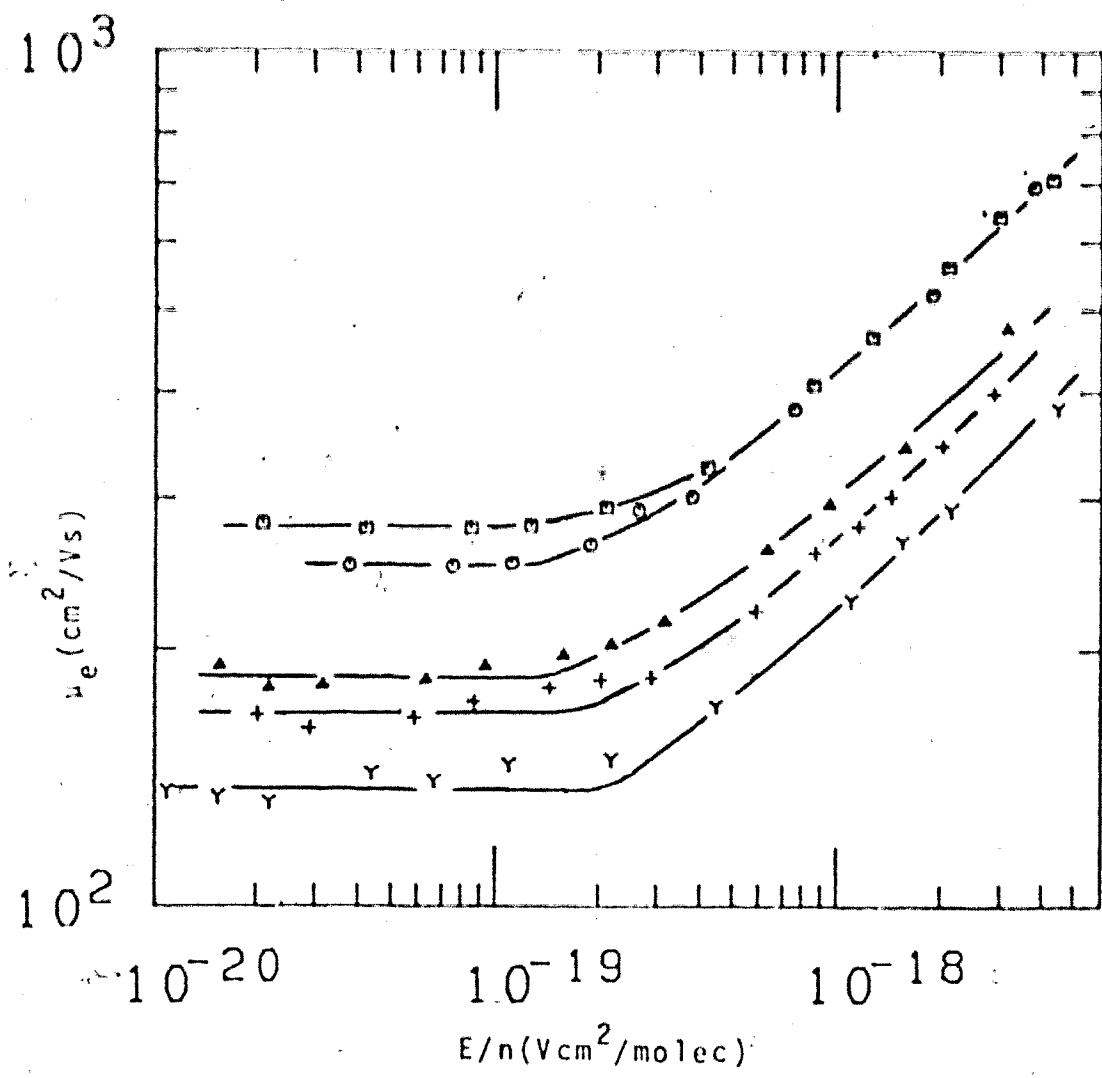


FIGURE III-9. Electron mobilities as functions of E/n in gaseous methane. Densities and temperatures ($n/10^{20}$ molec/cm³, T): \square (7.30, 154K), \circ (8.26, 157K), \triangle (9.87, 161K), $+$ (10.7, 163K), Y (14.1, 169K).

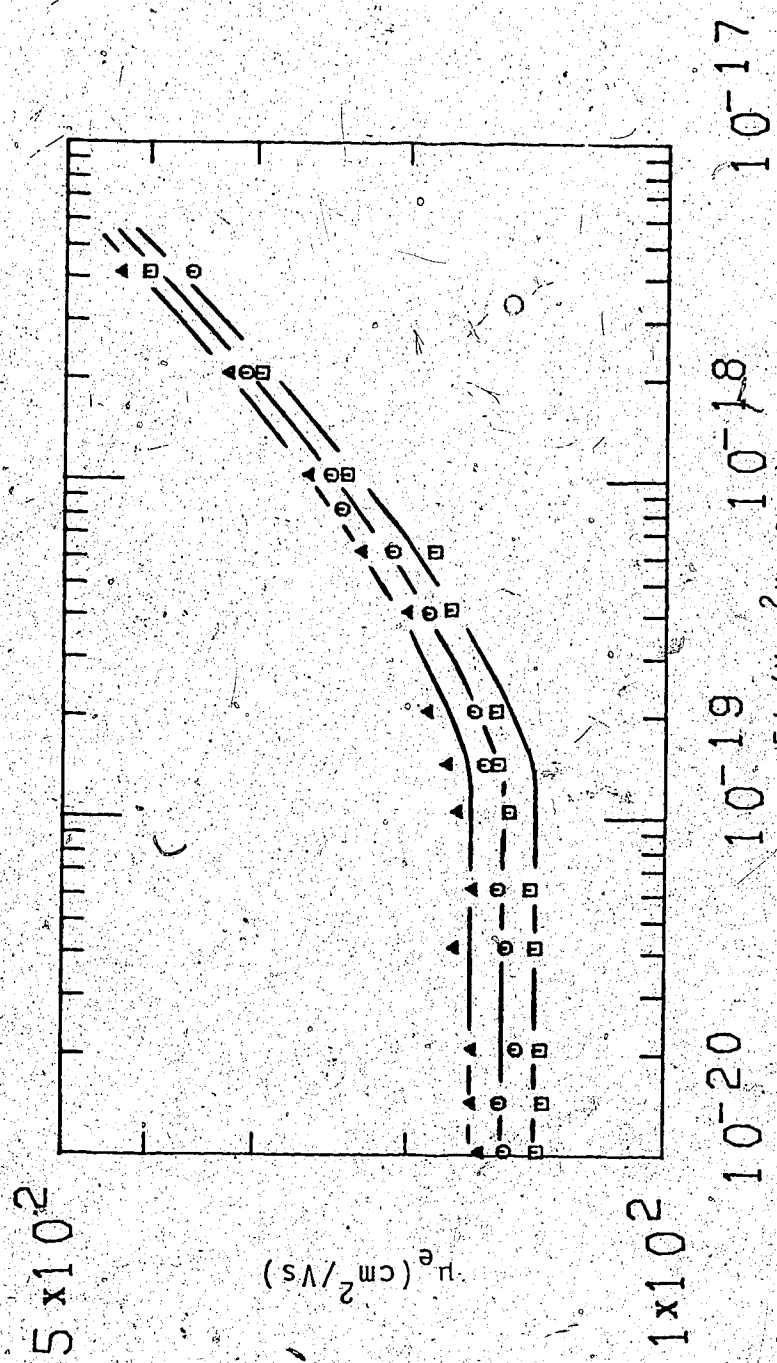


FIGURE III-10. Electron mobilities as functions of E/n in gaseous methane. $n = 1.48 \times 10^{21}$ molec/cm³. Temperatures: \square (174K), \circ (180K), Δ (187K).

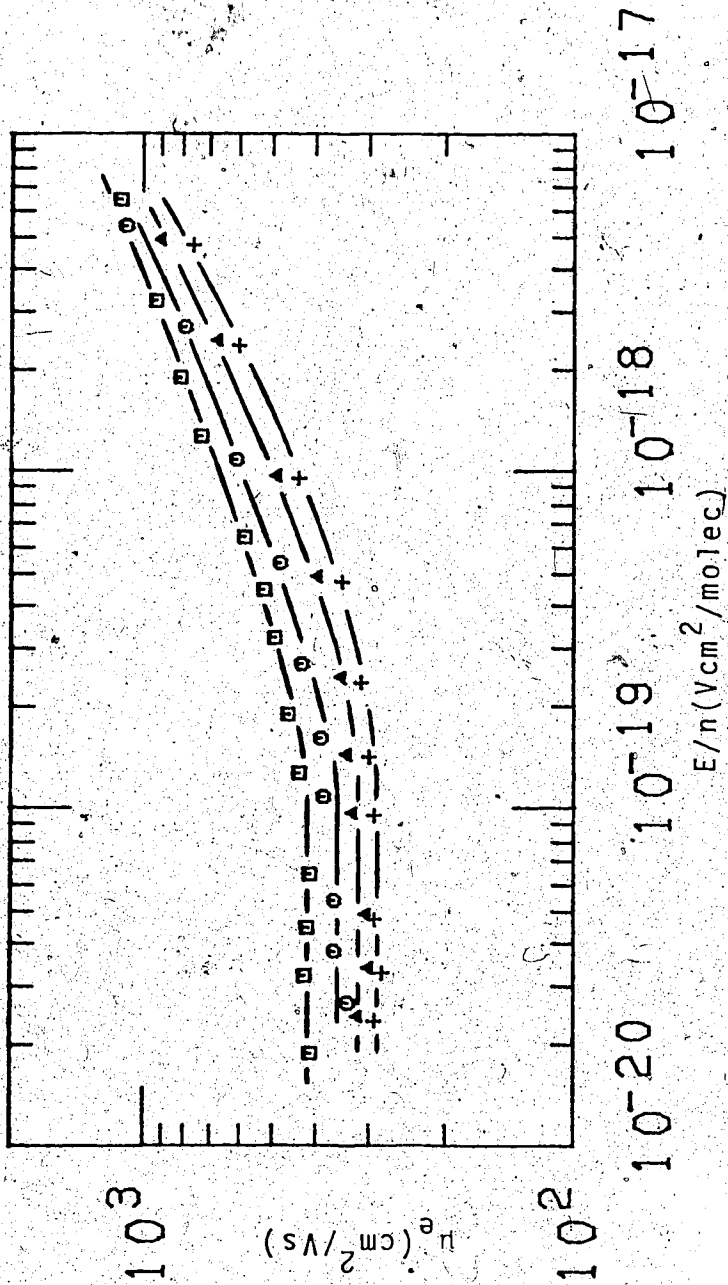


FIGURE III-11. Electron mobilities as functions of E/n in gaseous methane. Densities and temperatures ($n/10^{20} \text{ molec/cm}^3, T$): \square (4.88, 145K), \circ (5.78, 149K), \triangle (6.38, 151K), + (6.57, 153K).

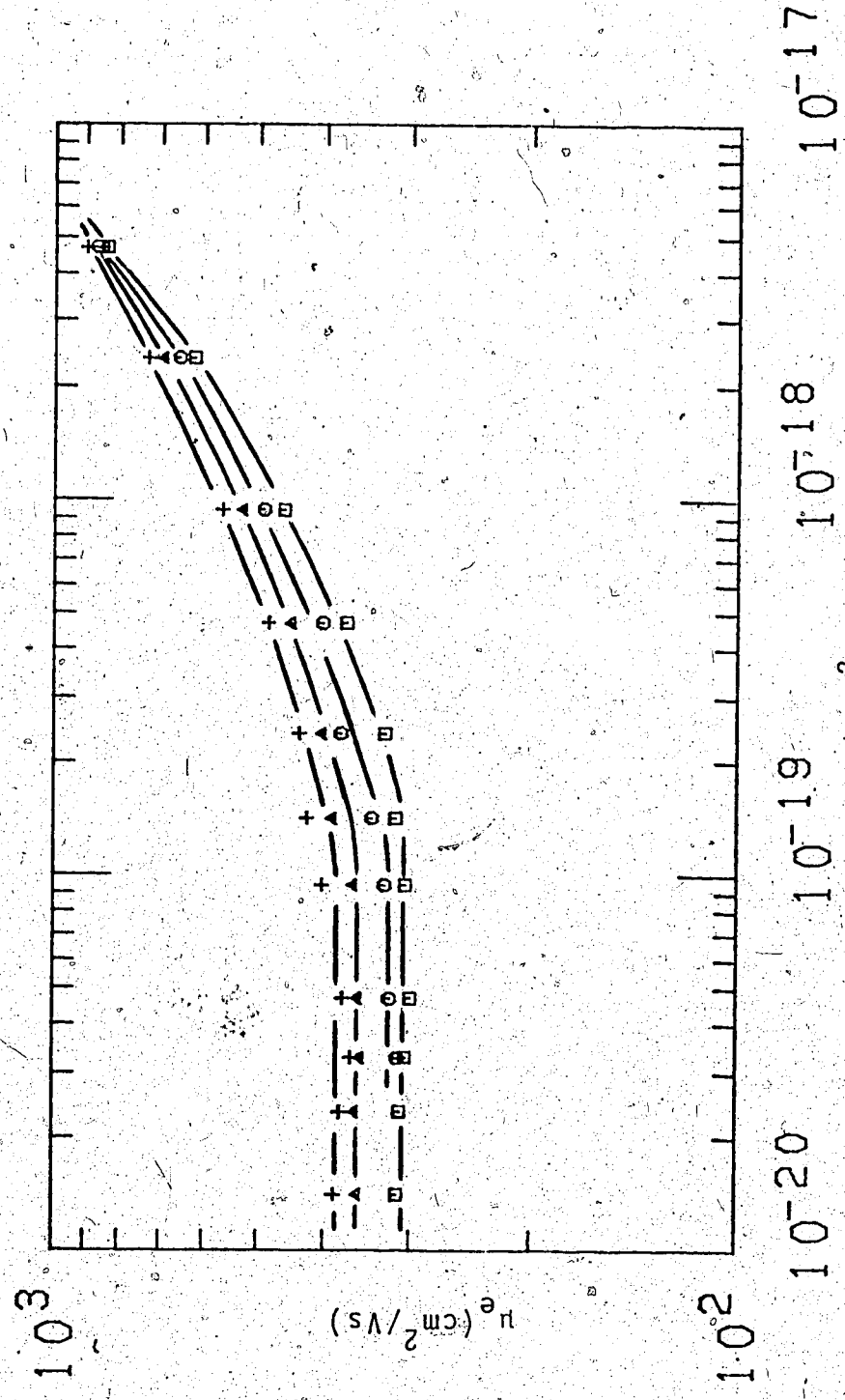


FIGURE III-12. Electron mobilities as functions of E/n in gaseous methane.
 $n = 6.57 \times 10^{20}$ molec/cm³. Temperatures: □ (159K), ○ (166K), Δ (187K), + (208K).

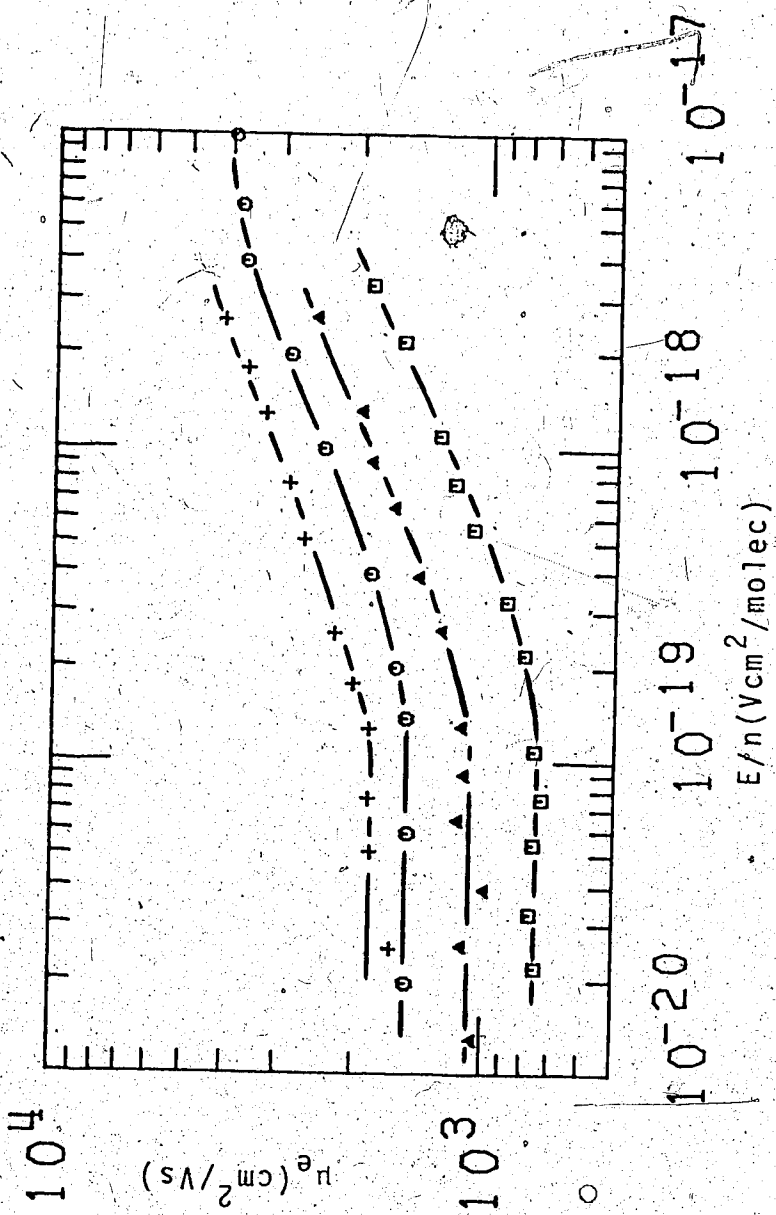


FIGURE III-13. Electron mobilities in gaseous methane as functions of E/n .
 Densities and temperatures ($n/10^{20}$ molec/cm³, T): + (1.22, 120K); O (1.58, 124K), Δ (2.40, 131K); \square (2.85, 134K).

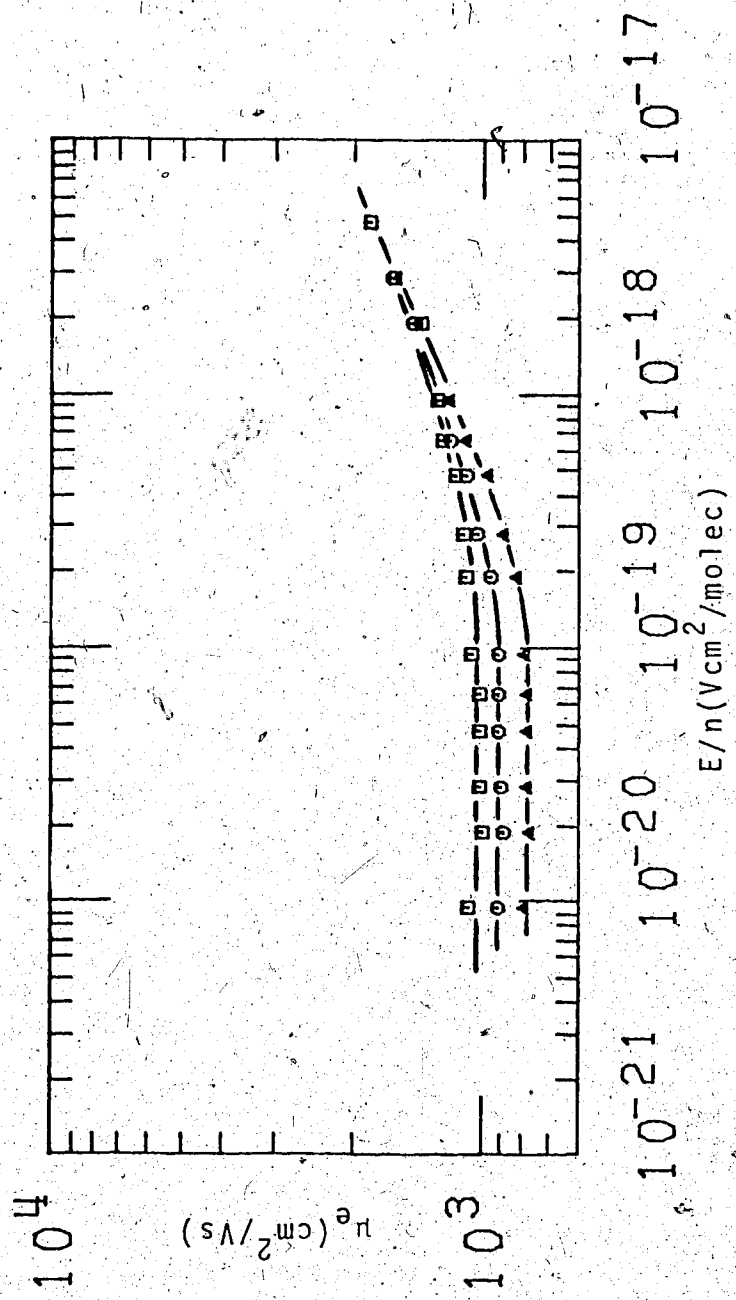


FIGURE III-14. Electron mobilities in gaseous methane as functions of E/n $n = 3.28 \times 10^{20}$ molec/cm³. Temperatures (T): □ (297K), ○ (220K), △ (181K).

leads to the same effects (Figure III-15). Variation of densities in Figures III-16 and III-17 leads to the same increase in low field mobilities and fairly constant threshold fields. At $n = 1.99 \times 10^{19}$ and $n = 3.57 \times 10^{19}$ molec/cm³, measurements could not be made at the lower fields to fix the low field mobility.

Except for the curves 3.09×10^{21} molec/cm³ at 185K (Figure III-7) and 6.57×10^{20} molec/cm³ at 153K and those specified as being at a constant density which were at temperatures above the co-existence curve, all the results were measured along the co-existence curve.

For all the gas phase results except those in Figures III-15 and III-16, gas type high pressure conductance cells were used (Figure II-5). The electrode separations were about 0.32 cm. For the measurements in Figures III-15 and III-16, a low pressure gas type conductance cell was used. The electrode separation was 1.00 cm. This allowed the measurement of more low voltage points and a better determination of low field mobility at the low densities.

A summary of the low field mobilities and the threshold voltages at the different temperatures and densities appears in Table III-1.

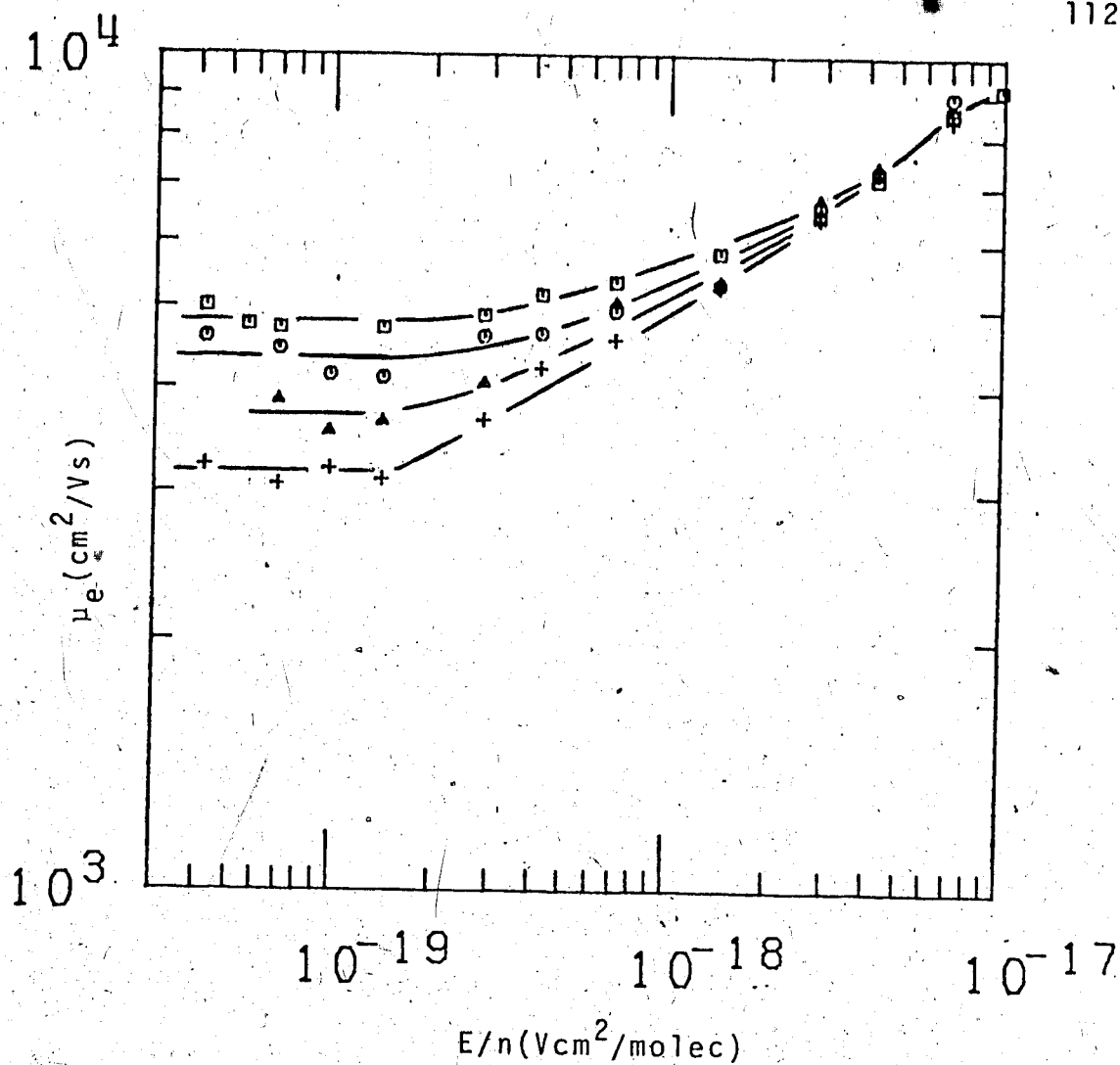


FIGURE III-15. Electron mobilities in gaseous methane as functions of E/n . $n = 7.13 \times 10^{19}$ molec/cm³.
 Temperatures (T): \square (297K), \circ (243K), \triangle (163K), $+$ (117K).

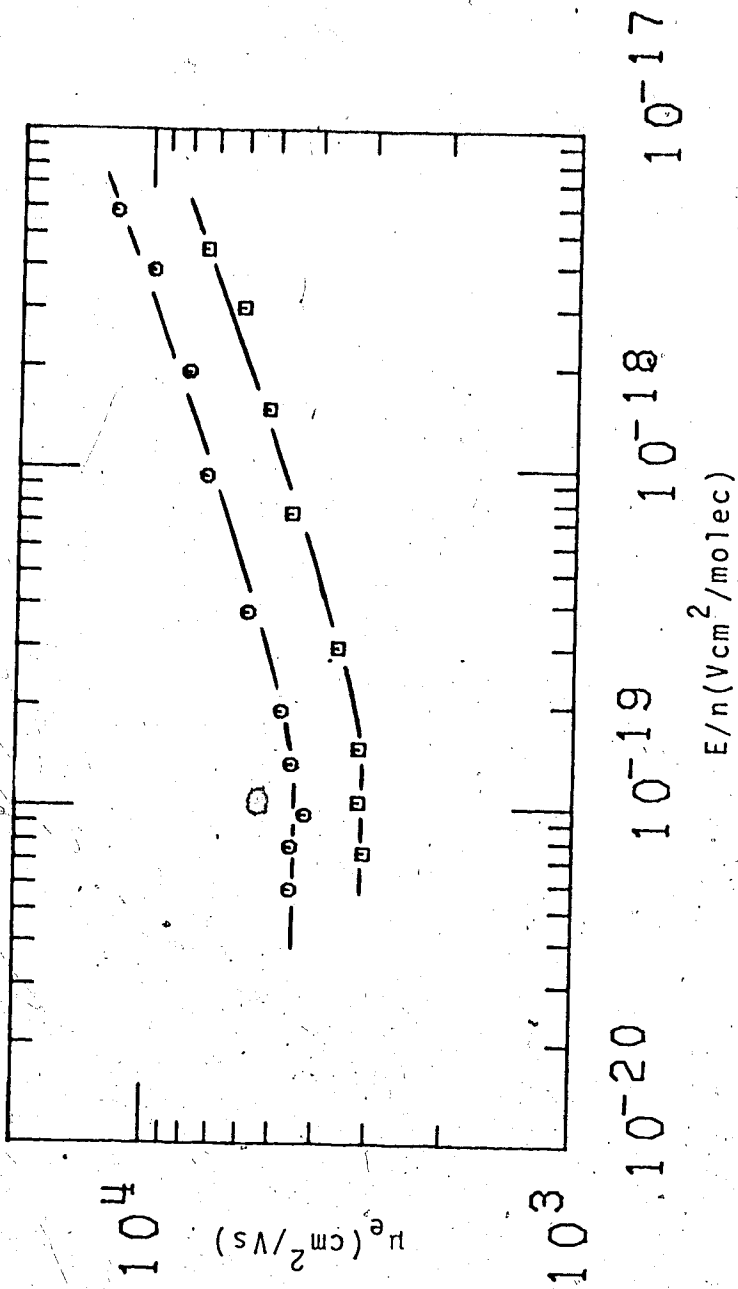


FIGURE III-16. Electron mobilities in gaseous methane as functions of E/n .

Densities and temperatures ($n/10^{19}$, T): □ (6.76, 112K),
 ○ (5.26, 108K).

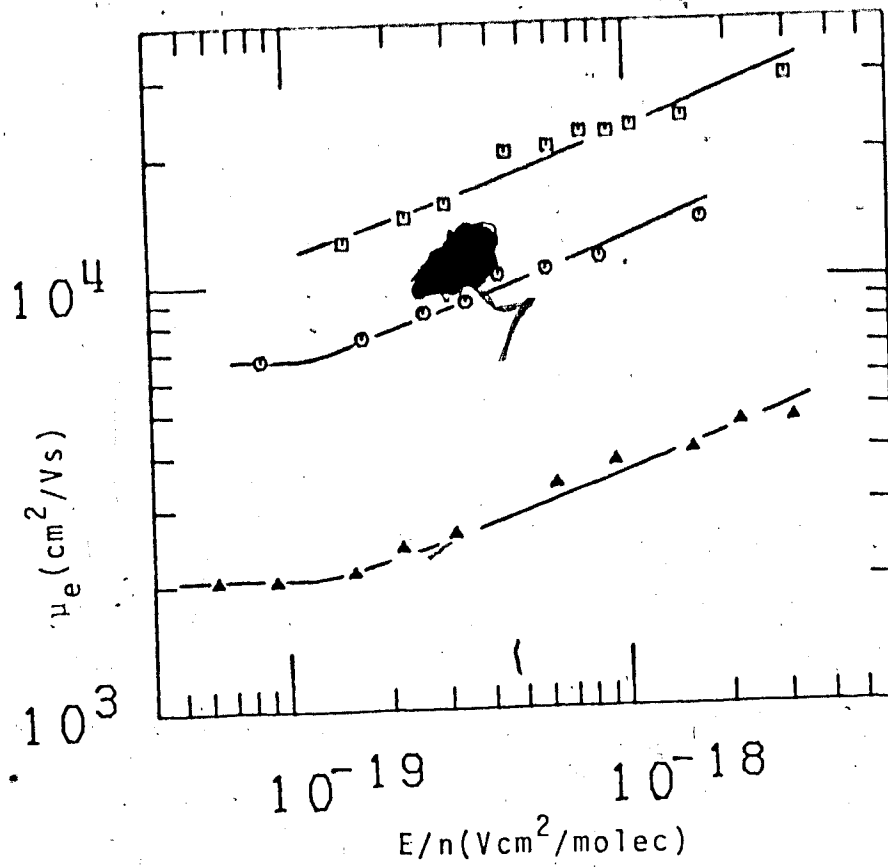


FIGURE III-17. Electron mobilities as functions of E/n in gaseous methane. Densities and temperature ($n/10^{19}$ molec/cm³, T): □ (1.99, 97K), ○ (3.57, 103K), Δ (9.91, 117K).

TABLE III-1
Summary of Methane Results^a

T (K)	n $10^{21} \frac{\text{molec}}{\text{cm}^3}$	μ_0 $\frac{\text{cm}^2}{\text{Vs}}$	$(\mu_0 n)$ $10^{23} \frac{\text{molec}}{\text{Vs cm}}$	$(E/n)_{\text{threshold}}$ $10^{-19} \frac{\text{Vcm}^2}{\text{molec}}$	$\frac{d \log \mu}{d \log E/n}$ ^b
181	10.2	938	95.7	1.2	minus
183	9.87	848	83.7	1.3	minus
187	8.93	571	51.0	1.5	minus
189	8.26	446	36.8	-	-
172	11.5	746	86.0	1.1	minus
178	10.7	938	100	1.2	minus
176	11.0	964	106	1.2	-0.66
173	11.4	946	108	1.2	-0.66
153	13.4	482	64.6	1.3	-0.46
122	15.5	396	61.4	1.5	-0.45
91	17.0	536	91.1	1.6	-0.50
170	11.8	826	97.2	1.2	-0.61
179	10.5	1040	109	1.2	-0.61
180	10.4	982	102	1.2	-0.61
192	6.1 ^c	46.7	2.85	3.9	0.45
195	6.1 ^c	60.7	3.70	2.1	0.36
196	6.1 ^c	61.6	3.76	1.7	0.29
173	1.71	109	1.86	2.4	0.33
184	2.87	63.4	1.82	3.2	0.35
188	3.66	54.8	2.01	3.8	0.44
190	4.47	48.2	2.15	3.9	0.45
168	1.5	125	1.69	2.1	0.36
172	1.63	105	1.71	2.3	0.38
178	2.15	85	1.83	2.4	0.39
185	3.09	71.8	2.22	2.5	0.43
188	3.09	76.6	2.37	1.6	0.36
191	3.09	82.4	2.55	1.3	0.31
194	3.09	93.5	2.89	1.2	0.31

(continued.....)

TABLE III-1 (continued)

196	3.09	97.2	3.00	1.2	0.31
154	0.73	280	2.04	1.2	0.32
157	0.826	252	2.08	1.3	0.32
161	0.987	186	1.84	1.4	0.32
163	1.07	168	1.80	1.5	0.33
169	1.41	137	1.93	2.0	0.33
174	1.48	141	2.09	1.4	0.29
180	1.48	154	2.28	1.3	0.27
187	1.48	168	2.49	1.3	0.25
145	0.488	415	2.03	1.2	0.17
149	0.578	354	2.05	1.2	0.17
151	0.638	312	1.99	1.3	0.18
153	0.657	288	1.89	1.3	0.20
159	0.657	306	2.01	1.2	0.17
166	0.657	320	2.10	1.1	0.16
187	0.657	358	2.35	1.1	0.15
208	0.657	381	2.50	1.0	0.14
120	0.122	1830	2.23	1.2	0.24
124	0.158	1500	2.37	1.2	0.24
131	0.240	1080	2.59	1.3	0.26
134	0.285	750	2.14	1.1	0.28
297	0.328	1030	3.38	1.1	0.19
220	0.328	911	2.99	1.1	0.21
181	0.328	784	2.57	1.1	0.23
297	0.0713	4800	3.42	1.8	0.12
243	0.0713	4330	3.09	1.6	0.19
163	0.0713	3700	2.64	1.4	0.22
117	0.0713	3160	2.25	1.4	0.24
112	0.0676	3150	2.13	1.5	0.27
108	0.0526	4500	2.37	1.3	0.27
97	0.0199	11700 ^d	2.33	-1 ^d	0.32
103	0.0357	6500	2.32	1.2	0.32

(continued.....)

TABLE III-1 (continued)

117	0.0991	2030	2.01	1.2	0.27
-----	--------	------	------	-----	------

a The numbers appear in this table in the same order of appearance as the figures. The results for Figure III-1 appear first, followed by III-2 and so forth, on to Figure III-17.

b Estimated at $E/n \approx 4(E/n)_{\text{threshold}}$

c $n_c = 6.1 \times 10^{21}$ molecule/cm³, $T_c = 191\text{K}$

d Estimated

2. Ethane

Electron mobilities plotted as functions of the density normalized electric field strength, E/n appear in Figures III-18 to III-27. Figures III-18 and III-19 do not show any field effect in the liquid phase. However, this is because the field strengths used were insufficient to show the transition. Previous workers (119) show that at about 1×10^5 V/cm, a positive dependence of the mobility on the field strength occurs over the range of temperatures of 111K to 216K. Further, at 294K, a negative dependence occurs at 8000 V/cm (129). These field strengths correspond to $E/n = 9 \times 10^{-18}$ V cm²/molec at 155K and 1.1×10^{-18} V cm²/molec at 294K. Variation of the temperature and density along the coexistence curve towards the critical point increases the low field mobility smoothly from about 0.08 at 148K to 54 at the critical point.

However, a small maximum is attained at 304K just below the critical point. In terms of density, this corresponds to a variation from 1.18×10^{22} molec/cm³ at 148K to 4.06×10^{21} molec/cm³ at the critical point. Data for these two figures were obtained using a liquid type high pressure conductance cell. In Figure III-20 measurements are shown for the gas phase near the critical point. Gas type high pressure conductance cells were used. The accessible field strength range has been

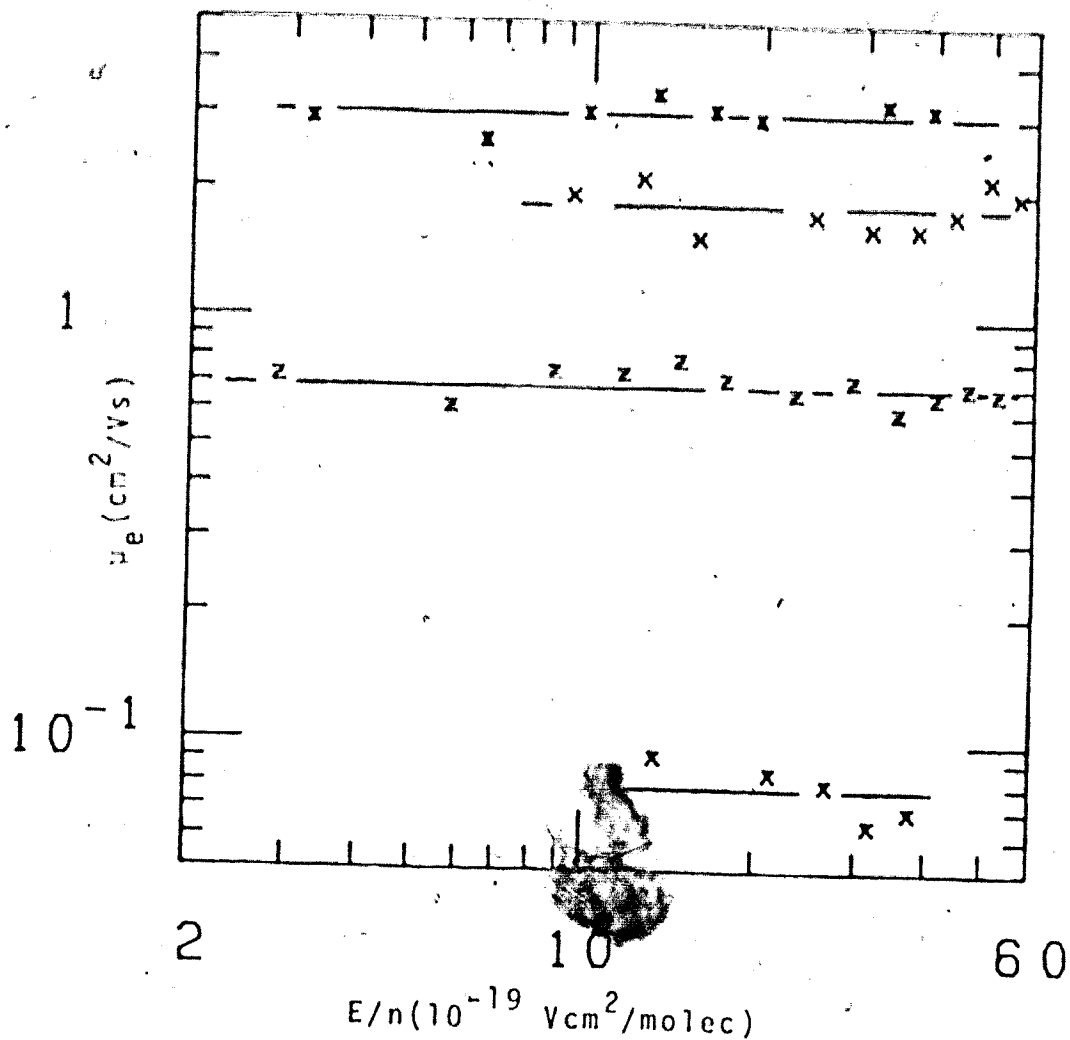


FIGURE III-18 Electron mobilities μ_e plotted as functions of E/n in liquid ethane. Densities are in molec/cm^3 . ($n/10^{21}$, T): **x** (11.8, 148K), **z** (10.9, 188K), **x** (10.1, 224K), **x** (9.56, 241K).

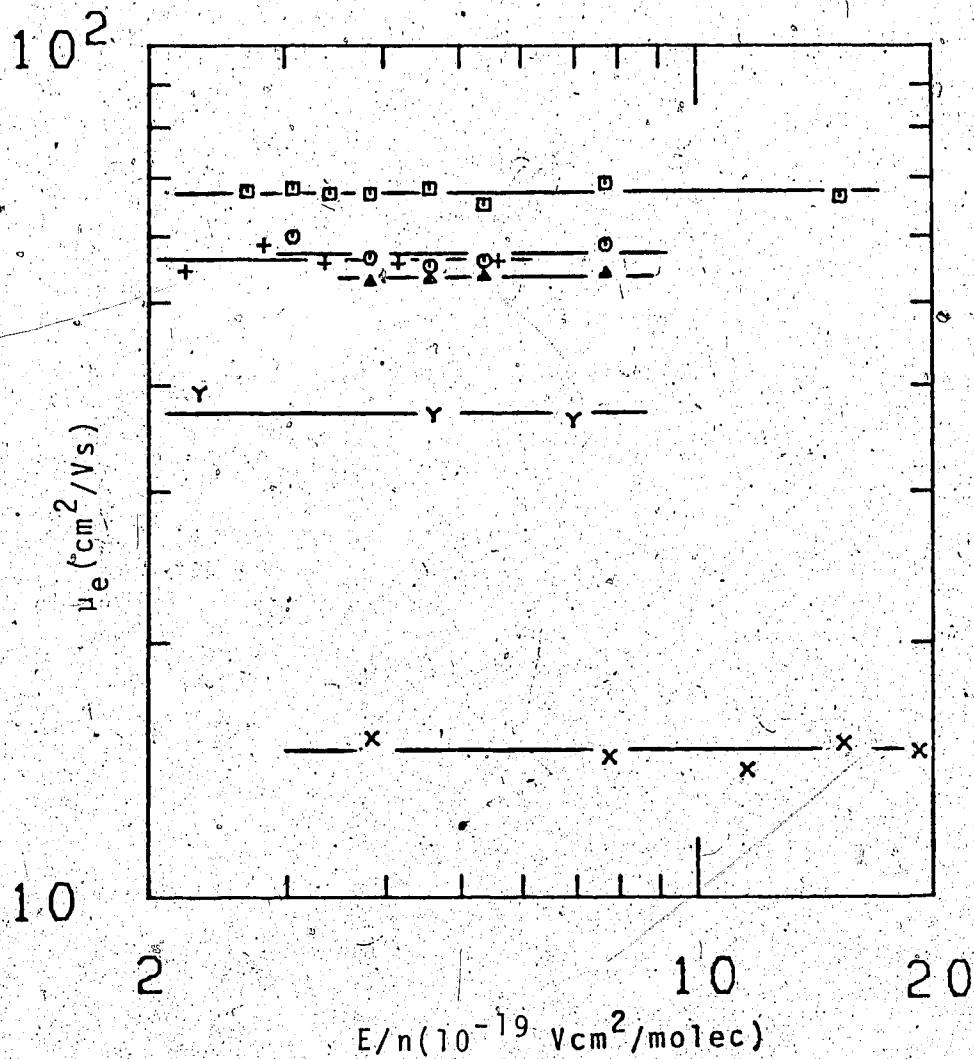


FIGURE III-19 Electron mobilities in liquid and supercritical ethane plotted against E/n .

Densities and temperatures ($n/10^{21}$, T):

X (8.04, 281K), Y (6.70, 298K), + (5.56, 304K), Δ (4.06, 306K), \circ (4.06, 307K), \square (4.06, 310K).

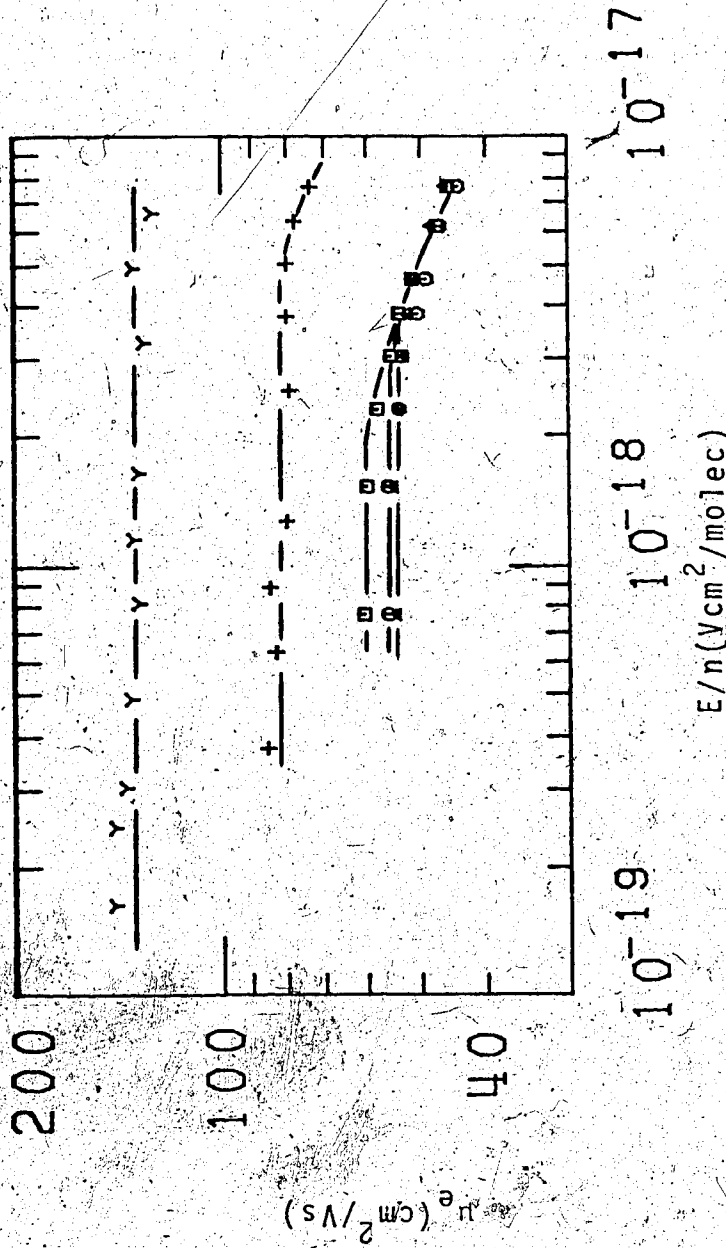


FIGURE III-20 Electron mobilities as functions of E/n in supercritical and gaseous ethane. Densities and temperatures ($n/10^{21}$, T):
 Y, (1.90, 296K), + (2.46, 302K), Δ (4.06, 306K), O (4.06, 307K), \square (4.06, 308K).

extended by an order of magnitude, and the negative mobility dependence on the field strength is seen to hold in the gas near the critical point, though the threshold field of $3.5 \times 10^{-18} \text{ V cm}^2/\text{molec}$ is considerably larger than that in the liquid at 294K (129).

Figure III-20 also shows the effect of temperature on a gas of the critical density. While the low field mobility increases, the threshold field decreases. At higher field strengths, the three mobility curves merge.

As the density decreases from that of the critical fluid, the mobility and the threshold field both increase. At $1.90 \times 10^{21} \text{ molec/cm}^3$ (296K), the threshold field could not be observed. This is in agreement to the data shown in Figure III-21. No clear field effect appears in the mobility curves for densities between 1.36×10^{21} to $2.02 \times 10^{21} \text{ molec/cm}^3$. The mobility increases as the density decreases. Increasing the temperature at $2.02 \times 10^{21} \text{ molec/cm}^3$ also leads to an increase in the mobility. When the density in the coexistence gas decreases down to $1.02 \times 10^{21} \text{ molec/cm}^3$, (Figure III-22), a field effect reappears. However, the mobility now increases at $E/n > (E/n)_{\text{threshold}}$ rather than decreasing as in the denser fluid. It is possible that the curve for $1.36 \times 10^{21} \text{ molec/cm}^3$ in Figure III-21 is already increasing slightly, though the increase is well within the scatter of the points. As the tempera-

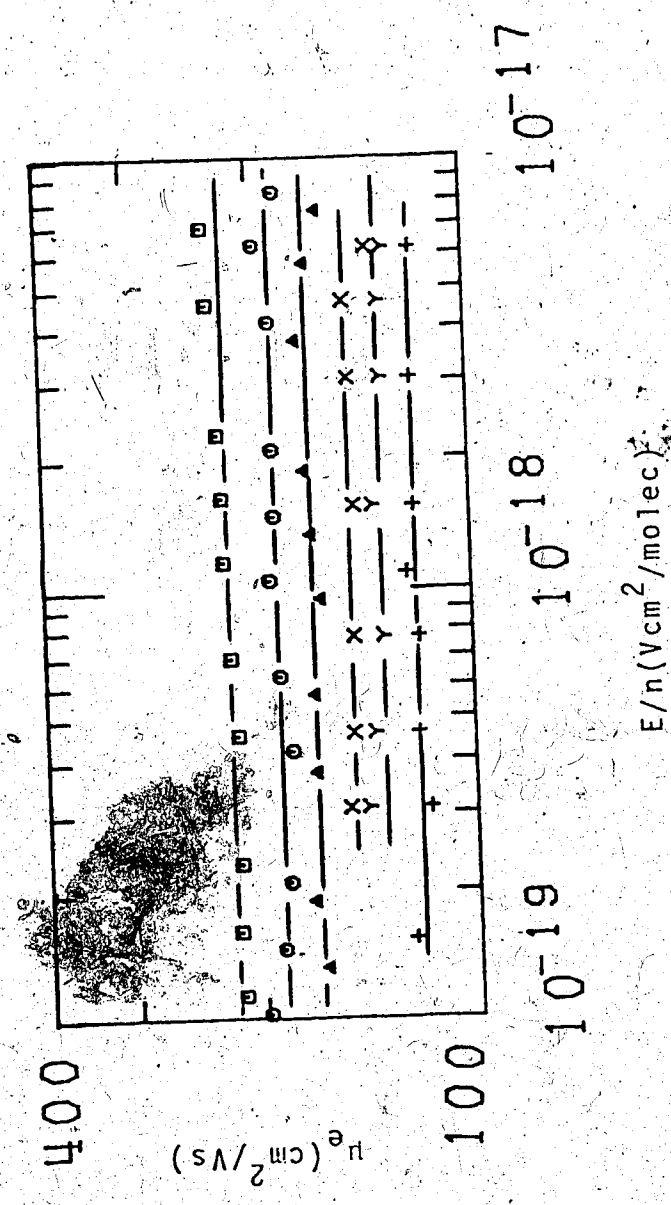


FIGURE III-21 Electron mobilities as functions of E/n in gaseous ethane. Densities and temperatures ($n/10^{21}$, T):
 □ (1.36, 286K), ○ (1.50, 289K), △ (1.62, 292K),
 + (2.02, 298K), × (2.02, 303K).

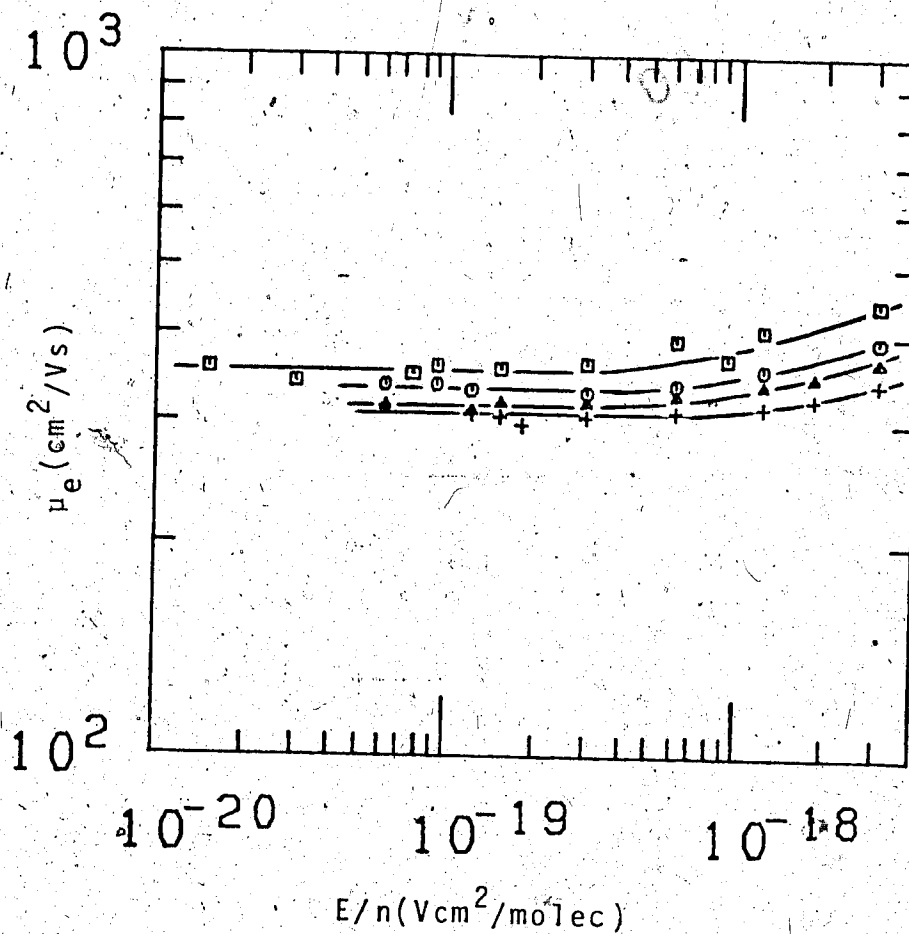


FIGURE III-22 Electron mobilities as functions of E/n in gaseous ethane $n = 1.02 \times 10^{21}$ molec/ cm^3 . Temperatures: \square (309K), \circ (297K); \triangle (283K), $+$ (276K).

ture increases at 1.02×10^{21} molec/cm³, the threshold field decreases, the low field mobility increases, and the increase of the mobility at the higher fields becomes more pronounced.

Figures III-23 and III-24 show the effect of further decreases in the density of the coexistence curve gas. The threshold field decreases slightly though the low field mobility is increasing roughly in inverse proportion to the density change. At densities lower than 5.31×10^{20} molec/cm³, the mobility curves begin to round off at the high field strengths. Figure III-25 shows the effect of temperature at 5.31×10^{20} molec/cm³. The low field mobility increases as the temperature increases. The threshold field also appears to increase slightly. The mobility curves merge at high fields.

When the density decreases down to 6.77×10^{19} molec/cm³, the complete mobility maximum can be seen (Figures III-26, III-27).

As the field strength increases from the low field region, the mobility stays constant up to $E/n \sim 2.5 \times 10^{-19}$ V cm²/molec. At higher fields, the mobility increases until a maximum is attained at $E/n \sim 4.5 \times 10^{-18}$ V cm²/molec. Further increases in field strength lead to a monotonic decrease in the mobility. The curve for $n = 6.21 \times 10^{21}$ molec/cm³ has the same

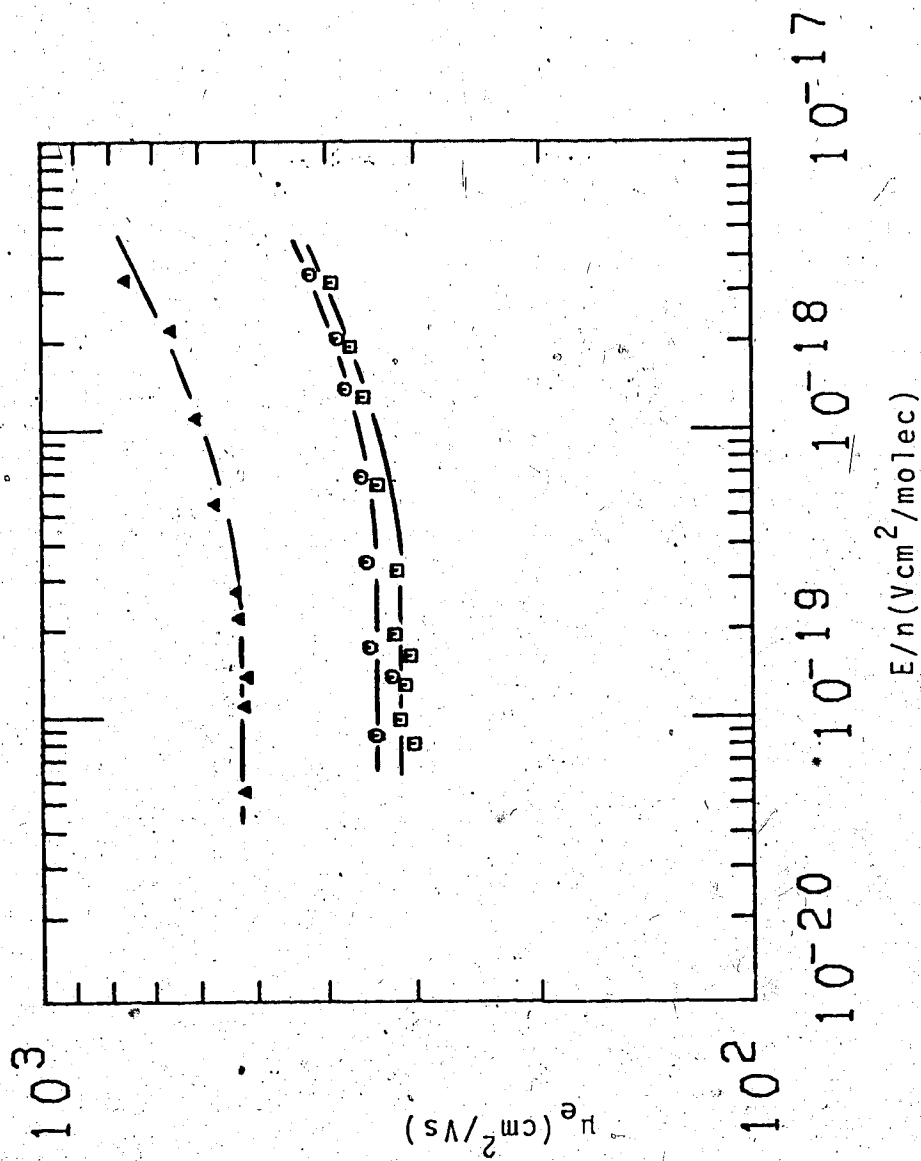


FIGURE III-23 Electron mobilities as functions of E/n in gaseous ethane. Densities and temperatures ($n/10^{20}$, T): \square (9.70, 274K), \circ (9.10, 272K), Δ (5.71, 256K).

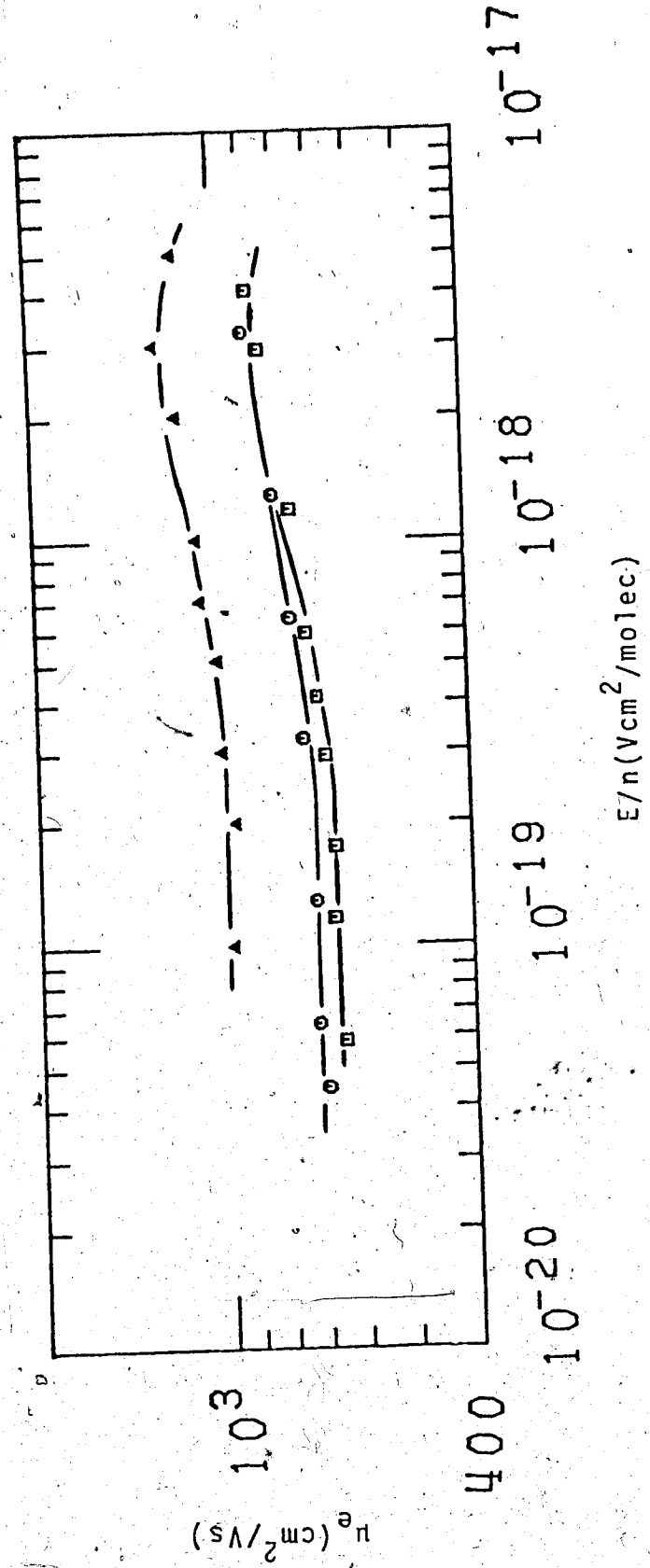


FIGURE III-24 Electron mobilities as functions of E/n in gaseous ethane. Densities and temperatures ($n/10^{20}$, T): \square (5.31, 254K), \circ (4.85, 251K), Δ (3.1, 236K).

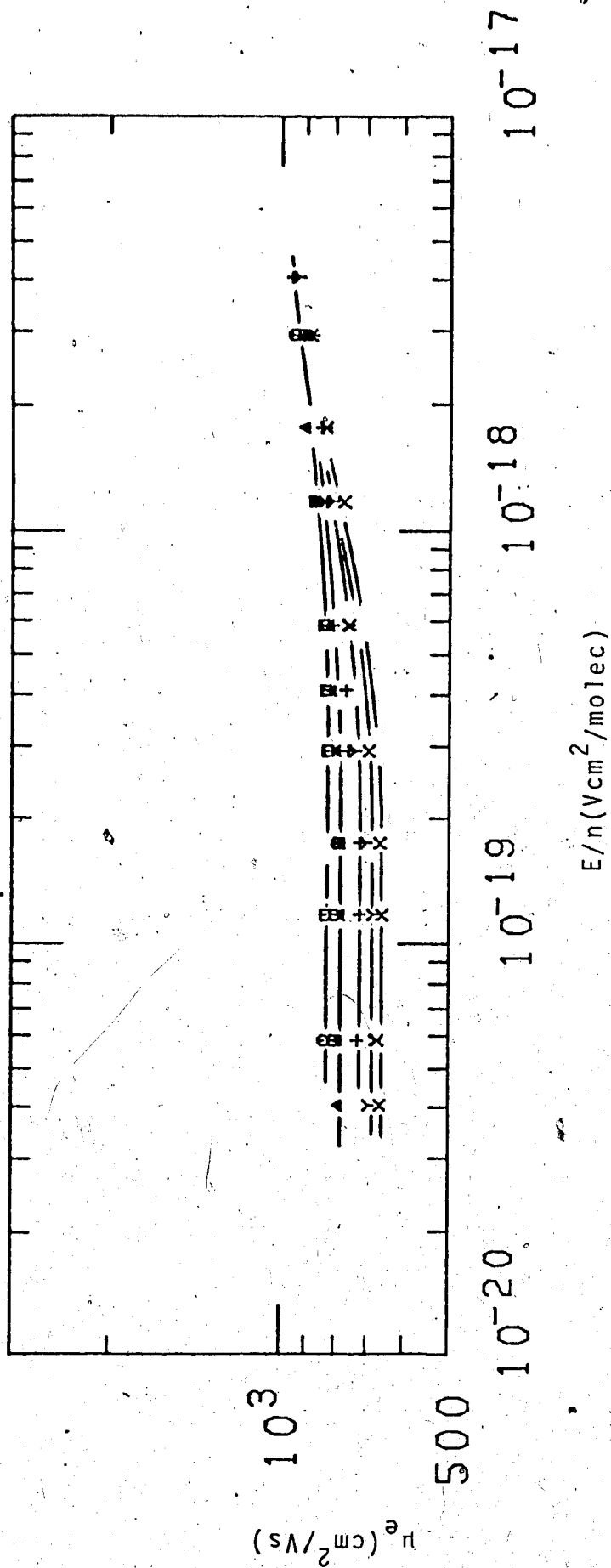


FIGURE III-25 Electron mobilities as functions of E/n in gaseous ethane
 $n = 5.31 \times 10^{20}$ molec/cm³. Temperatures (T): □ (325K), O (313K),
 Δ (296K), + (270K), Y (259K), X (255K).

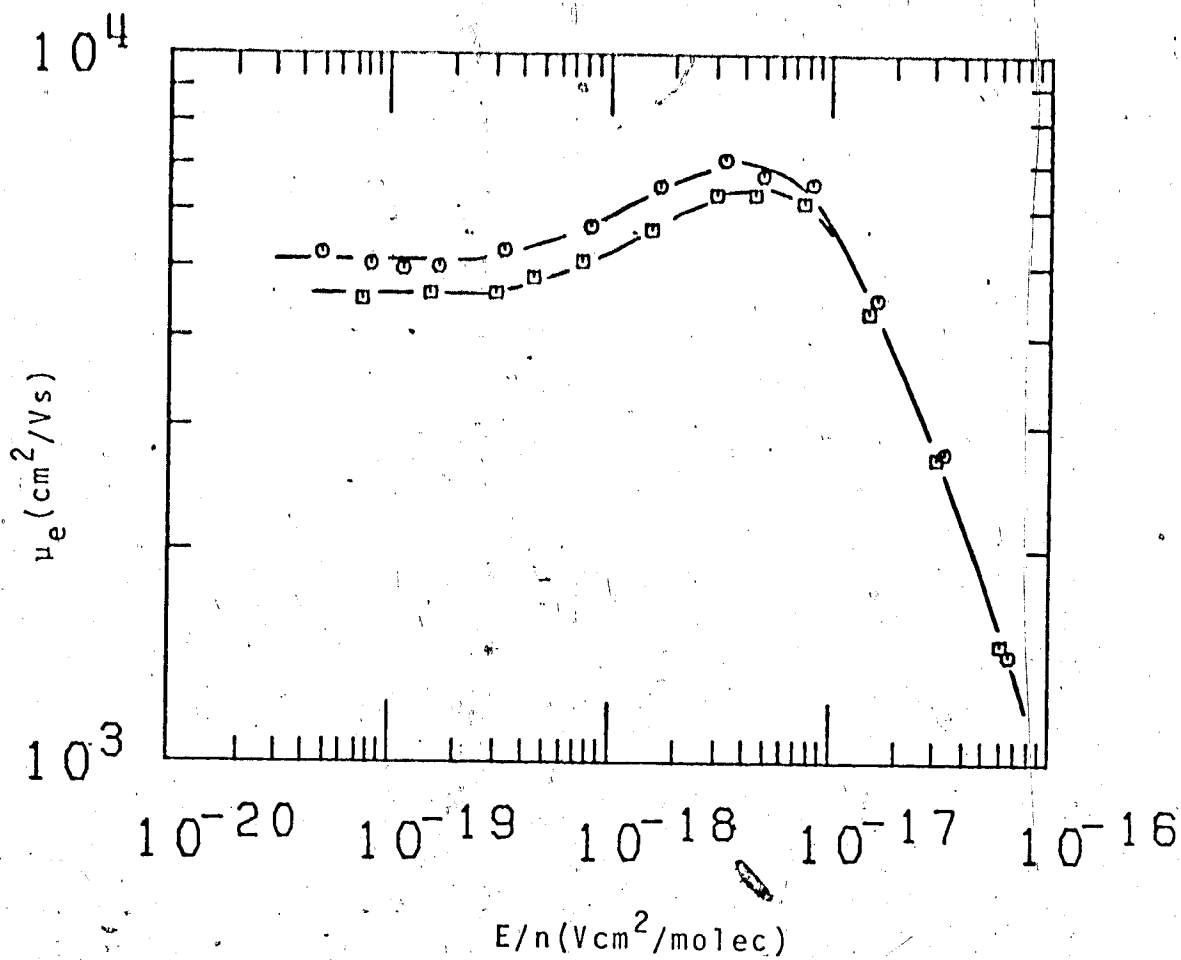


FIGURE III-26 Electron mobilities as functions of E/n in gaseous ethane. Densities and temperatures ($n/10^{19}$, T): \square (6.77, 197K), \circ (6.21, 193K).

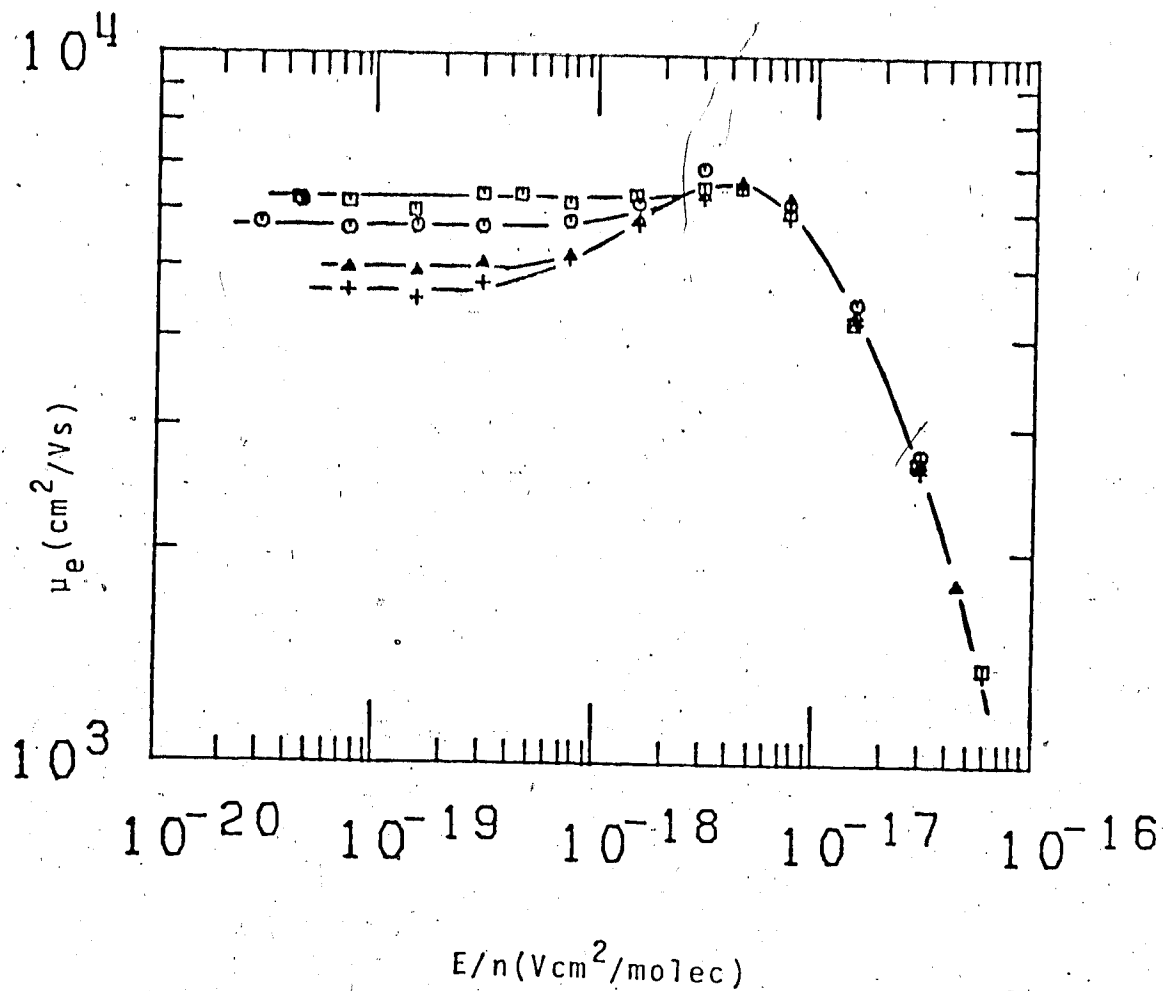


FIGURE III-27 Electron mobilities as functions of E/n in gaseous ethane $n = 6.77 \times 10^{19}$ molec/cm³.
 Temperatures (T): \square (326K), \circ (294K), $+$ (203K), \triangle (221K).

features as the curve for $n = 6.77 \times 10^{21}$ molec/cm³.

Heating the gas at $n = 6.77 \times 10^{21}$ molec/cm³ (Figure III-27) does not vary the mobility at the mobility maximum or at higher values of E/n . In the low field region, the mobility increases with the temperature. However, the threshold fields also increase. From the scatter of the points, the possibility exists that the mobility curves for the gases above the coexistence curves do not increase until they intersect the hump of the mobility curve of the coexistence gas of that density.

As previously mentioned, data for Figures III-20 to III-25 were obtained in high pressure gas type conductance cells. The data for Figures III-26 and III-27 were obtained using a low pressure gas type conductance cell. Data for the ethane figures are summarized in Table III-2. Data for 148K, 188K, 224K, and 241K in the liquid phase were obtained by the conductance method described in Chapter II. All other data were obtained by the time of flight measurement.

Electron mobility data for ethane are summarized in Table III-2.

TABLE III-2
Summary of Ethane Results^a

T °K	n $10^{21} \frac{\text{molec}}{\text{cm}^3}$	μ_0 $\frac{\text{cm}^2}{\text{Vs}}$	$\mu_0 n$ $10^{23} \frac{\text{molec}}{\text{Vs cm}}$	(E/n) threshold $10^{-19} \frac{\text{Vcm}^2}{\text{molec}}$	b $\frac{d \log \mu}{d \log E/n}$
148	11.8	0.0779	0.00752		
188	10.9	0.69	0.0919		
224	10.1	1.84	0.186		
241	9.56	3.03	0.290		
281	8.04	14.9	1.19		
298	6.70	37.1	2.49		
304	5.56	56.2	3.12		
306	4.06 ^c	53.6	2.18		
307	4.06 ^c	57.1	2.32		
310	4.06 ^c	67.6	2.74		
296	1.90	134	2.55		
302	2.46	81.6	2.01	45	
306	4.06 ^c	54.1	2.20	35	-0.26 ^d
307	4.06 ^c	55.6	2.26	29	-0.22 ^e
308	4.06 ^c	59.7	2.42	19	-0.22
286	1.36	221	3.01	-	-
289	1.50	188	2.82	-	-
292	1.62	168	2.72	-	-
298	2.02	120	2.44	-	-
303	2.02	134	2.71	-	-
308	2.02	148	2.99	-	-
309	1.02	354	3.61	3.7	0.12
297	1.02	335	3.42	4.5	0.10
283	1.02	317	3.23	4.5	0.098
276	1.02	307	3.13	5.0	0.095
274	0.970	312	3.03	3.8	0.13
272	0.910	337	3.06	3.8	0.14
256	0.571	522	2.98	2.6	0.13

(continued.....)

TABLE III-2 (continued)

254	0.531	659	3.50	2.2	0.14
251	0.485	707	3.43	2.2	0.11
236	0.310	991	3.07	2.7	0.14
325	0.531	822	4.36	3.5	0.070
313	0.531	822	4.36	3.5	0.070
296	0.531	778	4.13	2.7	0.092
270	0.531	722	3.83	2.4	0.11
259	0.531	687	3.65	2.2	0.14
255	0.531	661	3.51	2.2	0.15
197	0.0677	4600	3.11	2.6	0.16
193	0.0621	5100	3.17	2.4	0.16
326	0.0677	6300	4.27	15	plus
294	0.0677	5800	3.93	5.5	plus
221	0.0677	5000	3.38	4.1	0.20
203	0.0677	4700	3.18	2.4	0.20

a Results appear in the order of appearance in the preceding figures

b Estimated at $E/n \approx 4(E/n)_{\text{threshold}}$. Positive if the mobilities increase at the threshold; negative, if decreases

c $n_c = 4.06 \times 10^{21}$ molec/cm³, $T_c = 306K$.

d At $E/n \approx 2(E/n)_{\text{threshold}}$

e At $E/n \approx 3(E/n)_{\text{threshold}}$

3. Propane

Electron mobilities in propane plotted against the density normalized electric field strength E/n are given in Figures III-28 to III-34. Units for the mobilities are in cm^2/Vs , the densities molec/cm^3 , and the density normalized field strengths, $\text{Vcm}^2/\text{molec}$.

Figure III-28 shows the mobilities in liquid propane in the density range of 8.96×10^{21} to 6.00×10^{21} . No field dependence appears. A previous work (120) shows that the mobility should have a positive dependence on the field strength at $E > 1 \times 10^5 \text{ V/cm}$. This corresponds at 195K to $E/n > 1 \times 10^{-17}$. Variation of the mobility as the liquid is heated along the coexistence curve up to the supercritical fluid is given in Figure III-29. Decreasing the density increases the mobility. No clear field effect can be observed. The mobility increases with temperature in the supercritical fluid.

Mobilities in the supercritical fluid and in the coexistence gas at a density just below the critical density are shown in Figure III-30. High fields are seen to decrease the mobility in the supercritical fluid.

Increasing the temperature decreases the threshold field while the low field mobility decreases. At $n = 2.45 \times 10^{21}$, the field effect can no longer be seen. Figure III-31 indicates that the reason for the disappearance is that the field attained was just too low. Data for n between

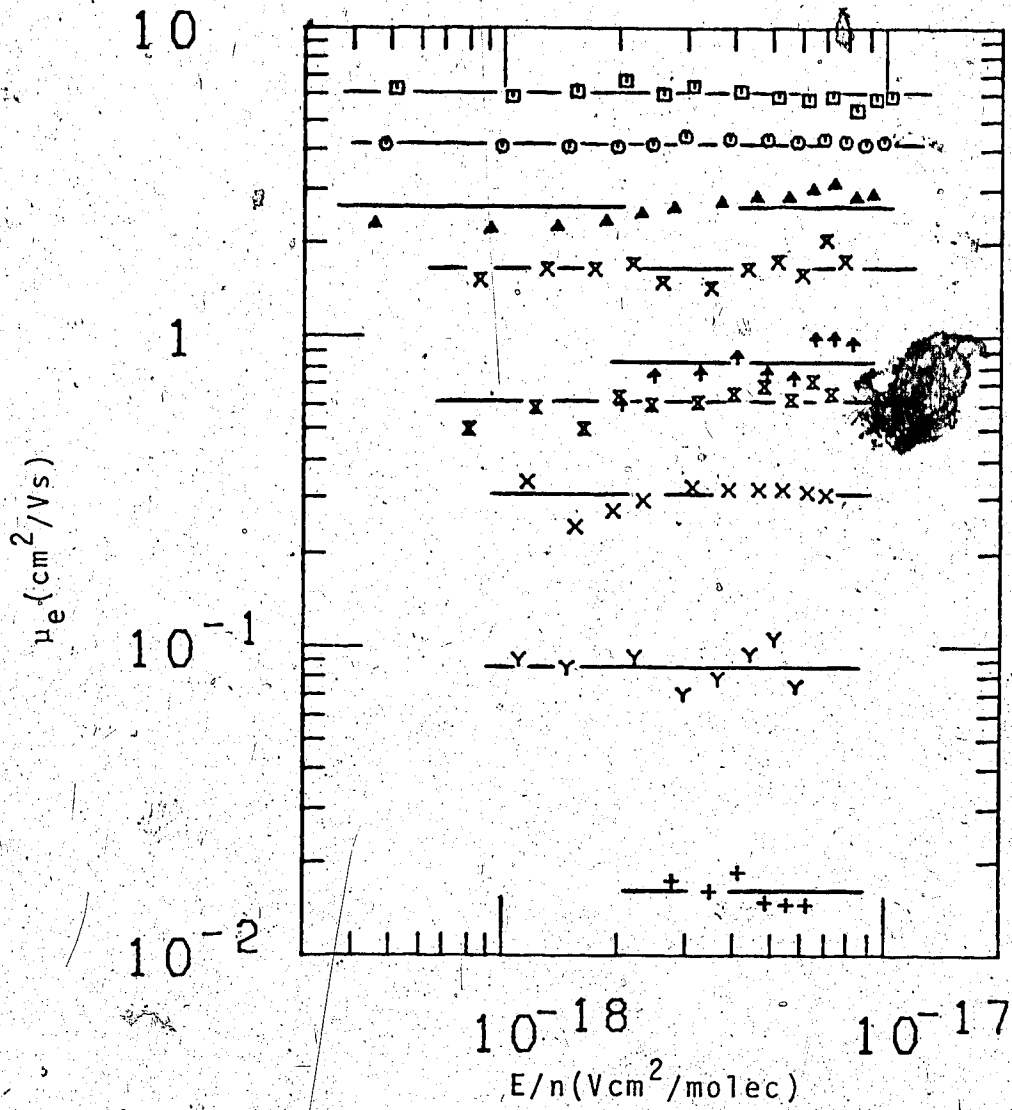


FIGURE III-28 Electron mobilities μ_e in liquid propane plotted against the density normalized electric field strength E/n . Densities and temperatures ($n/10^{21}$, T): \square (6.00, 328K), \circ (6.35, 315K), \triangle (6.76, 298K), \times (7.18, 276K), \blacktriangle (7.59, 252K), \blacktriangledown (7.73, 243K), \times (8.05, 224K), Y (8.48, 197K), $+$ (8.96, 169K).

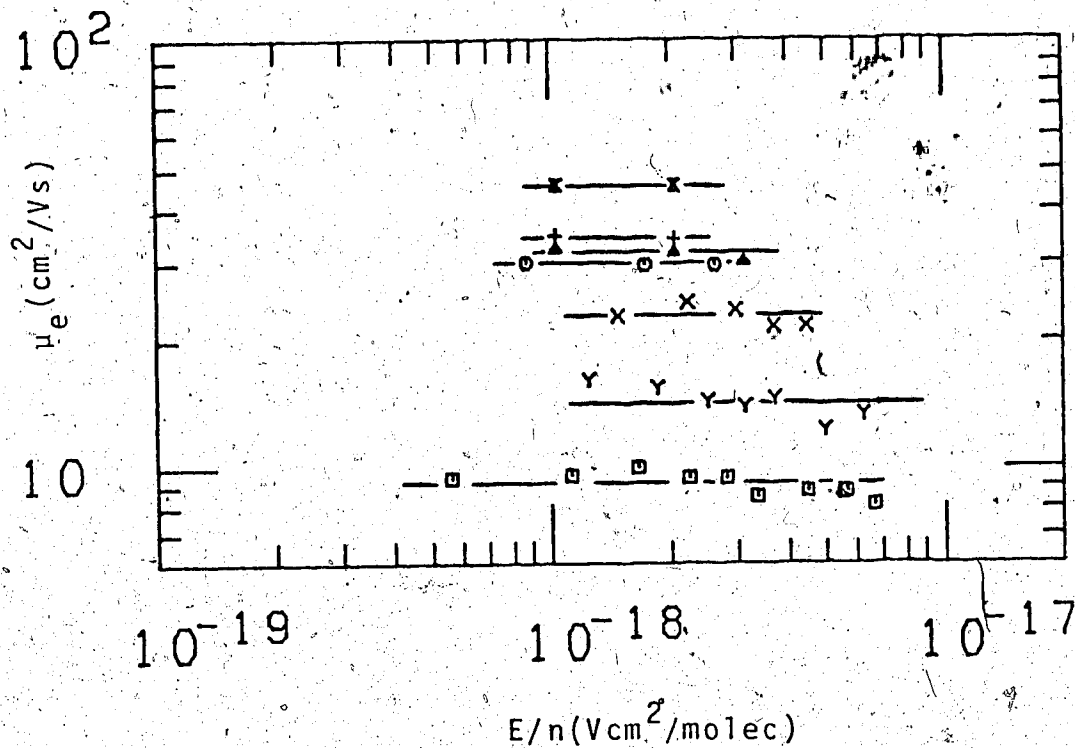


FIGURE III-29 Electron mobilities μ_e in liquid and supercritical propane plotted against the density normalized electric field strength E/n . Densities and temperature ($n/10^{21}$, T): \square (5.57, 340K), Y (4.99, 353K), X (4.17, 365K), O (3.54, 370K), Δ (3.00, 371K), + (3.00, 373K), * (3.00, 383K).

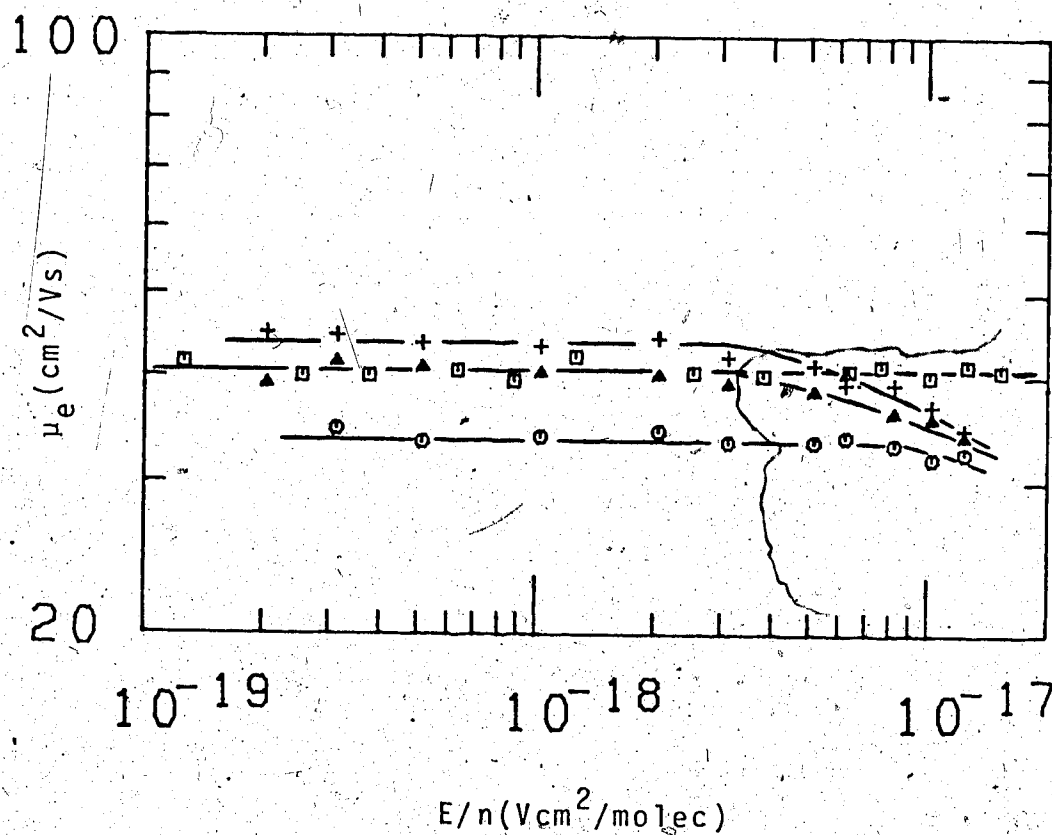


FIGURE III-30 Electron mobilities in gaseous propane as functions of E/n . Densities and temperatures ($n/10^{21}$, T): \square (2.45, 369K), \circ (3.00, 370K), Δ (3.00, 374K), $+$ (3.00, 377K).

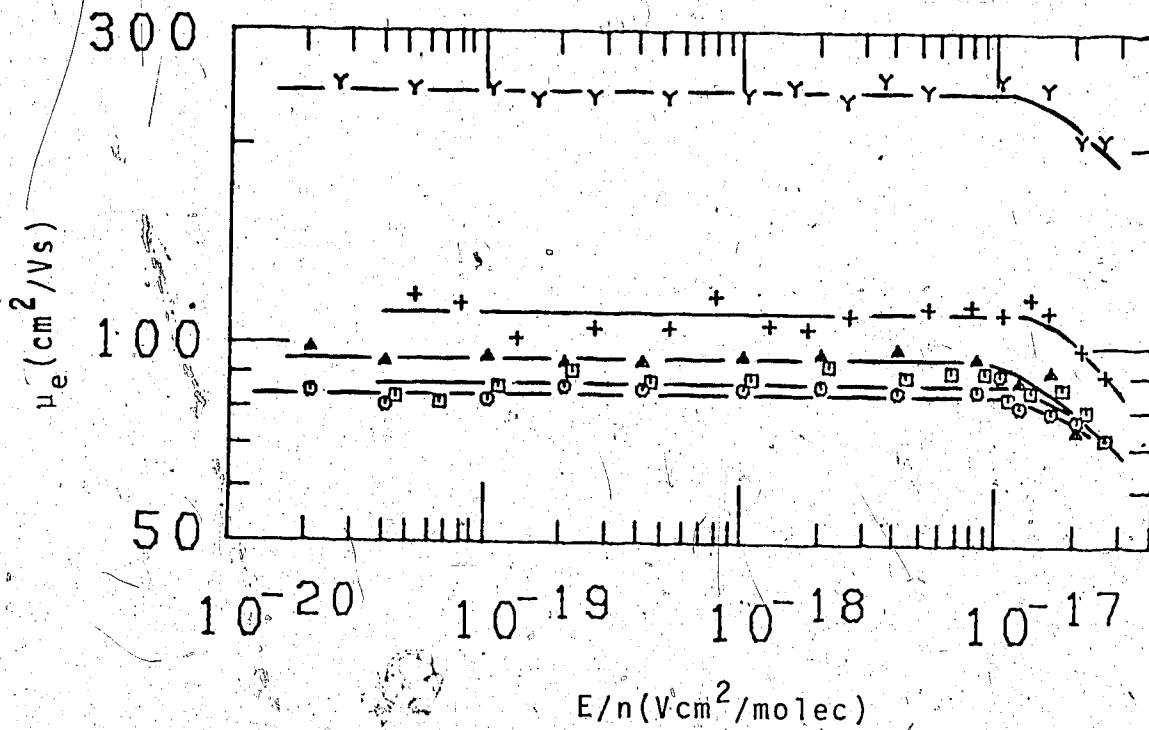


FIGURE III-31. Electron mobilities in gaseous propane as functions of E/n . Densities and temperatures ($n/10^{21}$, T): Y (0.593, 328K), + (1.16, 354K), □ (1.39, 360K), ○ (1.50, 372K), △ (1.50, 385K).

1.50×10^{21} and 5.93×10^{20} show that the threshold fields have shifted to $E/n > 10^{-17}$. The mobility varies inversely as the density. The two curves for $n = 1.50 \times 10^{21}$ show that the mobility at constant n is increasing with temperature. Both curves for $n = 1.5 \times 10^{21}$ are off the coexistence curve.

Figure III-32 shows that at $n = 7.50 \times 10^{20}$ the same trends exist. The increasing temperature also increases the low field mobility though the threshold field does not vary much. At $n = 4.50 \times 10^{20}$ though, the field effect cannot be seen against the scatter of the data.

Figure III-33 shows that the disappearance of the field effect at $n = 4.50 \times 10^{20}$ may represent a turning point. For $n = 3.41 \times 10^{20}$, the threshold field has decreased by an order of magnitude, and the sign of the field effect has inverted. Common features to the other figures include the inverse dependence of the mobility on the density, and the monotonic increase of the mobility with temperature at constant density. For $n = 3.41 \times 10^{20}$, the three mobility curves merge together at high fields.

Finally, Figure III-34 gives data for more dilute gases. The features are similar to those in Figure III-33. At $n = 6.69 \times 10^{19}$, heating the gas above the coexistence curve not only increases the mobility, but increases the threshold field. The mobility curves at the higher temperatures merge into those of the lower temperatures. The

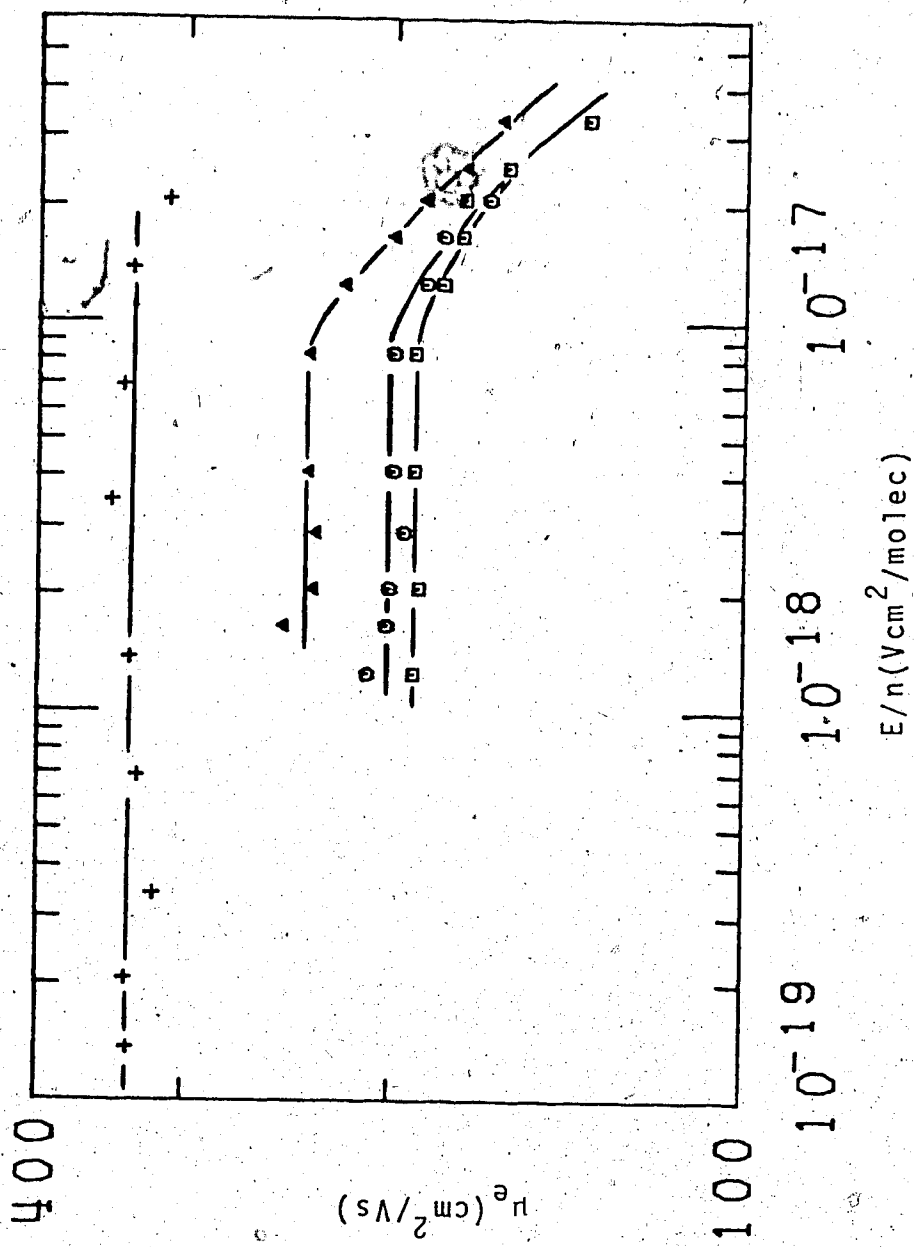


FIGURE III-32 Electron mobilities in gaseous propane as functions of E/n .
 Densities and temperatures ($n/10^{20}$, T): + (4.5, 317K), \square (7.50, 338K), \circ (7.50, 346K), Δ (7.50, 383K).

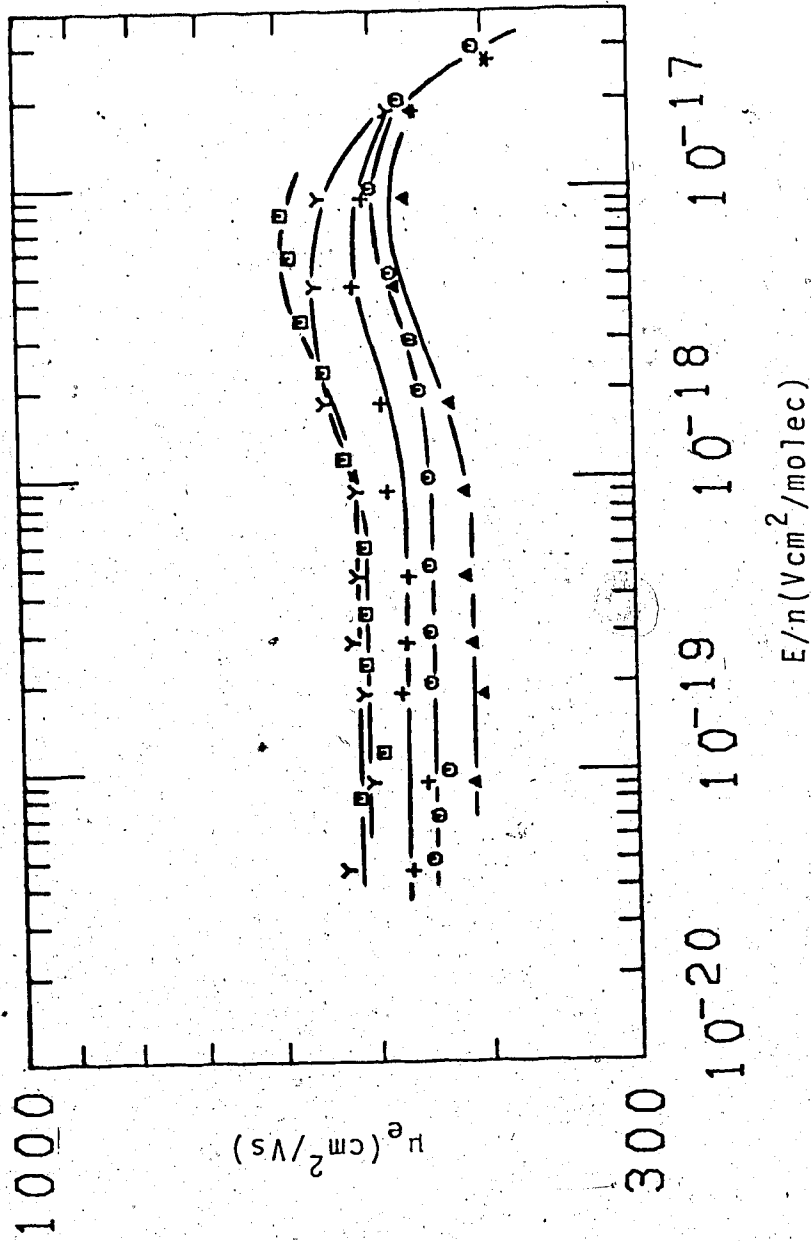


FIGURE III-33 Electron mobilities in gaseous propane as functions of E/n .
 Densities and temperatures ($n/10^{20}$, T): \square (2.69, 297K), \circ (3.11, 303K), Δ (3.41, 306K), $+$ (3.41, 358K), γ (3.41, 436K).

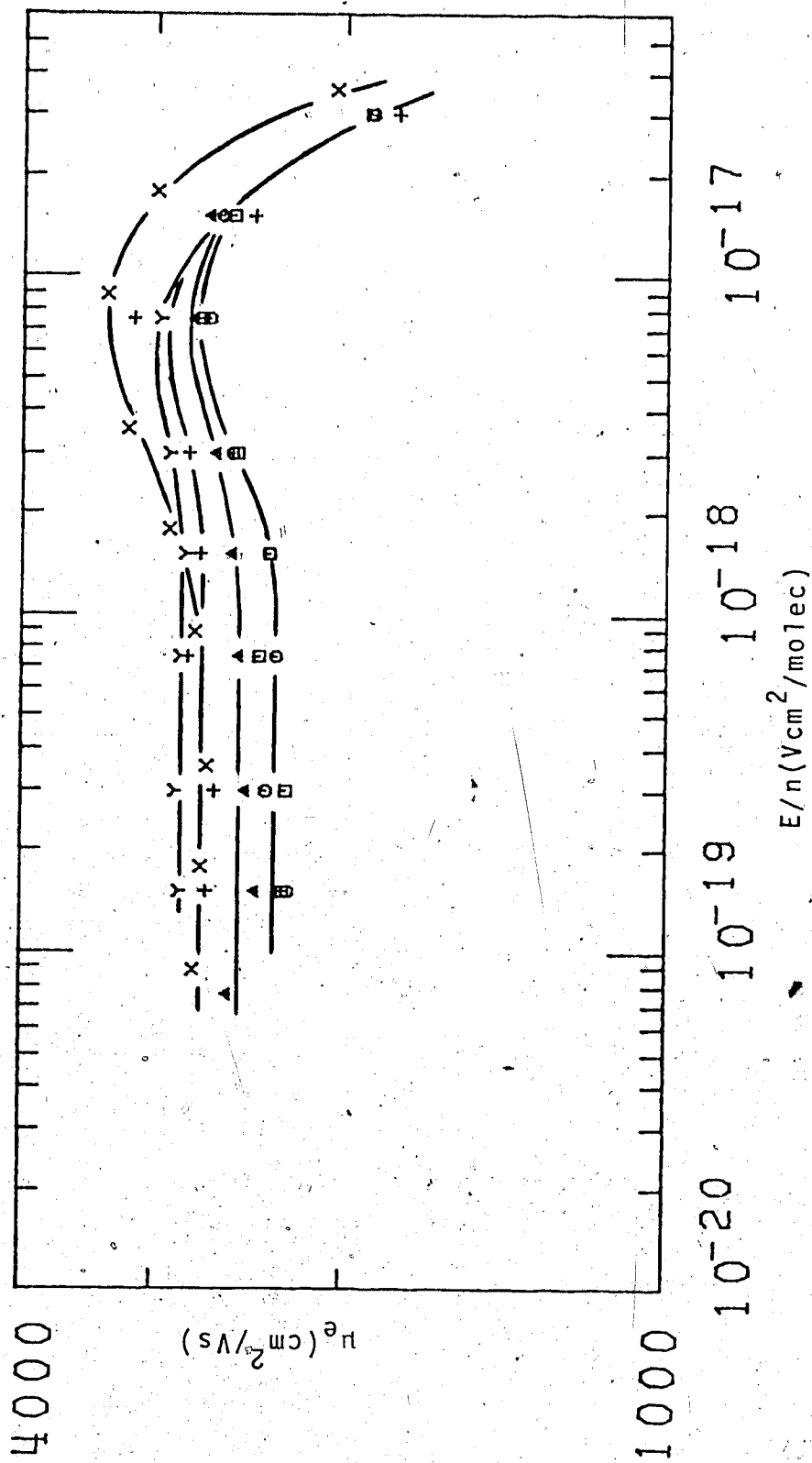


FIGURE III-34 Electron mobilities in gaseous propane as functions of E/n . Densities and temperatures ($n/10^{19}$, T): Y (6.69, 394K), + (6.69, 345K), Δ (6.69, 296K), O (6.69, 257K), \square (6.69, 253K), X (5.67, 245K).

mobility maximum at $E/n \approx 8 \times 10^{-18}$ agrees quite well with those of the higher densities (Figure III-33).

Measurements for Figure III-28 and III-29 were done in a liquid type high pressure conductance cell. All other measurements were done in gas type conductance cells. A low pressure cell was used for the data in Figure III-34. All other gas results were obtained in a high pressure cell. Data for propane are summarized in Table III-3. Data for the liquid phase at 276K and lower temperatures were obtained by the electron conductance method described in Chapter II. All other results were obtained by time of flight measurements.

TABLE III-3
Summary of Propane Results^a

T °K	n $10^{21} \frac{\text{molec}}{\text{cm}^3}$	μ_{O_2} $\frac{\text{cm}^2}{\text{Vs}}$	μ_{O_n} $10^{23} \frac{\text{molec}}{\text{Vscm}}$	(E/n) _{threshold} ^c $10^{-18} \frac{\text{Vcm}^2}{\text{molec}}$	b,c $\frac{d \log \mu}{d \log E/n}$
328	6.00	6.05	0.363		
315	6.35	4.21	0.267		
298	6.76	2.63	0.178		
276	7.18	1.65	0.118		
252	7.59	0.821	0.0623		
243	7.73	0.616	0.0476		
224	8.05	0.306	0.0246		
197	8.48	0.0861	0.00730		
169	8.96	0.016	0.00143		
340	5.57	9.16	0.510		
353	4.99	14.2	0.709		
365	4.17	22.6	0.942		
370	3.54	29.9	1.06		
371	3.00 ^d	31.5	0.945		
373	3.00 ^d	34.3	1.03		
383	3.00 ^d	45.5	1.36		
369	2.45	40.6	0.995		
370	3.00 ^d	33.9	1.02	8.0	minus
374	3.00 ^d	40.2	1.21	3.3	-0.21
377	3.00 ^d	43.7	1.31	2.7	-0.27
328	0.593	241	1.43	15	minus
354	1.16	111	1.29	12	minus
360	1.39	87.0	1.21	8.8	minus
372	1.50	84.6	1.27	10.6	minus
385	1.50	95.4	1.43	10.6	minus
317	0.450	335	1.51	-	-
338	0.750	192	1.44	8.4	-0.20
346	0.750	202	1.52	8.6	-0.26

(continued.....)

383	0.750	237	1.78	8.7	-0.34
297	0.269	508	1.37	0.62	0.19
303	0.311	446	1.39	0.97	0.25
306	0.341	412	1.40	0.88	0.38
358	0.341	472	1.61	0.88	0.20
436	0.341	518	1.77	0.89	0.20
394	0.0669	2830	1.89	1.7	0.065
345	0.0669	2740	1.81	1.5	0.073
296	0.0669	2490	1.67	1.0	0.083
257	0.0669	2320	1.55	1.1	0.093
253	0.0669	2320	1.55	1.1	0.093
245	0.0567	2720	1.54	0.77	0.13

^a Order of appearance of results in this table is the same as in the figures.

^b Estimated at $E/n = 4(E/n)_{\text{threshold}}$

^c Results were not obtained at high enough fields in the liquid phase to allow calculation of these quantities.

^d $n_c = 3.00 \times 10^{21}$ molec/cm³. $T_c = 370\text{K}$.

4. n-Butane

Electron mobilities in n-butane are plotted against the density normalized electric field strength E/n in Figures III-35 to III-45. The densities are in units of molec/cm³, the mobilities in units of cm²/Vs, and the normalized field strengths, in units of Vcm²/molec.

Data for the liquid phase appear in Figures III-35 to III-38. No field effect is observed. The mobility increases monotonically as the density decreases. Data for 356K and below were obtained by the electron conductance method described in Chapter II. All other liquid phase and all the gas phase results were obtained by the time of flight method. As the temperature increases in the supercritical fluid (Figure III-38), the mobility continues to increase.

More data in the supercritical fluid appear in Figure III-39. No field effect is observed for fields up to $E/n = 1 \times 10^{-17}$. As the density decreases from the critical density, the low field mobility increases. At $n = 9.74 \times 10^{21}$, 5.18×10^{21} and 3.42×10^{21} , sufficient field strength is attained to observe a decrease in mobility. The threshold field is $E/n \approx 1 \times 10^{17}$ for all three densities.

The temperature effect on the $n = 1.18 \times 10^{21}$ gas is shown in Figure III-40. The threshold field remains roughly constant. The low field mobility, however, increases with the temperature. The four mobility curves

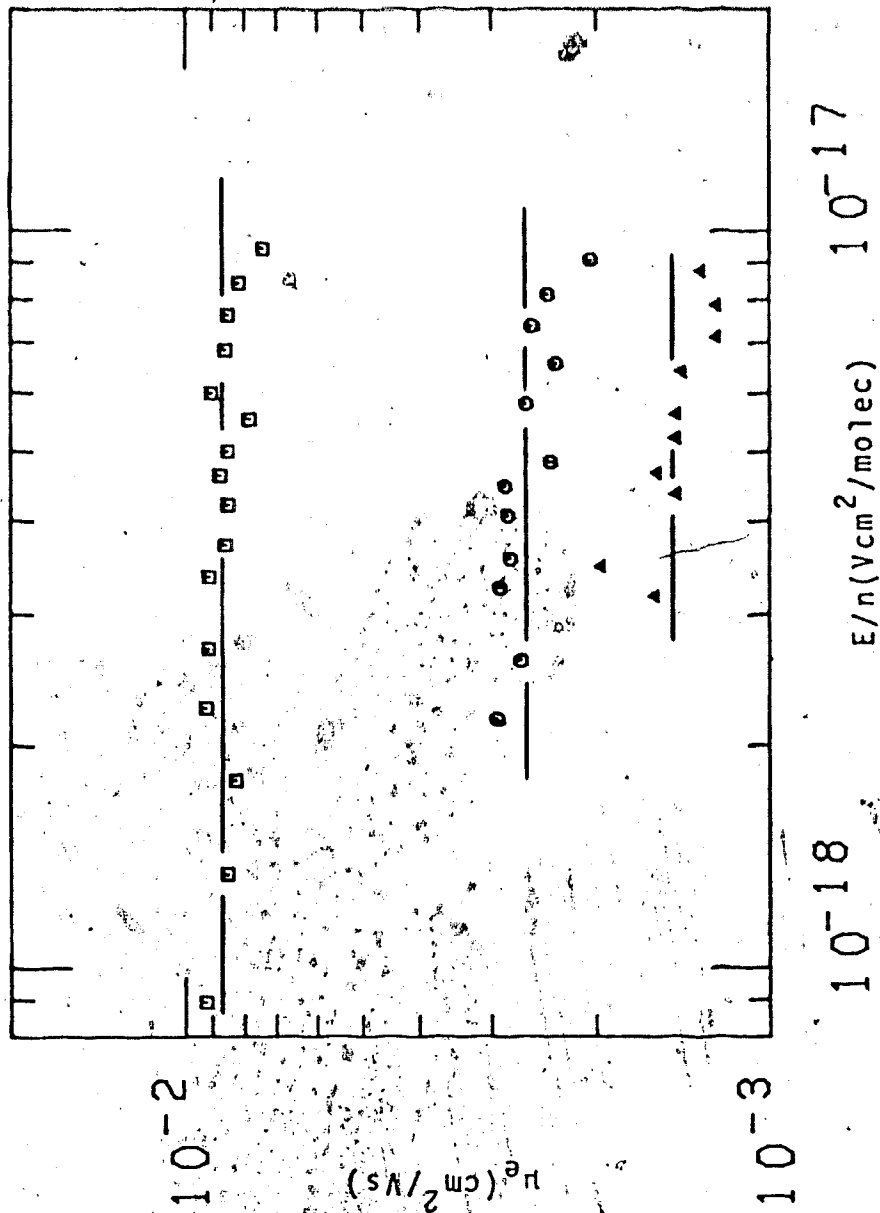


FIGURE III-35 Electron mobilities μ_e in liquid *n*-butane plotted against the density normalized electric field strength E/n . Densities and temperatures ($n/10^{21}$, T): \square (6.89, 203K), \circ (7.14, 177K), Δ (7.35, 154K).

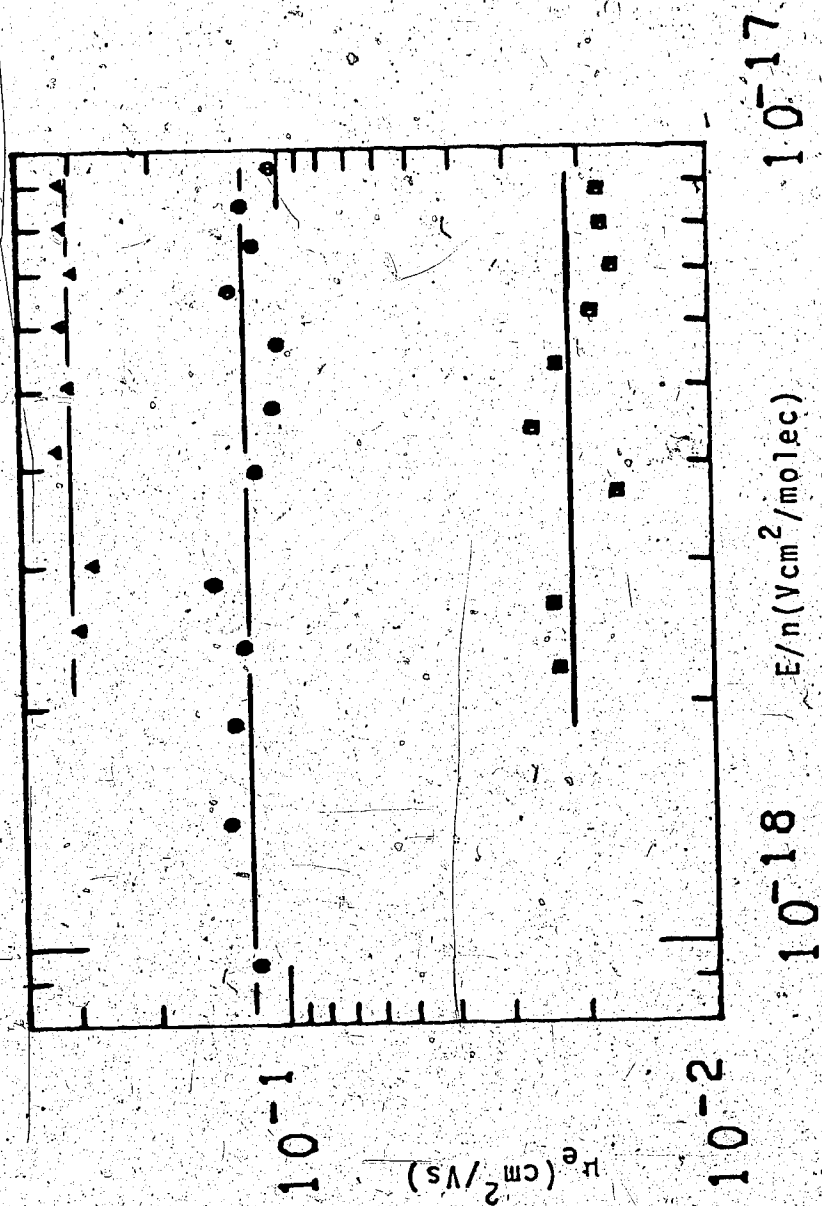


FIGURE III-36 Electron mobilities in liquid *n*-butane plotted against the density normalized electric field strength E/n . Densities and temperatures ($n/10^{21}$, T): Δ (5.98, 298K), \circ (6.28, 268K), \square (6.72, 222K).

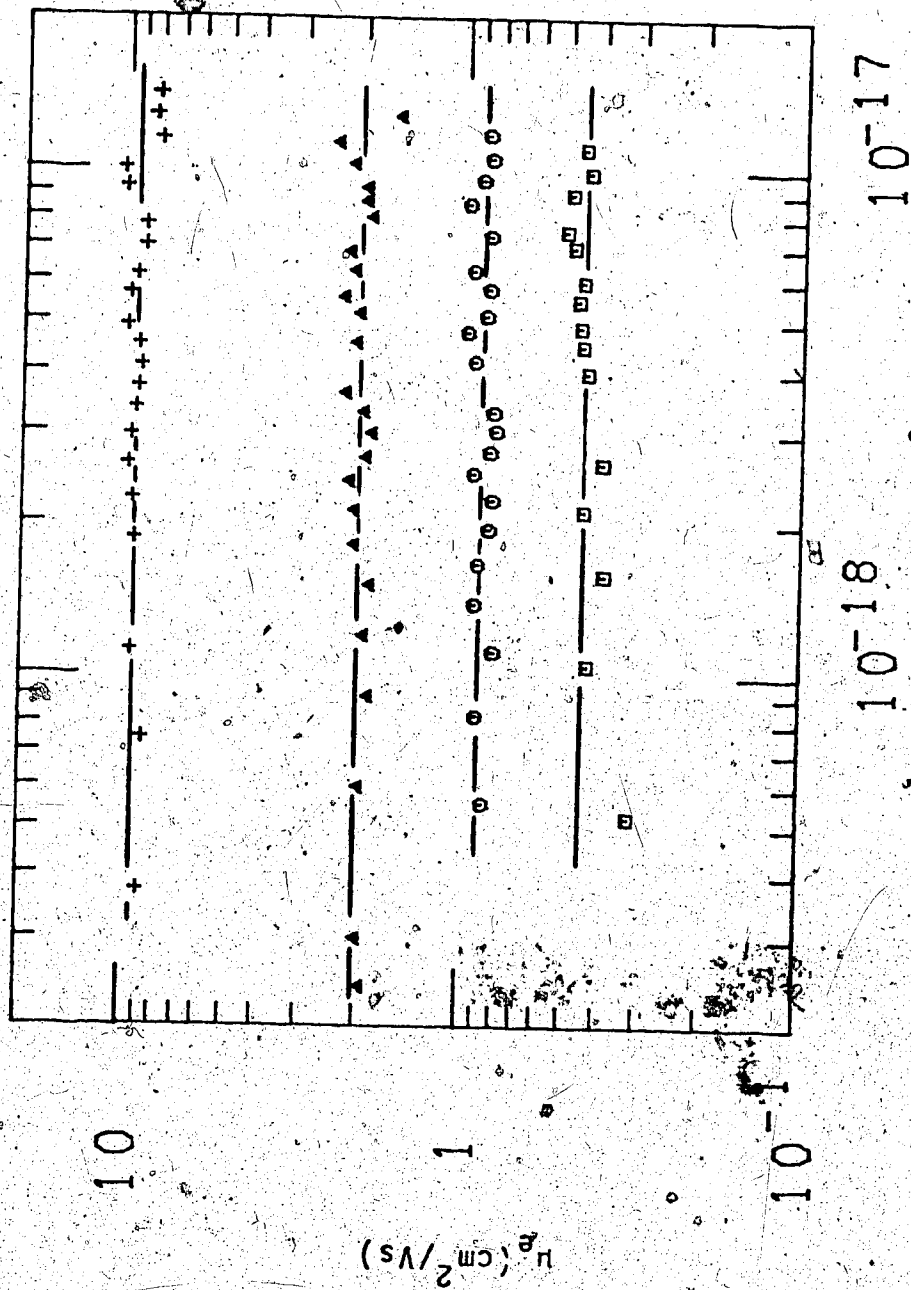


FIGURE III-37 Electron mobilities in liquid n-butane as functions of E/n .
 Densities and temperatures ($n/10^{21}$, T): \square (5.90, 305K), \circ (5.58, 330K), Δ (5.15, 356K), $+$ (4.17, 400K).

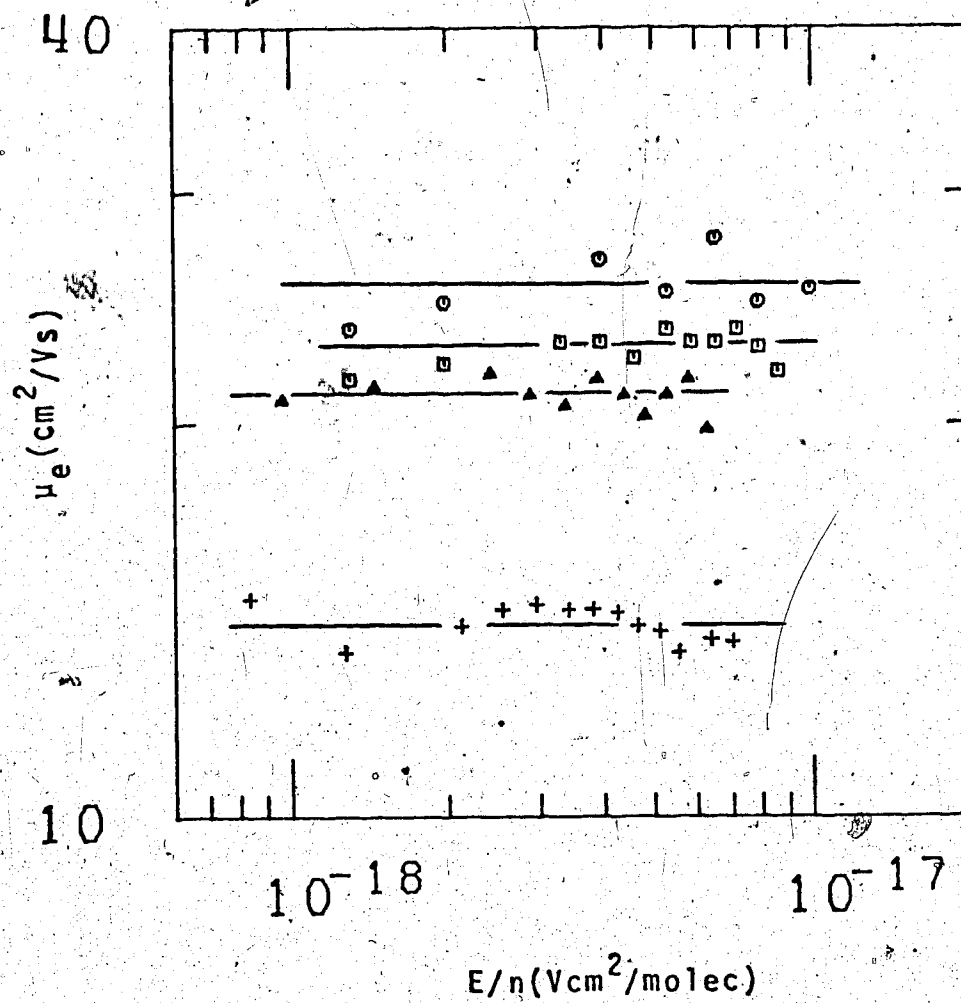


FIGURE I-38 Electron mobilities in liquid and supercritical n-butane as functions of E/n . Densities and temperatures ($n/10^{21}$, T): + (3.66, 414K), Δ (3.20, 421K), \square (2.36, 425K), \circ (2.36, 430K).

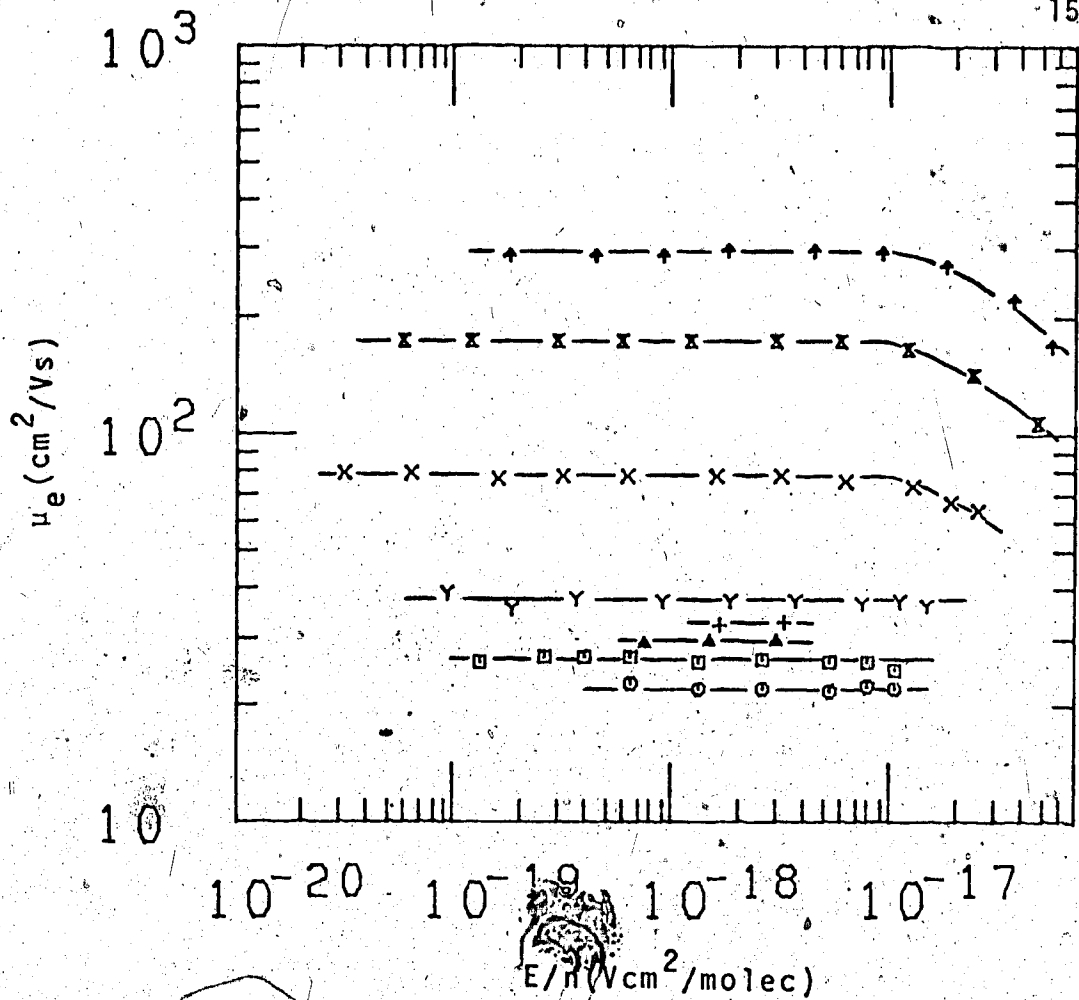


FIGURE III-39 Electron mobilities in gaseous and supercritical n-butane as functions of E/n. Densities and temperatures ($n/10^{21}$, T): \square (2.36, 430K), \circ (2.36, 425.5K), Δ (2.07, 424.8K), $+$ (1.87, 424.4K), γ (1.68, 424K), \bar{x} (0.974, 409K), \bar{x} (0.518, 384K), Φ (0.342, 365K).

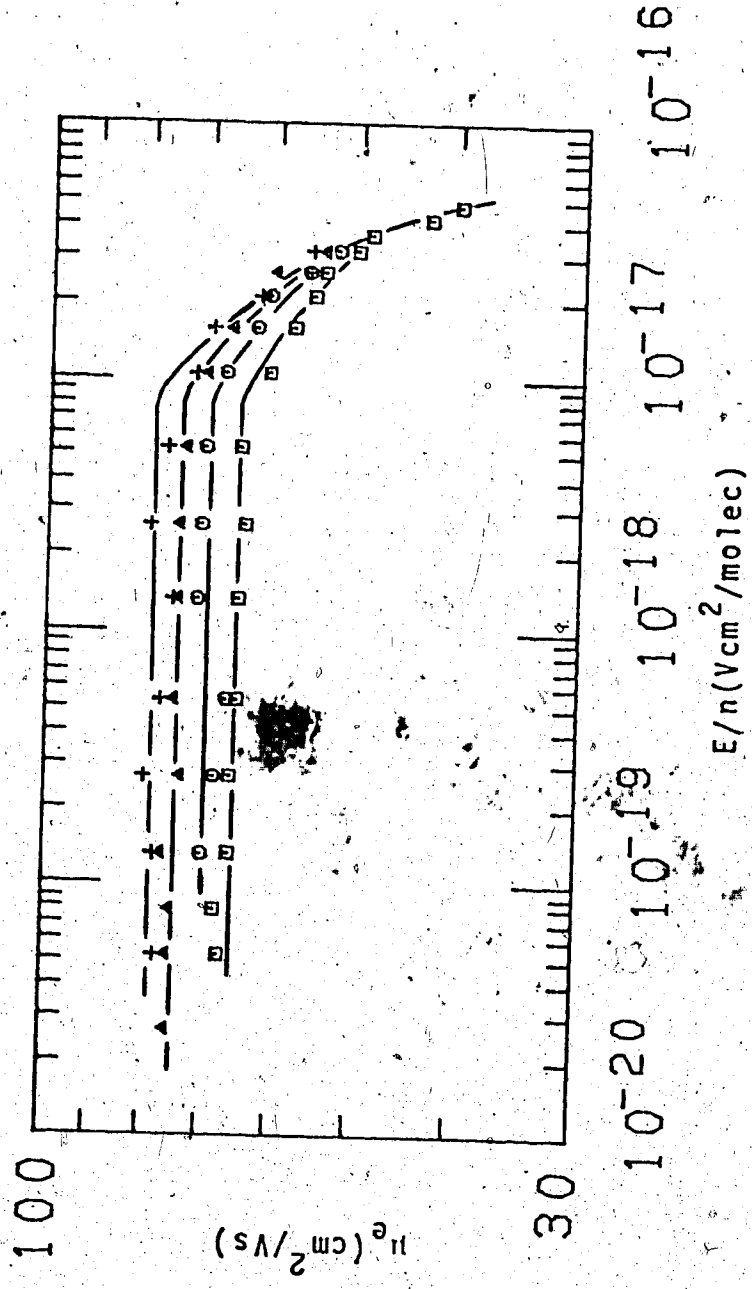


FIGURE III-40. Electron mobilities in gaseous n-butane as functions of $E/n, n = 1.18 \times 10^{21}$. Temperatures (Δ): \square (419K), \circ (428K), Δ (435K), + (440K).

merge together at high fields. Similar effects are observed for $n = 5.99 \times 10^{20}$ (Figure III-41). A difference is that there appears to be a slight decrease in the threshold field as the temperature increases. This decrease may be due to the scatter in the data.

Figure III-41 shows the result of further decrease in the density as well as the temperature effect for $n = 2.42 \times 10^{20}$. Variation of density from 2.42×10^{20} to 1.64×10^{20} does not vary the threshold field to any noticeable extent though the low field mobility is varying inversely with the density. The high fields bring the curves closer together. The temperature effect at $n = 2.42 \times 10^{20}$ is the same as those previously noted. The effect on the threshold field is observed. Varying the temperature from 430K to 450K only causes a slight increase of less than 1%. A single curve is drawn on Figure III-42 to include both temperatures.

Figures III-43 and III-44 give results in the dilute gases. No field effect can be clearly seen for $n = 6.09 \times 10^{19}$ or 6.84×10^{19} . For 7.56×10^{19} in Figure III-43, comparison with the temperature effects on $n = 7.56 \times 10^{19}$ leads to an estimate of threshold at $E/n \approx 10^{-17}$. Figure III-44 shows that variation of the temperature has little effect on the mobility. Single curves were drawn for 308K and 312K, 333K and 370K, and a separate curve drawn for 424K. The threshold field appears

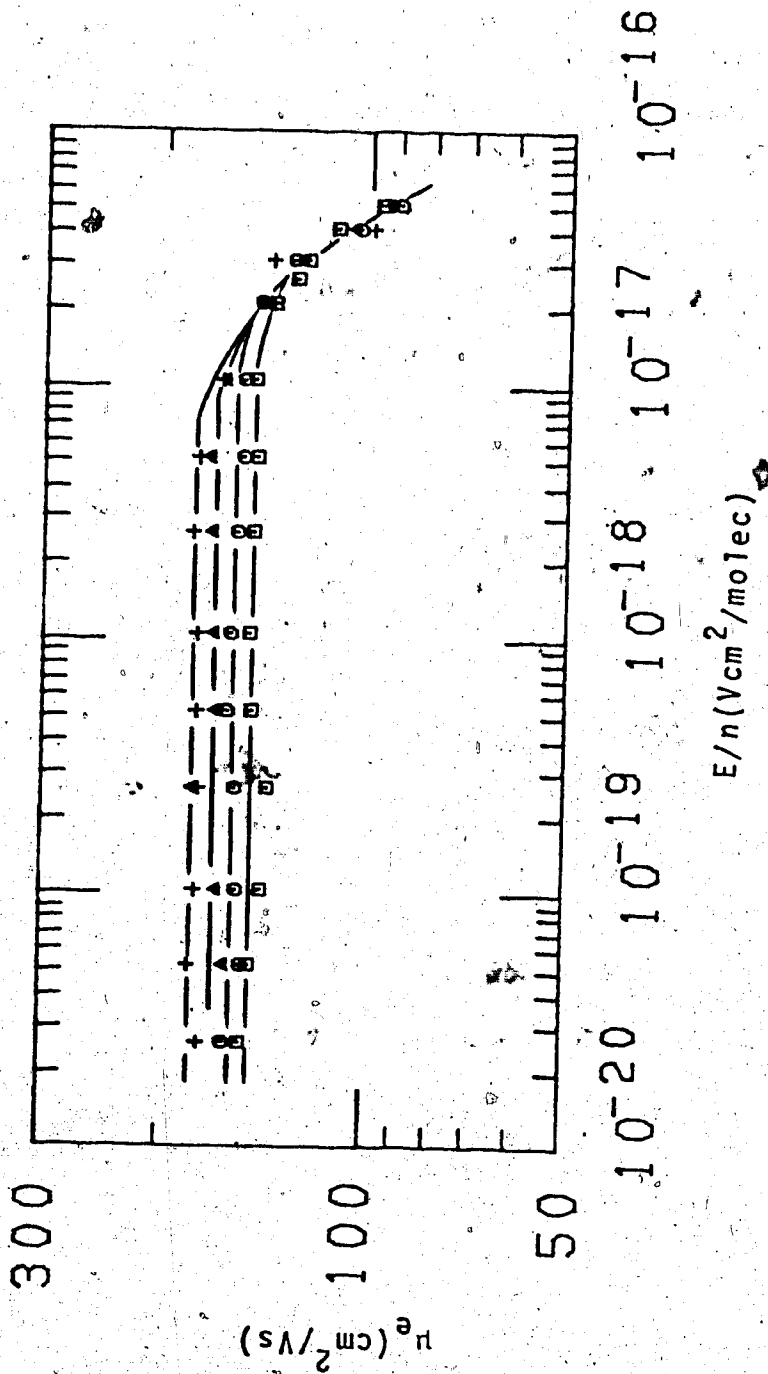


FIGURE III-41 Electron mobilities in gaseous n-butane as functions of E/n . $n = 5.99 \times 10^{20}$. Temperatures (T): \square (391K), \circ (407K), Δ (431K), $+$ (444K).

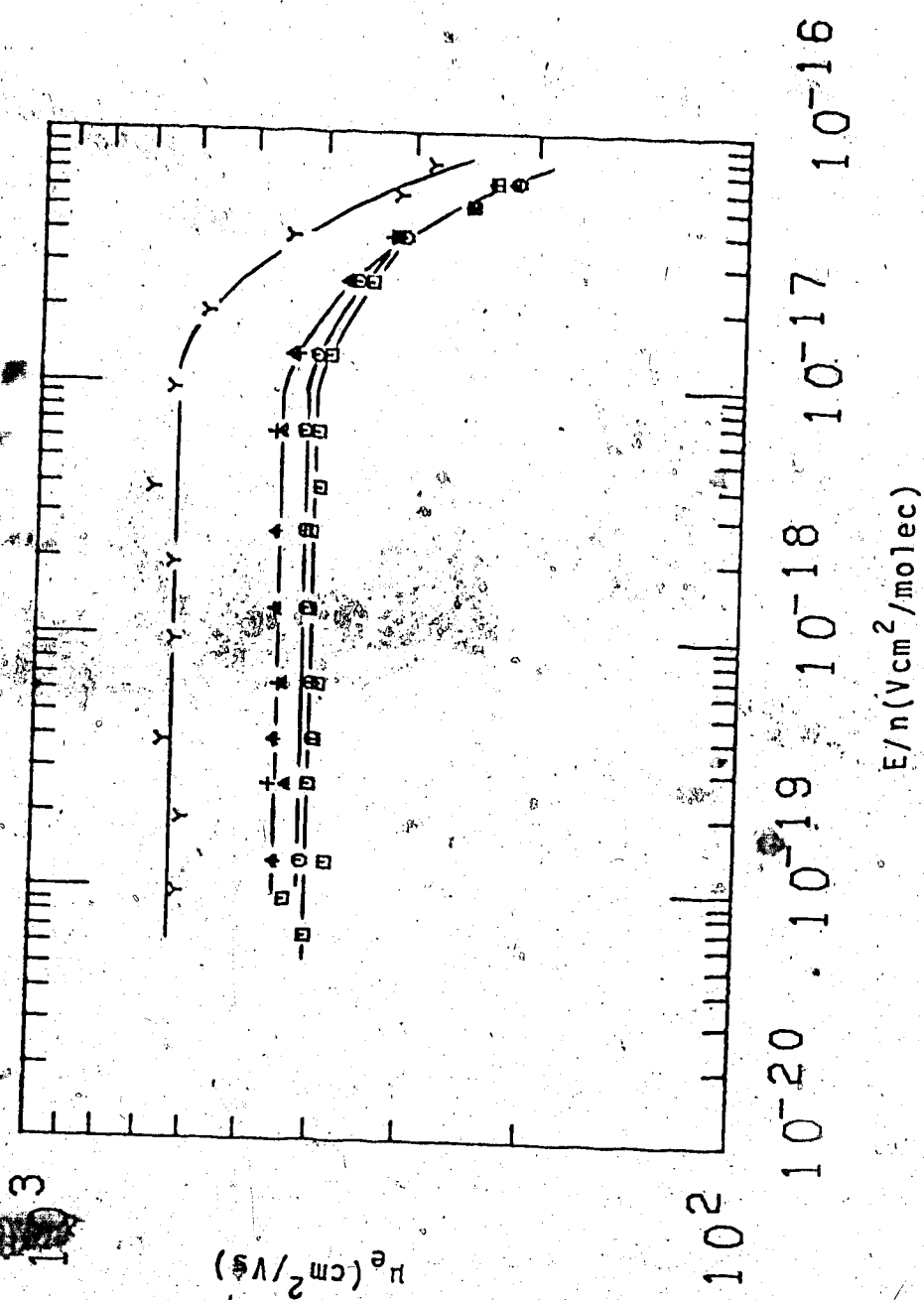


FIGURE III-42 Electron mobilities in gaseous *n*-butane as functions of E/n .
 Densities and temperatures ($n/10^{20}$, T): Y (1.64, 333K), □ (2.42, 355K), O (2.42, 367K), Δ (2.42, 430K), + (2.42, 458K).

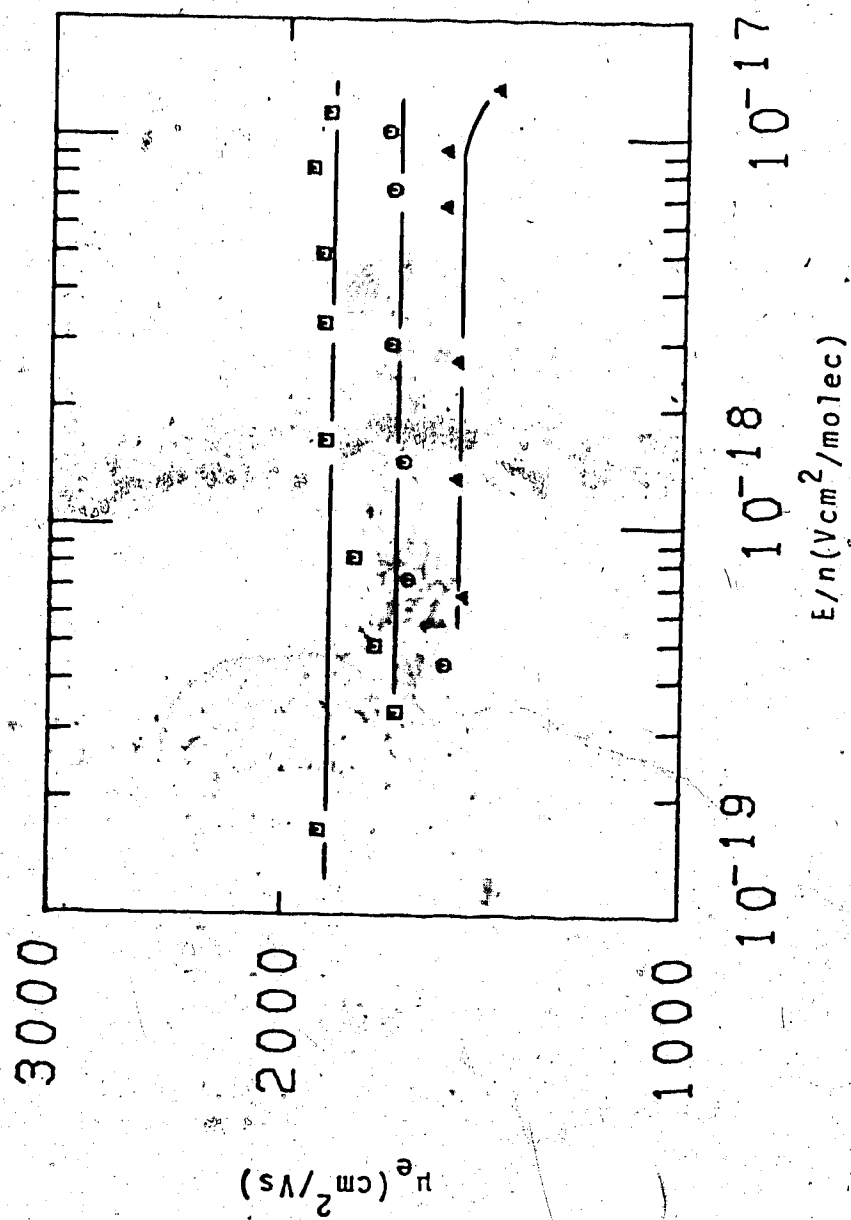


FIGURE III-43. Electron mobilities in gaseous *n*-butane as functions of

E/n . Densities and temperatures ($n/10^{19}$, T): □ (6.09, 296K),

○ (6.84, 300K), Δ (7.56, 304K).

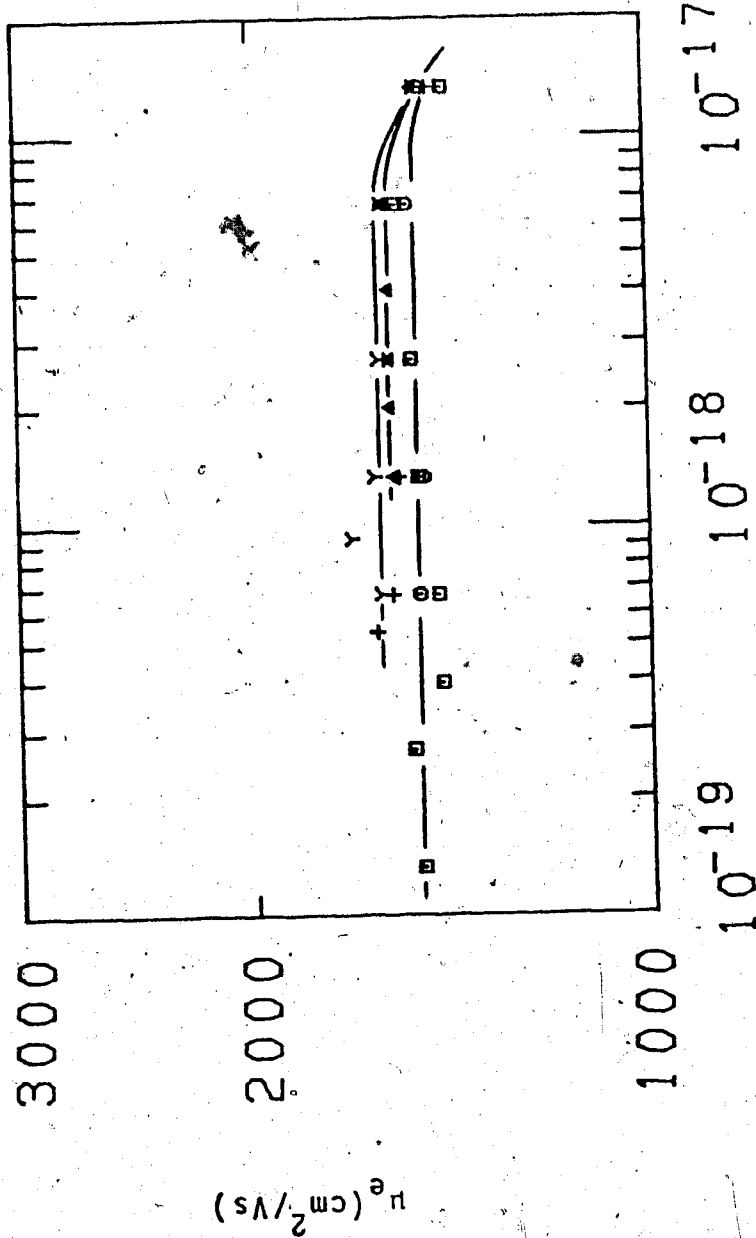


FIGURE III-44 Electron mobilities in gaseous n-butane as functions of E/n . $n = 7.56 \times 10^{19}$. Temperatures (T): □ (308K), ○ (312K), Δ (333K), + (370K), Y (424K).

to be about 9×10^{-18} .

A summary of the electron mobility data for n-butane appears in Table III-4. For $T > 298\text{K}$, a high pressure liquid type conductance cell was used. For $T \leq 298\text{K}$, a low pressure liquid type conductance cell was used. All gas phase results except data for Figures III-43 and III-44 were obtained in high pressure gas type conductance cells. Data of Figures III-43 and III-44 were obtained in low pressure gas type conductance cells.

TABLE III-4
 Summary of Results for n-Butane^a

T °K	n 10 ²¹ $\frac{\text{molec}}{\text{cm}^3}$	μ_0 $\frac{\text{cm}^2}{\text{Vs}}$	$\mu_0 n$ 10 ²² $\frac{\text{molec}}{\text{Vscm}}$	(E/n) _{threshold} 10 ⁻¹⁸ $\frac{\text{Vcm}^2}{\text{molec}}$	$d \log \mu^{b,c}$ d log E/n
203	6.89	0.00864	0.00595		
177	7.14	0.00262	0.00187		
154	7.35	0.00147	0.00108		
298	5.98	0.308	0.184		
268	6.28	0.121	0.0760		
222	6.72	0.0210	0.0141		
305	5.90	0.440	0.260		
330	5.58	0.880	0.491		
356	5.15	2.01	1.04		
400	4.17	9.24	3.85		
414	3.66	14.0	5.12		
421	3.20	21.0	6.72		
425	2.36 ^d	22.9	5.40		
430	2.36 ^d	25.5	6.02		
430	2.36 ^d	26.3	6.21		
425.5	2.36 ^d	22.0	5.19		
424.8	2.07	29.3	6.07		
424.4	1.87	32.4	6.06		
424	1.68	37.5	6.30		
409	0.974	77.7	7.57	10	minus
384	0.518	174	9.01	10	-0.48
365	0.342	295	10.1	10	-0.49
419	1.18	65.2	7.69	8.1	-0.20
428	1.18	69.6	8.21	8.5	-0.21
435	1.18	74.1	8.74	8.6	-0.24
440	1.18	77.7	9.17	8.4	-0.28
391	0.599	148	8.87	11	-0.27

(continued.....)

407	0.599	157	9.40	10	-0.30
431	0.599	167	10.0	8.8	-0.30
444	0.599	181	10.8	7.5	-0.30
333	0.164	632	10.4	10	-0.50
355	0.242	407	9.85	10	-0.24
367	0.242	417	10.1	10	-0.25
430	0.242	454	11.0	9.9	-0.38
458	0.242	458	11.1	9.9	-0.39
296	0.0609	1850	11.2	~10	minus
300	0.0684	1650	11.3	-	
304	0.0756	1480	11.2	~10	minus
308	0.0756	1500	11.3	~10	minus
312	0.0756	1500	11.3	~9	minus
333	0.0756	1570	11.9	~9	minus
370	0.0756	1580	11.9	~9	minus
424	0.0756	1600	12.1	~9	minus

^a Order of appearance as in figures.

^b Estimated at $4(E/n)_{\text{threshold}}$. Negative values indicates that the mobility decreases at $E/n > (E/n)_{\text{threshold}}$.

^c Field strengths attained were too low to allow observation of these effects in liquid phase n-butane.

^d $n_c = 2.36 \times 10^{21}$. $T_c = 425\text{K}$.

5. Isobutane (2-methylpropane)

Electron mobilities as functions of the density-normalized electric field strength E/n are shown in Figures III-45 to III-53. Densities are in units of molec/cm³, mobilities in units of cm²/Vs, and the normalized field strengths in units of Vcm²/molec.

Data obtained in the liquid phase are shown in Figures III-45, III-46 and III-47. Between the density range of 7.69×10^{21} to 6.07×10^{21} , the mobility increases as the density decreases (Figure III-46). As the density decreases towards the critical point, a mobility maximum is reached (Figure III-47) at $n = 2.92 \times 10^{21}$, followed by a decrease in mobility (Figure III-48) as the liquid approaches the critical point. In the critical fluid, the mobility increases as the temperature increases (Figure III-48 and III-49). No field effect is observed either for the liquid or for the critical fluid at E/n up to about $E/n = 1 \times 10^{-17}$ for the liquid, and up to $E/n \sim 2 \times 10^{-17}$ for the supercritical gas.

Figures III-48 and III-49 show the mobility in the vicinity of the critical point as well as the temperature effect on the $n = 2.30 \times 10^{21}$ and the $n = 1.15 \times 10^{21}$ isochores. The mobility increases as the density of the gas decreases along the coexistence curve. As the temperature is raised along an isochore, the mobility increases as well. A field effect cannot be distinctly

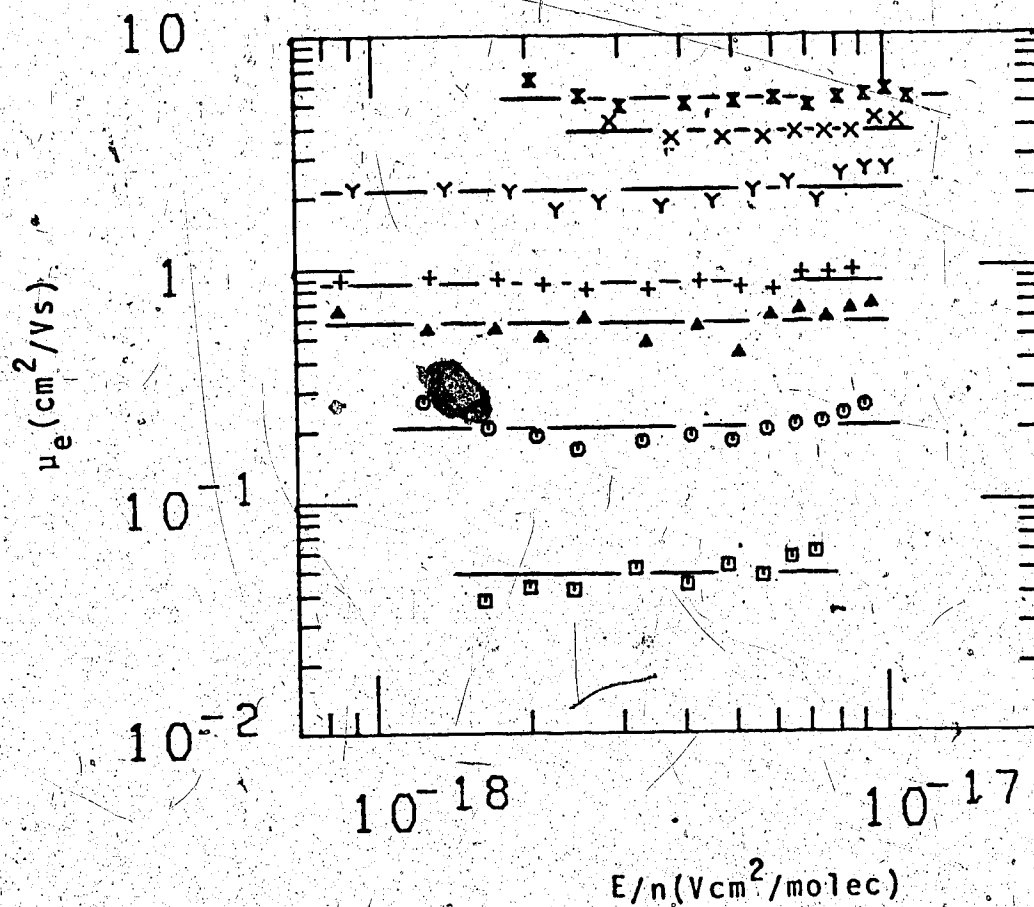


FIGURE III-45. Electron mobilities μ_e plotted against the density normalized electric field strength E/n in liquid isobutane. Densities and temperatures ($n/10^{21}$, T): \square (7.69, 140K), \circ (7.49, 155K), \triangle (7.26, 173K), $+$ (7.17, 181K), Y (6.73, 214K), X (6.42, 239K), \otimes (6.07, 270K).

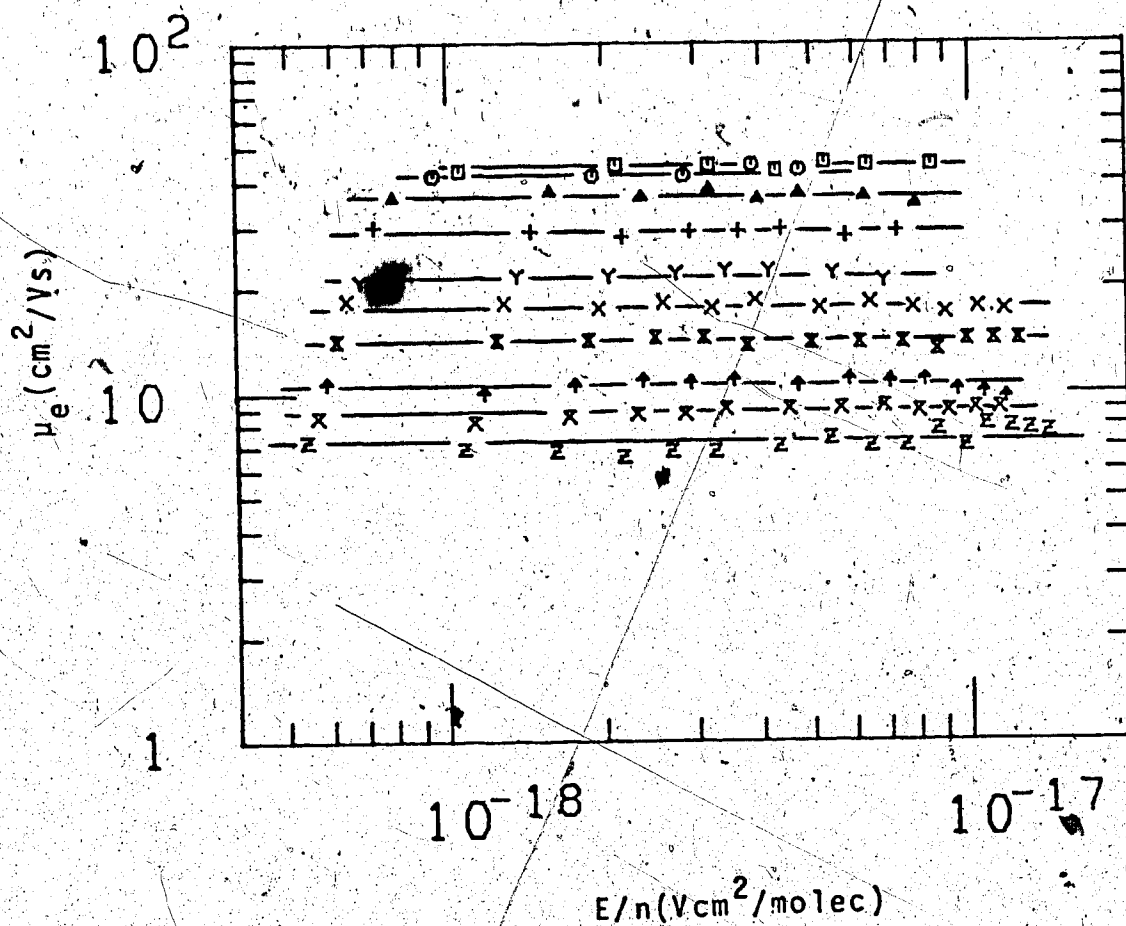


FIGURE III-46. Electron mobilities in liquid isobutane as functions of E/n . Densities and temperatures ($n/10^{21}$, T): z (5.73, 298K), X (5.45, 318K), \uparrow (5.28, 330K), $\&$ (5.00, 347K), X (4.79, 359K), Y (4.54, 371K), + (4.26, 382K), Δ (3.92, 392K), \circ (3.26, 403K), \square (2.92, 406.7K).

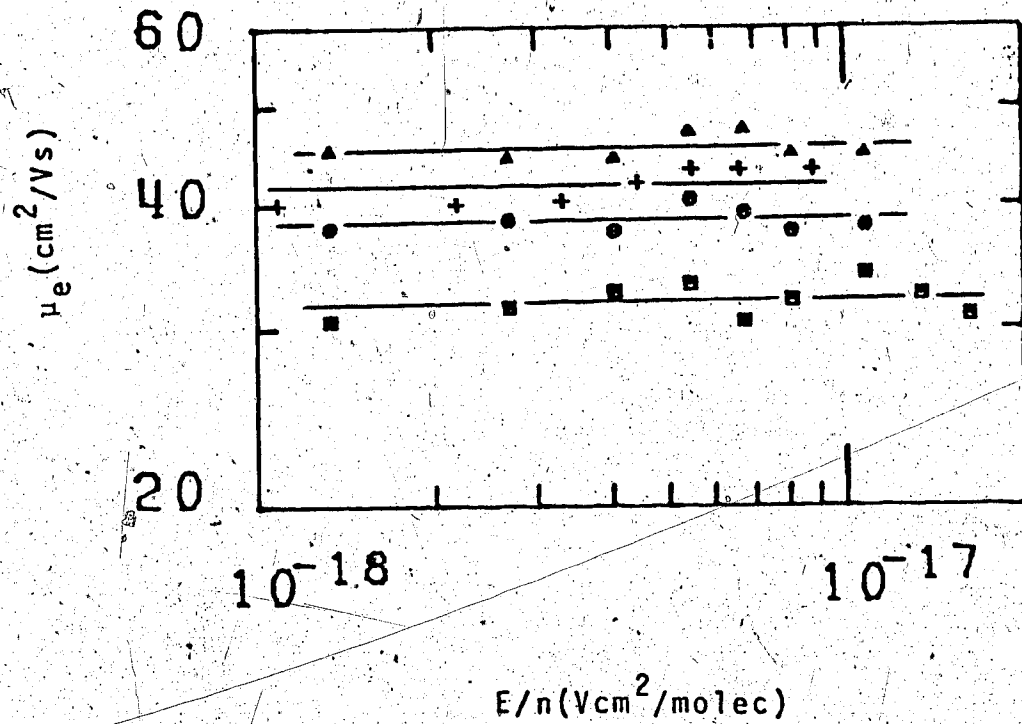


FIGURE III-47. Electron mobilities in liquid and supercritical isobutane as functions of E/n . Densities and temperatures ($n/10^{21}$, T): + (2.80, 407.4K), □ (2.30, 408.4K), ○ (2.30, 414K), △ (2.30, 423K).

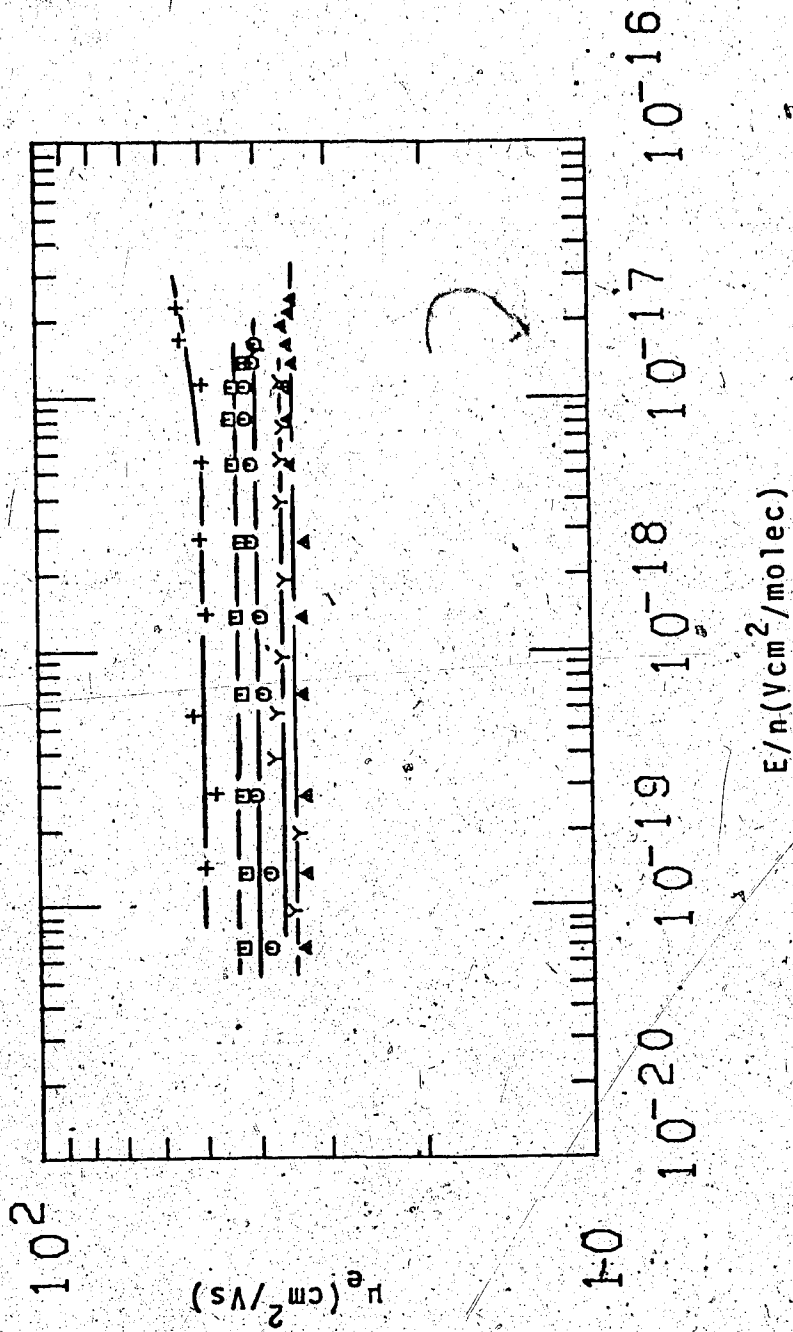


FIGURE III-48. Electron mobilities in supercritical and gaseous isobutane as functions of E/n . Densities and temperatures ($n/10^{21}$, T):

Δ (2.30, 408K), \circ (2.30, 415K), \square (2.30, 421K), γ (1.62, 406K),
 + (1.11, 398K).

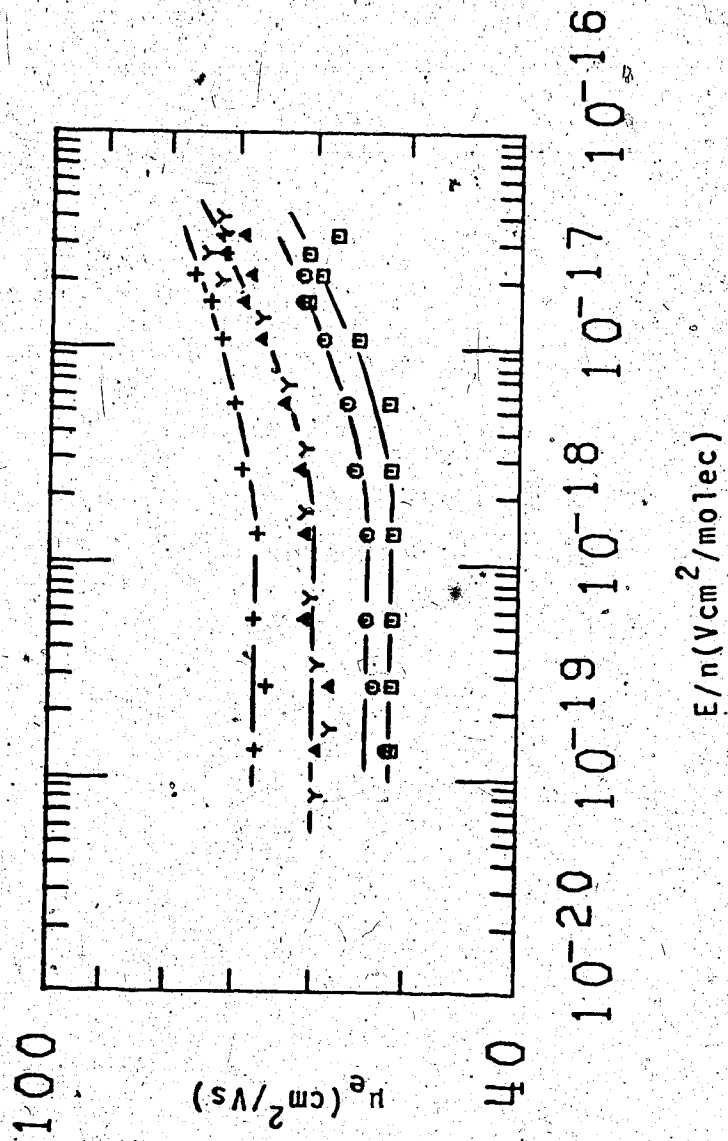


FIGURE III-49. Electron mobilities in gaseous isobutane as functions of E/n . Densities and temperatures ($n/10^{21}$, T): \square (1.15, 400K), \circ (1.15, 405K), Δ (1.15, 415K), $+$ (1.15, 425K), γ (0.922, 391K).

seen for the $n = 2.30 \times 10^{21}$ isochore (Figure III-48). No field effect stands out for the $n = 1.62 \times 10^{21}$ curve either. The high field end of the $n = 1.11 \times 10^{21}$ curve appears to be drifting upwards. Comparison with the $n = 1.15 \times 10^{21}$ curves (Figure III-49) would indicate that the upward drift on the $n = 1.11 \times 10^{21}$ curve can be taken as a real field effect. In Figure III-49, the density and temperature effects are the same as those drawn in the previous figure. The field effect is more pronounced. The second curve from the top was drawn through the points for both 415K of the isochore and 391K of the coexistence curve, since the μ_0 's for the two curves are within the experimental scatter.

In Figure III-50, the density is half of that in Figure III-49. The field effect is clear enough to show a rounding of the mobility curve. Raising the temperature increases the mobility at low fields more than at the higher fields. The mobility curves of the higher temperatures approach the curve near the coexistence state on a flat trajectory that increases only slightly as they go over the mobility maximum.

The same tendencies are shown in the more dilute gases. Figure III-51 shows that the amount of increase in the maximum is more in the more dilute gas. Variation of the mobility with density is as previously noted. Figure III-52 shows the temperature effect on the

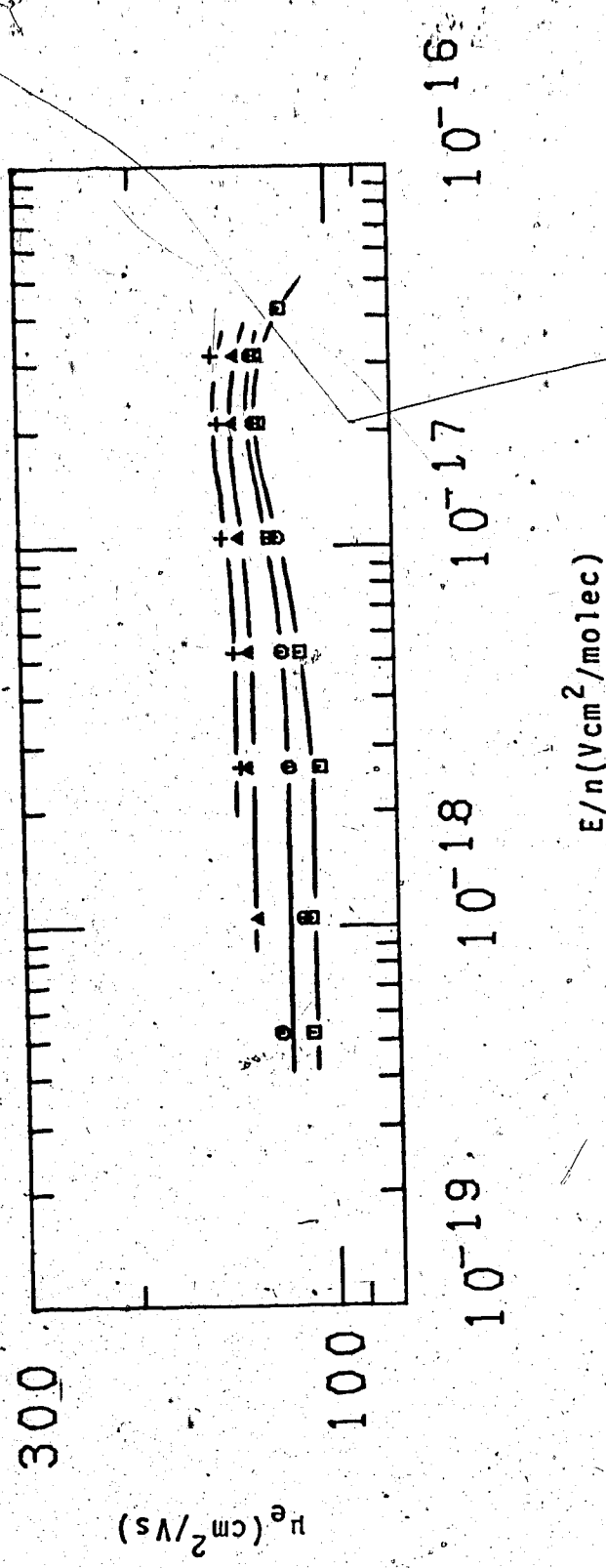


FIGURE III-50. Electron mobilities in gaseous isobutane as functions of E/n . $n = 5.91 \times 10^{20}$. Temperatures: \square (377K), \circ (388K), Δ (409K), $+$ (430K).

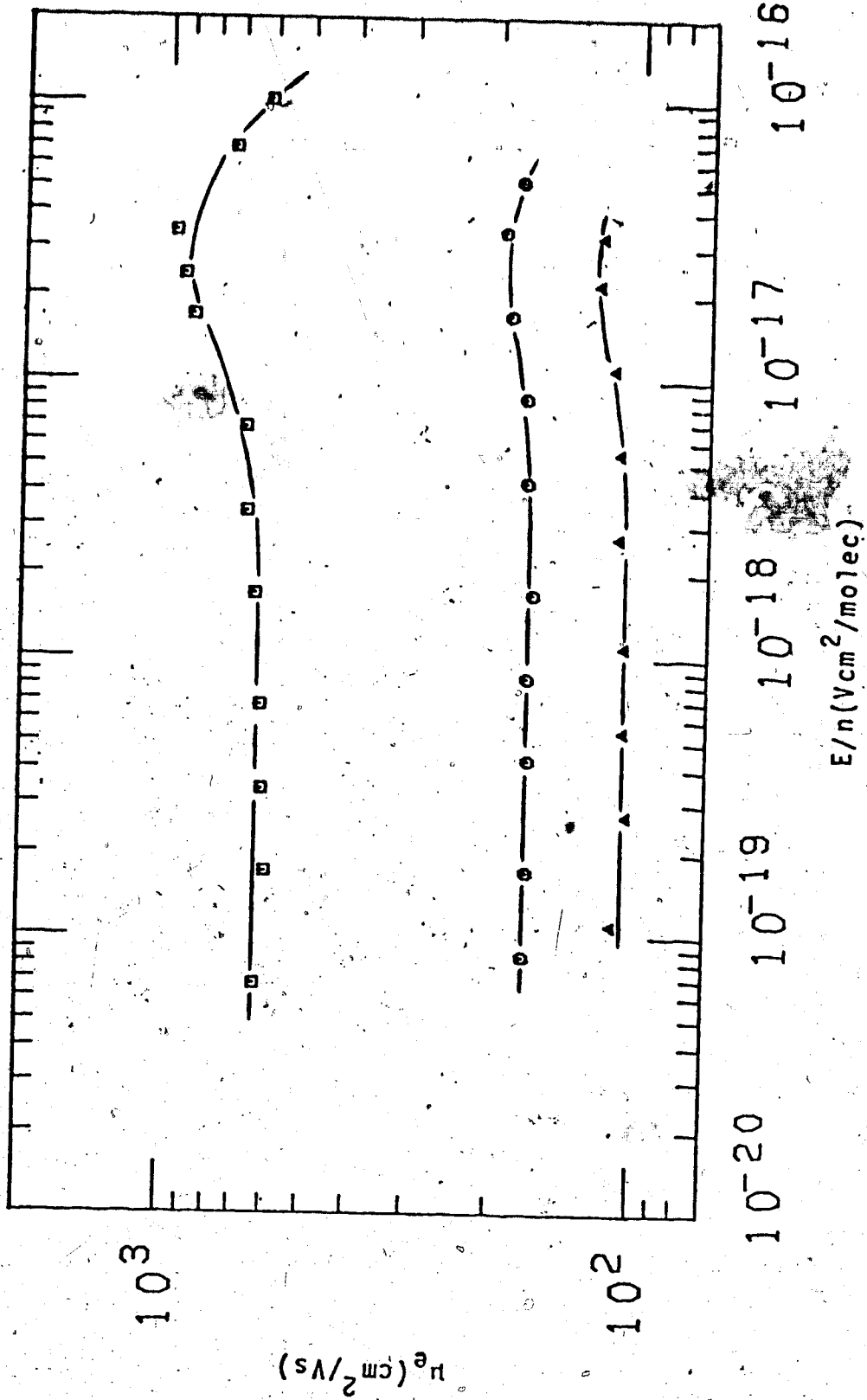


FIGURE III-51. Electron mobilities in gaseous isobutane as functions of E/n .
 Densities and temperatures ($n/10^{20}$, T): \square (0.922, 297K), \circ (3.63, 352K), \triangle (5.65, 371K).

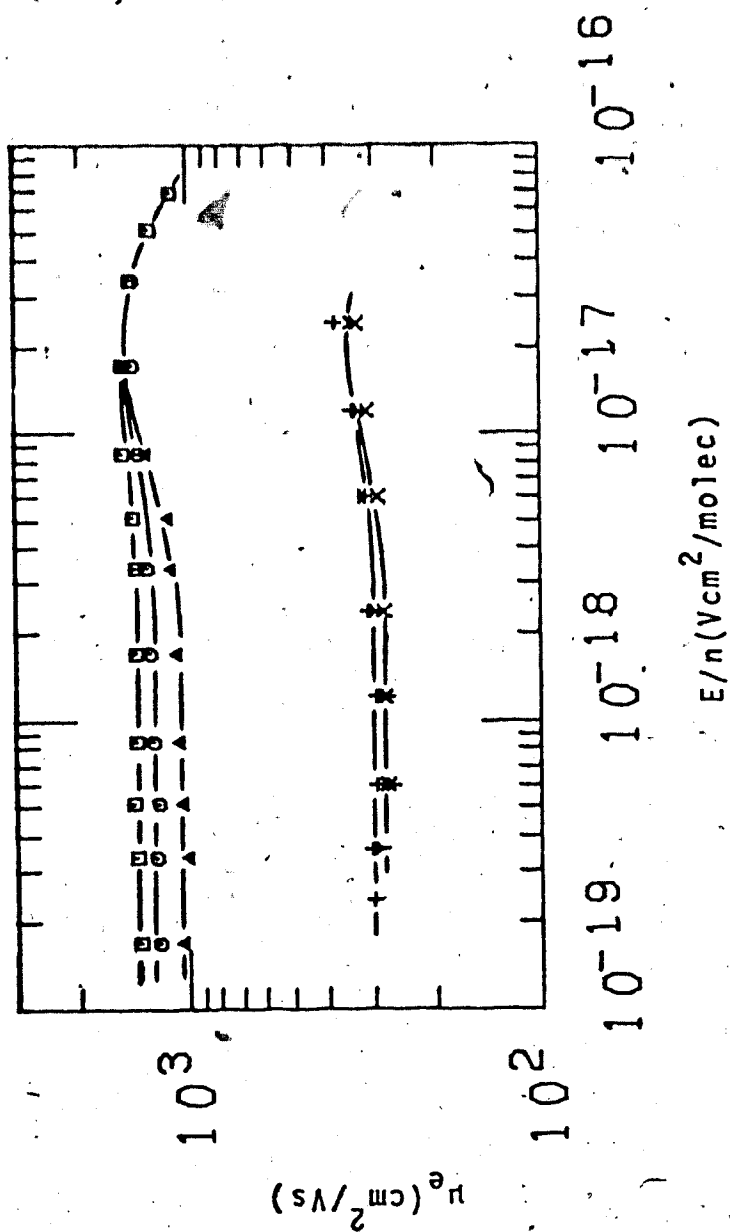


FIGURE III-52. Electron mobilities in gaseous isobutane as functions of E/n .

Densities and temperatures ($n/10^{20}$, T): + (2.59, 430K), γ (2.59, 398K),
 X (2.59, 365K), \square (0.591, 435K), \circ (0.591, 364K), Δ (0.591, 295K).

$n = 2.59 \times 10^{20}$ and the 5.91×10^{19} isochores. To avoid excess crowding, the line for 398K on the 2.59×10^{20} isochore was not drawn. The temperature effect on these constant density curves is the same as noted for Figure III-50. As can be seen from the upper curves, the flat trajectory of the low field mobilities seems to increase slightly before intersecting the lower temperature curve. Figure III-53 gives results along the coexistence curve. The features of the curves are as previously noted. As well, the density effect where the mobility varies inversely to the density is the same. The threshold field does not vary much with density.

Data for isobutane are summarized in Table III-5. Mobilities for $T \leq 270\text{K}$ were measured in a low pressure liquid type conductance cell. For $T \leq 214\text{K}$, the conductance method was used. High pressure liquid type conductance cells were used to collect the liquid phase data (Figures III-45, III-46, and III-47). Low pressure gas type conductance cells were used to collect the data where $n < 6 \times 10^{19}$ in Figures III-51 and III-52. All other gas phase results were obtained using high pressure gas type conductance cells.

2

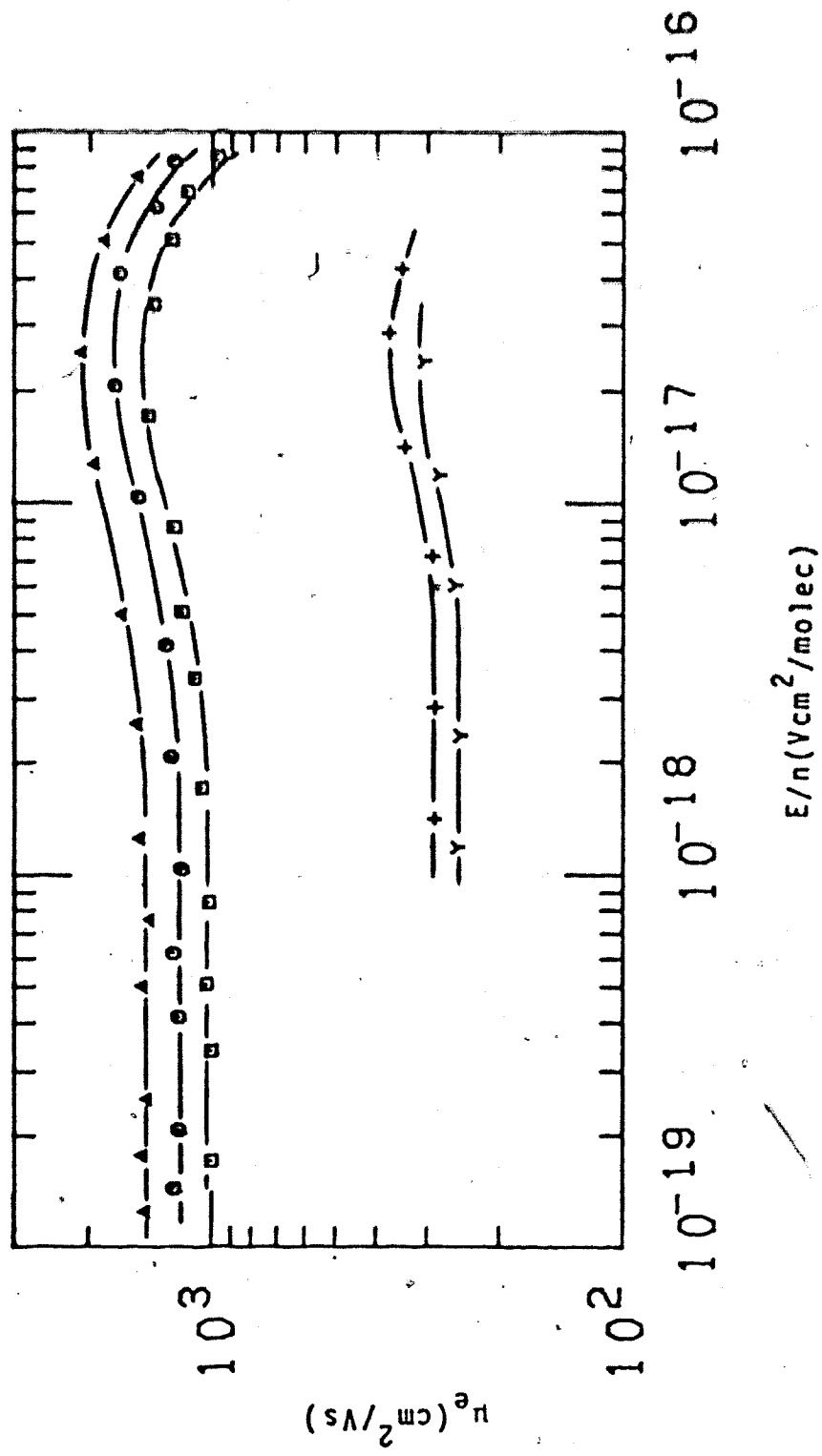


FIGURE III-53. Electron mobilities in gaseous isobutane as functions of E/n . Densities and temperatures ($n/10^{19}$, T): □ (5.91, 282K), O (4.87, 276K), Δ (3.99, 270K), Y (25.9, 340K), + (21.8, 330K).

TABLE III-5
 Summary of Results for Isobutane^a

T	n	μ_0	$\mu_0 n$	(E/n) threshold ^c	b
°K	$10^{20} \frac{\text{molec}}{\text{cm}^3}$	$\frac{\text{cm}^2}{\text{Vs}}$	$10^{22} \frac{\text{molec}}{\text{Vs cm}}$	$10^{-18} \frac{\text{Vcm}^2}{\text{molec}}$	$\frac{d \log \mu}{d \log E/n}$
140	76.9	0.0486	0.0373		
155	74.9	0.208	0.155		
173	72.6	0.581	0.108		
181	71.7	0.868	0.408		
214	67.3	2.14	1.44		
239	64.2	3.84	2.47		
270	60.7	5.31	3.22		
298	57.3	7.22	4.14		
318	54.5	8.77	4.77		
330	52.8	10.5	5.53		
347	50.0	14.0	7.01		
359	47.9	17.5	8.39		
371	45.4	21.4	9.71		
382	42.6	28.8	12.3		
392	39.2	36.4	14.3		
403	32.6	42.5	13.9		
406.7	29.2	44.3	13.0		
407.4	28.0	41.6	11.6	-	-
408.4	23.0 ^d	31.8	7.31	-	-
414	23.0 ^d	38.5	8.86	-	-
423	23.0 ^d	45.3	10.4	-	-
408	23.0 ^d	34.2	7.87	-	-
415	23.0 ^d	40.3	9.27	-	-
421	23.0 ^d	43.4	9.98	-	-
406	16.2	36.1	5.79	-	-
398	11.1	50.1	5.56	3	0.082
400	11.5	51.4	5.91	2.0	0.083

(continued.....)

TABLE III-5 (continued)

405	11.5	53.6	6.16	1.7	0.077
415	11.5	60	6.90	1.6	0.075
425	11.5	67.2	7.73	1.4	0.056
391	9.22	60	5.53	1.6	0.077
377	5.91	107	6.32	2.3	0.11
388	5.91	117	6.91	3.3	0.090
409	5.91	132	7.80	4.8	0.062
430	5.91	140	8.27	5.2	0.054
297	0.922	617	5.69	2.6	0.21
352	3.63	167	6.06	3.5	0.11
371	5.65	105	5.93	3.5	0.12
430	2.59	296	7.67	3.0	0.16
398	2.59	278	7.20	2.8	0.15
365	2.59	276	7.15	2.8	0.15
435	0.591	1390	8.21	3.0	0.077
364	0.591	1250	7.39	2.4	0.15
295	0.591	1050	6.21	2.1	0.20
282	0.591	1020	6.02	2.0	0.21
276	0.487	1220	5.94	2.0	0.21
270	0.399	1450	5.79	2.0	0.21
340	2.59	289	6.30	3.0	0.20
330	2.18	250	6.47	3.0	0.21

^a Order of appearance of data as in figures.

^b Estimated at $4(E/n)$ threshold

^c Insufficient field strength to determine these quantities in liquid phase isobutane.

^d $n_c = 2.30 \times 10^{21}$ molec/cm³. $T_c = 408K$.

6. Ethene

Electron mobilities determined in ethene are plotted as functions of the density normalized electric field strength E/n in Figures III-54 to III-58. Units of n are molec/cm³, mobilities, cm²/Vs and E/n , Vcm²/molec.

Figure III-54 gives liquid phase and supercritical results. The lowest three curves, which represent from the lowest curve upwards, 225K, 235K, 266K, were determined by the electron conductance transient method. All other ethene results were obtained by the time of flight method. There is no maximum of the electron mobility at a density greater than that of the critical fluid. The mobility increases smoothly as the liquid density decreases. Variation of the temperature by 1°K at the critical point does not noticeably change the mobility. Variation of the temperature to 1.3°K below the critical temperature decreases the mobility by almost 50% (22.3 at 283K to 12.0 at 281.7K).

Figure III-55 displays results at densities below that of the critical point. Variation of mobility with density is as observed in the previous systems. A decrease in density leads to an increase in mobility. The highest curve ($n = 2.19 \times 10^{21}$) displays a threshold of $E/n \sim 6 \times 10^{-18}$. The next curve down ($n = 2.62 \times 10^{21}$) may also display a (E/n) threshold but results are not clear against the scatter in the data. At 2.19×10^{21} molec/cm³, increasing the field strength above (E/n) threshold leads

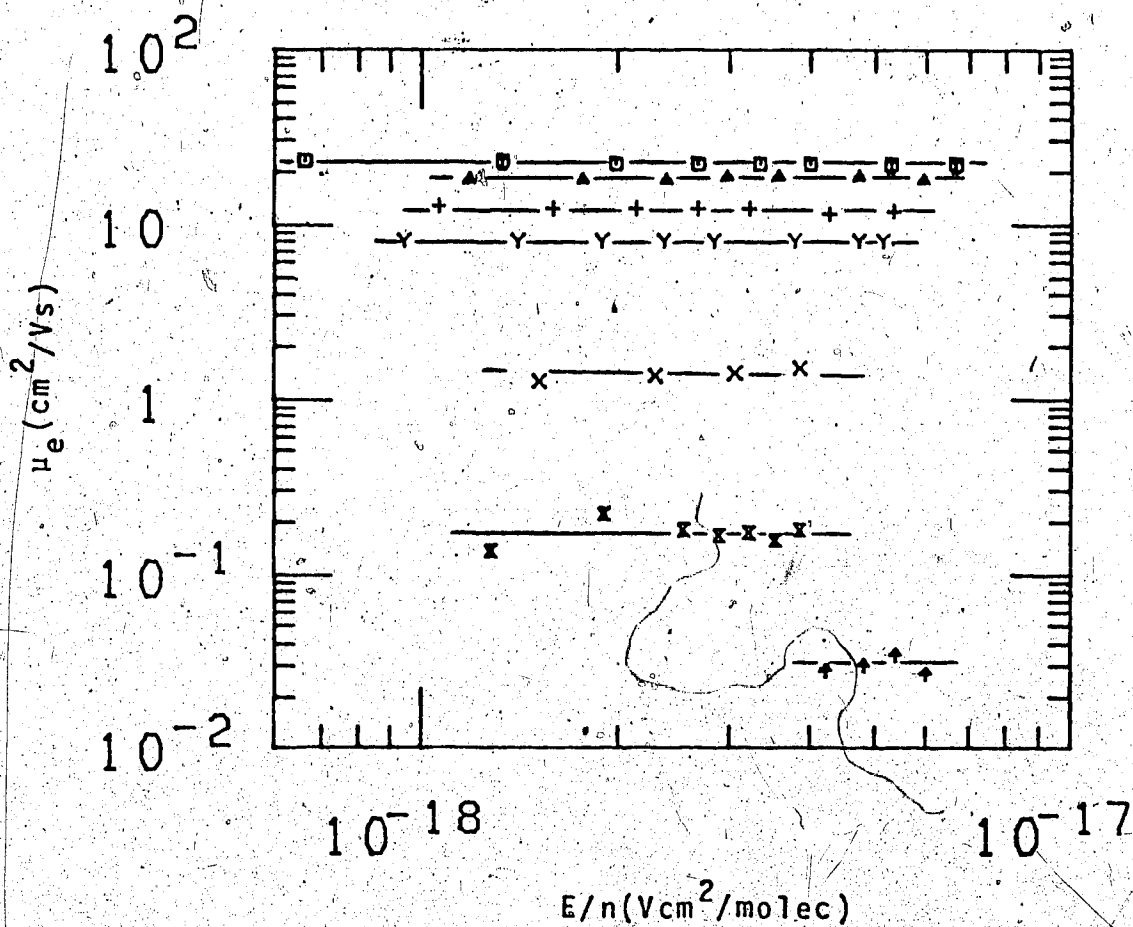


FIGURE III-54. Electron mobilities μ_e plotted against the density normalized electric field strength E/n in liquid and supercritical ethene. Densities and temperatures ($n/10^{21}$, T): \circ (4.66, 284.1K), \square (4.66, 283.0K), \triangle (5.22, 282.7K), $+$ (5.80, 281.7K), γ (6.57, 278.7K), x (8.11, 266K), δ (9.70, 239K), ∇ (10.3, 225K).

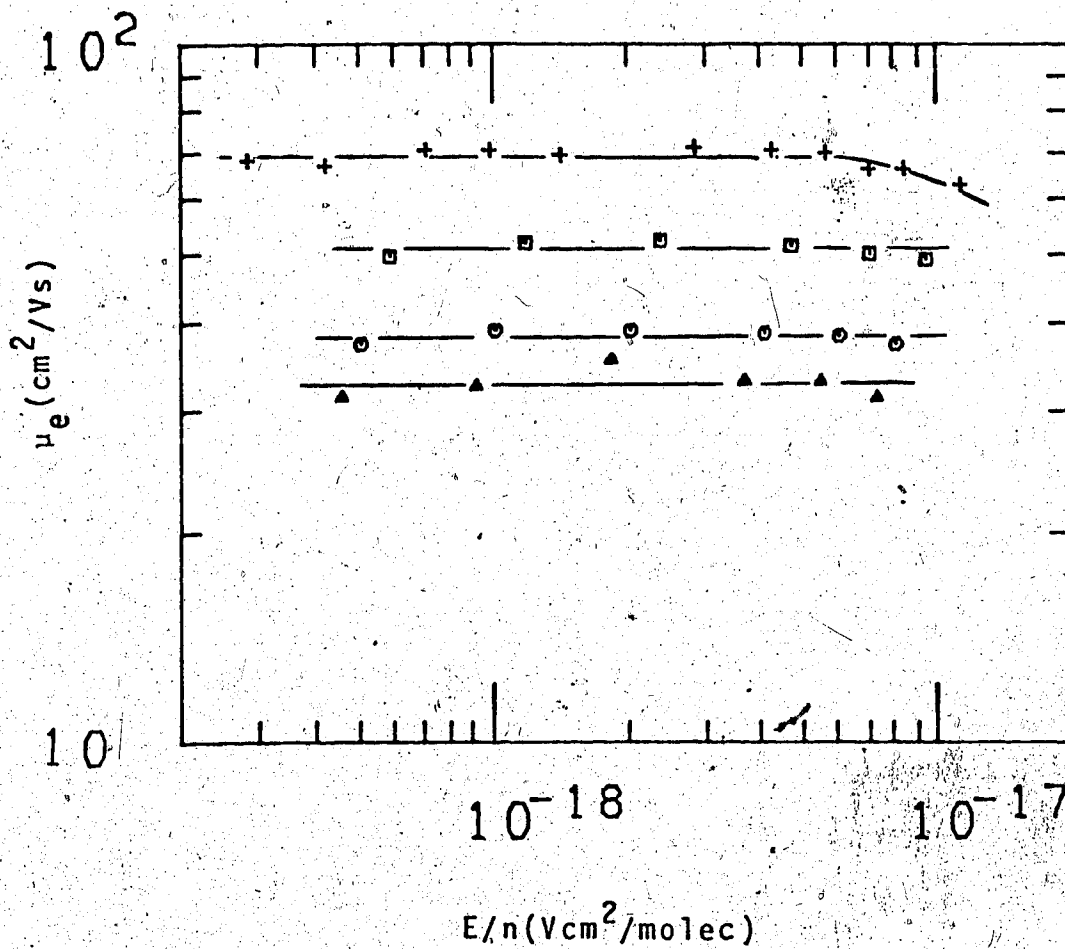


FIGURE III-55. Electron mobilities μ_e plotted against the density normalized electric field strength E/n in gaseous ethene. Densities and temperatures ($n/10^{21}$, T): Δ (3.37, 281.6K), \circ (3.05, 280.7K), \square (2.62, 287.7K), $+$ (2.19, 274.4K).

to a decrease in the mobility.

Figure III-56 shows mobilities at still lower densities as well as the temperature effect on the $n = 1.64 \times 10^{21}$ isochore. Variation of density shifts the mobility curves as before. Variation of temperature leads to very slight variations of the mobilities. The two lower curves are drawn through the 294K and the 268K points and represent a difference of 8%. The threshold fields are about constant.

Figure III-57 gives results after a further decrease in density. Decreasing the density leads to an increase of the mobility approximately in proportion. The lowest curves are drawn through the 296K, 254K and 245K mobility curves of the $n = 7.95 \times 10^{20}$ isochore. The difference between the μ_0 's of the three curves, obtained by an arithmetic average of the low field mobilities, differ by less than 5%. This is within the experimental scatter of the points.

The last figure of this set, Figure III-58, shows that the mobility continues to increase with decreasing density. The field strengths attained were insufficient to show the field effect. At $n = 1.89 \times 10^{20}$ the 296K, 236K, 207K, and 203K superimpose.

All measurements were made in high pressure conductance cells. Results in Figure III-54 were made in a liquid type cell. All other sets were made in gas type

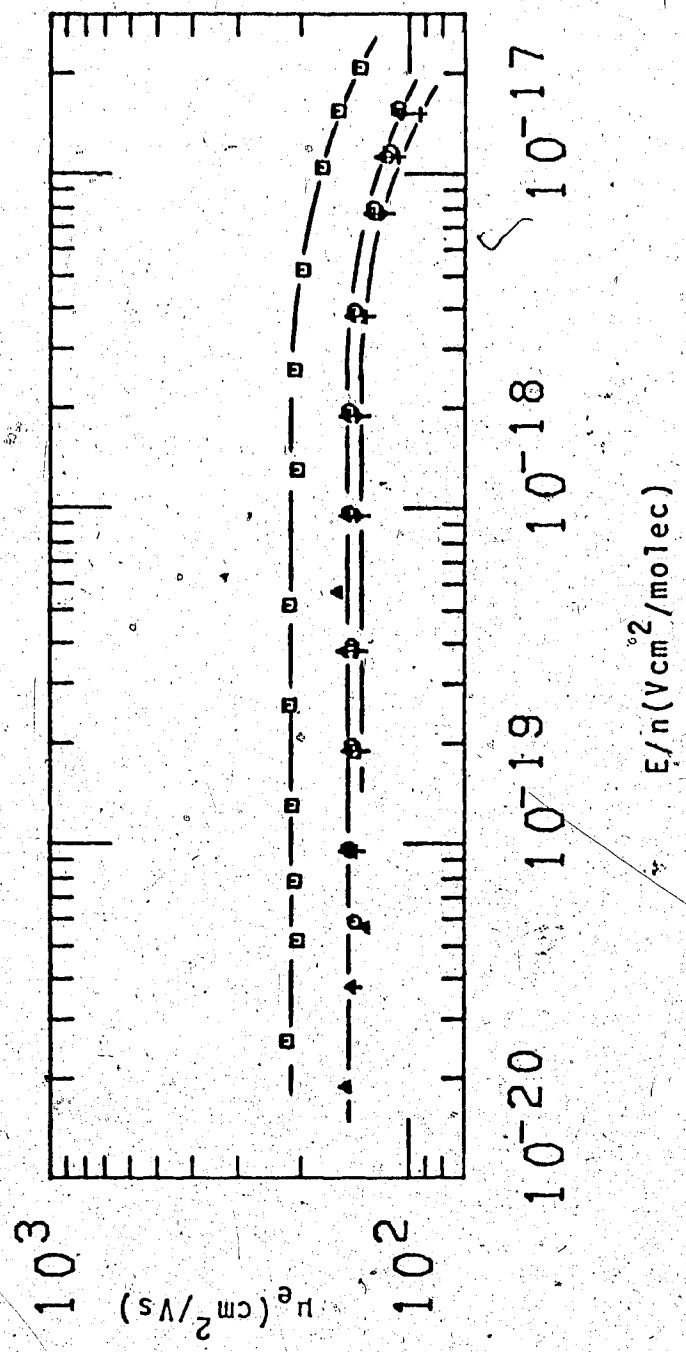


FIGURE III-56. Electron mobilities in gaseous ethene as functions of E/n .
 Densities and temperatures ($n/10^{21}$, T): \square (1.20, 256K), \circ (1.56,
 265K), \triangle (1.64, 294K), \times (1.64, 274K), γ (1.64, 268K).

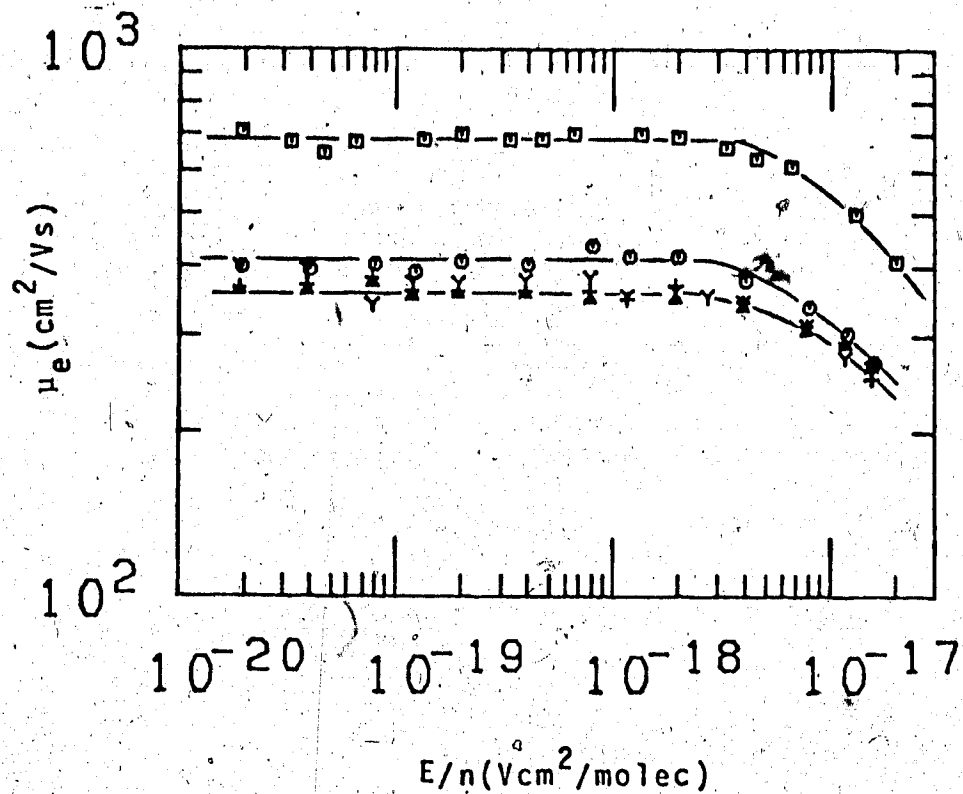


FIGURE III-57. Electron mobilities in gaseous ethene as functions of E/n . Densities and temperatures ($n/10^{20}$, T): □ (4.72, 227K), ○ (7.73, 241K), Δ (7.95, 245K), + (7.95, 254K), × (7.95, 296K).

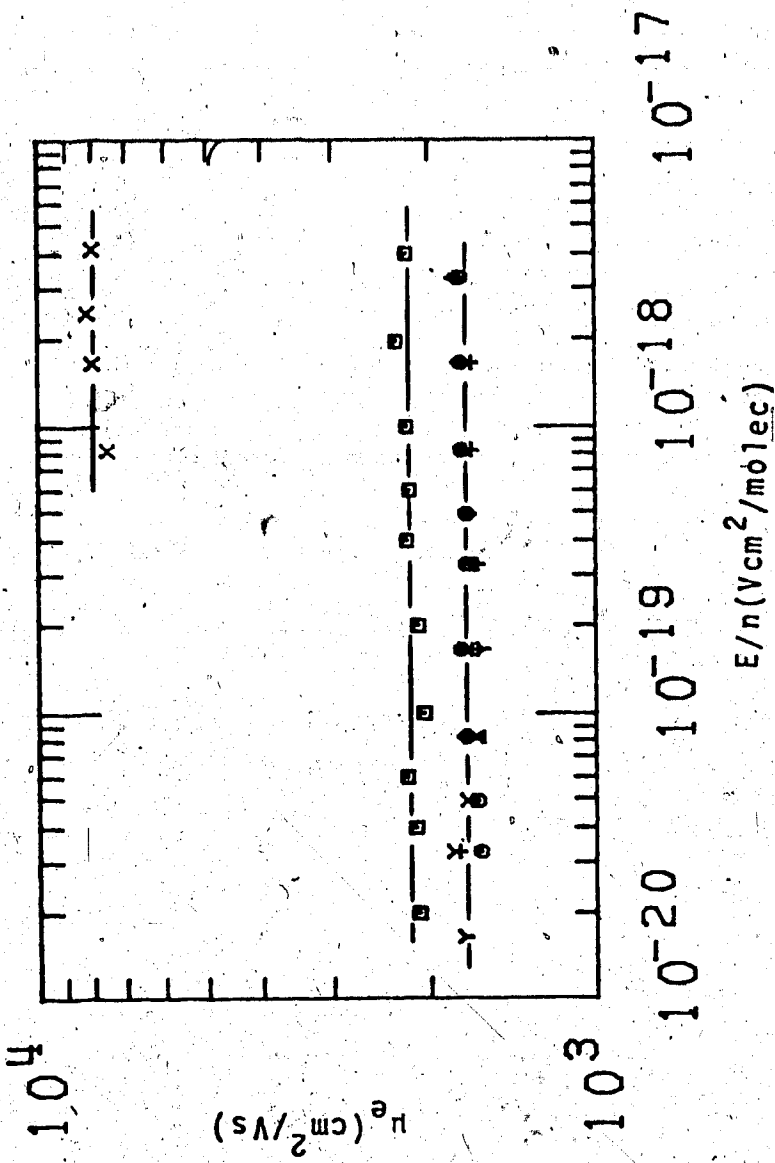


FIGURE III-58. Electron mobilities in gaseous ethene as functions of E/n .
 Densities and temperatures ($n/10^{20}$, T): \square (1.57, -196K), \circ (1.89, 203K),
 Δ (1.89, 207K), $+$ (1.89, 236K), γ (1.89, 298K), \times (0.376, 166K).

cells. Data from Figures III-54 to III-58 are summarized in Table III-6.

TABLE III-6

Summary of Results for Ethene^a

T °K	n 10 ²¹ molec cm ³	μ_0 cm ² Vs	$\mu_0 n$ 10 ²³ molec Vs cm	(E/n) _{threshold} ^c 10 ⁻¹⁸ V cm ² molec	b,c $\frac{d \log \mu}{d \log (E/n)}$
284.1	4.66 ^d	22.3	1.04		
283.0	4.66 ^d	22.3	1.04		
282.7	5.22	18.3	0.955		
281.7	5.80	12.0	0.696		
278.7	6.57	7.97	0.500		
266	8.11	1.37	0.111		
239	9.70	0.165	0.0160		
225	10.3	0.0305	0.00314		
281.6	3.37	32.6	1.10		
280.7	3.05	38.1	1.16		
287.7	2.62	50.8	1.33		
274.4	2.19	69.1	1.52	-6	minus
256	1.20	210	2.49	2.1	-0.24
265	1.59	144	2.29	2.5	-0.24
294	1.64	146	2.39	2.5	-0.21
274	1.64	138	2.26	2.5	-0.23
268	1.64	135	2.21	2.5	-0.24
227	0.472	686	3.24	3.6	-0.36
241	0.773	410	3.17	2.8	-0.22
245	0.795	358	2.85	2.6	-0.17
254	0.795	365	2.90	2.6	-0.17
296	0.795	374	2.97	2.6	-0.17
196	0.157	2160	3.39	-	-
203	0.189	1710	3.23	-	-
207	0.189	1720	3.25	-	-
236	0.189	1710	3.23	-	-

(continued.....)

TABLE III-6 (continued)

296	0.186	1710	3.23	-	-
166	0.0376	7940	2.99	-	-

a. Order of appearance of data as in figures

b. Estimated at $E/n \approx 4(E/n)_{\text{threshold}}$

c. Insufficient field strength in liquid or dense gas near the critical point for determination.

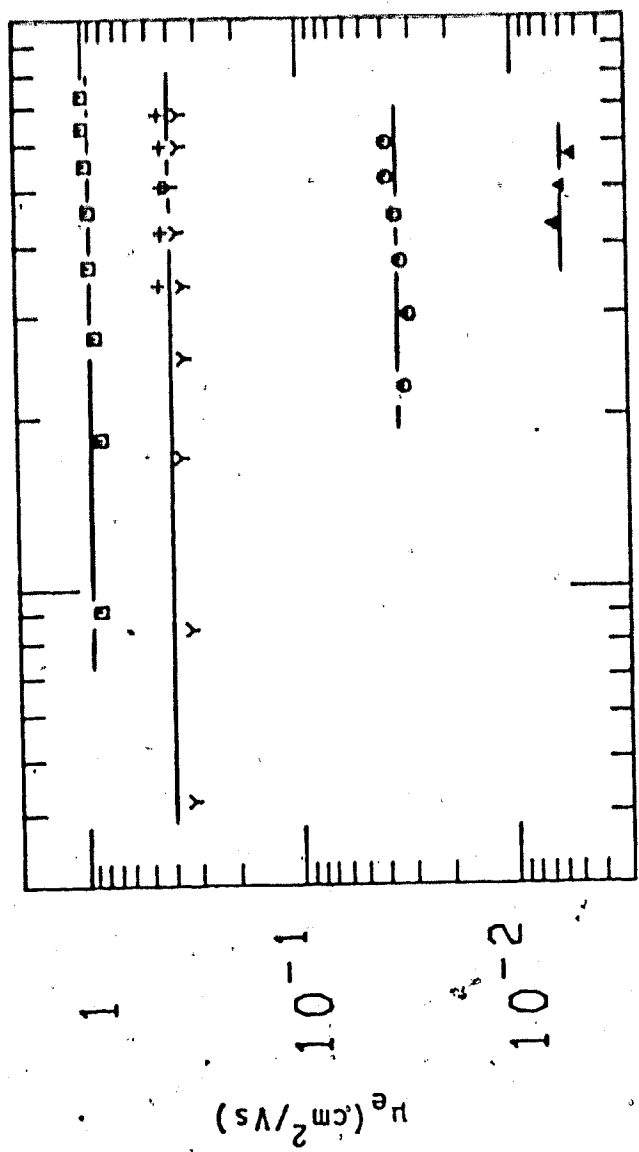
d. $n_c = 4.66 \times 10^{21}$ molecule/cm³. $T_c = 283\text{K}$.

7. Propene

Data obtained in propene are displayed in Figures III-59 to III-66. Densities are in units of molec/cm³, mobilities, of cm²/Vs, and density normalized electric fields, of Vcm²/molec. Plots are all of mobilities, μ_e , shown against the density normalized electric field strength E/n .

Liquid phase results are given in Figures III-59 and III-60. The second and third sets from the top in Figures III-59 are both at 296K. The higher points were obtained by the time of flight method. The lower points were obtained by the conductance method. The difference is less than 20%. The curves for 231K and 255K were also determined by the conductance method. All other propene results were obtained by the time of flight method. The highest three curves in Figure III-60 are for the supercritical gas. Throughout the liquid range, decreasing the density by increasing the temperature leads to an increase in the mobility.

Figure III-61 shows mobilities in gaseous propene at densities near the critical point. From Figures III-60 and III-61, increasing the temperature at the critical point increases the mobility. Decreasing the density away from the critical density increases the mobility. No field effect is observed over the field range covered.



10⁻¹⁸ 10⁻¹⁷

E/n (Vcm²/molec)

FIGURE III-59. Electron mobilities μ_e in liquid propene plotted against E/n . Densities and temperatures ($n/10^{21}$, T): \square (6.76, 318K), \triangle (7.33, 296K), γ (7.33, 296K), \circ (8.27, 255K), Δ (8.66, 231K).

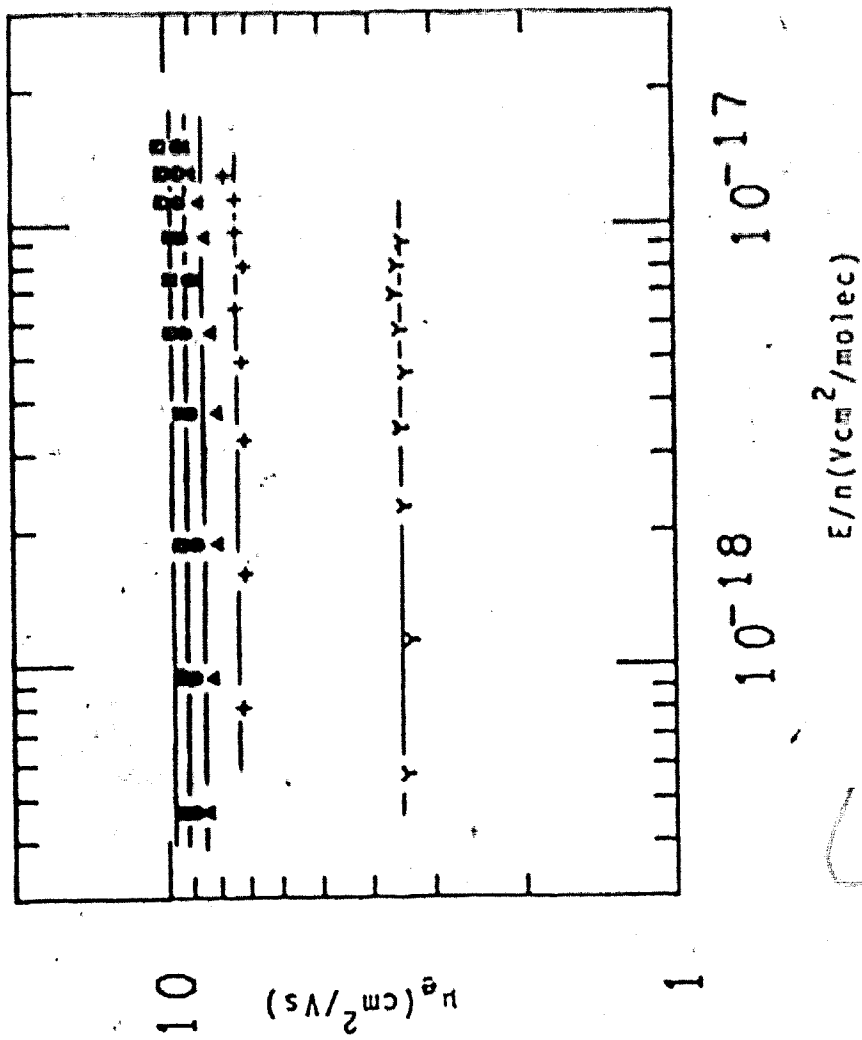


FIGURE III-60. Electron mobilities in liquid and supercritical propane

as functions of E/n . Densities and temperatures ($n/10^{21}$, T):

Y (5.44, 350K), + (3.86, 365K), Δ (3.32, 365.7K), \circ (3.32, 367.5K),

\square (3.32, 370K).

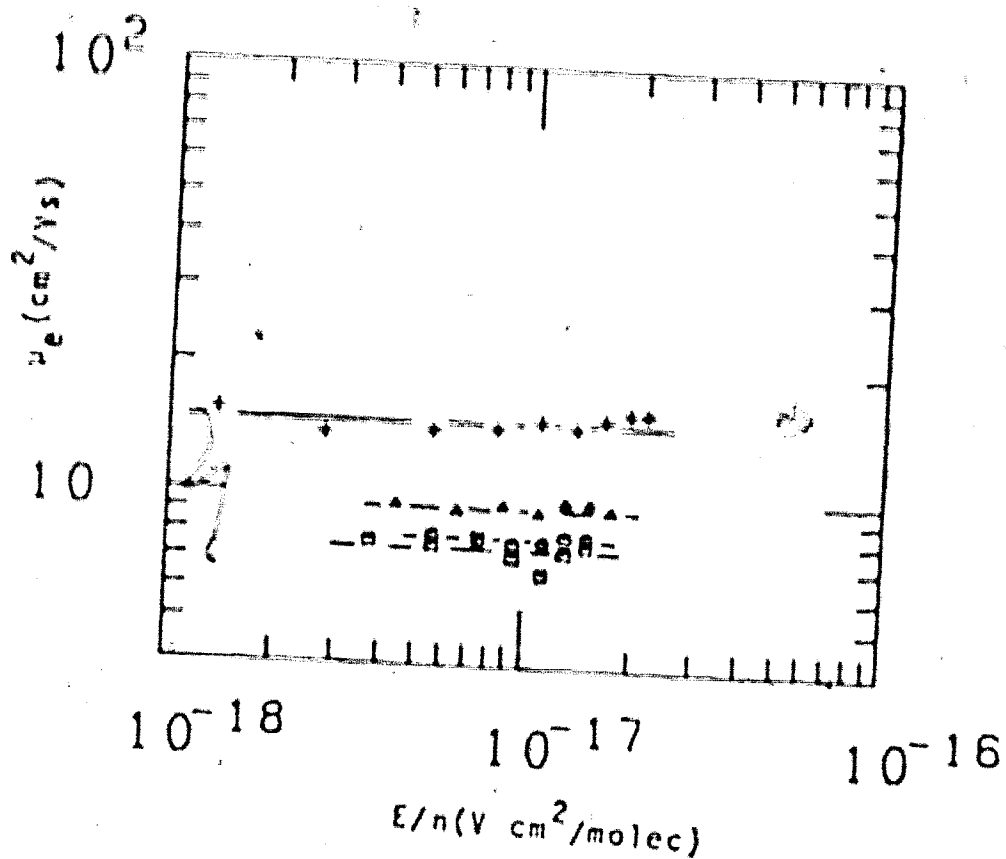


FIGURE III-61. Electron mobilities in supercritical and gas phase propene as functions of E/n . Densities and temperatures ($n/10^{21}$, T): O (3.32, 368K), square (3.32, 365.4K), + (2.86, 364K), triangle (2.26, 362K).

The temperature effect on the $n = 1.66 \times 10^{21}$ isochore is shown in Figure III-62. No field effect is observed at this density. Increasing the temperature leads to an increase in the mobility.

When the density decreases a bit more to the $n = 8.23 \times 10^{20}$ isochore, a field effect is observed (Figure III-63). Upon exceeding (E/n) threshold, the mobility increases with further increase in electric field, and reaches a maximum at $E/n \approx 3 \times 10^{-17}$ $\text{Vcm}^2/\text{molec}$. Increasing the temperature increases the mobilities, but the effect on (E/n) threshold is slight.

The same field effect carries over when the density is further reduced by a factor of about 2 (Figure III-64). As observed in the other systems, the mobilities increase with decrease in density. On the 4.15×10^{20} isochore, the increase in temperature leads to an increase in low field mobility, and little change in the threshold field. Unlike Figure III-63, the temperature also has little effect on the mobilities at higher fields. As a result, the four different curves are seen to merge.

The last two figures give results for the 6.61×10^{19} isochore as well as two curves at lower densities on the coexistence curve. The trends on the isochore are as noted for Figure III-64. The higher fields attained in this case allow a better picture of the mobility maximum. Figure III-66 shows that further

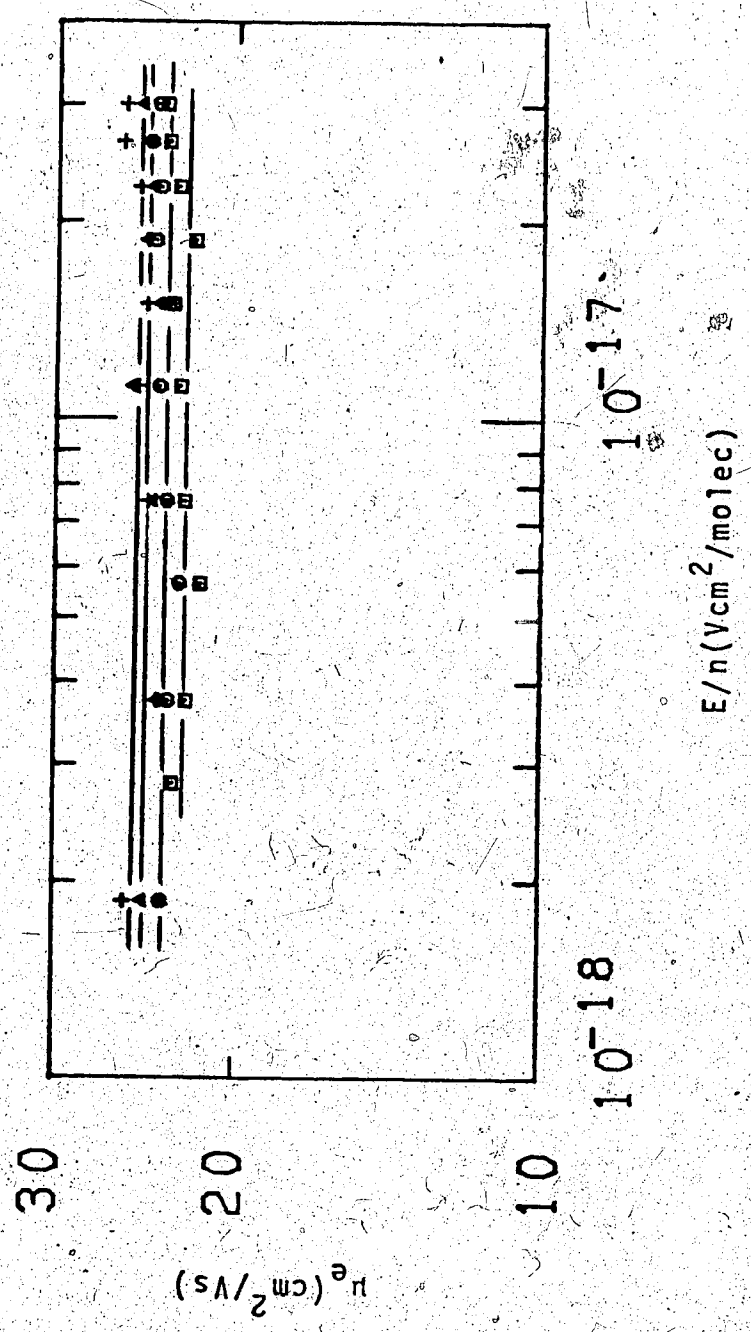


FIGURE III-62. Electron mobilities in gaseous propene as functions of E/n .
 $n = 1.66 \times 10^{21}$. Temperatures: \square (358K), \circ (362K), Δ (366K), + (368K).

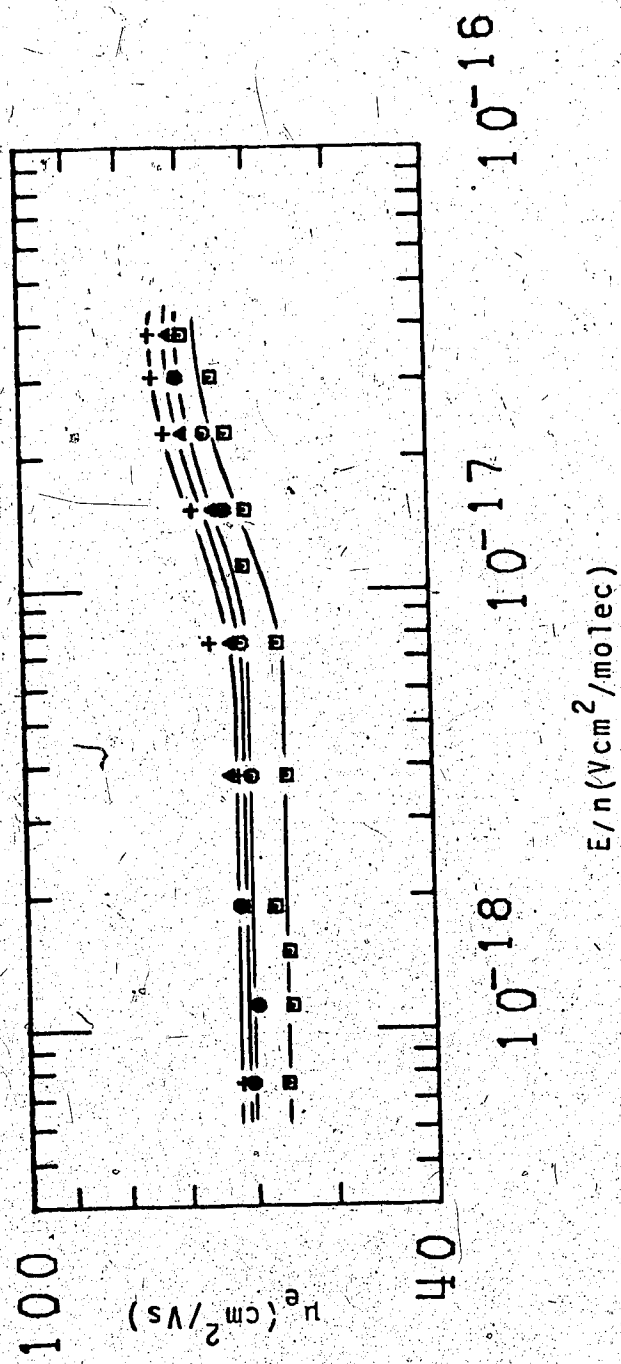


FIGURE III-63. Electron mobilities in gaseous propene as functions of E/n .

$n = 8.23 \times 10^{20}$. Temperatures: \square (323K), \circ (349K), Δ (368K), $+$ (389K).

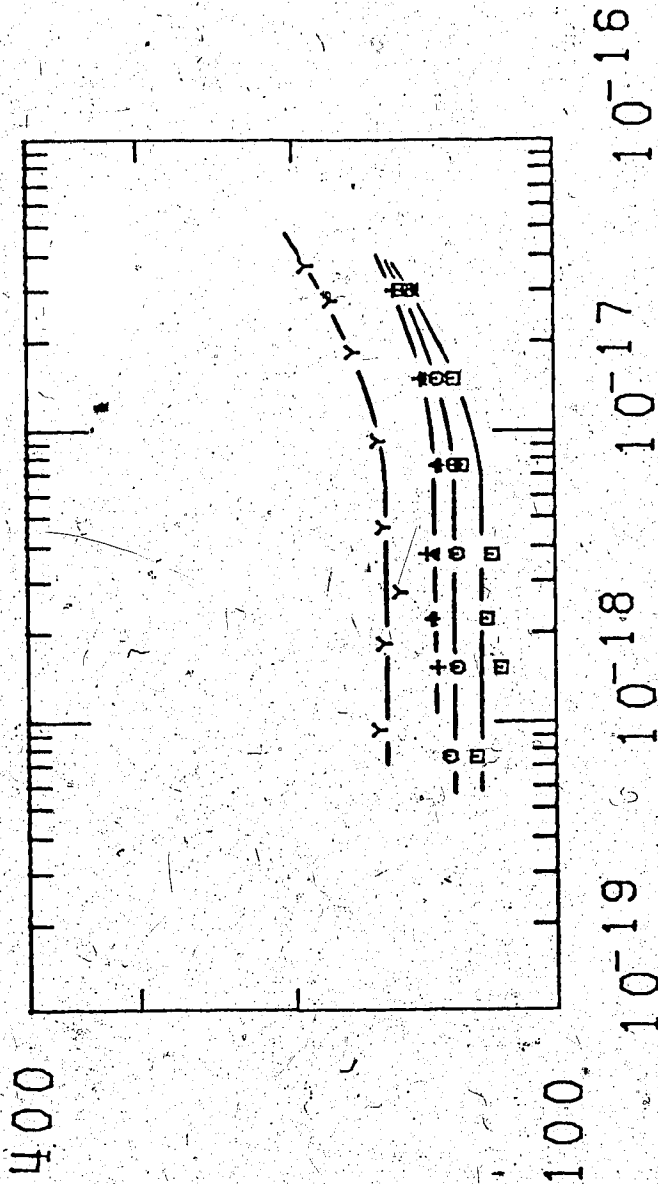


FIGURE III-64. Electron mobilities in gaseous propene as functions of E/n .
 Densities and temperatures ($n/10^{20}$, T): Y (3.37, 296K), □ (4.15, 305K),
 O (4.15, 318K), Δ (4.15, 357K), + (4.15, 382K).

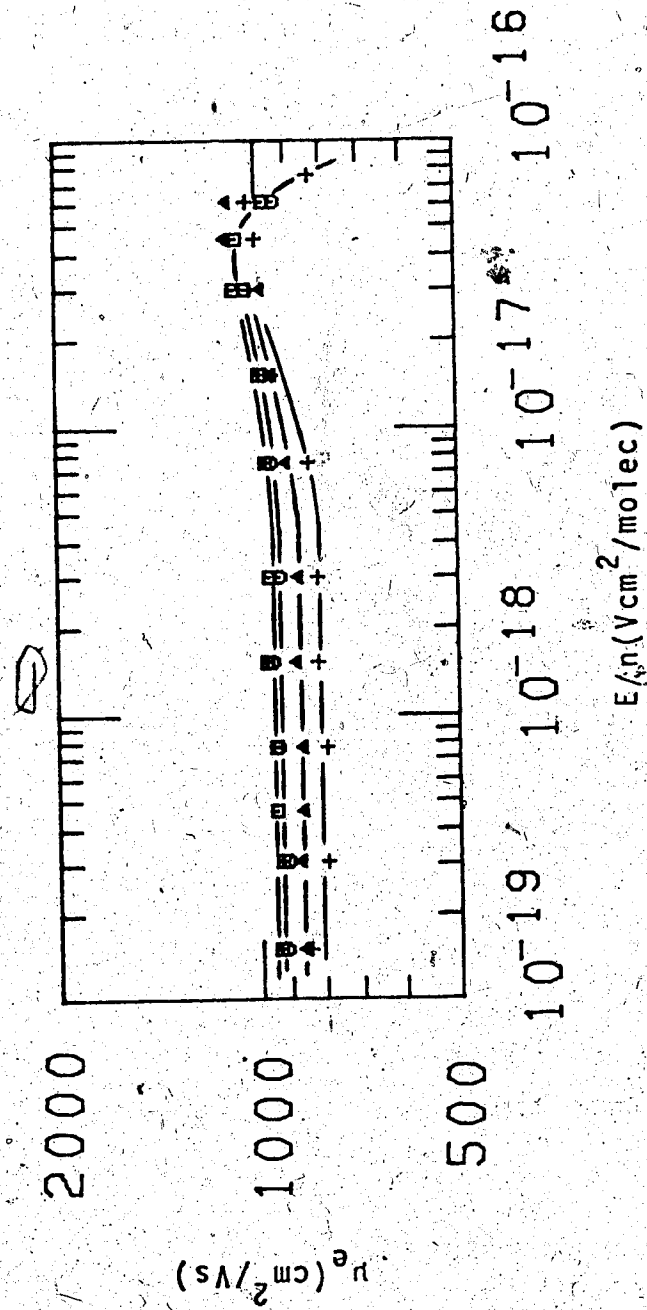


FIGURE III-65. Electron mobilities in gaseous propene as functions of E/n .

$n = 6.61 \times 10^{19}$. Temperatures: \square (393K), \triangle (294K), \circ (355K).

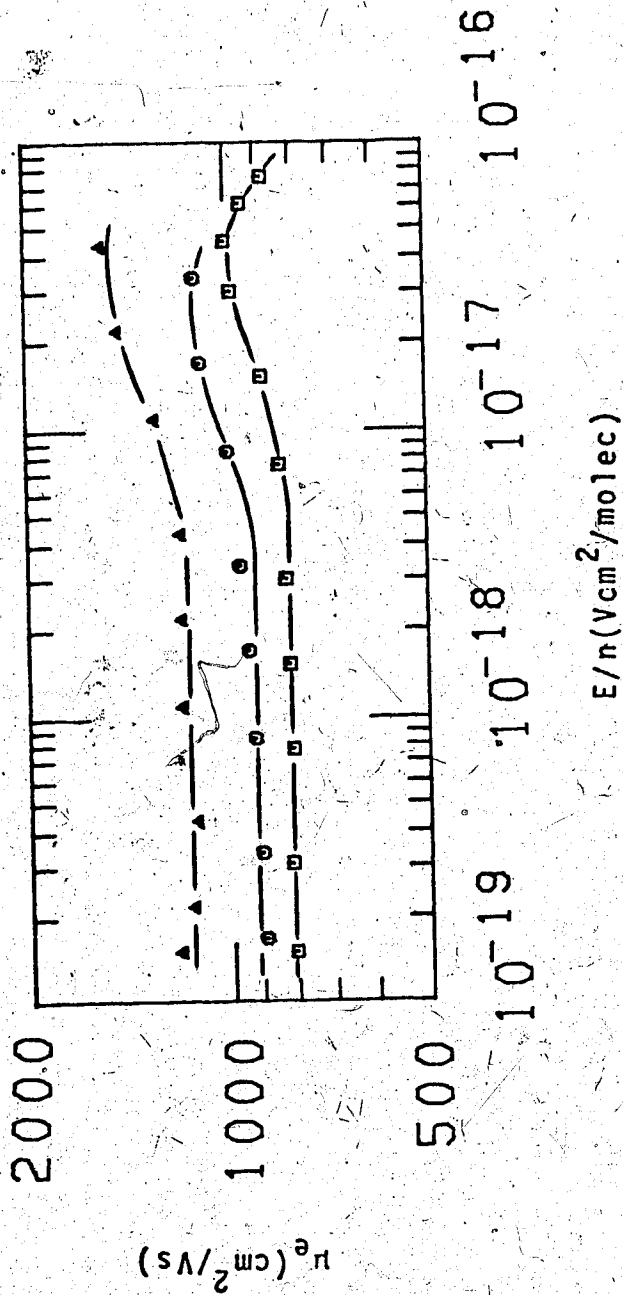


FIGURE III-66. Electron mobilities in gaseous propene as functions of E/n .
 Densities and temperatures ($n/10^{19}$, T): \square (6.01, 241K), \circ (6.61, 247K), Δ (4.61, 233K).

decreases in density lead to further increases in mobility. The lowest two densities do not clearly show the position of the maximum. The electric field strength position of the mobility maximum does not clearly change with the variation in temperature.

Electron mobility data for propene are summarized in Table III-7. All cells used except for the data of Figures III-65 and III-66 were the high pressure conductivity cells. Data of Figures III-59 and III-60 were obtained with liquid type cells. All other results were obtained with gas type cells. Data of Figures III-65 and III-66 were obtained with low pressure gas type cells.

TABLE III-7

Summary of Results for Propene^a

T °K	n $10^{21} \frac{\text{molec}}{\text{cm}^3}$	μ_0 $\frac{\text{cm}^2}{\text{Vs}}$	$\mu_0 n$ $10^{22} \frac{\text{molec}}{\text{Vscm}}$	(E/n) threshold	
				$10^{-18} \frac{\text{Vcm}^2}{\text{molec}}$	$\frac{d \log \mu}{d \log E/n}$
318	6.76	0.006	0.00608		
296	7.33	0.0349	0.0256		
255	8.27	0.39	0.323		
231	8.66	0.927	0.803		
350	5.44	3.45	1.15		
364.6	3.86	7.21	2.39		
365.7	3.32 ^d	8.42	2.80		
367.5	3.32 ^d	9.09	3.02		
370	3.32 ^d	9.73	3.23		
368	3.32 ^d	7.92	2.63		
365.4	3.32 ^d	7.47	2.48		
364	2.86	9.38	2.68		
362	2.26	14.8	3.34		
358	1.66	22.8	3.77		
362	1.66	23.5	3.90		
366	1.66	24.4	4.05		
368	1.66	24.9	4.13		
333	0.823	55.8	4.59	7.5	0.15
349	0.823	60.5	4.98	7.3	0.13
368	0.823	61.3	5.04	6.8	0.13
389	0.823	62.2	5.12	6.2	0.13
296	0.337	156	5.27	6.7	0.16
305	0.415	121	5.00	7.2	0.18
318	0.415	130	5.39	7.2	0.13
357	0.415	137	5.69	7.2	0.11
382	0.415	138	5.73	7.2	0.11
393	0.0661	946	6.25	4.7	0.064

(continued.....)

TABLE III-7 (continued)

355	0.0661	928	6.13	4.7	0.084
294	0.0661	865	5.72	4.5	0.14
252	0.0661	808	5.34	4.5	0.17
247	0.0661	808	5.34	4.7	0.14
241	0.0601	912	5.48	3.9	0.15
231	0.0461	1160	5.35	4.4	0.15

^a Data appears in the same order as in the figures

^b Estimated at $E/n \approx 4(E/n)_{\text{threshold}}$. Positive value if mobilities increase at $E/n > (E/n)_{\text{threshold}}$, and negative if mobilities decrease

^c May be slight increase at highest fields, but can not determine against the scatter.

^d $n_c = 3.32 \times 10^{21}$ molec/cm³. $T_c = 365\text{K}$

8. Cyclopropane

Electron mobilities obtained in cyclopropane appear in Figures III-67 to III-71. Densities are in molec/cm³, mobilities μ_e are in units of cm²/Vs and the density normalized electric field strengths E/n , are in units of Vcm²/molec.

Figures III-67 and III-68 show the liquid phase results. Data in Figure III-67 were all collected by the electron conductance method except the top curve. For the top curve, the leftmost three points were obtained by the conductance method. The rest of the curve, and the rest of the cyclopropane results were obtained by the time of flight method. In the liquid phase, heating the liquid along the coexistence curve towards the critical point leads to an increase in the electron mobility. Figure III-68 shows the mobilities within 5K of the critical point. From 4.97×10^{21} to 3.58×10^{21} , the mobility changes by a factor of about 2.8 while the density has only changed by a factor of 1.4. No variation of the mobility with field strength was observed.

The next Figure, III-69, shows results in gaseous cyclopropane near and at the critical point. The mobilities at 397.8K and at 398.4K are too scattered to display a significant difference. The discrepancy of ~11% between the values obtained in the gas type cell and those obtained from the liquid type cell may be due to the density gradi-

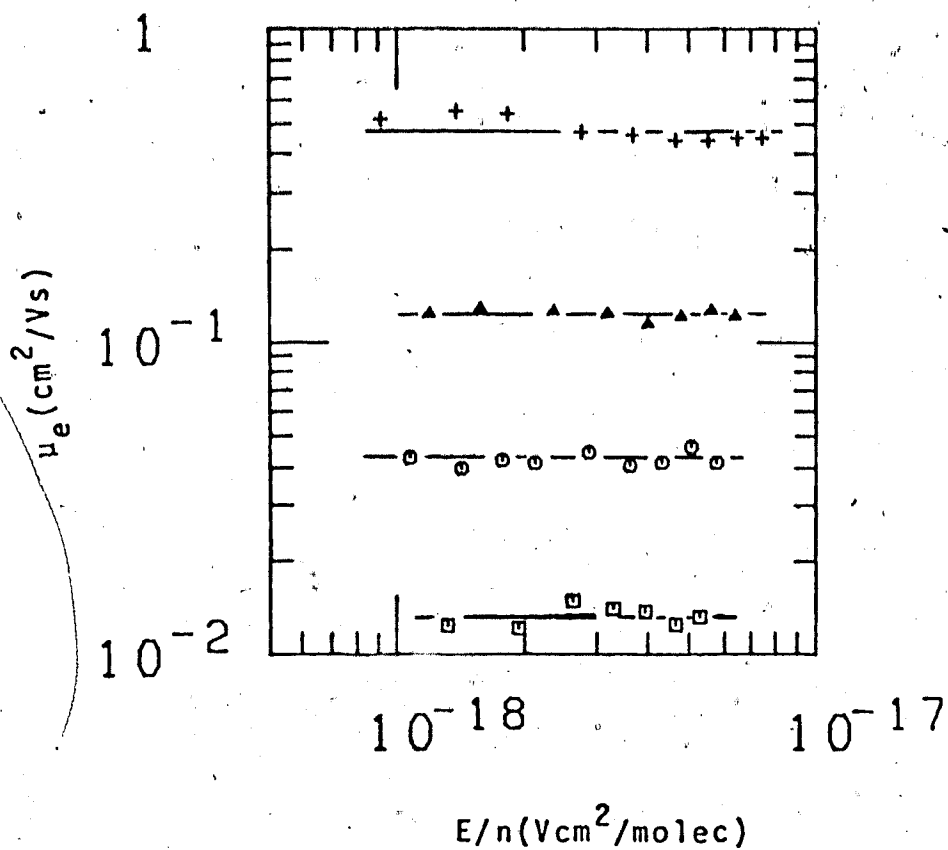


FIGURE III-67. Electron mobilities μ_e in liquid cyclopropane plotted against the density normalized electric field strength E/n . Densities and temperatures ($n/10^{21}$; T): \square (9.39, 254K), \circ (8.62, 297K), \triangle (7.79, 332K), $+$ (6.73, 367K).

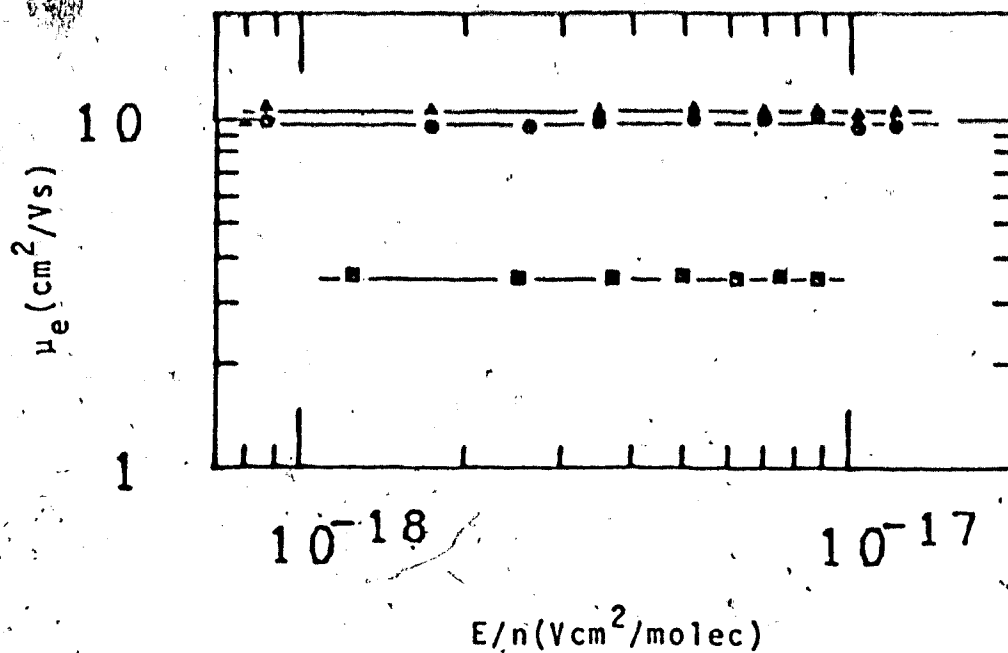


FIGURE III-68. Electron mobilities in liquid and supercritical cyclopropane as functions of E/n . Densities and temperatures ($n/10^{21}$, T): □ (4.97, 393K), ○ (3.55, 397.8K), Δ (3.55, 398.7K).

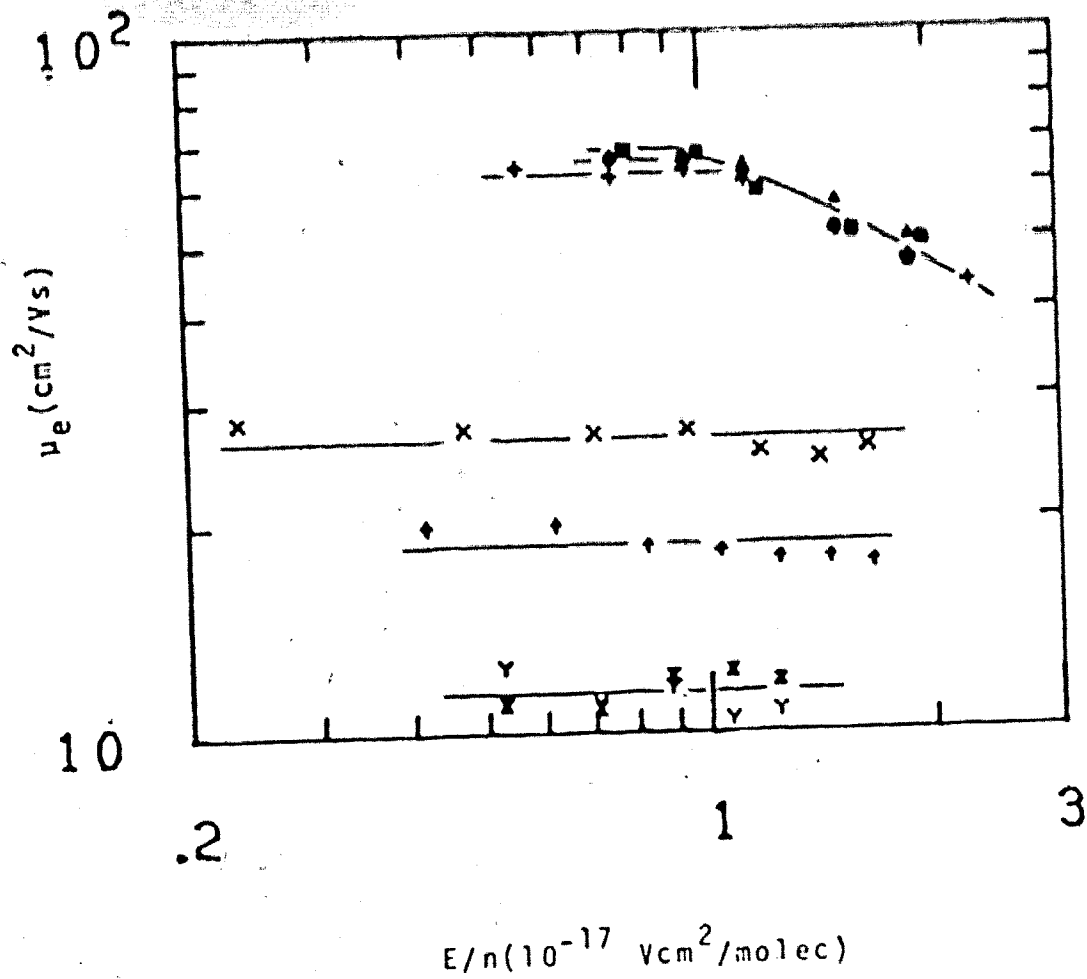


FIGURE III-69. Electron mobilities in supercritical and gaseous cyclopropane as functions of E/n . Densities and temperatures ($n/10^{21}$, T): z (3.55, 398.4K), Y (3.55, 397.8K), z (3.01, 397K), x (2.65, 395K), \square (1.57, 385K), + (1.64, 387K), \circ (1.64, 394K), Δ (1.64, 399K).

ent at the critical point. As previously noted, decreasing the density away from the critical density, increases the mobility. Figure III-69 also shows the temperature effect along the $n = 1.64 \times 10^{20}$ isochore. An increase of temperature leads to an increase in mobility. At high fields, the curves merge. The threshold field appears to decrease a bit as the temperature increases.

Figure III-70 gives mobilities measured in cyclopropane along the $n = 8.74 \times 10^{20}$ isochore and at $n = 8.30 \times 10^{20}$. The higher curve is drawn for $n = 8.30 \times 10^{20}$. Only a single curve is drawn for the isochore. Maximum spread in μ_0 along the isochore is less than 5%.

Figure III-71 shows the effect of decreasing the density from $n = 3.51 \times 10^{20}$ to $n = 1.76 \times 10^{20}$ as well as the effect of temperature along the $n = 3.51 \times 10^{20}$ isochore. From the left, the 2nd, 3rd, 4th, 6th, 7th, and eighth points contain a point from each of the four temperatures. The temperature effect is negligible. Further decrease of the density continues to increase the mobility. The mobility still has a negative field dependence. Of the other seven systems studied, ethene is the only other gas in which the mobility decreases at high fields, in the lower density fluids.

All the cyclopropane data were gathered using high pressure conductance cells. Data for Figures III-67 and III-68 required liquid type cells. The rest of

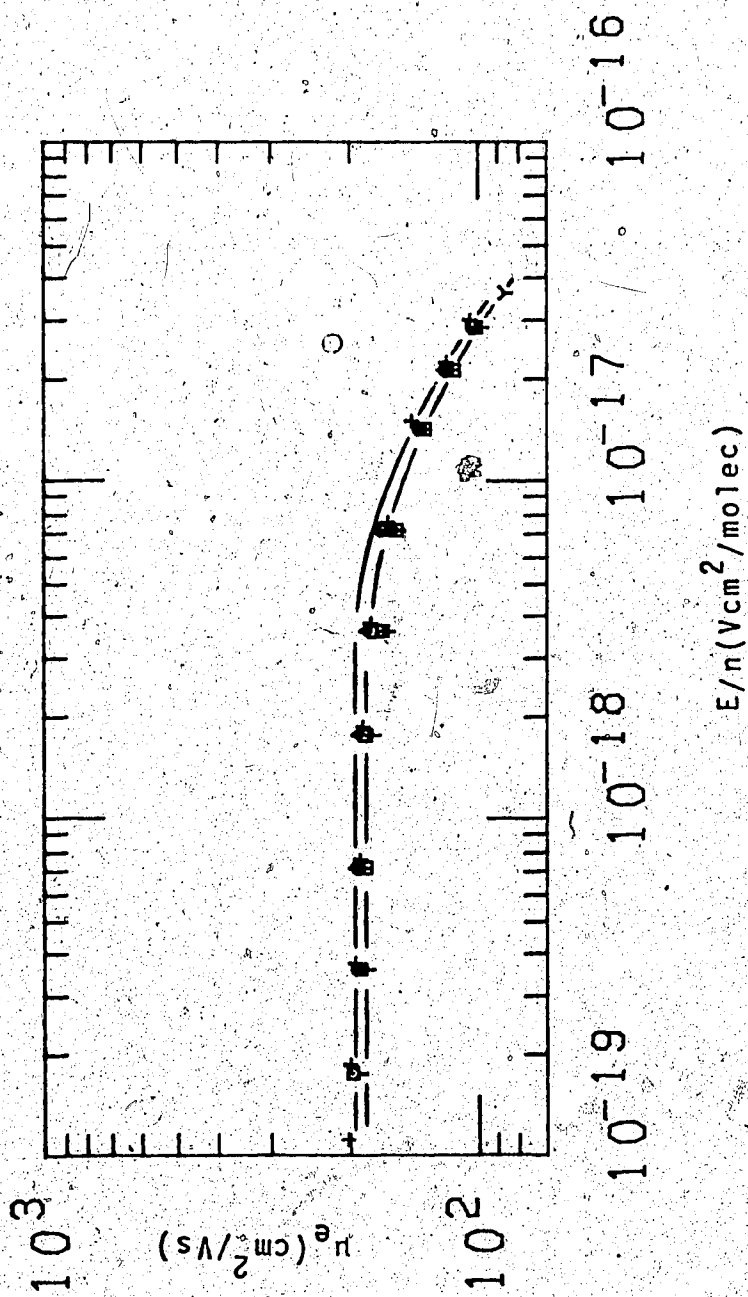


FIGURE III-70. Electron mobilities in gaseous cyclopropane as functions of E/n . Densities and temperatures ($n/10^{20}$, T): Δ (8.74, 405K), \circ (8.74, 395K), \square (8.74, 372K), γ (8.74, 360K), $+$ (8.30, 358K).

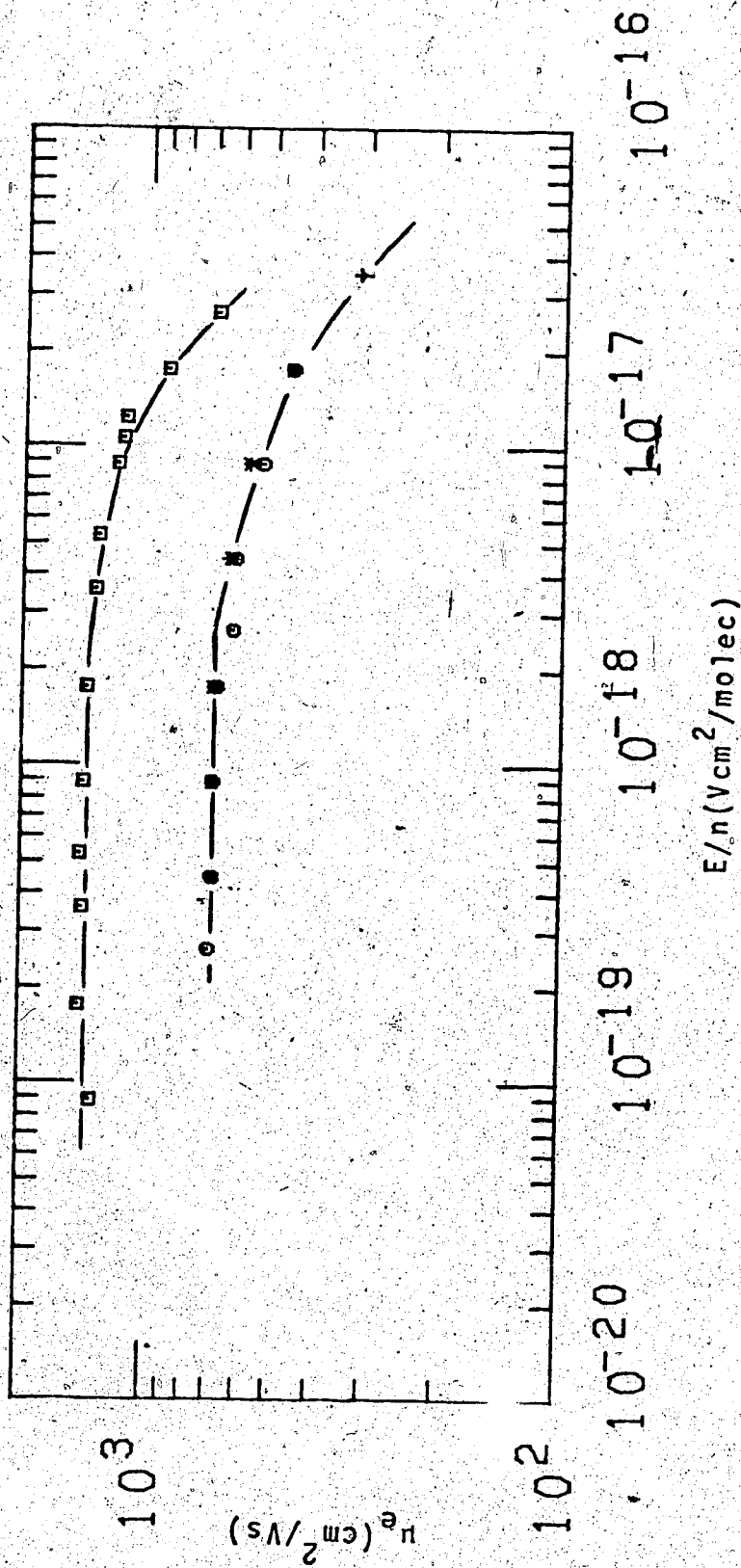


FIGURE III-71. Electron mobilities in gaseous cyclopropane as functions of E/n . Densities and temperatures ($n/10^{20}$, T): γ (3.51, 406K), Δ (3.51, 396K), Δ (3.51, 348K), \circ (3.51, 322K), \square (1.76, 296K):

205.

the data was collected using gas type cells.

TABLE III-8

Summary of Results for Cyclopropane^a

T °K	$10^{21} \frac{\text{molec}}{\text{cm}^3}$	μ_0 $\frac{\text{cm}^2}{\text{Vs}}$	$\mu_0 n$ $10^{20} \frac{\text{molec}}{\text{Vs cm}}$	(E/n) threshold ^c $10^{-18} \frac{\text{Vcm}^2}{\text{molec}}$	b
					$\frac{d \log \mu}{d \log E/n}$
254	9.39	0.013	0.012		
297	8.62	0.0423	0.0365		
332	7.79	0.123	0.0958		
367	6.73	0.466	0.314		
393	4.97	3.50	1.74		
397.8	3.55 ^d	9.73	3.45		
398.7	3.55 ^d	10.5	3.73		
398.4	3.55 ^d	11.6	4.12		
397.8	3.55 ^d	11.3	4.01		
397	3.01	18.5	5.56		
395	2.65	26.2	6.96		
385	1.57	67.3	10.6	9.3	minus
387	1.64	62.4	10.3		minus
394	1.64	64.4	10.6		minus
399	1.64	65.0	10.7	11	minus
405	0.874	192	16.8	3.7	-0.27
395	0.874	189	16.5	3.7	-0.27
372	0.874	188	16.4	3.7	-0.27
360	0.874	183	16.0	3.7	-0.27
358	0.830	194	16.1	3.7	-0.28
406	0.351	688	24.1	2.4	-0.24
396	0.351	688	24.1	2.4	-0.24
348	0.351	688	24.1	2.4	-0.24
322	0.351	686	24.1	2.4	-0.24
296	0.176	1390	24.6	2.2	-0.25

(continued.....)

Footnotes to Table III-8

- a Data appear in the same order as in the figures.
- b Estimated at $E/n = 4(E/n)_{\text{threshold}}$
- c Too low field strength to allow determination in the liquid phase or in the dense gas near the critical point.
- d $n_c = 3.55 \times 10^{21} \text{ molec/cm}^3$. $T_c = 398\text{K}$.

B. Ion Mobilities

In this section ion mobilities of the eight compounds are plotted against the density normalized field strength E/n . The ions are the slowest charge carriers in the systems and correspond to the positive ions. The exact identity of the ions is not known, though they are likely polymeric. Each compound is presented in a separate subsection. A table summarizing the results is included at the end of each subsection.

In all the ion plots, no field effect was found. The highest field strength used was typically 10^{-18} to 10^{-17} $\text{Vcm}^2/\text{molec}$. The absence of a field dependence is not totally unexpected. Recent work on alkali ion mobility in rare gases and in simple molecular gases (e.g. CO_2), as well as known ions in the parent fluid (e.g. NO_2^+ in NO_2) indicate that the field dependence occurs at fields in excess of 10^{-16} $\text{Vcm}^2/\text{molec}$. In all these cases, the ion mobility increases at $(E/n) > (E/n)_{\text{threshold}}$, which is characteristic of a heating effect (38,171,172). The threshold for hydrocarbons is likely intermediate between that in the rare gases and that in the polar molecular fluids, that is, $\sim 5 \times 10^{-16}$.

Throughout this section, the mobilities μ will be given in cm^2/Vs , the densities n , in molec/cm^3 , and the density normalized field strengths E/n , in $\text{Vcm}^2/\text{molec}$.

1. Methane

Data for methane are contained in Figures III-72 to III-77. Measurements were made along the coexistence curve in both the liquid and gas phases. Measurements were also made of the variation of mobility with temperature at the critical density and in the dilute gas (1.2% of the critical density).

From Figures III-72 and III-73, ion mobilities in liquid methane are seen to increase monotonically with the density. The low field mobility increases by a factor of 6.1 when the density and temperature are varied

Figure III-74 gives ion mobilities at densities at and near the critical point. Increasing the temperature at the critical density leads to an increase in the mobility. Decreasing the density along the coexistence curve also leads to an increase in mobility. The mobility in this range increases by a factor of 2.7 while the density has decreased by a factor of 3.6.

Figure III-75 shows the effect of a further decrease in density. In this range, the mobility increases in inverse proportion to the density decrease.

In Figure III-76, the effect of temperature on the 7.13×10^{19} isochore is seen. Increasing the temperature along the constant density line leads to an increase in the mobility. At the high temperature end of the curve,

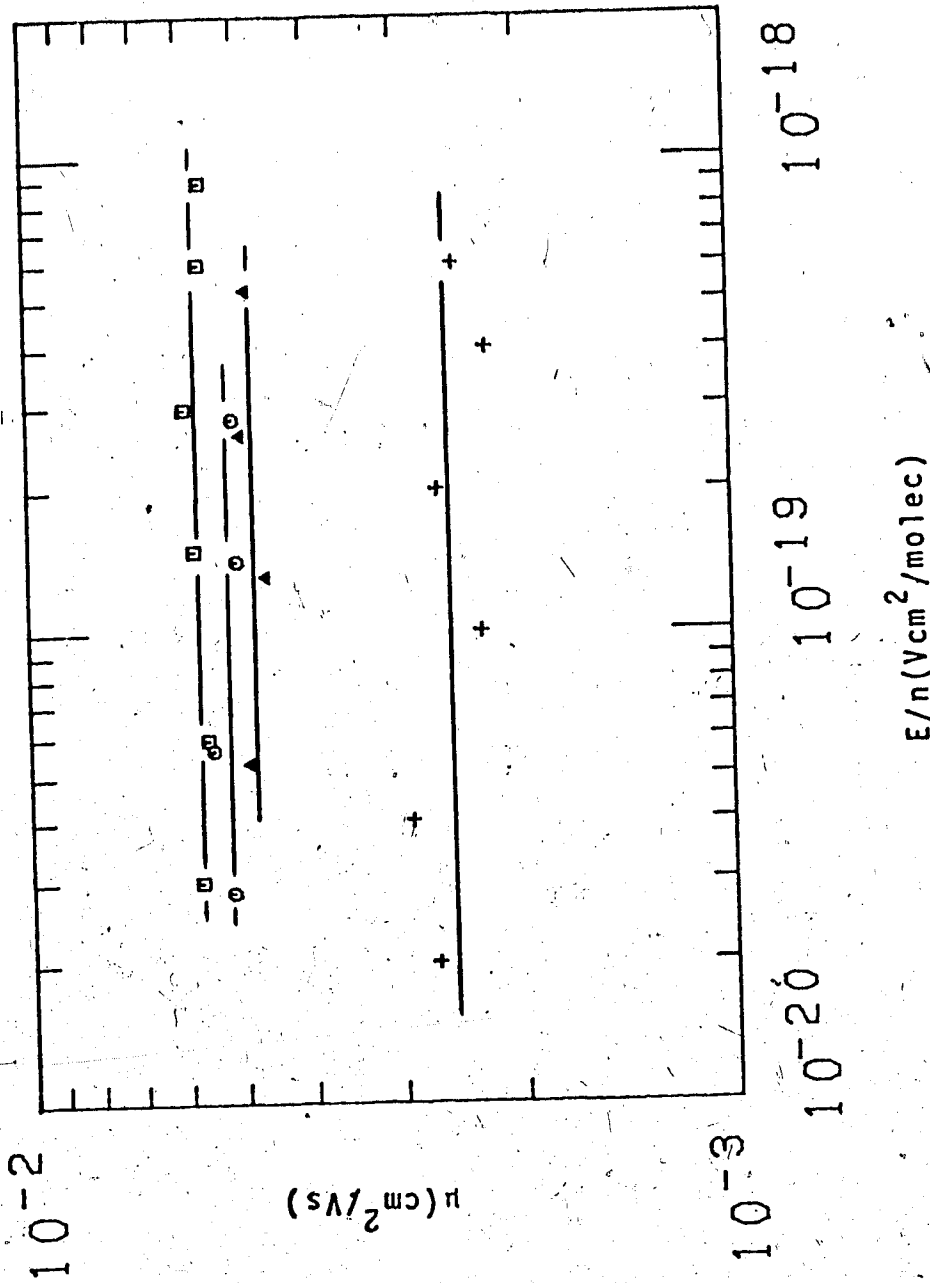


FIGURE III-72. Ion mobilities μ in liquid methane as functions of the density normalized electric field strength E/n . Densities and temperatures ($n/10^{21}$ molec/cm³, T): + (15.5, 122K), Δ (11.8, 170K), \circ (11.0, 176K), \square (10.4, 180K).

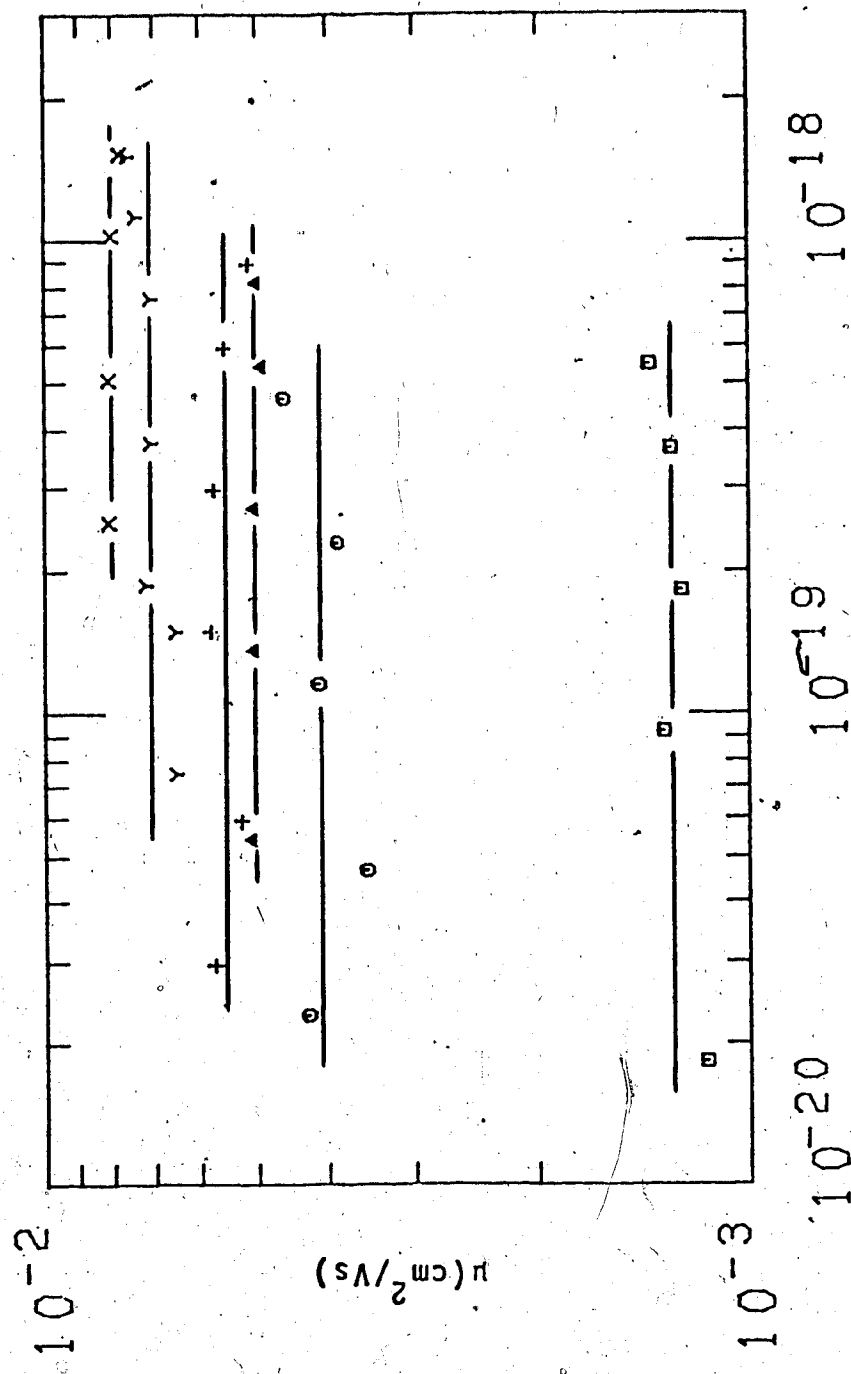


FIGURE III-73. Ion mobilities in liquid and supercritical methane as functions of E/n . Densities and temperatures ($n/10^{21}$ molec/ cm^3 , T): \square (17.0, 91K), \circ (13.4, 153K), Δ (11.4, 173K), $+$ (10.5, 179K), \times (8.26, 189K), \times (6.8, 195K).

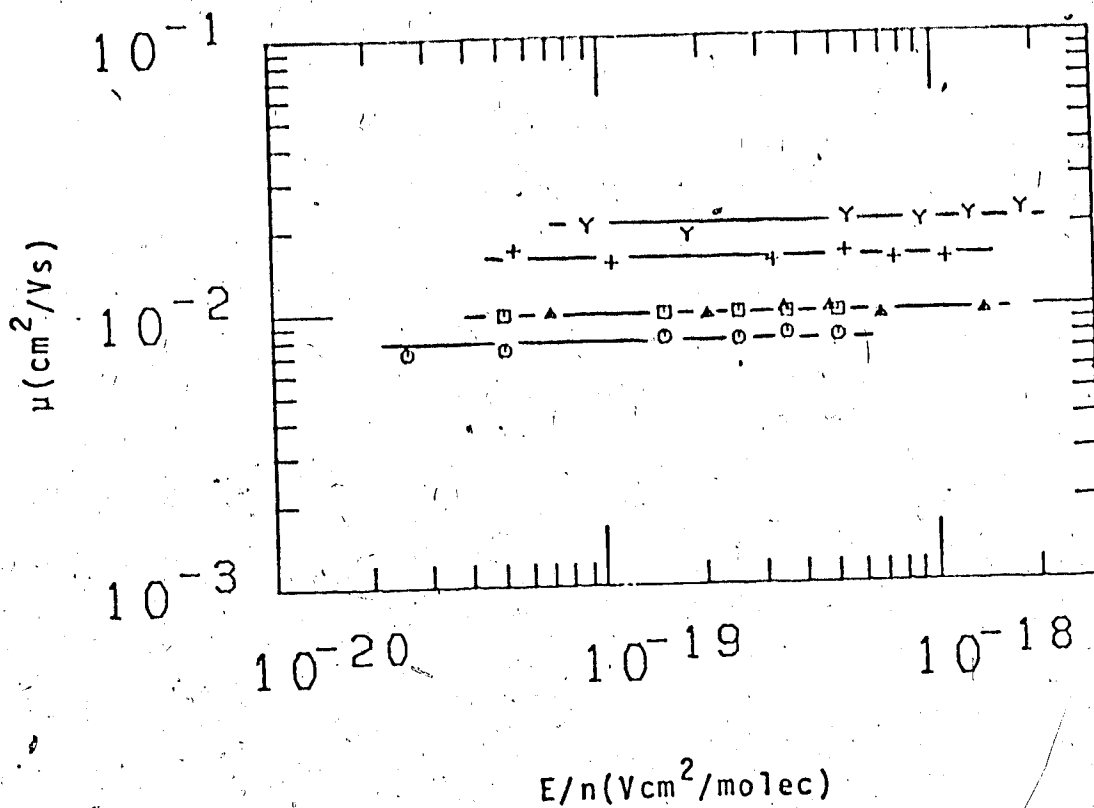


FIGURE III-74. Ion mobilities in gaseous and super-critical methane as functions of E/n . Densities and temperatures ($n/10^{21}$ molec/cm³, T): □ (6.1, 195K), ○ (6.1, 192K), Δ (4.47, 190K), + (2.87, 184K), Y (1.71, 173K).

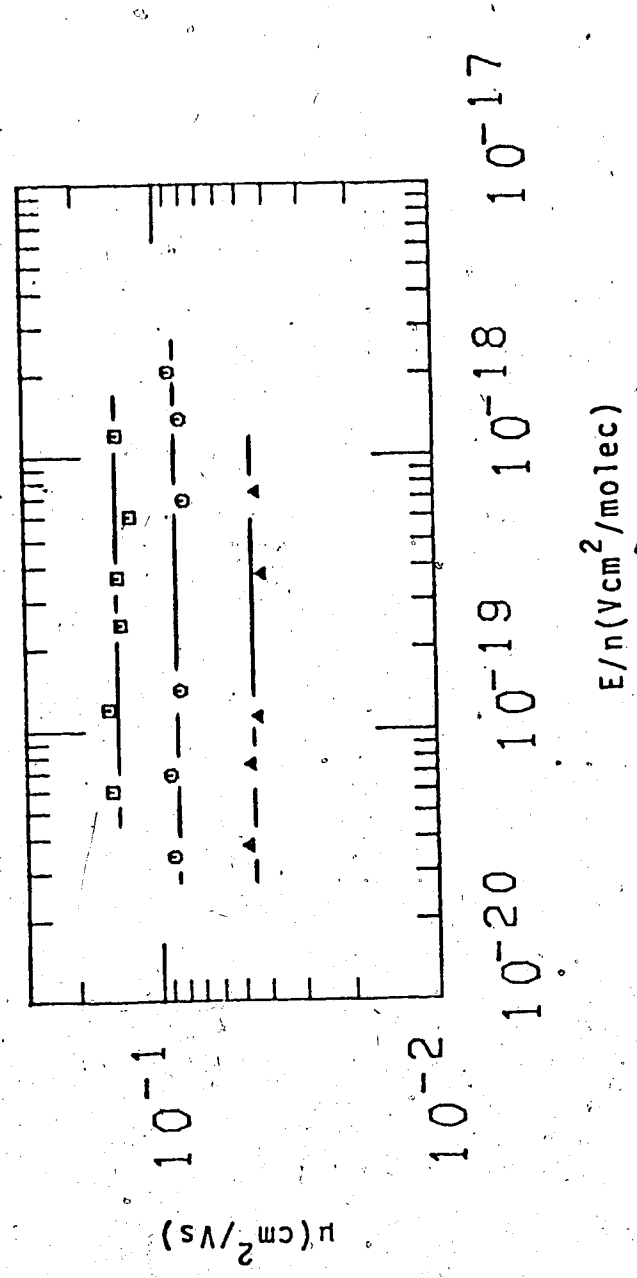


FIGURE III-75. Ion mobilities in gaseous methane as functions of E/n .
Densities and temperatures ($n/10^{20}$ molec/cm³, T): Δ (8.64, 158K), \square (4.66, 144K), \circ (2.67, 133K).

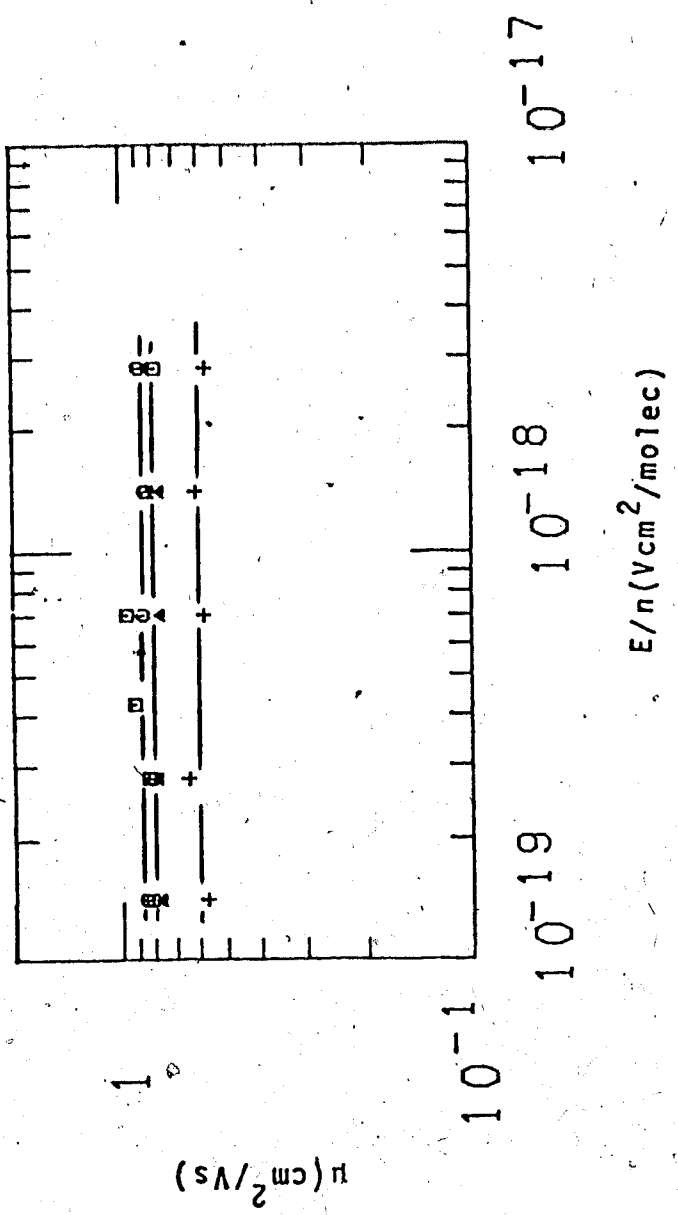


FIGURE III-76. Ion mobilities in gaseous methane as functions of E/n .
 $n = 7.13 \times 10^{19} \text{ molec/cm}^3$. Temperatures: \square (297K), \circ (243K),
 Δ (163K), $+$ (117K).

the mobilities appear to be levelling off.

In Figure III-77, the effect of a further variation of density along the coexistence curve is shown. The trends observed in Figure III-75 are continued. The mobility varies inversely with the density.

Measurements of the ion mobilities were all made in high pressure conductance cells except data contained in Figures III-76 and III-77 for which low pressure cells were used. For data in Figures III-72 and III-73 liquid type cells were used. For all other data gas type cells were used. The results for methane are summarized in Table III-9.

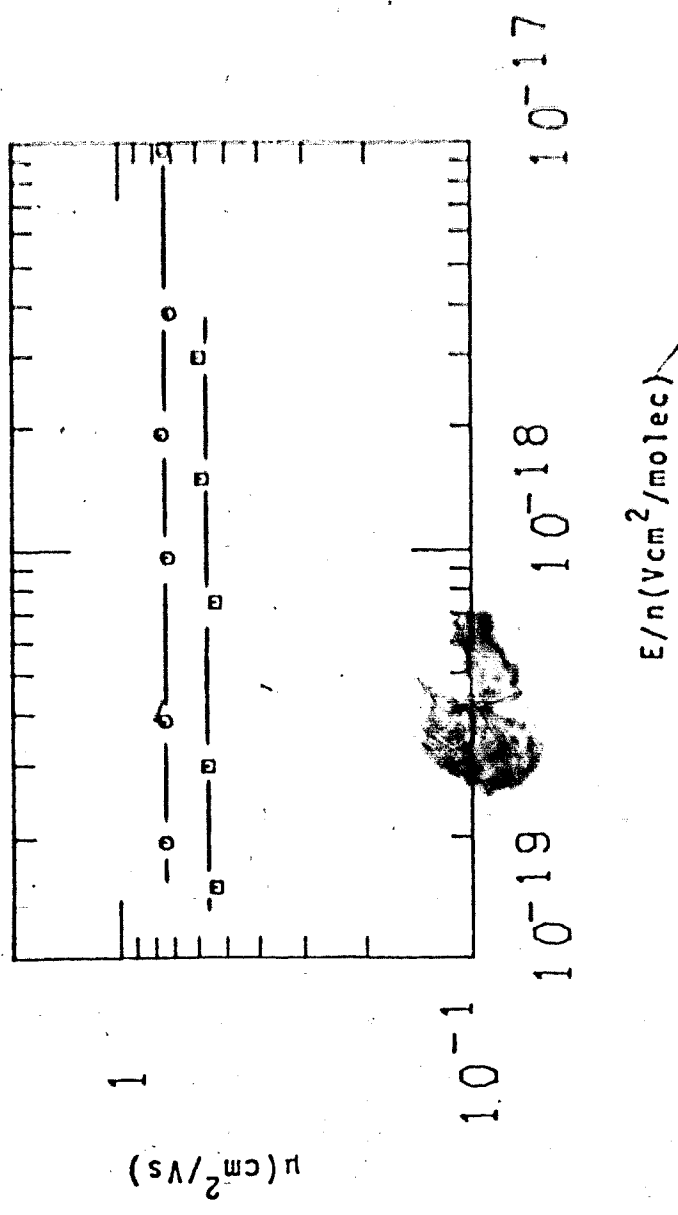


FIGURE III-77. Ion mobilities in gaseous methane as functions of E/n .
 Densities and temperatures ($n/10^{19}$ molec/cm³, T): □ (6.76, 102K),
 O (5.26, 108K).

TABLE III-9

Summary of Ion Results for Methane^a

T °K	n $10^{21} \frac{\text{molec}}{\text{cm}^3}$	μ_+ $10^{-3} \frac{\text{cm}^2}{\text{Vs}}$	$\mu_+ n$ $10^{19} \frac{\text{molec}}{\text{cmVs}}$
122	15.5	2.53	3.92
170	11.8	4.81	5.68
176	11.0	5.22	5.74
180	10.4	5.73	5.96
91	17.0	1.29	2.19
153	13.4	4.06	5.44
173	11.4	5.02	5.72
179	10.5	5.55	5.83
189	8.26	7.04	5.82
195	6.1 ^b	8.01	4.89
195	6.1 ^b	9.82	5.99
192	6.1 ^b	7.84	4.78
190	4.47	9.82	4.39
184	2.87	15.6	4.48
173	1.71	20.8	3.56
158	0.864	44.5	3.84
144	0.466	85.4	3.98
133	0.267	140	3.74
297	0.0713	861	6.14
243	0.0713	850	6.06
163	0.0713	792	5.65
177	0.0713	595	4.24
112	0.0676	559	3.78
108	0.0526	740	3.89

^a Order of appearance of data is the same as in the figures

^b $n_c = 6.1 \times 10^{21}$. $T_c = 191\text{K}$.

2. Ethane

Measurements have been made along the liquid-gas coexistence curve in both the liquid and the gas phases. Measurements were also made of the mobilities as functions of temperature along the critical, $n = 4.06 \times 10^{21}$ isochore and along the $n = 6.77 \times 10^{19}$ isochore. The results for ethane are contained in Figures III-78 to III-83.

Data in liquid phase ethane are contained in Figures III-78 and III-79. A high pressure, liquid type conductance cell was used for the measurements. As the system moves from the cold liquid towards the critical point, the mobility increases. Above the critical point, increasing the temperature leads to a further increase in mobility.

Figure III-80 shows the mobilities about the critical region in the gas phase. Once more, the temperature effect on the critical isochore can be seen. As well, moving the system away from the critical region along the coexistence curve also leads to an increase in the ion mobility in the gas phase. As the system continues to move along the coexistence curve (Figure III-81) the same trends as observed for the ions in methane (as well as the electrons in section III A) hold: the mobility increases steadily with the decrease in density. Data for the two figures were obtained in high pressure

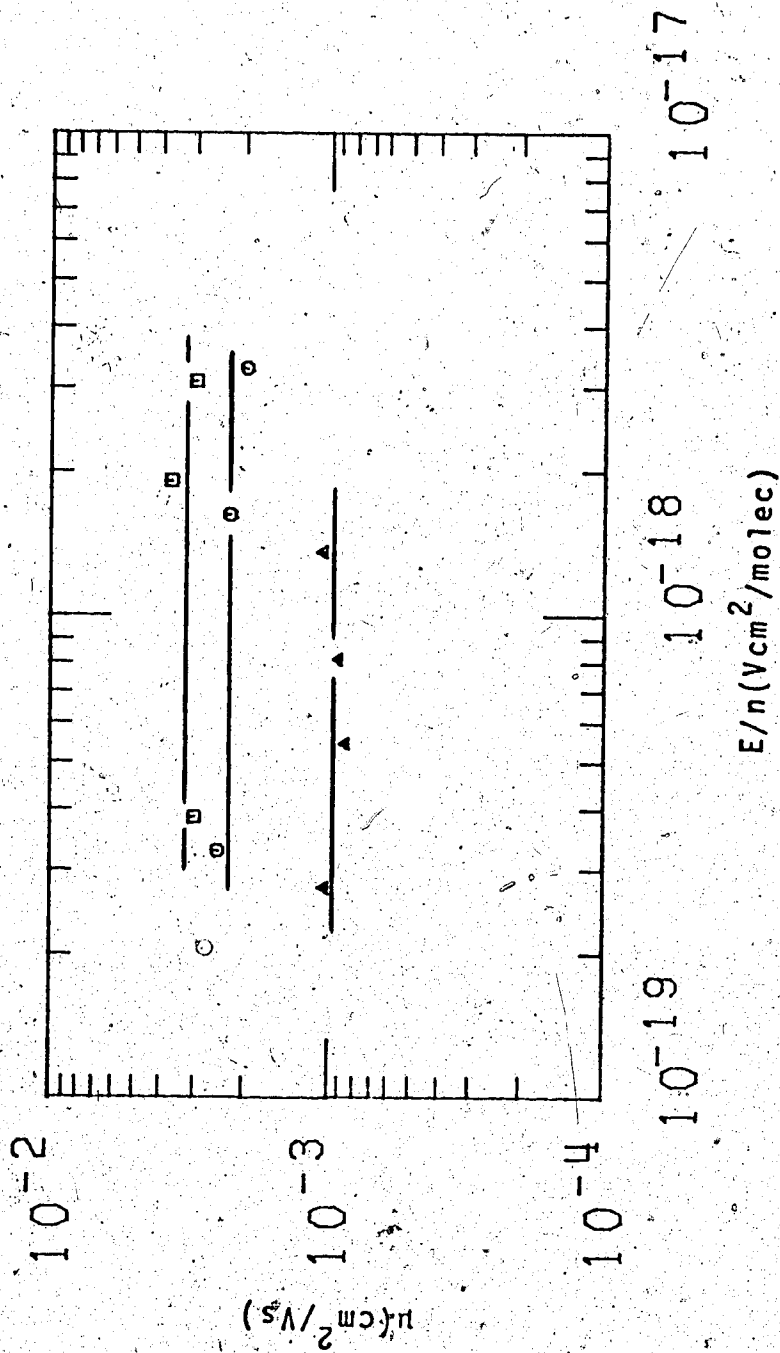


FIGURE III-78. Ion Mobilities μ in liquid ethane as functions of the density normalized electric field strength E/n . Densities and temperatures ($n/10^{21}$ molec/cm³, T): Δ (11.4, 166K), \circ (9.57, 242K), \square (8.09, 281K).

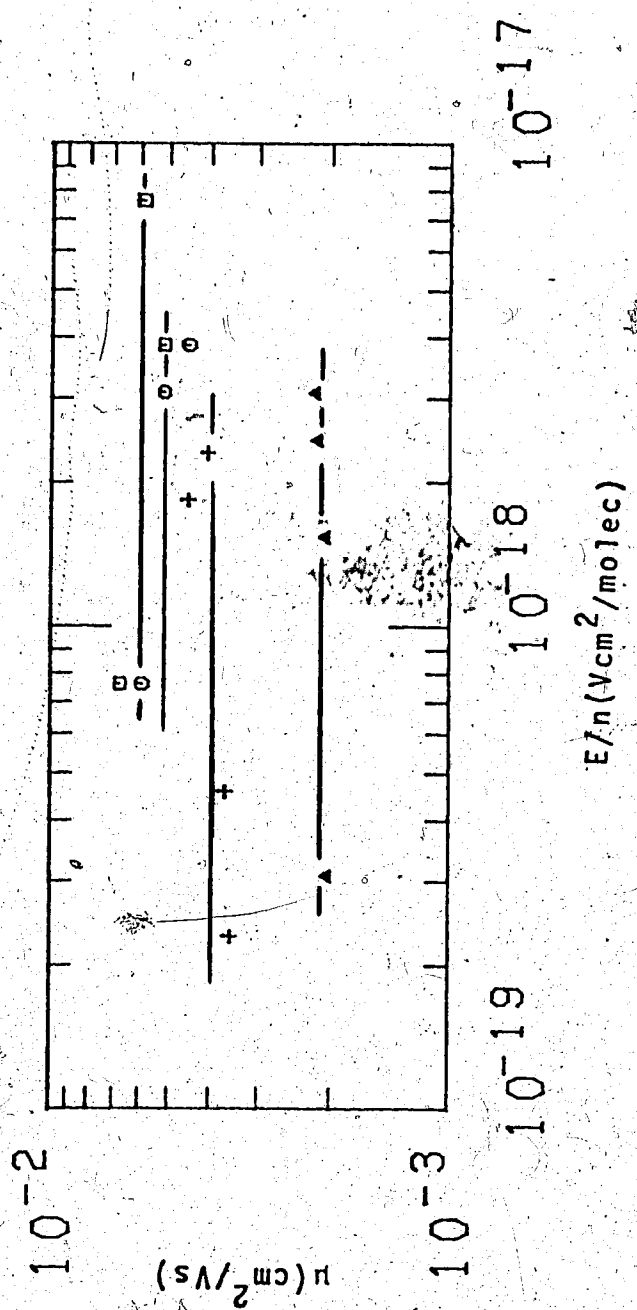


FIGURE III-79. Ion mobilities in liquid and gaseous ethane as functions of E/n . Δ Densities and temperatures ($n/10^{21}$ molec/cm³, T): Δ (10.1, 224K), + (6.77, 298K), \circ (4.06, 306K), \square (4.06, 309K).

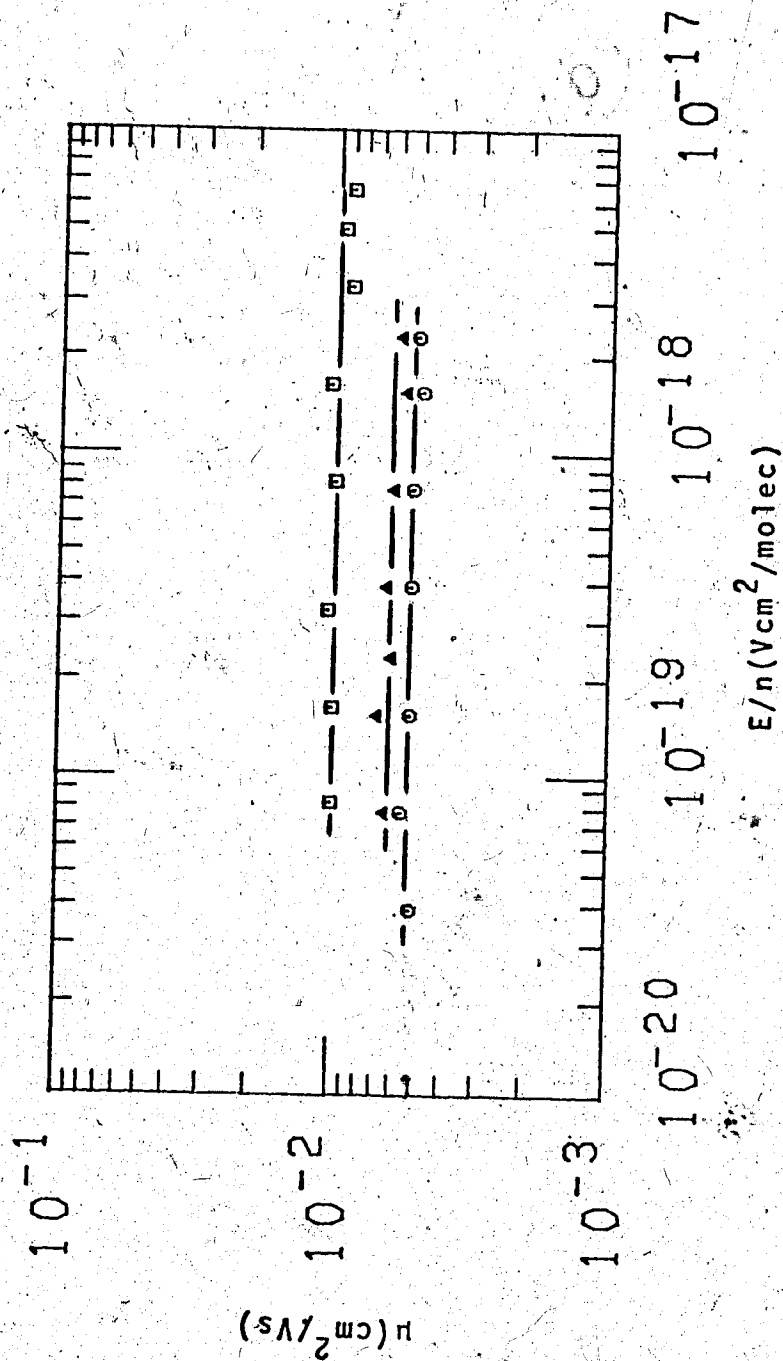


FIGURE III-80. Ion mobilities in gaseous and supercritical ethane as functions of E/n . Densities and temperatures ($n/10^{21}$ molec/cm³, T): Δ (4.06, 308K), O (4.06, 306K), □ (1.90, 296K).

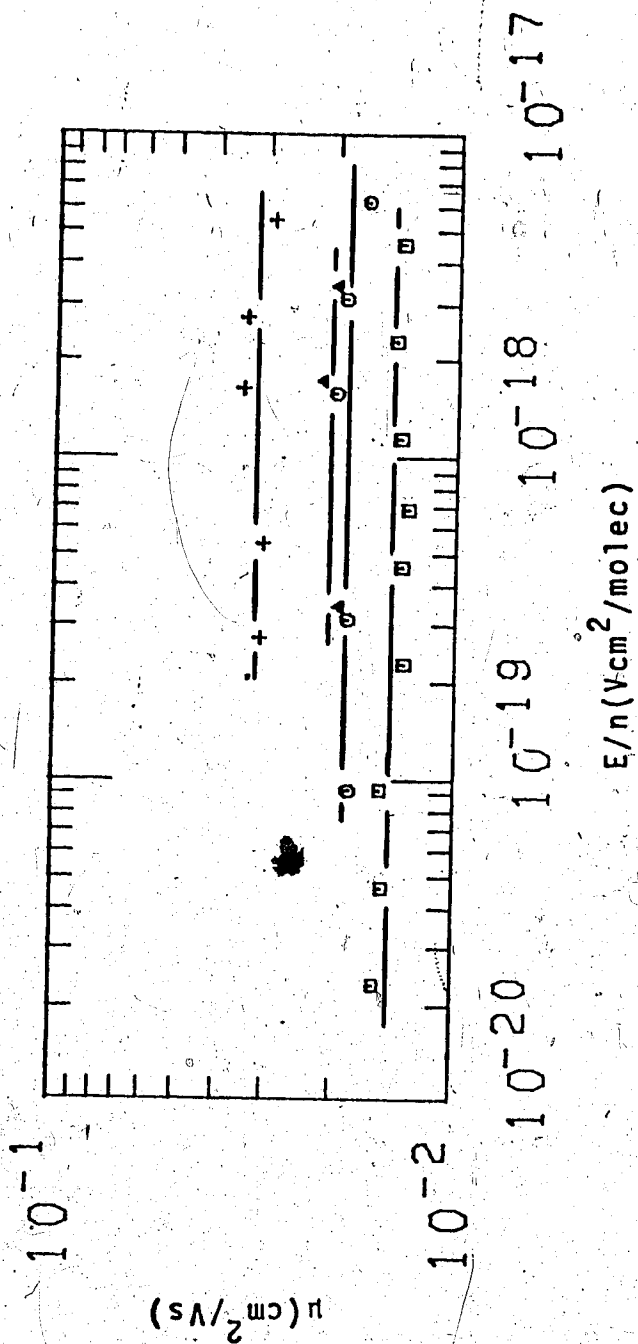


FIGURE III-81. Ion mobilities in gaseous ethane as functions of E/n .
 (Densities and temperatures ($n/10^{21}$, T): \square (1.36, 286K), \circ (1.02, 276K), Δ (0.910, 272K), + (0.571, 256K)).

gas type conductance cells.

In Figure III-82, the temperature effect on the dilute gas is seen. Increasing the temperature from 203K to 326K leads to a continuous increase in the ion mobility. Figure III-83 contains the lowest temperature examined along the isochore (197K). Decreasing the density to 6.21×10^{19} gives another increase in mobility. Data for these two figures were obtained in low pressure gas type conductance cells.

Results of these figures of the ion mobilities in ethane are summarized in Table III-10.

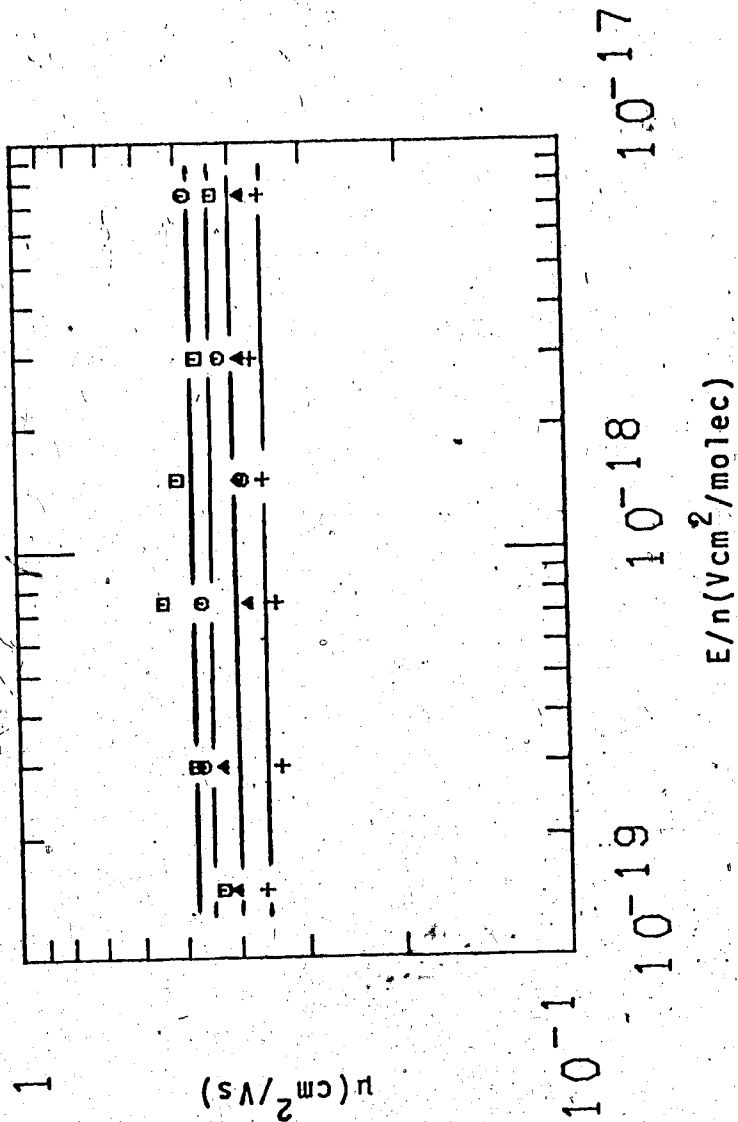


FIGURE III-82. Ion mobilities in gaseous ethane as functions of E/n .

$n = 6.77 \times 10^{19}$ molec/cm³. Temperatures: \square (326K), \circ (294K),

Δ (203K), + (203K).

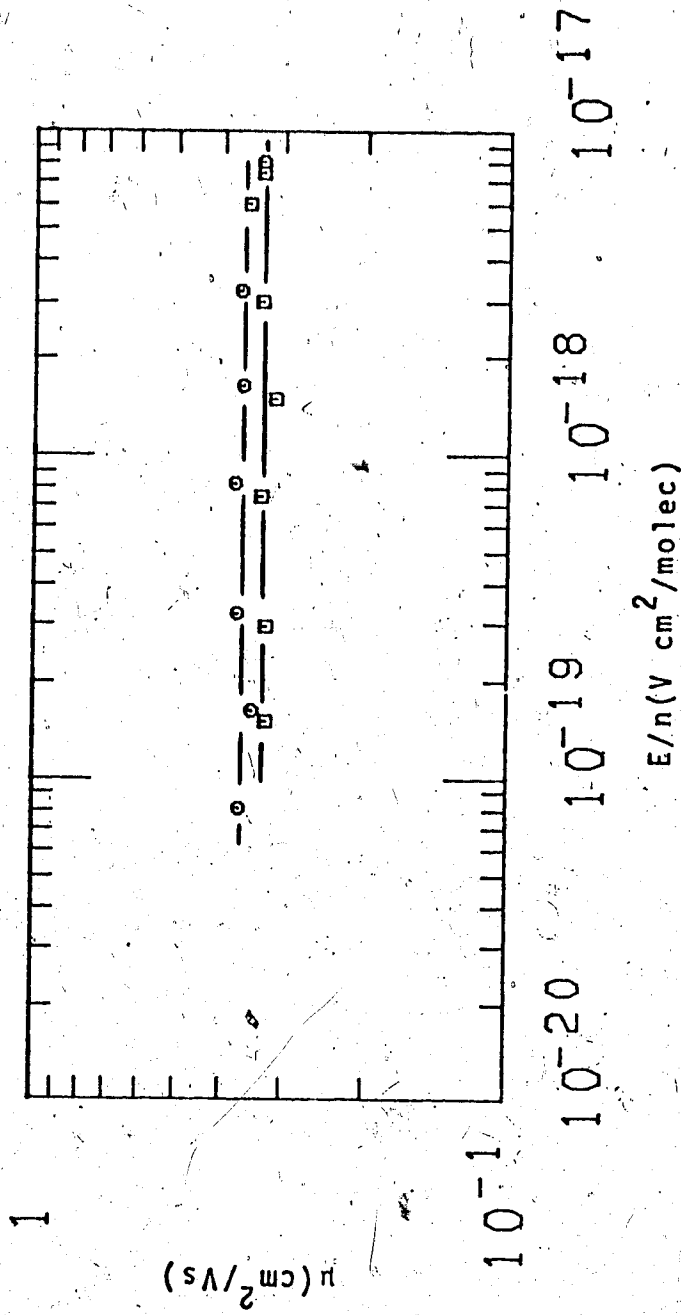


FIGURE III-83. Ion mobilities in gaseous ethane as functions of E/n .
 Densities and temperatures ($n/10^{19}$ molec/cm³, T): □ (6.77, 197K),
 ○ (6.21, 193K).

TABLE III-10

Summary of Ion Results for Ethane^a

T °K	n $10^{20} \frac{\text{molec}}{\text{cm}^3}$	μ_+ $10^{-3} \frac{\text{cm}^2}{\text{Vs}}$	$\mu_+ n$ $10^{19} \frac{\text{molec}}{\text{Vscm}}$
166	114	0.943	1.08
242	95.7	2.21	2.11
281	80.9	3.22	2.60
224	101	2.08	2.10
298	67.7	3.91	2.65
306 ^b	40.6	5.12	2.08
309 ^b	40.6	5.88	2.39
308 ^b	40.6	6.22	2.53
306 ^b	40.6	5.27	2.14
296	19.0	9.91	1.88
286	13.6	14.3	1.94
276	10.2	18.7	1.91
272	9.10	20.5	1.87
256	5.71	31.9	1.82
326	0.677	478	3.24
294	0.677	444	3.01
221	0.677	399	2.70
203	0.677	353	2.39
197	0.677	328	2.22
193	0.621	360	2.24

^a Order of appearance of data is the same as order of appearance of figures.

^b $n_c = 4.06 \times 10^{21}$. $T_c = 306\text{K}$.

3. Propane

Measurements have been made in propane in both the gas and the liquid phases along the gas-liquid coexistence curve, and as functions of temperature for a series of densities in the gas phase. Ion mobilities for propane are contained in Figures III-84 to III-93.

Ion mobilities in liquid propane are shown in Figures III-84 and III-85. The measurements were made in high pressure liquid type conductance cells. The mobility increases smoothly as the system moves from the cold liquid towards the critical point. Decreasing the density by a factor of 3.0 leads to an increase of mobility by a factor of 12. Unlike the gas, in the liquid phase, a considerable portion of the effect seems related to the change in temperature. At the critical region, increasing the temperature leads to an increase in mobility.

Figure III-86 displays mobilities in the critical region and in the gas phase just below the critical density. These results were obtained in high pressure gas type cells as was the data for the remaining portion of this section. The exceptions are Figures III-92 and III-93 for which low pressure gas type cells were used. The two effects, that of density and that of temperature are the same as previously noted for methane and for ethane.

As the system moves away from the critical region along the coexistence curve, the mobility increases as

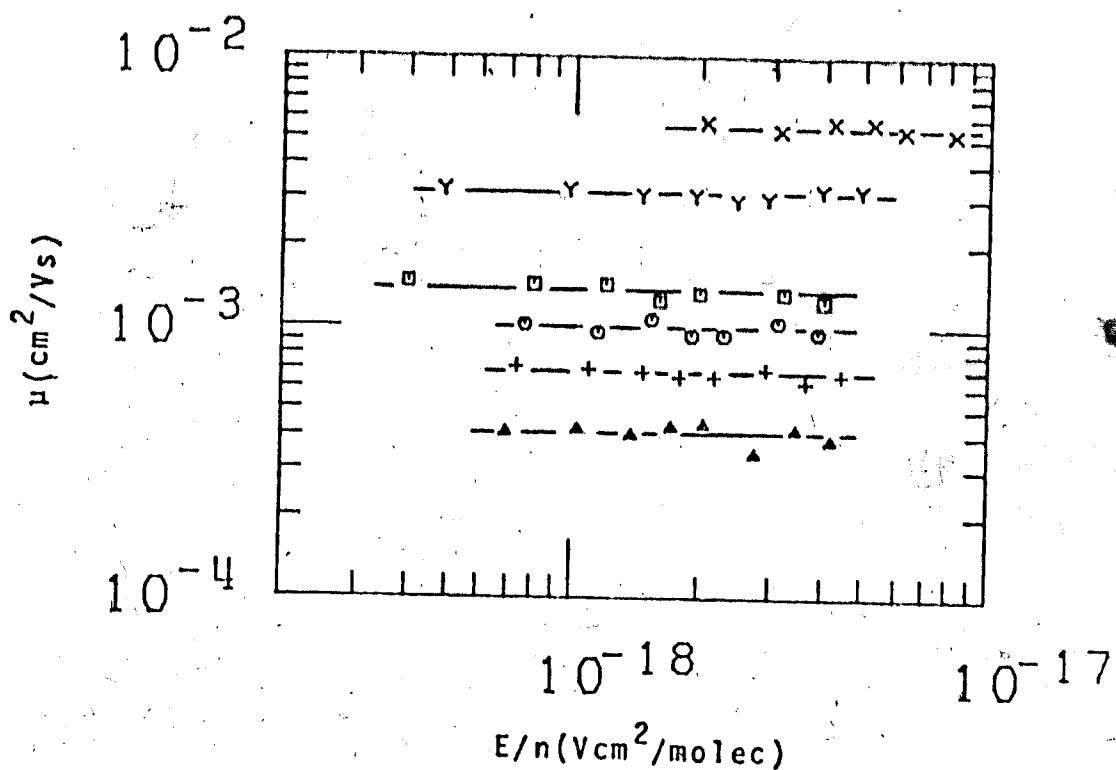


FIGURE III-84. Ion mobilities μ in liquid and supercritical propane plotted against the density normalized electric field strength E/n . Densities and temperatures ($n/10^{21}$ molec/cm³, T): Δ (8.96, 169K), + (8.48, 197K), O (8.05, 224K), \square (7.73, 243K), Y (6.35, 315K), X (3.00, 371K).

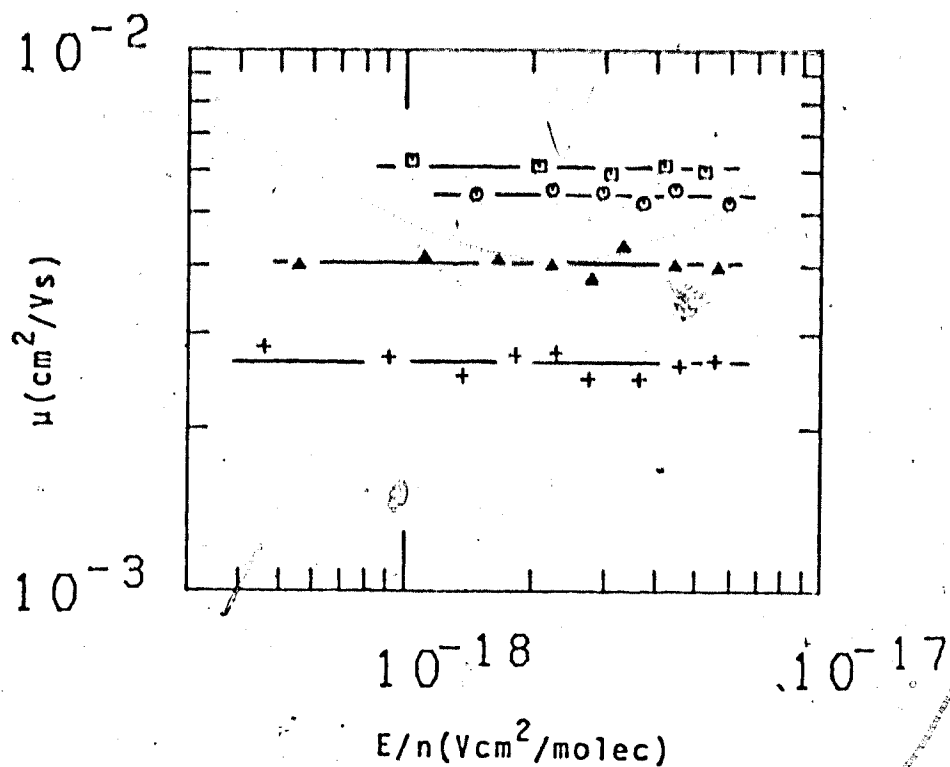


FIGURE III-85. Ion mobilities in liquid and supercritical propane plotted against the density normalized electric field strength E/n . Densities and temperatures ($n/10^{21}$ molec/cm³, T): + (6.76, 298K), Δ (5.57, 340K), \circ (4.17, 365K), \square (3.00, 373K).

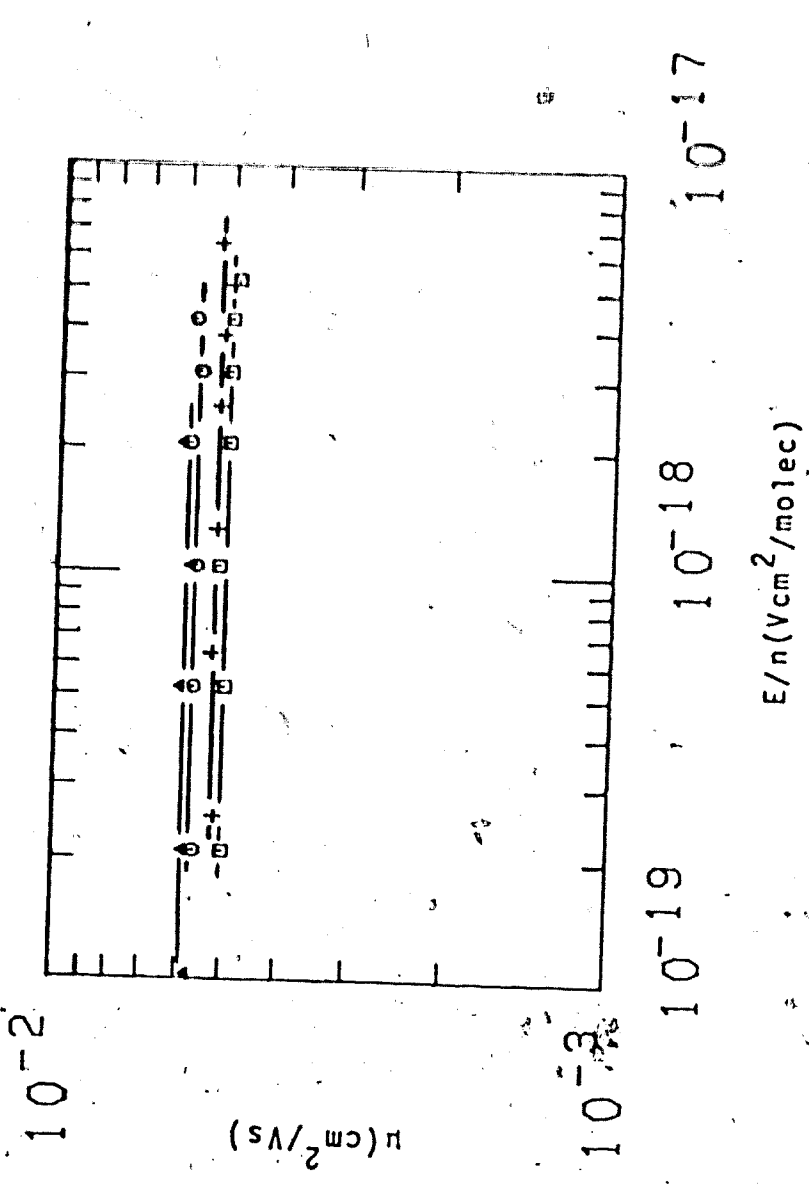


FIGURE III-86. Ion mobility in gaseous and supercritical propane as functions of E/n . Densities and temperatures ($n/10^{21}$ molec/ cm^3 , T): Δ (3.00, 377K), \square (3.00, 370K), \circ (3.00, 369K).

the density decreases. This is shown by Figures III-86, III-87, III-89, III-91 and III-93. When the system moves from the critical region (Figure III-86) to $T = 360\text{K}$ (Figure III-87), the density changes by a factor of 2.2, while the temperature only changes by about 3%. The sharp increase in mobility reflects the density variation. Over the entire density range outside the critical region, the mobility varies inversely to the density.

The other figures give the effect of temperature on fixed density lines. The isochores are of $0.50 n_c$ (Figure III-83), $0.25 n_c$ (Figure III-89), $0.11 n_c$ (Figure III-90), and of $0.022 n_c$ (Figure III-92). In all these cases, the effect of increasing the temperature along an isochore is to increase the mobility. The increase however depends on the temperature difference away from the coexistence curve. This is most clear in the most dilute ($0.022 n_c$) isochore. The ion mobility rises sharply near the coexistence curve, but then levels off. There is no variation in ion mobility as the temperature is raised from 345K to 394K. A single curve is drawn through the points of both temperatures.

Data for propane is summarized in Table III-11.

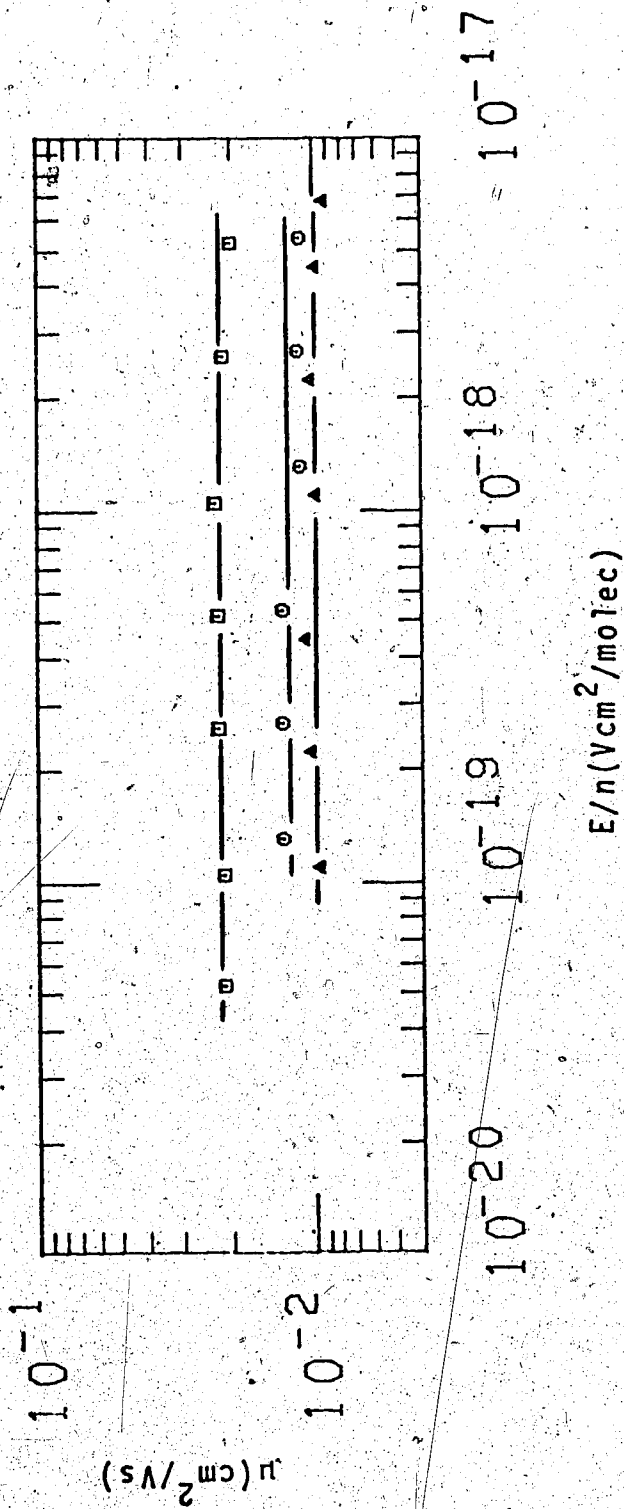


FIGURE III-87. Ion mobilities in gaseous propane as function of E/n .
 Densities and temperatures ($n/10^{21}$ molec/cm³, T): Δ (1.39, 360K),
 \circ (1.16, 354K), \square (0.593, 328K).

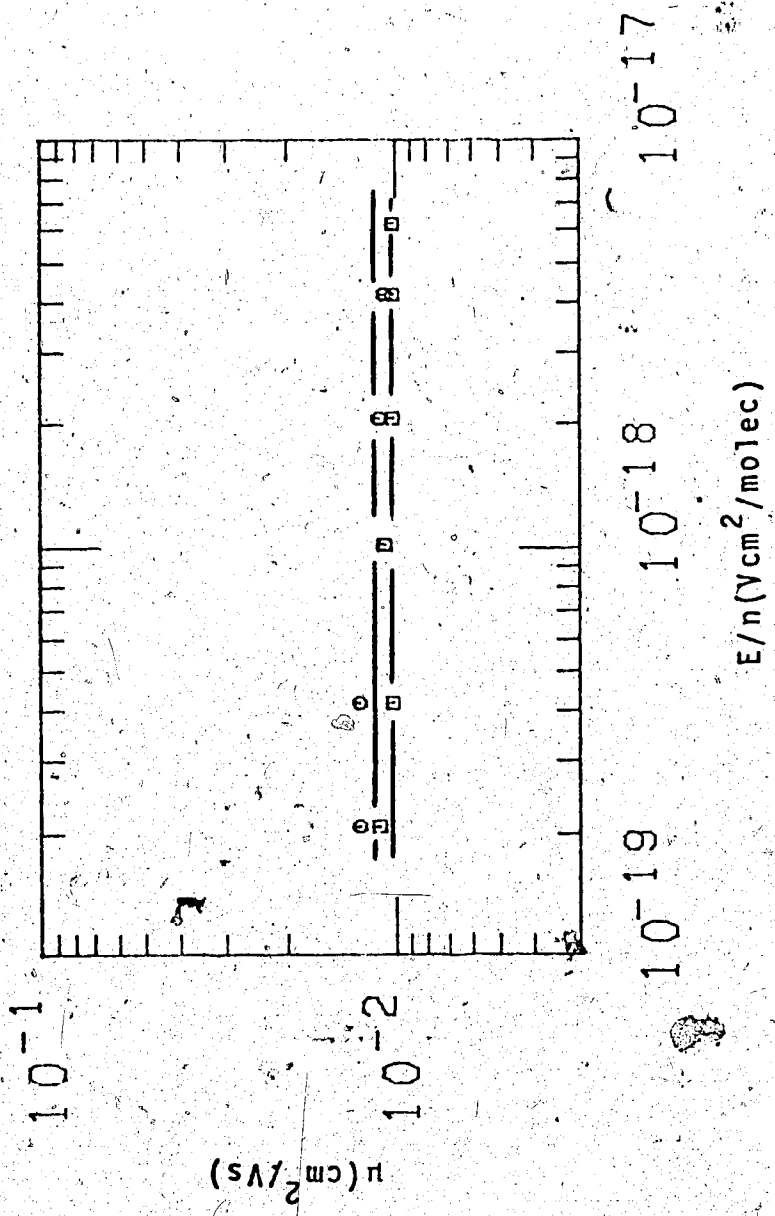


FIGURE III-88. Ion mobilities in gaseous propane as functions of E/n .
 ρ $n = 1.50 \times 10^{21}$ molec/cm³. Temperatures: \square (372K), \circ (385K).

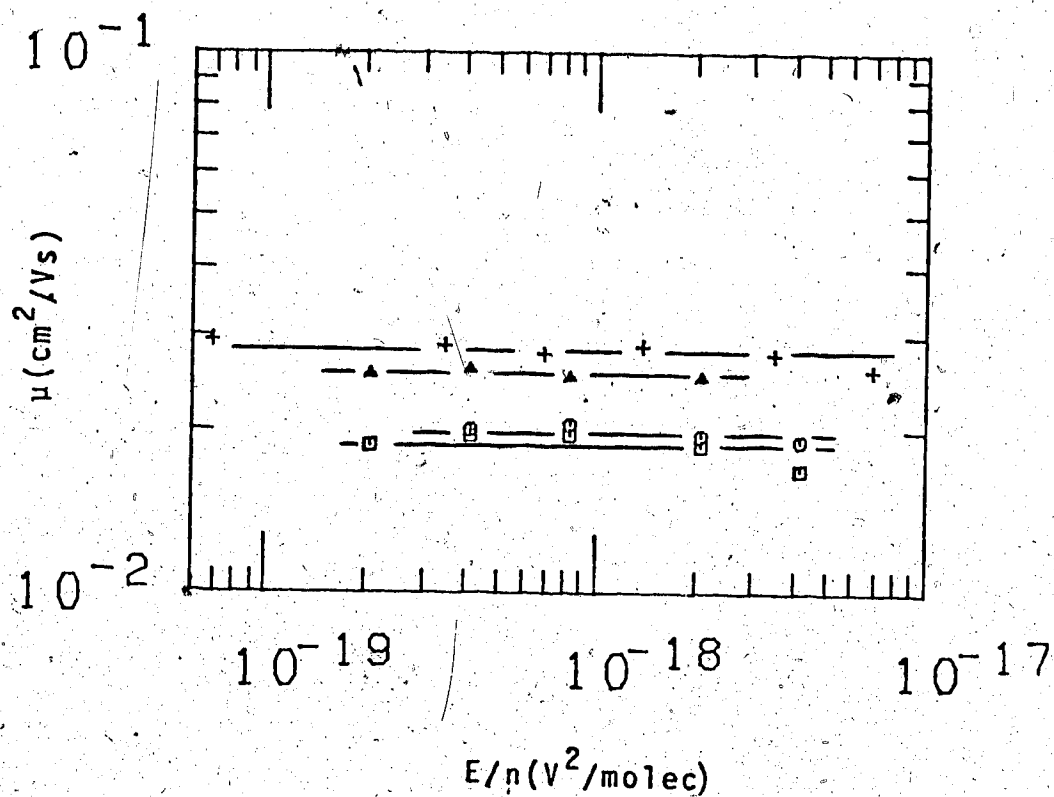


FIGURE III-89. Ion mobilities in gaseous propane as functions of E/n . Densities and temperatures ($n/10^{20}$, T): + (4.50, 317K), \square (7.51, 338K), \circ (7.51, 346K), Δ (7.51, 383K).

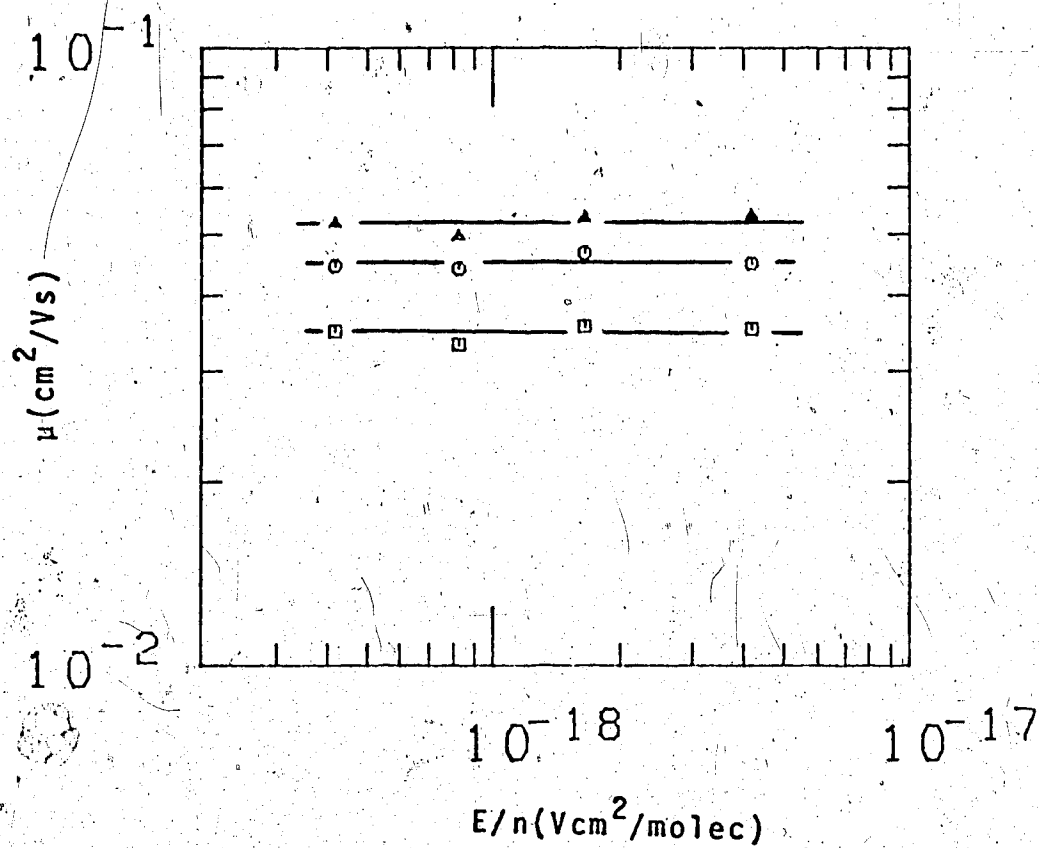


FIGURE III-90. Ion mobilities in gaseous propane as functions of E/n . $n = 3.41 \times 10^{20}$ molec/cm³. Temperatures: \square (306K), \circ (358K), Δ (426K).

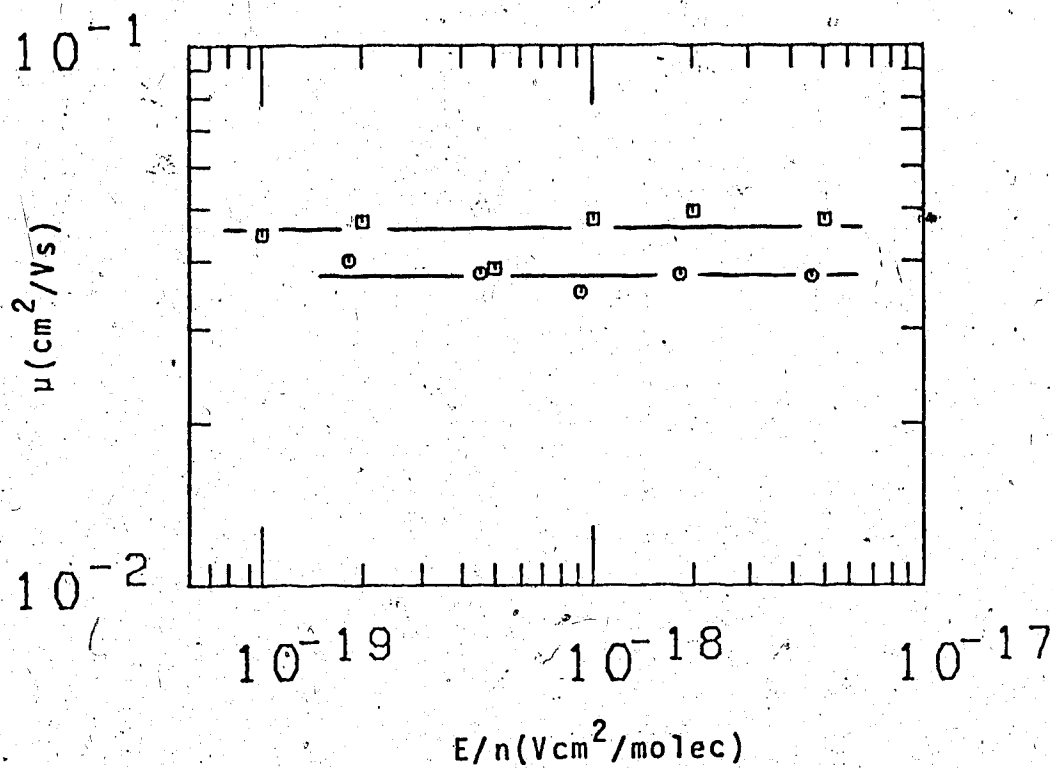


FIGURE III-91. Ion mobilities in gaseous propane as functions of E/n . Densities and temperatures ($n/10^{20}$ molec/cm³, T): □ (2.69, 297K), ○ (3.11, 303K).

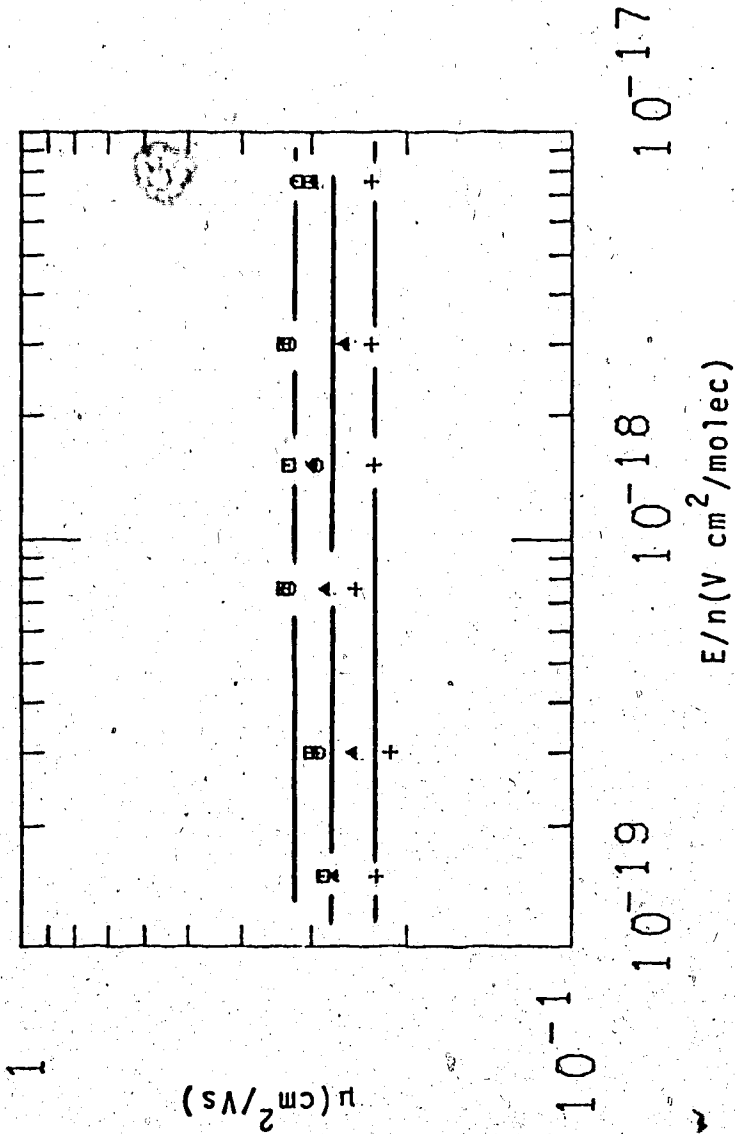


FIGURE III-92. Ion mobilities in gaseous propane as functions of E/n .
 $n = 6.69 \times 10^{19}$ molec/cm³. Temperatures: \square (394K), \circ (345K),
 Δ (295K), $+$ (257K).

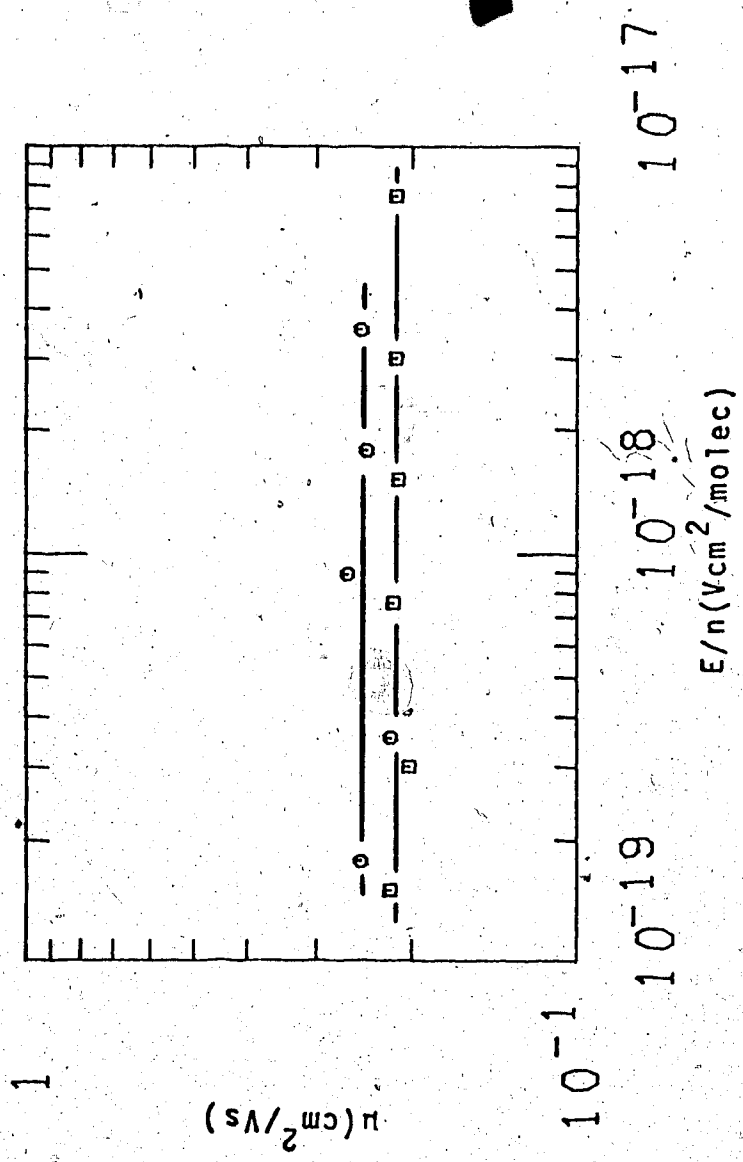


FIGURE III-93. Ion mobilities in gaseous propane as functions of

E/n . Densities and temperatures ($n/10^{19}$ molec/cm³, T).

□ (6.69, 253K), O (5.67, 245K).

TABLE III-11
Summary of Ion Results for Propane^a

T °K	n $10^{21} \frac{\text{molec}}{\text{cm}^3}$	μ_+ $10^{-3} \frac{\text{cm}^2}{\text{Vs}}$	$\mu_+ n$ $10^{19} \frac{\text{molec}}{\text{Vscm}}$
169	8.96	0.408	0.366
197	8.48	0.682	0.578
224	8.05	1.00	0.805
243	7.73	1.37	1.06
315	6.35	3.13	1.99
371	3.00	5.53	1.66
298	6.76	2.64	1.78
340	5.57	4.04	2.25
365	4.17	5.40	2.25
373	3.00 ^b	6.07	1.82
369	2.45	5.21	1.28
370	3.00 ^b	5.04	1.51
374	3.00 ^b	5.71	1.71
377	3.00 ^b	5.90	1.77
360	1.39	9.91	1.38
354	1.16	12.1	1.40
328	0.593	21.6	1.28
372	1.50	10.3	1.54
385	1.50	11.3	1.70
317	0.450	27.9	1.26
338	0.751	18.7	1.40
346	0.751	19.6	1.47
383	0.751	25.4	1.91
306	0.341	34.7	1.18
358	0.341	45.0	1.53
426	0.341	52.2	1.78

(continued.....)

TABLE III-11 (continued)

297	0.269	45.9	1.23
305	0.311	37.7	1.17
394	0.0669	319	2.13
345	0.0669	319	2.13
296	0.0669	272	1.82
257	0.0669	229	1.53
253	0.0669	213	1.42
245	0.0567	246	1.40

^a Data appear in same order as in figures.

^b $n_c = 3.00 \times 10^{21}$. $T_c = 370K$.

4. n-Butane

Measurements were made in n-butane in both the liquid and gas phases along the coexistence curve as well as at different temperatures on a number of isochores. Data are contained in Figures III-94 to III-102. Low pressure conductance cells were used for collecting the data in Figures III-94, III-95, III-101 and III-102. For the other figures high pressure conductance cells were used. For Figures III-94, III-95 and III-96 liquid type cells were used. For the rest, gas type cells were used.

In liquid phase n-butane, two components were found for the ion mobility at 208K, 266K and 298K. The faster component is shown in Figure III-94 and the slower in Figure III-95. The faster species is the negative ion while the slower is the more usually observed positive ion. For 208K and 266K, μ_-/μ_+ is 1.9 and 2.1 respectively, in agreement with the observation in other hydrocarbon systems (195) that $\mu_-/\mu_+ \sim 2$ in the normal liquids.

For 298K, this ratio has increased to 3.1. When the liquid is heated to 365K, the fast component disappears. Throughout the liquid range, the mobility increases as the temperature increases. When the critical region is reached, increasing the temperature continues to increase the mobility.

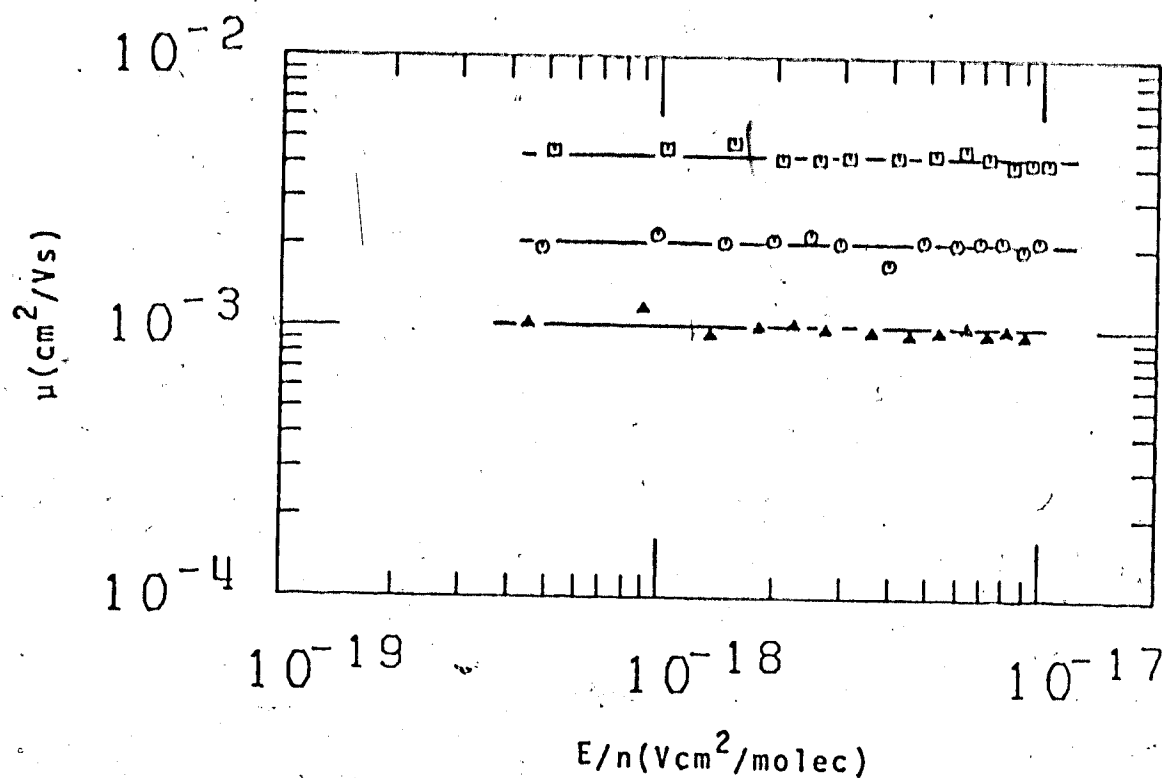


FIGURE III-94. Ion mobilities in liquid *n*-butane plotted against the density normalized electric field strength E/n . Fast component. Densities and temperatures ($n/10^{21}$ molec/cm³, T): \square (5.99, 298K), \circ (6.31, 266K), \triangle (6.86, 208K).

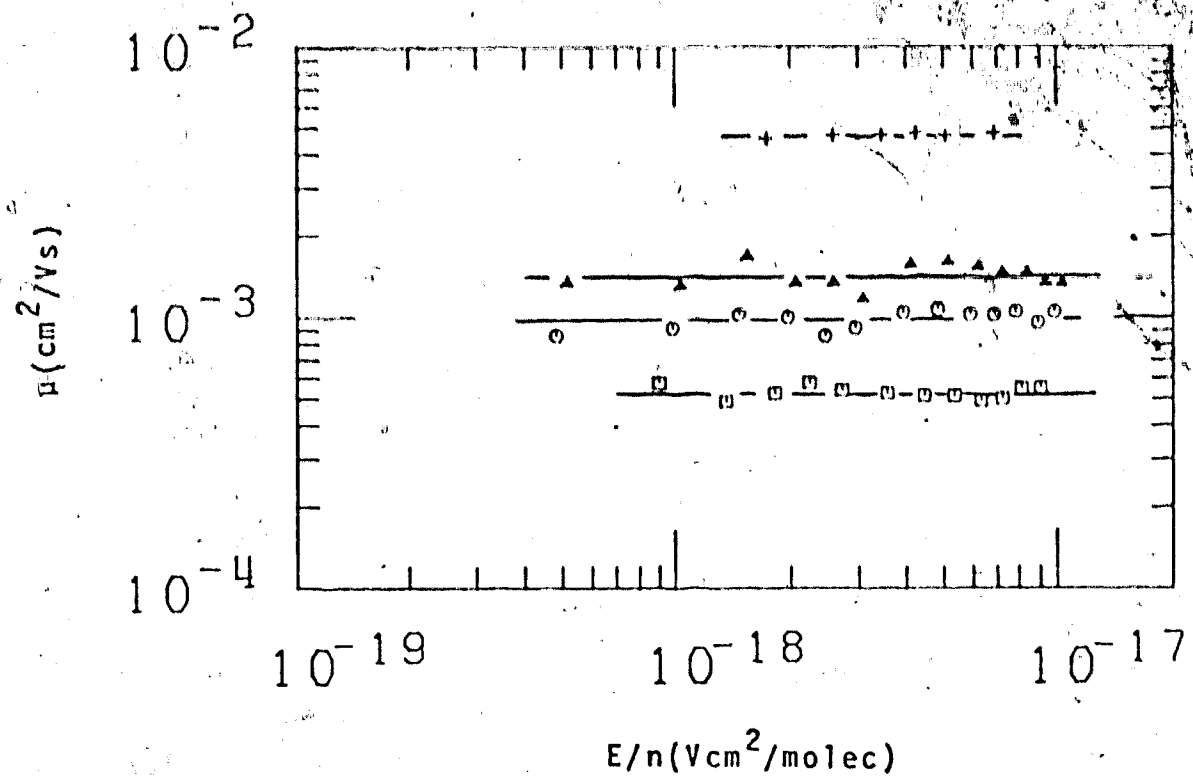


FIGURE III-95. Ion mobilities in liquid *n*-butane plotted against the density normalized electric field strength E/n . Densities and temperatures ($n/10^{21}$ molec/cm³, T): \square (6.86, 208K), \circ (6.31, 266K), Δ (5.99, 293K), $+$ (3.61, 415K).

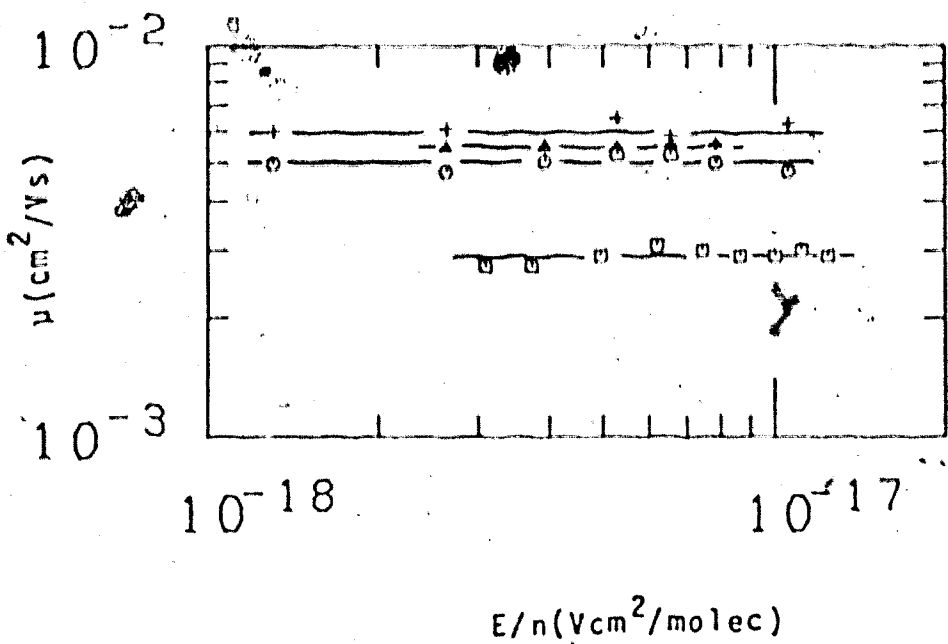


FIGURE IIV-96. Ion mobilities in liquid and supercritical n-butane as functions of E/n. Densities and temperatures ($n/10^{21}$ molec/cm³, T): \square (4.99, 365K), \circ (2.36, 427K), \triangle (2.36, 432K), $+$ (2.36, 443K).

In the gas phase (Figures III-97 to III-102), the mobility varies in the same way as the other systems previously discussed when the density or temperature (at constant density) is changed. The density effect along the coexistence curve can be extracted from Figures III-97, III-99 and III-102. The density range covered is $n/n_c = 1.0$ (Figure III-97) to 0.026 (Figure III-102). Initially the mobility increases by a factor less than that of the decrease in density. When the density drops below about $n/n_c \sim 0.5$, the mobility varies inversely with the density decrease.

The mobility was also measured at different temperatures along five isochores where $n/n_c = 1.0$ (Figure III-97), 0.50 (Figure III-98), 0.25 (Figure III-99), 0.10 (Figure III-100) and 0.032 (Figure III-101). In all cases, the mobility increases with the temperature. The initial rate of increase also decreases as n/n_c decreases. For the $n/n_c = 0.10$ and 0.032 isochores, the mobilities at the higher temperatures are levelling off. In order to avoid crowding, some of the curves were not drawn. On Figure III-98, the top curve is at 440K. The curve for 435K which was not drawn, is 4% lower than that of 440K. On Figure III-101, the three curves drawn are, from the top, for 424K, 312K, and 304K. The curve for 370K would be 0.6% lower than that of 424K. Within the scatter, the two curves are the same. The curve for 333K lies between

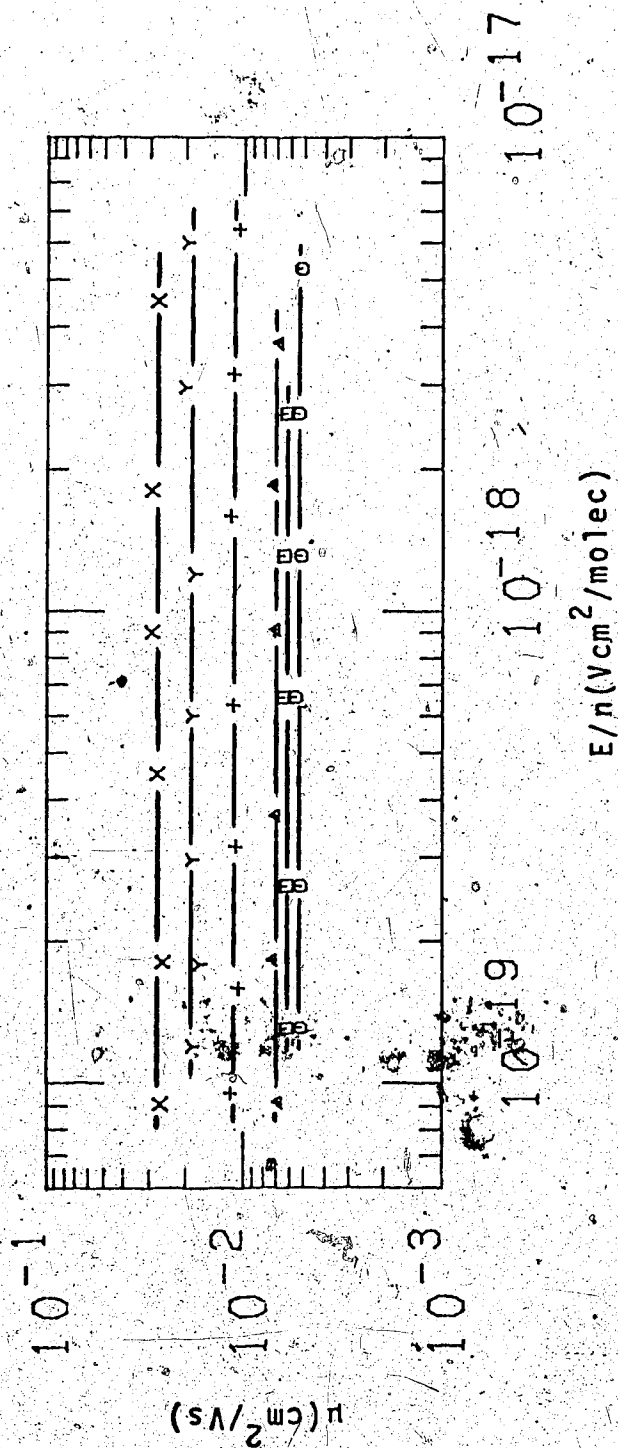


FIGURE III-97. Ion mobilities in gaseous and supercritical n-butane as functions of E/n . Densities and temperatures ($n/10^{20}$ molec/ cm^3 , T): \square (23.6, 430K), Δ (16.8, 424K), \circ (9.74, 409K), γ (5.18, 384K), \times (3.42, 365K).

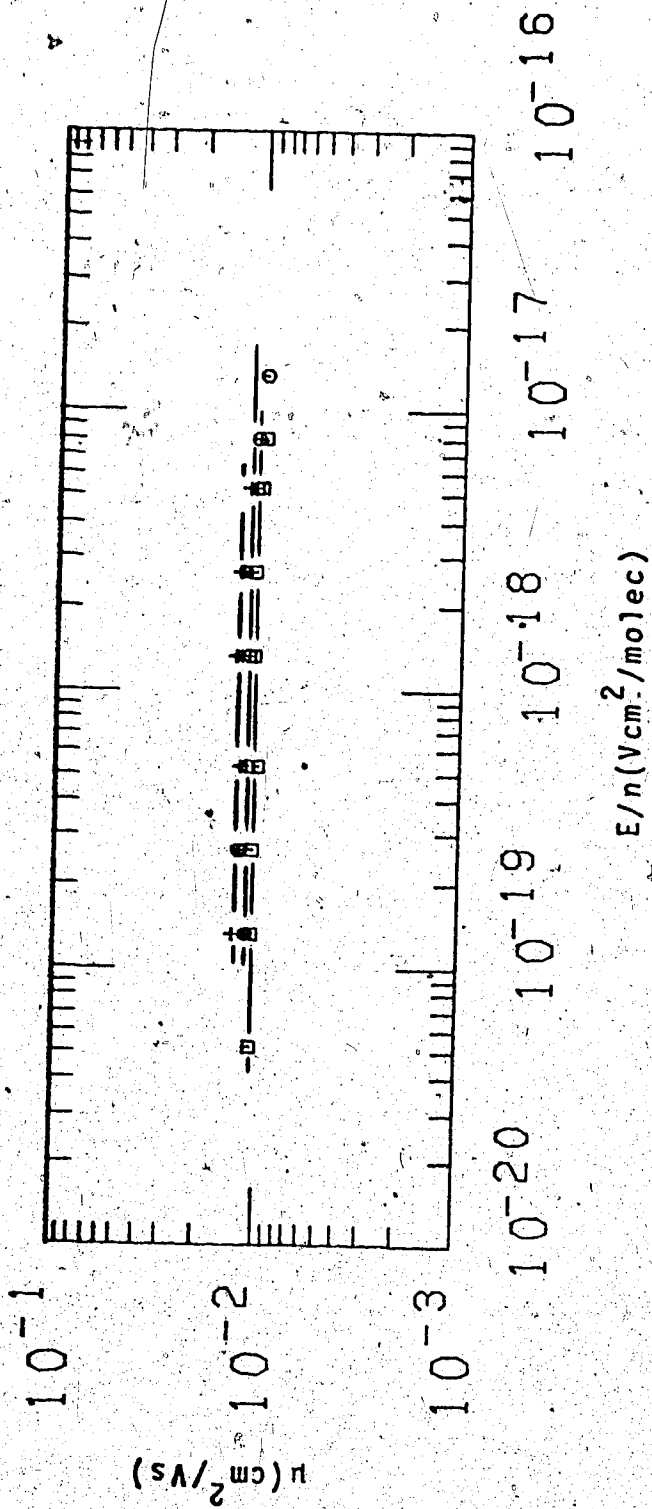


FIGURE III-98. Ion mobilities in gaseous *n*-butane as functions of E/n .

$n = 1.18 \times 10^{21}$ molec/cm³. Temperatures: \square (419K), \circ (428K), Δ (435K),
 + (440K).

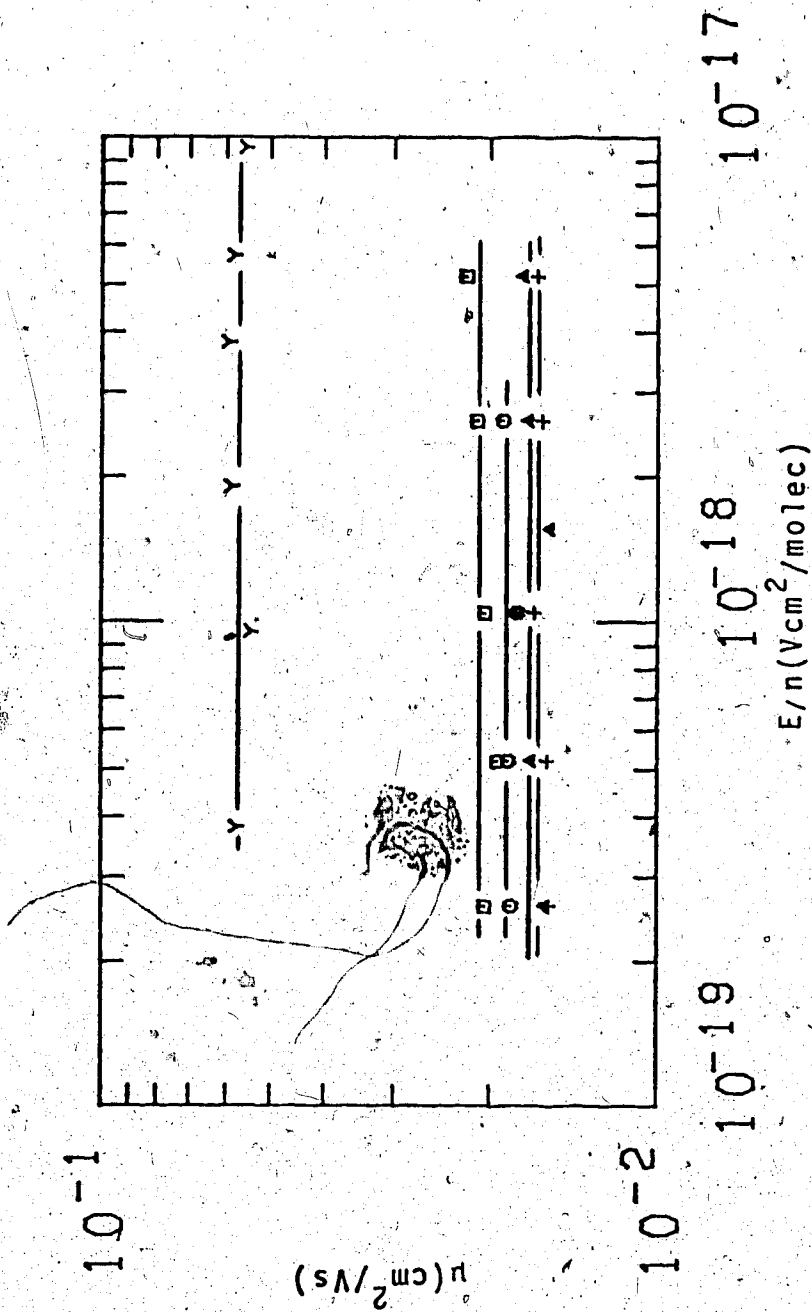


FIGURE III-99. Ion mobilities in gaseous n-butane as functions of E/n .
 Densities and temperatures ($n/10^{20}$, T): Y (1.64, 333K), + (5.99, 391K),
 Δ (5.99, 407K), ○ (5.99, 431K), □ (5.99, 444K).

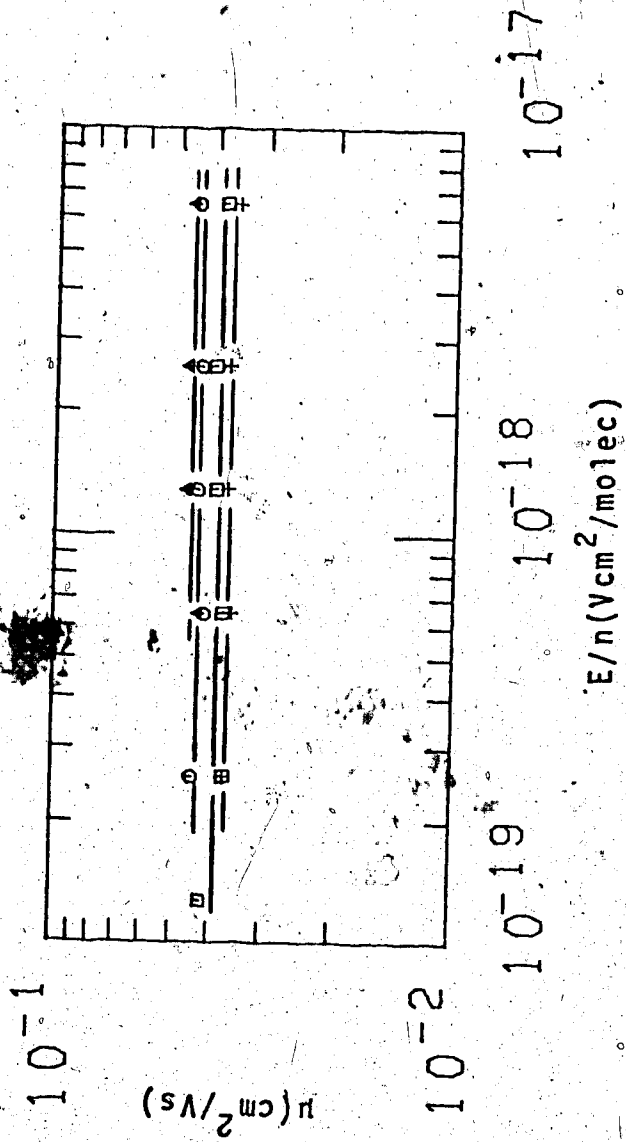


FIGURE III-100. Ion mobilities in gaseous n-butane as functions of E/n .
 $n = 2.42 \times 10^{20}$. Temperatures: + (355K), Δ (367K), O (430K),
 □ (458K).

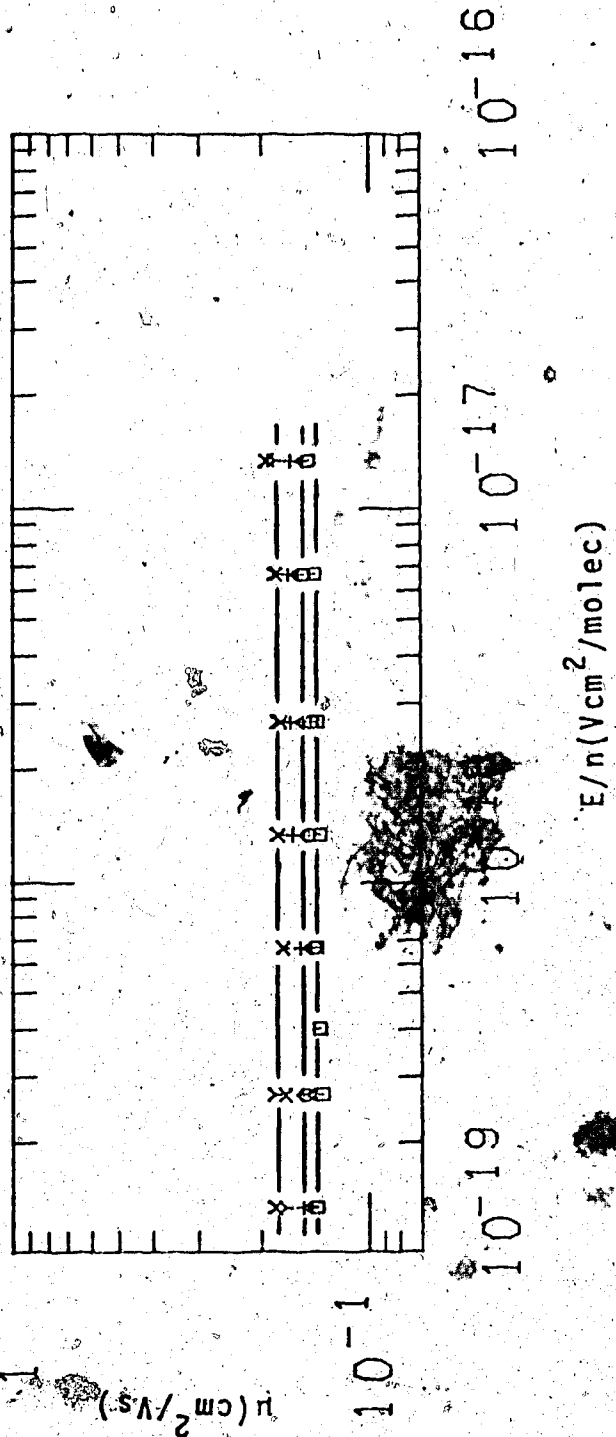


FIGURE III-101. Ion mobilities in gaseous n-butane as functions of E/n .
 $n = 7.56 \times 10^{19}$. Temperatures: \square (308K), Δ (312K), $+$ (333K),
 γ (370K), \times (424K).

B

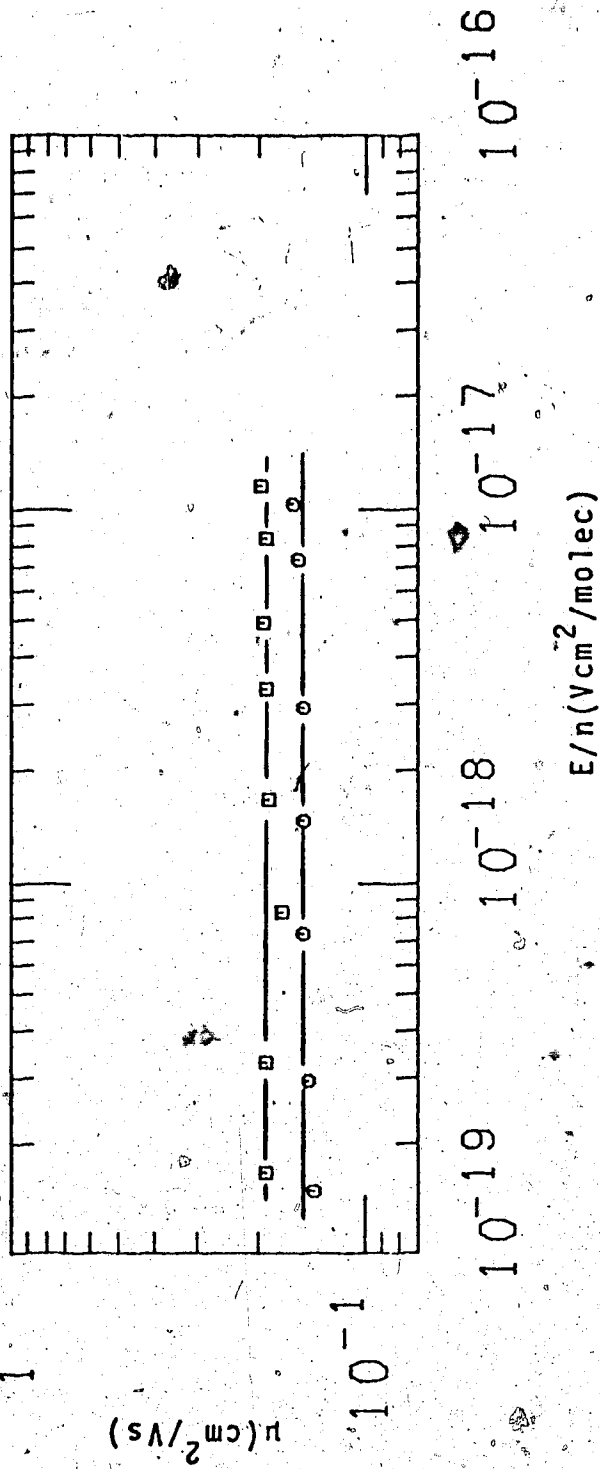


FIGURE III-102. Ion mobilities in gaseous n-butane as functions of E/n .
 Densities and temperatures ($n/10^{19}$, T): O (6.84, 300K), □ (6.06, 296K).

that of 424K and 312K. It is 6% above that of 312K. The curve for 308K lies between that of 304K and that of 312K. It is 4% above that of 304K.

TABLE III-12

Summary of Ion Results for n-Butane ^a

T °K	n $10^{20} \frac{\text{molec}}{\text{cm}^3}$	μ_+ $10^{-2} \frac{\text{cm}^2}{\text{Vs}}$	$\mu_+ n$ $10^{19} \frac{\text{molec}}{\text{Vscm}}$
298	59.9	0.435	2.61 [†]
266	63.1	0.205	1.29 [†]
208	68.6	0.100	0.686 [†]
208	68.6	0.0524	0.359
266	63.1	0.0983	0.620
298	59.9	0.142	0.851
415	36.1	0.466	1.68
365	49.9	0.289	1.44
427	23.6 ^b	0.501	1.18
432	23.6 ^b	0.552	1.30
443	23.6 ^b	0.593	1.40
430	23.6 ^b	0.619	1.46
425.5	23.6 ^b	0.529	1.25
424	16.8	0.692	1.16
409	9.74	1.12	1.09
384	5.18	1.81	0.938
365	3.42	2.71	0.927
419	11.8	1.05	12.4
428	11.8	1.13	13.3
435	11.8	1.23	14.5
440	11.8	1.28	15.1
333	1.64	5.71	9.36
391	5.99	1.63	9.76
407	5.99	1.69	10.1
431	5.99	1.85	11.1
444	5.99	2.08	12.5
355	2.42	3.64	8.81

(continued....)

TABLE III-12 (continued)

367	2.42	3.90	9.44
430	2.42	4.35	10.5
458	2.42	4.56	11.0
304	0.756	13.9	10.5
308	0.756	14.5	11.0
312	0.756	15.0	11.3
333	0.756	16.0	12.1
370	0.756	17.9	13.5
424	0.756	18.0	13.6
300	0.684	14.9	10.2
296	0.606	18.9	11.5

^a Data appears in the same order as in the figures.

^b $T_c = 425K$, $n_c = 23.6 \times 10^{20}$

† Fast component

5. iso-Butane (2-methylpropane)

Ion mobilities in iso-butane are contained in Figures III-103 to III-111. Low pressure conductance cells were used to collect the data in Figures III-103, III-110, and III-111. High pressure cells were used for all the rest. As well, cells used to gather the data in Figures III-103, III-104, and III-105 were liquid type whereas all the rest were gas type cells.

The liquid phase results are shown in Figures III-103, III-104 and III-105. Much more variation with density is shown than in *n*-butane (preceding section). As the system moves from 140K to 408K, the mobility increases by a factor of 50 for a density increase of a factor of 3. Varying the temperature between 140K and 270K (Figure III-103) leads to a continuous increase in mobility. However, between 298K and 330K, (Figure III-104), the mobility varies only slightly. There is no mobility maximum in front of the critical point (Figures III-104, III-105). Above 359K, the mobility rises continuously towards the critical region.

In the gas phase, upon attaining the critical point increasing the temperature leads to an increase in mobility (Figures III-105, III-106). Increasing the temperature along the other isochores where $n/n_c = 0.50$ (Figure III-108), 0.26 (Figure III-109), 0.026 (Figure III-110) leads in each case to an increase in

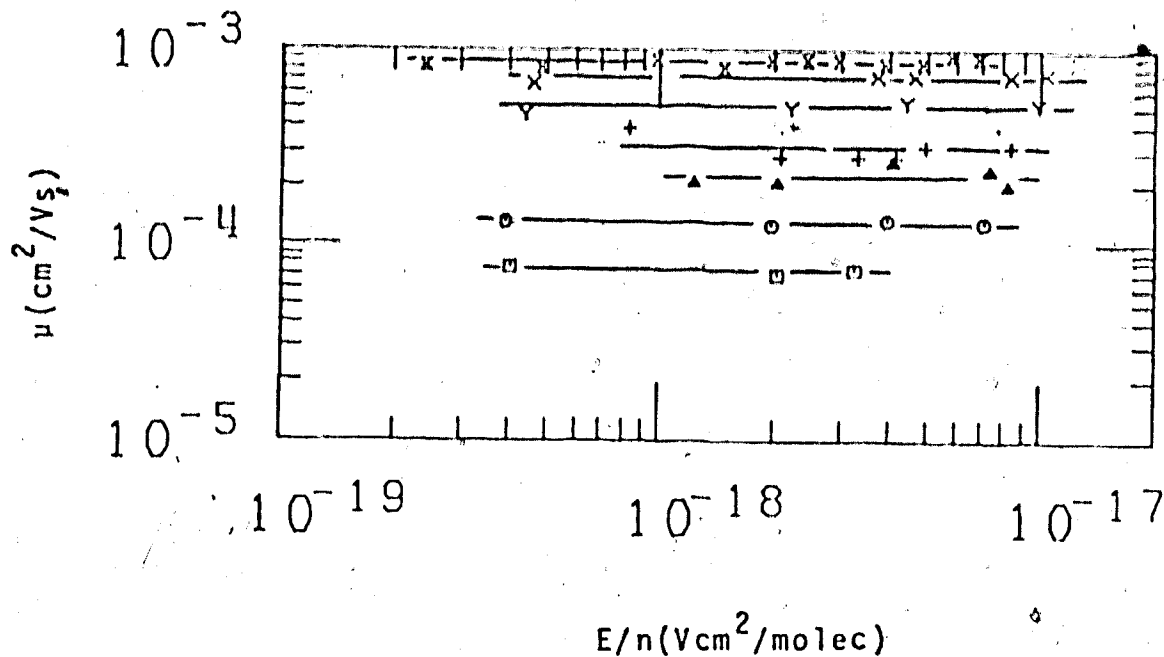


FIGURE III-103. Ion mobilities μ in liquid iso-butane as functions of E/n . Densities and temperatures ($n/10^{21}$ molec/ cm^3 , T): \square (7.69, 140K), \circ (7.49, 154K), Δ (7.26, 173K), + (7.17, 181K), Y (6.74, 214K), X (6.41, 239K), \bar{X} (6.07, 270K).

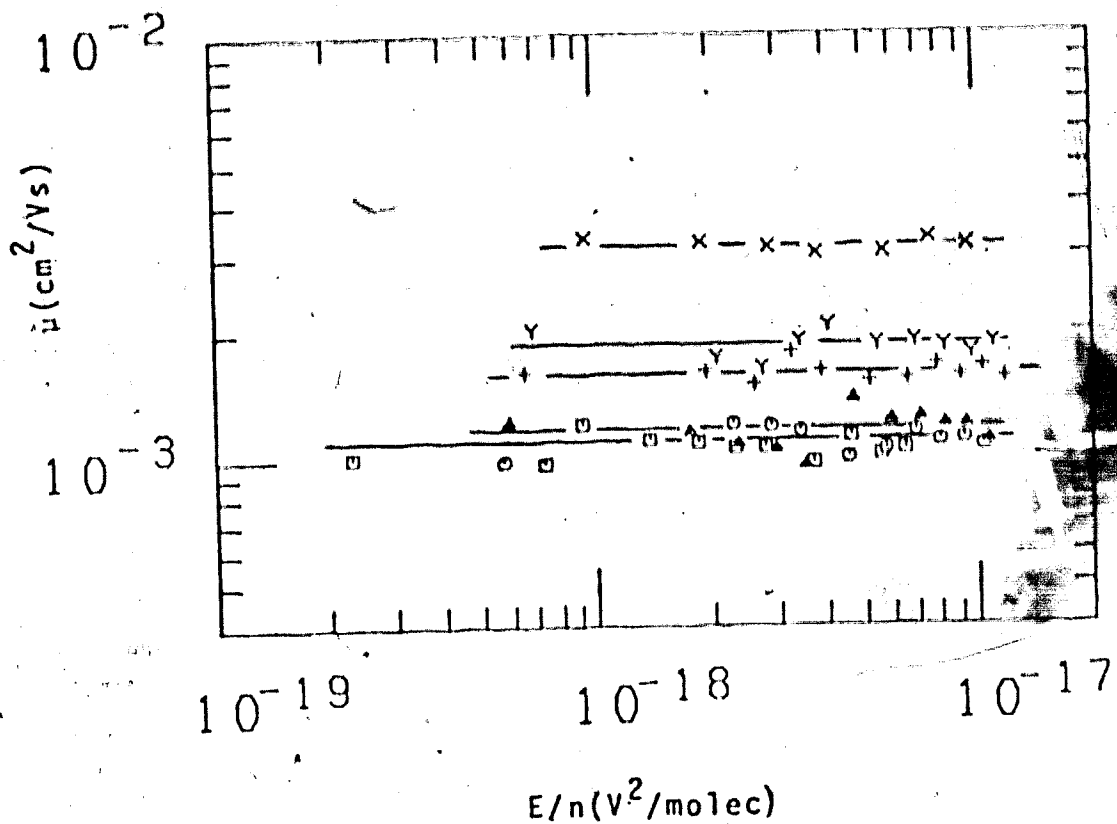


FIGURE III-104. Ion mobilities in liquid iso-butane as functions of E/n . Densities and temperatures ($n/10^{21}$ molec/ cm^3 , T): \square (5.73, 298K), \circ (5.45, 318K), Δ (5.28, 330K), + (4.79, 359K), Y (4.54, 371K), X (3.26, 403K).

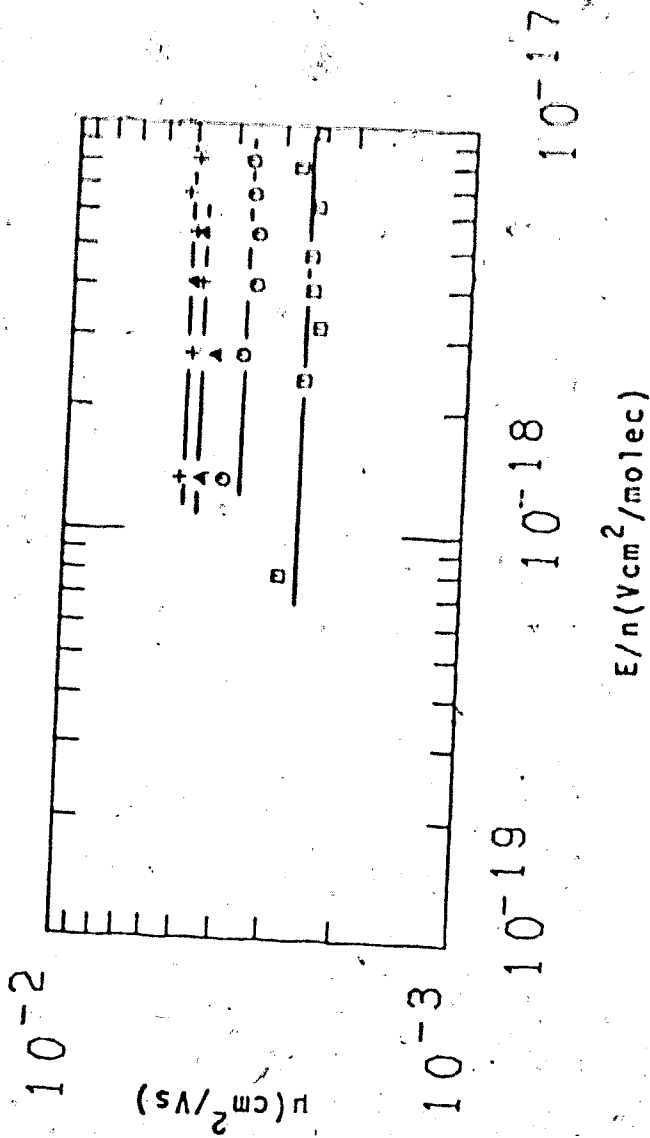


FIGURE III-105. Ion mobilities in liquid and supercritical iso-butane as functions of E/n. Densities and temperatures ($n/10^{21}$ molec/cm³, T):
 □ (3.92, 393K), ○ (2.30, 408K), Δ (2.30, 423K).

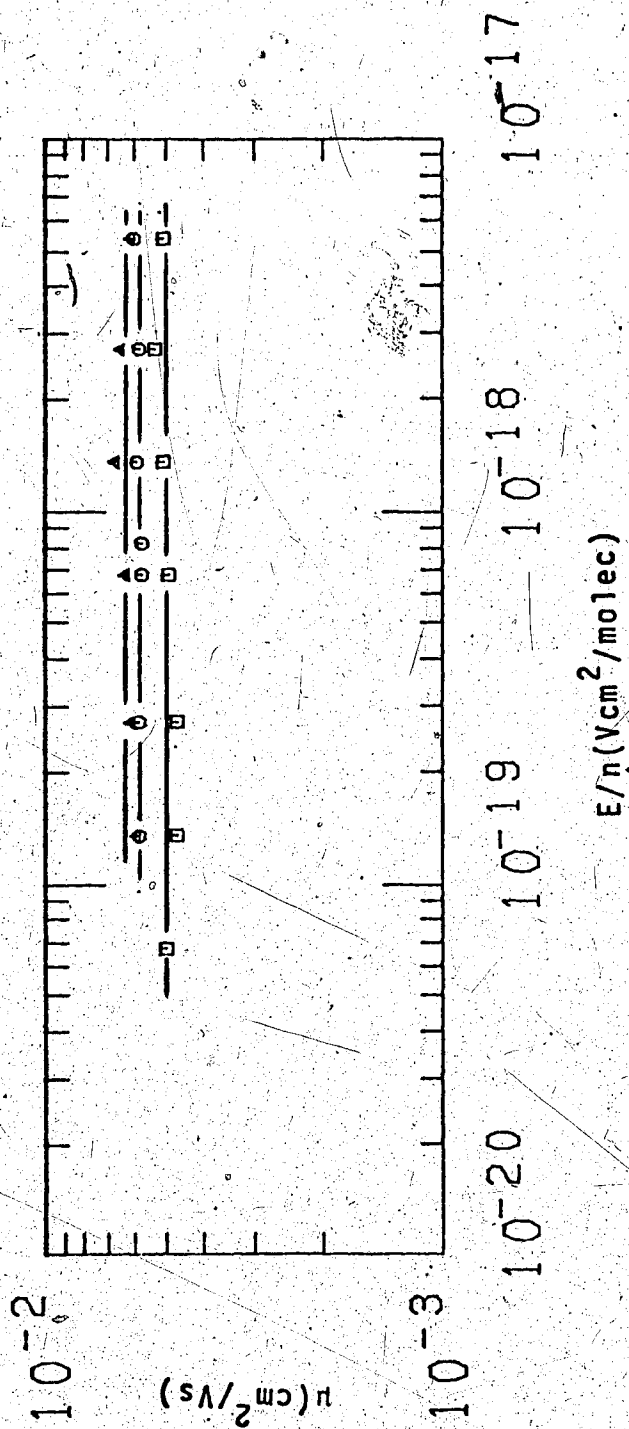


FIGURE III-106. Ion mobilities in supercritical iso-butane as functions of E/n . $n = 2.30 \times 10^{21}$ molec/cm³. Temperatures: \square (408K), \circ (415K), Δ (421K).

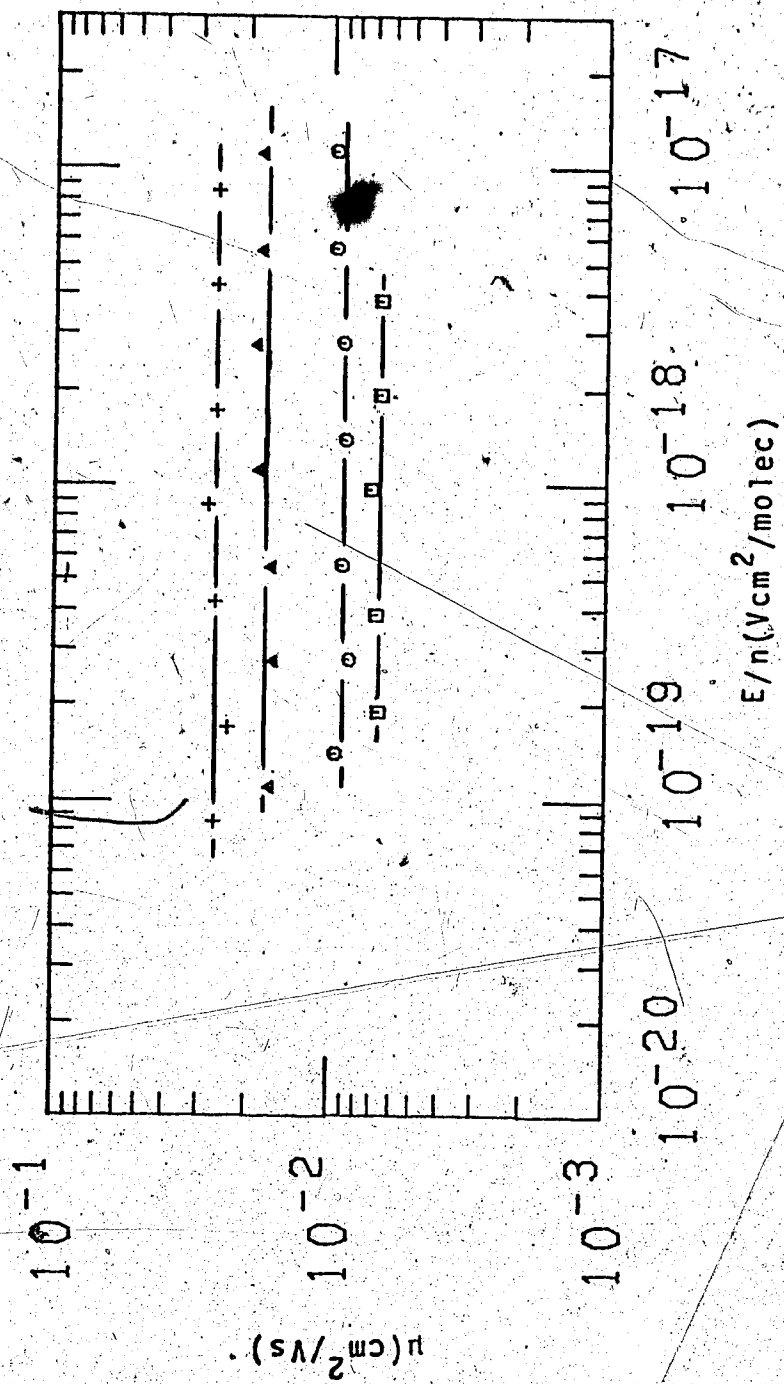


FIGURE III-107. Ion mobilities in gaseous iso-butane as functions of E/n .
 Densities and temperatures ($n/10^{20}$ molec/ cm^3 , T): \square (16.2, 406K),
 \circ (11.1, 398K), Δ (5.65, 371K), + (3.63, 352K).

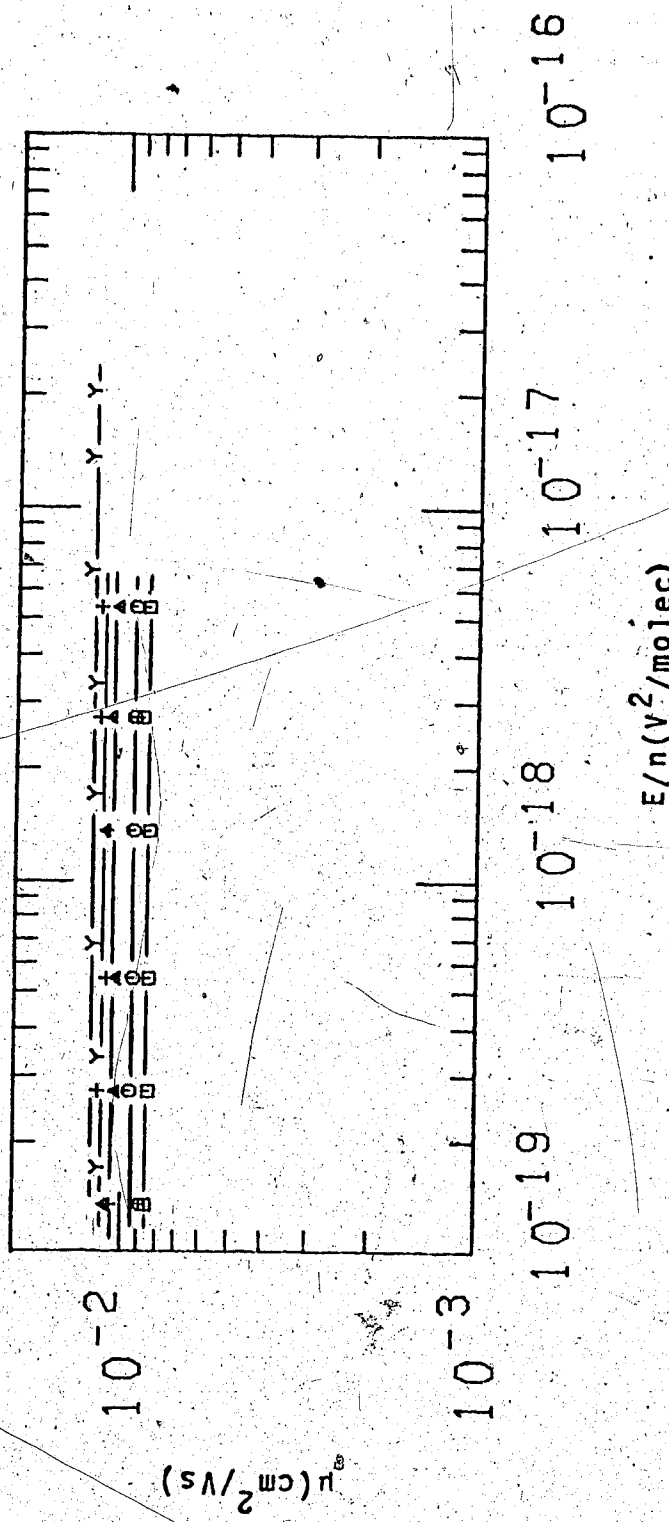


FIGURE III-108. Ion mobilities in gaseous iso-butane as functions of E/n .
 Densities and temperatures ($n/10^{20}$, T): \square (11.5, 400K), \circ (11.5, 405K), Δ (11.5, 415K), $+$ (11.5, 425K), γ (9.22, 391K).

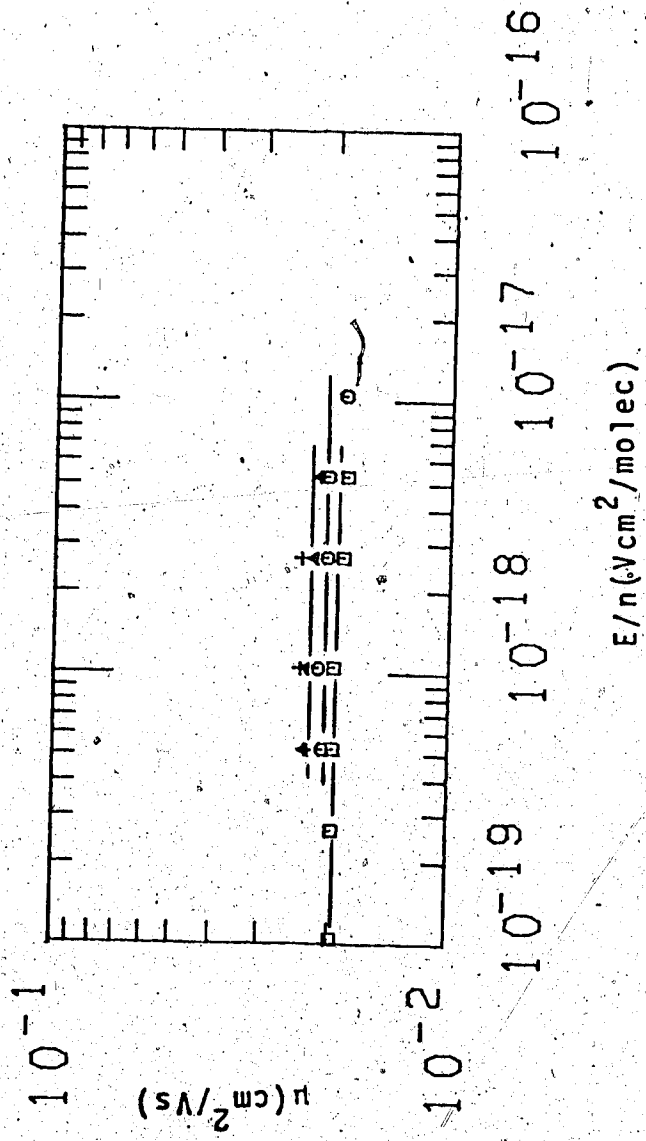


FIGURE IPI-109. Ion mobilities in gaseous iso-butane as functions of

E/n. n = 5.91 x 10²⁰ molec/cm³. Temperatures: □ (377K), ○ (388K), △ (409K), + (430K).

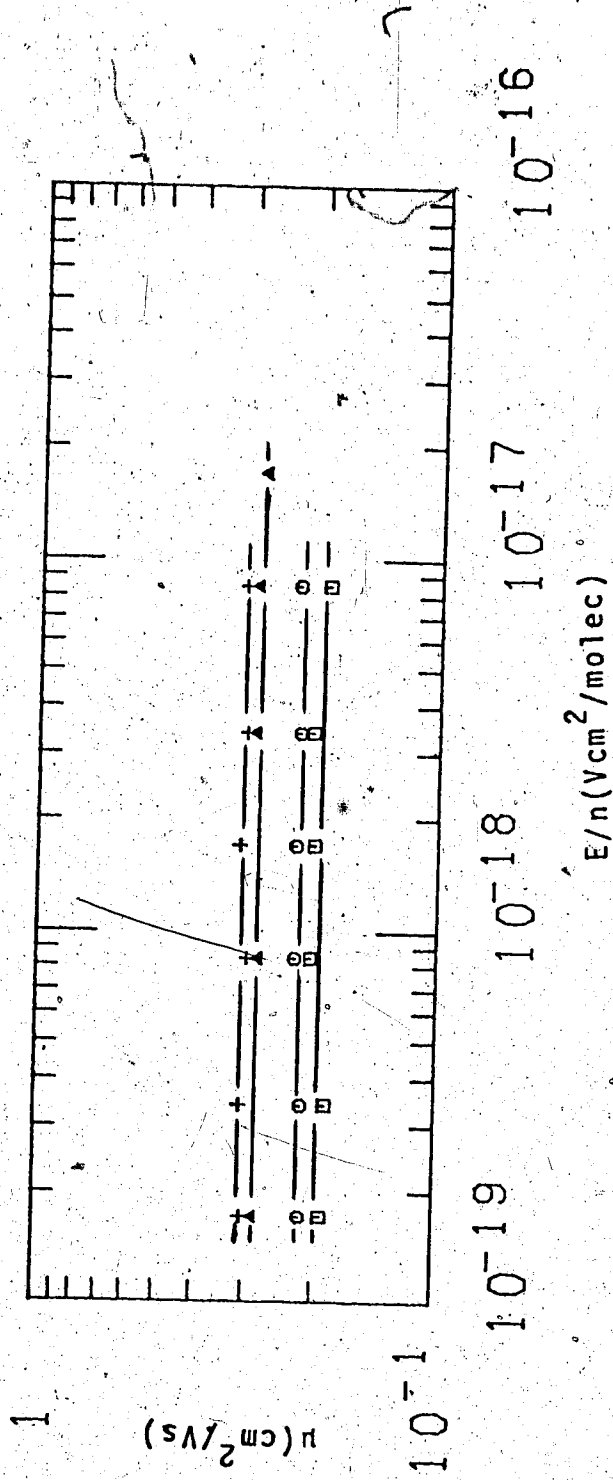


FIGURE III-110. Ion mobilities in gaseous iso-butane as functions of E/n .
 $n = 5.91 \times 10^{19}$ molec/cm³. Temperatures: \square (283K), \circ (295K),
 Δ (364K), $+$ (435K).

mobility. In the case of n-butane, the mobility curve along the $n/n_c = 0.032$ isochore levels off at higher temperatures. This is also the case for propane and ethane. However, in the same manner as methane, the dilute gas isochore in iso-butane does not level off at the higher temperatures even though the curve is beginning to bend towards a plateau.

From Figures III-107, III-111, and from the 391K curve on Figure III-108, it is seen that moving the system away from the critical region along the coexistence curve towards the dilute gas leads to the same trends observed in the other hydrocarbons. The mobility initially increases at a rate less than the density is decreasing, but then at $n/n_c < 0.5$, the mobility varies inversely proportional to the density change.

Data for iso-butane are summarized in Table III-13.

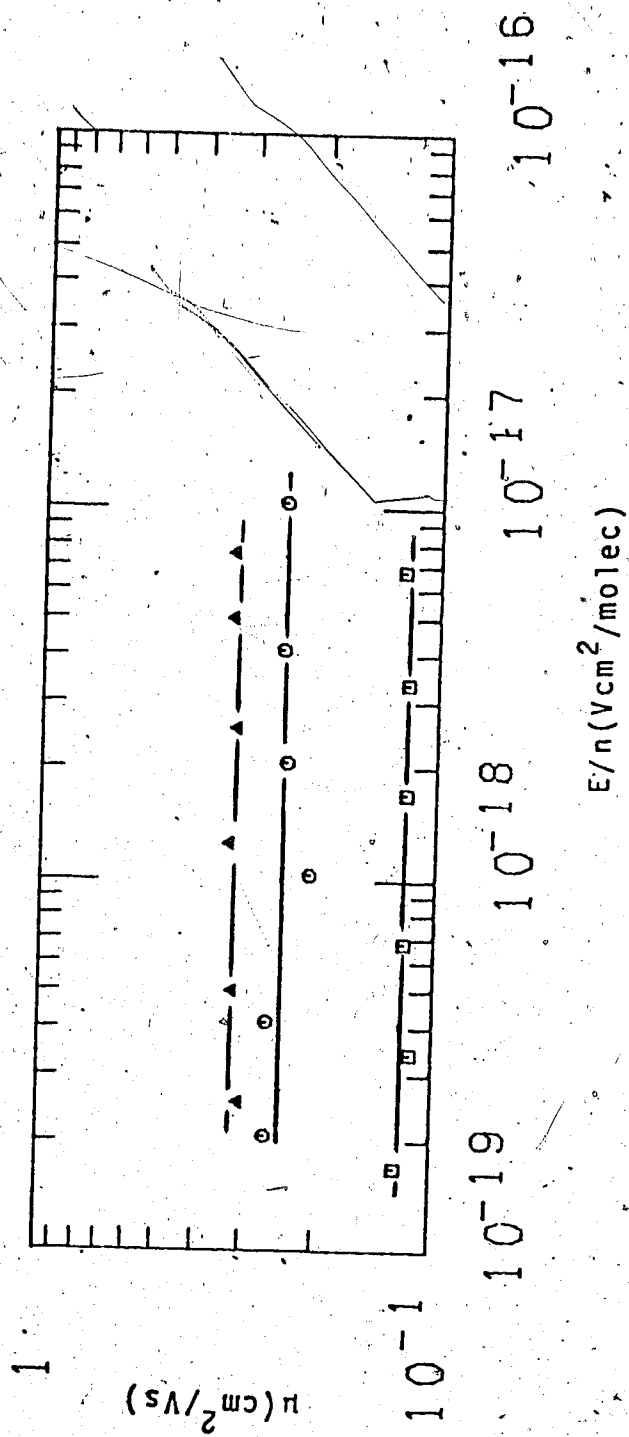


FIGURE III-111. Ion mobilities in gaseous iso-butane as functions of E/n .
 Densities and temperature. ($n/10^{19}$, T); \square (9.22, 297K), \circ (4.87,
 276K), Δ (3.99, 270K).

TABLE III-13

Summary of Ion Results for iso-Butane ^a

T °K	n $10^{20} \frac{\text{molec}}{\text{cm}^3}$	μ_+ $10^{-2} \frac{\text{cm}^2}{\text{Vs}}$	$\mu_+ n$ $10^{19} \frac{\text{molec}}{\text{Vs cm}}$
140.	76.9	0.00734	0.0564
154	74.9	0.0130	0.0974
173	72.6	0.0222	0.161
181	71.7	0.0312	0.224
214	67.4	0.0502	0.342
239	64.1	0.0723	0.463
270	60.7	0.0863	0.524
298	57.3	0.110	0.630
318	54.5	0.110	0.600
330	52.8	0.116	0.612
359	47.9	0.159	0.762
371	45.4	0.184	0.835
403	32.6	0.318	0.841
393	39.2	0.258	1.25
408	23.0 ^b	0.366	0.842
414	23.0 ^b	0.465	1.07
423	23.0 ^b	0.500	1.15
408	23.0 ^b	0.494	1.14
415	23.0 ^b	0.582	1.34
421	23.0 ^b	0.623	1.43
406	16.2	0.664	1.08
398	11.1	0.902	1.00
371	5.65	1.69	0.955
352	3.63	2.62	0.951
400	11.5	0.851	0.979
405	11.5	0.929	1.07
415	11.5	1.06	1.22

(continued.....)

TABLE III-13 (continued)

425	11.5	1.13	1.30
391	9.22	1.21	1.12
377	5.91	1.92	1.13
388	5.91	2.04	1.21
409	5.91	2.26	1.34
430	5.91	2.32	1.37
283	0.591	19.7	1.16
295	0.591	22.2	1.31
364	0.591	28.0	1.65
435	0.591	30.7	1.81
297	0.922	12.0	1.11
276	0.487	24.2	1.18
270	0.399	32.4	1.29

^a Data appear in the same order as in the figures.

^b $n_c = 2.30 \times 10^{21}$. $T_c = 408K$.

6. Ethene

Data for ethene are contained in Figures III-112 to III-116. The ion mobilities were all measured in high pressure conductance cells. All the results were obtained using gas type cells except for the results of Figure III-112 for which a liquid type cell was used.

Liquid phase results appear in Figure III-112. Raising the temperature from 173K along the coexistence curve towards the critical region leads to an increase in mobility by a factor of 3.1 for a density decrease in the same range of a factor of 2.6. There is no mobility maximum below the critical region.

In the gas phase, measurements were made along the $n/n_c = 1.0$ (Figures III-112, III-113), 0.35 (Figure III-114), 0.17 (Figure III-115), and 0.041 (Figure III-116) isochores. In each case, the mobility increases with temperature. At the higher temperatures of the isochores (except $n/n_c = 1$) the mobilities do not increase at as great a rate as near the coexistence curve.

Figures III-113, III-115, and III-116 show curves for temperatures along the coexistence curve. Decreasing the density along the coexistence away from the critical fluid towards that of the dilute gas leads to an increase in the mobility. The mobility increases at a rate less than the density decrease at $n/n_c > 0.6$, and at the same rate as the density decrease at $n/n_c \lesssim 0.6$.

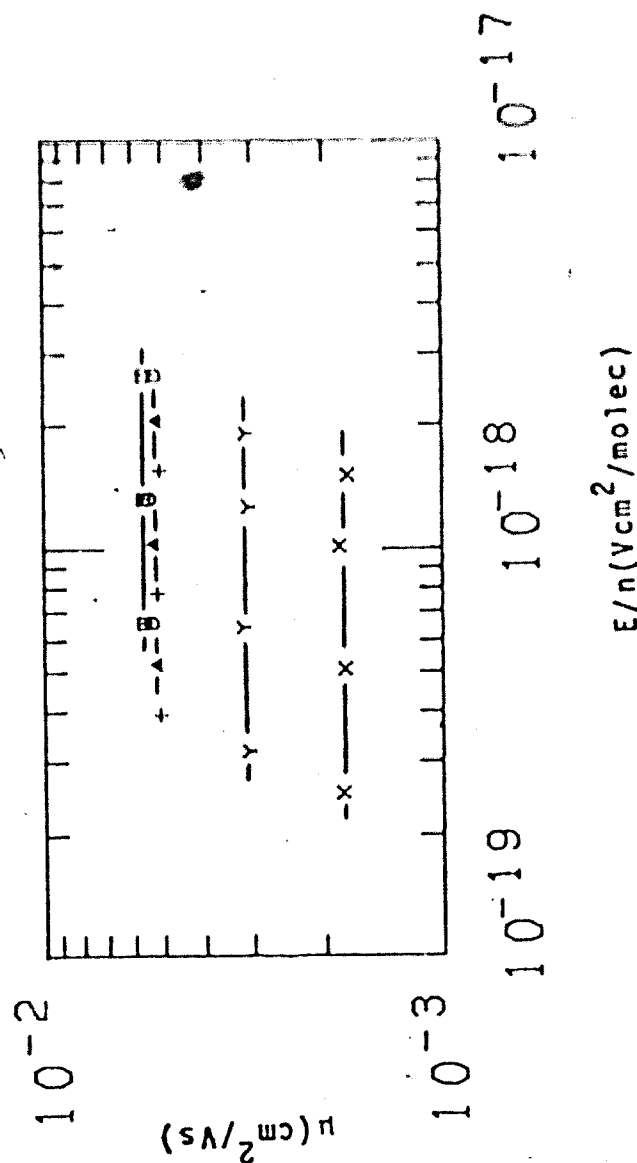


FIGURE III-112. Ion mobilities as functions of E/n in liquid and supercritical ethene. Densities and temperatures ($n/10^{24}$ molec/cm³, T); X (12.2, 173K), Y (9.70, 238K), + (7.90, 279K), Δ (5.97, 282K), O (4.65, 283K), \square (4.65, 284K).

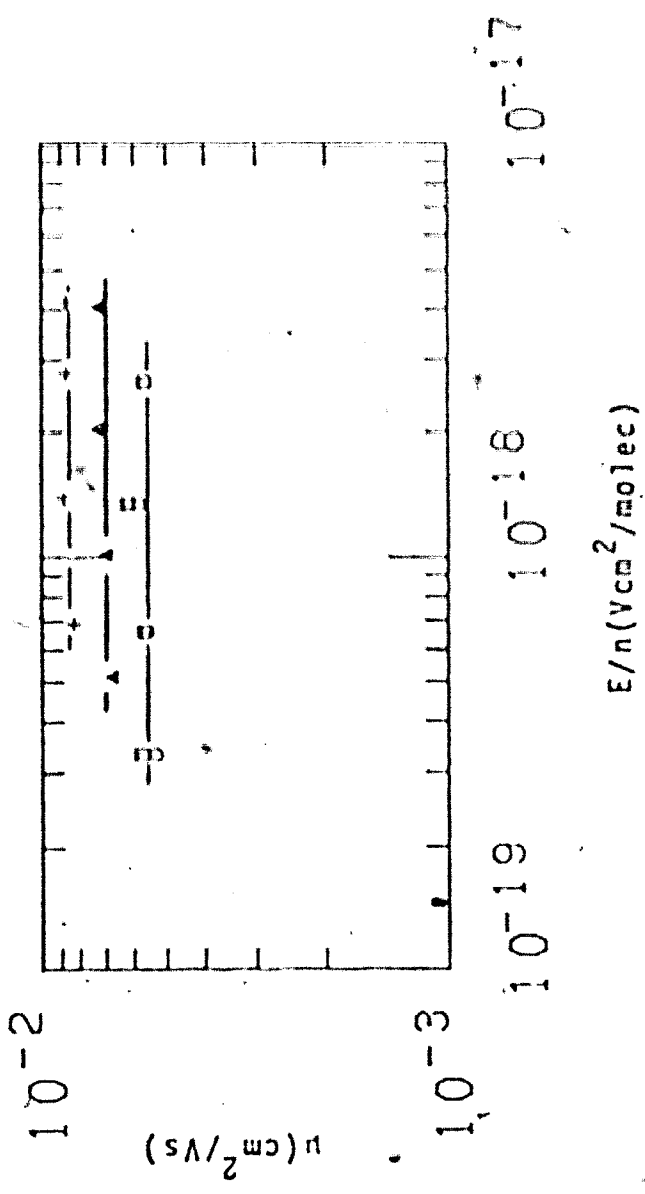


FIGURE III-113. Ion mobilities in gaseous and super-critical ethene as functions of E/n . Densities and temperatures ($n/10^{21}$ molec/cm³, T): □ (4.66, 285K), ○ (4.66, 253K), Δ (3.05, 281K), + (2.25, 275K).

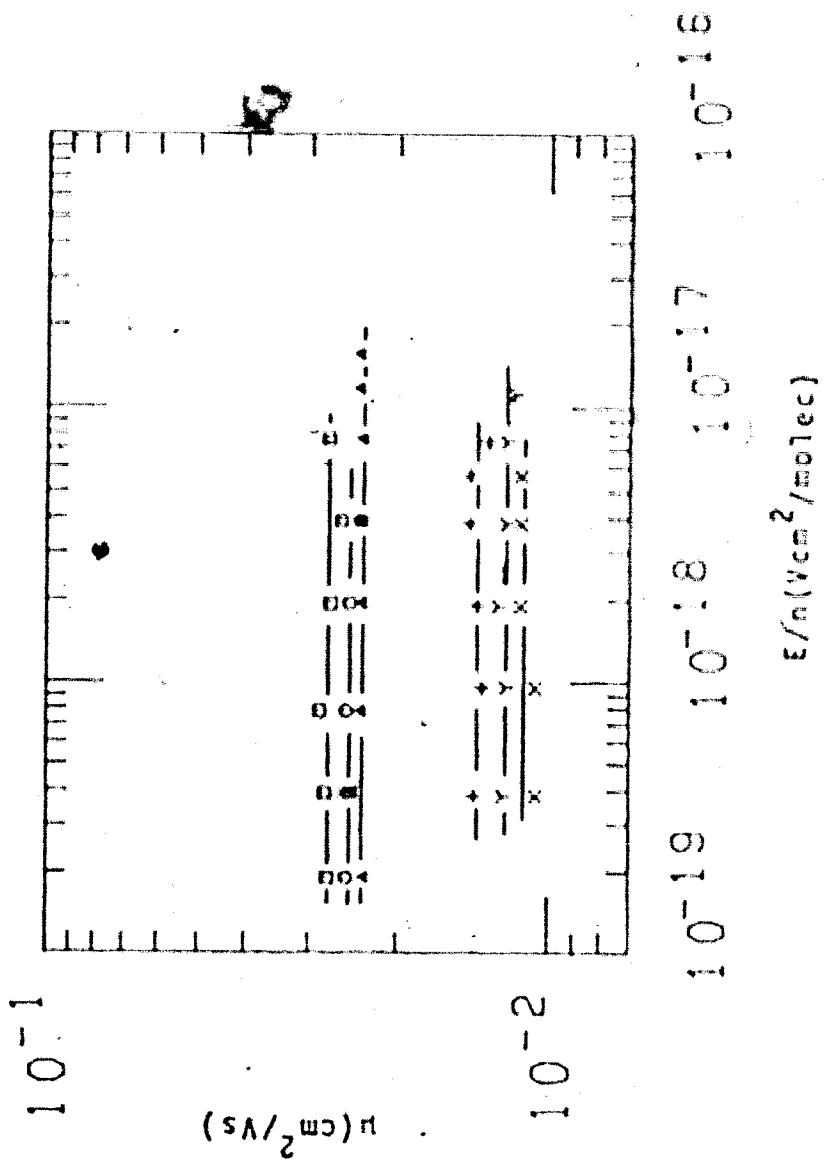


FIGURE III-114. Ion mobilities in gaseous ethene as functions of ϵ/n .

Open symbols: $n = 7.95 \times 10^{20} \text{ molec/cm}^3$. Stick symbols:
 $n = 1.64 \times 10^{21} \text{ molec/cm}^3$. Temperatures: \bullet (274K), γ (274K),
 \times (268K), \square (296K), \circ (254K), Δ (245K).

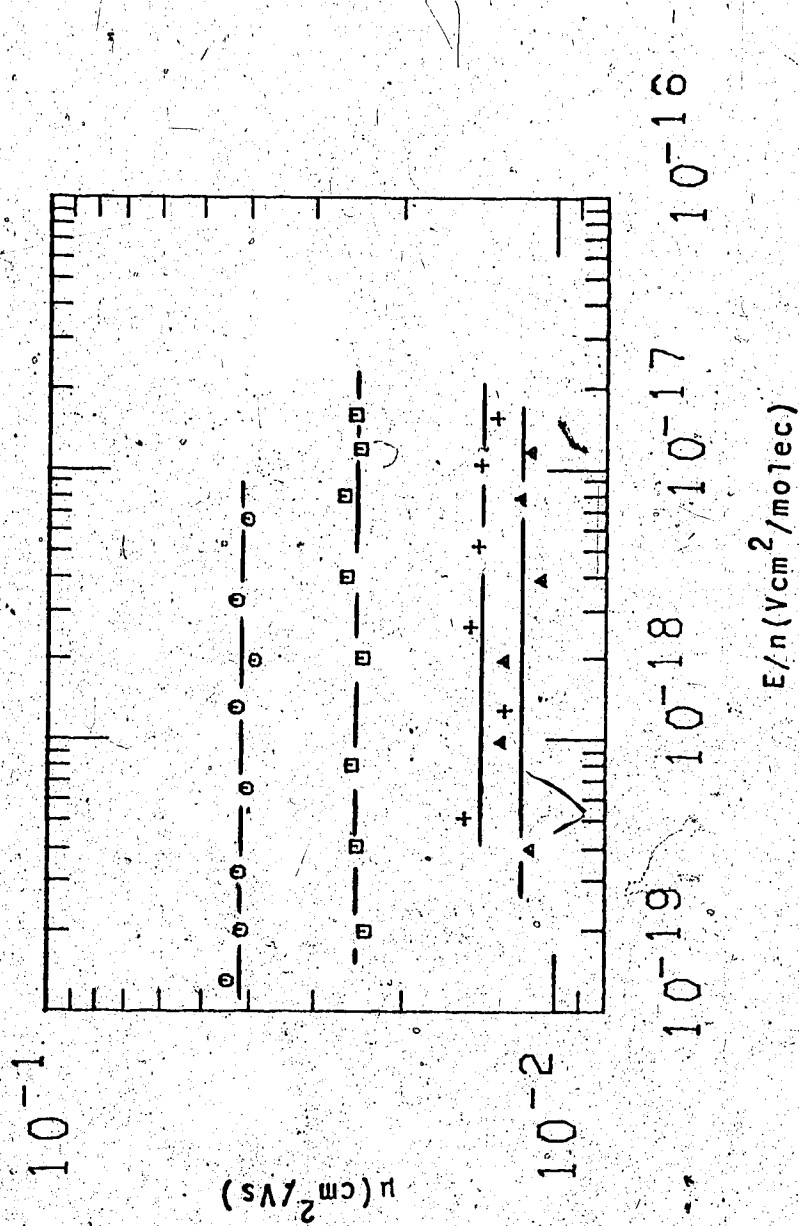


FIGURE III-115. Ion mobilities in gaseous ethene as functions of E/n .

Densities and temperatures ($n/10^{20}$ molec/cm³, T): □ (4.72, 227K),

○ (7.73, 241K), + (12.0, 256K), Δ (15.9, 265K).

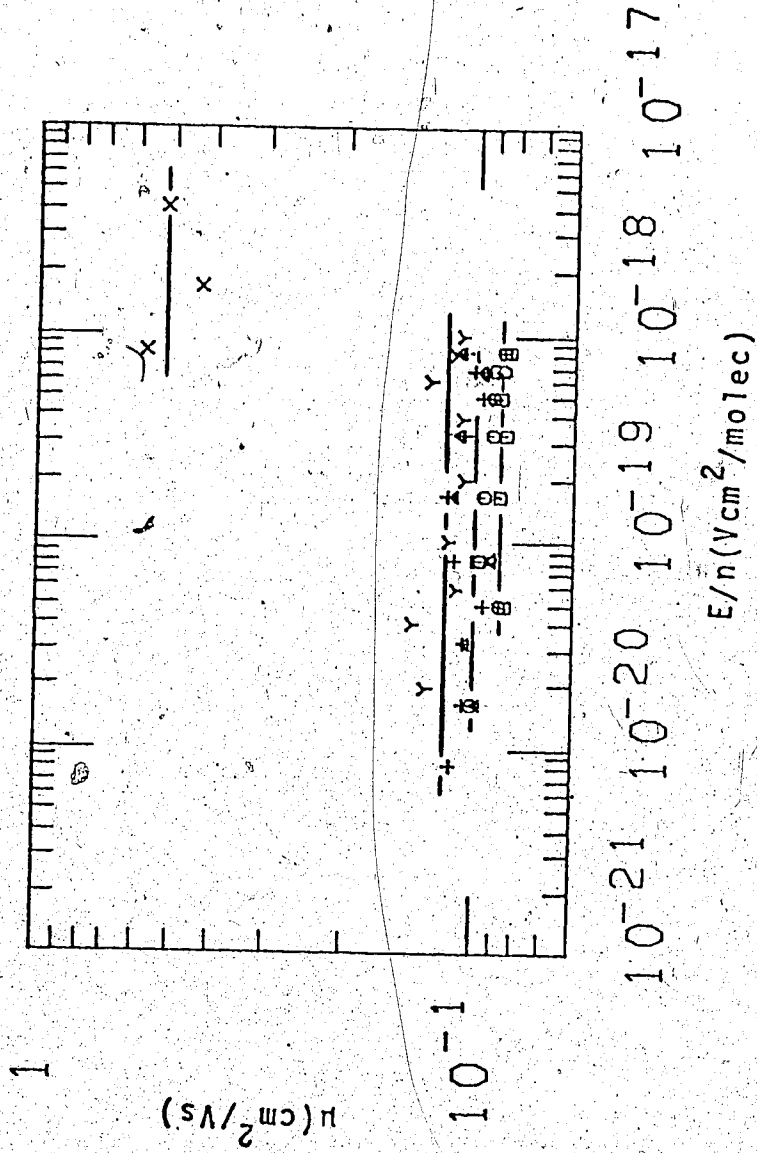


FIGURE III-116. Ion mobilities in gaseous ethene as functions of E/n .
 Densities and temperatures ($n/10^{20}$ molec/ cm^3 , T): \square (1.89, 203K),
 \circ (1.89, 207K), Δ (1.89, 236K), + (1.89, 298K), γ (1.57, 196K),
 \times (0.376, 166K)

Not all the curves were drawn through the figures in order to avoid excess crowding. On Figure III-112, the curve second from the top is for 282K. The arithmetic averages of the 283K and of the 279K curves are respectively 3% above and 2% below that of the 282K curve. On Figure III-113, the lowest curve is drawn for 283K. The curve for 285K based on the arithmetic average of the points would be 4% above the curve for 285K. On Figure III-116, the bottom curve is drawn for 203K, the second, for 236K, and the third, for 196K. The curves (based on the arithmetic averages) would be for 298K 7% above that of 236K, and for 207K, 4% above that of 203K.

Data for ethene are summarized in Table III-14.

TABLE III-14

Summary of Ion Results for Ethene ^a

T °K	n $10^{21} \frac{\text{molec}}{\text{cm}^3}$	μ_+ $10^{-3} \frac{\text{cm}^2}{\text{Vs}}$	$\mu_+ n$ $10^{19} \frac{\text{molec}}{\text{Vs cm}}$
173	12.2	1.76	2.15
238	9.70	3.12	3.03
279	6.48	5.13	3.29
282	5.97	5.23	3.12
283	4.66 ^b	5.39	2.51
284	4.66 ^b	5.62	2.62
285	4.66 ^b	5.79	2.70
283	4.66 ^b	5.59	2.60
281	3.05	6.99	2.13
275	2.25	8.59	1.93
294	1.64	13.9	2.28
274	1.64	12.2	2.00
268	1.64	11.2	1.84
296	0.795	27.3	2.17
254	0.795	24.8	1.97
245	0.795	23.5	1.87
227	0.472	41.6	1.96
241	0.773	24.8	1.92
256	1.20	14.0	1.68
265	1.59	11.7	1.86
298	0.189	110	2.08
236	0.189	102	1.93
207	0.189	92.0	1.74
203	0.189	88.4	1.67
196	0.157	117	1.84
166	0.0376	51.0	1.92

^a Data appear in the same order as in the figures.

^b $n_c = 4.66 \times 10^{21}$. $T_c = 283\text{K}$.

7. Propene

Ion mobilities in propene are contained in Figures III-117 to III-122. Data for Figures III-121 and III-122 were obtained in low pressure gas type conductance cells. Data for Figure III-117 were obtained in high pressure liquid type conductance cells. The rest of the results were obtained in high pressure gas type conductance cells.

Liquid phase results appear in Figure III-117. As the sample is heated along the coexistence curve from 231K towards the critical region the mobility increases by a factor of 5.4. In this same region, the density decreases by a factor of 2.6. Increasing the temperature leads to a smooth increase in the mobility. There is no mobility maximum below the critical region.

On reaching the critical region (Figures III-117 and III-118), the mobility increases with temperature at a larger rate than in the liquid phase just below the critical region.

In Figure III-117, the second curve from the top is drawn through the points for 365.7K. The points for 365K (liquid phase) are negligibly different. Other isochores examined include those where $n/n_c = 0.50$ (Figure III-119), 0.25 (Figure III-120), 0.13 (Figure III-121), and 0.020 (Figure III-122). In all these cases increasing the temperature along the isochore leads to an increase in mobility with the rate of increase becoming less at the higher temperatures.

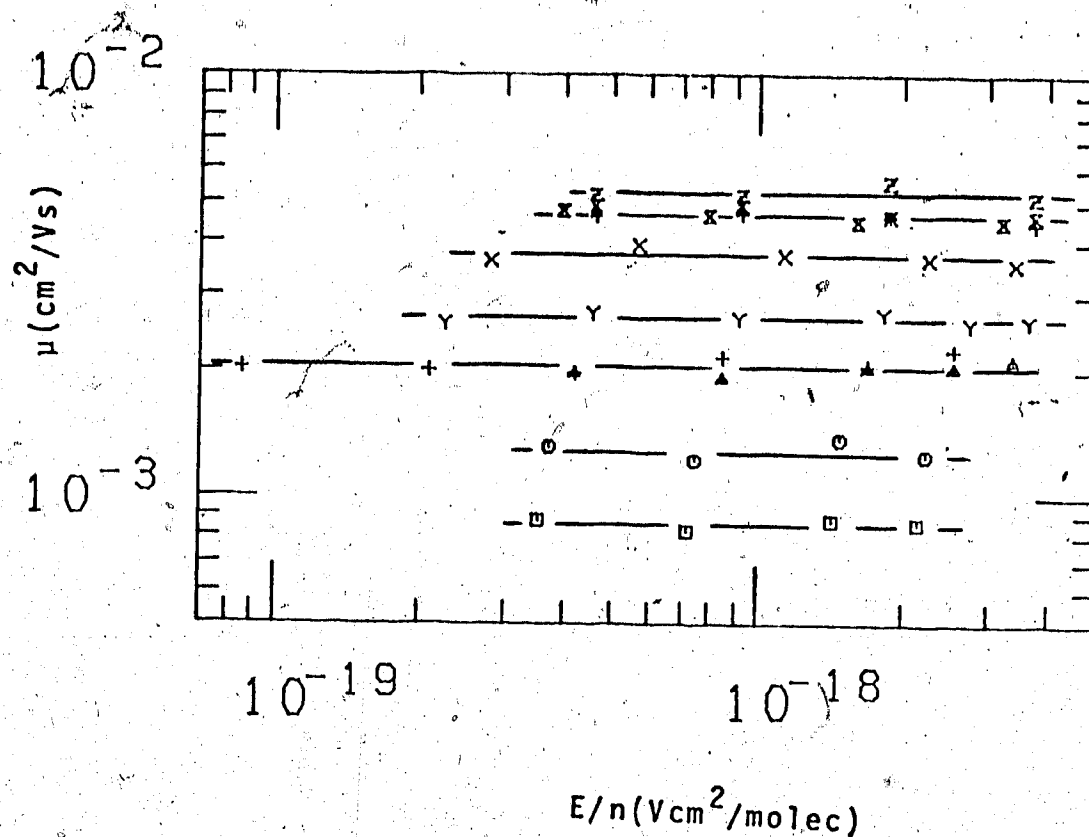


FIGURE III-117. Ion mobilities in liquid propene as functions of E/n . Densities and temperatures ($n/10^{21}$ molec/cm³, T): \square (8.66, 231K), \circ (8.27, 255K), Δ (7.33, 296K), $+$ (7.33, 296K), Y (6.76, 318K), X (5.44, 350K), \bar{X} (3.86, 364.6K), Φ (3.32, 365.7K), \bar{X} (3.32, 367.5K), Z (3.32, 370K).

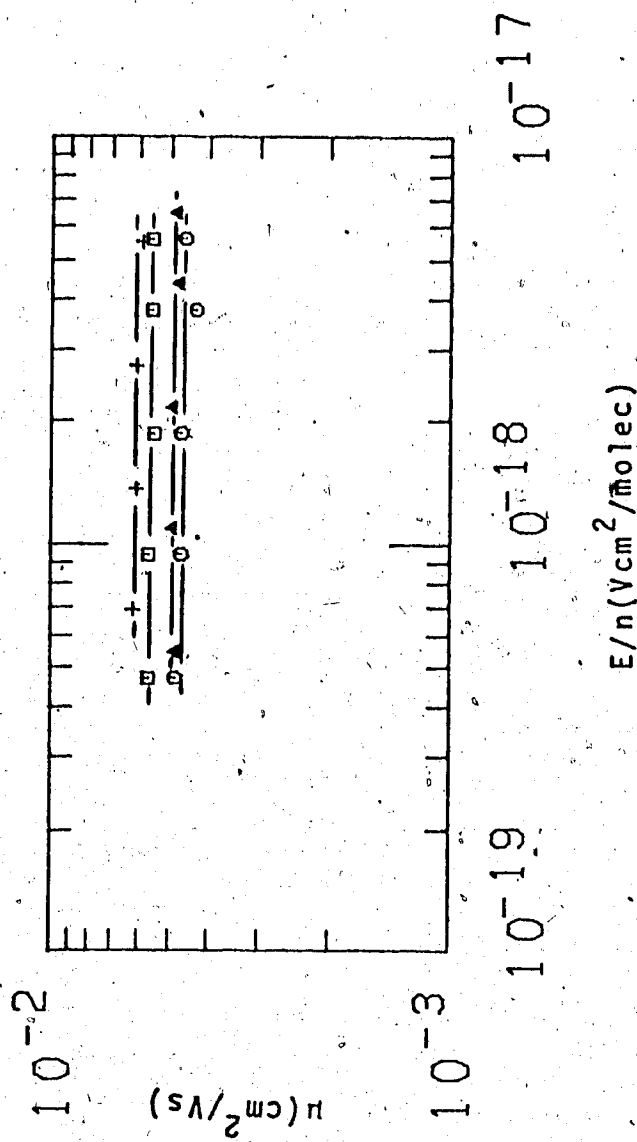


FIGURE III-118. Ion mobilities in gaseous and supercritical propene as functions of E/n . Densities and temperatures ($n/10^{21}$ molec/cm³, T): \square (3.32, 368K), \circ (3.32, 365.4K), Δ (2.86, 364.2K), $+$ (2.26, 362K).

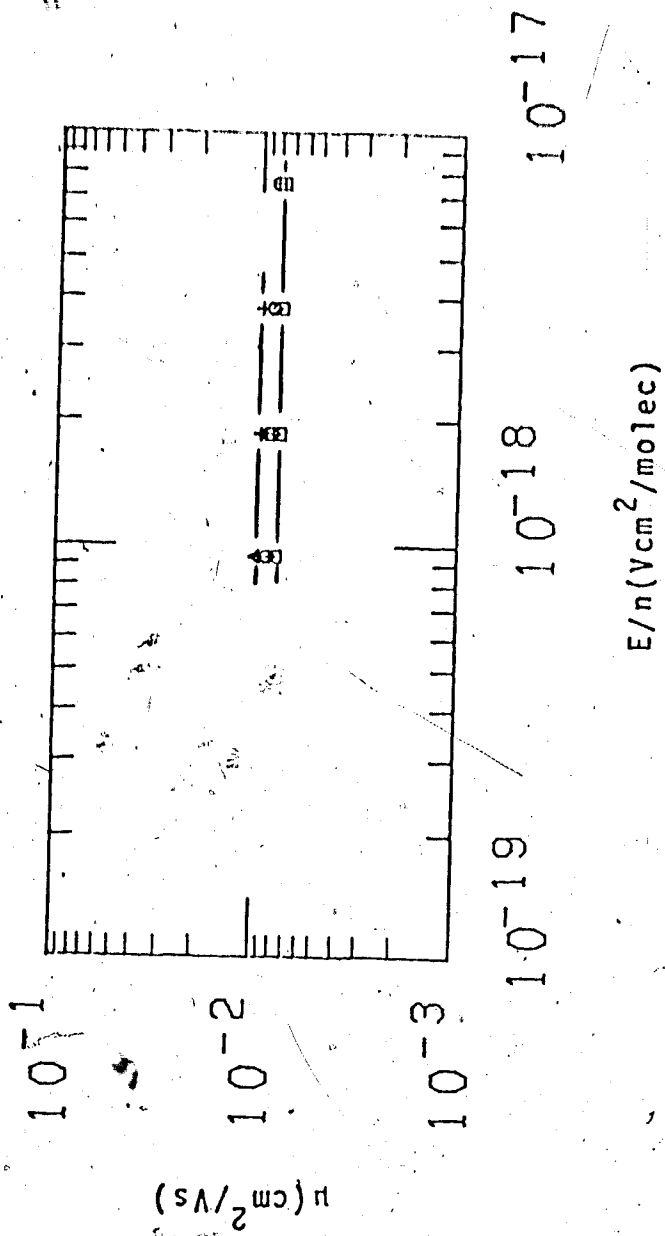


FIGURE III-119. Ion mobilities in gaseous propene as functions of E/n .
 $n = 1.66 \times 10^{21}$ molec/cm³. Temperatures: \square (358K), \circ (362K),
 Δ (366K), $+$ (368K)

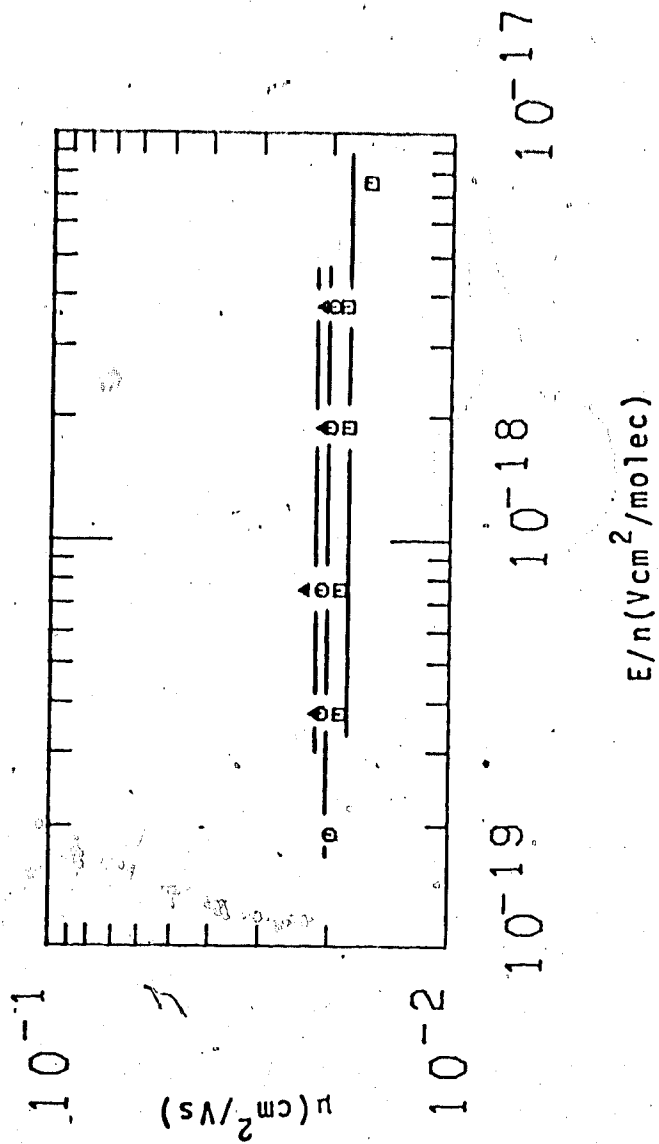


FIGURE III-120. Ion mobilities in gaseous propene as functions of E/n .

$n = 8.23 \times 10^{20}$ molec/ cm^3 . Temperatures: □ (349K), ○ (368K), Δ (389K).

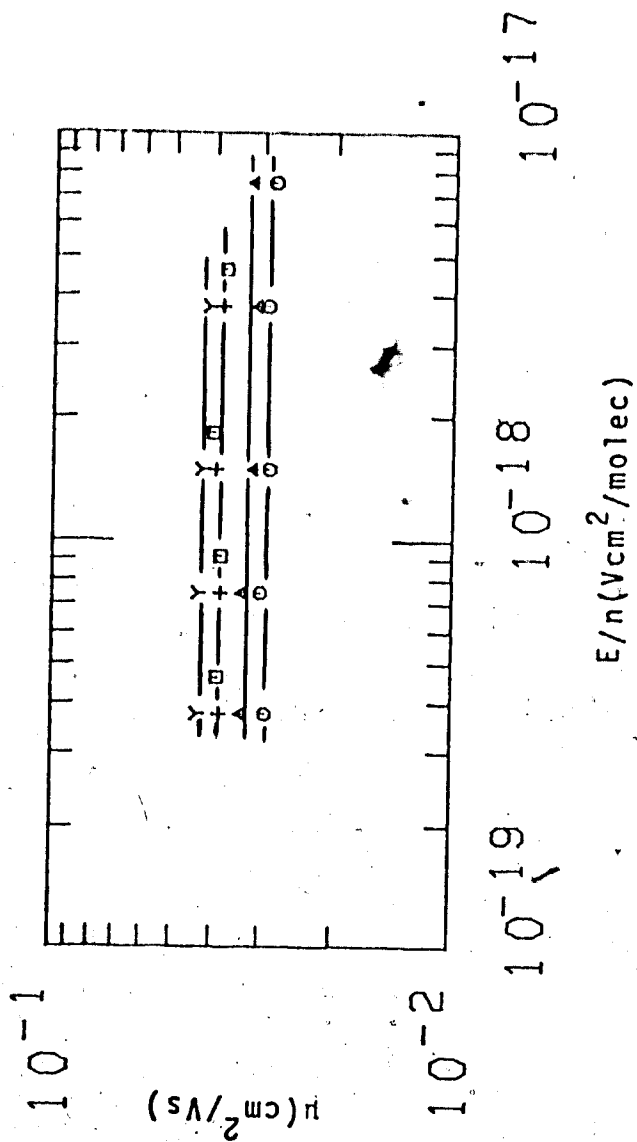


FIGURE III-121. Ion mobilities in gaseous propene as functions of E/n .
 Densities and temperature ($n/10^{20}$ molec/ cm^3 , T): \square (3.37, 296K),
 \circ (4.15, 305K), Δ (4.15, 318K), + (4.15, 358K), Y (4.15, 382K).

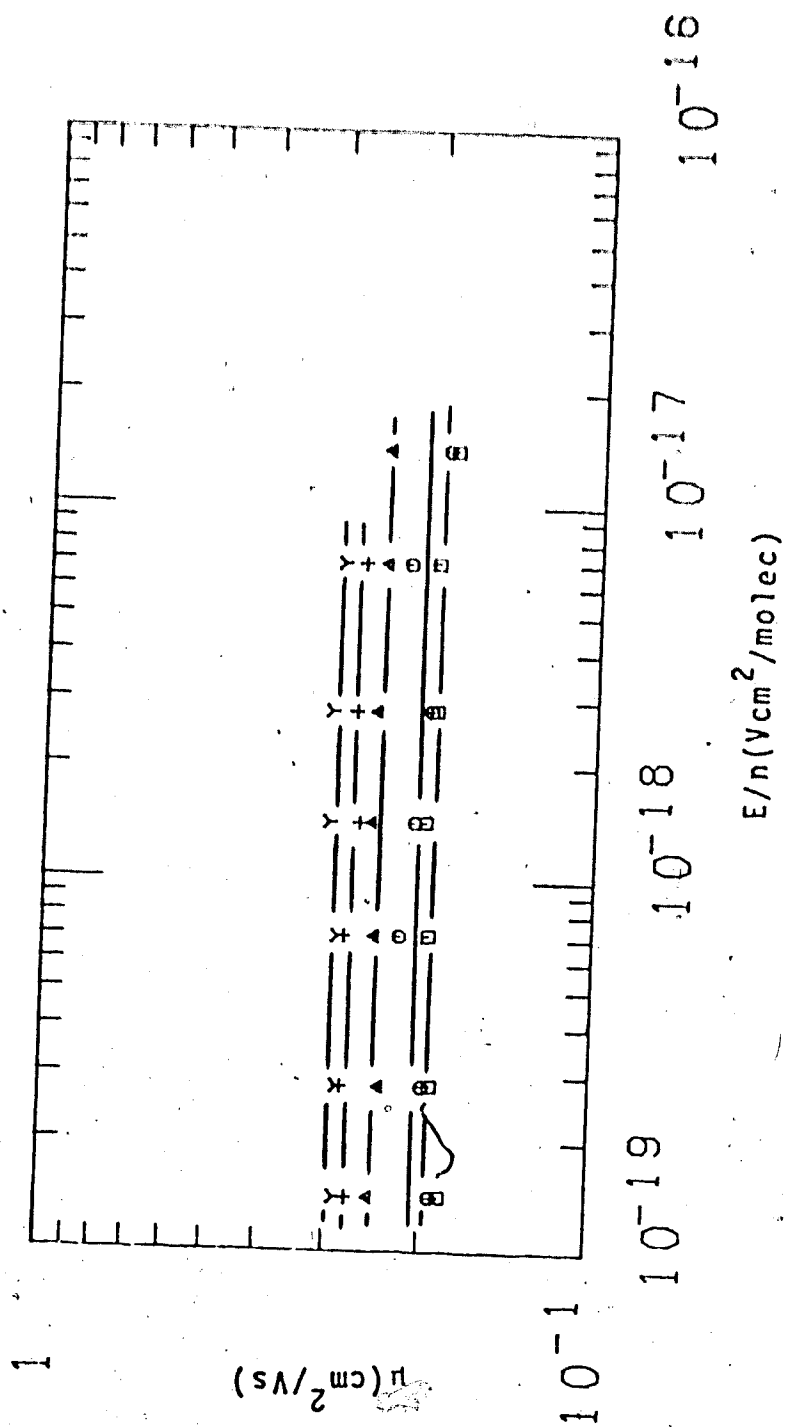


FIGURE III-122. Ion mobilities in gaseous propene as functions of E/n .
 $n = 6.61 \times 10^{19}$ molec./ cm^3 . Temperatures: \square (294K), \circ (355K), Δ (393K).

The effect of decreasing the density along the co-existence curve can be obtained from figures III-118, III-121 and III-123. Below $n/n_c \sim 0.8$, the mobility increases inversely proportionally with the decrease in density. Between $n/n_c = 1$ and $n/n_c = 0.8$, the mobility increases at a slower rate than the decrease in density.

Three curves were not drawn. They are the curves for 362K and 366K (both on Figure III-119) and the curve for 358K (Figure III-121). On Figure III-119, the curve for 362K is 9% above that of the curve for 358K. The curve for 366K is 3% below that of the curve for 368K. On Figure III-121, the curve for 358K is only 2% higher than that of 296K (based on arithmetic average). On the scale of figure the two curves would coincide.

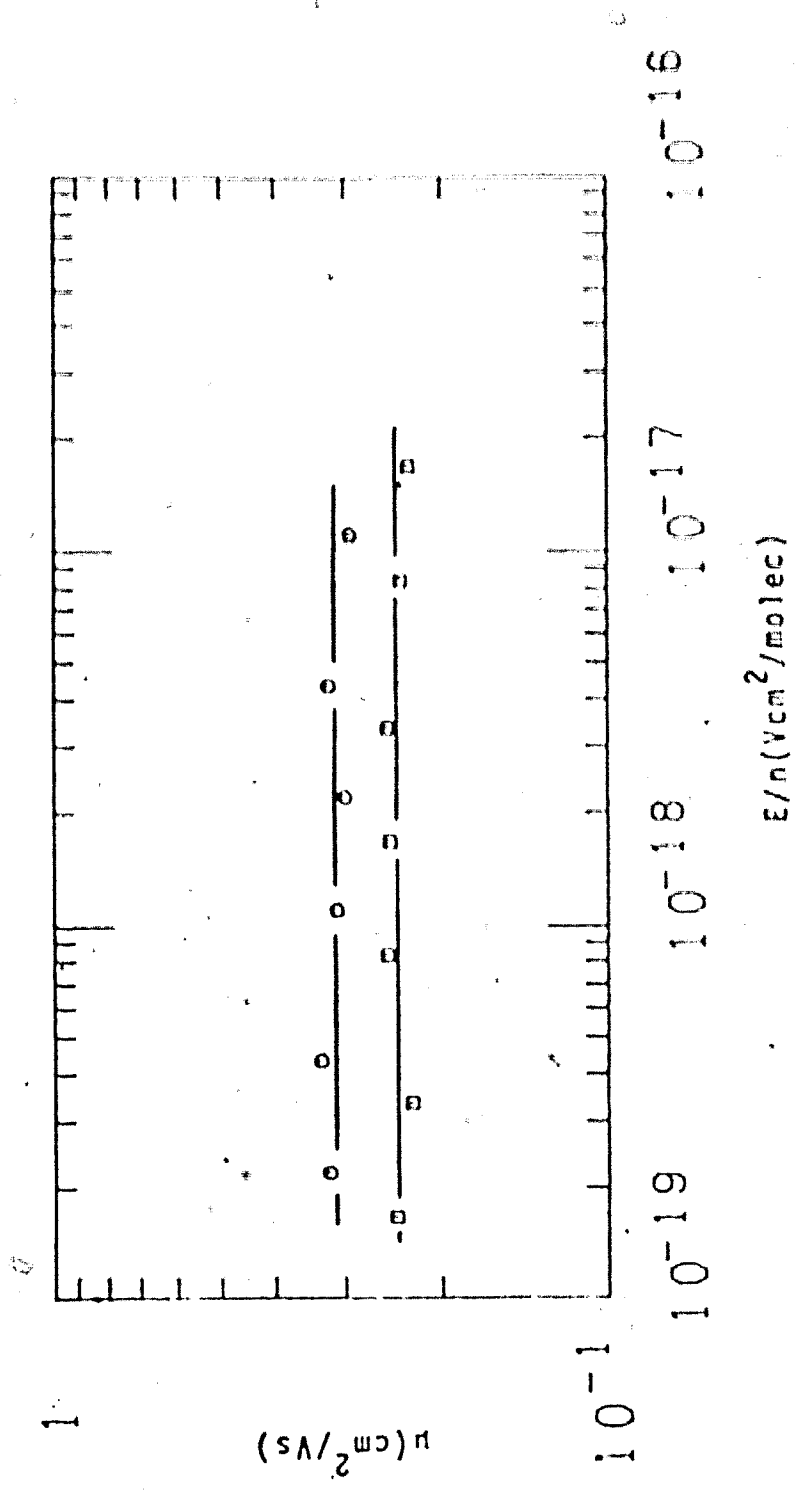


FIGURE III-123. Ion mobilities in gaseous propene in functions of E/n .
Densities and temperatures ($n/10^{19}$, T): ◻ (5.01, 240K), ○ (4.51,
233K).

S

TABLE III-15

Summary of Ion Results for Propene ^a

T °K	n 10 ²¹ molec cm ³	ν_i 10 ⁻¹⁷ cm ² Vs	$\mu_i n$ 10 ¹⁹ molec Vs cm
231	8.66	0.0859	0.744
255	8.27	0.129	1.07
296	7.33	0.203	1.49
318	6.76	0.264	1.78
350	5.44	0.372	2.02
364.6	3.86	0.461	1.78
365.7	3.32 ^b	0.462	1.53
367.5	3.32 ^b	0.475	1.58
370	3.32 ^b	0.526	1.75
368	3.32 ^b	0.557	1.85
365.4	3.32 ^b	0.462	1.53
364.2	2.86	0.485	1.39
362	2.26	0.607	1.37
368	1.66	0.973	1.62
366	1.66	0.946	1.57
362	1.66	0.865	1.44
358	1.66	0.787	1.31
389	0.823	2.16	1.78
368	0.823	2.03	1.67
349	0.823	1.79	1.47
382	0.415	4.24	1.76
358	0.415	3.85	1.60
318	0.415	3.23	1.34
305	0.415	2.92	1.21
296	0.337	3.78	1.27
393	0.0661	29.5	1.95
355	0.0661	27.6	1.82
294	0.0661	24.7	1.63

(continued.....)

TABLE III-15 (continued)

252	0.0661	20.7	1.37
247	0.0661	19.5	1.29
240	0.0603	24.0	1.44
233	0.0461	31.2	1.44

a Data appear in the order of appearance in the figures.

b $n_c = 3.32 \times 10^{21}$. $T_c = 365K$.

8. Cyclopropane

Results for cyclopropane are contained in Figures III-124 to III-129. All measurements were made in high pressure conductance cells. Cells used to collect data in Figures III-124 and III-125 were liquid type. The other results were obtained in gas type cells.

Liquid phase results are shown in Figure III-124. Increasing the temperature along the coexistence curve leads to a steady increase in mobility between 254K and 393K. When the sample is heated to the critical temperature (Figure III-125), the mobility increases. A further increase in temperature leads to another increase in mobility.

Figure III-126 shows the variation in the mobility in the gas phase as the sample is cooled from the supercritical fluid. The mobility first decreases, passes through the critical point, then increases again at below the critical point.

Measurements along other isochores where $n/n_c = 0.46$ (Figure III-127), 0.25 (Figure III-128), and 0.099 (Figure III-129) show that over the temperature range examined, the mobility continues to rise with temperature. From Figures III-126 to III-129, the gas phase ion mobilities in cyclopropane are seen to increase as the density is decreased along the coexistence curve in the same manner as in the other seven compounds. Below

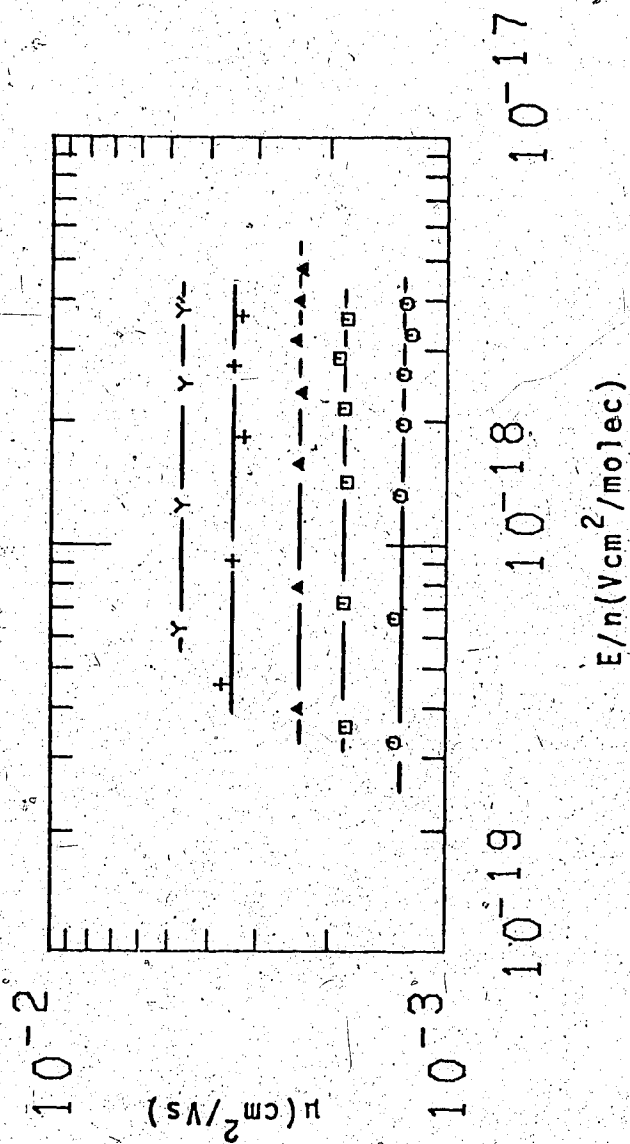


FIGURE III-124. Ion mobilities in liquid cyclopropane as functions of E/n .

Densities and temperatures ($n/10^{21}$ molec/cm³, T): O (9.39, 254K)

\square (8.62, 297K), Δ (7.79, 332K), + (6.73, 367K), γ (4.97, 393K).

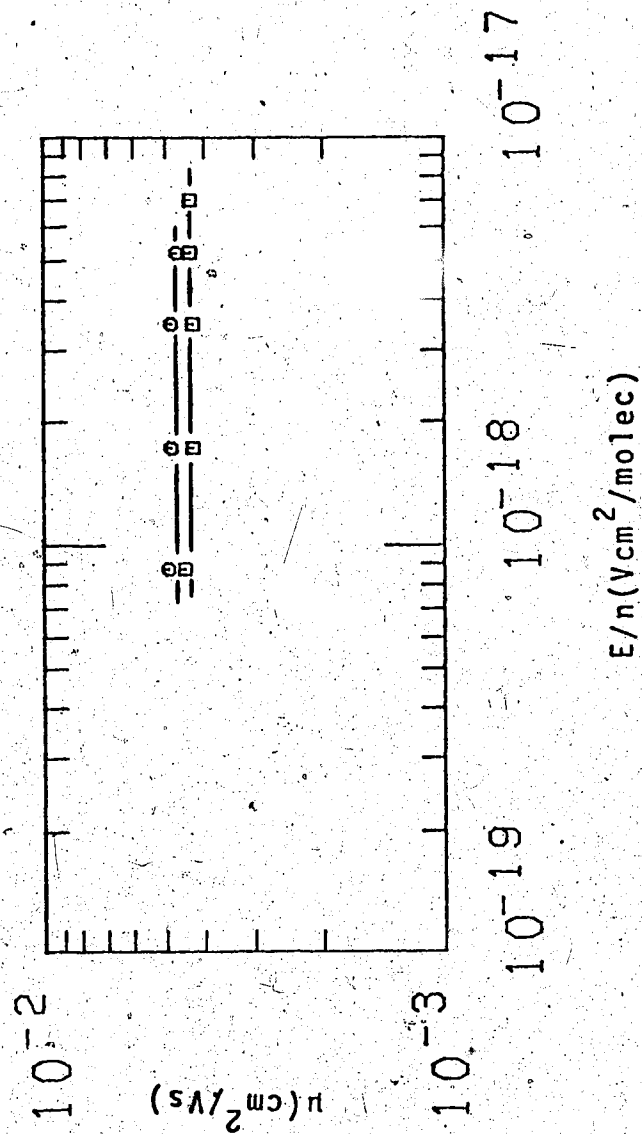


FIGURE III-125. Ion mobilities in supercritical cyclopropane as functions of E/n . $n = 3.55 \times 10^{21}$ molec/cm³. Temperatures: □ (397.8K), O (398.7K).

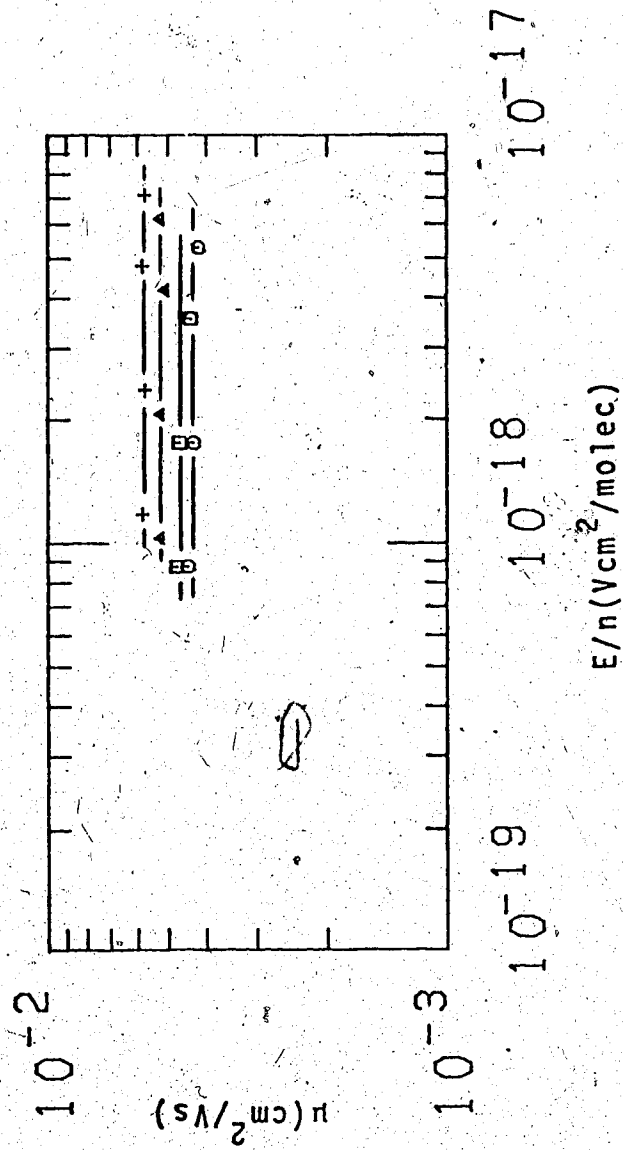


FIGURE III-126. Ion mobilities in gaseous and supercritical cyclopropane as functions of E/n . Densities and temperatures ($n/10^{21}$ molec/cm³, T): \square (3.55, 398.4K), \circ (3.55, 397.8K), \triangle (3.01, 397K), $+$ (2.65, 395K).

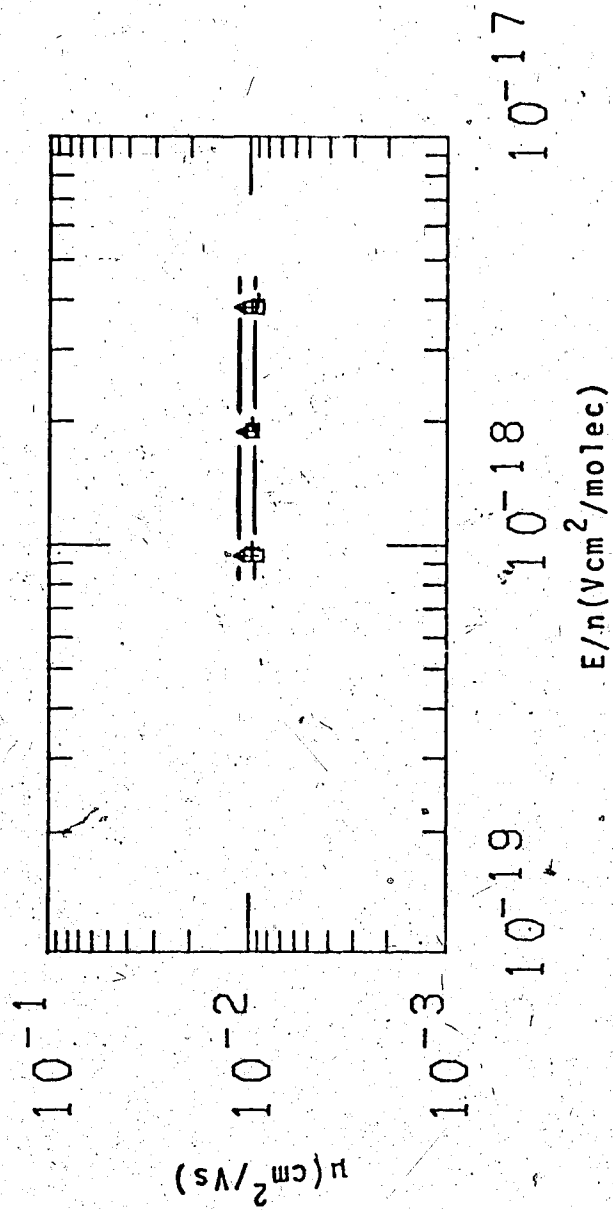


FIGURE III-127. Ion mobilities in gaseous cyclopropane as functions of E/n .

Densities and temperatures ($n/10^{21}$ molec/cm³, T): \square (1.57, 385K),

\square (1.64, 387K), \triangle (1.64, 399K).

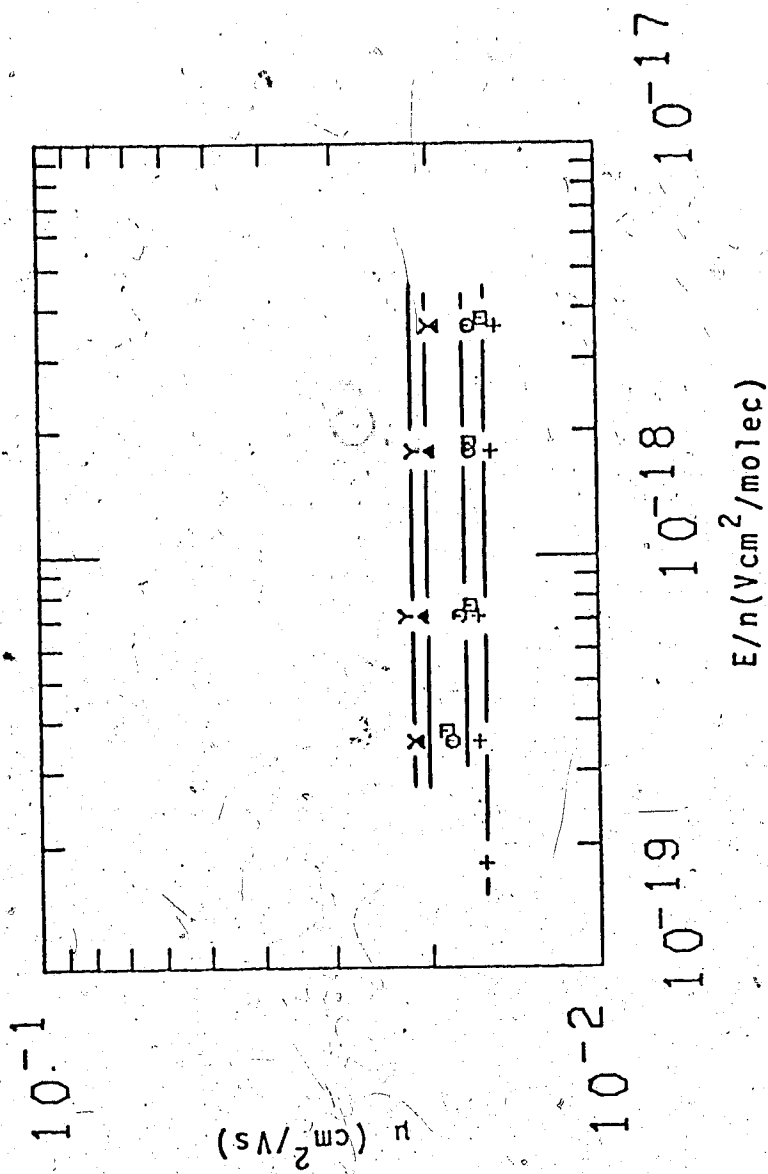


FIGURE III-128. Ion mobilities in gaseous cyclopropane in functions of E/n .

Densities and temperatures ($n/10^{20}$ molec/ cm^3 , T): □ (8.30, 358K),

+ (8.74, 360K), O (8.74, 373K), Δ (8.74, 395K), Y (8.74, 405K).

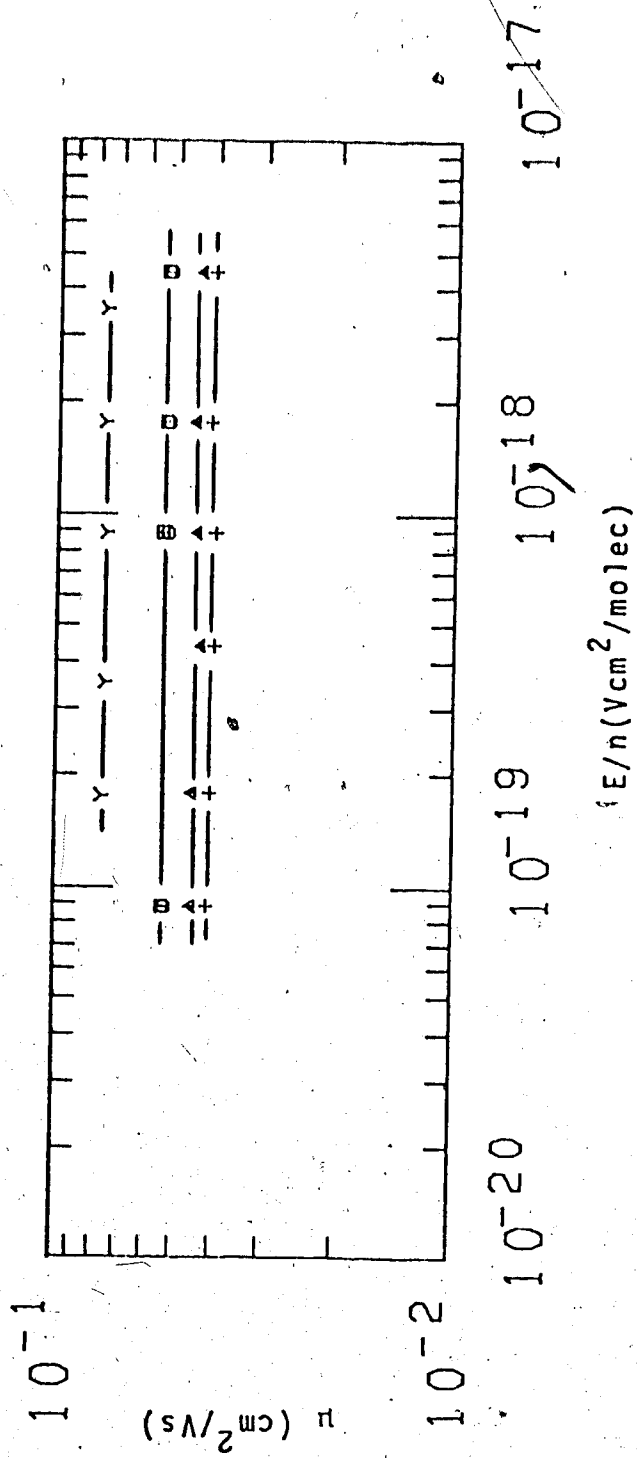


FIGURE III-129. Ion mobilities in gaseous cyclopropane as functions of E/n .
 Densities and temperatures ($n/10^{20}$ molec/cm³, T): Y (1.76, 296K),
 + (3.51, 322K), Δ (3.51, 348K), O (3.51, 396K), \square (3.51, 406K).

$n/n_c \sim 0.4$, the mobility varies inversely proportionally with the density. Between $1 > n/n_c > 0.4$ the mobility is increasing at a lesser rate than the decrease in density.

On Figure III-127, the curve for 387K and that for 394K were omitted. The curve for 387K is 2% lower than that of 385K. The curve for 394K is 4% higher than that of 385K. On Figure III-128, the curves for 358K and 372K are within 2% of each other. The curve for 372 was drawn. On Figure III-129, curves for 396K and 406K are within 2% of each other. On the scale of the figure, they superimpose. The curve drawn is for 406K.

Data for cyclopropane are summarized in Table III-

16.

TABLE III-16

Summary of Ion Results for Cyclopropane^a

T °K	\bar{n} $10^{21} \frac{\text{molec}}{\text{cm}^3}$	μ_+ $10^{-3} \frac{\text{cm}^2}{\text{Vs}}$	$\mu_+ \bar{n}$ $10^{19} \frac{\text{molec}}{\text{Vs cm}}$
254	9.39	1.30	1.22
297	8.62	1.81	1.56
332	7.79	2.35	1.83
367	6.73	3.45	2.32
393	4.97	4.66	2.32
397.8	3.55 ^b	4.35	1.54
398.7	3.55 ^b	4.70	1.67
398.4	3.55 ^b	4.63	1.64
397.8	3.55 ^b	4.34	1.54
397	3.01	5.20	1.57
395	2.65	5.78	1.53
385	1.57	9.55	1.50
387	1.64	9.38	1.54
394	1.64	10.2	1.67
399	1.64	11.0	1.80
358	0.830	17.1	1.42
360	0.874	16.0	1.40
372	0.874	17.5	1.53
395	0.874	20.2	1.77
405	0.874	21.3	1.86
296	0.176	76.0	1.34
322	0.351	40.4	1.42
348	0.351	44.3	1.55
396	0.351	52.9	1.86
406	0.351	53.8	1.89

^a Data appear in the order of appearance as in the figures.

^b $n_c = 3.55 \times 10^{21}$. $T_c = 397.8\text{K}$.

C. Free Ion Yields

Free ion yields were measured in the eight hydrocarbon systems along the vapor-liquid co-existence curve in both phases as well as in the supercritical fluid. With the exceptions of methane and ethane, measurements were also made along a number of isochores where $n/n_c < 1$. The effect of an electron scavenger, SF_6 , on the free ion yields in isobutane (2-methylpropane) was also examined.

The experimental free ion yields were calculated in the manner described in Chapter II. The solid curves drawn through the figures of this section were calculated with a model that will be described in Chapter IV. By this model, the most probable distance b that the epithermal electrons travel during thermalization can be extracted.

The free ion yields are plotted against the electric field strength since that is the relevant parameter in the model. Further, common practice involves a comparison of bd , where d is the density in g/cm^3 , so all the densities in this section are cited in g/cm^3 . G_{fi}^0 and G_{tot} are fitting parameters.

Data will be presented in the same manner as the mobilities. Tables summarizing the results will be given after each subsection.

1. Methane

Free ion yields in liquid methane appear in Figures III-130 to III-133. In all the figures, the free ion yields increase sharply with electric field up to about 10 kV/cm and then tend towards levelling off. There is a difference between the results obtained with a positive applied electric field and that obtained using a negative voltage supply. The positive voltage results are consistently above those of the negative voltage supply. This difference has been previously noted in other high mobility liquids (150). Also in agreement with the earlier work, the difference between the two sets of results increases with increasing voltage. The difference has been attributed to positive field penetration into the region between the collector and guard electrodes that removes some of the highly mobile electrons from that dead volume, which permits the positive ions then to drift towards the collector. A negative applied field would push extra electrons into the dead volume, but there would not be additional positive ions to neutralize. The extra electrons would eventually diffuse to the collector and guard, relatively unaffected by entry into the dead volume. As corroborating evidence, it was pointed out that this difference is not observed for liquids where the electron mobilities are low, and that the difference is also smaller when the cell volume is smaller. The same observations about the

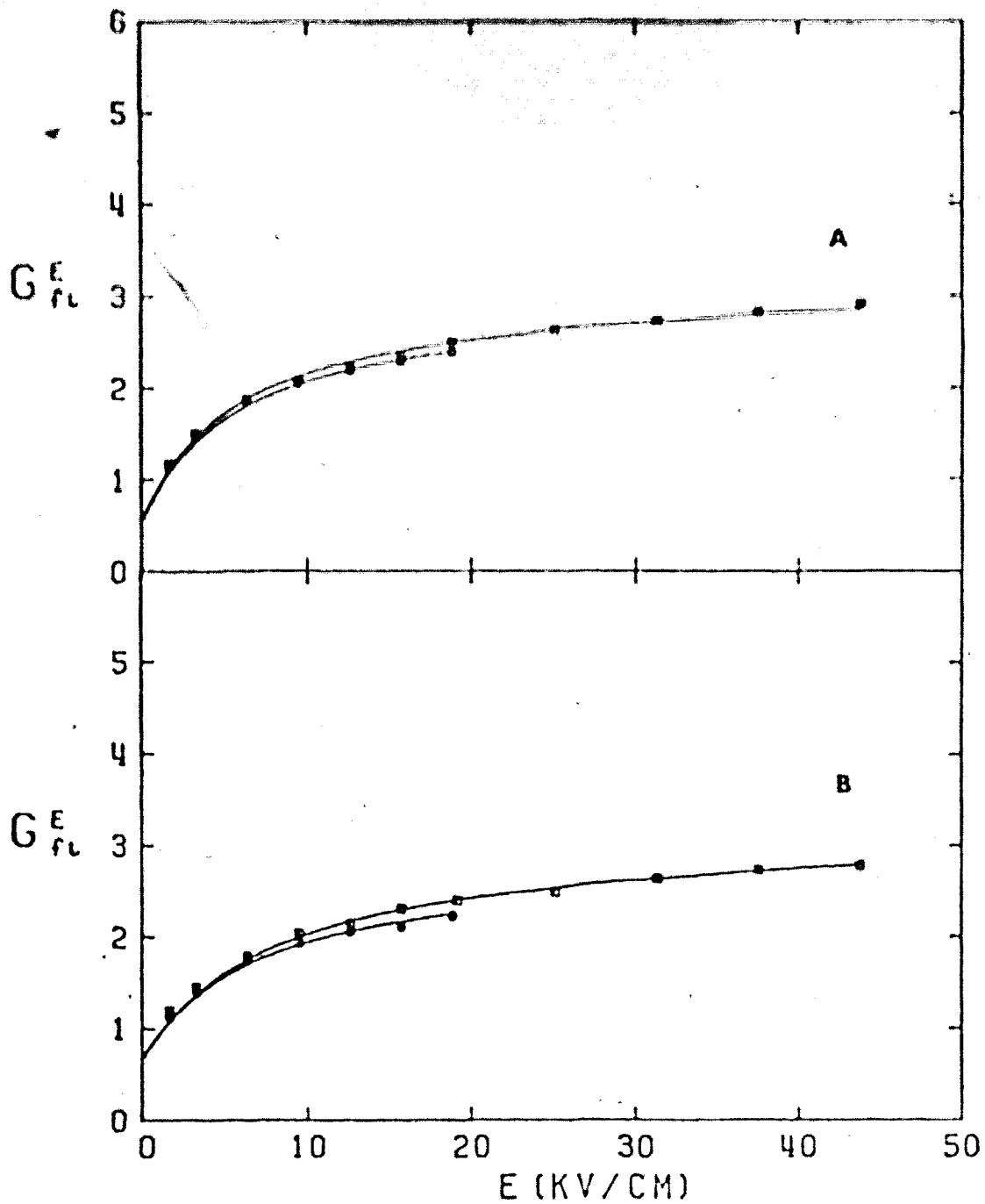


FIGURE III-130. Free ion yields G_{fi}^E as functions of electric field strength E in liquid methane. \square is (+) applied voltage. \circ is (-) applied voltage.

A: 91K and 0.453 g/cc.

B: 118K and 0.412 g/cm³.

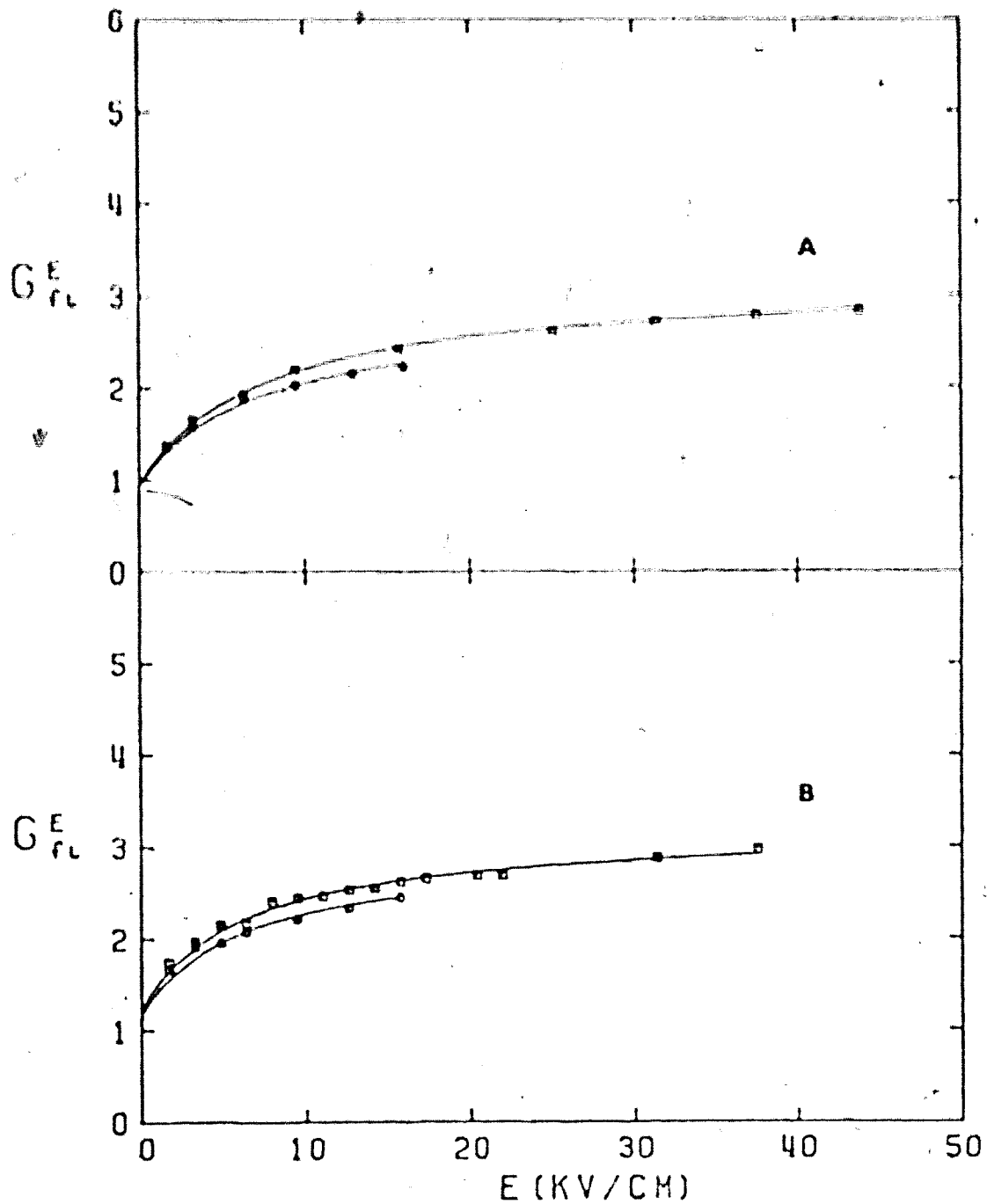


FIGURE III-131. Free ion yields G_{fi}^E as function of electric field strength E in liquid methane. \square is (+) applied voltage. \circ is (-) applied voltage.

A: 153K and 0.357 g/cm³.

B: 170K and 0.314 g/cm³.

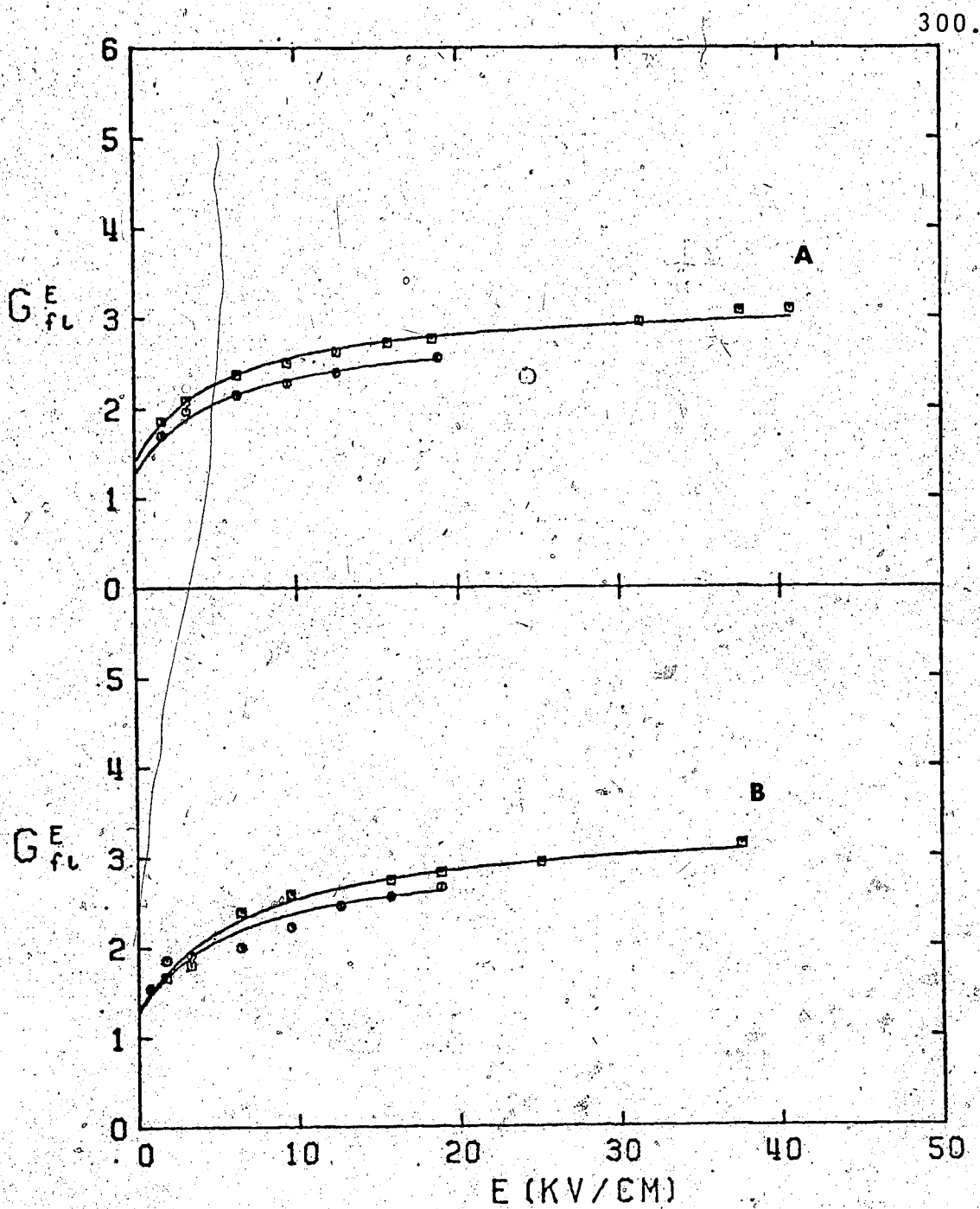


FIGURE III-132. Free ion yields as functions of electric field strength in liquid methane. □ is (+) applied voltage. ○ is (-) applied voltage.

A: 173K and 0.303 g/cm³.

B: 179K and 0.280 g/cm³.

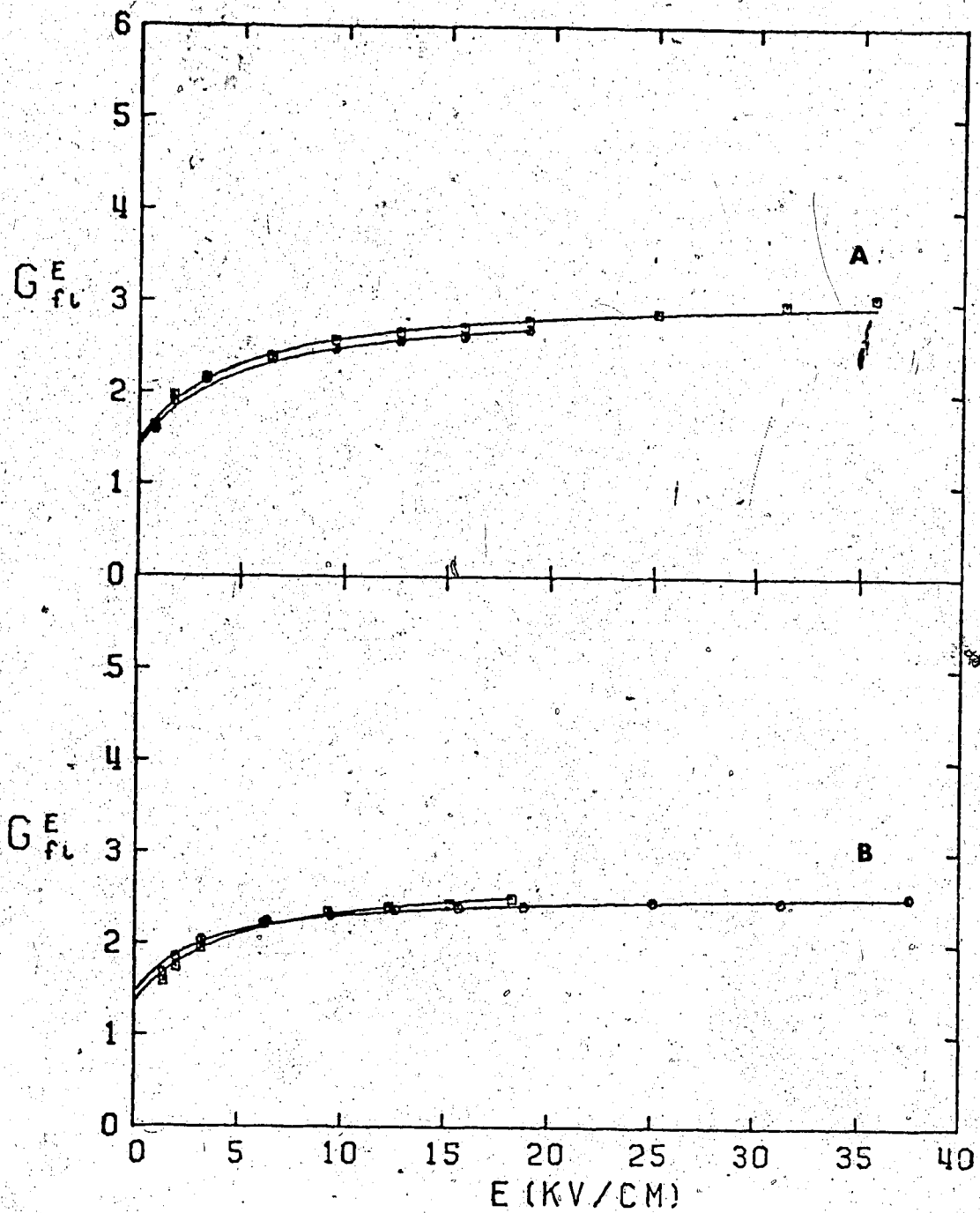


FIGURE III-133. Free ion yields as functions of E in liquid methane. \square is (+) applied voltage. \circ is (-) applied voltage.

A: 180K and 0.276 g/cm³.

B: 188K and 0.220 g/cm³.

sign difference were also noted by another worker (137).

The free ion yields in methane change very little over the entire liquid range. In this behavior it is much more like the liquified rare gases than the other hydrocarbon compounds. In the other seven systems the free ion yield will be seen to change much more drastically as the liquid is heated along the co-existence curve.

From section III-A, the electron mobility can be seen to drop an order of magnitude over a few degrees (Figures III-1 and III-5). As the liquid is heated into the critical region, the voltage sign effect disappears (Figure III-134). Increasing the temperature from 192K to 194K leads to little increase in the free ion yield. Later sections will show that in all the eight compounds, increasing the temperature along an isochore leads to little variation of the free ion yield.

Figures III-135 and III-136 show the effect of cooling the gas along the co-existence curve first to 0.119 g/cm^3 near the critical region, and then down to 0.023 g/cm^3 ($d/d_c \approx 0.14$). For the higher densities there is no voltage sign effect. For the 0.023 g/cm^3 , a voltage sign effect may be appearing though the difference is not large. The curves are also arching more. The high voltage free ion yields are increasing as the density decreases.

Figure III-137 shows free ion yields in much more dilute gases. The voltage difference between positive and

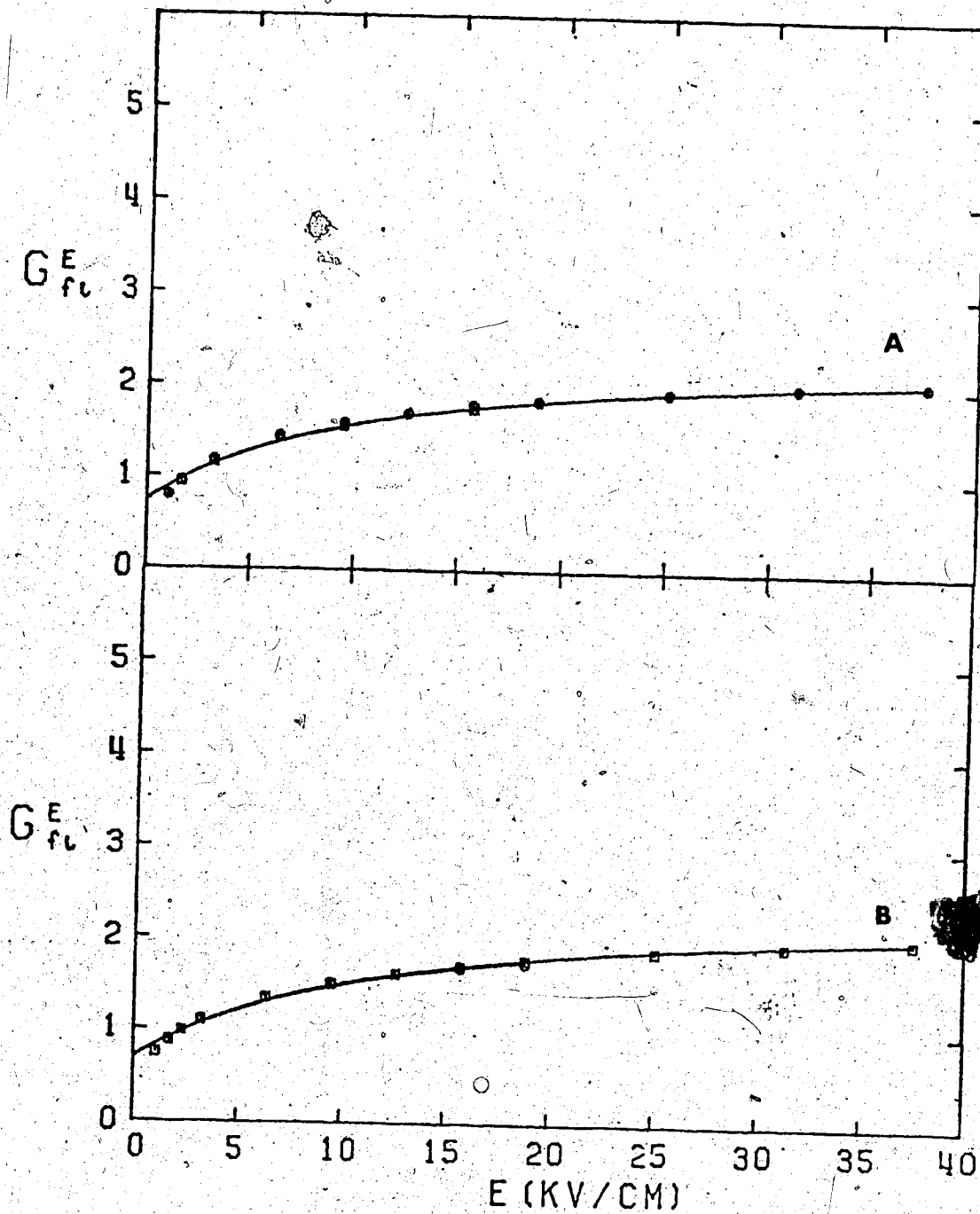


FIGURE III-134. Free ion yields as functions of E in supercritical methane $d = 0.162 \text{ g/cm}^3$.

A: \square (-) applied voltages, \circ (+) applied voltage
194K.

B: \square (+) applied voltage, \circ (-) applied voltage
192K.

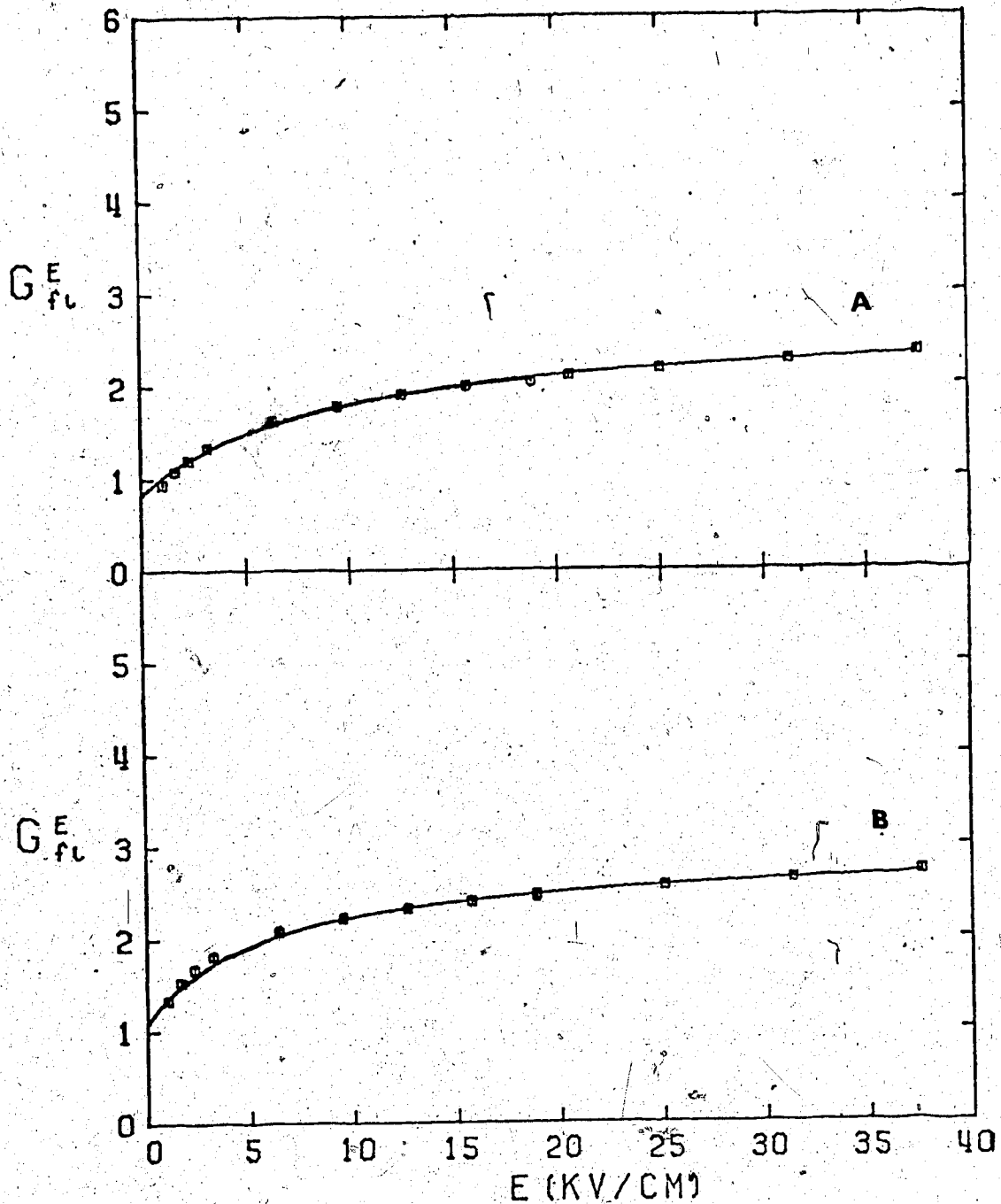


FIGURE III-135. Free ion yields as function of E in gaseous methane. \square is (+) applied voltage \circ is (-) applied voltage.

A: 190K and 0.119 g/cm³.

B: 183K and 0.0765 g/cm³.

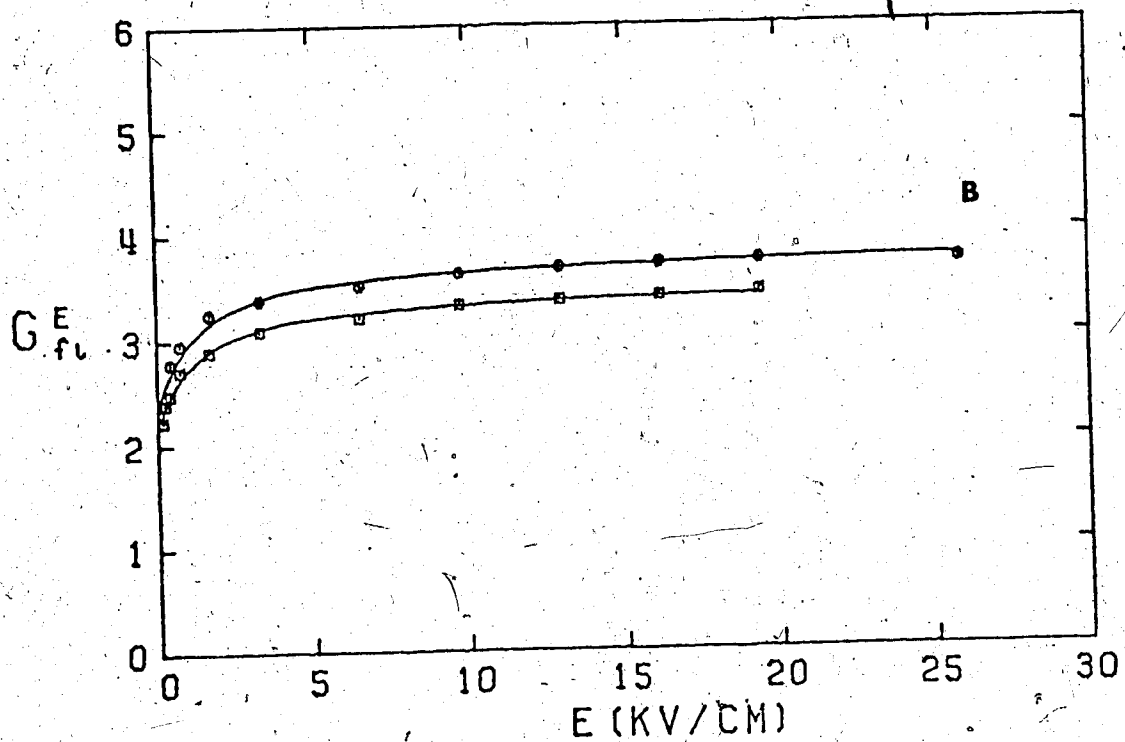
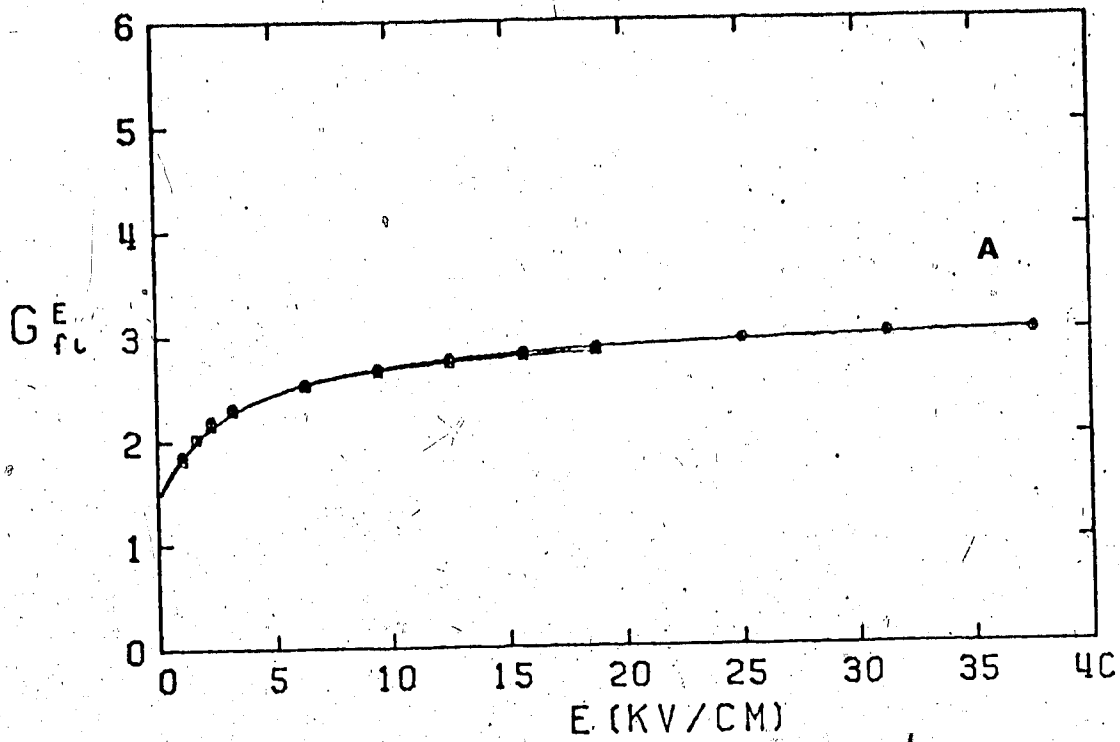


FIGURE III-136. Free ion yields as functions of E in gaseous methane. \square is (-) applied voltage. \circ is (+) applied voltage.

A: 173K and 0.0455 g/cm³.

B: 158K and 0.023 g/cm³.

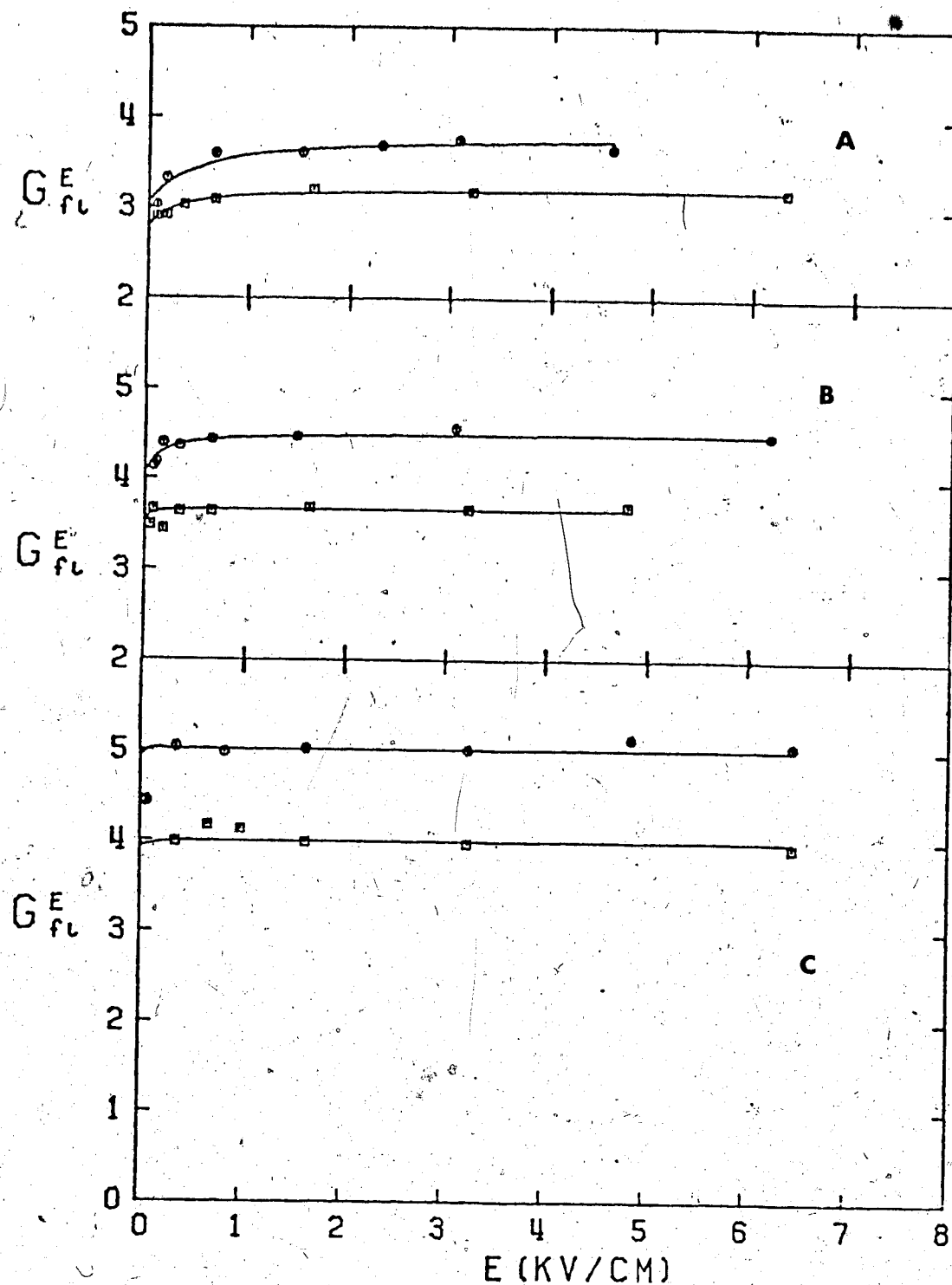


FIGURE III-137. Free ion yields in gaseous methane as functions of E . □ is (-) applied voltage. O is (+) applied voltage.

A: 144K and $0.0124 g/cm^3$.

B: 133K and $0.0071 g/cm^3$.

C: 123K and $0.0039 g/cm^3$.

negative applied voltage results can once more be seen. The conclusion of (150) appears to be supported, that is the negative voltage in such a situation is more correct. Assuming that saturation has occurred at the highest fields, the total free ion yield G_{tot} at the lowest densities are 3.3, 3.6 and 4.0 for 0.0124, 0.0071 and 0.0039 g/cm³, respectively, for the negative applied voltage results. Though the G_{tot} may still be changing, they are within 10% of the low density gas phase $G_{tot} = 3.6$ obtained for methane by other methods (see Table I-1). At these low densities, the model fitting is inappropriate. Variation of b with G_{fi}^0/G_{tot} is too drastic to allow unique determination of b .

Data for methane is summarized in Table III-17.

TABLE III-17

Summary of Free Ion Results for Methane ^a

T K.	d g/cm ³	ϵ^b	G_{fi}^o	G_{tot}	$10^{-8} b^c$ cm	$10^{-8} bd$ g/cm ²
91	0.453	1.72	0.59 (0.61)	3.0 (3.0)	560 (570)	250 (260)
122	0.412	1.65	0.70 (0.70)	2.8 (3.1)	540 (500)	220 (200)
153	0.357	1.54	0.97 (1.0)	2.9 (3.1)	590 (570)	210 (200)
170	0.314	1.47	1.2 (1.3)	3.0 (3.2)	690 (680)	220 (210)
173	0.303	1.45	1.3 (1.4)	2.9 (3.2)	780 (780)	240 (240)
179	0.280	1.42	1.3 (1.3)	3.0 (3.4)	750 (660)	210 (180)
180	0.276	1.41	1.4 (1.5)	3.0 (3.1)	860 (870)	240 (240)
188	0.220	1.31	1.4 (1.5)	2.8 (2.5)	930 (1300)	200 (280)
194	0.162 ^d	1.22	0.75 (0.75)	2.4 (2.4)	540 (550)	88 (88)
192	0.162 ^d	1.22	0.70 (0.70)	2.4 (2.4)	510 (520)	83 (84)
190	0.119	1.16	0.85 (0.86)	2.7 (2.7)	590 (590)	70 (71)
183	0.0765	1.09	1.1 (1.1)	2.8 (2.9)	860 (800)	66 (61)
173	0.0455	1.05	1.5 (1.5)	3.1 (3.0)	1200 (1300)	55 (59)
158	0.023	1.03	2.3 (2.5)	3.5 (3.7)	2300 (2500)	54 (58)

(continued....)

TABLE III-17 (continued)

144	0.0124	1.02	2.8 (3.1)	3.3 (3.7)
133	0.0071	1.01	3.6 (4.1)	3.6 (4.6)
123	0.0039	1.01	3.9 (5.0)	4.0 (5.1)

a Positive applied voltage results in brackets.

b Static dielectric constant

c Most probable thermalization distance

d $T_c = 191K$, $d_c = 0.162 \text{ g/cm}^3$

ii) Ethane

Free ion yield results for ethane are contained in Figures III-138 to III-142. Data in Figures III-138 and III-139 (except 306K) were obtained using a high pressure liquid type cell. The rest of the data was obtained in a high pressure gas type cell.

The liquid phase results are shown in Figure III-138. At low temperatures the free ion yields G_{fi} vary linearly with the electric field strength. As the liquid is heated along the co-existence curve from 166K, the free ion yields become sublinearly dependent upon the electric field strength. There is also much more variation in the liquid phase G_{fi} values than in methane. From Table III-18, it can be seen that G_{fi}^0/G_{tot} for methane is always greater than 0.1. In ethane at 166K, this ratio is 0.02. In the subsequent sections, the other hydrocarbon systems will be seen to resemble ethane in this regard rather than methane. This ratio increases with the temperature and the extent of curvature.

In Figure III-139, free ion yields in supercritical ethane are shown. The top curves (A) and the higher curve of B (307K) were obtained in a liquid type cell using positive applied voltages. More recent results using a gas type cell and a negative applied voltage are given in B for comparison. Possible reasons for the discrepancy have already been given in the discussion

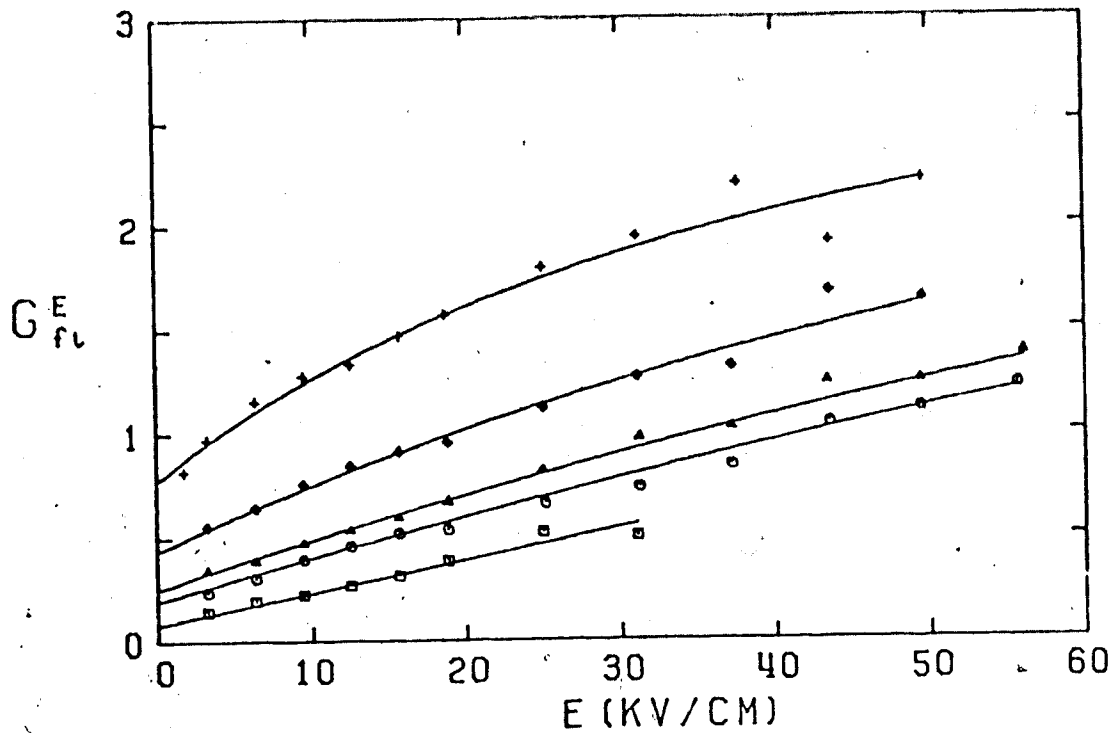


FIGURE III-138. Free ion yields in liquid ethane plotted against the electric field strength. Temperatures and densities (K, d): □ (166, 0.571), ○ (224, 0.503), △ (242, 0.476), ◇ (281, 0.430), + (298, 0.338).

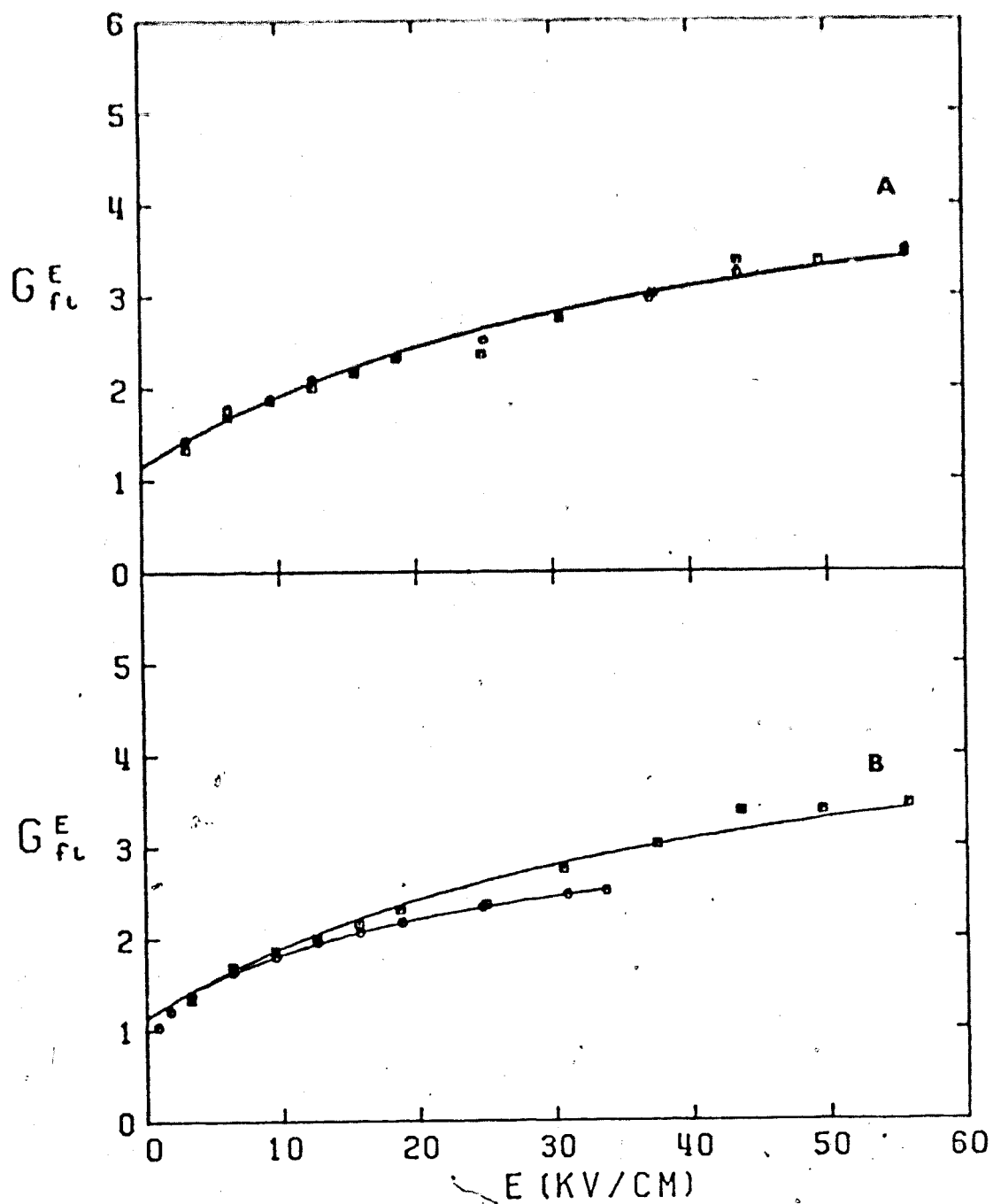


FIGURE III-139. Free ion yields in supercritical ethane as functions of E . $d = 0.203 \text{ g/cm}^3$. Temperatures:
 A: □ (307K), ○ (310K).
 B: □ (307K), ○ (306K).

for methane (section III C (1)). The gas type cell shows no difference between positive and negative applied voltage (Figure III-140 (B) and (C)) in the supercritical fluid. It may be that the dead space in the liquid cell is much larger than that of the gas cell. The results from the gas cell are preferred for the critical density.

The top curves in figure III-140 in the A box are at a density less than that of the supercritical fluid. The free ion yields at the higher fields have increased to a lesser extent than those at lower fields. The overall effect is a more pronounced bending of the free ion curve. Further decreases in density appear in Figures III-141 and III-142. The threshold field at which the free ion yields level off appears to shift from about 15 kV/cm at 0.095 g/cm³ to about 8 at 0.068 g/cm³ to about 6 at 0.028 g/cm³. This value remains the same when the density decreases to 0.051 and 0.046 g/cm³. The high field free ion yields for the three lowest densities are all within about 10% of each other. The difference between the (+) and (-) applied voltages are likely due to experimental scatter. The fitting parameter G_{tot} for these densities is $4.0 \pm 5\%$. This agrees with the total ionization yield obtained in low density gases by other methods of 4.1 (see Table I-1).

Data for ethane are summarized in Table III-18.

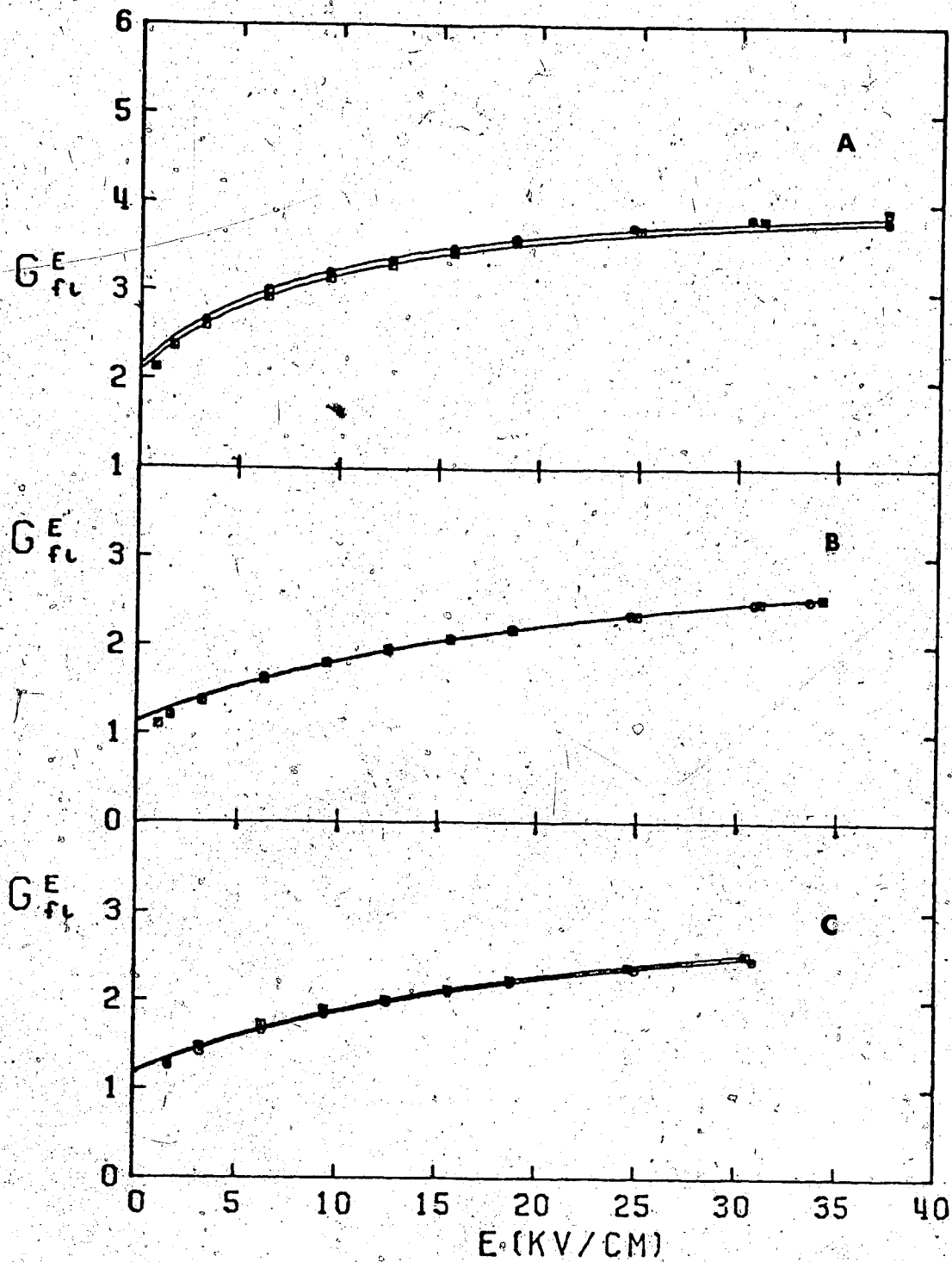


FIGURE III-140. Free ion yields in gaseous and supercritical ethane. Temperatures and densities are: A: (296, 0.095), B: (306, 0.203). C: (308, 0.203). The polarities of the applied voltages are (□, ○): A (+, -), B (-, +), C (+, -).

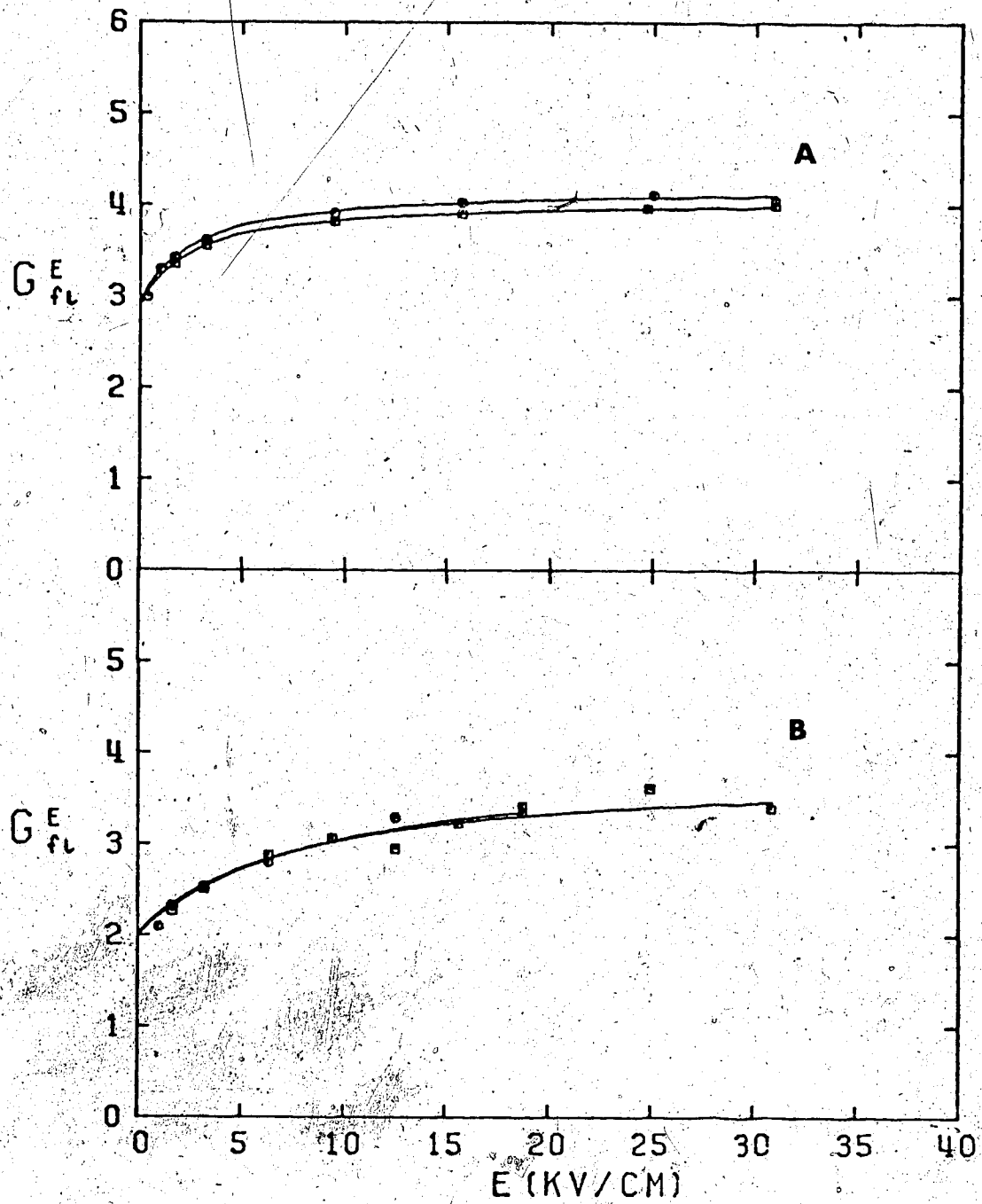


FIGURE III-141. Free ion yields in gaseous ethane.

Temperature and density and polarities of the applied voltages (T, d, □, ○) are:

A (256, 0.028, -, +),

B (286K, 0.068, -, +)

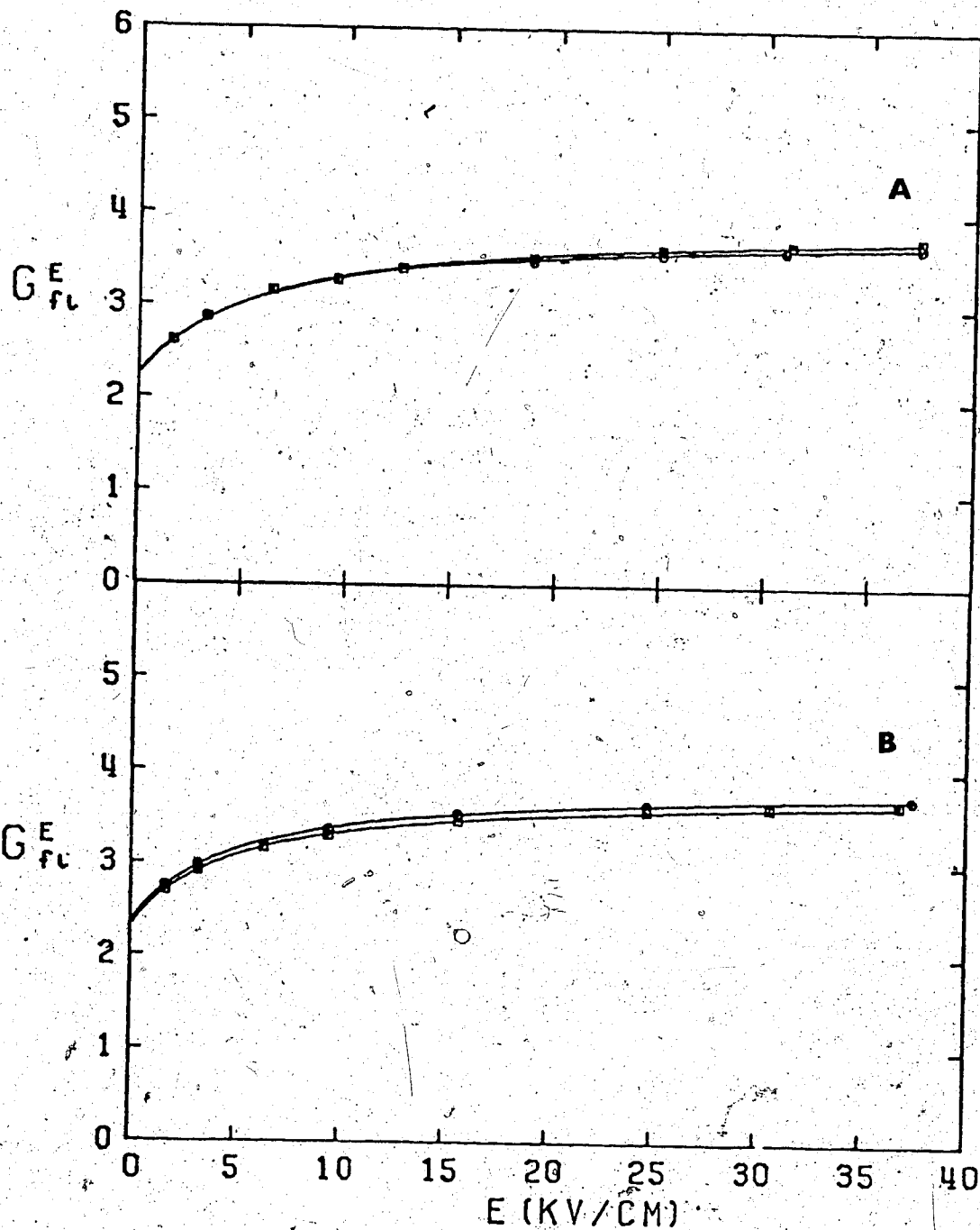


FIGURE III-142. Free ion yields in gaseous ethane as functions of E . Temperature, density and polarities of the applied voltages are (T, d, □, ○):
A (276, 0.051, -, -),
B (273, 0.046, -, +)

TABLE III-18

Summary of Free Ion Results for Ethane ^a

T (K)	d (g/cm ³)	ϵ^b	G _{fi} ^o	G _{tot}	$10^{-8} \text{ cm}^{b,c}$	$10^{-8} \text{ g/cm}^2 \text{ }^{bd}$
166	0.571	1.82	(0.081)	(4.0) ^e	(93)	(53)
224	0.503	1.70	(0.20)	(4.0) ^e	(105)	(53)
242	0.476	1.65	(0.25)	(4.0) ^e	(110)	(54)
281	0.430	1.54	(0.44)	(4.0) ^e	(140)	(58)
298	0.338	1.44	(0.78)	(3.5)	(230)	(76)
307	0.203 ^d	1.25	(1.2)	(5.0)	(260)	(52)
310	0.203 ^d	1.25	(1.2)	(5.0)	(260)	(52)
306	0.203 ^d	1.25	1.1	3.5	350	72
		1.25	(1.1)	(3.5)	(350)	(71)
308	0.203 ^d	1.25	1.2	3.5	370	75
			(1.2)	(3.5)	(360)	(74)
296	0.095	1.12	2.2	4.3	710	67
			(2.1)	(4.2)	(703)	(67)
286	0.063	1.07	2.0	3.9	790	54
			(2.0)	(3.9)	(810)	(55)
256	0.038	1.03	2.9	4.0	2100	58
			(3.0)	(4.2)	(1900)	(53)
276	0.051	1.06	2.3	3.9	1040	53
			(2.3)	(4.0)	(980)	(50)
273	0.046	1.05	2.3	3.8	1200	55
			(2.4)	(3.8)	(1250)	(57)

^a Positive voltage results in brackets.

^b Static dielectric constant

^c Most probable thermalization distance

^d T_c = 306K, d_c = 0.203 g/cm³

^e Assumed equal to low density gas phase value.

3. Propane

Free ion yields determined in propane appear in Figures III-143 to III-151. Data in Figures III-143 to III-145 excluding the negative voltage results in III-145 were obtained in a liquid type high pressure conductance cell. The remainder of the results were obtained in a gas type high pressure conductance cell.

Liquid phase data in Figures III-143 to III-145 show the same general features as the free ion yields in ethane. However, low enough temperatures were attained to show an effect that was not apparent in the ethane set. The lowest three curves 149, 169 and 197K in Figure III-143 are increasing superlinearly with electric field. At 252K, the free ion yield curve is linear with respect to E and at 276K, the free ion yields are beginning to bend sublinearly.

Figure III-144 shows that the extent of bending increases with the temperature. The electron field reached (60 kV/cm) was not sufficient to totally collect all the ions. This trend continues into the critical region (Figure III-145). There is no noticeable difference between results obtained using different polarities. The (+) voltage results in III-144 (B) were obtained in a liquid type cell whereas the (-) results were obtained in a gas type cell. No difference can be noted up to about 36 kV/cm which was the maximum field attained in the gas type cell.

Further results in the supercritical fluid appear in

Figure III-146. A seven degree variation leads to little change in the free ion yields.

Decreasing the density along the co-existence curve (Figure III-147 (A), III-148, III-150(A), III-151) raises the high field voltages but increases the low field voltage results more. The field where the free ion yield seems to level off shifts downwards as the density decreases in a similar manner to the behavior in ethane.

The temperature effect along isochores can be seen in Figures III-147(B), III-149, and III-150(B). The temperature has been increased 13, 50 and 130K for the isochores $n/n_c = 0.5, 0.25$ and 0.15 , respectively. The variation in free ion yield is slight. There may be a slight increase. The apparent voltage sign effect is likely due to scatter.

The fitting parameter G_{tot} (Table III-19) for $d < 0.0557 \text{ g/cm}^3$ is fairly constant and equals 4.0. This agrees well with the low density gas phase total ionization yield of 4.1 (see Table I-1).

Data for propane are summarized in Table III-19.

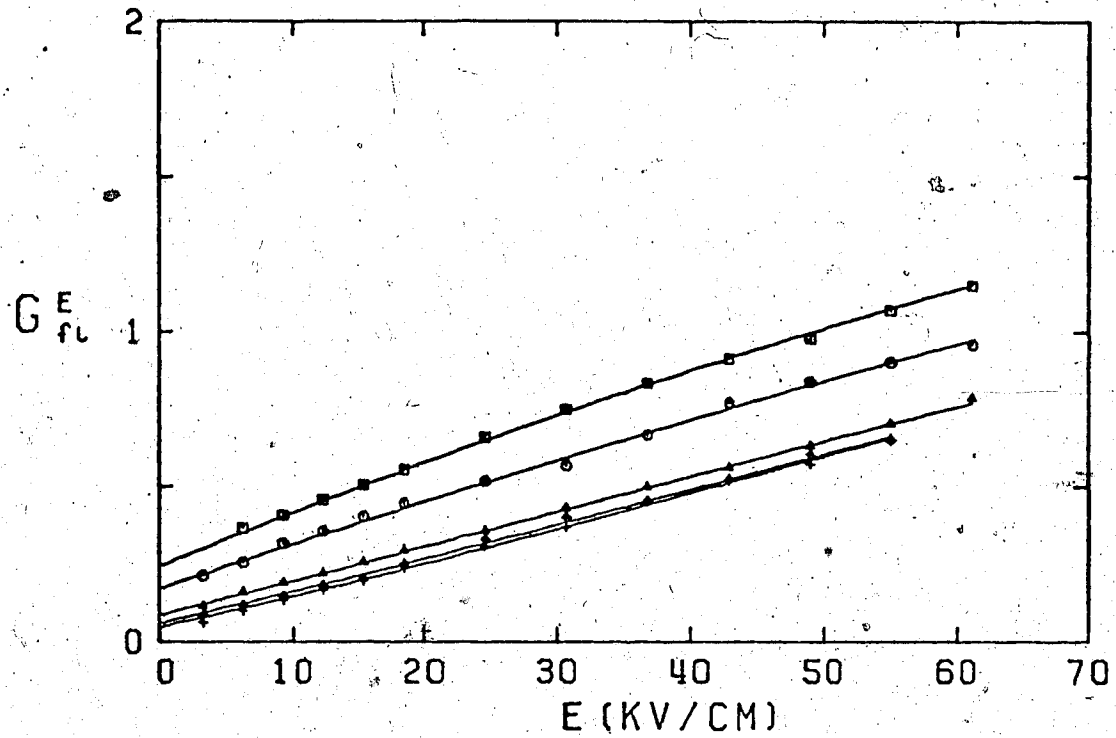


FIGURE III-143. Free ion yields in liquid propane as functions of E . Temperature and density (T, d):
 + (149, 0.680), \diamond (169, 0.656), \triangle (197, 0.621),
 \circ (252, 0.556), \square (276, 0.526).

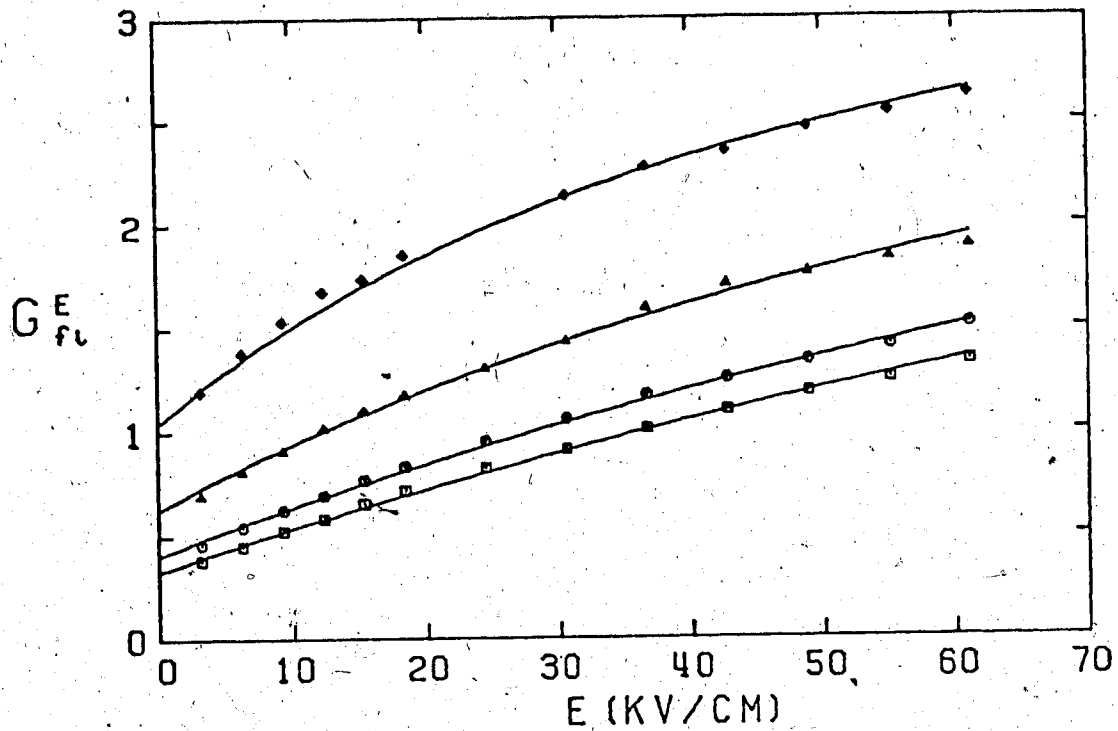


FIGURE III-144. Free ion yields in liquid propane as functions of E . Temperatures and densities (T,d): □ (297, 0.495), ○ (314, 0.465), △ (340, 0.408), ◇ (365, 0.305).

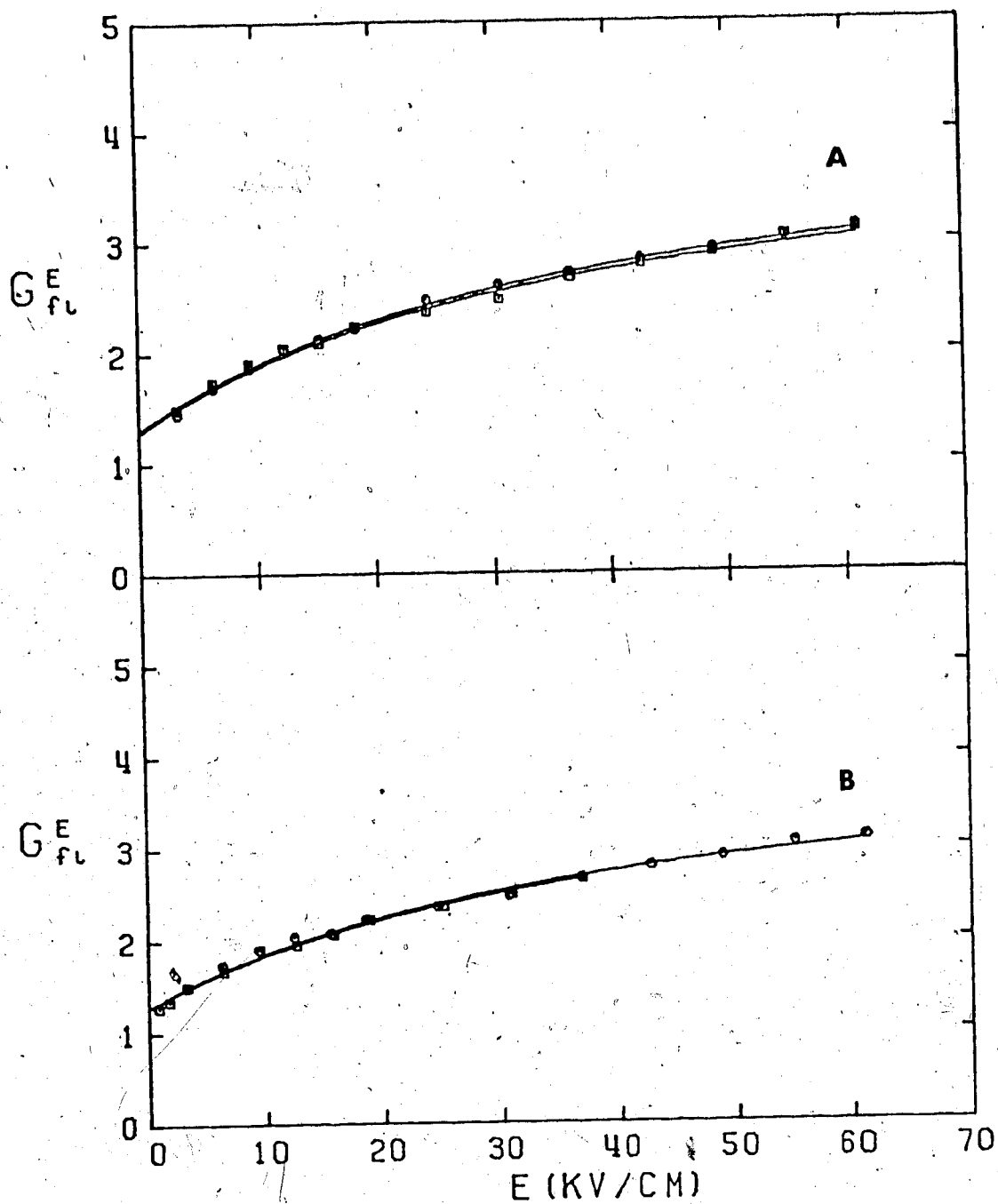


FIGURE III-145. Free ion yields in supercritical propane as functions of E . $d = 0.220$. Temperatures and polarities of the applied voltages:

A, \square (370K, +), \circ (371K, +).

B, \square (370, -), \circ (370, +).

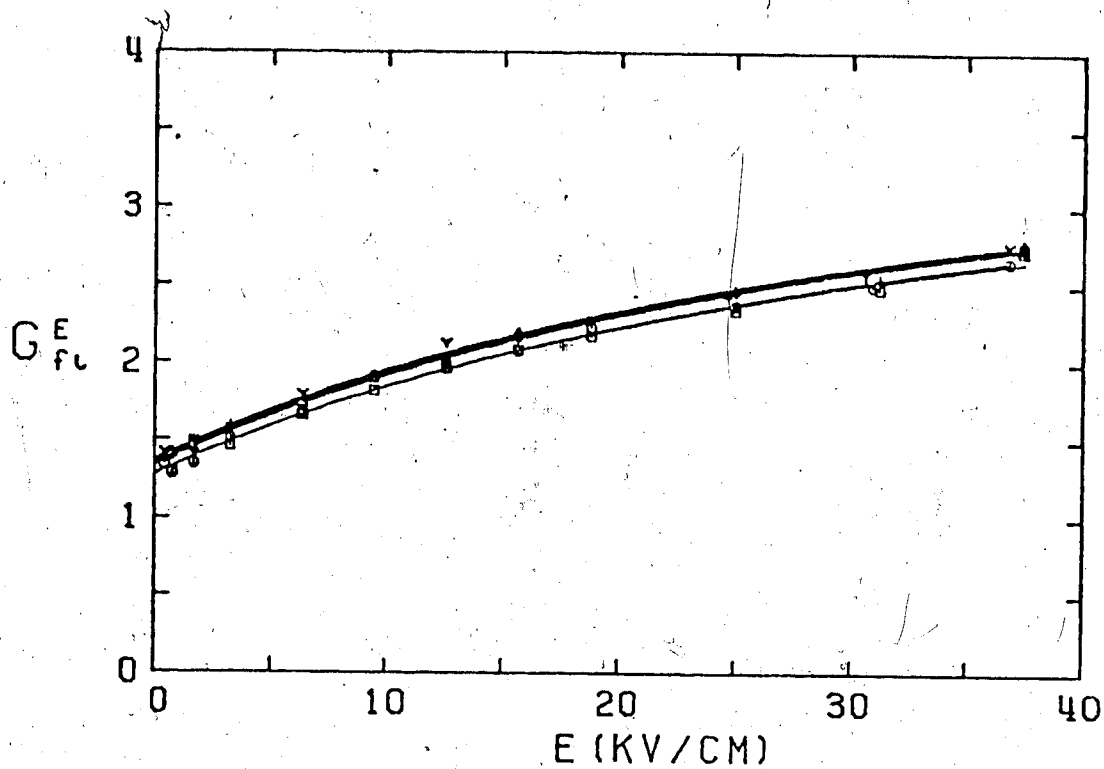


FIGURE III-146. Free ion yields in supercritical propane as functions of E . $d = 0.220 \text{ g/cm}^3$. Temperatures and polarities of the applied voltages: Y (377, -), + (377, +), ◇ (374, +), △ (374, -), ○ (370, -), □ (370, +).

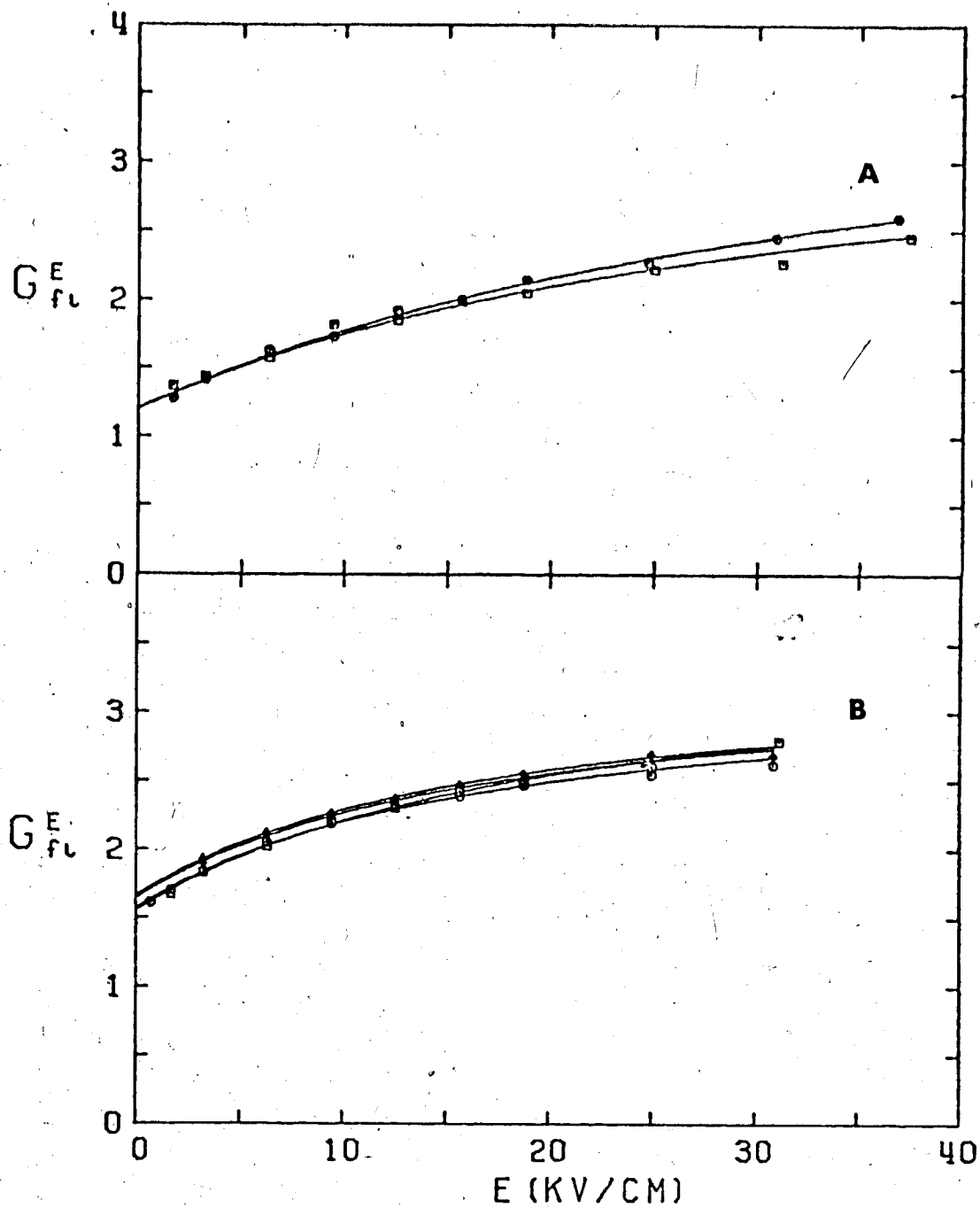


FIGURE III-147: Free ion yields in gaseous propane as functions of E . Temperatures, densities and polarities of the applied voltages (T , d , V):

A: □ (369K, 0.180, -), ○ (369K, 0.180, +).

B: □ (372K, 0.110, +), ○ (372K, 0.110, -), △ (385K, 0.110, -), ◇ (385K, 0.110, +).

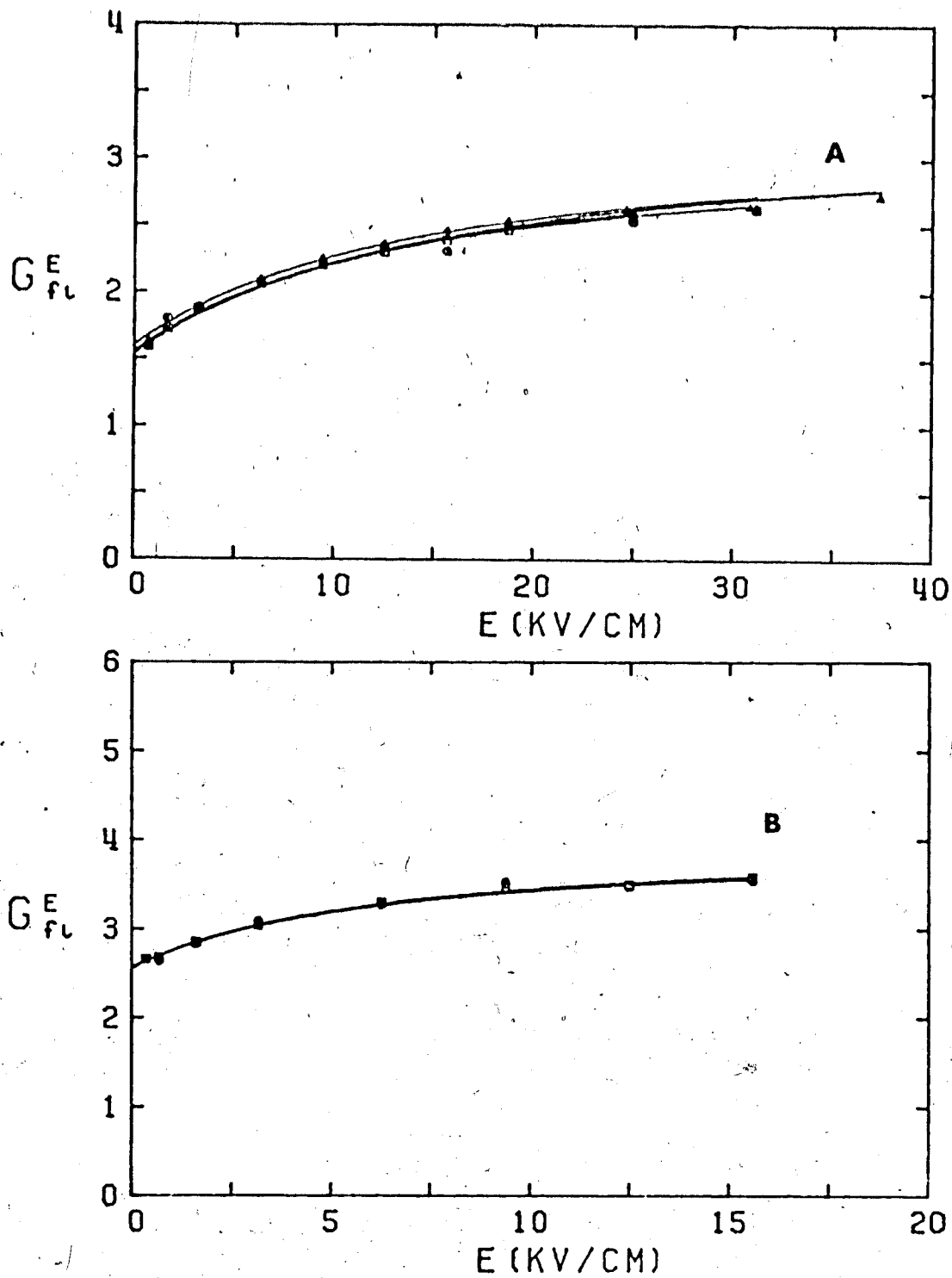


FIGURE III-148. Free ion yields in gaseous propane as functions of E . Temperatures, densities and polarities of the applied voltages (T , d , V):
 A: \square (354K, 0.085, -), \circ (354K, 0.085, +), \triangle (360K, 0.102, -) B: \square (328K, 0.0435, -), \circ (328, 0.0435,+).

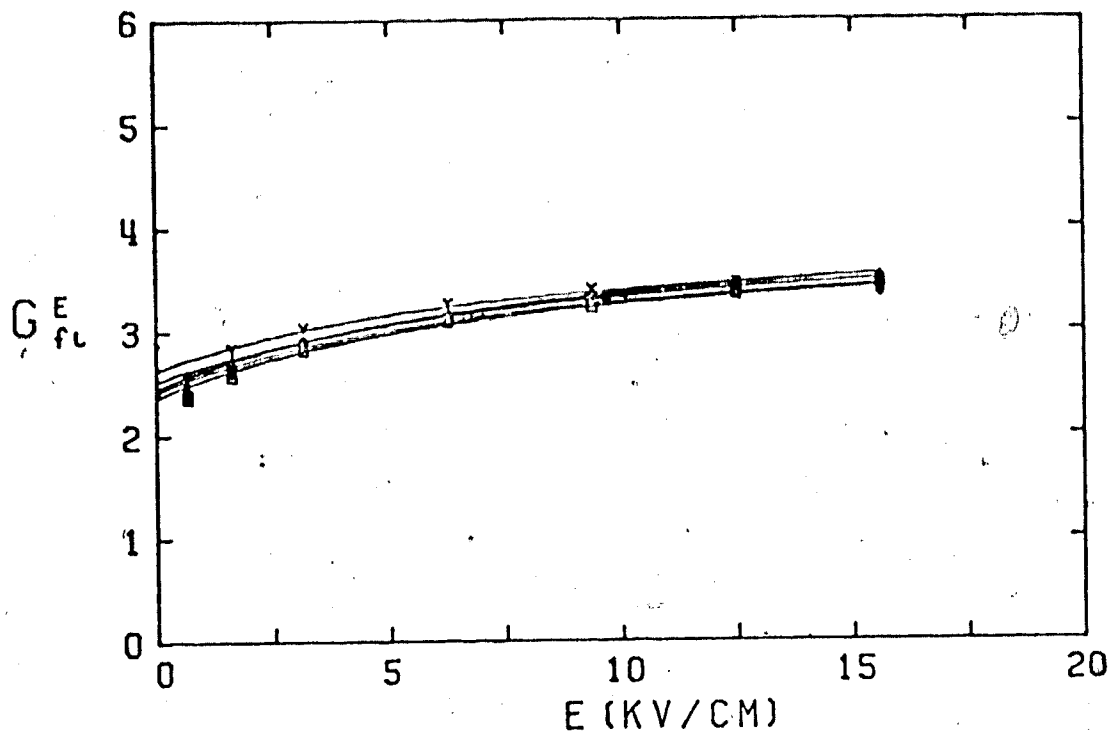


FIGURE III-149. Free ion yields in gaseous propane as functions of E . $d = 0.0557 \text{ g/cm}^3$. Temperatures and polarities of the applied voltages (T,V): \square (338K, +), \circ (338K, -), \triangle (346K, -), \diamond (346K, +), $+$ (383K,+), \times (383K, -).

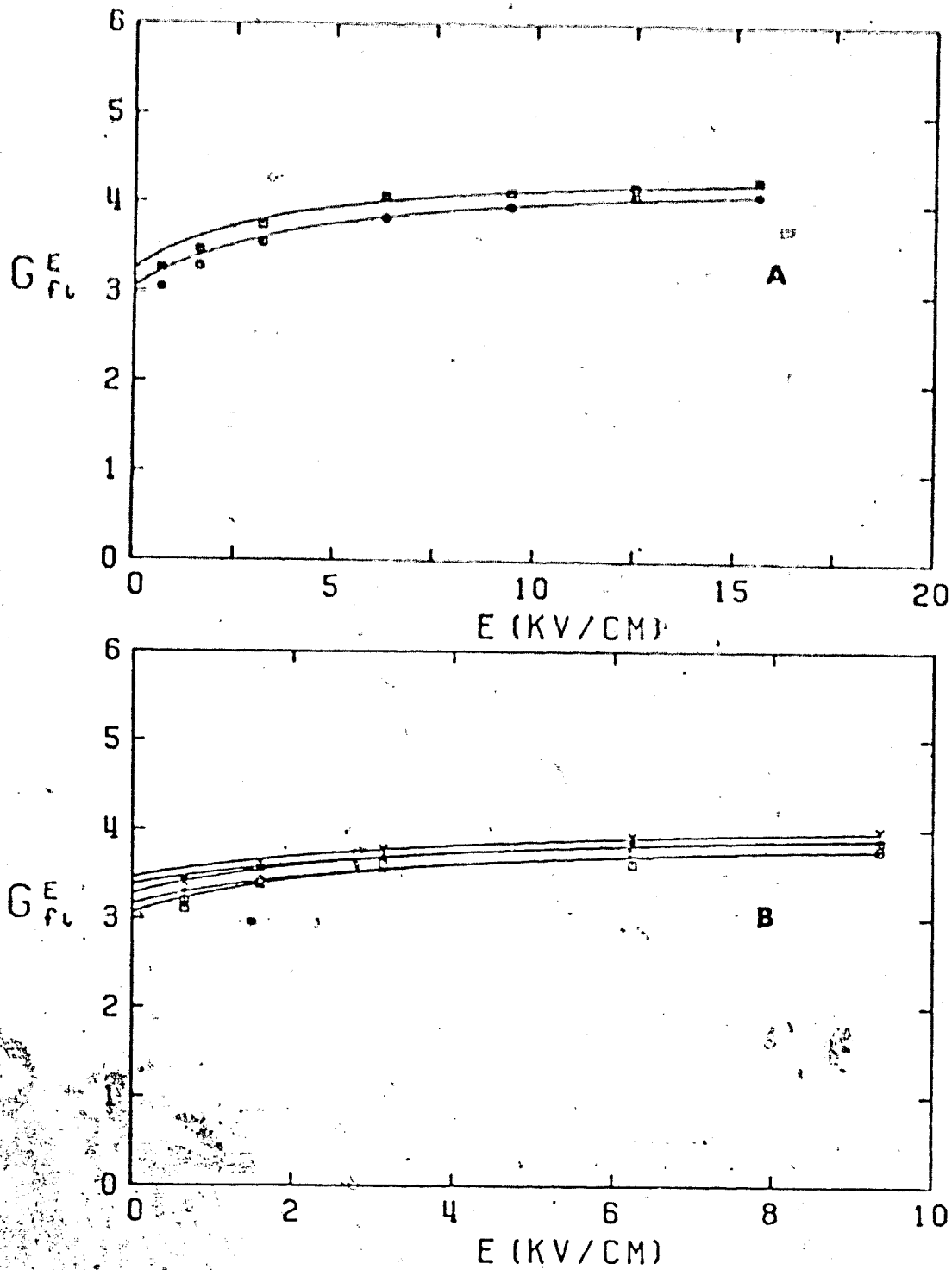


FIGURE III-150. Free ion yields in gaseous propane as functions of E . A: $d = 0.033 \text{ g/cm}^3$, $T = 317\text{K}$, \square is (-) and \circ is (+) applied voltage. B: $d = 0.025 \text{ g/cm}^3$. Temperature and polarities of applied voltages: X (436K,-), Y (436K,+), + (358K,+), \circ (358K,-), Δ (306K, -), \square (306K, +).

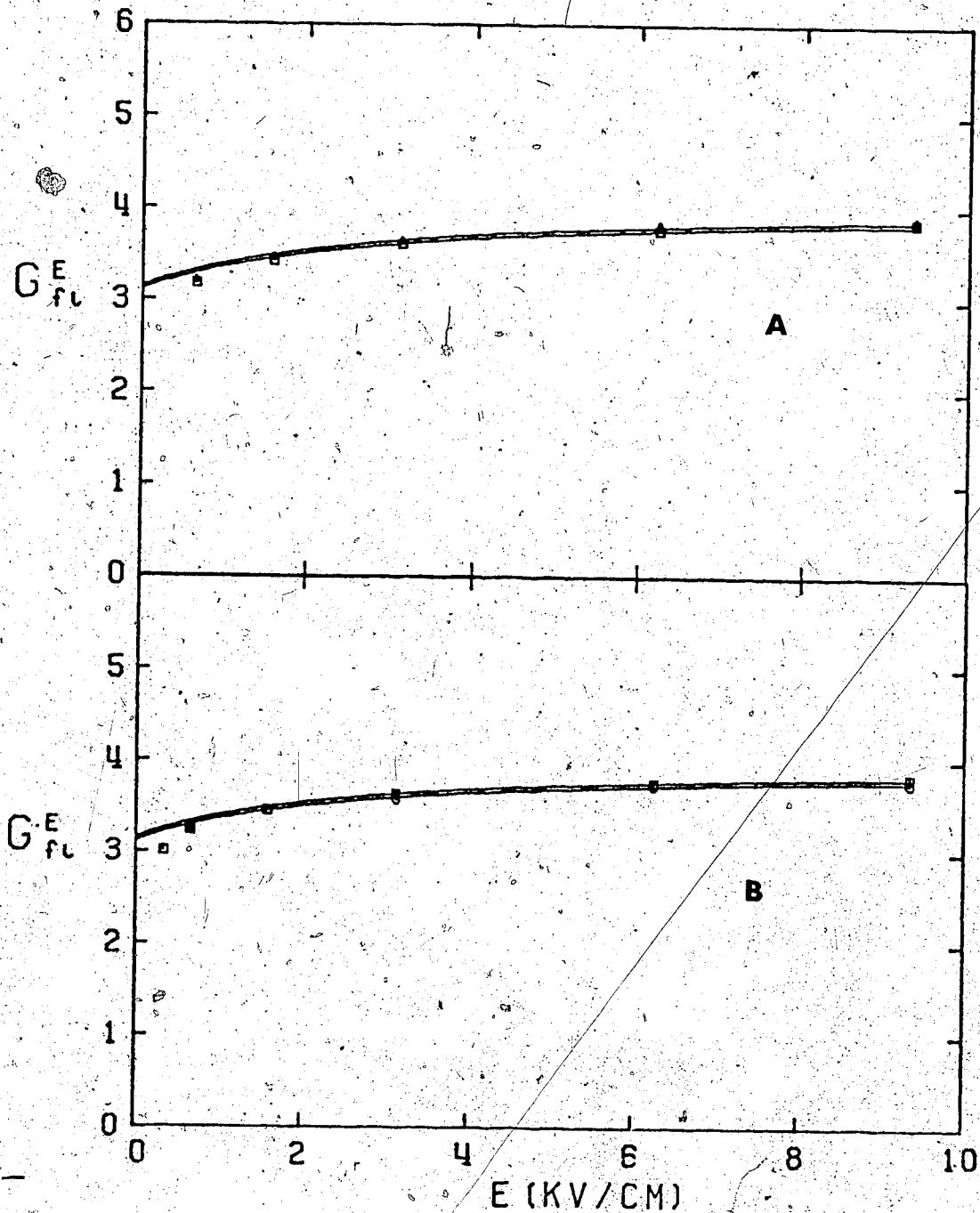


FIGURE III-151. Free ion yields in gaseous propane as functions of E . A: $d = 0.0228 \text{ g/cm}^3$, $T = 303\text{K}$, □ is - and △ is + applied voltage. B: $d = 0.0197 \text{ g/cm}^3$, $T = 297\text{K}$, □ is (+) and ○ is (-) voltage.

TABLE III-19

Summary of Free Ion Yield Results for Propane^a

T (K)	d ^c (g/cm ³)	ϵ^b	G_{fi}^0	G_{tot}	b^c 10^{-8} cm	b^d /cm ²
149	0.680	2.00	(0.047)	(4.1) ^e	(75)	(51)
169	0.656	1.95	(0.061)	(4.1) ^e	(75)	(49)
197	0.621	1.88	(0.085)	(4.1) ^e	(76)	(47)
252	0.556	1.76	(0.17)	(4.1) ^e	(85)	(47)
276	0.526	1.72	(0.25)	(4.1) ^e	(93)	(49)
297	0.495	1.65	(0.33)	(4.1) ^e	(104)	(51)
314	0.465	1.62	(0.41)	(4.1) ^e	(110)	(52)
340	0.408	1.53	(0.63)	(4.1) ^e	(140)	(58)
365	0.305	1.38	(1.05)	(4.1)	(210)	(65)
370	0.220 ^d	1.26	(1.3)	(4.1)	(280)	(62)
371	0.220 ^d	1.26	(1.3)	(4.1)	(280)	(63)
377	0.220 ^d	1.26	1.4	4.1	290	64
			(1.4)	(4.1)	(290)	(64)
374	0.220 ^d	1.26	1.3	4.2	280	61
			(1.3)	(4.1)	(290)	(63)
370	0.220 ^d	1.26	1.3	4.1	280	61
			(1.3)	(4.1)	(280)	(61)
369	0.180	1.21	(1.2)	4.1	270	49
			(1.2)	(3.6)	(310)	(56)
372	0.110	1.12	1.6	3.3	510	56
			(1.6)	(3.6)	(450)	(49)
385	0.110	1.12	1.7	3.3	530	59
			(1.7)	(3.3)	(540)	(60)
360	0.102	1.11	1.6	3.3	530	54
			(1.6)	(3.2)	(580)	(59)
354	0.085	1.09	1.5	3.2	560	48
			(1.6)	(3.1)	(600)	(51)

(continued.....)

TABLE III-19 (continued)

328	0.0435	1.05	2.6 (2.6)	3.9 (3.9)	1200 (1200)	51 (51)
383	0.0557	1.06	2.6 (2.5)	4.0 (4.0)	990 (890)	55 (50)
346	0.0557	1.06	2.5 (2.4)	4.0 (3.9)	930 (950)	52 (53)
338	0.0557	1.06	2.5 (2.4)	4.0 (3.9)	940 (930)	53 (52)
317	0.033	1.04	3.3 (3.1)	4.4 (4.4)	1700 (1400)	57 (47)
436	0.025	1.03	3.4 (3.5)	4.1 (4.2)	2020 (2010)	51 (50)
358	0.025	1.03	3.2 (3.3)	4.0 (4.1)	1980 (2080)	50 (52)
306	0.025	1.03	3.1 (3.1)	4.0 (4.0)	2100 (2100)	52 (52)
303	0.0228	1.03	3.1 (3.2)	4.0 (4.0)	2200 (2300)	51 (53)
297	0.0197	1.02	3.1 (3.2)	3.9 (3.9)	2500 (2700)	50 (53)

a Positive applied voltage results in brackets

b Static dielectric constant

c Most probable thermalization distance

d $T_c = 370K$, $d_c = 0.220 \text{ g/cm}^3$

e. Assumed

4. n-Butane

Free ion yields for n-butane are given in Figures III-152 to III-161. Data in Figure III-152 were obtained in a low pressure liquid type cell. Results in Figures III-153 and III-154 (except the negative voltage set in Figure III-154(B)) were obtained in a high pressure liquid type cell.

In the cold liquid (Figure III-152), the free ion yields can be seen to climb superlinearly with the electric field strength at the lowest temperatures. The differences between the 203K and 222K results at the lowest electric fields may be just due to scatter in the data. Above 203K, the curves straighten out. Above 299K (Figure III-153), the free ion curves begin bending over in the same manner as the free ion curves in propane. The extent of the curvature appears less than in propane.

Results in the supercritical fluid are shown in Figures III-154 and III-155. The difference between the (+) and (-) applied voltages are likely due to scatter. The temperature increase of 14K (Figure III-154(A)) changes the free ion yields by less than 7%. The 5K increase does not vary the free ion yield to any noticeable extent.

Figures III-156, III-159 and III-161 show the effect of decreasing the density along the co-existence curve. The same features appear as for ethane and propane. The high field free ion yields level off. The electric field

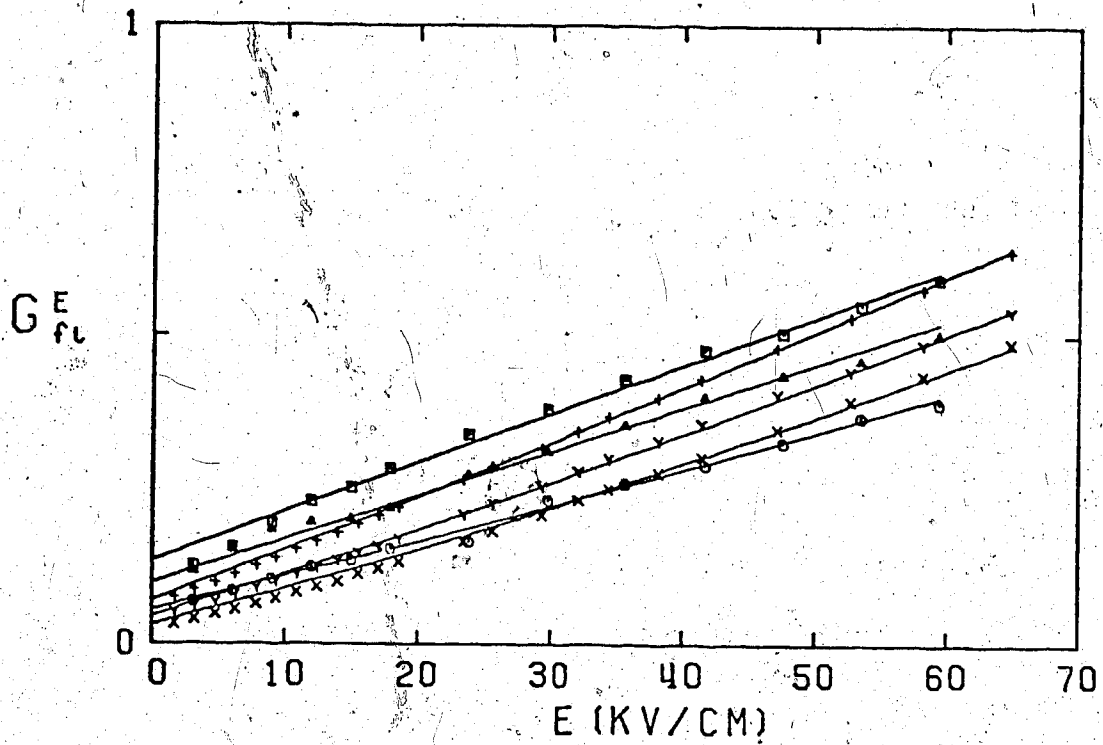


FIGURE III-152. Free ion yields in liquid n-butane as functions of E . Temperatures and densities (T, d):
 X (154K, 0.710), Y (176K, 0.690), + (203K, 0.666),
 O (222K, 0.649), Δ (268K, 0.607), □ (298K, 0.578).

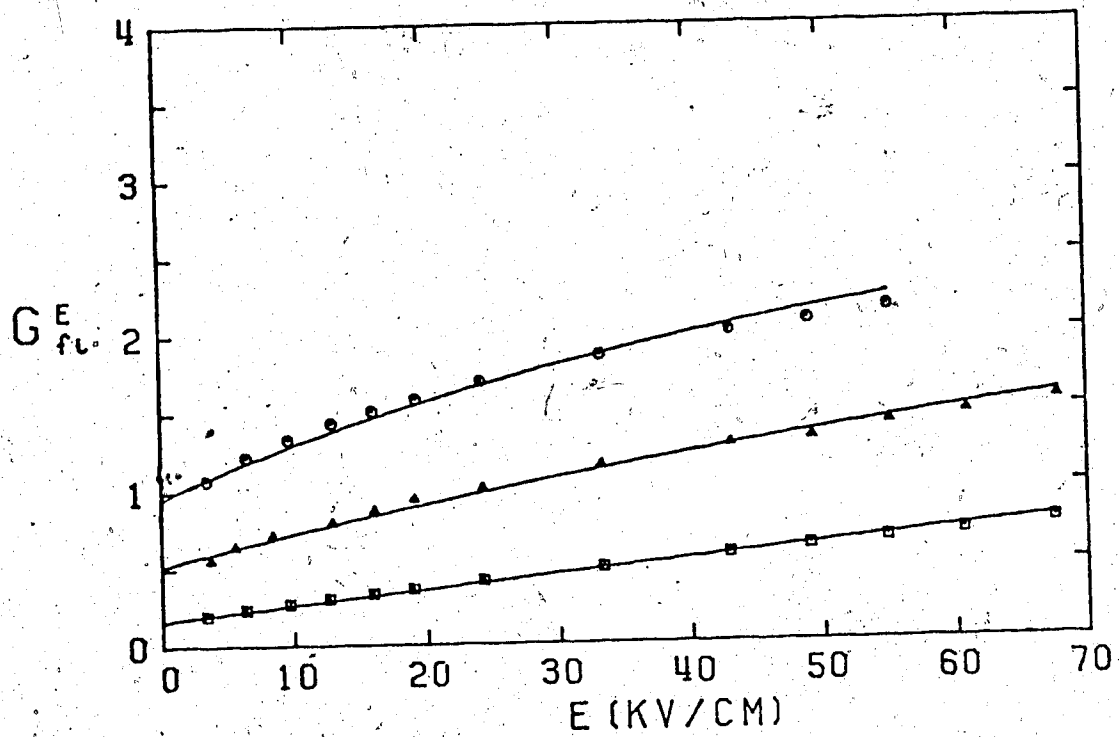


FIGURE III-153. Free ion yields in liquid *n*-butane as functions of E . Temperatures and densities (T, d):
 \square (299K, 0.576), \triangle (352K, 0.443), \circ (421K, 0.309).

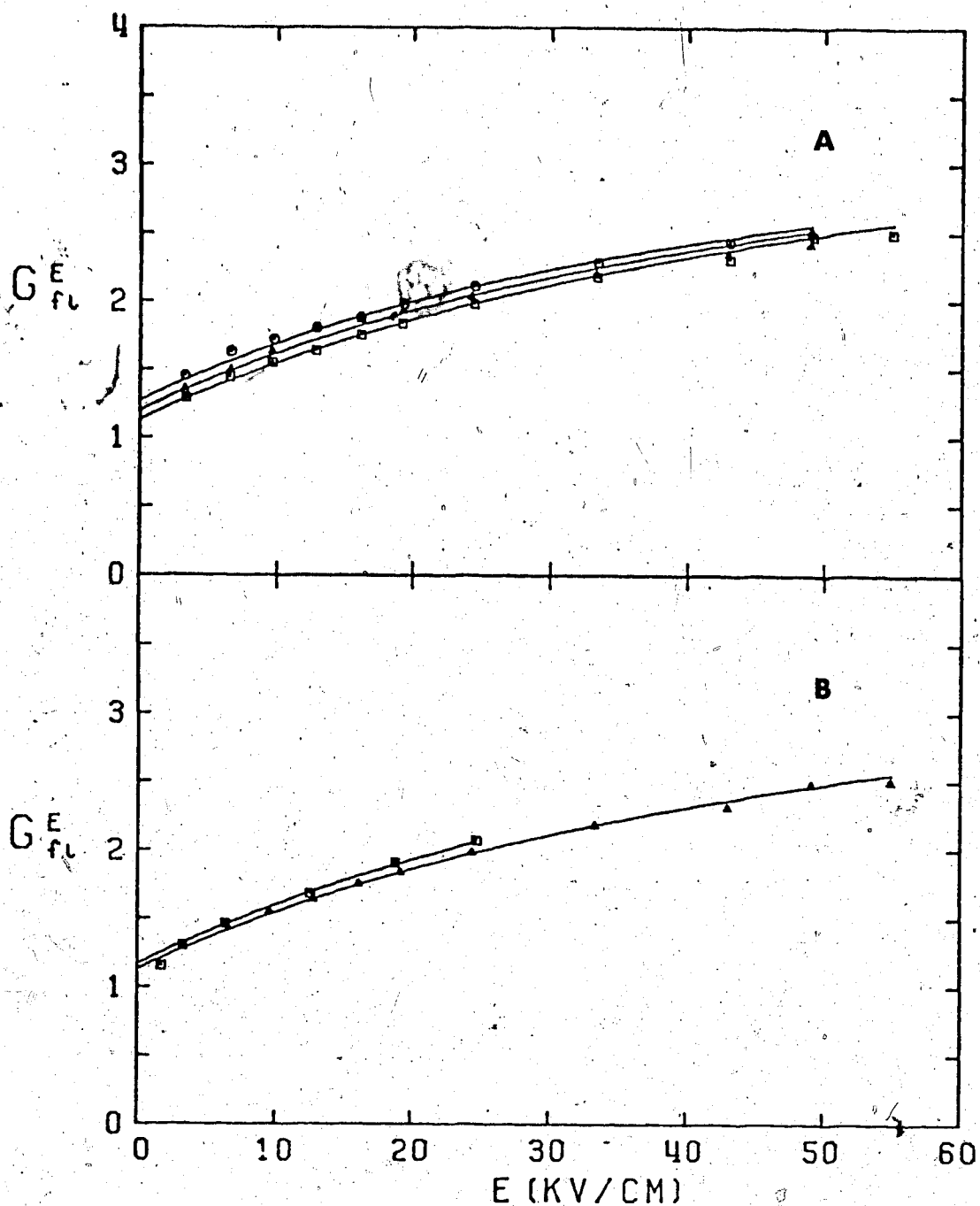


FIGURE III-154. Free ion yields in supercritical n -butane as functions of E . $d = 0.228 \text{ g/cm}^3$. Temperatures and polarities of applied voltages (T,V): A: \square (427,+), \triangle (434, +), \circ (441K, +). B: \square (425K, -), \triangle (427K, +).

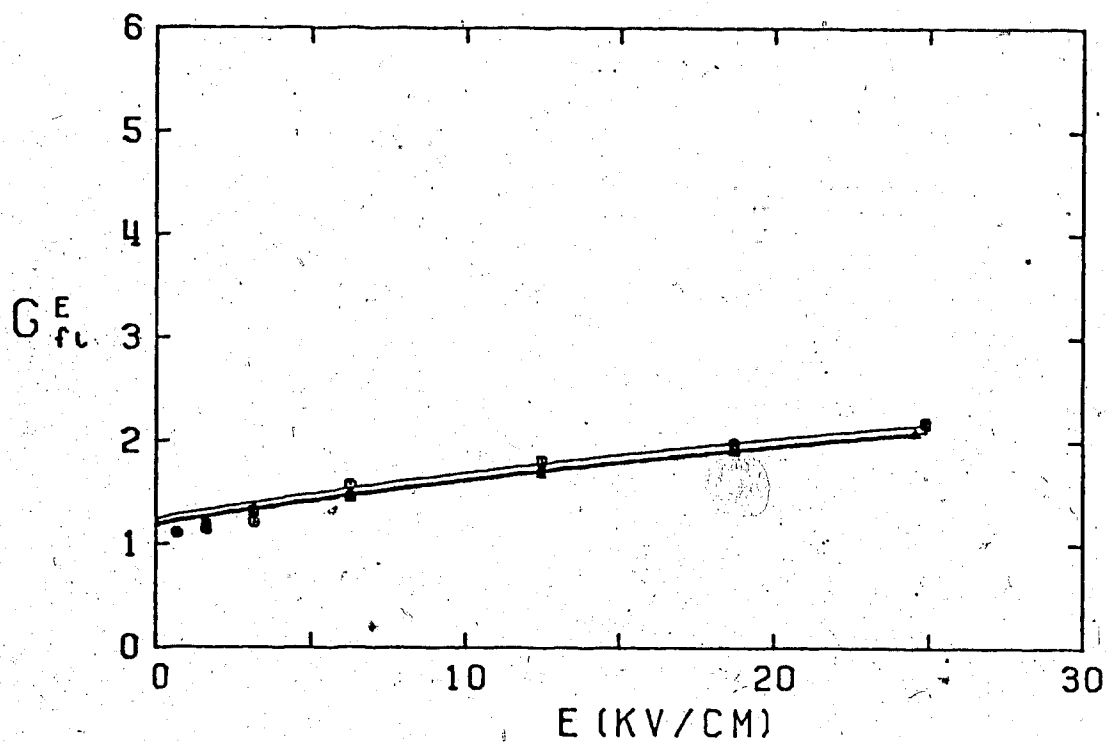


FIGURE III-155. Free ion yields in supercritical n-butane as functions of E . $d = 0.228 \text{ g/cm}^3$. Temperatures and polarities of the applied voltages (T,V): + (430K,-), \circ (430K, +), Δ (425K, -), \square (425, +).

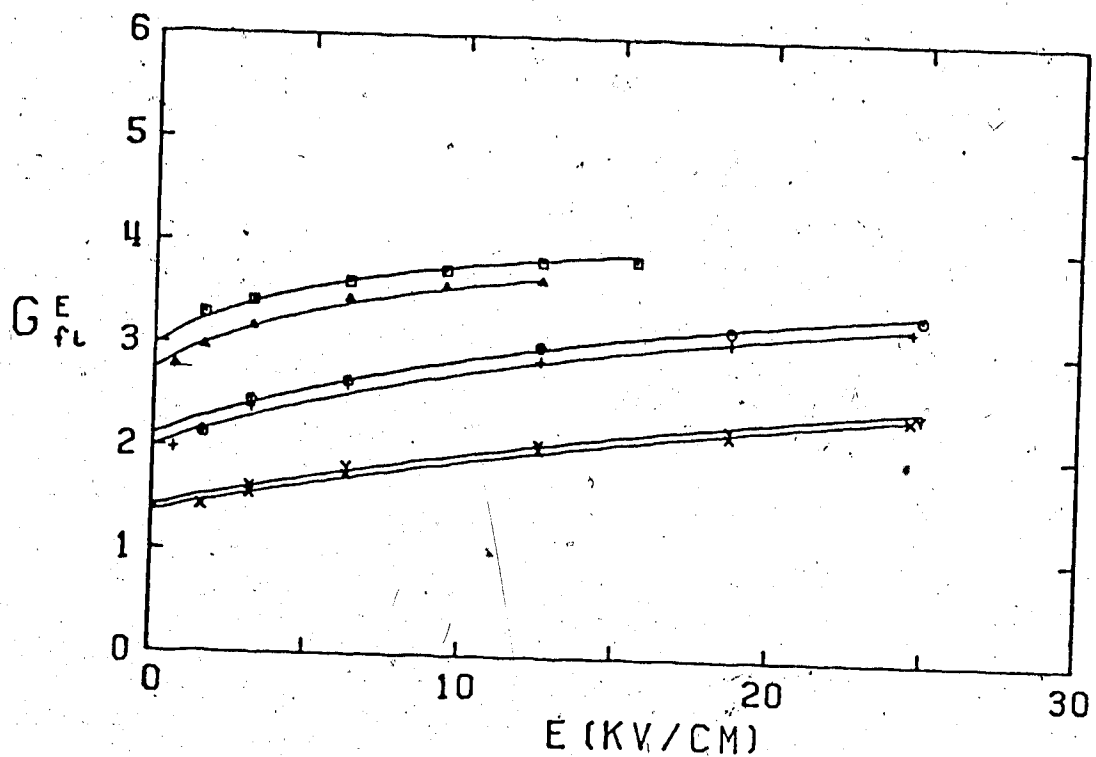


FIGURE III-156. Free ion yields in gaseous n-butane as functions of E/n . Temperatures, densities and polarities of the applied voltages (T, d, V):
 X (423K, 0.168, -), Y (423K, 0.168, +), + (409K, 0.094, -), ○ (409K, 0.094, +), △ (384K, 0.050, -), □ (384K, 0.050, +).

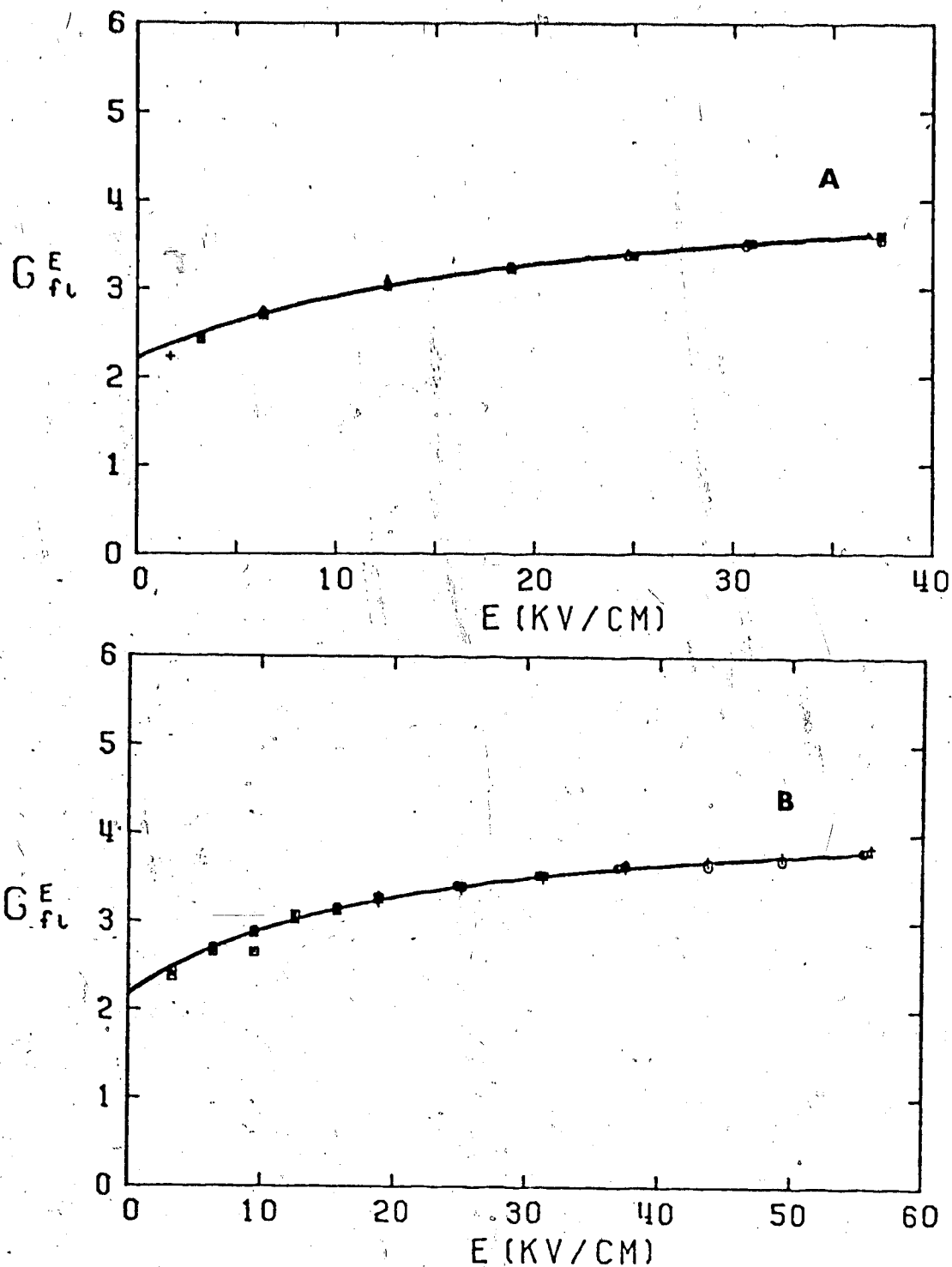


FIGURE III-157. Free ion yields in gaseous n -butane as functions of E . $d = 0.114 \text{ g/cm}^3$. Temperatures and polarities of the applied voltages (T,V) are:
 A: + (441K, +), \circ (441K, -), Δ (436K, -), \square (436K, +).
 B: + (428K, +), \circ (428K, -), Δ (420K, -), \square (420K, +).

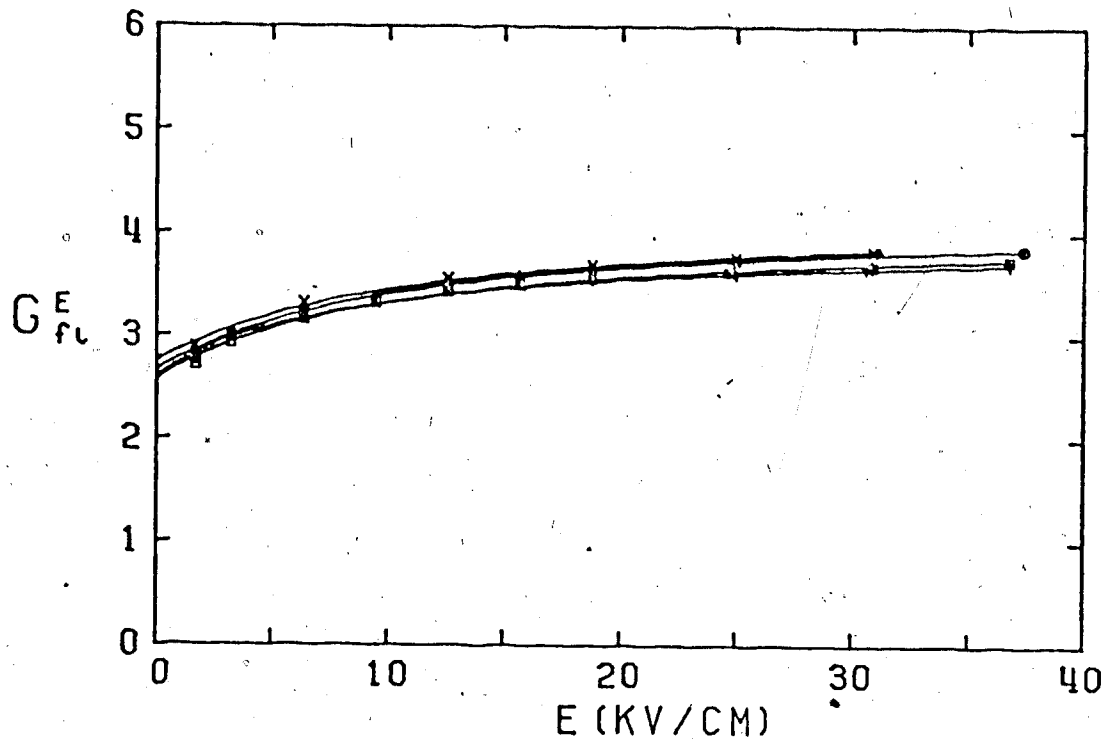


FIGURE III-158. Free ion yields in gaseous *n*-butane as functions of E . $d = 0.0575 \text{ g/cm}^3$. Temperatures and polarities of the applied voltages (T,V): X (444K, +), Y (444K, -), + (427K, -), O (427K, +), Δ (407K, +), □ (407K, -).

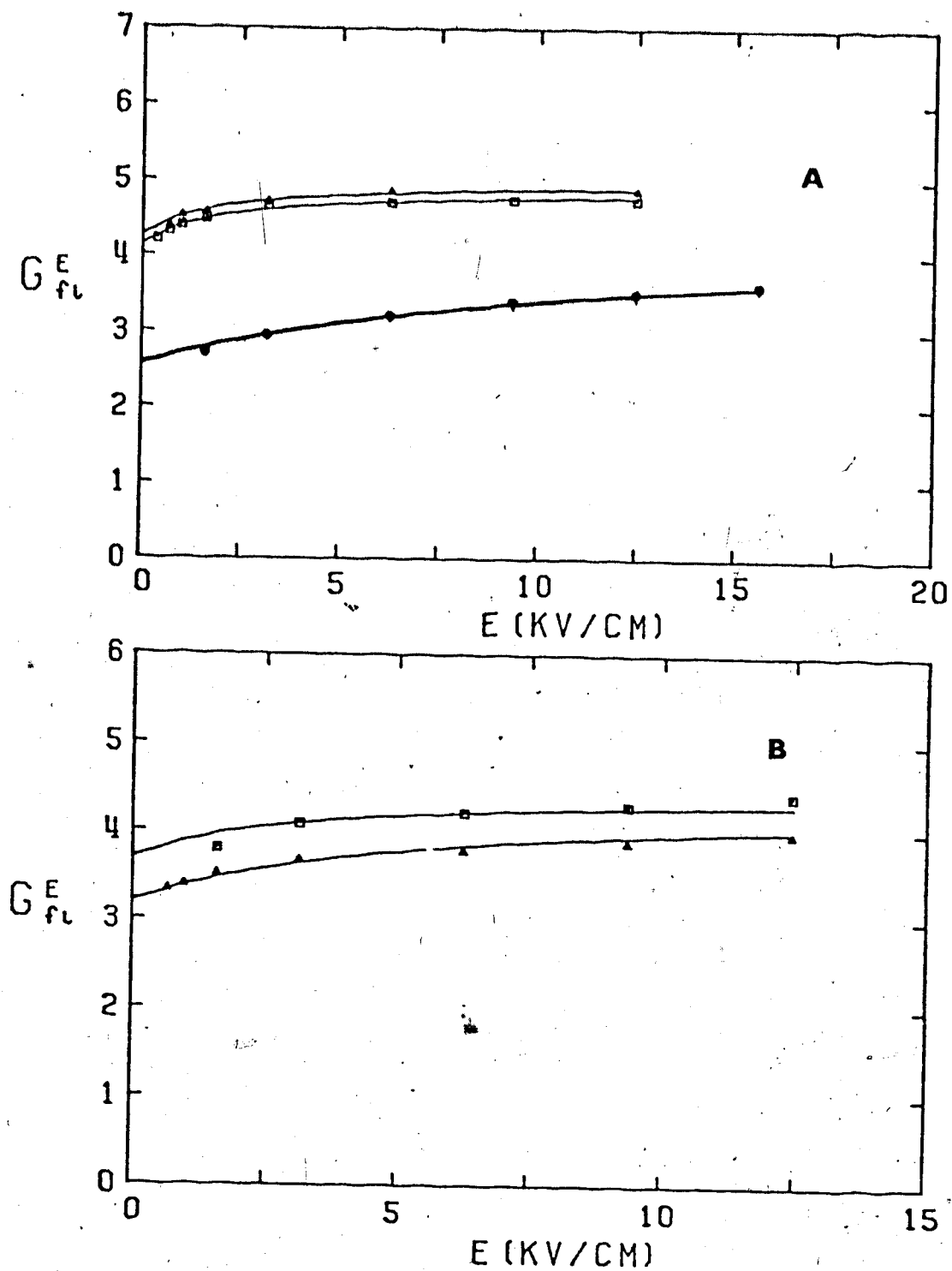


FIGURE III-159. Free ion yields in gaseous *n*-butane as functions of E . Temperatures, densities and polarities of the applied voltages (T, D, V) are A: + (391K, 0.0575, -), \circ (391K, 0.0575, +), Δ (333K, 0.0158, +), \square (333K, 0.0158, -) and B: \square (365K, 0.033, +), Δ (365K, 0.033, -).

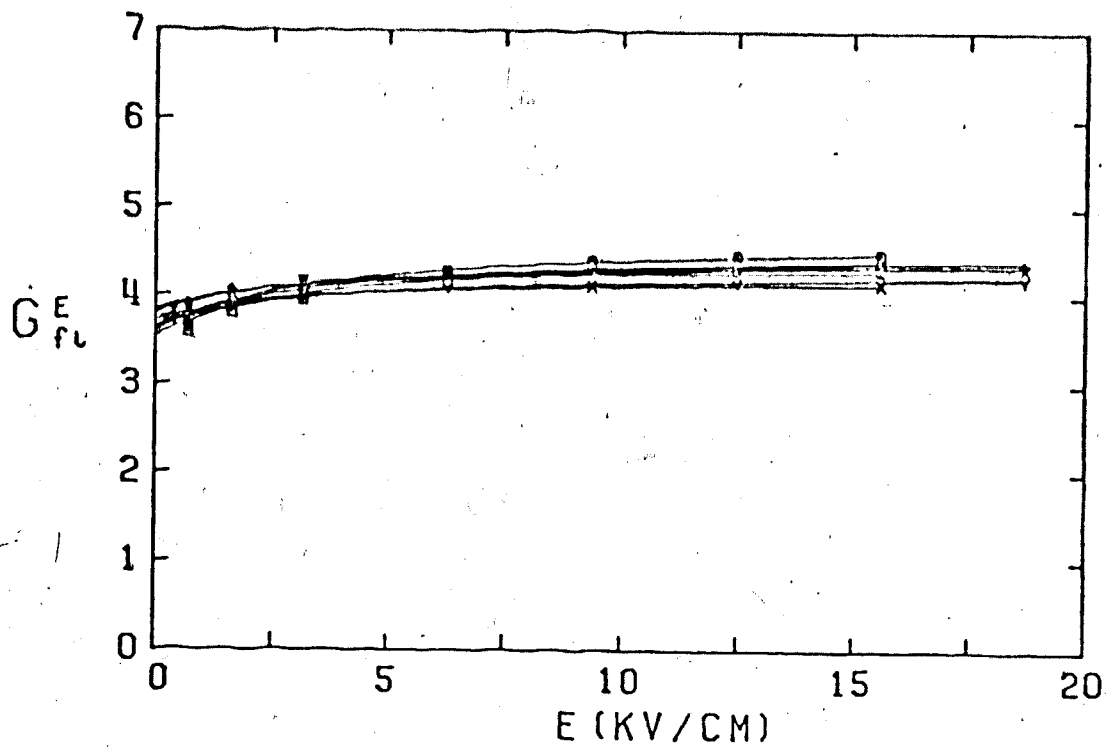


FIGURE III-160. Free ion yields in gaseous n-butane as functions of E . $d = 0.0234 \text{ g/cm}^3$. Temperature and polarities (T,V): λ (458K, +), Φ (458K, -), \times (430K, -), γ (430K, +), $+$ (366K, +), \circ (366K, -), Δ (354K, -), \square (354K, +).

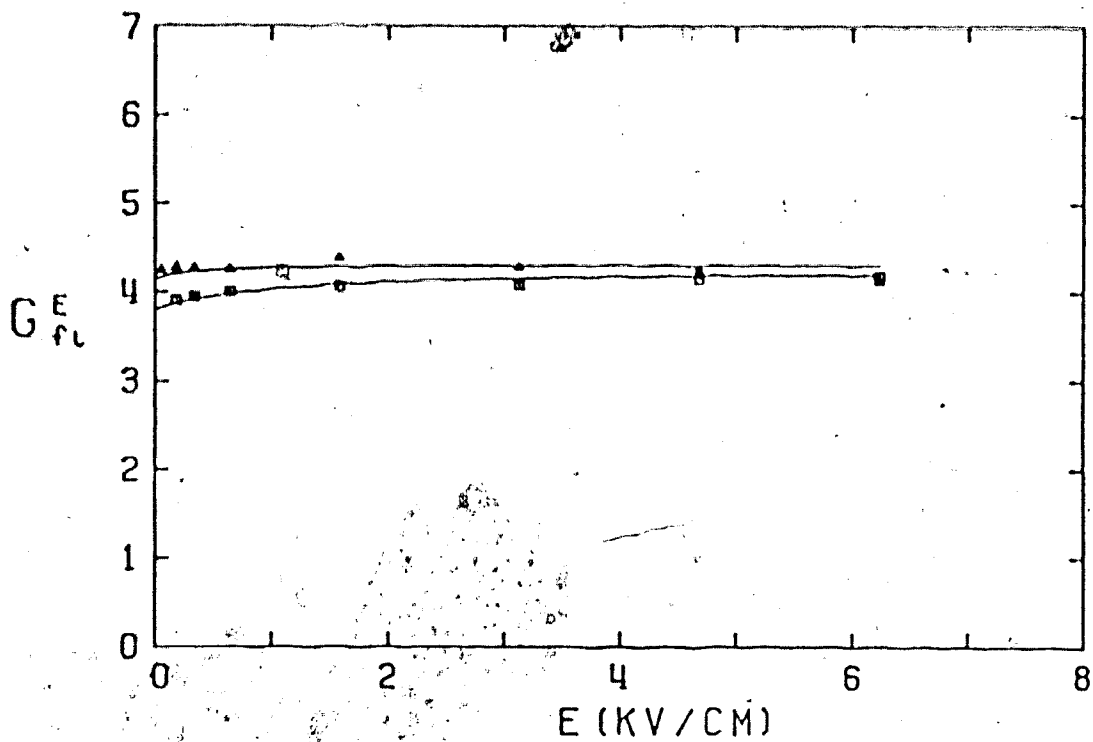


FIGURE III-161. Free ion yields in gaseous n-butane as functions of E ; $d = 0.0059 \text{ g/cm}^3$. Temperature and polarities (T,V): \square (295K, -), \triangle (295K, +).

strength where this occurs decreases as the density decreases:

The effect of temperature along isochores is shown in Figures III-157, III-158 and III-160, respectively. The shape of the curves is like those on the co-existence curve. Temperature changes of 21, 37 and 104K for the isochores where $n/n_c = 0.50, 0.25$ and 0.10 , respectively, did not vary the free ion yields beyond the scatter of the data set.

The fitting parameter G_{tot} equals 4.3 in good agreement with the low density gas phase value (see Table I-1).

Data for n-butane are summarized in Table III-20.

TABLE III-20

Summary of Free Ion Results for n-Butane^a

T (K)	d_3 g/cm ³	ϵ^b	G_{fi}^o	G_{tot}	b^c 10 ⁻⁸ cm	b^d 10 ⁻⁸ g/cm ²
154	0.710	2.00	(0.031)	(3.8)	(64)	(45)
176	0.690	1.96	(0.045)	(4.0)	(65)	(45)
203	0.666	1.92	(0.070)	(4.3)	(66)	(44)
222	0.649	1.89	(0.055)	(3.8)	(58)	(38)
268	0.607	1.82	(0.099)	(3.8)	(63)	(38)
298	0.578	1.77	(0.14)	(4.3)	(63)	(36)
299	0.576	1.76	(0.16)	(4.3)	(69)	(39)
352	0.443	1.56	(0.52)	(4.2)	(110)	(48)
421	0.309	1.39	(0.96)	(4.2)	(170)	(52)
427	0.228 ^d	1.26	(1.1)	(4.2)	(210)	(48)
434	0.228 ^d	1.26	(1.2)	(4.0)	(230)	(52)
441	0.228 ^d	1.26	(1.3)	(3.9)	(240)	(55)
430	0.228 ^d	1.26	1.2	4.3	210	49
			(1.3)	(4.3)	(220)	(51)
425	0.228 ^d	1.26	1.18	4.3	210	49
			(1.19)	(4.3)	(210)	(49)
423	0.168	1.19	1.4	4.3	260	45
			(1.4)	(4.3)	(260)	(45)
409	0.094	1.10	2.0	4.3	460	43
			(2.1)	(4.3)	(500)	(47)
384	0.050	1.05	2.8	4.3	920	46
			(3.0)	(4.3)	(1100)	(57)
441	0.114	1.12	2.2	4.3	500	57
			(2.2)	(4.3)	(500)	(57)
4.36	0.114	1.12	2.2	4.3	500	57
			(2.2)	(4.3)	(500)	(57)
428	0.114	1.12	2.2	4.3	500	57
			(2.2)	(4.3)	(500)	(57)

(continued.....)

TABLE III-20 (continued)

420	0.114	1.12	2.2 (2.2)	4.3 (4.4)	500 (480)	57 (55)
444	0.0579	1.06	2.7 (2.7)	4.0 (4.2)	880 (840)	51 (49)
427	0.0579	1.06	2.6 (2.7)	4.1 (4.1)	810 (860)	47 (50)
407	0.0579	1.06	2.6 (2.6)	4.0 (4.1)	880 (880)	51 (51)
391	0.0579	1.06	2.6 (2.6)	4.3 (4.3)	770 (770)	45 (45)
333	0.0158	1.02	4.1 (4.3)	4.8 (4.9)	3500 (3800)	56 (59)
365	0.033	1.04	3.2 (3.7)	4.3 (4.3)	1500 (3100)	50 (101)
458	0.0234	1.03	3.7 (3.8)	4.3 (4.3)	2600 (3400)	60 (79)
430	0.0234	1.03	3.7 (3.5)	4.3 (4.3)	2400 (3300)	57 (76)
366	0.0234	1.03	3.6 (3.6)	4.5 (4.6)	2100 (2000)	50 (46)
354	0.0234	1.03	3.6 (3.6)	4.5 (4.5)	2010 (2100)	47 (50)
295	0.0059	1.01	4.2 (3.8)	4.3 (4.3)	17000 (5000)	100 (29)

^a Positive polarity results in brackets.

^b Static dielectric constant.

^c Most probable thermalization distance.

^d $T_c = 425K$, $d_c = 0.228 \text{ g/cm}^3$.

5. Isobutane

Free ion yields in isobutane appear in Figures III-162 to III-172. Liquid type high pressure cells were used to obtain the data in the first four figures except the negative voltage set in Figure III-165(B). Gas type high pressure cells were used for the rest of this data set.

Liquid phase results are contained in Figures III-162 to III-164. Like propane and n-butane, the free ion yields at the lowest temperatures increase with electric field strength to a much greater extent than the higher temperatures (Figure III-162). The lowest temperature 140K increases superlinearly with electric field, then appears to bend over once more. A similar result occurs for 154K, but to a lesser degree. At 173K, the superlinear initial increase no longer occurs. The free ion yields for 173K, 181K, 214K, and 239K are very similar (Figures III-162 and III-163). Increasing the temperature to 270K separates the free ion yield curve more distinctly.

In Figure III-164, free ion yields between 298K to just below the critical point are shown. The 298K does not show a levelling of the free ion curve even at 93 kV/cm. The extent of the bending seems more pronounced as the temperature increases.

Data in the supercritical fluid appear in Figures III-165 and III-166. The earlier, liquid type cell results show a slight increase for a 15K rise in temperature

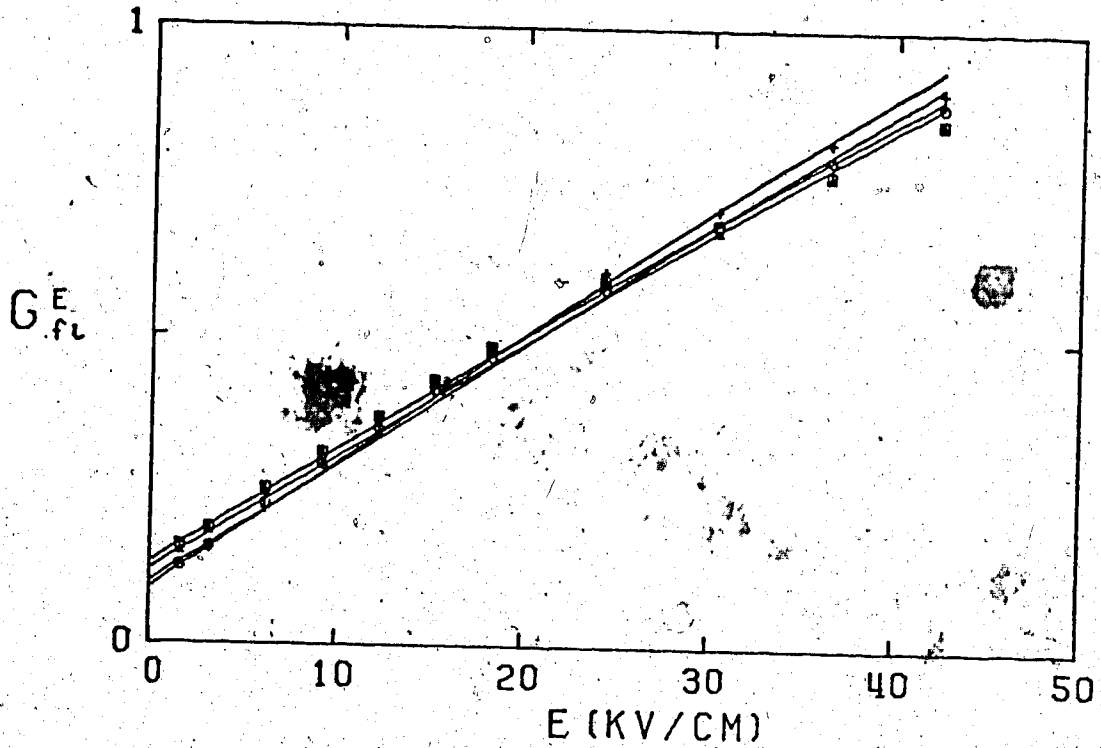


FIGURE III-162 Free ion yields in liquid isobutane as functions of E . Temperatures and densities (T, d): ∇ (146K, 0.742), \circ (154K, 0.723), \triangle (173K, 0.701), \square (181K, 0.692).

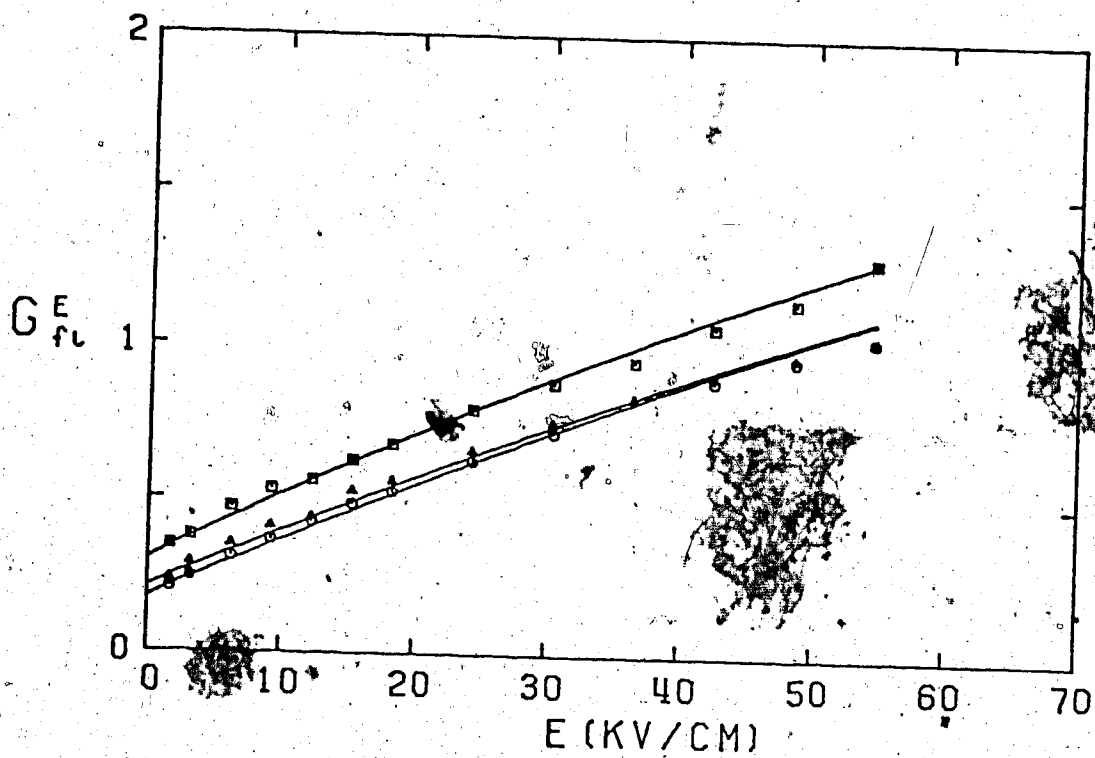


FIGURE III-163 Free ion yields in liquid isobutane as functions of E . Temperatures and densities (T, d):
○ (214K, 0.650), △ (239K, 0.620), □ (270K, 0.586).

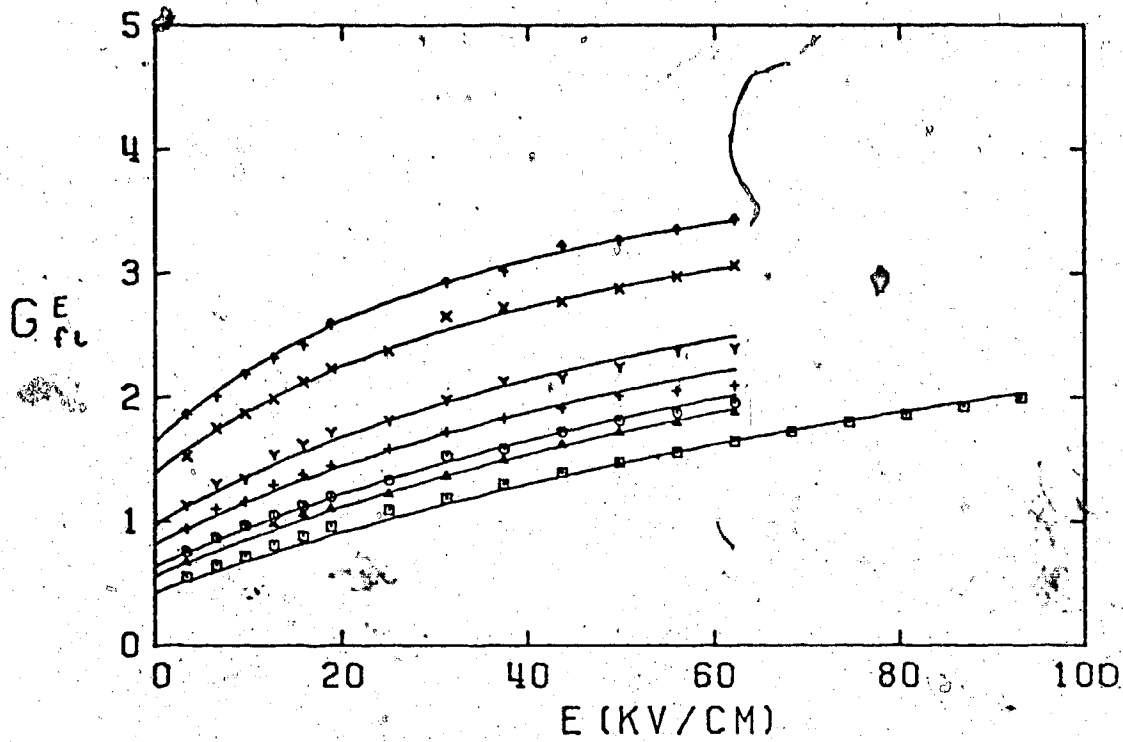


FIGURE III-164. Free ion yields in liquid isobutane as functions of E . Temperatures and densities (T, d): \square (293K, 0.553), \triangle (318K, 0.526), \circ (330K, 0.510), $+$ (359K, 0.462), Y (371K, 0.438), X (393K, 0.378), \diamond (403K, 0.315)

(Figure III-165(A)). The discrepancy in Figure III-165(B) between the liquid and gas cell results is likely as noted in methane and ethane. The difference between the two sets of results is about 20%. The gas cell results (Figure III-166) also show an increase with the temperature rise. No difference can be noted between the (+) and (-) applied voltages. The shapes of the curves between the two sets are similar.

Gas phase results along the co-existence curve can be seen from Figures III-167, III-169, III-171 and III-172. The effect of decreasing the density is as for the other systems. The high field results approach a plateau and the field where this bending occurs goes to a lower value. The initial zero field value increases.

Figures III-168 and III-172 show the usual minor importance of the temperature effect on the free ion yield compared to that of the density. Increases of 20 and 52 degrees cause little variation in the free ion yields.

There is also no polarity effect on the isochore results. In Figure III-169, the lower two curves also belong to the $n/n_c = 0.5$ isochore. Superpositioning this curve with Figure III-168 would have all the results falling between the (+) and (-) results of the 399K curve. The polarity effect in Figure III-171 can be due to scatter. The positive voltage results may lie a bit higher

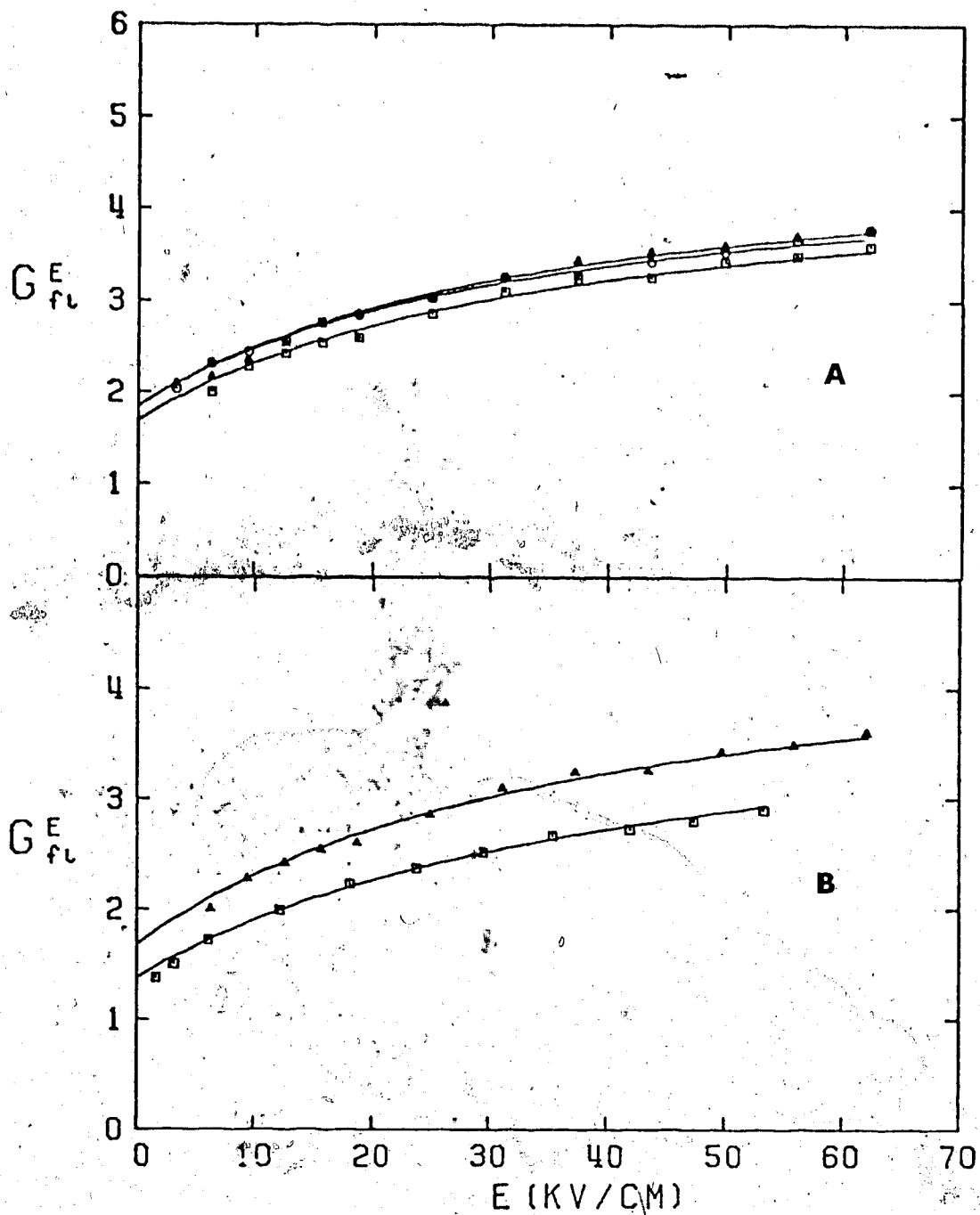


FIGURE III-165. Free ion yields in supercritical isobutane as functions of E . $d = 0.222 \text{ g/cm}^3$. A: all (+) polarity results. Temperatures: \square (408K), Δ (414K), \circ (423K). B: $T = 408\text{K}$. Polarity of applied voltage \square (-), Δ (+).

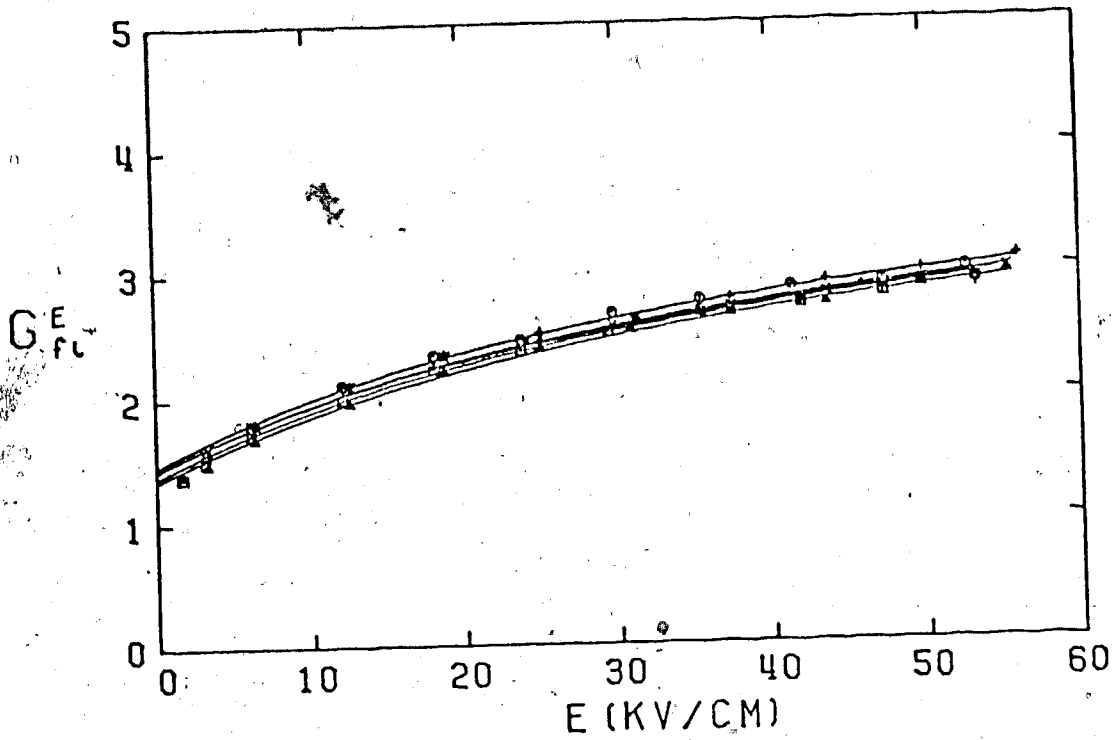


FIGURE III-166. Free ion yields in supercritical isobutane as functions of E . $d = 0.222 \text{ g/cm}^3$. Temperatures and polarities: □ (408K, -), △ (408K, +), ○ (414K, -), + (414K, +), Y (420K, -), X (420K, +).

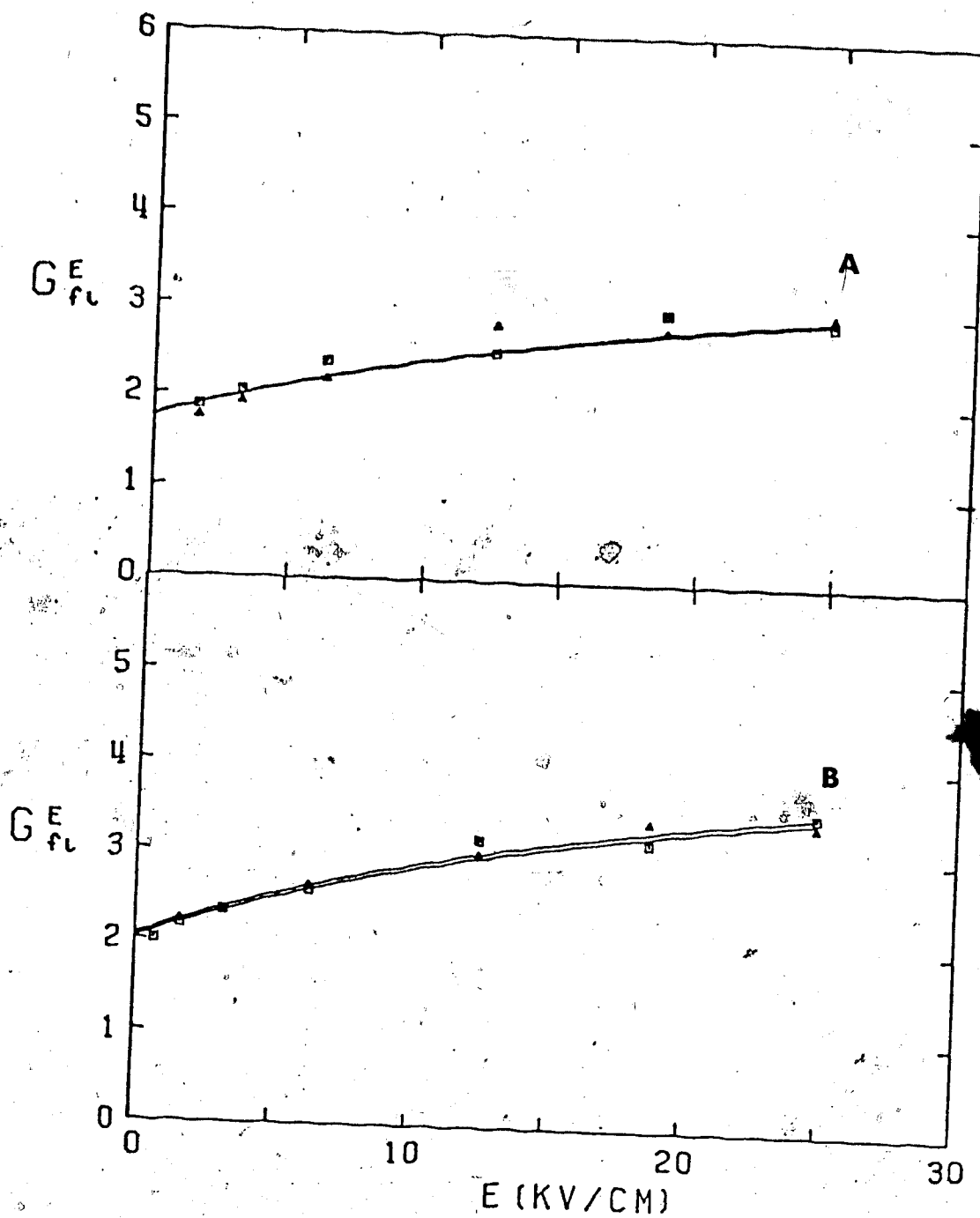


FIGURE III-167. Free ion yields in gaseous isobutane as functions of E . \square is (-) and Δ is (+) applied voltage. Temperatures and densities: A (406K, 0.156), B (398K, 0.107).

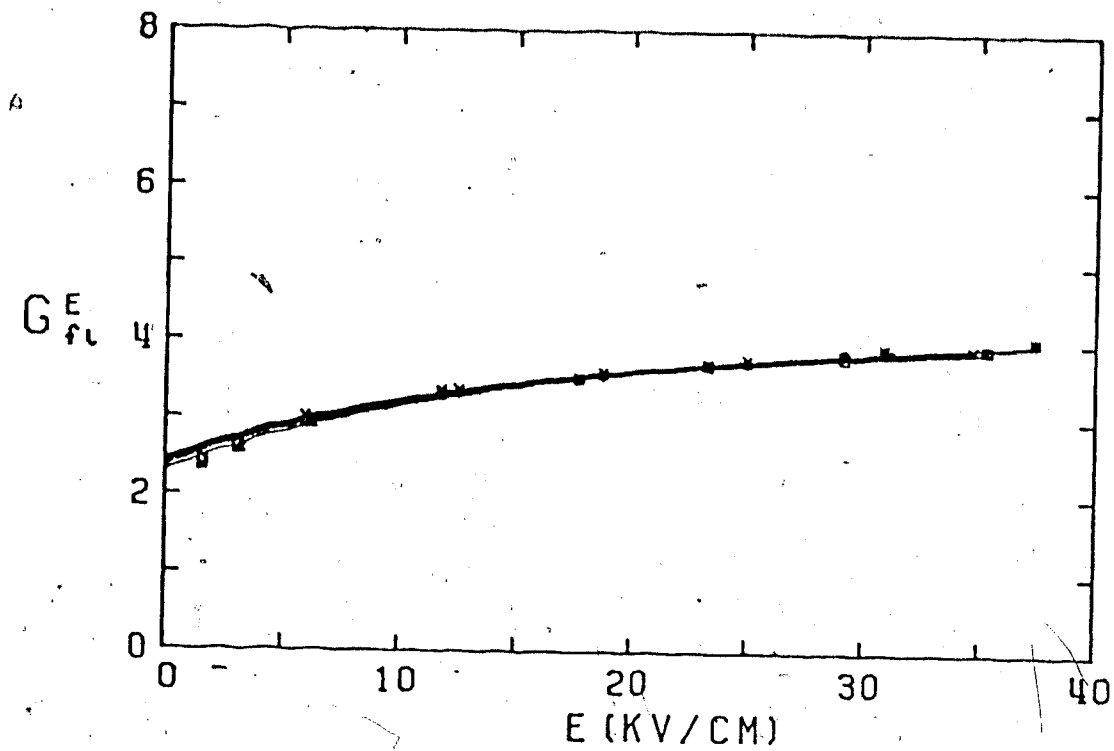


FIGURE III-168. Free ion yields in gaseous isobutane as functions of E . $d = 0.111 \text{ g/cm}^3$. Temperatures and polarities of applied voltage: X (424K, +), Y (424K, -), + (414K, +), O (414K, -), Δ (404K, +), \square (404K, -).

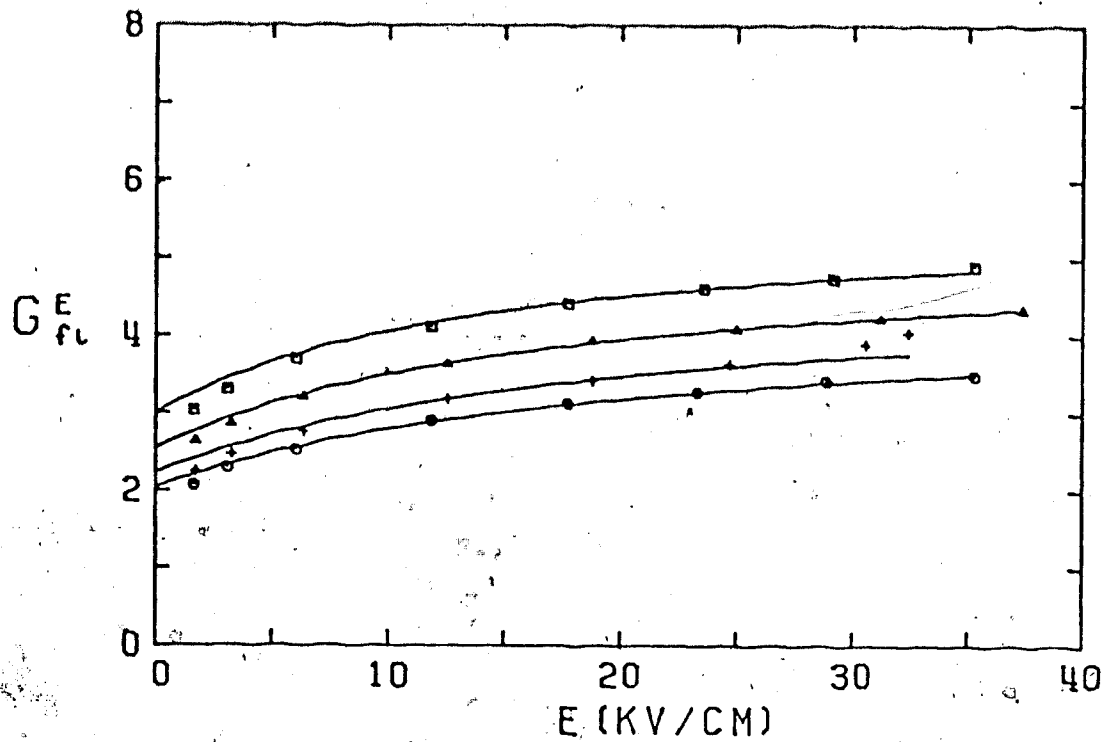


FIGURE.III-169. Free ion yields in gaseous isobutane as functions of E . Temperatures, densities and polarities of applied voltages (T, d, V): \square (391K, 0.089, +), \triangle (391K, 0.089, -), + (399K, 0.111, +), \circ (399K, 0.111, -)

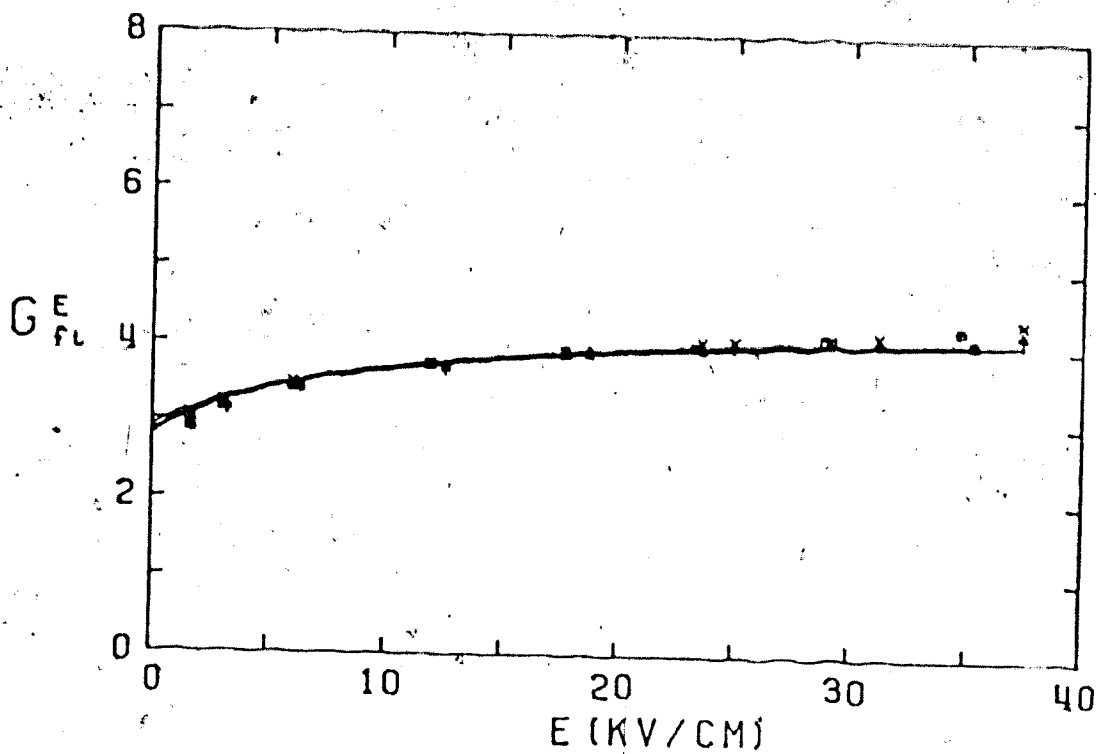


FIGURE III-170. Free ion yields in gaseous isobutane as functions of E . $d = 0.0565 \text{ g/cm}^3$. Temperatures and polarities of the applied voltages: X (428K, +), Y (409K, -), + (387K, +), O (387K, -), Δ (376K, +), \square (376K, -).

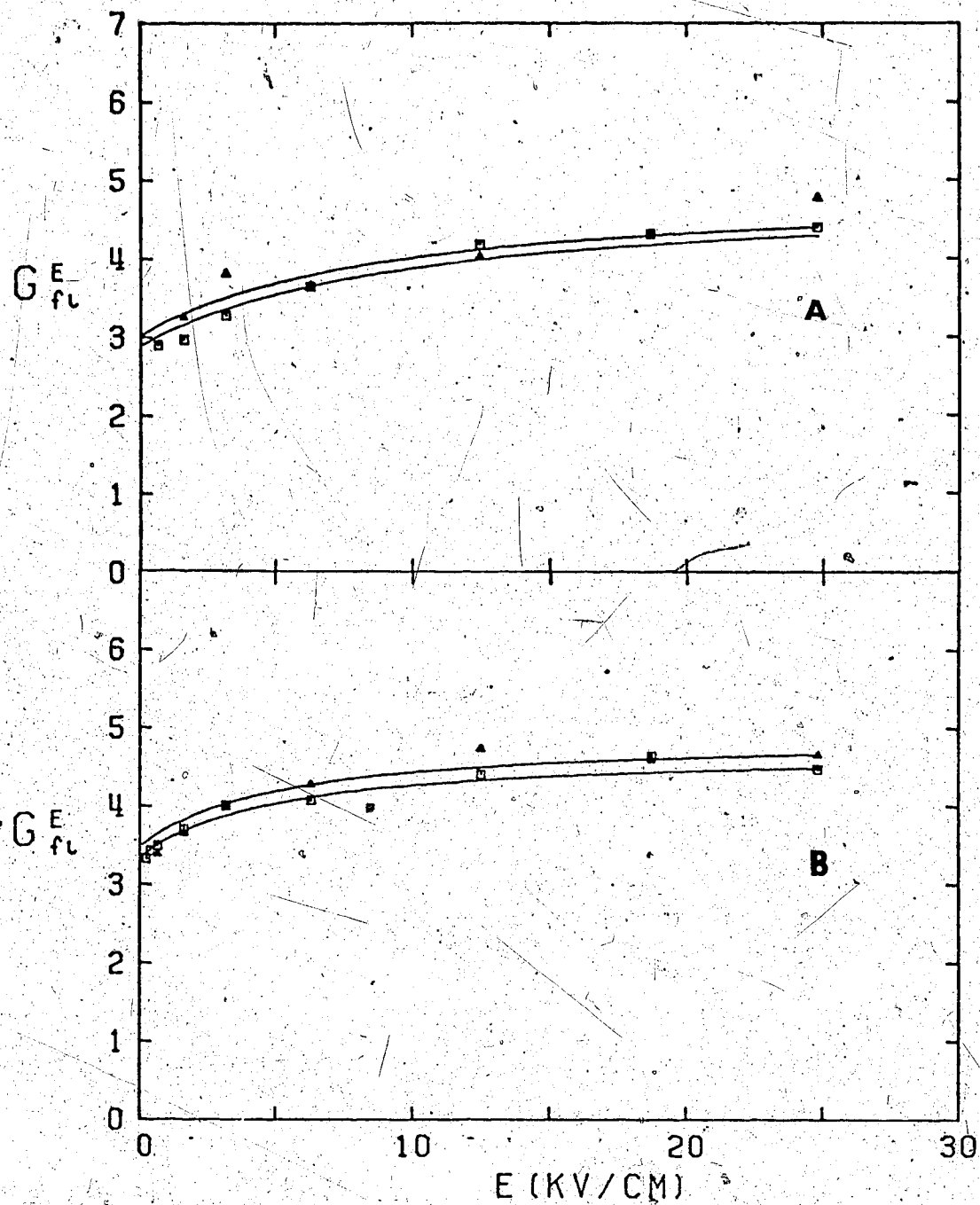


FIGURE III-171. Free ion yields in gaseous isobutane as

functions of E . \square is (-) and \triangle is (+) applied voltage. A: $T = 371K$, $d = 0.0545 \text{ g/cm}^3$.

B: $T = 352K$, $d = 0.0350 \text{ g/cm}^3$.

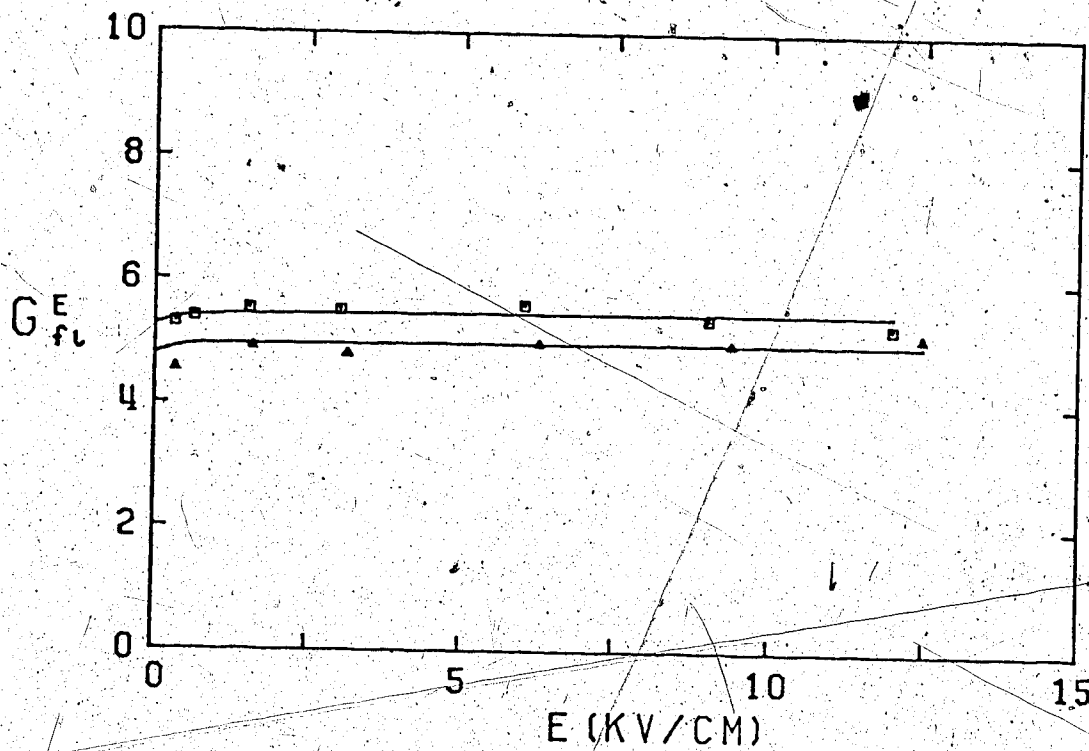


FIGURE III-172. Free ion yields in gaseous isobutane as functions of E . $T = 297K$, $d = 0.0089 \text{ g/cm}^3$.
 \square is (-) and Δ is (+) applied voltage.

than that of the negative voltage. In both the 391K curve (Figure III-169) and the 297K curve (Figure III-172) there is an apparent difference between the results of about 12%. However, in the 391K, the positive applied voltage result is greater than the negative, and in the 297K, the reverse is true. The negative voltage curve is greater than the positive. The difference, once more may be due to scatter.

The fitting parameter G_{tot} from Table III-21 equals 4.7 (using all values where $d \leq 0.089 \text{ g/cm}^3$). Previous values of the low density total ionization yield give 4.3 (see Table I-1). The present result is 9% higher. Agreement can be considered to be fair...

Data for isobutane are summarized in Table III-21.

TABLE III-21

Summary of Free Ion Yield Results for Isobutane^a

T K	d g/cm ³	ϵ^b	G_{fi}^c	G_{tot}	10^{-8} cm^{bc}	$10^{-8} \text{ q/cm}^2 \text{ }^{bd}$
140	0.742	2.12	(0.091)	(3.9)	(100)	(74)
154	0.723	2.07	(0.101)	(4.4)	(92)	(66)
173	0.701	2.02	(0.12)	(4.2)	(92)	(64)
181	0.692	2.01	(0.13)	(4.2)	(92)	(63)
214	0.650	1.92	(0.18)	(4.0)	(94)	(61)
239	0.620	1.86	(0.21)	(4.0)	(94)	(58)
270	0.586	1.80	(0.30)	(4.2)	(99)	(58)
298	0.553	1.72	(0.44)	(4.3)	(110)	(62)
318	0.526	1.68	(0.57)	(4.4)	(120)	(65)
330	0.510	1.65	(0.65)	(4.4)	(130)	(67)
359	0.462	1.59	(0.83)	(4.2)	(150)	(71)
371	0.438	1.54	(0.99)	(4.2)	(170)	(76)
393	0.378	1.48	(1.4)	(4.3)	(230)	(88)
403	0.315	1.37	(1.6)	(4.5)	(280)	(88)
408	0.222 ^d	1.25	(1.7)	(4.6)	(302)	(67)
414	0.222 ^d	1.25	(1.85)	(4.8)	(310)	(69)
423	0.222 ^d	1.25	(1.86)	(4.8)	(310)	(69)
420	0.222 ^d	1.25	1.44	4.2	270	60
			(1.44)	(4.2)	(270)	(60)
414	0.222 ^d	1.25	1.47	4.2	280 ^e	62
			(1.47)	(4.2)	(280)	(62)
408	0.222	1.25	1.38	4.2	270	59
			(1.35)	(4.2)	(260)	(58)
406	0.156	1.18	1.8	4.2	370	58
			(1.8)	(4.4)	(350)	(55)
398	0.107	1.12	2.0	4.8	410	44
			(2.0)	(4.8)	(410)	(44)
424	0.111	1.12	2.5	4.6	540	60
			(2.5)	(4.8)	(504)	(56)

(continued.....)

Table III-21 (continued)

414	0.111	1.12	2.4 (2.4)	4.7 (4.9)	520 (470)	58 (52)
404	0.111	1.12	2.4 (2.3)	4.6 (4.9)	550 (470)	61 (52)
399	0.111	1.12	2.0 (2.2)	4.2 (4.6)	490 (490)	55 (55)
391	0.089	1.11	3.0 (2.6)	5.5 (5.2)	630 (530)	56 (46)
428	0.0565	1.06	(2.9)	(4.3)	(940)	(53)
409	0.0565	1.06	2.9	4.3	990	56
387	0.565	1.06	2.9 (2.8)	4.3 (4.3)	990 (990)	56 (56)
376	0.0565	1.06	2.8 (2.8)	4.3 (4.3)	990 (990)	56 (56)
371	0.0545	1.06	2.9 (3.0)	4.8 (4.8)	830 (920)	45 (50)
352	0.0350	1.04	3.4 (3.5)	4.6 (4.8)	1500 (1500)	52 (52)
297	0.0089	1.01	5.3 (4.8)	5.4 (5.0)	-	-

a. Positive voltage results in brackets

b. Static dielectric constant

c. Most probable thermalization range.

d. $T_c = 408K$ $d_c = 0.222 \text{ g/cm}^3$

6. Ethene

Data for ethene appear in Figures III-173 to III-181. No polarity effect beyond the scatter of the data ($\sim 10\%$) exists. Results in Figures III-173 and III-174(A) were obtained with a high pressure liquid type conductance cell. The rest were obtained with a high pressure gas type cell.

Liquid phase results appear in Figure III-173. The lowest two curves are varying superlinearly with electric field strength. The upper two are varying linearly with E . At 2 degrees below the critical point, the free ion yields are still small compared to the low density gas G_{tot} , which equals 3.9 (see Table I-1). This is true even at 30 kV/cm. In the previous five alkane systems, the free ion yield in the liquid just before the critical point was much higher. The low values reflect the greater ability of the alkene to capture the ion pairs before they can escape the geminate cage than the alkanes.

Figure III-174 shows the free ion yields in the supercritical fluid. At high fields (>30 kV/cm), the curves are starting to bend. Note that the free ion yield has changed a fair amount in the liquid from 279K to 281K and over the two degree range from 281K to 283K.

The effect of decreasing the density along the co-existence curve can be seen from Figures III-175, III-177, III-179 and III-181. The density attained is low enough that a fairly flat plateau can be seen (Figures

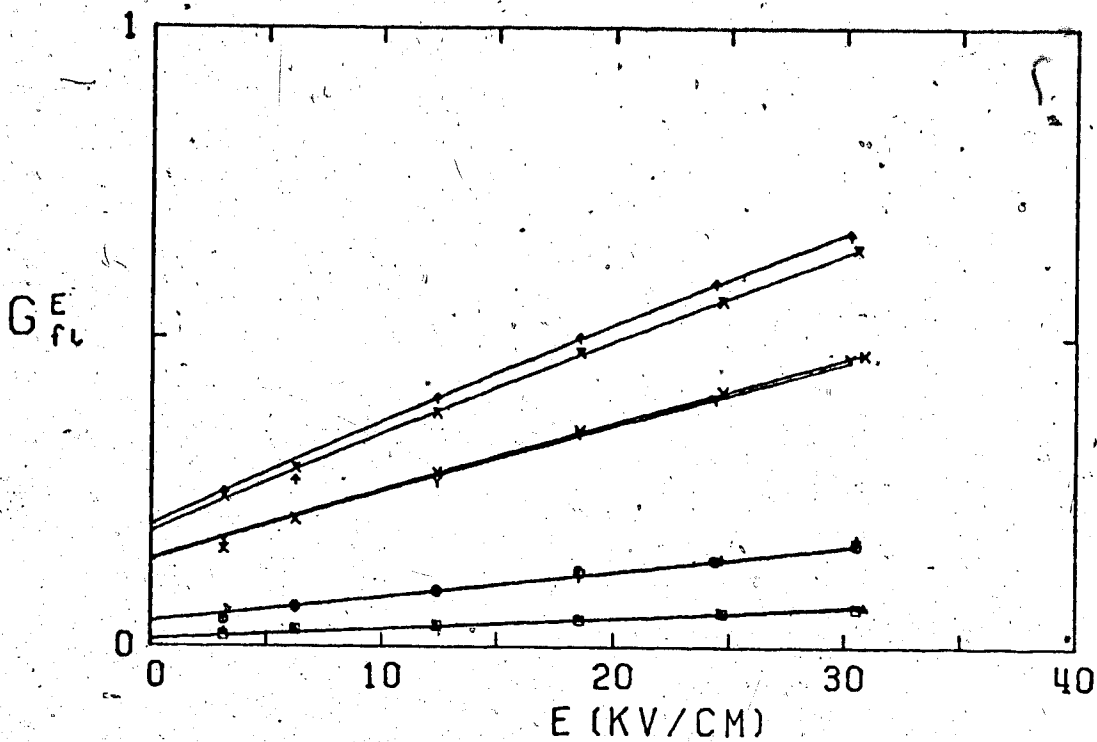


FIGURE III-173. Free ion yields as functions of E in liquid ethene. Temperature, densities and polarities of the applied voltages (T,d,V): \square (173K, 0.566, -), Δ (173K, 0.566, +), \circ (239K, 0.452, -), $+$ (239K, 0.452, +), γ (279K, 0.368, -), X (279K, 0.368, +), ∇ (281K, 0.278, -), $*$ (281K, 0.278, +).

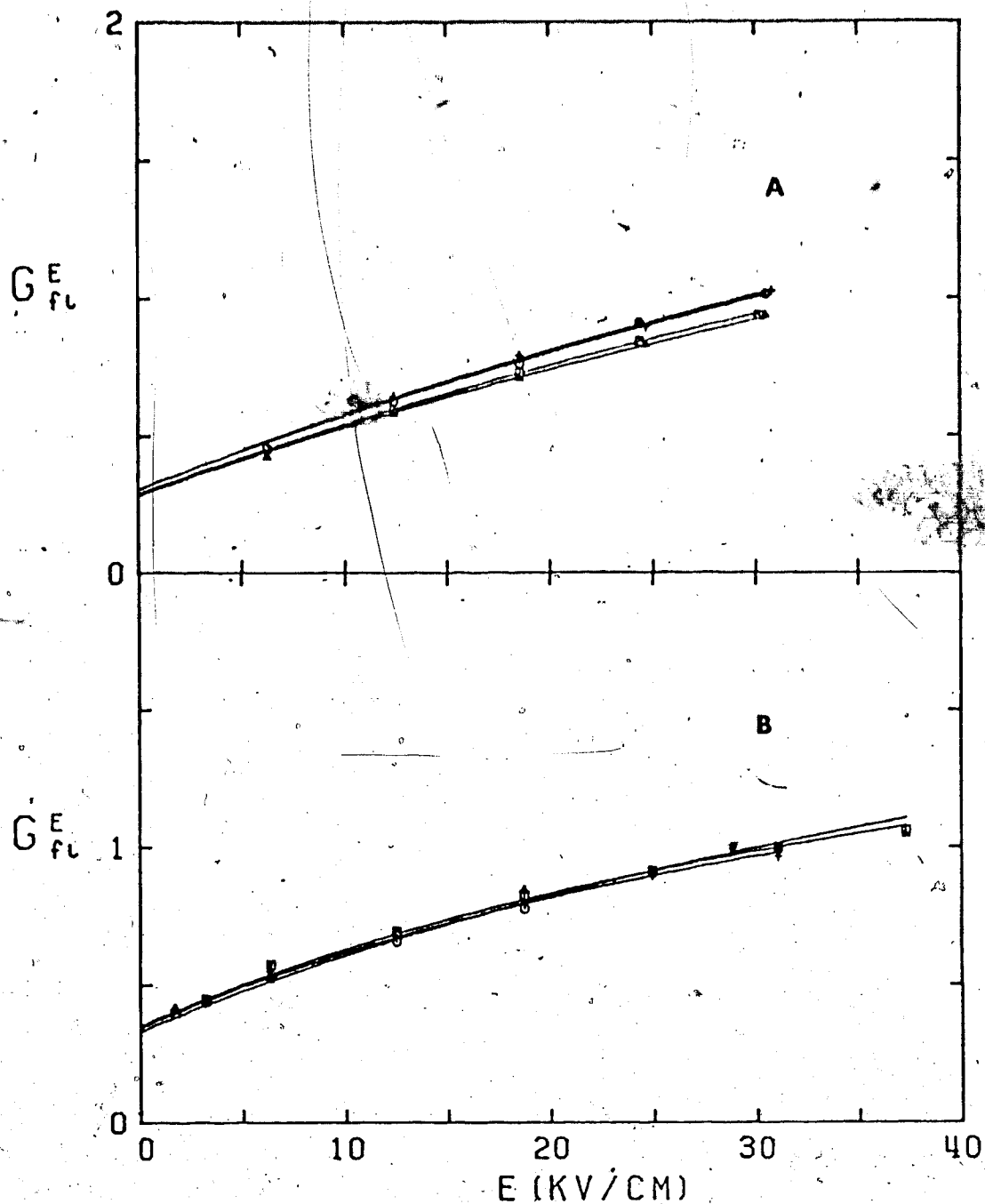


FIGURE III-174. Free ion yields as functions of E in supercritical ethene. $d = 0.22 \text{ g/cm}^3$. Temperatures and polarities of the applied voltages (T, V):

A: \square (283K, -) Δ (283K, +) \circ (284K, -) + (284K, +)
Liquid type cell results

B: \square (284K, -) Δ (284K, +), \circ (285K, -) + (285K, +)
Gas type cell results.

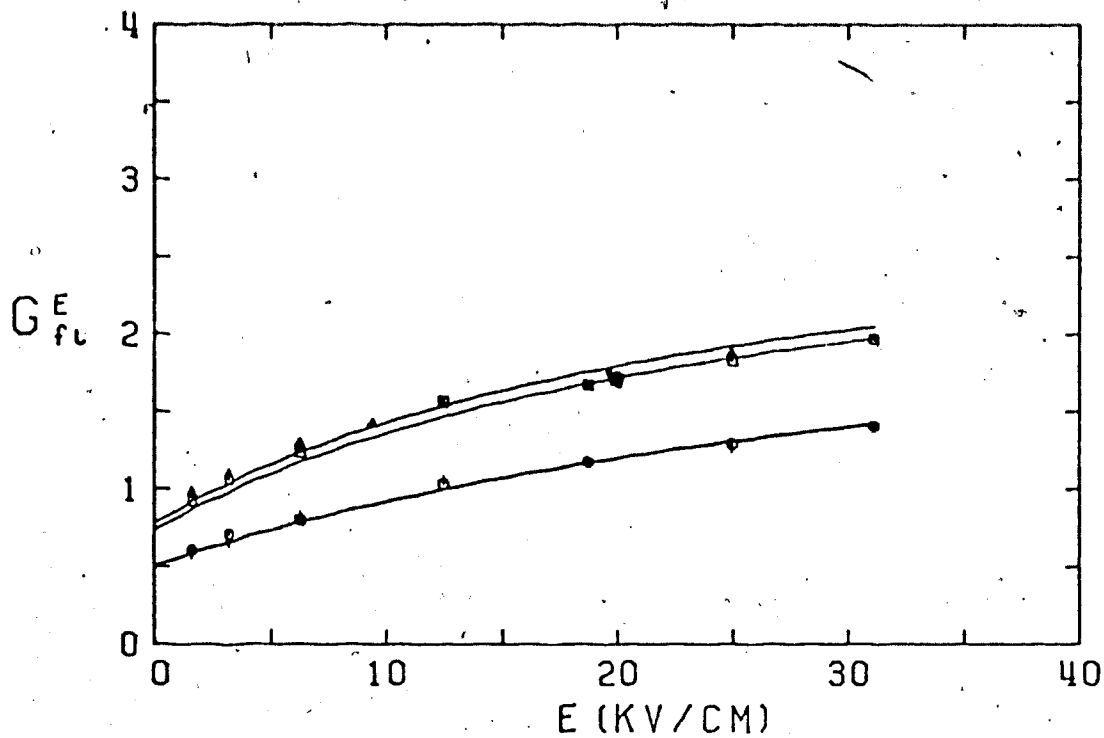


FIGURE III-175. Free ion yields in gaseous ethene as functions of E . Temperatures, densities and polarities of the applied voltages (T, d, V) : \circ (282K, 0.157, +), \triangle (282K, 0.157, -), \square (275K, 0.105, +), \diamond (275K, 0.105, -)

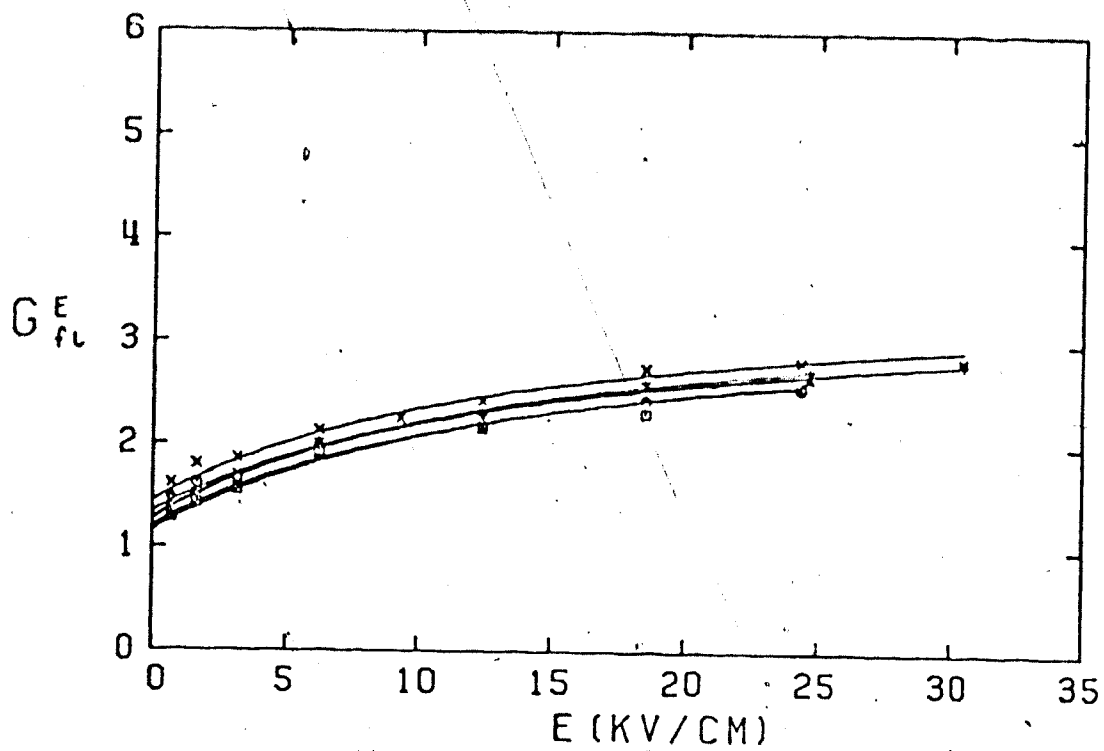


FIGURE III-176. Free ion yields in gaseous ethene as functions of E . $d = 0.0762 \text{ g/cm}^3$. Temperatures and polarities of the applied voltages (T,V): X (294K, +), Y (294K, -), + (274K, +), O (274K, -), Δ (268K, +), \square (268K, -).

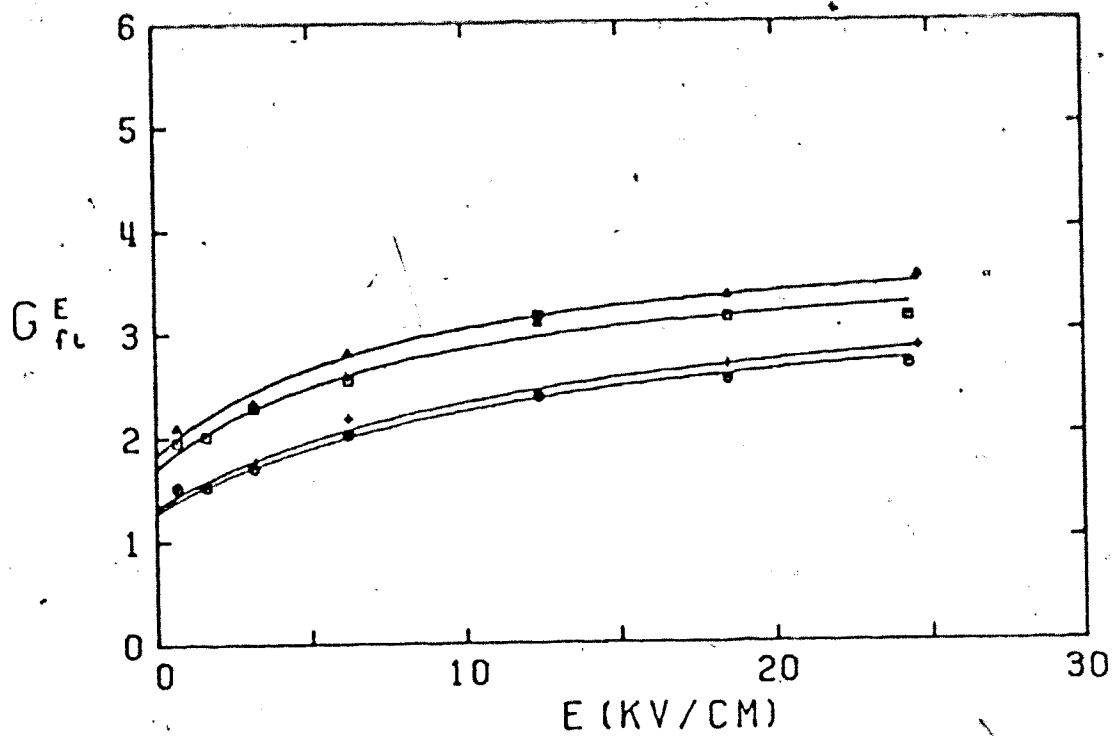


FIGURE III-177: Free ion yields in gaseous ethene as functions of E . Temperatures, densities and voltages (T,d,V):
 + (265K, 0.074, +), O (265K, 0.074, -) Δ (256K, 0.056, +), □ (256K, 0.056, -).

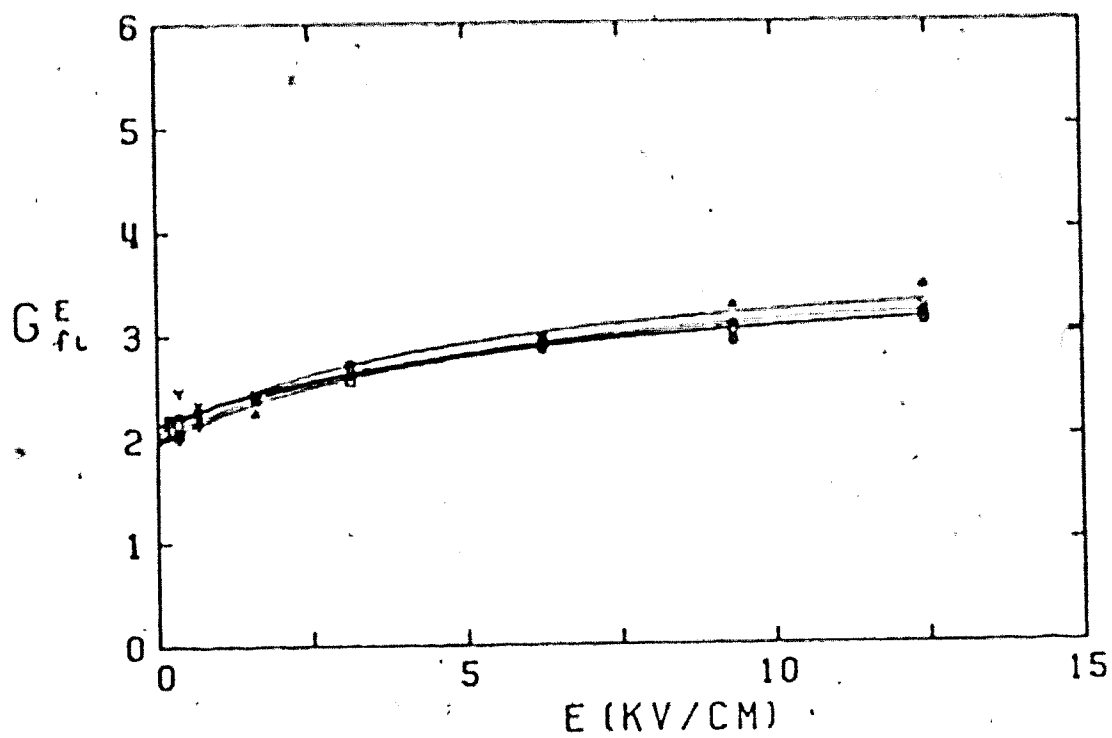


FIGURE III-178. Free ion yields in gaseous ethene as functions of E . $d = 0.037 \text{ g/cm}^3$. Temperatures and polarities of the applied voltages (T,V): X (295K, +), Y (295K, -), + (254K, +), ○ (254K, -), △ (244K, +), □ (244K, -).

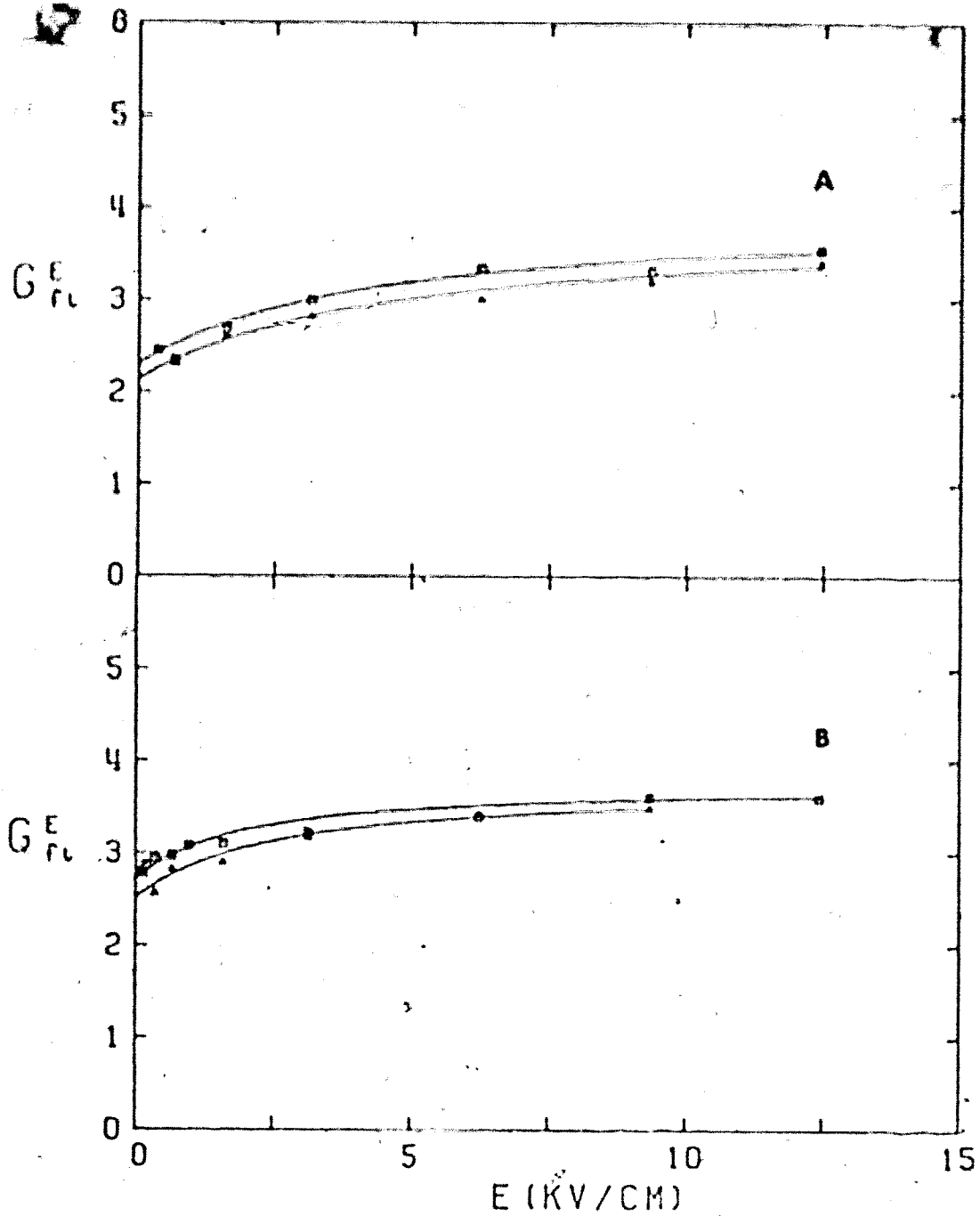


FIGURE III-179. Free ion yields in gaseous ethene as functions

of E . \square is (-) and \triangle is (+) applied voltage.

A: $T = 241K$, $d = 0.036 \text{ g/cm}^3$.

B: $T = 226K$, $d = 0.022 \text{ g/cm}^3$.

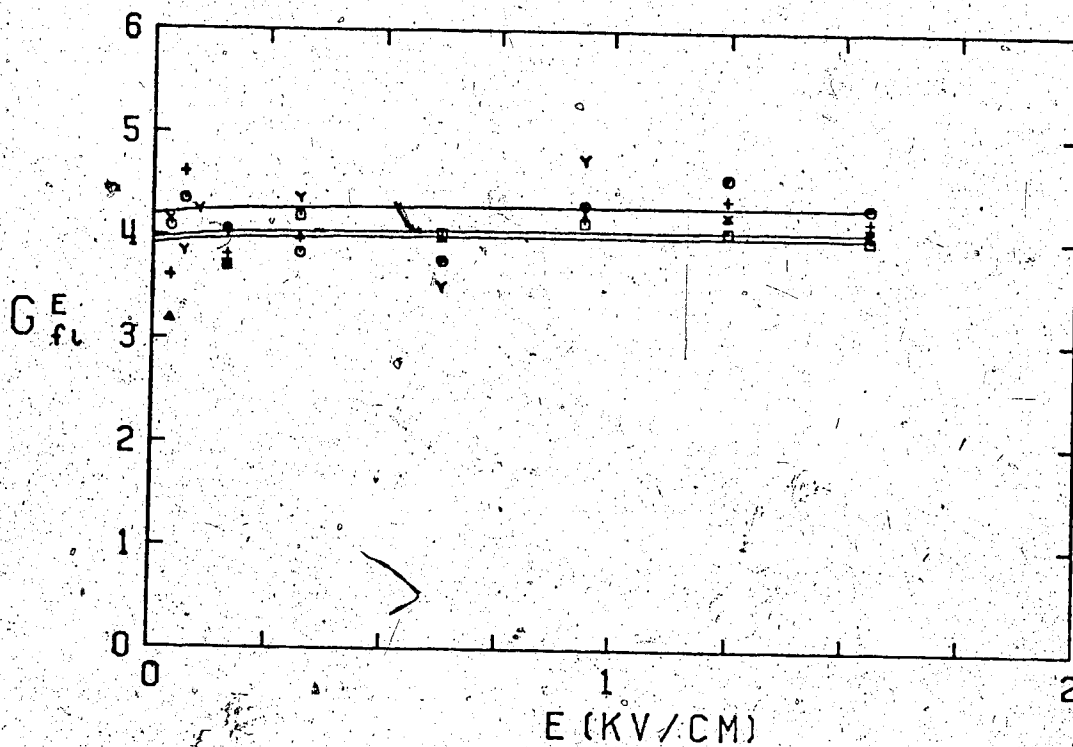


FIGURE III-180. Free ion yields in gaseous ethene as functions of E . $d = 0.0088 \text{ g/cm}^3$. Temperatures and polarities of the applied voltages (T,V): Y (297K, +), + (236K, +), O (236K, -), Δ (206K, +), \square (206K, -).

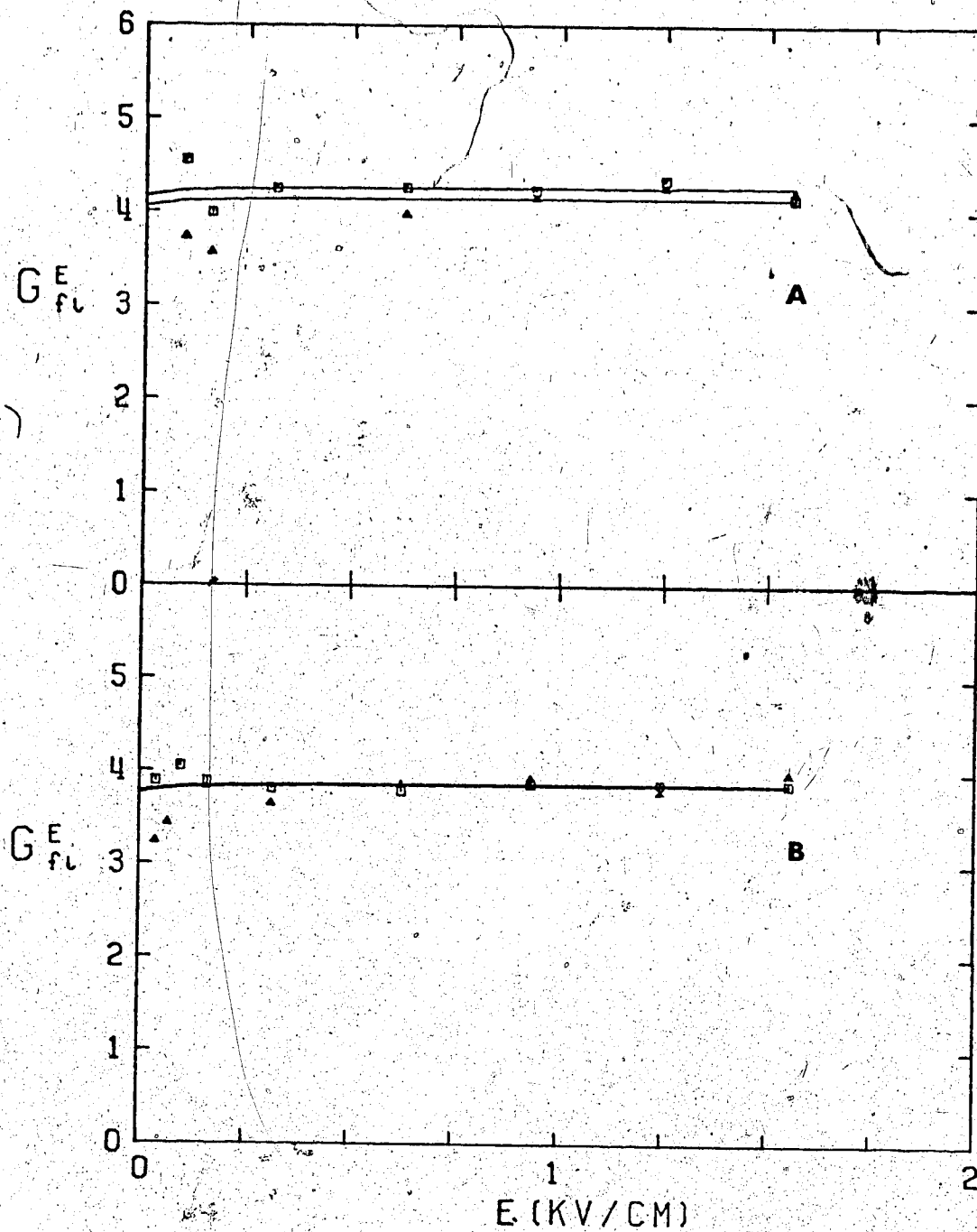


FIGURE III-181. Free ion yields in gaseous ethene as functions of E . \square is (-) and \triangle is (+). Applied voltage:
 A: $T = 203K$ $d = 0.0088 \text{ g/cm}^3$
 B: $T = 195K$ $d = 0.0073 \text{ g/cm}^3$

III-180 and III-181); otherwise, the curves have qualitative features as the alkanes. Decreasing density leads to an increase of the high field free ion yields up to a maximum. The field at which this maximum is attained shifts to a lower value as the density decreases.

Figures III-176, III-178 and III-180 show the temperature effect along isochores where $n/n_c = 0.35$, 0.17 and 0.04 , respectively. There may be an increase for $n/n_c = 0.35$, but the other two show no clear variation greater than the scatter in the data sets.

The free ion yields in the last two figures seem independent of the field strength at high fields. The experimental points are clustered about 4.0 . This agrees well with the total ionization yield obtained in the low density gas of 3.9 (see Table I-1).

Data for ethene are summarized in Table III-22.

Table III-22

Summary of Free Ion Results for Ethene^a

T	d	ϵ^b	G_{fi}^0	G_{tot}	b^c	bd
K	g/cm ³				10 ⁻⁸ cm	10 ⁻⁸ g/cm ²
173	0.566	1.82	0.011 (0.010)	2.0 (2.0)	53 (52)	30 (30)
239	0.452	1.62	0.040 (0.039)	2.0 (2.0)	71 (71)	32 (32)
279	0.302	1.49	0.14 (0.14)	3.0 (3.0)	95 (95)	29 (29)
281	0.278	1.35	0.20 (0.19)	3.5 (3.5)	110 (110)	31 (31)
283	0.22 ^d	1.27	0.29 (0.28)	3.0 (3.0)	160 (155)	35 (34)
284	0.22 ^d	1.27	0.31 (0.31)	3.4 (3.4)	150 (150)	33 (33)
285	0.22 ^d	1.27	0.35 (0.35)	2.0 (2.0)	220 (220)	48 (48)
284	0.22 ^d	1.27	0.33 (0.35)	2.5 (2.0)	190 (220)	41 (48)
282	0.157	1.19	0.51 (0.51)	2.5 (2.5)	270 (270)	42 (42)
275	0.105	1.11	0.75 (0.79)	3.0 (3.0)	340 (360)	36 (38)
294	0.0762	1.08	1.35 (1.45)	3.5 (3.6)	510 (540)	39 (41)
274	0.0762	1.08	1.2 (1.3)	3.4 (3.5)	500 (520)	38 (40)
268	0.0762	1.08	1.2 (1.27)	3.5 (3.5)	480 (520)	37 (40)
265	0.074	1.08	1.3 (1.30)	3.5 (3.6)	540 (540)	40 (40)
256	0.054	1.06	1.7 (1.8)	3.8 (3.9)	730 (790)	41 (44)

TABLE III-22 (continued)

295	0.037	1.04	2.2 (2.1)	3.6 (3.6)	1040 (1020)	39 (38)
254	0.037	1.04	2.0 (2.0)	3.7 (3.7)	1020 (1020)	38 (38)
244	0.037	1.04	2.0 (2.1)	3.7 (3.8)	1010 (1050)	37 (39)
241	0.036	1.04	2.3 (2.2)	3.9 (3.8)	1300 (1100)	45 (41)
226	0.022	1.03	2.7 (2.5)	3.7 (3.8)	2400 (1800)	53 (39)
297	0.0088	1.01		(4.1)		
236	0.0088	1.01		4.0 (4.1)		
206	0.0088	1.01		4.0 (4.0)		
203	0.0088	1.01		4.2 (4.2)		
195	0.0073	1.01		3.9 (3.9)		

- a. Results from positive applied voltage in brackets.
 b. Static dielectric constant
 c. Most probable thermalization length
 d. $T_c = 283K$ $d_c = 0.22 \text{ g/cm}^3$

vii) Propene

Data for propene appear in Figures III-182 to III-189. Results in Figures III-182, III-183 and III-184(A) were obtained with a high pressure liquid type cell. The rest were obtained with a high pressure gas type cell. No polarity effect exists.

The trends in the liquid phase resemble those in ethene. Throughout the liquid range, the free ion yields remain low. In the lowest two temperatures, 231K and 254K (Figure III-182), the free ion yield curve is increasing superlinearly with the electric field. At 296K (Figures III-182 and III-183), the curve is almost linear though there may be a slight upward bend. The curve for 318K is linear, while that of 350K may have a slight downwards bend (Figure III-183). The curve at 364.5K is definitely bending downwards. The free ion yield has increased smoothly as the temperature was increased.

Above the critical point, there is little difference between results obtained in a liquid type cell or a gas type cell (Figure III-184). Increasing the temperature from 365K to 368K to 370K does not noticeably raise the free ion yield. The bend in the curve is slight.

The temperature effect on isochores where $n/n_c = 0.5, 0.25,$ and 0.13 can be seen from Figures III-186, III-187 and III-188, respectively. There may be a slight increase, but most likely any difference is due to scatter.

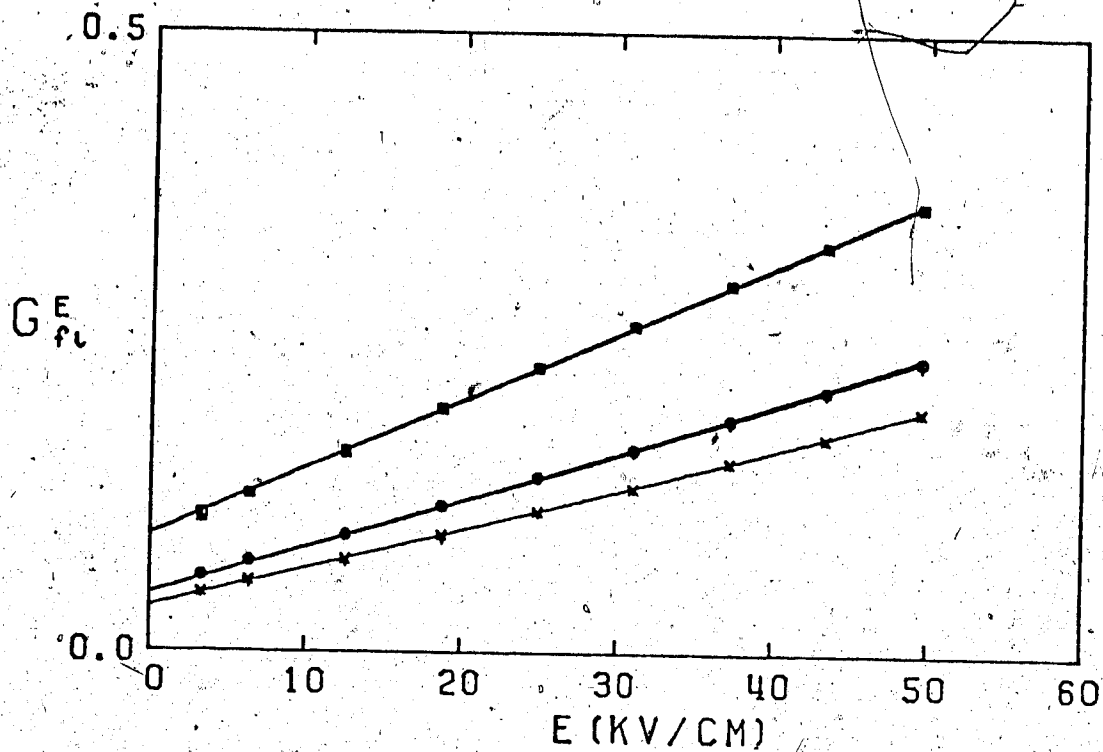


FIGURE III-182. Free ion yields in liquid propene as functions of E . Temperatures, densities and polarities of the applied voltages (T, d, V): x (231K, 0.605, +), γ (231K, 0.605, -), + (254K, +), \circ (254K, -), Δ (296K, +), \square (296K, -).

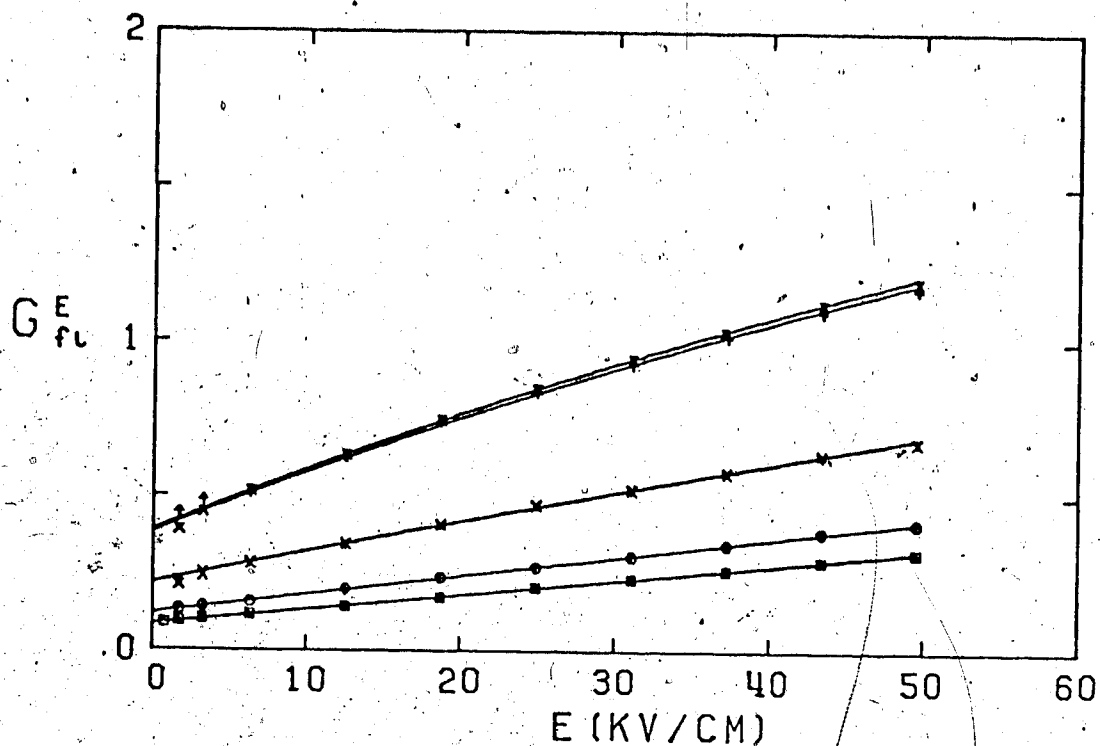


FIGURE III-183. Free ion yields in liquid propene as functions of E . Temperatures, densities and polarities of the applied voltages: □ (296K, 0.512, +), Δ (296K, -0.512, -), ○ (318K; 0.472, -); + (318K, 0.472, +), γ (350K, 0.380, +), X (350K, 0.380, -), ♣ (364.5K, 0.270, -), ⌘ (364.5K, 0.270, +).

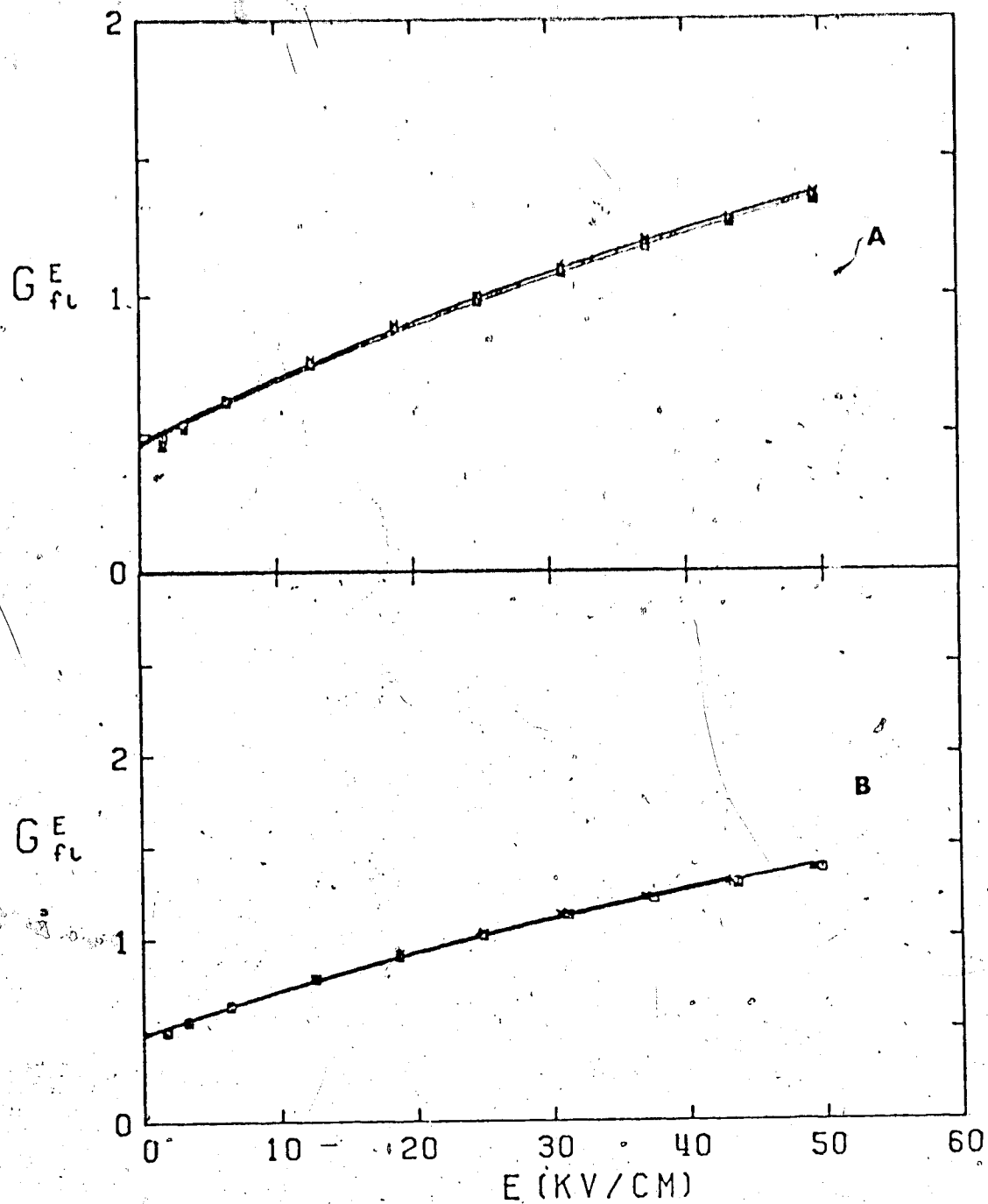


FIGURE III-184. Free-ion yields in supercritical propene as functions of E , $d = 0.232 \text{ g/cm}^3$. Temperatures and polarities of the applied voltages (T,V)

A: □ (365K, +), △ (365K, -), ○ (368K, -), + (368K, +), • (370K, +), x (370K, -) Liquid cell results.

B: * (368K, -) ○ (368K, +), △ (365K, -), □ (365, +) Gas cell results.

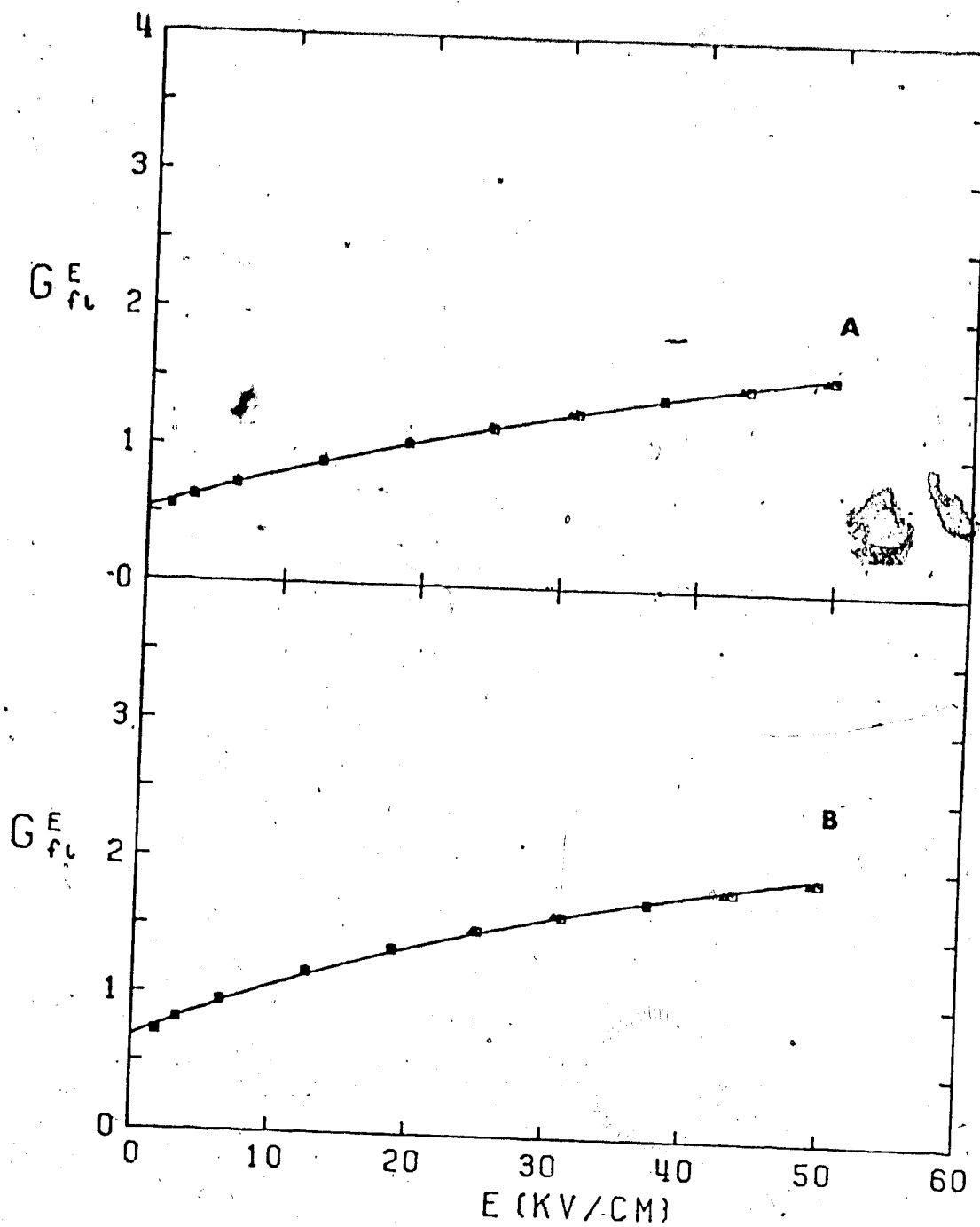


FIGURE III-185. Free ion yields in gaseous propene as functions of E . \square is (+) and \triangle is (-) applied voltage.

A: $T = 364K$ $d = 0.200 \text{ g/cm}^3$

B: $T = 361K$ $d = 0.158 \text{ g/cm}^3$

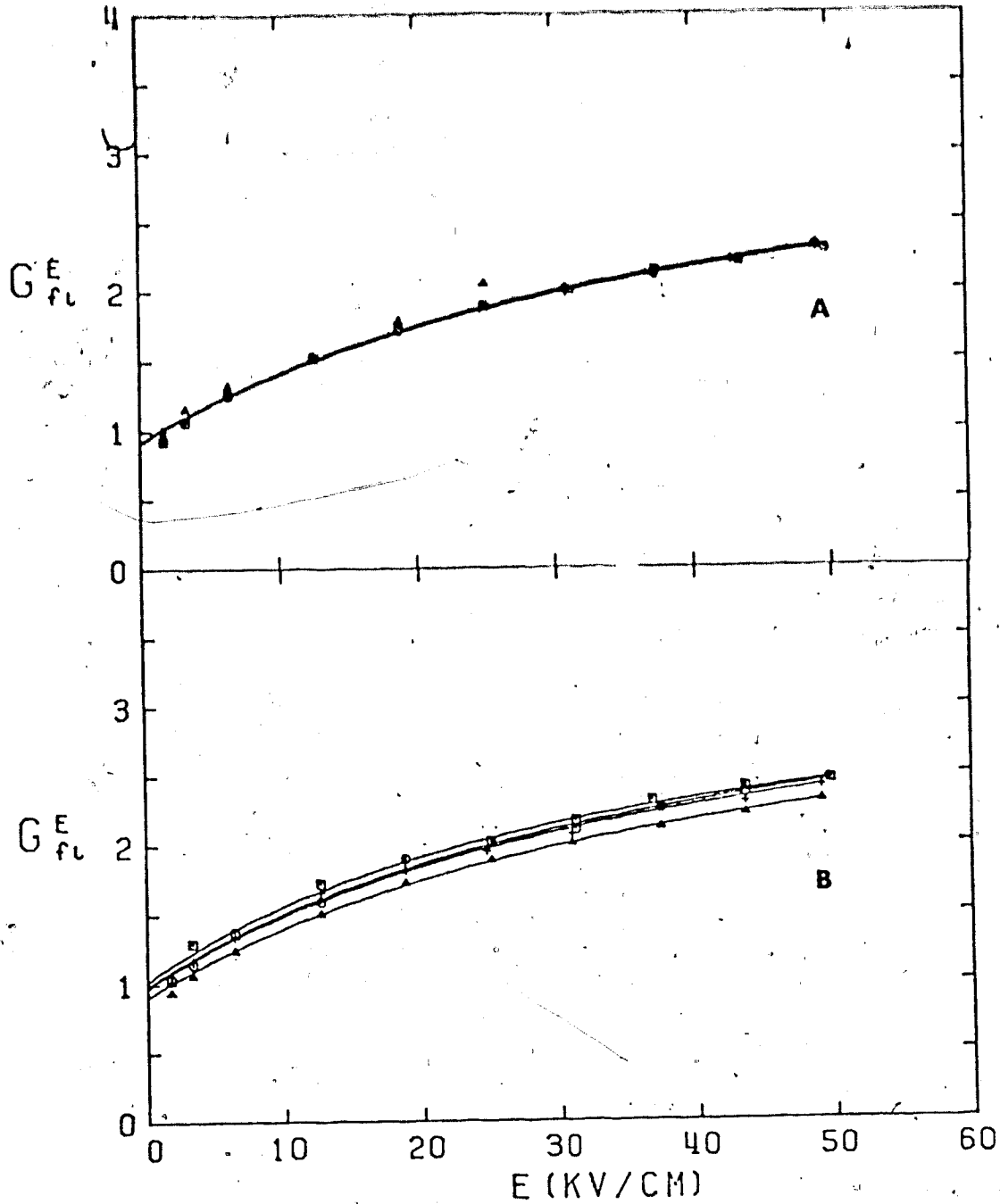


FIGURE III-186. Free ion yields in gaseous propene as functions of E . $d = 0.116 \text{ g/cm}^3$. Temperature and polarities of applied voltages (T,V):

A: \square (366K, +), Δ (366K, -), \circ (368K, +), $+$ (368K, -).

B: \square (358K, +), Δ (358K, -), \circ (362K, +), $+$ (362K, -).

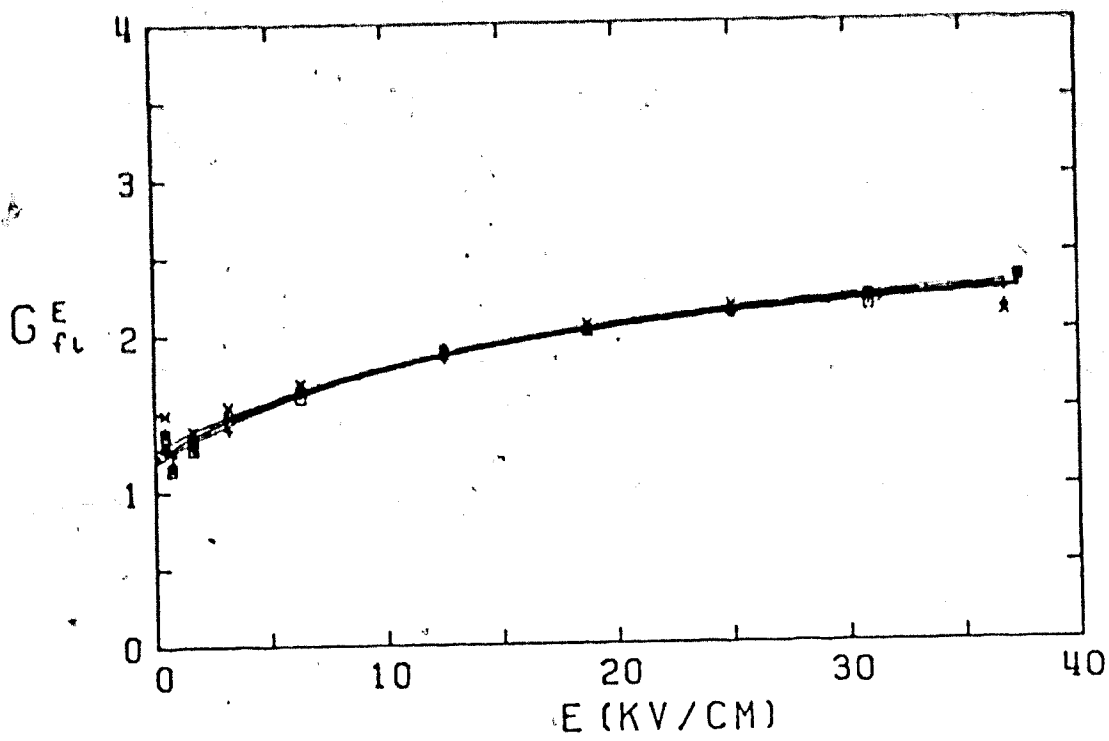
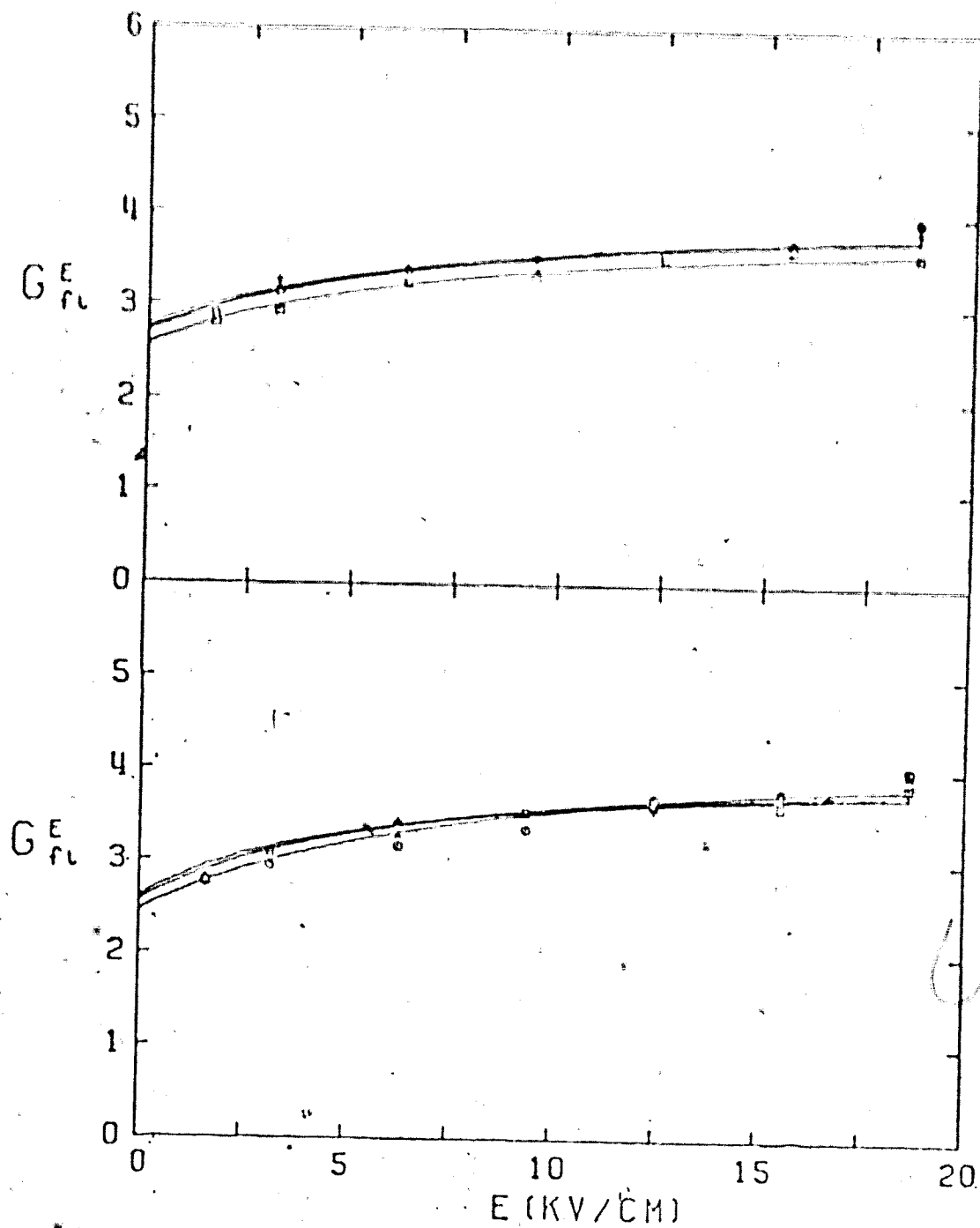


FIGURE III-187. Free ion yields in gaseous propene as functions of E . $d = 0.0575 \text{ g/cm}^3$. Temperature and polarities of the applied voltages (T,V): X (388K, -), Y (388K, +), + (367K, -) ○ (367K, +), △ (348K, -), □ (348K, +).



* FIGURE III-108. Free ion yields in gaseous propene as functions of E . $d = 0.029 \text{ g/cm}^3$. Temperatures and polarities of the applied voltages^o (T,V):

A: + (381K, -), \circ (331K, +), Δ (357K, -), \square (357K, +)

B: + (318K, -), \circ (318K, +), Δ (305K, -), \square (305K, +)

Examination of the gas phase results (Figures III-184 to III-189) shows similar trends to those noted in the other hydrocarbon systems. Decreasing the gas density from the supercritical fluid to 0.200 g/cm^3 , then 0.153 g/cm^3 (Figure III-185) leads to a definite bending of the free ion yield curve. At lower densities, the free ion yields are bending over towards a maximum but insufficient field strength did not allow the value to be actually reached, as in ethene (Figure III-181). Even at $d = 0.235 \text{ g/cm}^3$, $E = 16 \text{ kV/cm}$ was not quite enough to attain the maximum plateau (Figure III-189).

The value of the fitting parameter G_{tot} equals 3.1 for curves where $d \leq 0.029 \text{ g/cm}^3$ or 3.6 for $d \leq 0.116 \text{ g/cm}^3$. The low density gas phase total ionization yield is 4.0 (see Table I-1). Agreement is within about 10%.

Data for propene is summarized in Table III-23.

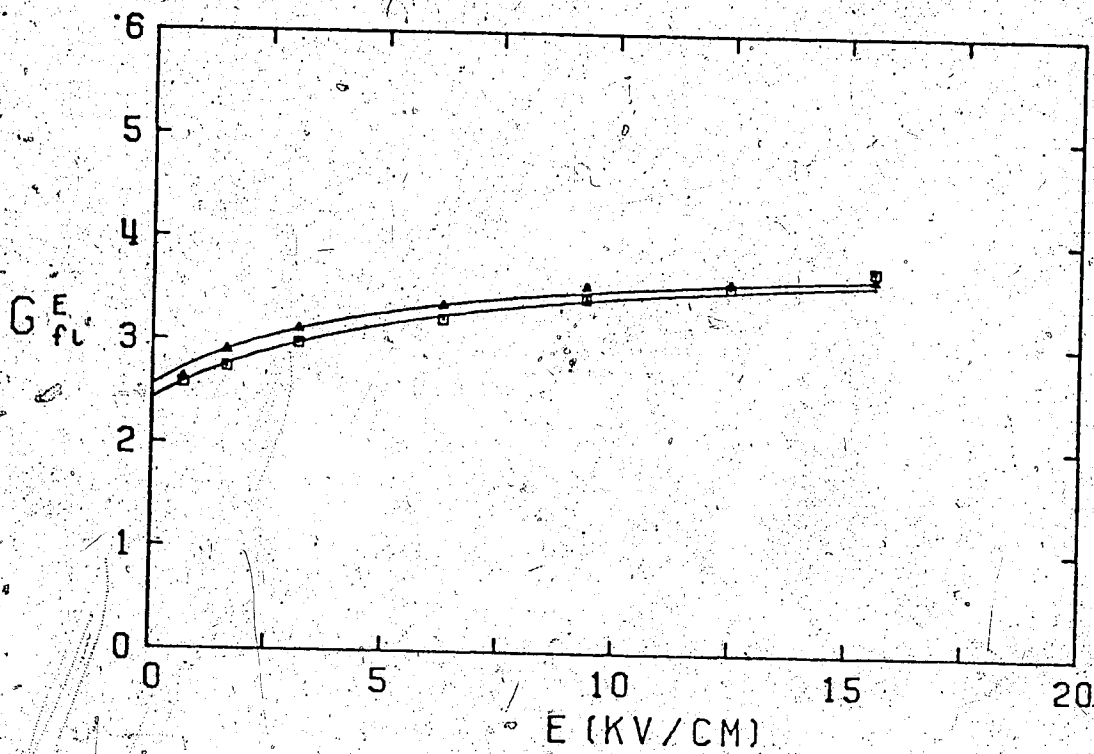


FIGURE III-189. Free ion yields in gaseous propene as functions of E . $T = 296K$. $d = 0.0235 \text{ g/cm}^3$. \square is (+) and \triangle is (-) applied voltage.

TABLE III-23

Summary of Free Ion Yield Results for Propene^a

T K	d g/cm ³	ϵ^b	G_{fi}^0	G_{tot}	b^c 10 ⁻⁸ cm	bd 10 ⁻⁸ g/cm ²
231	0.605	2.05	0.037 (0.037)	3.8 (3.8)	44 (44)	27 (27)
254	0.578	1.82	0.047 (0.47)	3.8 (3.8)	50 (50)	29 (29)
296	0.512	1.87	0.095 (0.095)	3.8 (3.8)	55 (55)	28 (28)
			0.083 (0.085)	3.8 (3.8)	52 (52)	27 (27)
318	0.472	1.80	0.12 (0.12)	3.8 (3.8)	58 (58)	27 (27)
350	0.380	1.61	0.22 (0.22)	3.8 (3.8)	76 (76)	29 (29)
364.5	0.270	1.34	0.38 (0.39)	3.8 (3.8)	120 (120)	32 (32)
365	0.232 ^d	1.33	0.46 (0.46)	3.6 (3.6)	135 (135)	31 (31)
368	0.232 ^d	1.33	0.47 (0.47)	3.6 (3.6)	135 (135)	31 (31)
370	0.232 ^d	1.33	0.47 (0.47)	3.6 (3.6)	135 (135)	31 (31)
368	0.232 ^d	1.33	0.48 (0.48)	3.6 (3.6)	140 (140)	32 (32)
365	0.232 ^d	1.33	0.48 (0.47)	3.6 (3.6)	140 (140)	32 (32)
364	0.200	1.24	0.54 (0.53)	3.6 (3.6)	160 (160)	32 (32)
361	0.158	1.13	0.68 (0.68)	3.5 (3.5)	210 (210)	33 (33)
368	0.116	1.12	0.92 (0.93)	3.5 (3.5)	270 (270)	31 (31)

TABLE III-23 (continued)

366	0.116	1.12	0.93 (0.92)	3.5 (3.5)	270 (270)	31 (31)
362	0.116	1.12	0.98 (0.99)	3.6 (3.6)	280 (280)	32 (32)
358	0.116	1.12	0.91 (1.0)	3.4 (3.4)	280 (310)	32 (36)
388	0.0575	1.07	1.3 (1.3)	2.8 (2.7)	490 (510)	28 (29)
367	0.0575	1.07	1.2 (1.2)	2.7 (2.7)	520 (520)	30 (30)
348	0.0575	1.07	1.2 (1.2)	2.7 (2.8)	540 (490)	31 (28)
381	0.029	1.03	2.8 (2.7)	4.1 (4.1)	1090 (1040)	32 (30)
357	0.029	1.03	2.7 (2.6)	4.1 (4.0)	1090 (1020)	32 (30)
318	0.029	1.03	2.6 (2.5)	4.2 (4.3)	1030 (890)	30 (26)
305	0.029	1.03	2.6 (2.6)	4.1 (4.0)	1100 (1200)	32 (35)
296	0.0235	1.03	2.6 (2.4)	3.9 (4.0)	1300 (1100)	31 (26)

a. Positive voltage results in brackets

b. Static dielectric constant

c. Most likely thermalization distance

d. $T_c = 365K$ $d_c = 0.232 \text{ g/cm}^3$

8. Cyclopropane

Free ion yields for cyclopropane appear in Figures III-190 to III-197. Data in Figures III-190 and III-191 were collected by a liquid type high pressure conductance cell. The other results were obtained with a gas type high pressure cell. No difference between results obtained with positive or negative voltage is apparent for $d \geq 0.058 \text{ g/cm}^3$. The difference between the results at lower densities is likely due to scatter.

In the liquid (Figures III-190 and III-191), the free ion yield curves are like those of the alkenes. The values of the free ion yields are low up to the critical point, though near the critical region (393K), and at the critical region, the value is greater than in propene. This intermediate behavior between that of the alkanes and that of the alkenes is another example of the dual nature of cyclopropane. (At 254K (Figure III-190), the free ion yield is noticeably superlinear with respect to E. At 296K, this is still true but is less noticeable. At 332K, the free ion yield is linearly dependent upon E. Further heating of the liquid to 367K, then to 393K (Figure III-191) leads to the onset of bending of the free ion yield curve. In the critical region (398K), the bending is fairly noticeable. Increasing the temperature 1K leads to no separation. Higher temperatures were not attempted since the high critical pressure can easily shatter the conductance cell.

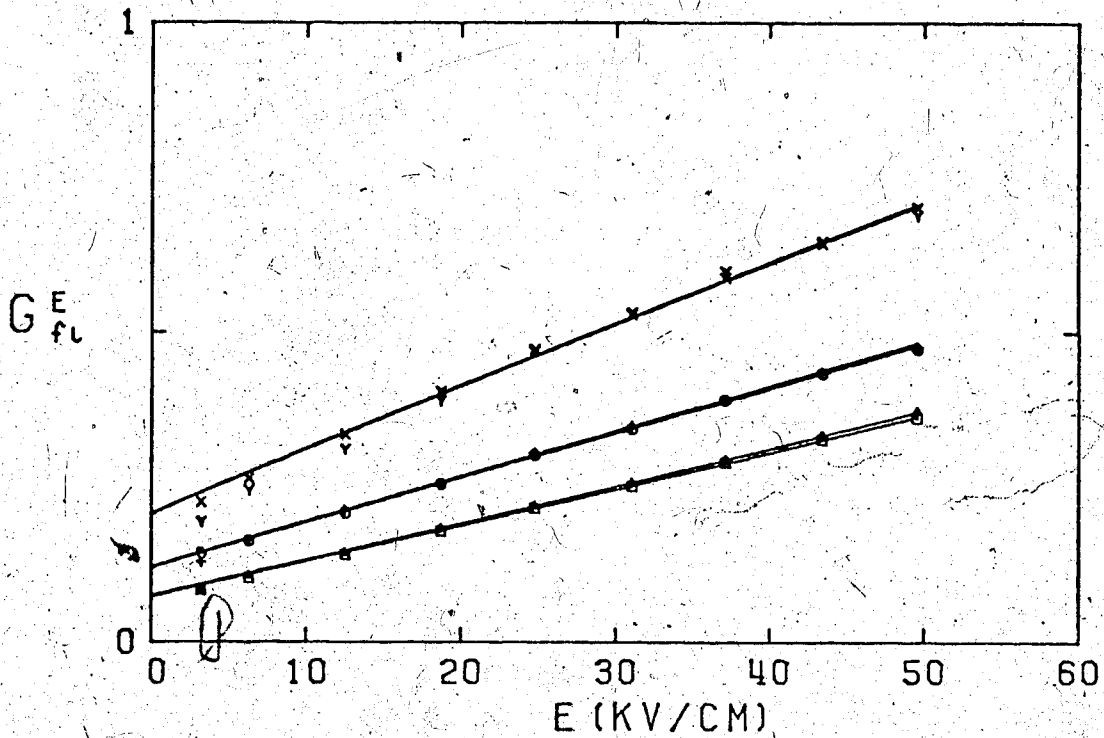


FIGURE III-190. Free ion yields in liquid cyclopropane as functions of E . Temperatures, densities and polarities of the applied voltages (T, d, V): □ (254K, -), △ (254K, +), ○ (296K, -), + (296K, +), γ (332K, -), x (332K, +).

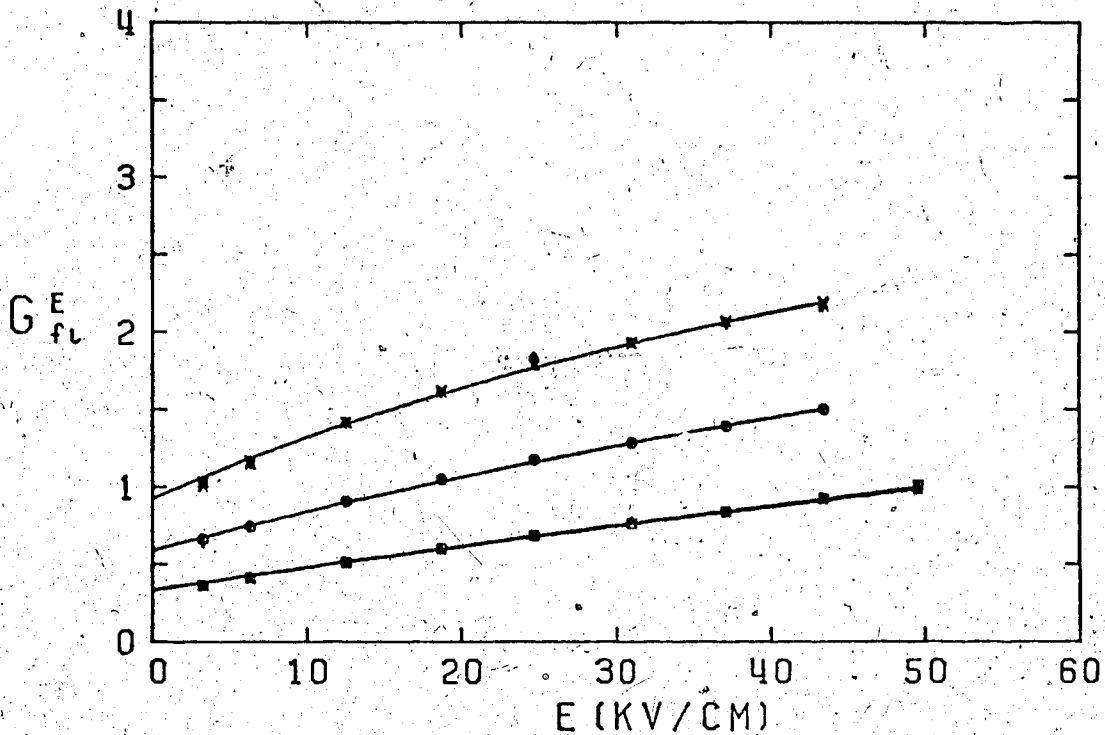


FIGURE III-191. Free ion yields in liquid and supercritical cyclopropane as functions of E . Temperatures, densities and polarities of the applied voltages (T, d, V): \square (367K, 0.470, +), Δ (367K, 0.470, -), \circ (393K, 0.347, -), $+$ (393K, 0.347, +), γ (398K, 0.248, -), x (398K, 0.248, +), ∇ (399K, 0.248, +), \times (399K, 0.248, -).

Results obtained in the gas cell for the supercritical fluid appear in Figure III-192. The 10% difference compared to the liquid cell results is due to the gravity effect.

In the gas phase the behavior parallels that in ethene. No temperature effect occurs along isochores where $n/n_c = 0.46$ (Figure III-194(A)), 0.25 (Figure III-195), or 0.099 (Figure III-197). For $n/n_c = 0.099$, the apparent difference is due to the high degree of scatter at that density. Decreasing the density along the co-existence curve leads to the appearance of a free ion yield plateau at high field strengths. As before, the threshold field shifts to a lower value as the density decreases. A unique value for the threshold field cannot be determined due to the gentleness of the bend. At 297.7K (Figure III-193), the bend is a little more than in the supercritical fluid. At 396K, the bend is a bit more noticeable. At 385K (Figure III-194), the higher field portion of the curve is flattening off. At 358K this is a bit more noticeable (Figure III-196). The zero field free ion yield has been increasing all the while. At 296K, the plateau dominates. The plateau seems to have already dominated the curve by 321K (Figure III-197).

The high field free ion yields at the lower two densities appear scattered about 5.0. This is also the needed value of the fitting parameter G_{tot} for $d \leq 0.11$ g/cm³ (Table III-24). This value is 19% higher than the low density total ionization yield of 4.2 (see Table I-1).

Data for cyclopropane are summarized in Table III-24.

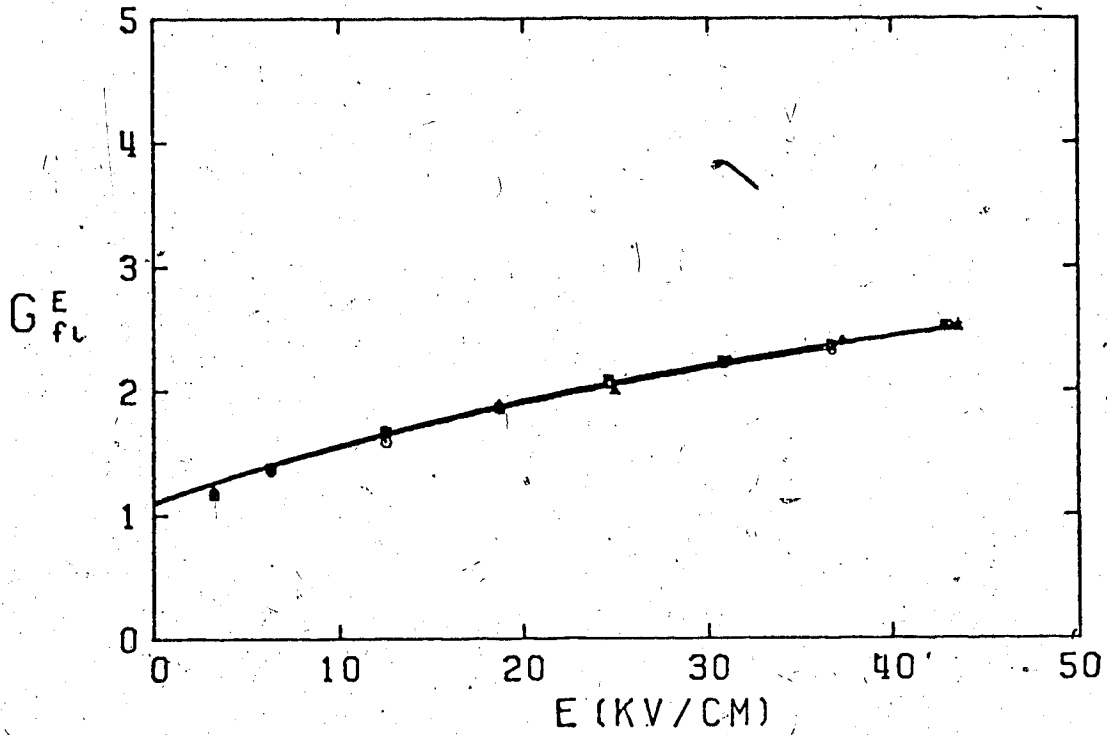


FIGURE III-192: Free ion yields in supercritical cyclopropane as functions of E . $d = 0.248 \text{ g/cm}^3$. Temperatures and polarities of the applied voltages (T,V): □ (398K, -), △ (398K, +), ○ (399K, -), + (399K, +).

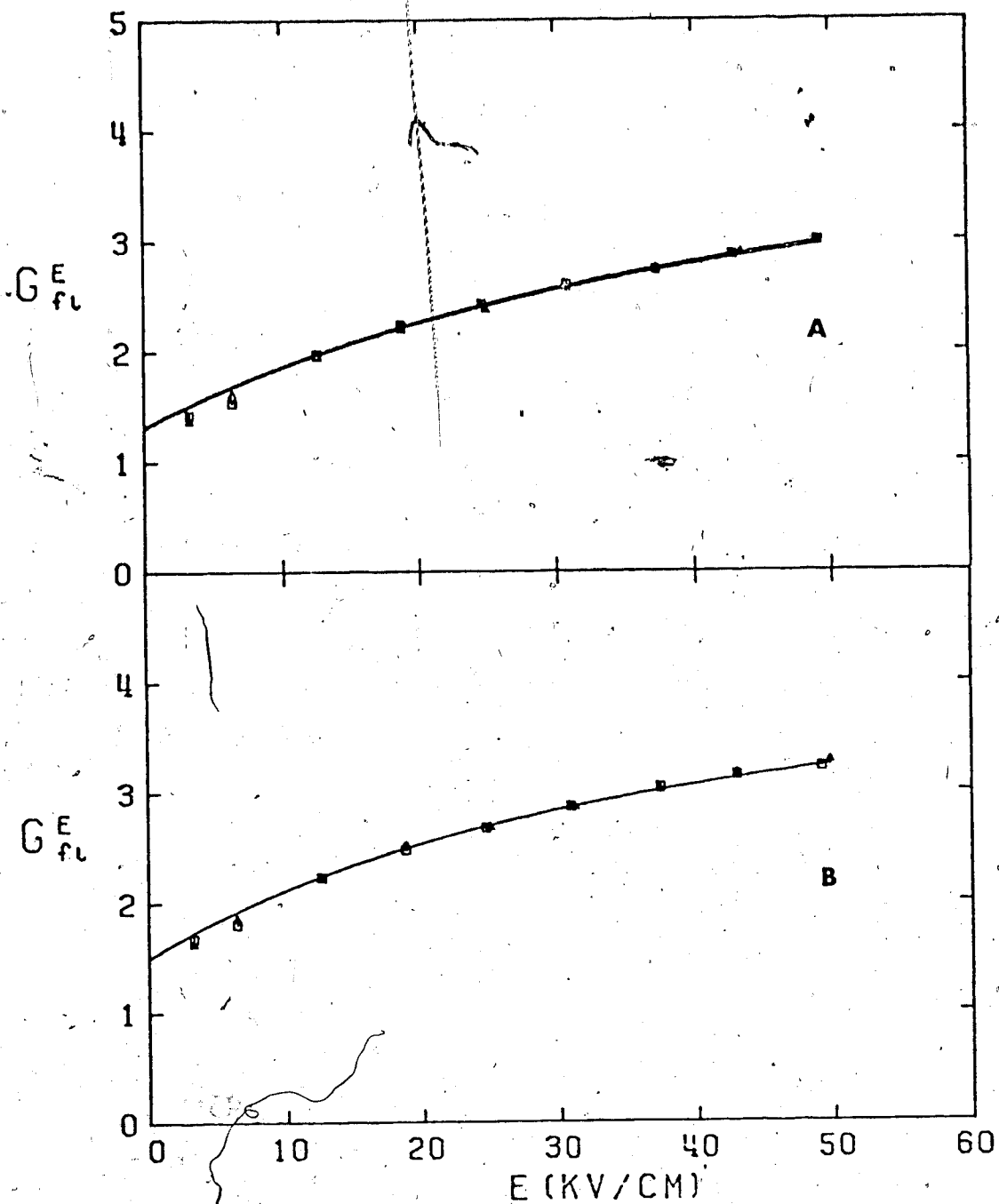


FIGURE III-193. Free ion yields in gaseous cyclopropane as functions of E . \square is (-) and Δ is (+) applied voltage.

A: $T = 397.7K$ $d = 0.21 \text{ g/cm}^3$

B: $T = 396K$ $d = 0.185 \text{ g/cm}^3$

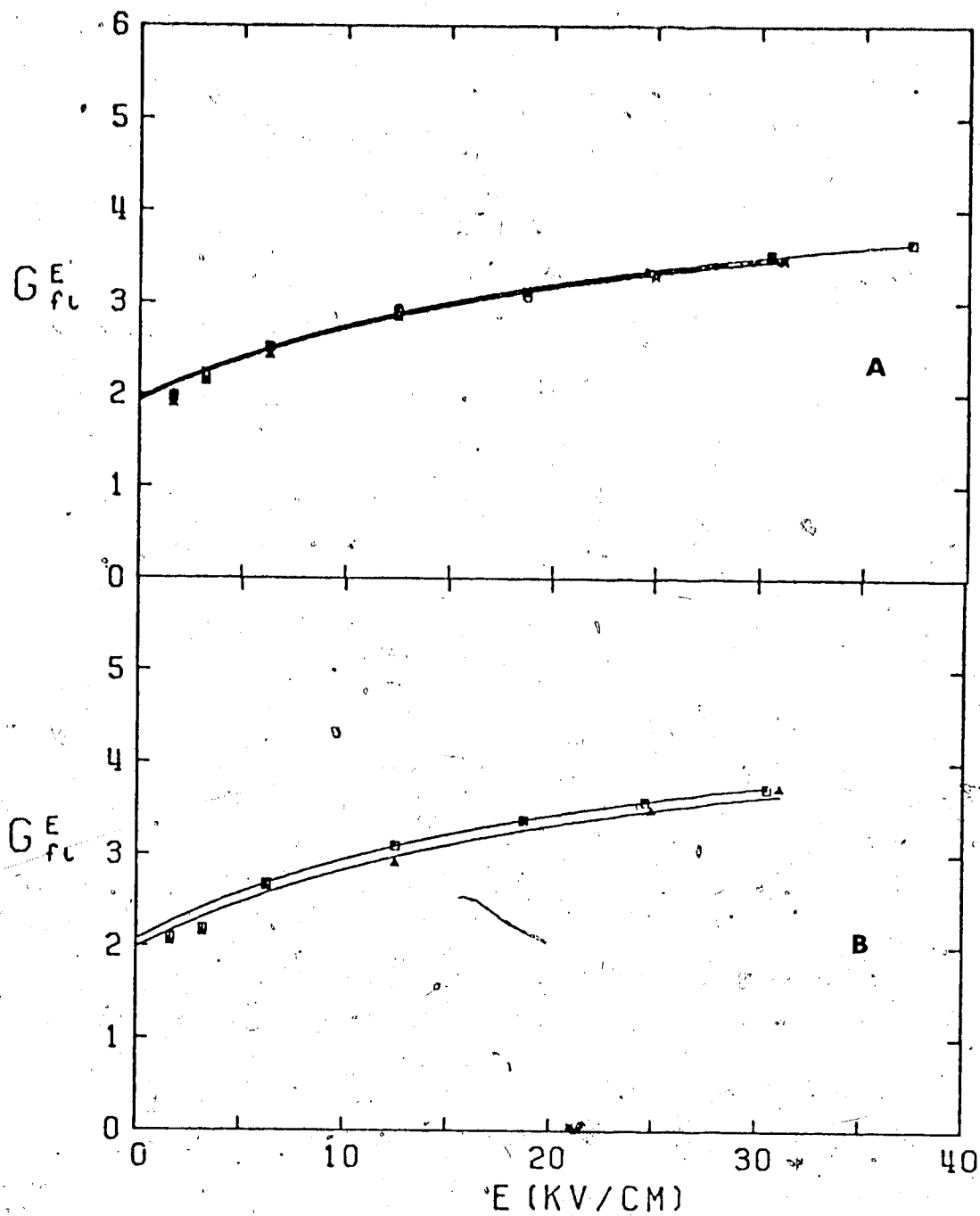


FIGURE III-194. Free ion yields in gaseous cyclopropane as functions of E . Temperatures and polarities of the applied voltages: A: X (398K, +), Y (398K, -), + (394K, +), ○ (394K, -), △ (387K, +), □ (387K, -) $d = 0.115 \text{ g/cm}^3$
 B: □ (385K, -), △ (385K, +) $d = 0.11 \text{ g/cm}^3$

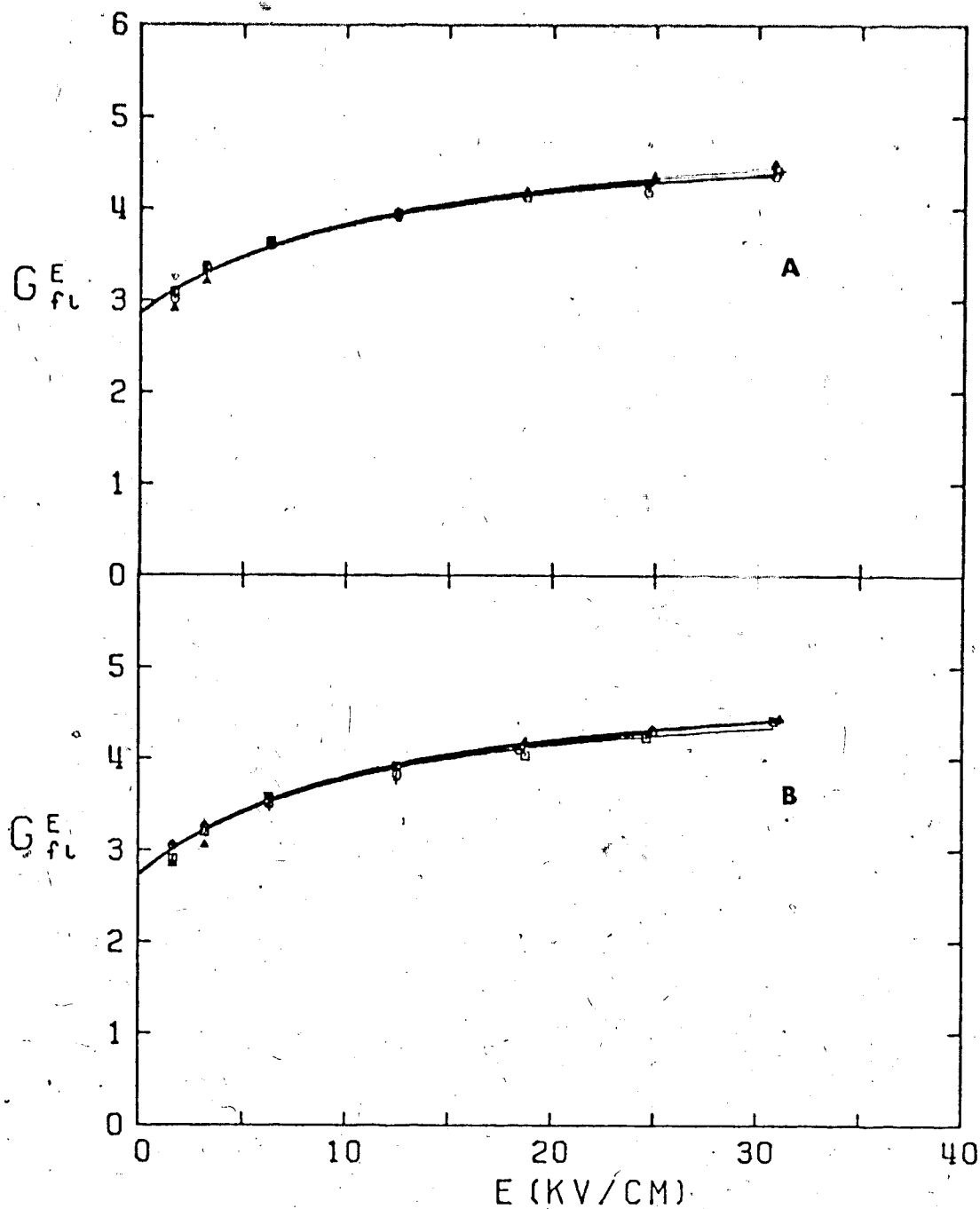


FIGURE III-195. Free ion yields in gaseous cyclopropane as functions of E . $d = 0.0611$. Temperatures and polarities of the applied voltages:

A: + (404K, +), \circ (404K, -), Δ (395K, +), \square (395K, -)

B: + (371K, +), \circ (371K, -), Δ (360K, +), \square (360K, -)

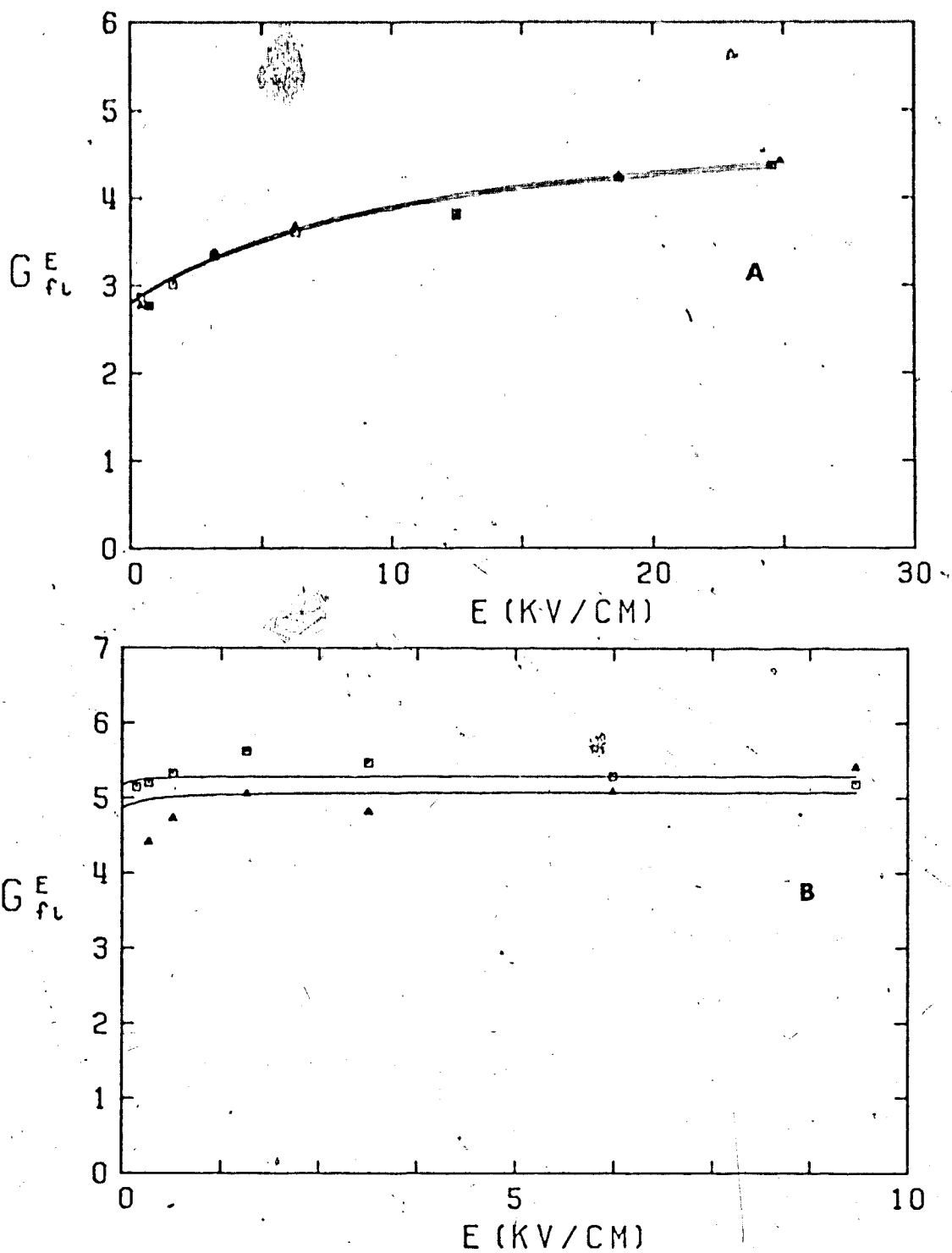


FIGURE III-196. Free ion yields in gaseous cyclopropane as functions of E . \square is (-) and \triangle is (+) applied voltage.

A: $T = 358K$ $d = 0.053 \text{ g/cm}^3$

B: $T = 296K$ $d = 0.0123 \text{ g/cm}^3$

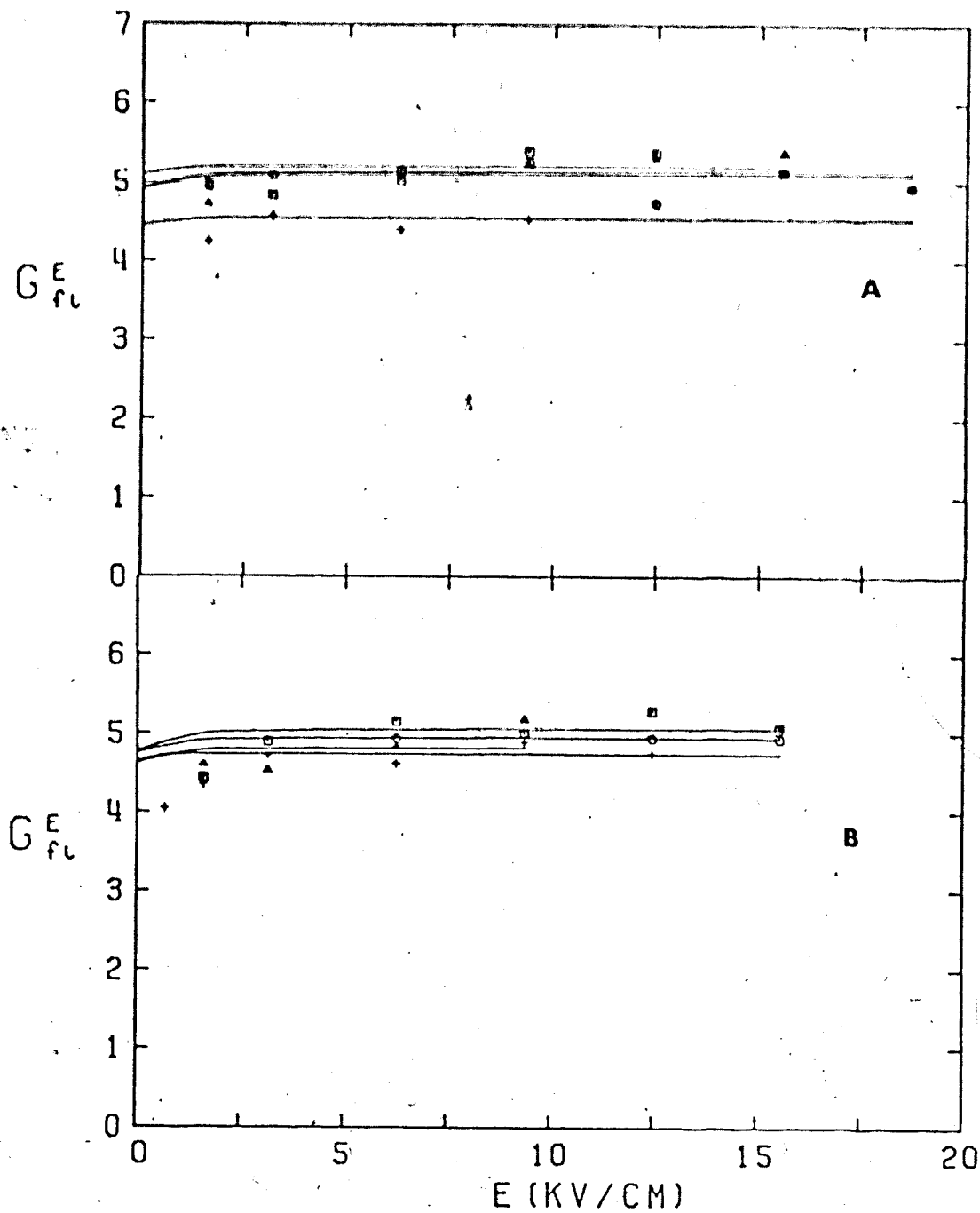


FIGURE III-197. Free ion yields in gaseous cyclopropane as functions of E . $d = 0.0245 \text{ g/cm}^3$. Temperatures and polarities of the applied voltages:

A: + (406K, +), ○ (406K, -) △ (396K, +), □ (396K, -)

B: + (348K, +), ○ (348K, -); △ (321K, +), □ (321K, -)

TABLE III-24

Summary of Free Ion Yields in Cyclopropane^a

T K	d g/cm ³	b	G _{FI} ⁰	G _{tot}	b ^c 10 ⁻⁸ cm	bxl 10 ⁻⁸ g/cm ²
254	0.656	1.85	0.073 (0.075)	4.6 (4.6)	54 (54)	35 (35)
296	0.602	1.76	0.12 (0.12)	4.6 (4.6)	59 (59)	36 (36)
332	0.544	1.67	0.21 (0.21)	5.0 (5.0)	67 (67)	36 (36)
367	0.470	1.57	0.33 (0.34)	4.8 (4.8)	82 (83)	39 (39)
393	0.347	1.40	0.60 (0.59)	4.8 (4.8)	120 (120)	41 (41)
398	0.248 ^d	1.27	0.93 (0.93)	4.6 (4.6)	180 (180)	44 (44)
399	0.248 ^d	1.27	0.93 (0.93)	4.6 (4.6)	180 (180)	44 (44)
399	0.248 ^d	1.27	1.1 (1.1)	4.6 (4.6)	200 (200)	50 (50)
398	0.248 ^d	1.27	1.1 (1.1)	4.6 (4.6)	200 (200)	50 (50)
397.7	0.21	1.25	1.3 (1.3)	4.6 (4.6)	240 (240)	51 (51)
396	0.185	1.22	1.5 (1.5)	4.6 (4.6)	280 (280)	52 (52)
398	0.115	1.13	2.0 (1.9)	4.7 (4.7)	400 (390)	46 (45)
394	0.115	1.13	1.9 (1.9)	4.6 (4.6)	410 (410)	47 (47)
387	0.115	1.13	2.0 (1.9)	4.6 (4.6)	420 (410)	48 (47)

Table III-24 (continued)

385	0.11	1.11	2.1	5.0	420	46
			(2.0)	(5.0)	(390)	(43)
404	0.0611	1.06	2.9	4.9	730	44
			(2.9)	(4.9)	(730)	(44)
395	0.0611	1.06	2.9	5.0	710	43
			(2.9)	(5.0)	(710)	(43)
371	0.0611	1.06	2.8	5.0	690	42
			(2.8)	(5.0)	(690)	(42)
360	0.0611	1.06	2.7	5.0	700	43
			(2.8)	(5.0)	(710)	(43)
358	0.058	1.06	2.8	5.0	740	43
			(2.8)	(5.0)	(740)	(43)
296	0.0123	1.01		5.3		
				(5.0)		
406	0.0245	1.03		4.5		
				(5.0)		
396	0.0245	1.03		5.1		
				(5.1)		
348	0.0245	1.03		4.9		
				(4.7)		
321	0.0245	1.03		5.0		
				(4.8)		

a. Positive applied voltage results in brackets

b. Static dielectric constant

c. Most likely thermalization distance

d. $T_c = 398K$ $d_c = 0.248 \text{ g/cm}^3$

9. Isobutane with Sulfur Hexafluoride (SF_6)

Known volumes of SF_6 at atmospheric pressure were condensed into a high pressure cell. Isobutane was added so that the total number of moles equalled n_c for pure isobutane. The total amount of SF_6 added equalled 0.15, 1.2, 4.9 and 9.5 mol % when the entire sample was in the gas phase. All the results in Figures III-198 to 201 were obtained with positive applied voltage. Sample negative voltage measurements for the 1.2 and the 4.9 % samples agree within 2% to the positive voltage results at all temperatures measured. Free ion yields were determined in the liquid phase at a number of temperatures between room temperature and the supercritical region. The results are summarized in Table III-25.

The exact solubility of the SF_6 in isobutane is not known. A previous calculation (232) for measurement of free ion yields in neopentane with SF_6 (142) assumed that the solubility will be the same as cyclohexane. The solubility in cyclohexane about room temperature is about 0.054 mol % for a partial pressure of 1 atmosphere. Assuming no isobutane is in the cell, the pressure corresponding to the number of moles of SF_6 added at the measured temperature can be calculated from the figures in Chapter 3 and the appendix in ref. (231). These values are tabulated in Table III-25. Since the solubilities in cyclohexane decrease with temperature, and room temperature is a higher

reduced temperature (T/T_c) for isobutane ($T_c = 550\text{K}$ for cyclohexane compared to 408K for isobutane), the solubility of SF_6 is likely less (for a partial pressure of 1 atmosphere). On the other hand the high pressures for the samples with more SF_6 are likely to increase the solubility of the SF_6 . Also the solubility curve is known to rise as the critical point is approached. If the amount of SF_6 dissolved does not exceed about 50% of the total number of moles of SF_6 , this represents no more than 5% of the total number of moles of SF_6 in the sample. For the calculations of the free ion yields the bulk density was assumed to be about the same as the pure isobutane at that temperature. Even about the critical point in the 9.5% sample, this would introduce an error of no more than about 20%. The minor role of the SF_6 on the P-V-T properties of the mixtures can be seen from the temperature where the sample went gaseous. The apparent critical points were $408 \pm 1\text{K}$ for the 0.15, 1.2, and the 2.5% samples, and $406 \pm 1\text{K}$ for the other two. Calculating the expected critical point by the method of C. C. Li cited on p.140 of ref. (231) leads to a value of 401K which is a difference of 1% from that observed.

Examining the curves, the addition of SF_6 is seen to have decreased the free ion yields in comparison to those of pure isobutane over the same temperature range (Figures III-164 and III-165). The shapes of the curves

have also changed. For the 0.15% sample all the curves are still sublinearly dependent on E (Figures III-198). Little change is noted as the amount of SF_6 added goes to 1.2% (Figure III-199). For the 4.9% mixture the free ion yields decreases yet more (Figure III-200).

There is another decrease though less, when the amount of SF_6 is increased to 9.5% (Figure III-201). At the lower temperatures of the 9.5%, the free ion yields are super-linearly increasing with E .

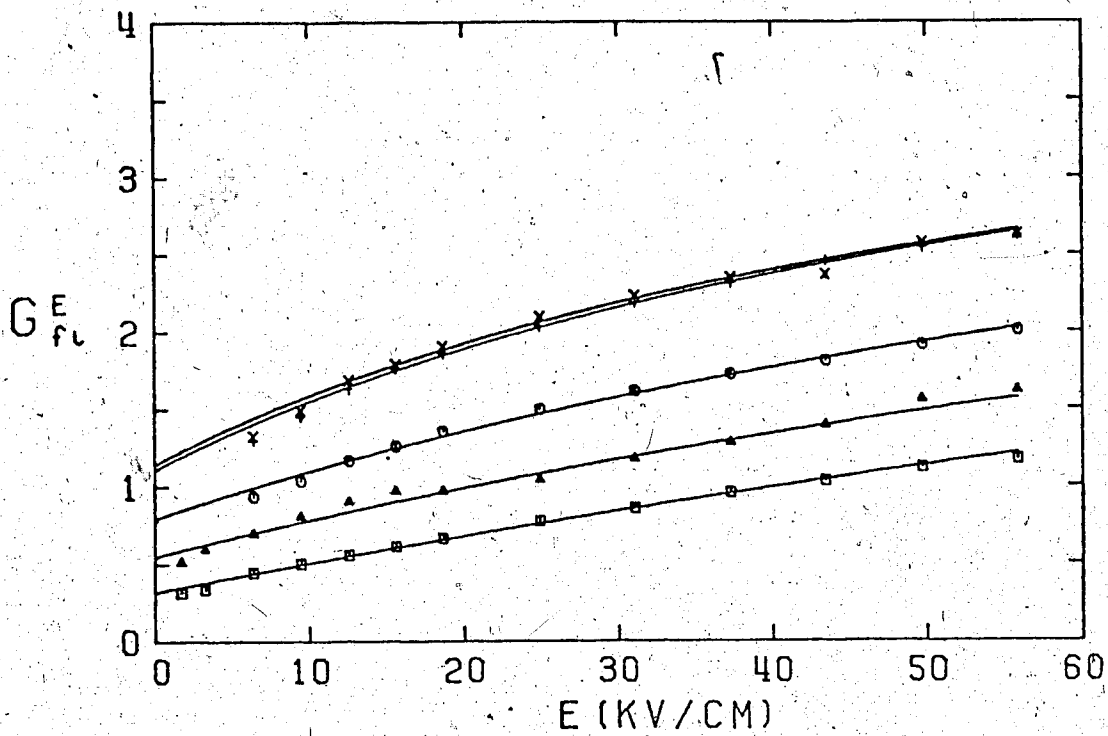


FIGURE III-198. Free ion yields in liquid isobutane + SF_6 .
 $[SF_6] = 0.15$ mol % when $\dagger \geq T_c$ (408K). Temperatures are:
 \square (298K), Δ (366K), \circ (395K), $+$ (408K), γ (412K).

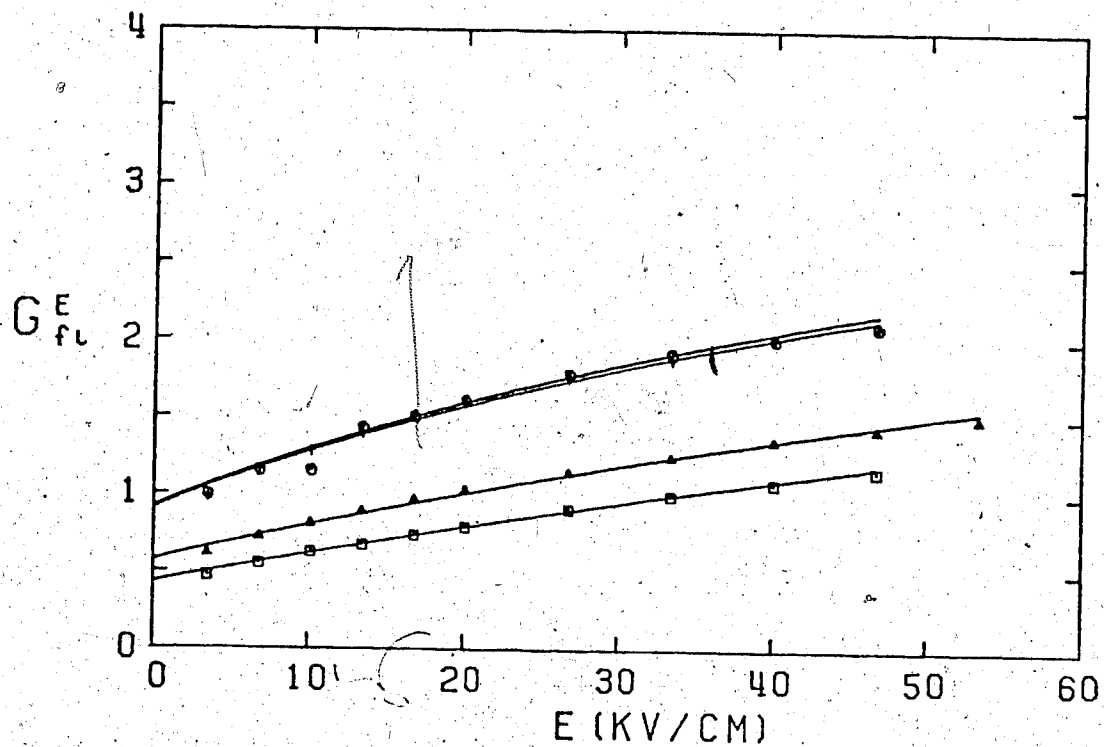


FIGURE III-199. Free ion yields in liquid isobutane + SF₆.

[SF₆] = 1.2 mol % when $T \geq T_c$ (408K). Temperatures are:

□ (363K), Δ (392K), ○ (408K), + (411K).

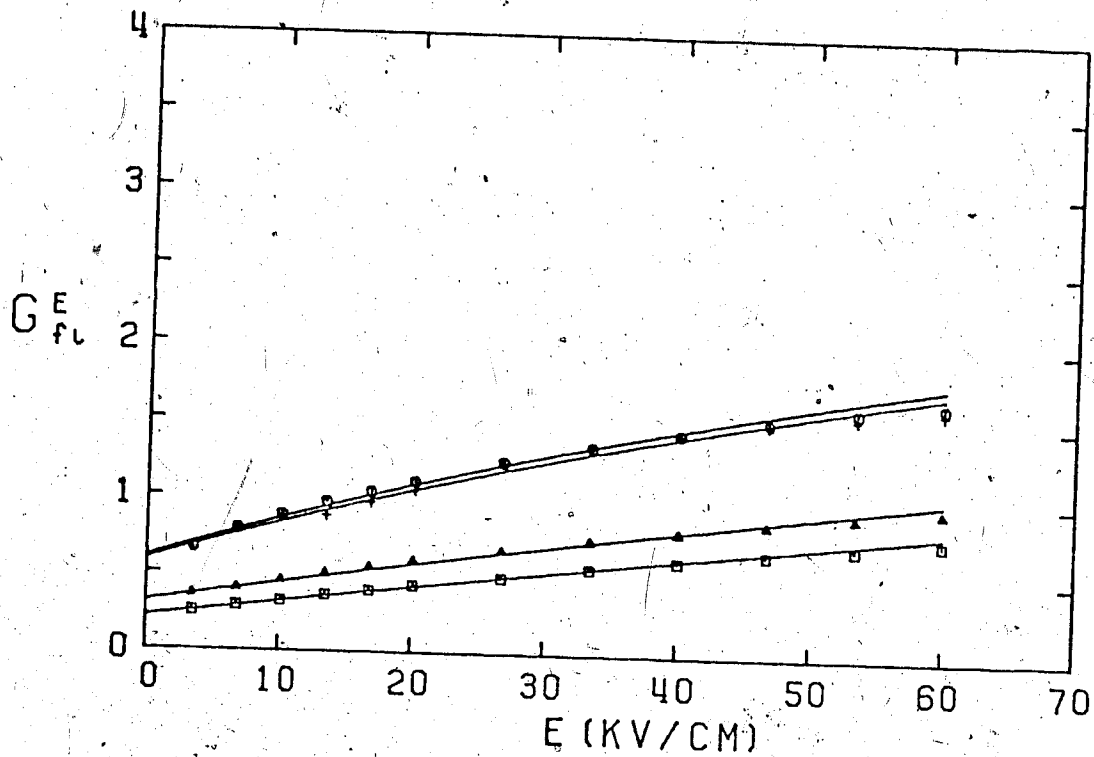


FIGURE III-200. Free ion yields in liquid isobutane + SF₆.
 [SF₆] = 4.9 mol % above the critical point. Temperatures
 are: □ (338K), △ (380K), ○ (408K), + (411K).

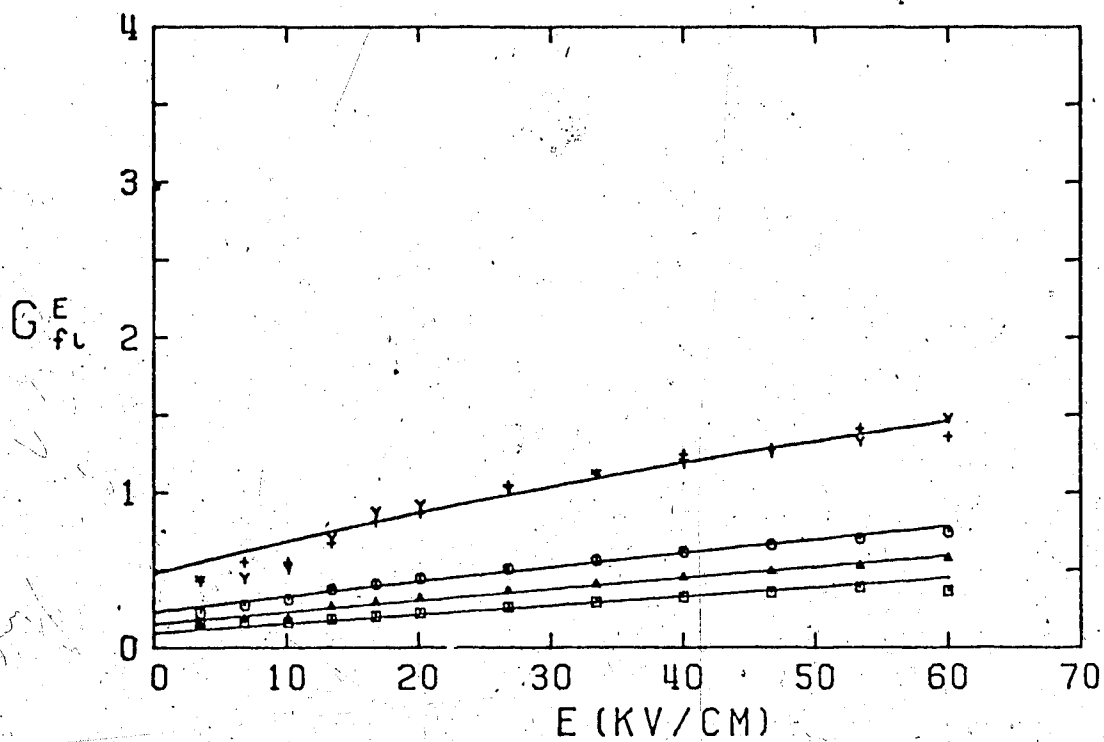


FIGURE III-201. Free ion yields in liquid isobutane + SF₆.

[SF₆] = 9.6 mol % above the critical point. Temperatures are:

□ (298K), △ (335K), ○ (376K), + (409K), γ (412K).

TABLE III-25

Summary of Free Ion Yields in Isobutane + SF₆

T K	d g/cm ³	ϵ^a	G _{fi} ^o	G _{tot} ^d	b 10 ⁻⁸ cm	bd 10 ⁻⁸ g/cm ²	p ^c atm
(1) 0.15 mol% SF ₆							
298	0.553	1.74	0.32	4.2	95	52	0.49
366	0.443	1.57	0.55	4.2	120	52	0.60
395	0.371	1.46	0.79	4.2	150	54	0.65
408	0.22 ^b	1.26	1.1	4.3	200	44	0.67
412	0.22 ^b	1.26	1.14	4.3	220	48	0.68
(2) 1.2 mol% SF ₆							
363	0.459	1.59	0.43	4.2	100	46	5.0
392	0.378	1.47	0.57	4.2	120	45	5.4
408	0.23 ^b	1.26	0.92	4.2	180	41	5.6
411	0.23 ^b	1.26	0.91	4.2	180	41	5.7
(3) 4.9 mol% SF ₆							
338	0.497	1.65	0.22	4.2	74	37	18
380	0.416	1.52	0.31	4.2	85	35	20
408	0.25 ^b	1.26	0.60	4.2	140	35	22
411	0.25 ^b	1.26	0.59	4.2	134	34	22
(4) 9.5 mol% SF ₆							
298	0.553	1.74	0.096	4.2	56	31	26
335	0.520	1.69	0.15	4.2	62	32	33
376	0.425	1.54	0.23	4.2	73	31	38
409	0.27 ^b	1.26	0.48	4.2	120	32	42
412	0.27 ^b	1.26	0.48	4.2	120	32	42

a. Used values from pure isobutane

b. Calculated by a linear mole fraction interpolation

IV DISCUSSION

A. Electron Mobility

1. Methane

The two variables investigated were the electric field strength and the temperature. Each will be discussed first for the low density gas. The variation of the effects will then be examined as a function of fluid density.

a. Electric Field Effect

i) Low Density

The electron mobility in methane at 6×10^{20} molec/cm³ is field dependent at $E/n \geq 0.012$ Td (Table III-1). The drift velocity at (E/n) threshold is usually compared to the low frequency velocity of sound c_0 in the saturated vapor (70,71,233,234). At $2 \times 10^{19} < n < 100 \times 10^{19}$, c_0 is 280 ± 10 m/s (225). A number of methane mobility curves from Chapter III are plotted as drift velocities in Figure IV-1. The curves furthest to the right along the E/n axis are for the lowest densities. At the low densities, the drift velocity becomes superlinear with E/n , that is electron heating becomes noticeable, at a threshold velocity of 270 ± 30 m/s. The ratio $(v_d)_{\text{threshold}}/c_0$ equals 1.0 ± 0.1 , implying that the dominant process moderating the electron energy in this density range is elastic collisions (178,180). Increased inelastic contributions would increase this ratio (70). A third

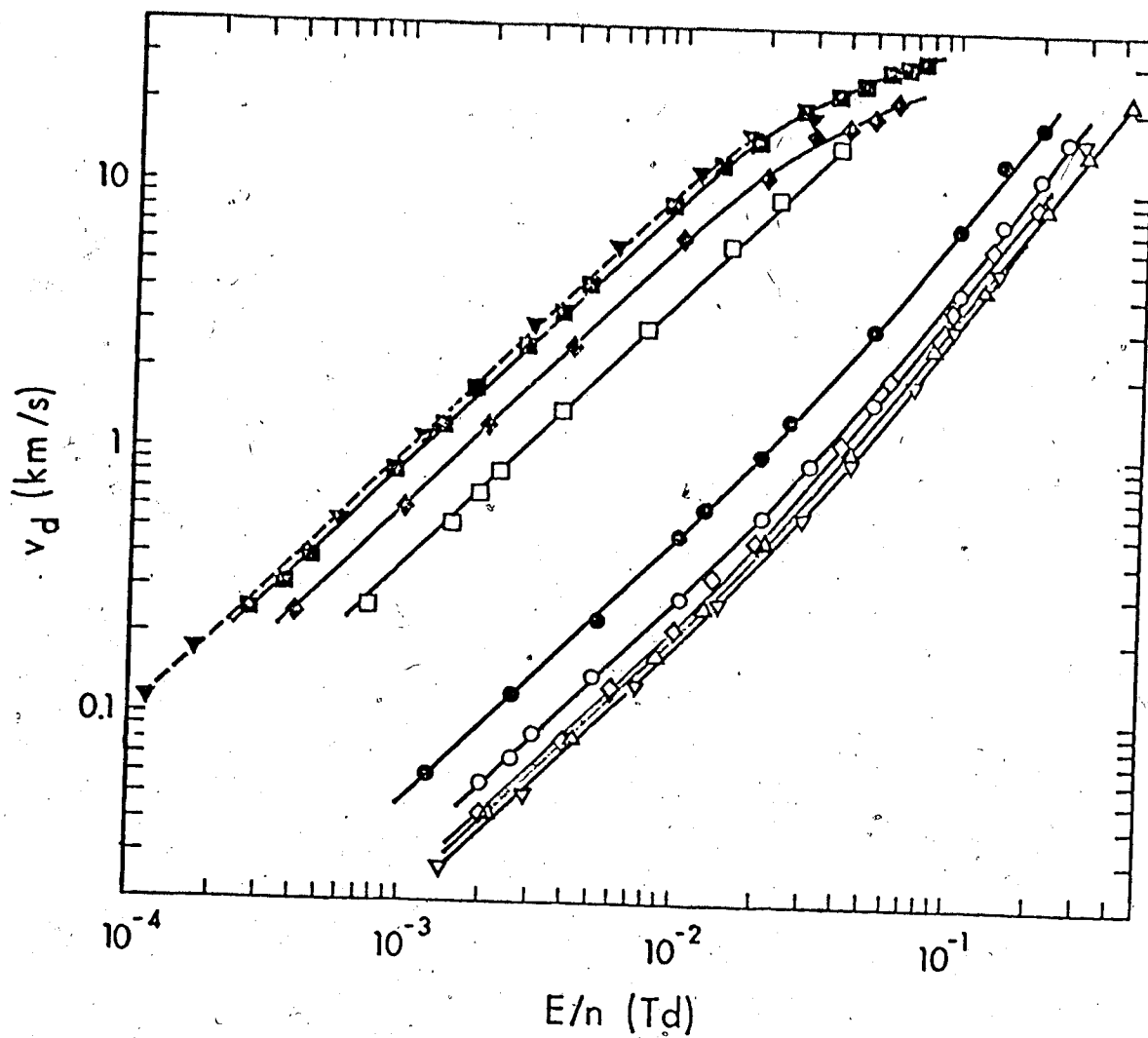


FIGURE IV-1 Electron drift velocity plotted against (E/n) in liquid and gaseous methane ($1 \text{ Td} = 10^{-17} \text{ V cm}^2/\text{molec}$). Densities and temperatures ($n/10^{21}$, T): \blacksquare , 17.0 molec/ cm^3 , 91K; \blacklozenge , 15.5, 122K; \blacktriangledown , 10.7, 178K; \square , 8.3, 189K; \circ , 6.1, 193K; \bullet , 6.1, 196K; \blacktriangledown , 2.2, 178K; \triangle , 0.73, 154K; \diamond , 0.16, 124K.

quantity that is constant at low densities is μ along the coexistence curve.

ii) Effect of Density

Plots of $(E/n)_{\text{threshold}}$ and $(v_d)_{\text{threshold}}$, $(v_d)_{\text{threshold}}/c_0$, and μ as functions of density are shown in Figures IV-2 to IV-4. Increasing n above 8×10^{20} leads to a change in all four quantities. The decrease in μ is attributed to quasilocalization of the electrons by Van der Waals clusters of molecules (233). This is an inelastic process which causes an increase in the other three quantities. At $n > 6 \times 10^{21}$ a sharper increase to a cusp at $\sim 8 \times 10^{21}$ occurs for the threshold curves. Only the μ curve increases smoothly through this density, by more than an order of magnitude, to reach a maximum at 11×10^{21} molec/cm³. This large increase is caused by conduction band formation. These features are similar to those of the Xe μ curve (also shown in Figure IV-4).

The cusp in $(E/n)_{\text{threshold}}$ and $(v_d)_{\text{threshold}}$ occurs because $d\mu/dE$ changes sign at 8×10^{21} molec/cm³ (see Table III-1). At 8×10^{21} increases in electron energy cause little effect on the mobility. On the high density side of the cusp, the $(E/n)_{\text{threshold}}$ returns to a value near that of the low density gas, consistent with the single-scatterer approximation of the Cohen-Lekner model of electron transport in liquids of sphere-like molecules (178,180). It should be noted that the scale of the $(v_d)_{\text{threshold}}$ curve on the high density side of the cusp

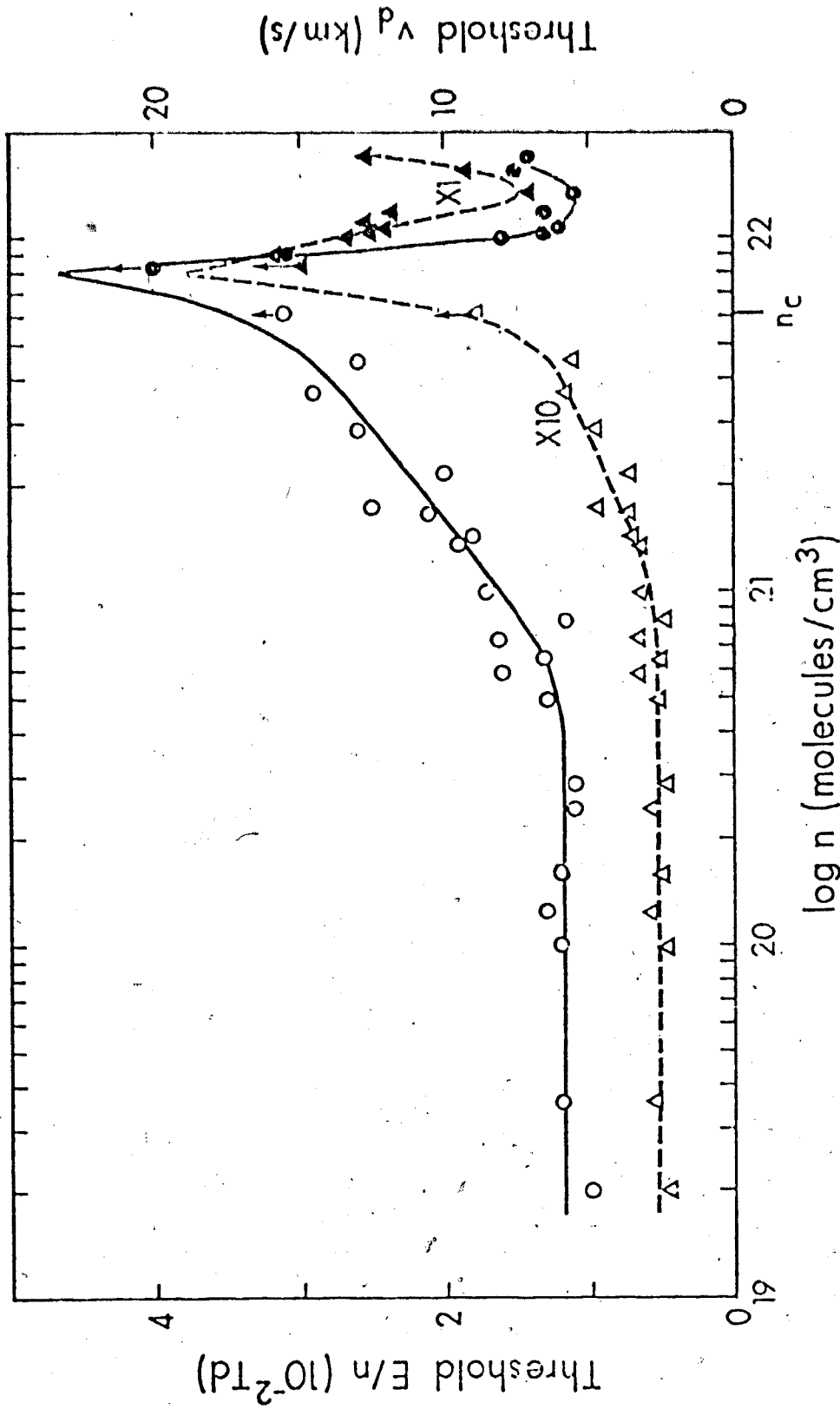


FIGURE IV-2. Threshold electric field strength (O, gas; ●, liquid) and threshold electron drift velocity (Δ , $10 v_d$, gas; \blacktriangle , v_d , liquid) above which electron heating occurs, plotted against the coexistence fluid density. O dW/dE = positive; ●, dW/dE = negative. The thresholds at the critical density n_c were measured at $T_c + 2K$ and are lower limits for the values at T_c . The thresholds in the liquid at $n = 8.3 \times 10^{21}$ are also lower limits.

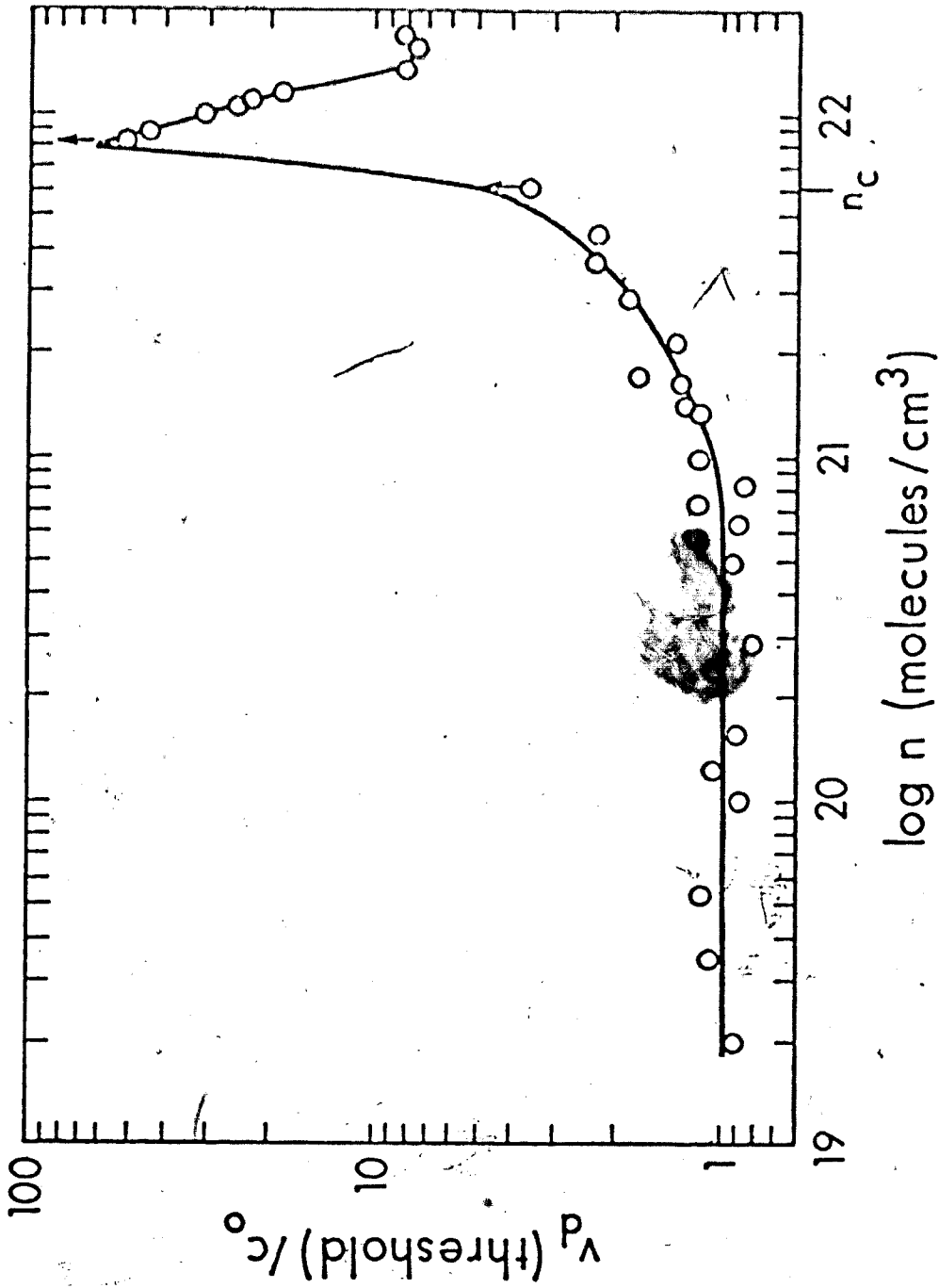


FIGURE IV-3 Ratio of the threshold drift velocity for electron heating to the speed of low frequency sound, $v_D(\text{threshold})/c_0$, plotted against the density of the coexistence fluids.

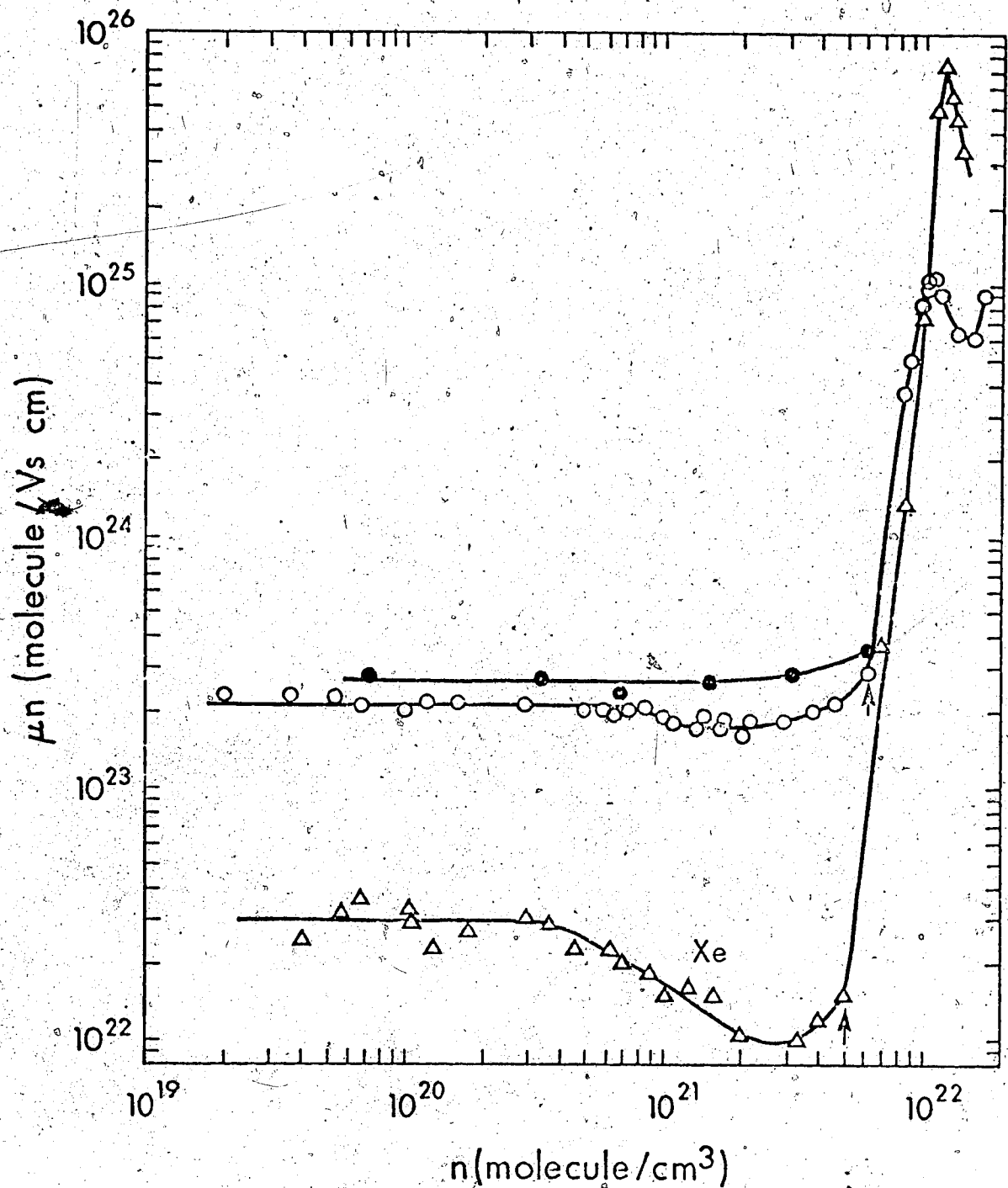


FIGURE IV-4. Plot of μn (low field strength limit) against n for thermal electrons in the coexistent liquid and gas phases of methane (\circ) and xenon (Δ , ref. 233). The arrows mark n_c . Some of the methane points are averages of two sets of results at the same density. \bullet , methane at $T_c + 3 = 194\text{K}$.

is 1/10 of the scale on the low density side (Figure IV-2). There is a 40-fold increase (also can be seen from Figure IV-1). This difference is once more consistent with the Cohen-Lekner model which has worked well for simple liquids near their triple points (185,234). The scattering cross-section of the molecules is assumed to be reduced by the long wavelength limit of the structure factor, $S(0)$, so that the electron mobility at high densities μ_{hd} is reduced from the low density mobility μ_{ld} by the increase of this factor.

$$\mu_{hd} = \mu_{ld}/S(0) \quad (1)$$

$$S(0) = nkT\chi_T \quad (2)$$

where k is the Boltzmann's constant, and χ_T is the isothermal compressibility at n and T (235). At low densities $S(0) \approx 1$. According to this model

$$\left(\nu_d\right)_{\text{threshold}} = \left(\nu_d\right)_{\text{threshold}}/S(0)_{hd} \quad (3)$$

at high densities at low densities

In liquid methane at 95K, $n = 1.67 \times 10^{22}$ and $S(0) = 0.033$ (236). A 30 fold increase can be expected which accounts for much of the 40 fold increase observed.

The $(\nu_d)_{\text{threshold}}/c_0$ curve returns to 8 near the triple point. In liquid argon, krypton and xenon where inelastic scattering is negligible, the ratio is approximately unity (234). The much larger value in liquid methane indicates the greater role of inelastic processes

in moderating the electron energies even at $\epsilon < 0.1$ eV.

b. Temperature Effect

i) Low Density Gas

An Arrhenius plot of the gas phase mobility from Table III-1 is given in Figure IV-5. The variation of the low field mobility with temperature can be used to get the energy variation of the electron-molecule scattering cross-section σ_v . Values of σ_v (estimated from the curve labelled 0.71 in Figure IV-5) are shown in Figure IV-6. Earlier results (17,18,52,53,56) are reliable at $\epsilon > 0.1$ eV but not at lower values since experimental measurements were made at $E/n > 0.2$ Td (above thermal energies) only. The Maxwellian distribution for 200K indicates that the energy range that affects the transport of the thermal electrons is $\sim 0.002 < \epsilon < 0.2$ eV. Use of equations (19) to (21) of Chapter 1 gives

$$\sigma_v = 0.0102 v^{-1.88} \text{ cm}^2 \quad (4)$$

over the temperature range $117 < T < 297\text{K}$, where v is $59.3 \times 10^6 \text{ e}^{1/2}$. Taking an average cross-section (assuming a Maxwellian distribution) leads to

$$\sigma_{av} = \langle v \rangle / \langle v / \sigma_v \rangle$$

$$= \left(\frac{m_e}{2kT} \right)^{1/2} (1-j)/2 / b_j \Gamma(5/2-j/2) \quad (5)$$

where e is the electronic mass, k Boltzmann's constant, $\Gamma(5/2 - j/2)$ a gamma function and j and b_j are fitting

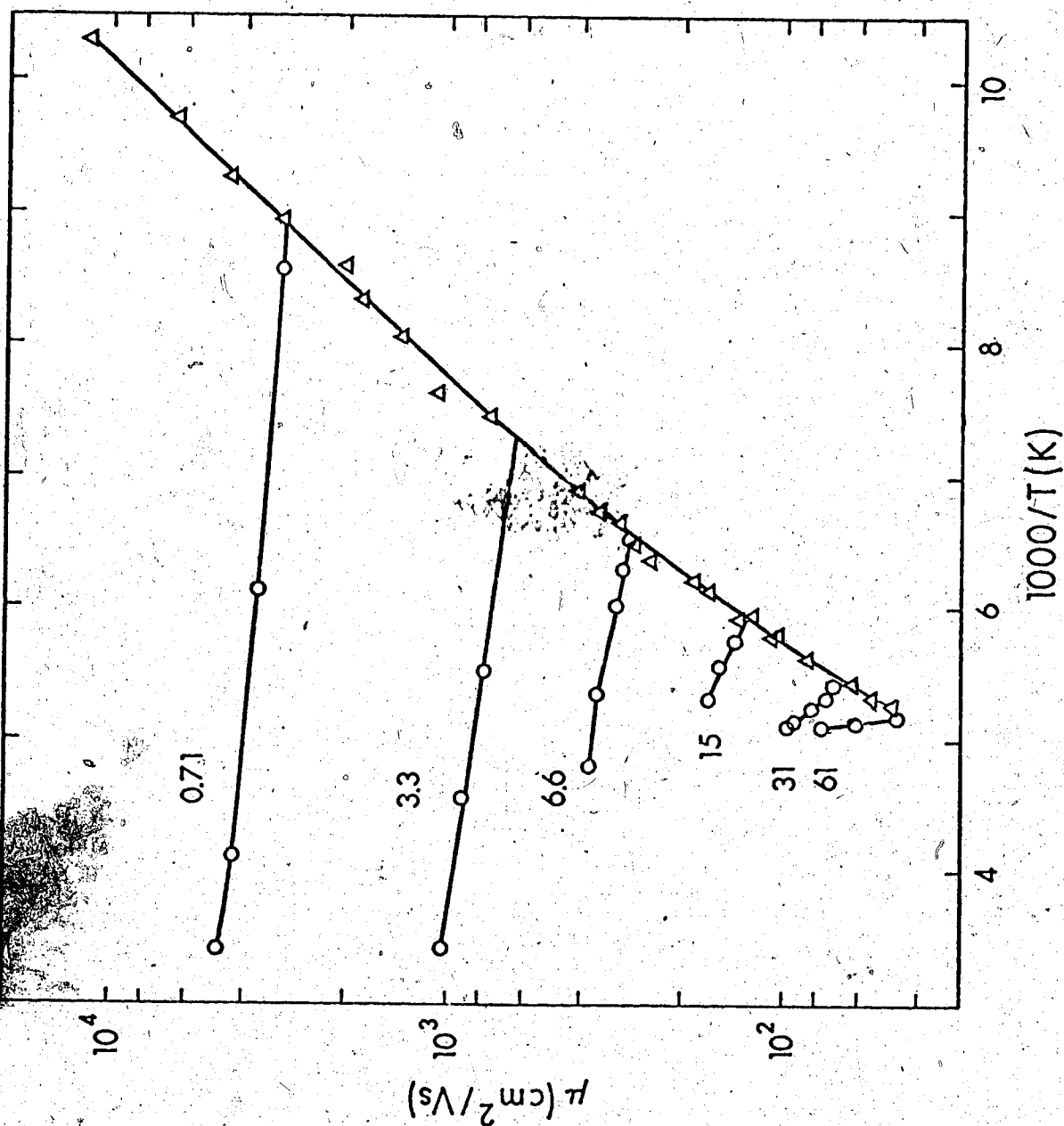


FIGURE IV-5. Arrhenius plot of thermal electron mobilities (low field strength limits) in methane gas at different densities (O). The numbers labelling the lines are the densities in units of 10^{20} molecule/cm³. Mobilities in the gas along the vapor/liquid coexistence curve are represented by Δ . The line through the data for 7.1×10^{19} molecules/cm³ was calculated from equation (20) of Chapter I.

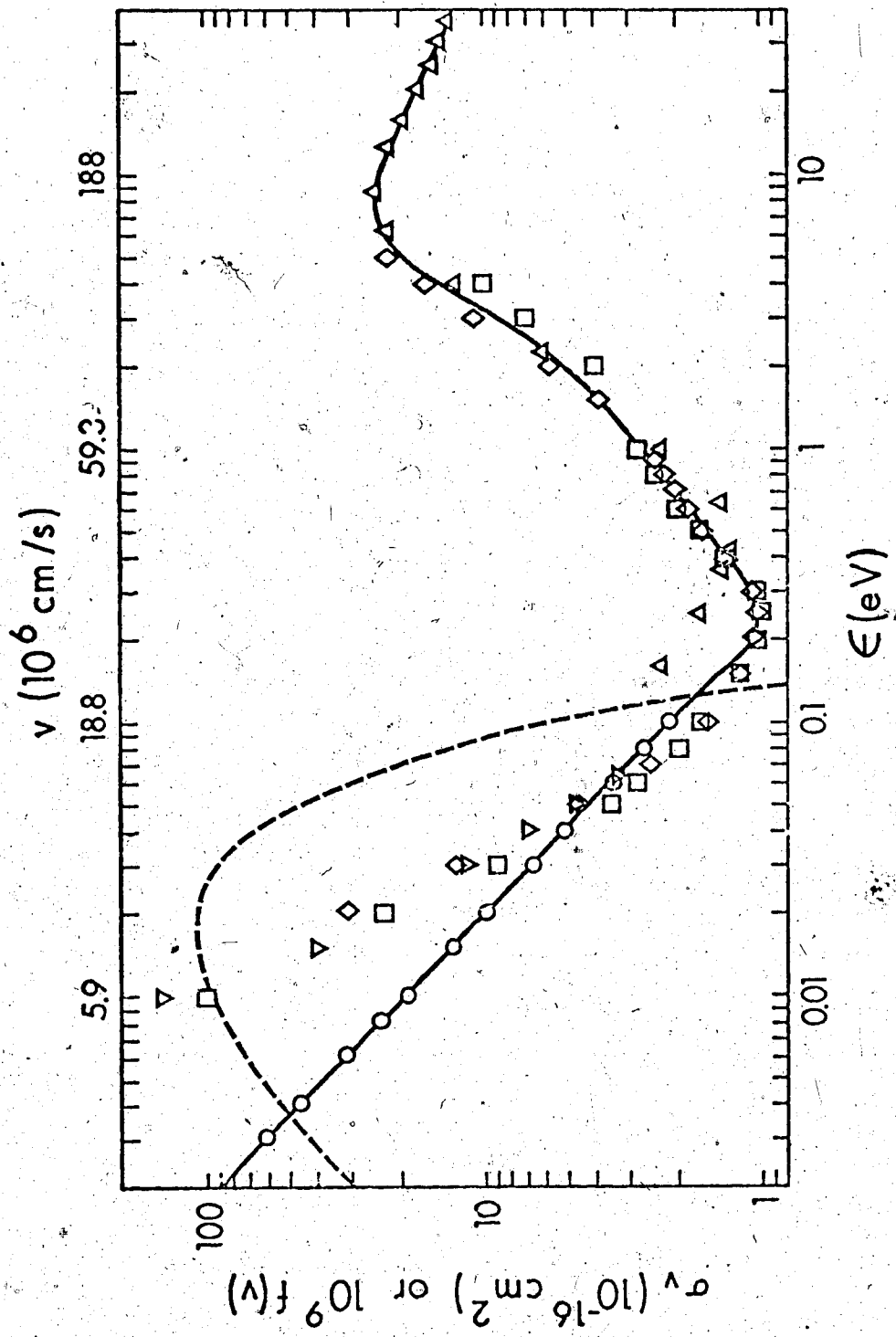


FIGURE IV-6. Momentum transfer cross section σ_v of low density methane gas as a function of electron energy ϵ and velocity v . \circ , present work; ∇ , ref. 52; \diamond , ref. 53; \square , ref. 56; \triangle , total cross section, ref. 18. — represents the favored values of σ_v . ---- represents $f(v) = N^{-1} \frac{dN(v)}{dv}$ for a Maxwellian distribution of electrons at 200K, where $f(v)dv$ represents the fraction of electrons that have velocities between v and $v + dv$.

parameters defined as for equations (19) to (21) of Chapter 1. For methane at 300K, $\sigma_{av} = 4.0 \times 10^{-16} \text{ cm}^2$.

ii) Effect of Density

The effect of density on μn can be seen from Figure IV-4 and has been briefly discussed above. The variation of mobility at $n > 6.1 \times 10^{21}$, is more clearly shown in Figure IV-7. The mobility drops as the density is increased along the co-existence vapor (open circles). A minimum is reached in the vicinity of the critical region. Further increases in density (dark circles) lead to an increase of more than an order of magnitude. A maximum is attained. Further increases in density lead to a minimum, and then another increase. The sharp rise in mobility at $n > 6.1 \times 10^{21}$ is due to the conduction band formation. The maximum indicates the position where the long range attractive forces and the short range repulsive forces best balance each other. At higher densities the decrease is due to the dominant short range repulsions. Liquid phase measurements of earlier workers are shown for comparison.

Through the range $0.6 < n < 6.1 \times 10^{21} \text{ molec/cm}^3$, the quasifree electron mobility μ^0 is increasing (58) although μn is decreasing at $0.6 < n < 2 \times 10^{21}$ (Figure IV-4). If the low field ($E/n < 0.06 \text{ Td}$) mobility at 293K is used as a measure of μ^0 (58), the ratio of $(\mu^0 n)_n /$

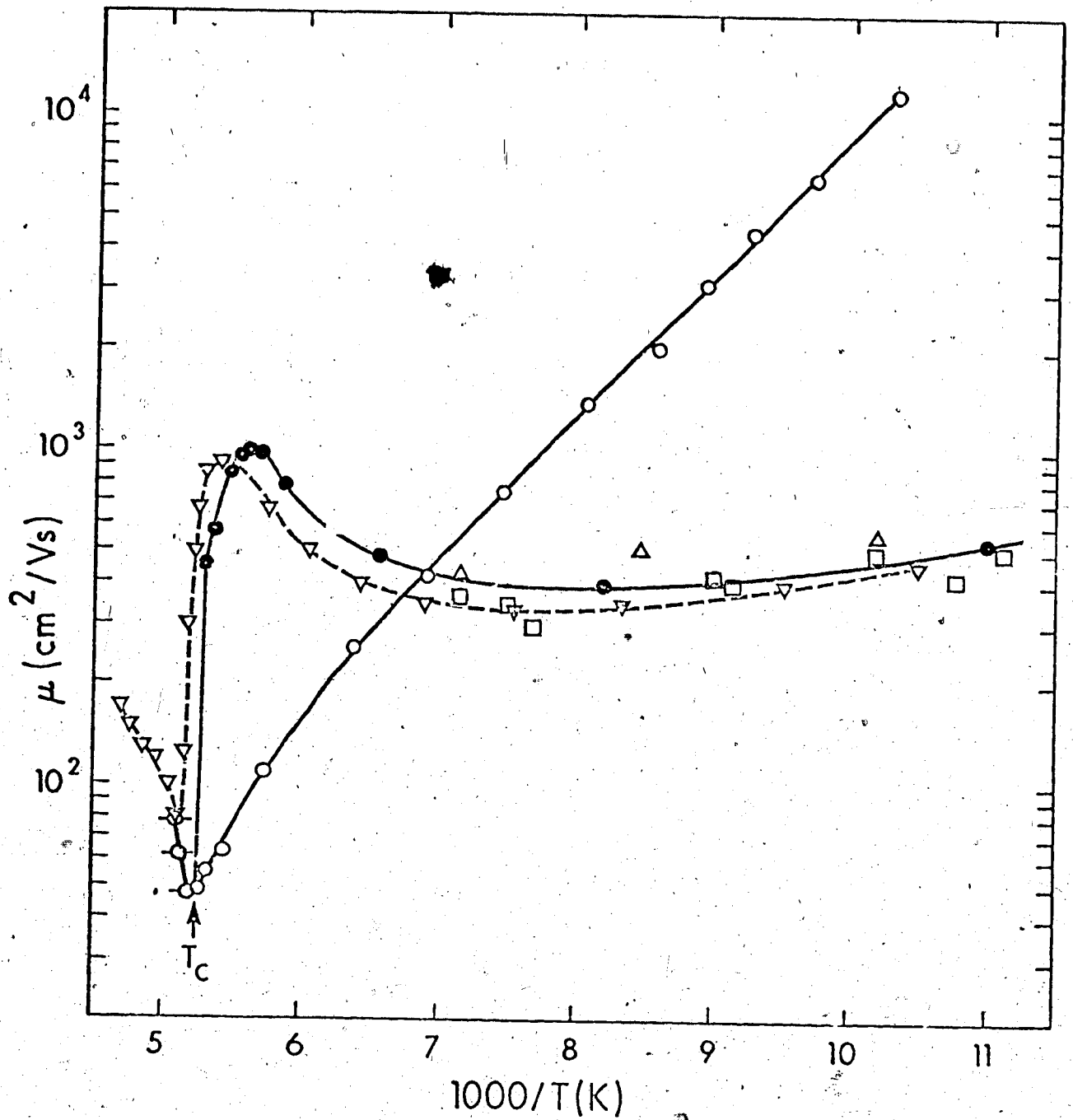
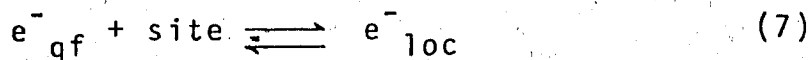


FIGURE IV-7. Arrhenius plot of thermal electron mobilities (low field strength limits) in the coexistent liquid (●) and gas (○) phases. Values in the superheated gas at the critical density are indicated by ○. Results from references 127 (▽, 5.1 MPa), 96 (□) and 109 (△) are included for comparison.

$(\mu^0_n)_{\text{low density}}$ is 1.05, 1.25 and 3 ± 1 (extrapolated) for $n = 2 \times 10^{20}$, 11×10^{20} and 61×10^{20} , respectively. The μ_n at any value of n and T depends on the fraction of electrons in the quasifree state. In the dense gas, the localization occurs on sites which may be regarded as density fluctuations.



where e^-_{qf} is the quasifree electron and e^-_{loc} the localized electron. The concentration of the site depends on the free energy change of equation 6, that is

$$k_6 = [\text{site}] = \exp[-\Delta G_6/RT] \quad (8)$$

where k_6 is the equilibrium constant, and R is the gas constant. The equilibrium constant, for equation 7 is

$$k_7 = \frac{[e^-_{\text{loc}}]}{[e^-_{\text{qf}}][\text{site}]} \quad (9)$$

and since the fraction of quasifree electrons f is

$$\begin{aligned} f &= \{e^-_{\text{qf}}/[e^-_{\text{qf}}] + [e^-_{\text{loc}}]\} \\ &= \{1 + [e^-_{\text{loc}}]/[e^-_{\text{qf}}]\}^{-1} \\ &= \{1 + [\text{site}]k_7\}^{-1} \end{aligned}$$

and since $\mu_n = (\mu^0_n)f$

then

$$\left\{ \left[\frac{(\mu^0_n)_n}{\mu n} \right] - 1 \right\} = [\text{site}] k_7 \quad (10)$$

and by using equation 8

$$\log \left\{ \left[\frac{(\mu^0_n)_n}{\mu n} \right] - 1 \right\} = \frac{-(\Delta G_6 + \Delta G_7)}{RT}$$

$$= \frac{\Delta S}{R} - \frac{\Delta H}{RT} \quad (11)$$

where $\Delta S = \Delta S^0_6 + \Delta S^0_7$ and $\Delta H = \Delta H^0_6 + \Delta H^0_7$. A plot of $\log \left\{ \left[\frac{(\mu^0_n)_n}{\mu n} \right] - 1 \right\}$ versus T^{-1} gives a line with a slope of $(\Delta H/R)$ and an intercept at $T^{-1} = 0$ of $(\Delta S/R)$. The $(\mu^0_n)_n$ at a given n and T was estimated using the 0.71 curve of Figure IV-5 to get $(\mu^0_n)_{\text{low density}}$ and multiplying it by $(\mu^0_n)_n / (\mu^0_n)_{\text{low density}}$ from reference 58. Values are tabulated in Table IV-1. At each density $\Delta H \approx T\Delta S$, or $\Delta G \approx 0$ as expected near the co-existence curve. $\Delta S/S(0)$ is approximately -19 J/mol-K . ΔS is approximately proportional to $S(0)$ which is related to the magnitude of the density fluctuations. The density fluctuations and hence the [site] and extent of quasilocalization are largest in the co-existence vapor and decrease as the gas is heated at constant density. The black dots in Figure IV-4 show μn at $T > T_{\text{co-existence}}$. There is no noticeable difference between μn at $n = 1 \times 10^{21}$ compared to 7×10^{19} . The decrease in quasilocalization upon heating is also reflected in a decrease in threshold E/n values as the temperature is increased along an isochore (see for example the decrease

TABLE IV-1

Temperature Coefficients of Thermal Electron Mobilities

in Methane Gas at Different Densities

Density (10^{20} molecule/cm ³)	T range (K)	E_{μ}^a (kJ/mol)	$-\Delta H^b$ (kJ/mol)	$-\Delta S^b$ (J/mol K)	$S(0)^c$	$-\Delta S$ $S(0)$
0.71	117-297	0.6	-	-	1.0	-
3.3	135-295	1.1	-	-	1.1	-
6.6	153-208	1.5	3.2	27	1.4	19
15.	170-187	3.7	7.1	43	2.3	19
31	185-196	9.	22.	117	6.	20
61	192-196 ^d	40.	100.	493	29.	17

a. From Figure IV-5.

b. From equation 11.

c. From equation 2, at the average temperature in the range.

d. $T_c = 191K$.

at $n=6.1 \times 10^{21}$ when the temperature was changed from 192K to 196K in Table III-1). The decreasing threshold field is a reflection of the decreasing threshold drift velocity.

2. n-Alkanes

Data for ethane, propane and n-butane are taken from Tables III-2, III-3 and III-4, respectively.

a. Electric Field Effect

i) Low Field Strengths

The mobility is constant at low field strengths. In Figure IV-8 the low field values of μn are plotted against n for the coexistence fluids. The arrows indicate the critical points. The curves for the different systems do not cross. Increasing the length of the carbon chain increases the average cross-section at all densities. At all densities the curve for ethane is above that for propane, which is above that for n-butane.

There are similarities between the different systems. At low densities μn is independent of n . In this region the electron-molecule scattering cross-section is determined by single body interactions. At higher densities quasilocalization occurs, leading to a decrease in μn . This happens at $n/n_c = 0.37$ (ethane), 0.25 (propane) and 0.13 (n-butane). As n is increased further, conduction band formation causes μn to increase once more. The curves pass smoothly through the critical region, attain a maximum and then drop steeply. The sharp decrease is caused by electron localization.

ii) Threshold Field Strengths

Figure IV-9 shows the threshold fields $(E/n)_{\text{threshold}}$. At $n < 6 \times 10^{20}$ the threshold field in ethane is about

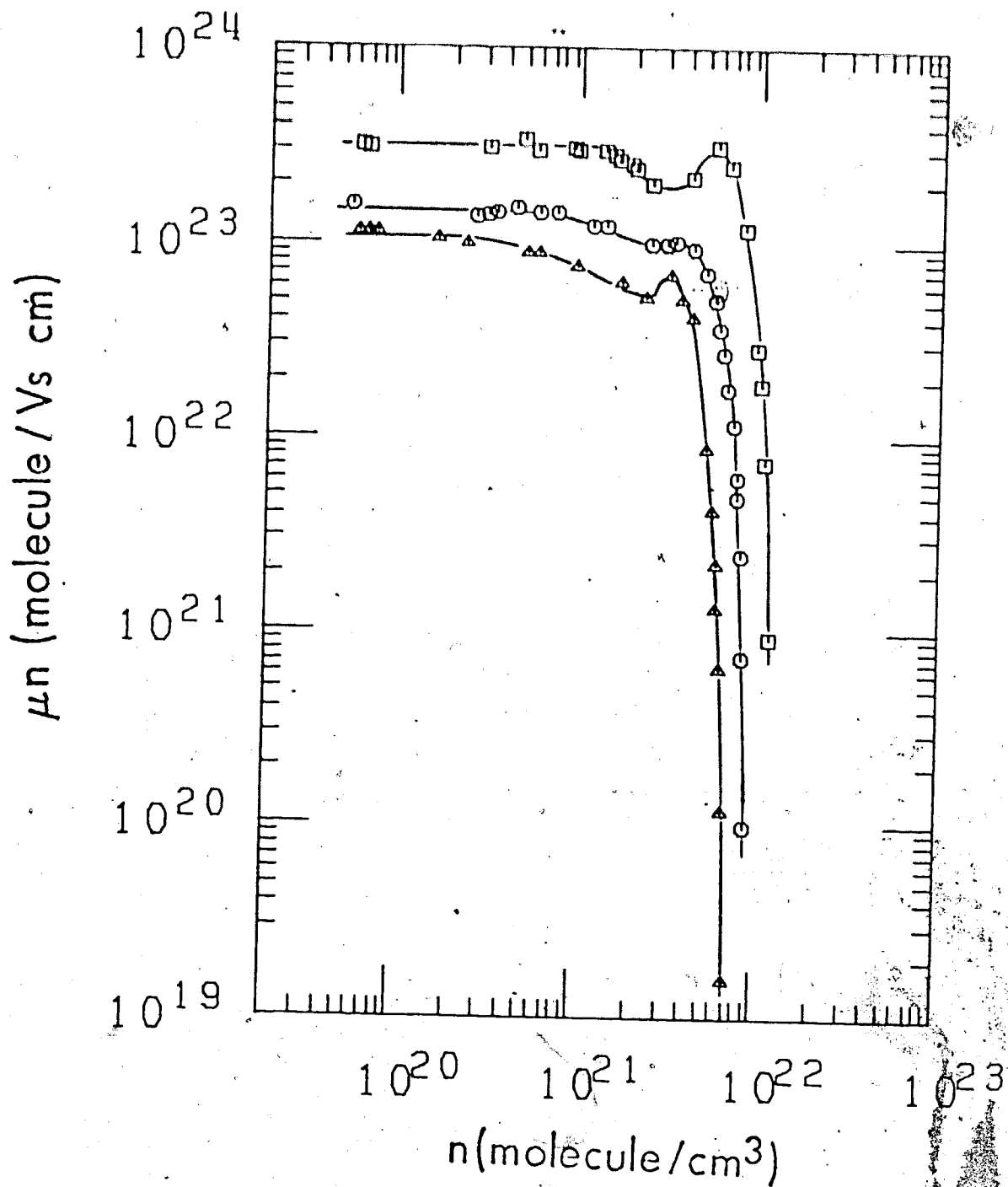


FIGURE IV-8. Density-normalized mobility plotted against n . The symbols represent ethane (\square), propane (O) and n-butane (Δ).

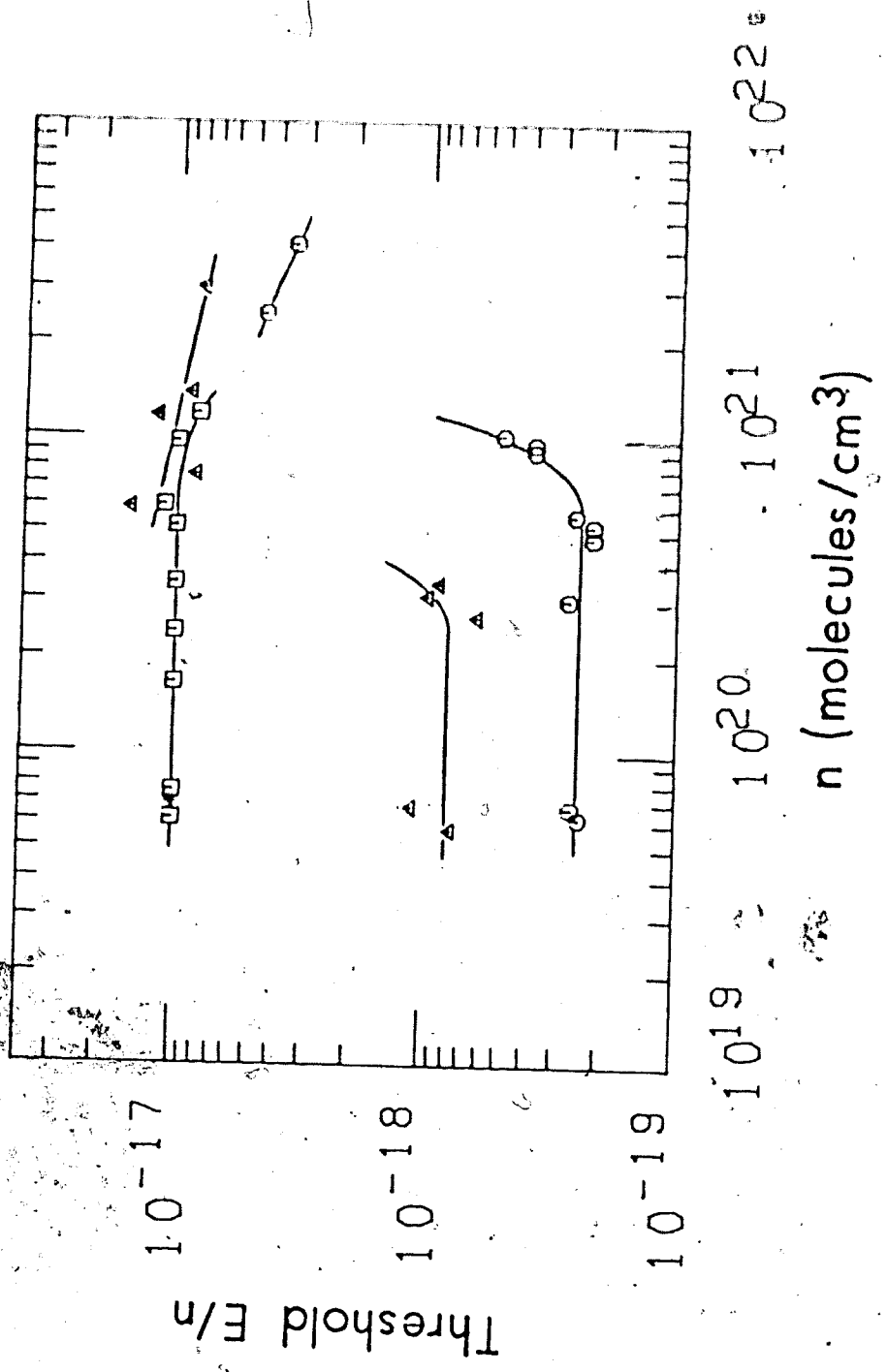


FIGURE IV-9. Threshold (E/n) plotted against n. Symbols represent ethane (O), propane (Δ) and n-butane (\square).

0.024 Td, a factor of 2 larger than in methane (0.012 Td). μn is 3.2×10^{23} molec/Vcms so that $(v_d)_{\text{threshold}}$ is 770 cm/s. Since the low frequency sound velocity c_0 is 250 ± 5 m/s (226), $(v_d)_{\text{threshold}}/c_0$ equals 3.1, reflecting the greater importance of inelastic processes in ethane compared to methane. As for methane, $d\mu/dE$ on the low density side of the cusp is positive, and on the high density side of the cusp, negative. At the cusp, $d\mu/dE \sim 0$ which can be taken to mean that the Ramsauer-Townsend minimum is at thermal energy. In liquid ethane at 294K, $d\mu/dE$ is still negative and $(E/n)_{\text{threshold}}$ is 0.1 Td(129). Between 4.1×10^{21} (306K) $< n < 7.1 \times 10^{21}$ (294K), the threshold decreases from 0.35 to 0.1 Td. At $n > 1.0 \times 10^{22}$ and $T < 216$ K, $d\mu/dE$ is positive again. The positive field effect at high densities is related to field assisted escape from the localized states (120,129,202-204). This threshold occurs at fields near 10^2 kV/cm.

In low density propane gas, the threshold E/n is about 0.08 Td, a factor of 3 larger than in ethane. A cusp occurs at a density near 4.5×10^{20} (also see Table III-3). The $d\mu/dE$ is positive on the low density side of the cusp, negative on the high density side, and zero at the cusp. The threshold field changes by an order of magnitude across the cusp. At $T < 218$ K, a positive field effect due to field assisted release from the electron traps is observed (120). In analogy to ethane, a transition to a negative field dependence should occur at a temperature between 218K and the critical temperature (370K).

In n-butane, $d\mu/dE$ is positive for the entire density range. No cusp is observed. Measurements could not be extended to densities near the critical region. No liquid phase threshold fields have been reported. A previous result, reported at $n = 3.5 \times 10^{18}$, also showed $d\mu/dE$ as positive with a threshold field of about 0.9 Td (64) in fair agreement to the present estimate of 1 Td. Even at low densities, the position of the Ramsauer-Townsend minimum has either not shifted to thermal energy, or else the dip may be too small to allow determination from the experimental data. From the temperature dependence of the low field drift velocity the energy of the minimum had been estimated to occur at $\epsilon = 0.13$ eV and to be of a sharp parabolic shape (64). The position of the minimum is about the same as that of ethane. The sharp minimum cannot be correct else the field effect would be much more pronounced. The temperature variations of the low field mobility in both the previous (64) and present (Figure IV-12) works are too small to indicate a drastic change in cross-section over the range of the Maxwellian distribution ($\epsilon \leq 0.2$ eV):

b. Temperature Effect

i) Gas Phase

Gas phase thermal electron mobilities along the co-existence curve are plotted in Figures IV-10 to IV-12 as functions of T^{-1} . From the isochores, the mobility

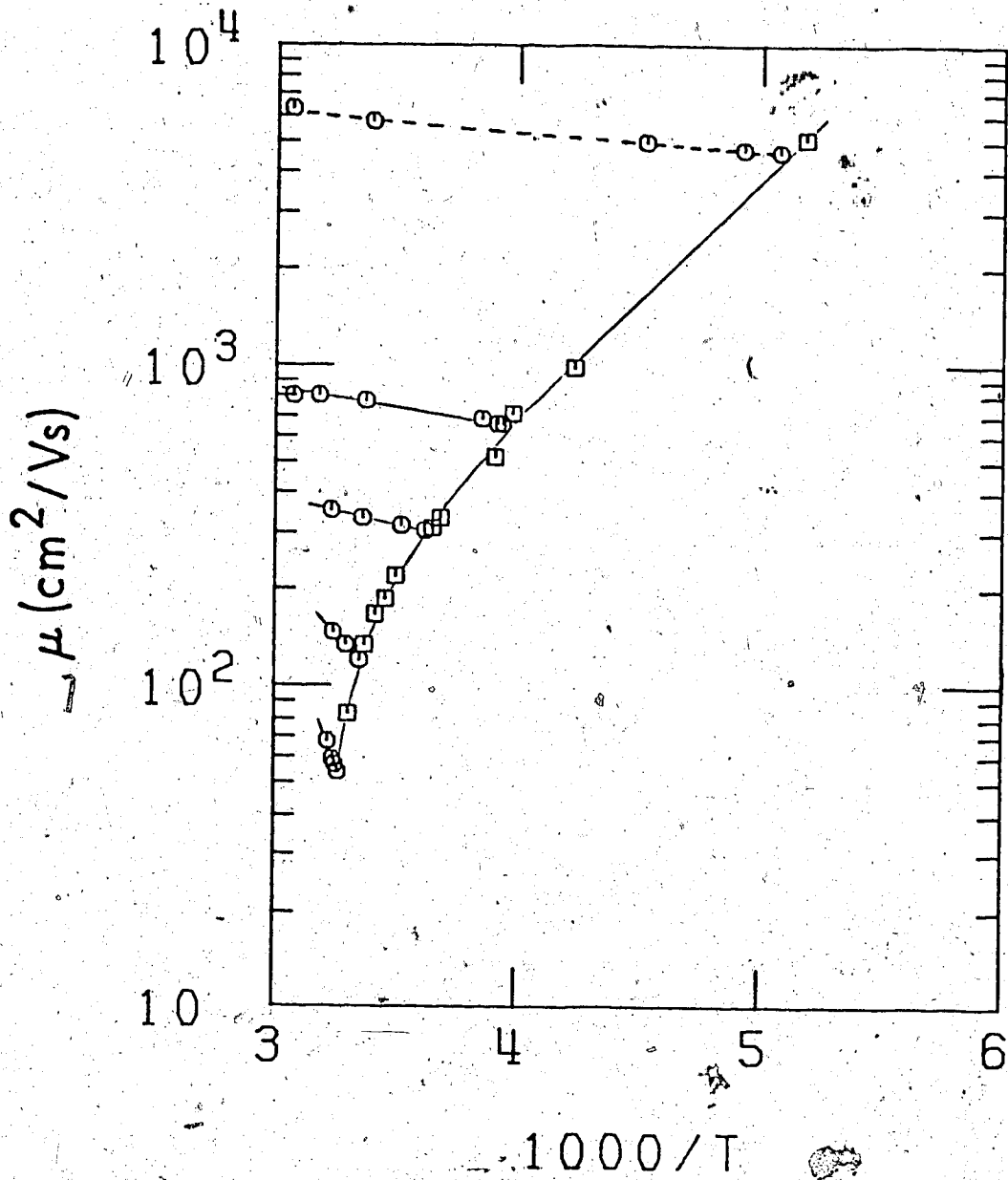


FIGURE IV-10. Electron mobility in gaseous ethane along the co-existence curve (\square) and above it (\circ) plotted against T^{-1} . The dashed line was calculated using equation 20 of Chapter I.

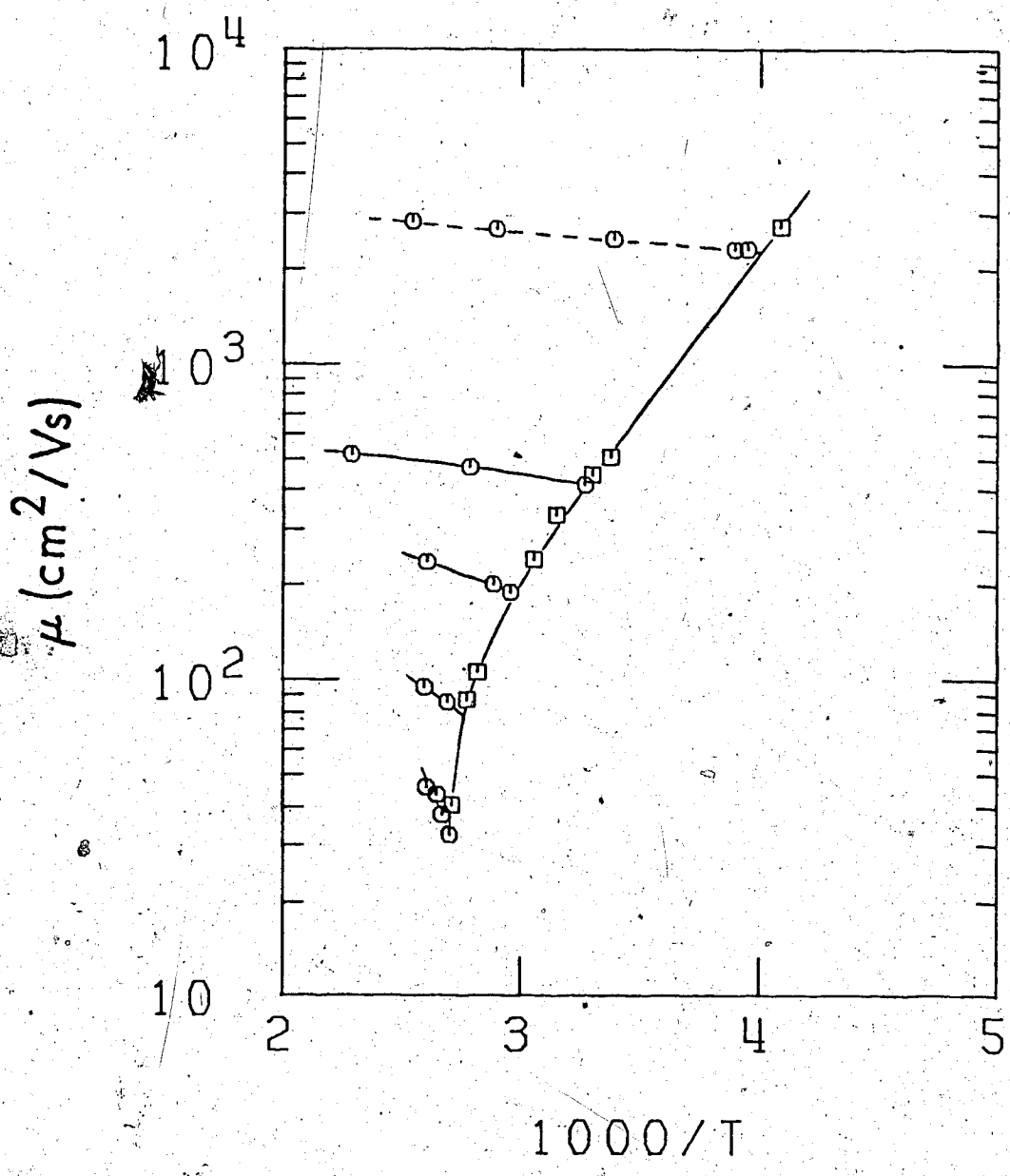


FIGURE IV-11. Electron mobility in gaseous propane along the coexistence curve (\square) and above it (\circ), plotted against T^{-1} . The dashed line was calculated using equation 20 of Chapter I.

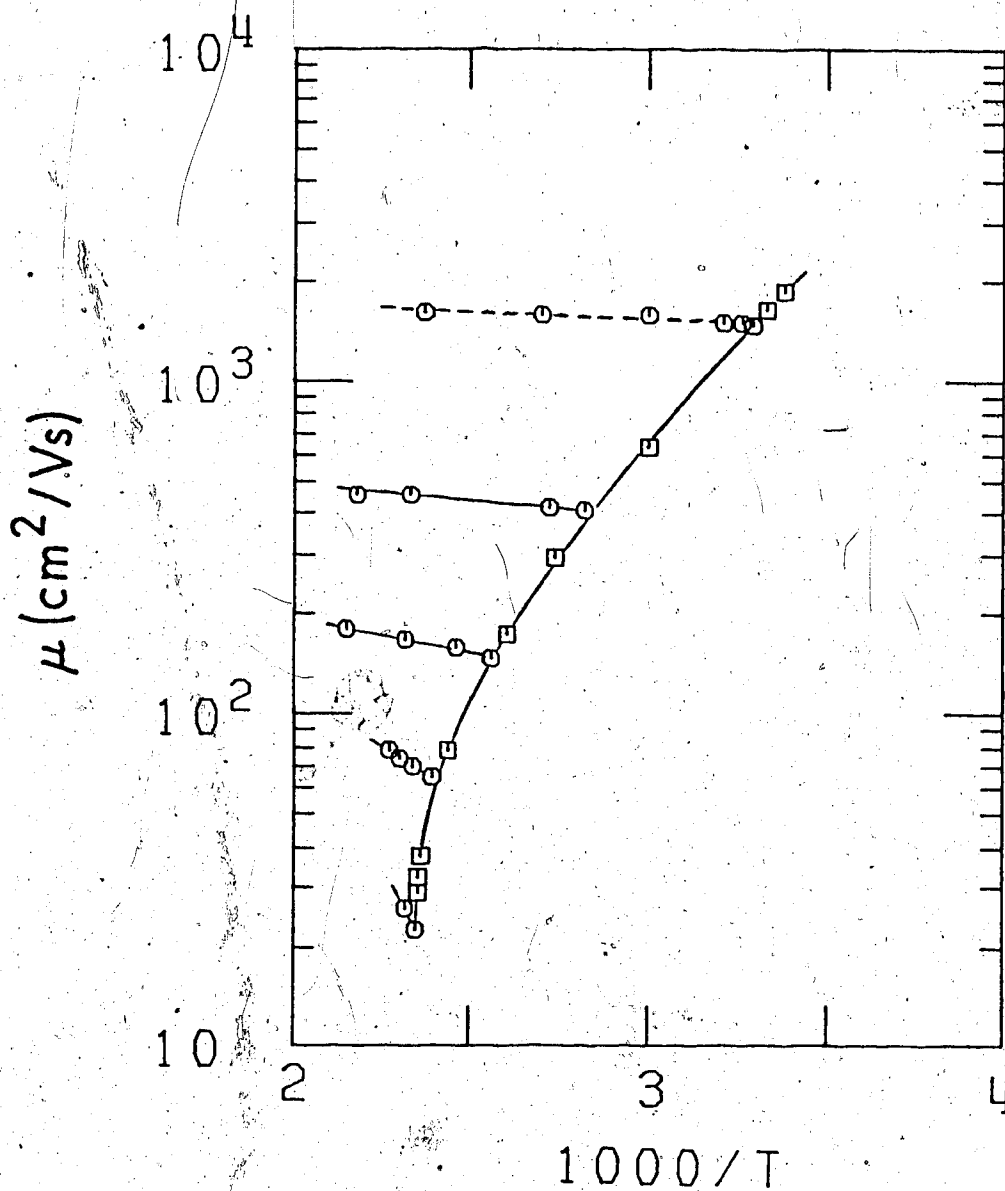


FIGURE IV-12. Electron mobility in gaseous *n*-butane along the coexistence curve (\square) and above it (\circ) plotted against T^{-1} . The dashed line was calculated using equation 20 of Chapter I.

can be seen to increase at all densities with temperature. The decrease for the co-existence conditions reflects the increase in n with the increase in T .

The low density mobility as a function of T can be used to extract the average cross-sections for the three alkanes in the same manner as for methane. The variation of the momentum-transfer cross-sections with electron velocity v can be expressed as

$$\text{ethane } \sigma_v = 1.72 v^{-2.20} \quad (12)$$

$$\text{propane } \sigma_v = 4.08 \times 10^{-2} v^{-1.92} \quad (13)$$

$$\text{n-butane } \sigma_v = 2.70 \times 10^{-5} v^{-1.45} \quad (14)$$

which, when integrated by equation 5, give average cross-sections (in units of 10^{-16} cm^2) of 3.9 (ethane), 11 (propane) and 13 (n-butane), all at 300K.

Increasing the density increases the temperature coefficient along the isochores. The values are given in Table IV-2. Application of the quasilocalization model (equations 6 to 11) can only be applied to ethane. $(\mu^0 n)_n$ can be obtained or extrapolated from the low field data in reference 66. For propane, the electrons at the lower fields are still localized. No data for n-butane exist. For ethane, application of equation 11 allows the calculation of ΔH and ΔS . As before $\Delta H \sim T\Delta S$. The ratio of $\Delta S/S(0)$ is about 20, nearly the same value as in methane. Values of the activation energies and the other

TABLE IV-2

Thermal Parameters of the n-Alkane Gases

	$n/10^{20}$ molec/cm ³	E^a kJ/mol	$-\Delta H^b$ kJ/mol	$-\Delta S^b$ J/mol	$S(0)^c$	$-\frac{\Delta S}{S(0)}$	$(\sigma_{av})^d$ 10^{-16} cm ²
C ₂ H ₆	0.68	1.3	-	-	-	-	3.9
	5.3	2.4	-	-	-	-	
	10	3.8	18	36	2.0	18	
	20	16	58	180	7.9	23	
C ₃ H ₈	41	38	140	440	25	18	
	0.67	1.2					11
	3.4	2.6					
	7.5	5.4					
n-C ₄ H ₁₀	15	12					
	30	38					
	0.76	0.7					13
	2.4	1.7					
	6.0	4.6					
	12	13					
	24	37					

a. From Figures IV-10 to IV-12 b. From Equation 11. c. From Equation 2. d. From Equation 5 for the low density gas

parameters are given in Table IV-2.

ii) Liquid Phase

In the liquid phase, where electron localization dominates the mobility, the temperature is a more important parameter than the density. Arrhenius plots of the thermal electron mobilities are given in Figure IV-13. A localization model developed from work on ethers (Chapter I, subsection C: The ether model) works quite well over the entire liquid range away from the critical region (131,195). The electrons are assumed to be in two states - an ion-like state or an extended (high mobility) state. In the ion-like state the mobility is of the order of 10^{-3} cm²/Vs. In the extended state the mobility is 10^4 to 10^5 times larger. The relevant equations of the model are

$$\mu = (1-x)\mu_{il}^0 \exp[-E_{il}/kT] + x\mu_h^0 \quad (15)$$

(equation 26 of Chapter 1)

$$x = \int_{-\infty}^{\infty} N(E) [1 + \exp(E/kT)]^{-1} dE \quad (16)$$

$$N(E) = \pi^{-1/2} \sigma^{-1} \exp[-(E - E_0)^2 / \sigma^2] \quad (17)$$

$$E_0 = E(0) - aT \quad (18)$$

$$\sigma = \sigma(0) + bT \quad (19)$$

$$\mu_h^0 = \mu_{ref}^0 (d_{ref} / d_T)^2 (T_{ref} / T) \quad (20)$$

x is the fraction of electrons in the extended mobility state with a mobility of μ_h^0 . The μ_{il}^0 and E_{il} are

respectively the pre-exponential factor and activation energy of the localized (ion-like) state. $N(E)dE$ is the relative number of localized electrons that require energies between E and $E + dE$ to be excited into the conduction band. The distribution of excitation energies is assumed to be Gaussian centered about E_0 with a dispersion σ . Both E_0 and σ are assumed to vary linearly with temperature. The quasifree electron mobility μ_h^0 is assumed to vary inversely with the temperature and as the square of the density. μ_{ref}^0 is μ_h^0 at temperature T_{ref} and density d_{ref} .

Unique values of the parameters could not be obtained by fitting the experimental data. To reduce the amount of flexibility in the calculation, $E(0)$ is anchored at 0.60 eV and μ_{ref}^0 at $30 \text{ cm}^2/\text{Vs}$ at 295K. For ethane, $\mu_{ref}^0 = 74$ at 185K (the boiling point for ethane).

The calculated curves (solid lines) are given in Figure IV-13. The parameters used are in Table IV-3. There does not seem to be a simple pattern to the values. $a/E(0)$ is calculated since the analogous quantity for the optical absorption energies in ethers is constant at 1.7×10^{-3} . The n-alkane values are about 25% higher (131).

Two other points can be noted from Figure IV-13. The apparent activation energy along the liquid curve is larger if the mobility is smaller. This is consistent with the above picture. A larger apparent activation energy means a deeper trap and fewer electrons in the

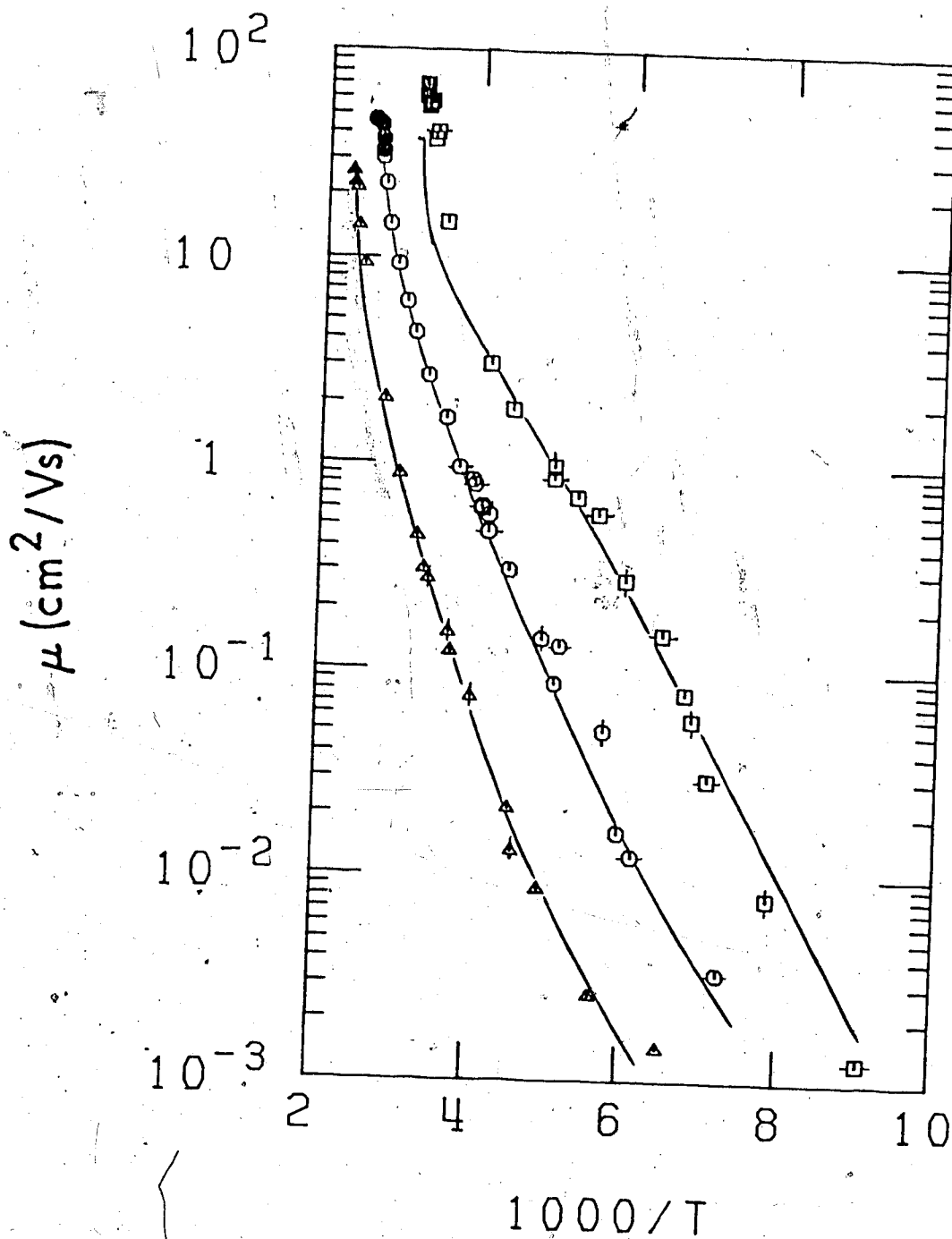


FIGURE IV-13. Electron mobilities plotted against T^{-1} for ethane (\square), propane (\circ), and *n*-butane (\triangle), both in the liquid phase (open symbols) and the supercritical fluid (solid symbols). Symbols with a horizontal bar through them are taken from ref. 120 and 129. Symbols with a vertical bar are from ref. 109.

TABLE IV-3

Liquid Phase Mobility Model Parameters[†]

	a (meV/K)	$\sigma(0)$ (meV)	b (meV/K)	a/E(0) (10^{-3} k^{-1})	μ_{ij}^0 ($\frac{\text{cm}^2}{\text{Vs}}$)	E_{ij} (eV)	T_{bp}^*	$(E_0/\sigma)_{bp}$	μ_{bp} ($\frac{\text{cm}^2}{\text{Vs}}$)
C_2H_6	1.2	50	1.0	2.0	0.04	0.04	185	1.6	0.56
C_3H_8	1.45	125	0.15	2.4	0.1	0.07	231	1.7	0.36
n- C_4H_{10}	1.17	135	0.015	2.0	0.1	0.07	273	2.0	0.15
C_2H_4	1.85	48	0	3.1	0.03	0.03	169	6.0	0.003 ^{**}
$\text{C}_3\text{H}_6^{-1}$	1.05	0	0.555	1.8	0.1	0.1	225	2.9	0.005
c- C_3H_6	0.97	126	0	1.6	0.1	0.1	240	2.9	0.006
i- C_4H_{10}	0.50	7	1.6	0.8	0.1	0.1	261	1.1	4.9

* normal boiling points taken from reference² 231

[†] $\mu_{ref} = 30 \text{ cm}^2/\text{V s}$ at 295K for all compounds except ethane (74 at 185K), ethene (54 at 169K) and isobutane (100 at 140K).

** ref. 109

extended state. Secondly, the mobility at the critical point decreases with the length of the carbon skeleton.

3. Ethene, Propene and Cyclopropane

Data are taken from Tables III-6 (ethene), III-7 (propene) and III-8 (cyclopropane).

a. Electric Field Effect

Available threshold field strengths normalized by n are plotted in Figure IV-14. Over the density range shown, $d\mu/dE$ is negative for ethene and cyclopropane, and positive for propene. This means at $(E/n) > (E/n)_{\text{threshold}}$, the mobility decreases with E/n in ethene and cyclopropane, and increases in propene. This is in agreement with previous cross-sections for the low density gases published by Duncan and Walker (67, 78). They reported that increasing the electron energy from 0.02 eV led to an increase in cross-sections in ethene and cyclopropane. For propene, the cross-section decreases and has a minimum at 0.2 eV. The effect of high electric field strengths is to increase the energy of the electrons.

The values of the low density threshold field strengths are 0.27 Td (ethene), 0.44 Td (propene) and ~0.22 Td (cyclopropane) (Figure IV-4). The ethene threshold had been previously reported as 0.3 Td in the low density gas at $4 \times 10^{17} < n < 1.9 \times 10^{19}$, invariant with density (78). These values, compared to the values for ethane (0.024 Td) and propane (0.08 Td) from Figure IV-9, indicate the greater ability of the double

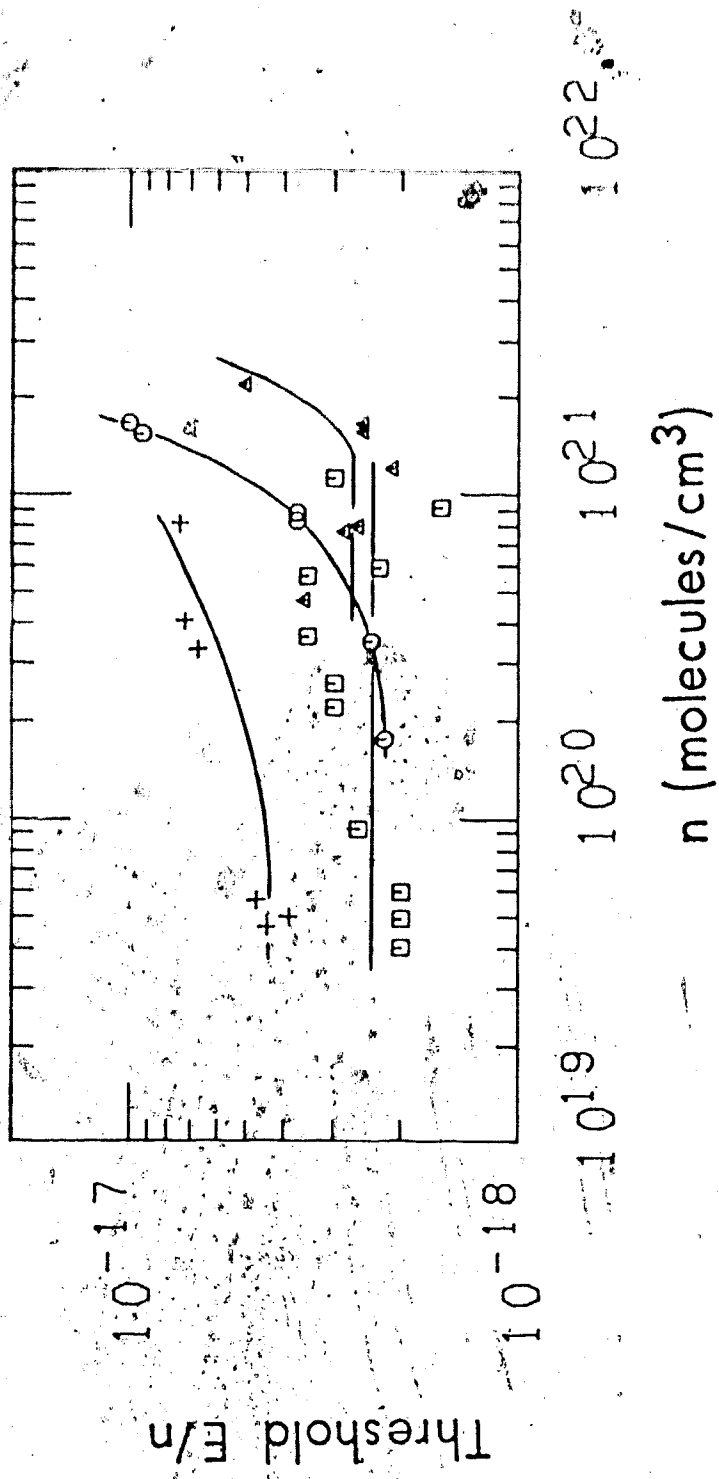


FIGURE IV-14. Threshold (E/n) plotted against n . The symbols represent Δ (ethene), $+$ (propene), O (cyclopropane), and \square (isobutane).

bonded compounds to thermalize hot electrons. The cyclopropane bonds are not solely single or double bond in character, hence the intermediate value of the threshold field (between that of propane and that of propene).

b. Density-normalized Mobility

Values of μn are plotted against n in Figures IV-15 and IV-16. The propane data are reproduced in Figure IV-15 to allow comparison between the C_3 hydrocarbons.

At low values of n , μn is constant, with values, in units of 10^{23} molec/cm Vs, of 3.3 (ethene), 2.4 (cyclopropane), 1.5 (propane) and 0.54 (propene). In cyclopropane and propene, μn decreases gently with n at $n > 4 \times 10^{20}$ (Figure IV-15). In ethene the decrease occurs at $n > 5 \times 10^{20}$ (Figure IV-16). The decrease continues until the critical density is reached, in the vicinity of which there is a tendency for the direction of the change to reverse. The μn vs n curves contain an inflection point in the vicinity of the critical density n_c . At $n > 1.3 n_c$, μn drops sharply with increasing n .

The initial decrease in μn at $n \sim 5 \times 10^{20}$ in the saturated vapor occurs at a density where the average center to center distance between the molecules is about 1 nm. This is larger than either the Van der Waal diameter of the molecules (~ 0.4 nm) or the electron-molecule collision diameter (~ 0.2 nm) (see Table IV-4).

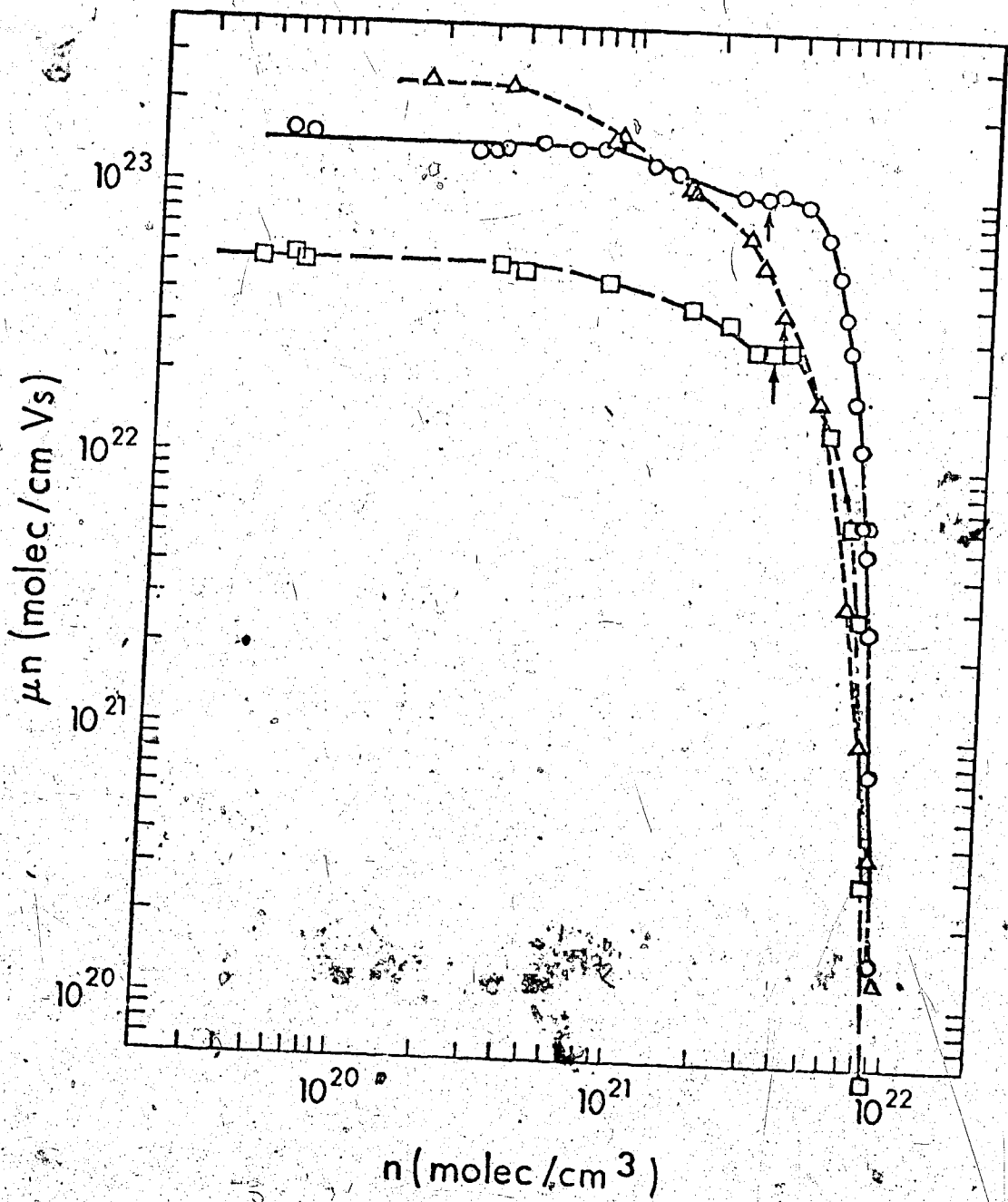


FIGURE IV-15 Density normalized mobilities μn of electrons in the coexistent liquid and vapor phases, plotted against the fluid density. O, propane; Δ , cyclopropane; \square , propene. The arrows indicate the critical densities.

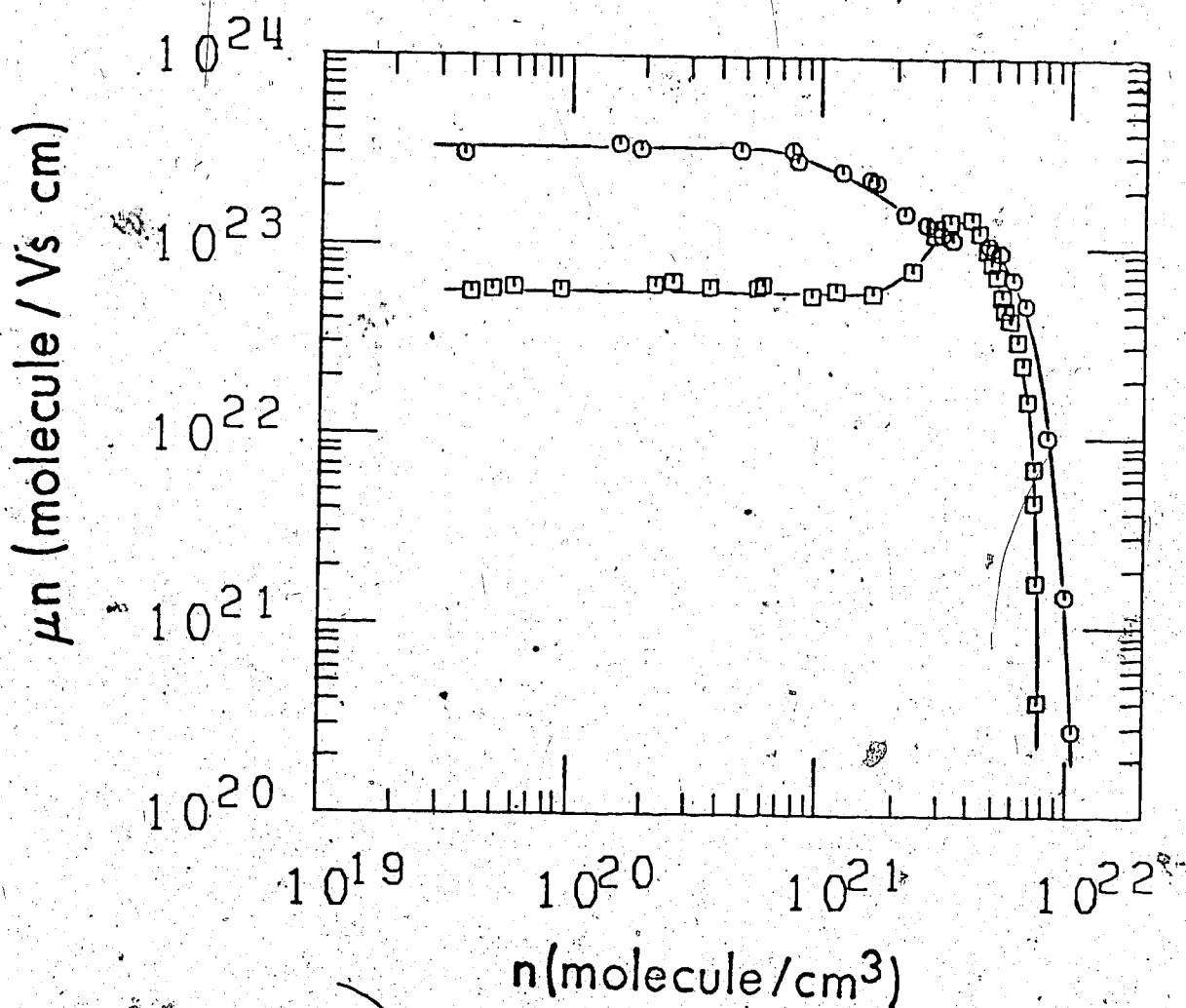


FIGURE IV-16. Density-normalized electron mobility in ethene (O) and isobutane (□) plotted against n .

TABLE IV-4

Molecular Properties for the C₃ Hydrocarbons and Ethene

	VDW ^a (nm)	(σ_{av}) ^b 300K (10 ⁻¹⁶ cm ²)	d ^c (nm)	(α^a) ^d (10 ⁻²⁴ cm ³)
C ₂ H ₄	0.36	4.4	0.12	2.1
C ₃ H ₈	0.40	11	0.19	0.9
C ₃ H ₆ -1	0.40	32	0.32	2.1
c-C ₃ H ₆	0.4	6	0.15	1.45

a. Van der Waal diameter

$$d = 2 \times \left[\frac{3b}{4\pi N} \right]^{1/3}$$

b is the VDW volume constant in cm³/mol, and N Avogadro's number.

$$= 0.2 \times (0.099b)^{1/3} \text{ nm.}$$

b. Calculated by Equation 5.

$$c. r = (\sigma_{av})_{300K} / \pi)^{1/2}$$

d. Anisotropy of polarizability reference 238.

The decrease in μn cannot, therefore, be attributed to the simultaneous interaction of several uncorrelated molecules. The electrons have to be slowed by some process such as those represented by equations 6 and 7. The mobility is reduced because the electrons undergo a quasilocalization process with density fluctuations. The previous sections for methane and ethane have shown that $\Delta S/S(0)$ is about constant, indicating that the entropy change is mostly associated with the formation of the localization sites. The extent of quasilocalization is an indication of the ability of the fluid to form fluctuations of the correct size to localize the electron.

The lack of importance of the double bond at low densities can be observed by comparing μn for ethene (3.3×10^{23}) with that of ethane (3.2×10^{23} molec/V cm s). The ethene structure is slightly more compact so that the cross-section can be slightly smaller, giving rise to a larger μn . The same is observed in comparing cyclopropane (2.4×10^{23}) to propane (1.5×10^{23}). The lower μn for propene compared to propane can be attributed to the presence of the dipole moment (237) rather than to the double bond.

As the density is increased, the differences between the cyclopropane and the propane μn curves increase. The extent of molecular clustering should be similar in the two vapors at the same value of n/n_c . The greater

decrease in cyclopropane indicates that the trap depths are deeper in cyclopropane than in propane for density fluctuations of the same magnitude. The cross-over of μn values occurs at $n = 1.3 \times 10^{21}$ molec/cm³ ($n/n_c = 0.4$). In the liquid phase the traps continue to be deeper in cyclopropane than in propane. However, in liquids well below the critical point the electron mobilities are stronger functions of temperature than of density. Due to the relatively compact structure of the cyclopropane molecules, the density of liquid cyclopropane is greater than that of propane at a given temperature. The propene curve crosses that of cyclopropane at $n = 5.0 \times 10^{21}$ molec/cm³, indicating stronger electron localization in liquid cyclopropane than in propene. The various crossings at the high density end of the μn curves ($n > 7 \times 10^{21}$ molec/cm³) are caused mainly by the temperature differences.

The ethene and ethane curves also diverge as the density is increased. The ethene curve drops below that of ethane at $n \sim 6.5 \times 10^{20}$ molec/cm³ ($n/n_c = 0.14$). The ratio of μn at the low densities to that at the critical density is twice as large in ethene as in ethane. These results indicate the greater importance of the double bond in localizing electrons at the higher densities.

Superposition of figure IV-15 and IV-16 would show that the ethene curve lies above those of the C₃ hydrocarbons

at all densities. For the liquid phase densities it has already been noted above that the temperature effect dominates. At a given density the temperature decreases in the order cyclopropane > propene > propane > ethene. The Arrhenius plot for the liquid phase mobilities is discussed in the following section.

c. Temperature Effect

i) Gas Phase

The Arrhenius plots of gas phase electron mobilities in ethene, propene and cyclopropane are given in Figures IV-17 to IV-19, respectively. For both ethene and cyclopropane, the temperature coefficients at the lowest density isochores are about 0. Propene has a slight increase but the temperature coefficient of 0.6 kJ/mol is only half of that in propane (1.2 kJ/mol) at the same density. These curves were used to obtain the velocity dependence of the momentum transfer cross-section as for the n-alkanes. The fitting equations are:

$$\text{ethene} \quad \sigma_v = 2.59 \times 10^{-9} v^{-0.95} \quad (21)$$

$$\text{propene} - \quad \sigma_v = 3.97 \times 10^{-3} v^{-1.72} \quad (22)$$

$$\text{cyclopropane} \quad \sigma_v = 5.54 \times 10^{-9} v^{-0.98} \quad (23)$$

which give average cross-sections at 300K, in units of 10^{-16} cm^2 , of 4.4, 32 and 6, respectively (Table IV-4).

At higher densities the temperature coefficient seems to increase slightly, but the extent is much less than in

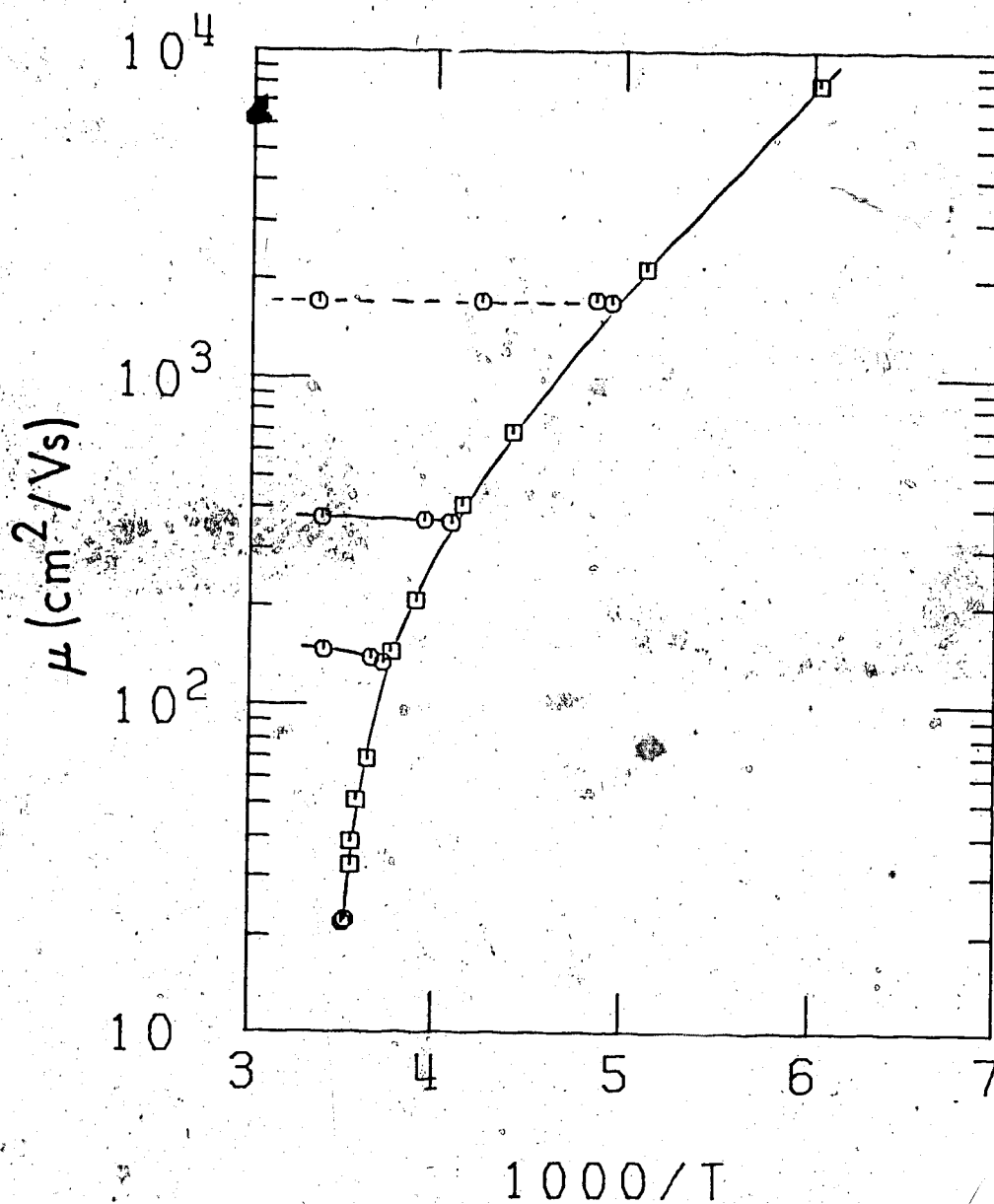


FIGURE IV-17. Electron mobility in gaseous ethene along the co-existence curve (\square) and above it (\circ), plotted against T^{-1} . The dashed line was calculated using equation 20 of Chapter I.

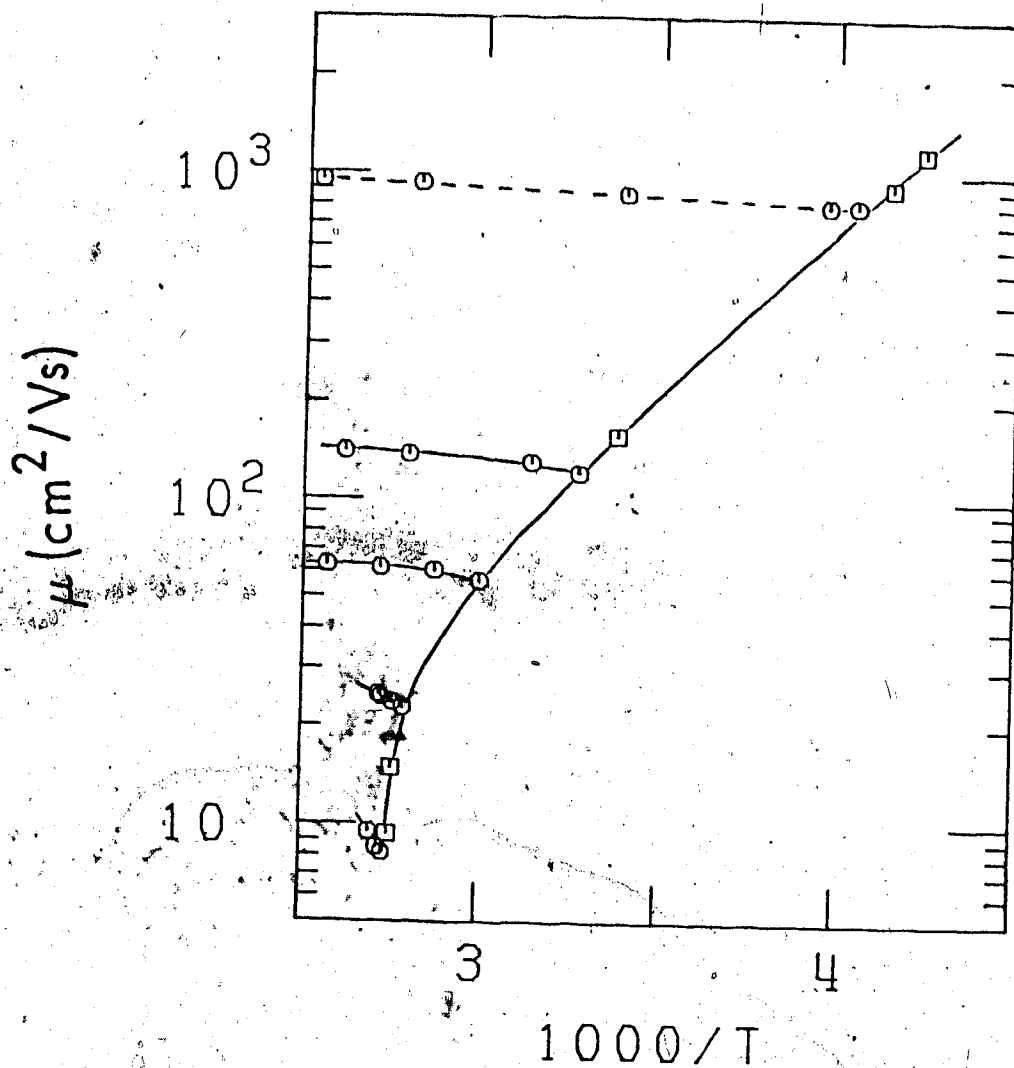


FIGURE IV-18. Electron mobility in gaseous propene, along the coexistence curve (\square) and above it (\circ), plotted against T^{-1} . The dashed line was calculated using equation 20 of Chapter I.

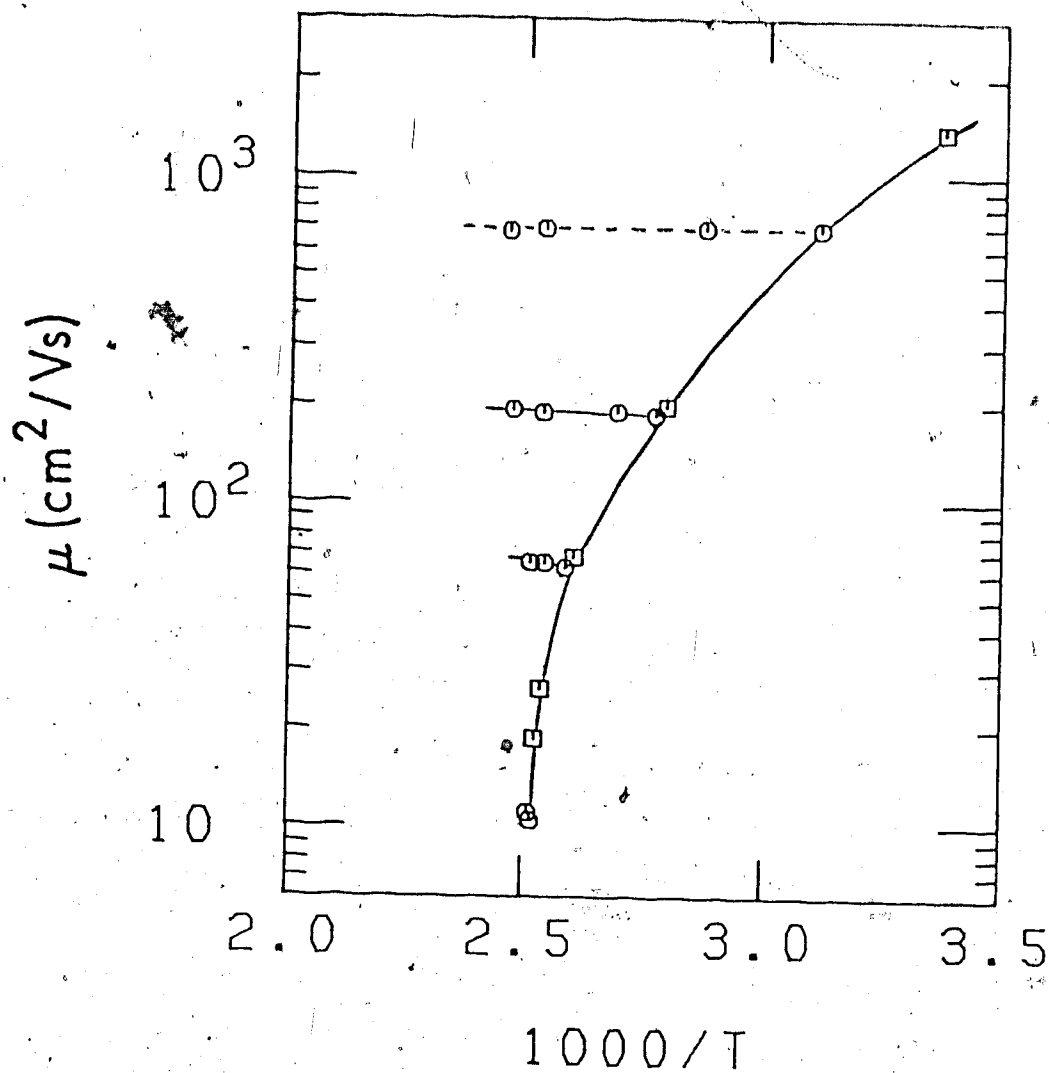


FIGURE IV-19. Electron mobility in gaseous cyclopropane, along the co-existence curve (\square) and above it (\circ), plotted against T^{-1} .

The dashed line was calculated using equation 20 of Chapter I.

the n-alkanes (Table IV-2). Even in propene the temperature coefficient appears much less than in propane (Figure IV-11). The cross-sections determined by Duncan and Walker (67,78) can be used to explain these results as follows.

The electron mobility is determined by an integral over $(v^3/\sigma_v) \exp(-mv^2/2kT)dv$ where v is the electron velocity, m the electron mass, σ_v the scattering cross-section at velocity v and k Boltzmann's constant. Increasing the temperature shifts the Maxwellian distribution to higher energies so that σ_v at large velocities becomes important. For 300K, the relevant range of energies is about $0.005 < \epsilon < 0.15$ eV. There is a minimum in propane at $\epsilon \sim 0.1$ eV and in propene at $\epsilon \sim 0.2$ eV. The minimum is both deeper and wider in propane. The same relative temperature increase can be expected to increase (v^3/σ_v) to a greater extent, for thermal electron velocities, for the propane distribution than for the propene. Heating along the isochore then gives a greater increase in mobility in propane.

In ethene and cyclopropane there is no pronounced minimum in the scattering cross-sections (67,68). At higher energies, the cross-section increases. This would lead to the expectation that heating the gas along an isochore would lead to a decrease in electron mobility. This is not observed (Figures IV-17 and IV-19). This indicates the presence of a competitive process which

is increasing the mobility and counterbalancing the heating effect, or which is cooling the electron distribution.

ii) Liquid Phase

Arrhenius plots of the liquid phase electron mobilities are given in Figures IV-20 and IV-21. The solid curves are calculated by the model discussed earlier (equations 15-20). The parameters used are given in Table IV-3.

Unlike the density plot (Figure IV-15), the C_3 temperature plot curves do not cross (Figure IV-20). The ethene curve is plotted separately to avoid conjection (Figure IV-21). Plotting ethene on Figure IV-20 would have it cut across all the C_3 hydrocarbon curves.

Comparison of the C_3 hydrocarbons shows an odd behavior on the part of cyclopropane. It does not have a dipole moment. Even with the π -like electron behavior of its bonds it is not expected to capture electrons more efficiently than propene. In the liquid phase, the mobilities are dependent upon α^a , the anisotropy of polarizability (107). From the values of α^a (Table IV-4), the mobilities at a density away from the critical region would be expected to fall in the order propane > cyclopropane > propene. However, the observed order is propane > propene > cyclopropane. The cyclopropane value is anomalously low, indicating an exceptionally stable

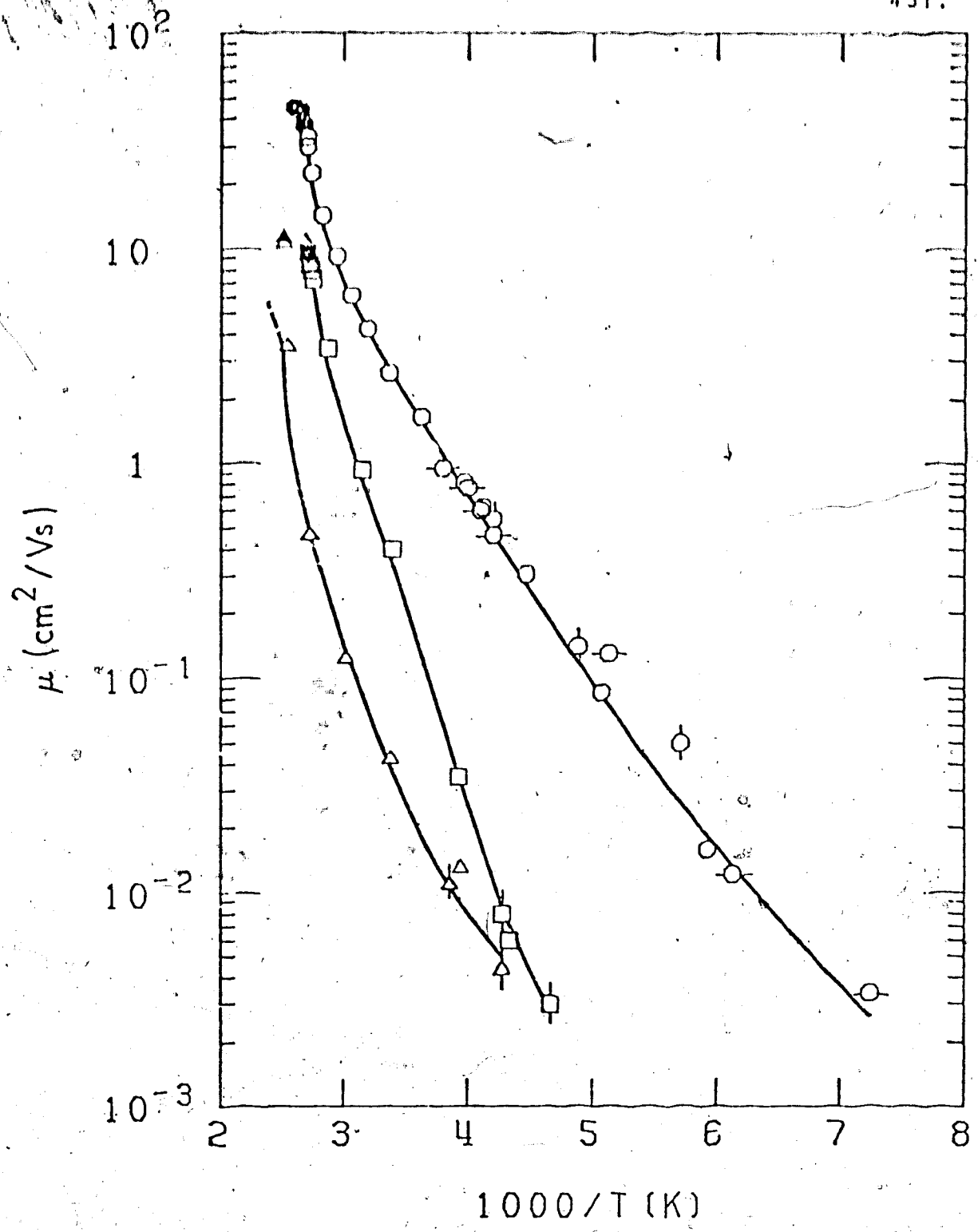


FIGURE IV-20. Arrhenius plots of electron mobilities in liquid propane (●), cyclopropane (Δ) and propene (□). Filled points represent supercritical gases at the critical densities. ○, △ and □ are propane, cyclopropane and propene data from reference 109. ○ are propane data from reference 120. The lines were calculated from equations 15-19, using the parameter values in Table IV-3.

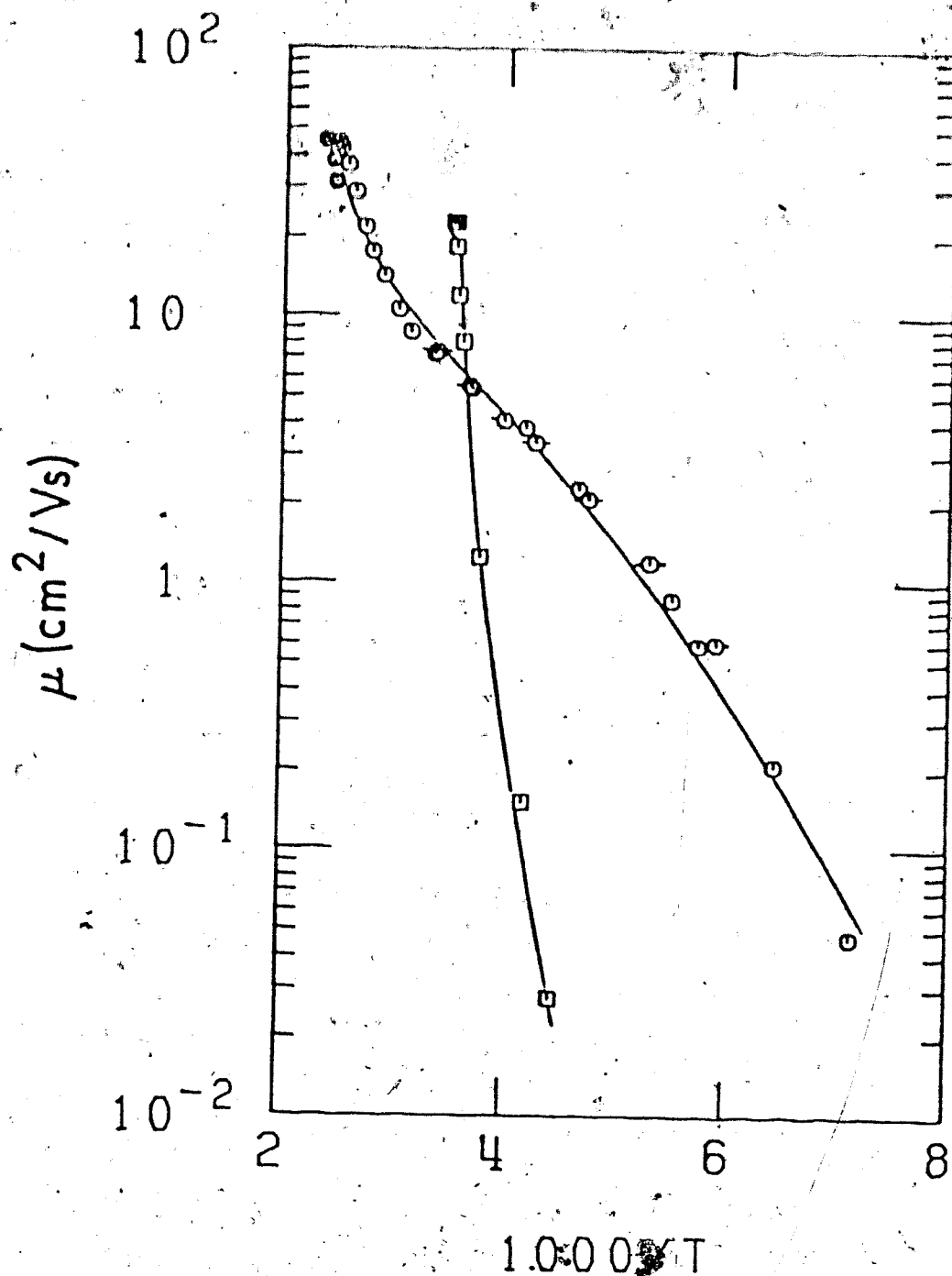


FIGURE IV-21. Electron mobilities in liquid ethene (\square) and isobutane (\circ) plotted against T^{-1} . Solid symbols are for the supercritical fluid. (\circ) are isobutane data from ref. 114. The solid lines were calculated from equations 15-19, using the parameter values in Table IV-3.

localized state. The importance of the ion-like state can be seen from the sharp drop of the mobility as the cyclopropane liquid is cooled from the critical region.

The cyclopropane type behavior also exists in ethene. Indeed the decrease is more rapid in ethene. Decreasing T/T_c from 1 to 0.8 decreases the mobility in ethene by 800 fold compared to a factor of 150 in cyclopropane and 9 in propane. While both ethene and cyclopropane have π -electron character, neither has a permanent dipole moment. Propene does. In the gas phase, the mobility varies inversely as the dipole moment (236). That the reverse applies in the liquid shows that another process must be overcoming the effect of the permanent dipole. This is similar to the finding in the butenes (108,131). The mobility of electrons in liquid cis-butene-2, which has a dipole moment of 0.3 debyes, is larger than that in liquid trans-butene-2 (Table IV-5). Comparison between behavior in n-butane and the butenes is even more interesting. Putting a double bond in the C_4 molecule results in a higher mobility in cis-butene-2 and isobutene and in a lower mobility in trans-butene-2 and butene-1. The dipole moment is about the same in cis-butene-2 and in butene-1 yet the mobility in cis-butene-2 is larger than in the alkane, and smaller, in butene-1. This can be included in the framework of the other hydro-

TABLE IV-5

Mobilities and Dipole Moments for C₄ Hydrocarbons at 296K^a

	D (debyes)	μ_e (cm ² /V s)
<u>trans</u> -Butene-2	0.0	0.029
Butene-1	0.34	0.064
<u>n</u> -Butane	0.0	0.30
Isobutene	0.50	1.5
<u>cis</u> -Butene-2	0.3	2.2

a. Data except for n-butane taken from ref. 131.

carbons by noting that the double bond fixes the carbon skeleton, in the case of cis-butene-2 and isobutene, into more sphere-like molecules than n-butane. A higher degree of sphericity tends to result in a higher mobility (107, 108). The trans-butene and butene-1 are fixed into rod-like shapes which would tend towards lower mobilities.

Sphericity by itself cannot explain the ethene, cyclopropane and propene results. Cyclopropane and ethene are more spherical compounds. Both are small molecules which are tightly packed together in the liquid. Away from the critical fluid, the number density of ethene in molec/cm³ at a given reduced temperature is greater than that in cyclopropane which in turn is greater than that in propene. The tighter packing in ethene and cyclopropane in the liquid may enhance temporary negative ion formation.

The behavior may be related to that in carbon dioxide at 293K (239). At $n > 3.5 \times 10^{20}$, the ratio of the electron drift velocity at a pressure p to that at 66 kPa, which will be labelled q , sharply decreased. At $n < 3.5 \times 10^{20}$, q was about 500 times that of the ratio of ion drift velocity at pressure p to the electron drift velocity at 66 kPa. At $n \sim 1 \times 10^{21}$, $v_d(\text{electron}) / v_d(\text{ion})$ is 3-4. Carbon dioxide like ethene and cyclopropane is a symmetrical molecule with π character electrons. The enhanced trapping is a function of

density, not of temperature. It was suggested that the CO_2 formed a negative ion which was stabilized by solvation at higher densities. Negative ion formation in the liquid phase has also been postulated for trans-butene-2 (131) and benzene (110). It may be that the low mobilities in ethene and cyclopropane are due to temporary negative ion formation.

4. Isobutane

Data for isobutane are taken from Table III-5.

a. Electric Field Effect

The threshold field strengths for isobutane are included in Figure IV-14. The value appears to be 0.24 Td, invariant of density for $n < 1.5 \times 10^{21}$. This value is in agreement to a previous value of 0.25 Td reported at 100 torr (68). The low field μ_n is also invariant of density for the range, and has a value of 5.9×10^{22} molec/V cm s (Figure IV-16). This gives a threshold drift velocity of 1.4 km/s. No sound velocity values are available for isobutane. In the low density gas, the low frequency velocity of sound, c_0 is given by (240)

$$c_0 = (\gamma P/D)^{0.5} \quad (24)$$

where $\gamma = C_p/C_v$ is the heat capacity ratio, P (dyne/cm²) the pressure and D (gm/cm³) the density. Assuming $\gamma = 1.1$ (70,71) gives $c_0 \approx 210$ m/s at 283K and 297K for isobutane.

The ratio v_d/c_0 is hence about 7, twice the value in ethane, and a bit larger than that in neopentane which was reported as 5 (70). Values for isopentane and *n*-pentane were also reported as 15 and 100. Values of c_0 in propane and *n*-butane from equation (24) are 240 and 220 m/s (at $T < 297K$). Using data of section 2 gives ratios of 5 and 50 respectively. As noted in the methane section, an increase in $(v_d)_{\text{threshold}}/c_0$ reflects a greater importance of inelastic processes. From the values above, it can be noted that the less rigid the carbon skeleton, the larger the ratio. This can be attributed to the possibility of greater rotational modes of energy loss and hence a greater ability to cool the electron distribution.

b. Density-normalized Electron Mobility

Values of μ_n are included in Figure IV-16. There is no quasilocalization dip as in the *n*-alkanes. The low density value of 5.9×10^{22} molec/cm³ Vs is less than that in propane (1.5×10^{23}) though isobutane is a larger molecule. The same curious effect has been noted in the pentane series (70). Isopentane and *n*-pentane both have larger μ_n values than neopentane. As well, neopentane displays no minimum (70,73). It was noted that increasing E/n at low densities leads to the μ_n in both isopentane and neopentane approaching the value in *n*-pentane.

Increasing n leads to the same effects as in the other compounds. Formation of the conduction band decreases the scattering cross-section and increases μn . There is a pronounced maximum. At higher densities μn decreases as the short range repulsive forces gain in importance.

c. Temperature Effect

The Arrhenius plot of the gas phase mobilities is shown in Figure IV-22. The temperature coefficient for the isochores with $n/n_c = 1.0, 0.5, 0.26, 0.11$ and 0.026 are 37, 15, 8.3, 2.8, and 2.2 kJ/mol, respectively. The values for the $n/n_c > 0.1$ isochores are similar to that of the other alkanes (Table IV-2). Isobutane however has a much larger value for the $n/n_c = 0.026$ curve. This would support the notion of a thermally activated localization process even at low densities. In a similar fashion the activation energy in low density neopentane stays at a much larger value than in isopentane or n-pentane (70). The controlling factor appears related to the shape of the carbon skeleton.

The low density isochore (dashed line) in Figure IV-22 was analyzed for the cross-section as in the other compounds. The appropriate cross-section is

$$\sigma_v = 8.96 \times 10^2 v^{-2.47} \quad (25)$$

giving an average cross-section of $25 \times 10^{-16} \text{ cm}^2$ at 300K.

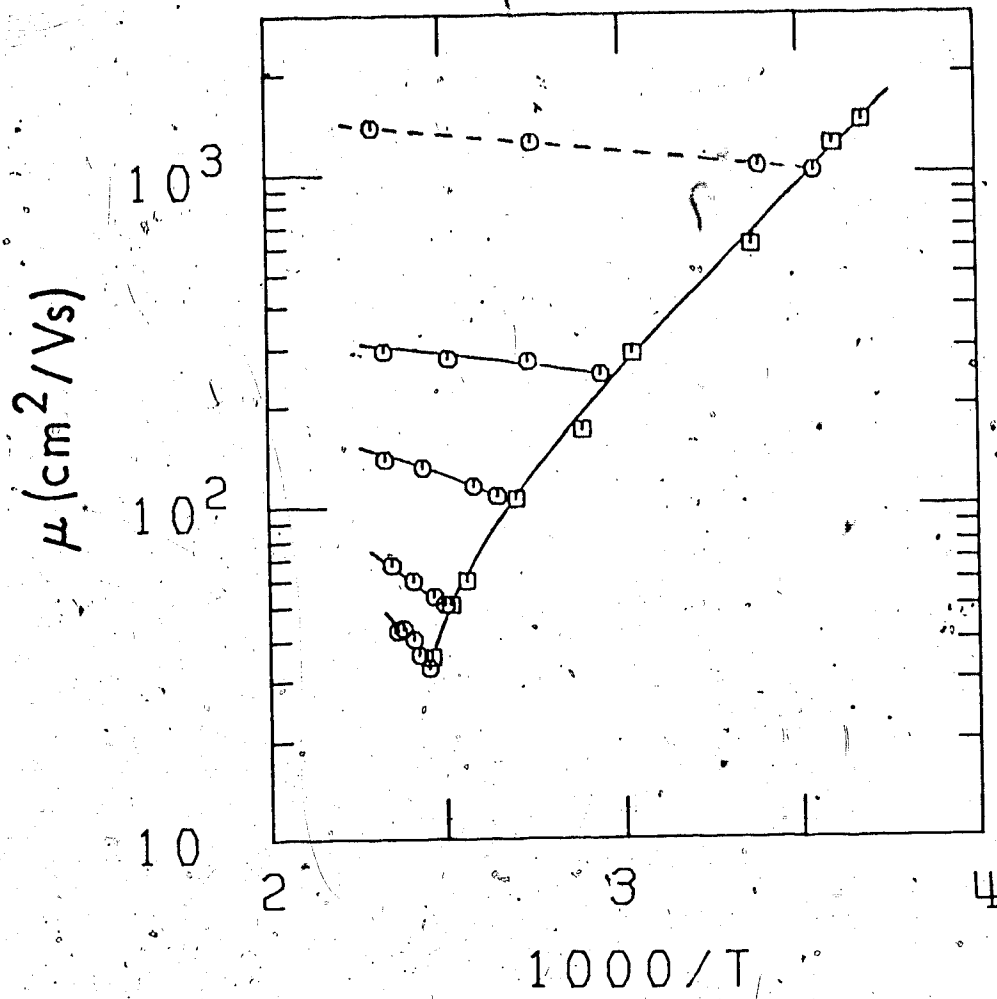


FIGURE IV-22 Electron mobility in gaseous isobutane, along the co-existence curve (\square) and above it (O), plotted against T^{-1} . The dashed line was calculated using equation 20 of Chapter I.

The Arrhenius plot for liquid phase mobilities in isobutane is shown in Figure IV-21. Mobilities in the liquid greater than $1 \text{ cm}^2/\text{V s}$ are usually considered large. Isobutane, with a value near its boiling point, of 4.9 resembles other sphere-like hydrocarbons in that the mobility in the region of the boiling point is large (107,114). Another trait shared by these hydrocarbons is that the electron mobilities possess a maximum below the critical temperature (130,132). The greater degree of sphericity seems to provide a smoother potential surface for the electrons. As a result, they are less readily localized. At lower temperatures there appears to be a transition in the isobutane curve. As a result the mobility drops fairly sharply.

The solid line through the isobutane mobilities is calculated as for the other compounds. The parameters are included in Table IV-3. Due to the large value of the mobility near its boiling point, a reference mobility of $110 \text{ cm}^2/\text{V s}$ at the lowest temperature, 140K, was used. This corresponds to a reference mobility of 83 at the boiling point.

5. Liquid Phase Model Parameters

Due to the degree of flexibility in the choice of the liquid phase mobility model parameters (Table IV-3), it is difficult to draw firm conclusions. To attempt reduction of this flexibility, μ_{ij}^0 and ϵ_{ij} are fixed to

values near the average in the hydrocarbons. In ethane and ethene the values are sufficiently different that values from the experimental curves (data in next section - Ion Mobilities) are used. As well, while μ_h^0 is usually taken as $30 \text{ cm}^2/\text{Vs}$ at 295K, larger values are used for ethane and ethene since their critical points are below 295K. The large experimental values of the electron mobility in isobutane near 295K also imply a larger μ_h^0 .

The ratio $a/E(0)$ has no simple value. In ethers, the corresponding ratio is about $1.7 \times 10^{-3} \text{ K}^{-1}$ (131). $E(0)$ is held to 0.6 eV for all the liquids. The ratio reflects the effect of the temperature on the mean trap depth. In previous works the value of (E_0/σ) at 300K, was used (71,132) since 300K was in the region of the boiling points. Since the boiling points for the present systems can be far from 300K, the ratio in Table IV-3 is calculated at the boiling point. The ratio is larger when the mobility at that temperature is smaller. A larger ratio indicates a deeper trap(71).

B. Ion Mobility

1. Electric Field Strength

For all the systems investigated the ion mobility is independent of applied electric field strength up to values of E/n of 0.5 Td (1 Td = 10^{-17} Vcm²/molec) in the normal liquids and 2 ± 1 Td in the normal vapors. The mobility vs E/n plots have been given in Chapter III, Section B. The ion mobility results are summarized in Tables III-9 to III-16.

2. Density-normalized Mobility

The density-normalized ion mobility μ_+n is plotted against n in Figures IV-23 and IV-24. The liquid and gas cell values in the supercritical fluid are averaged and that average used to adjust mobilities about the critical region so that the liquid and gas phase curves merge smoothly. Typical adjustments are in the order of 10% or less. In isobutane, the gas phase results are considered more reliable at the critical point. Liquid phase results at $2.3 \times 10^{21} < n < 5.5 \times 10^{21}$ molec/cm³ are increased by 28%, bringing them in line with the gas phase results and liquid phase results at $n > 5.5 \times 10^{21}$.

a. Low Density

In contrast to the low density values of μn for electrons, which vary over an order of magnitude between the different systems, the μ_+n values vary over a factor of 4 (Figure IV-23 and IV-24). The presence of dipole moments and the shape of the molecules have little effect.

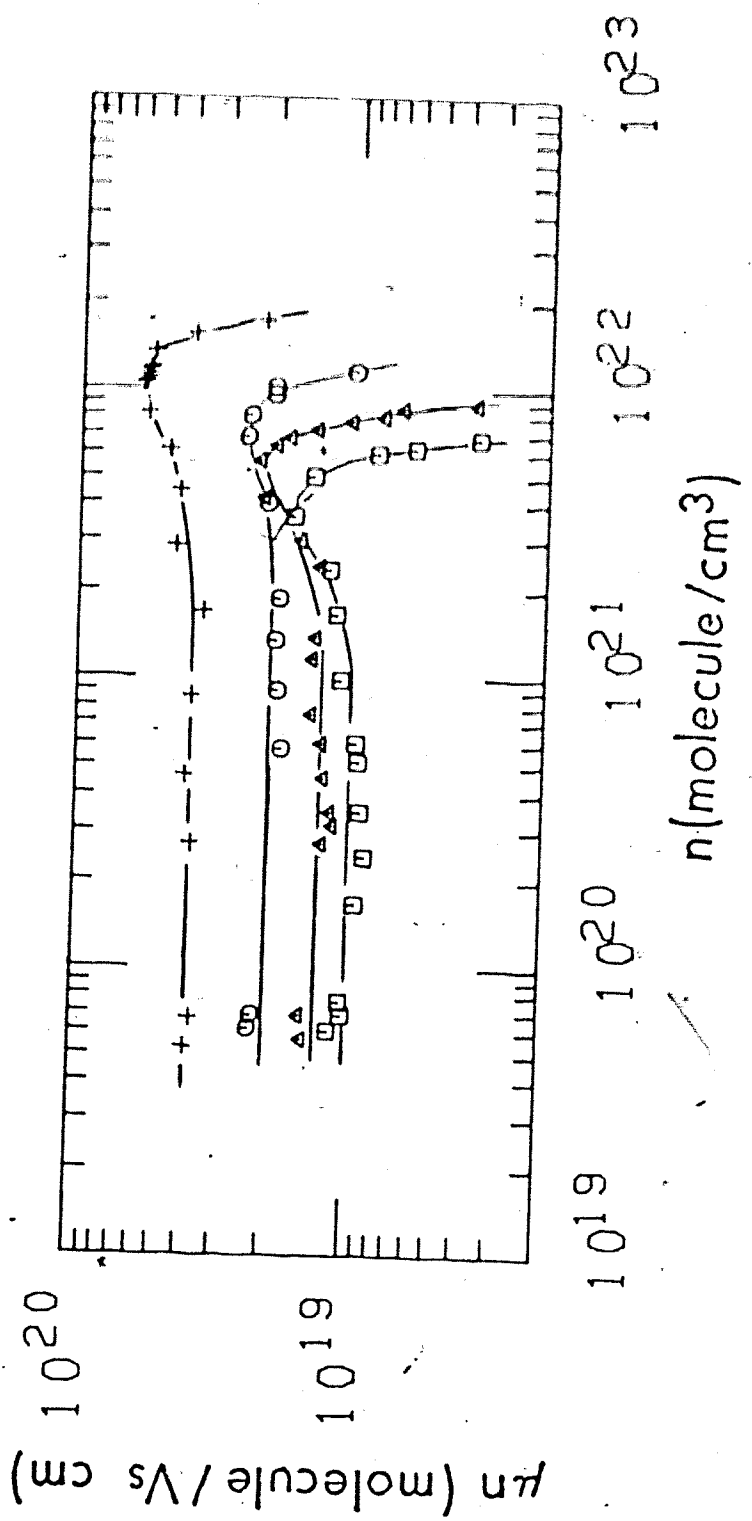


FIGURE IV-23 Density normalized ion mobility plotted against n for methane (+), ethane (O), propane (Δ) and n-butane (\square).

[Handwritten mark]

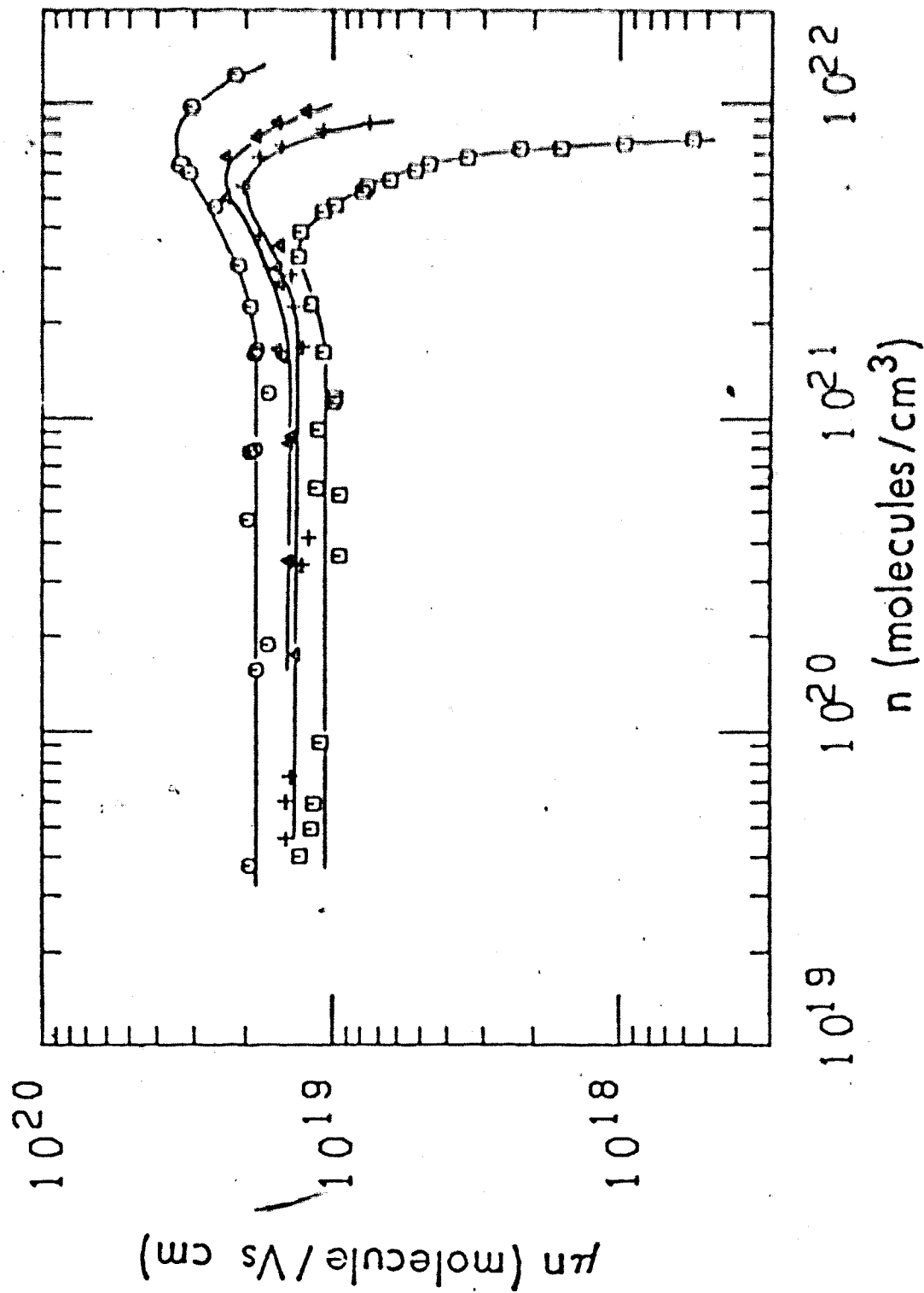


FIGURE IV-24. Density normalized ion mobility plotted against n for ethene (O), propene (\ast), cyclopropane (Δ) and isobutane (\square).

The main factor seems to be the physical size of the molecules. Methane has a μ_{+n} value of 3.9×10^{19} . Ethane which is about twice the size of methane has a value of 2.0×10^{19} . Propane and *n*-butane have correspondingly smaller values. The lack of importance of factors such as unsaturation of carbon-carbon bonds, dipole moments and branching can be seen from comparing the compound curves in Figure IV-24 to the corresponding *n*-alkane in Figure IV-23. Ethane and ethene have similar values at low densities as do propane and propene, and *n*-butane and *i*-butane. The slightly larger value of μ_{+n} in cyclopropane compared to that in propane can be attributed to the more compact structure of the cyclic molecule.

b. Effect of Density

As the density is increased from dilute gas values, the value of μ_{+n} does not change until the critical region is approached. Near the critical region μ_{+n} increases in value, passes through a maximum at a $n = n_c$, and then decreases. The initial increase has been attributed to destructive interference of attractive electrostatic interactions when the ion is near to more than one molecule at a time, and the subsequent decrease at high density, to obstruction of translational motion of the ion by the now closely spaced repulsive cores (174).

3. Temperature Dependence

a. Low Density

Arrhenius plots of the ion mobility vs T^{-1} for the eight hydrocarbon systems are given in Figures IV-25 to IV-31. The temperature dependences of the ion mobility along isochores at low densities are used to obtain average cross-sections. The dependences are obtained by least-squares fit of the logarithm of the mobility against the logarithm of the temperature. These curves are shown by dashed lines in Figures IV-25 to IV-31. The expression for the density-normalized mobility of Viehland and Mason (171,172) has been reduced by gamma functions (174) to

$$\mu_+ n = \frac{3\pi^{1/2}}{4A_\alpha} \frac{1}{\Gamma(3-\alpha/2)} \frac{e}{M_r} \left(\frac{2kT}{M_r} \right)^{(\alpha-1)/2} \quad (26)$$

where e is the electronic charge, M_r the reduced mass of the ion-molecule system, k Boltzmann's constant, T the temperature, A_α and α constants and Γ , ($\Gamma(x) = (x-1)!$) is a gamma function. It has also been assumed that $\sigma_v = A_\alpha v^{-\alpha}$ where v is the relative velocity between the ion and the molecule. From the least-squares fitting of $\log \mu_+$ vs $\log T$, A_α is obtained from the intercept at $\log T = 0$ and α from the slope. The average cross-section is then

$$\begin{aligned} \sigma_{av} &= \langle v \rangle / \langle v / \sigma_v \rangle \\ &= A_\alpha (M_r / 2kT)^{\alpha/2} / \Gamma(2 + \alpha/2) \quad (27) \end{aligned}$$

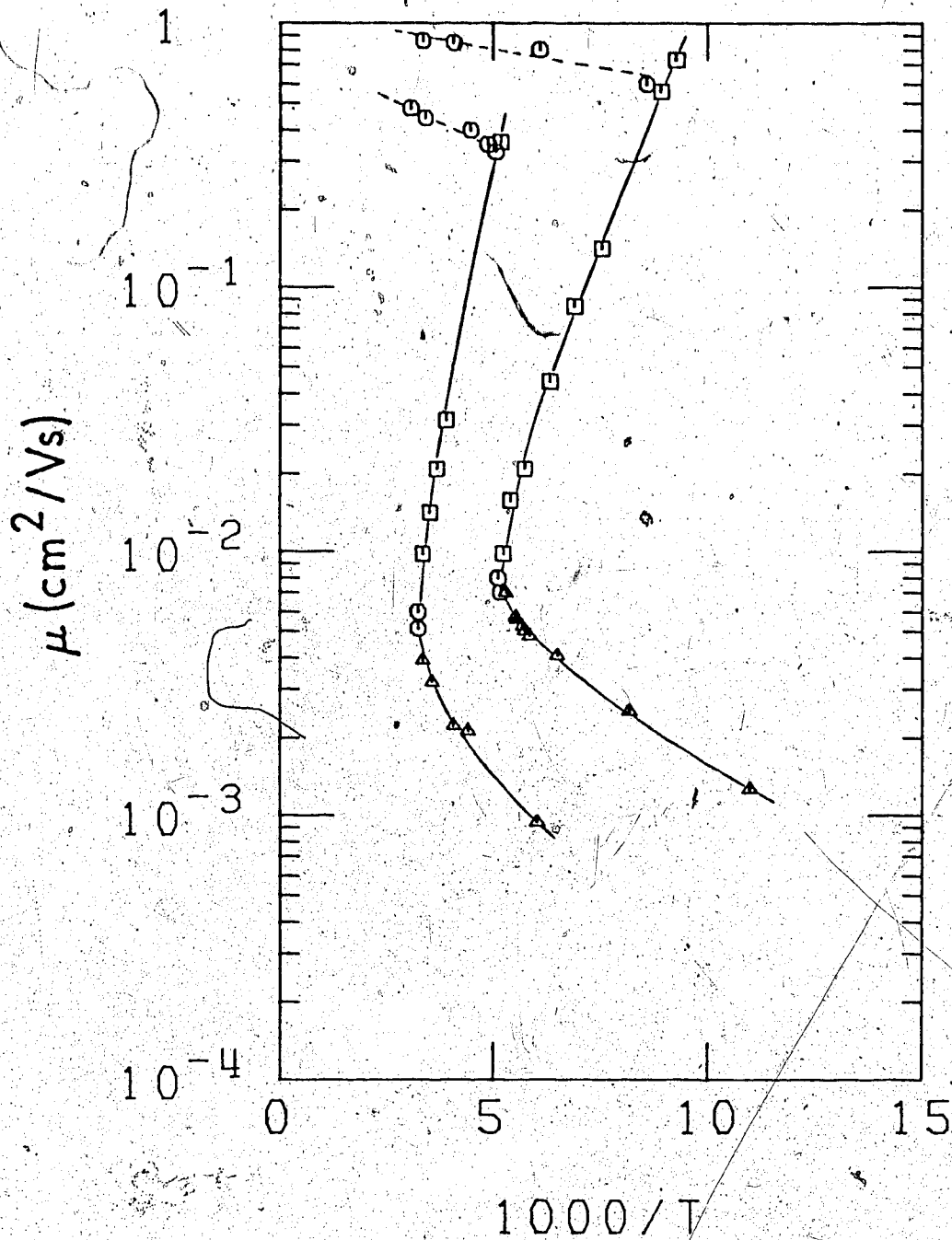


FIGURE IV-25. Arrhenius plot of the ion mobilities in methane (open symbols) and ethane (solid symbols). Data represent values in the co-existence curve gas (\square), co-existence curve liquid (Δ) and along isochores in the gas (\circ). The dashed lines was calculated using equation 26.

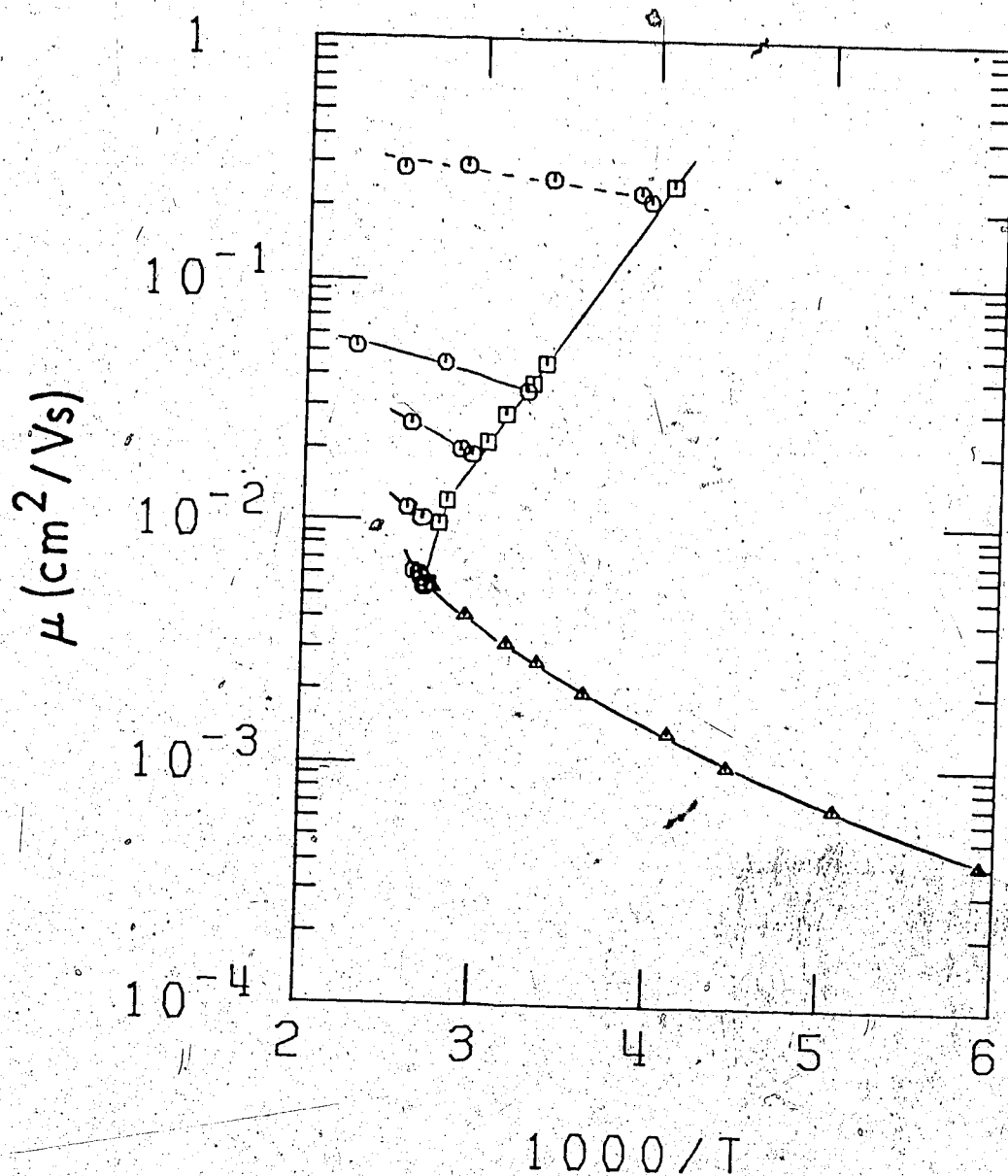


FIGURE IV-26. Arrhenius plot of the ion mobility in propane. Data are for the co-existence curve vapor (\square), co-existence curve liquid (Δ) as well as along isochores in the gas phase (\circ). The dashed line was calculated using equation 26.

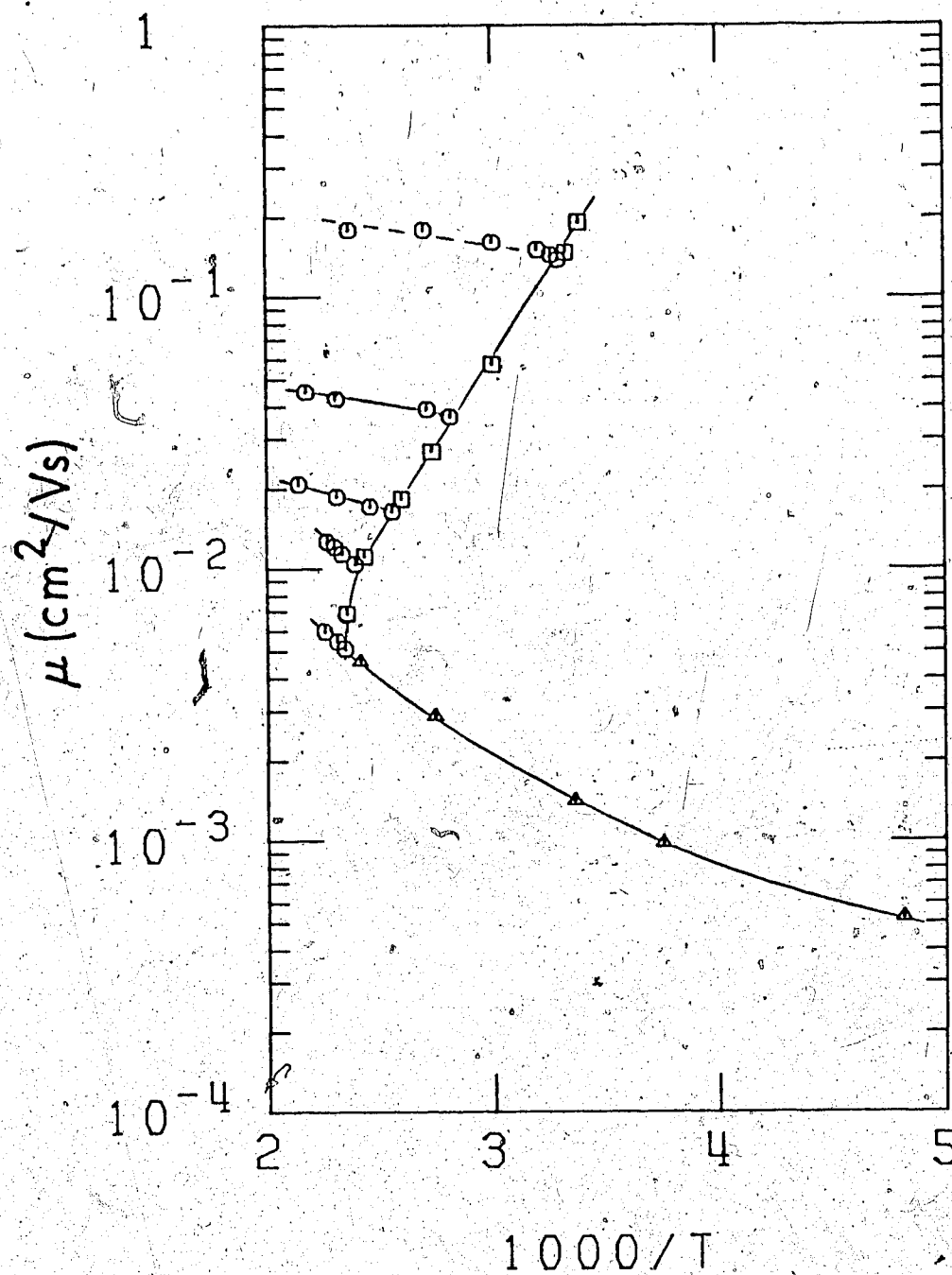


FIGURE IV-27. Arrhenius plot of the ion mobility in *n*-butane. Data are for the co-existence curve gas (\square), co-existence curve liquid (Δ) as well as along isochores in the gas (\circ). The dashed line was calculated using equation 26.

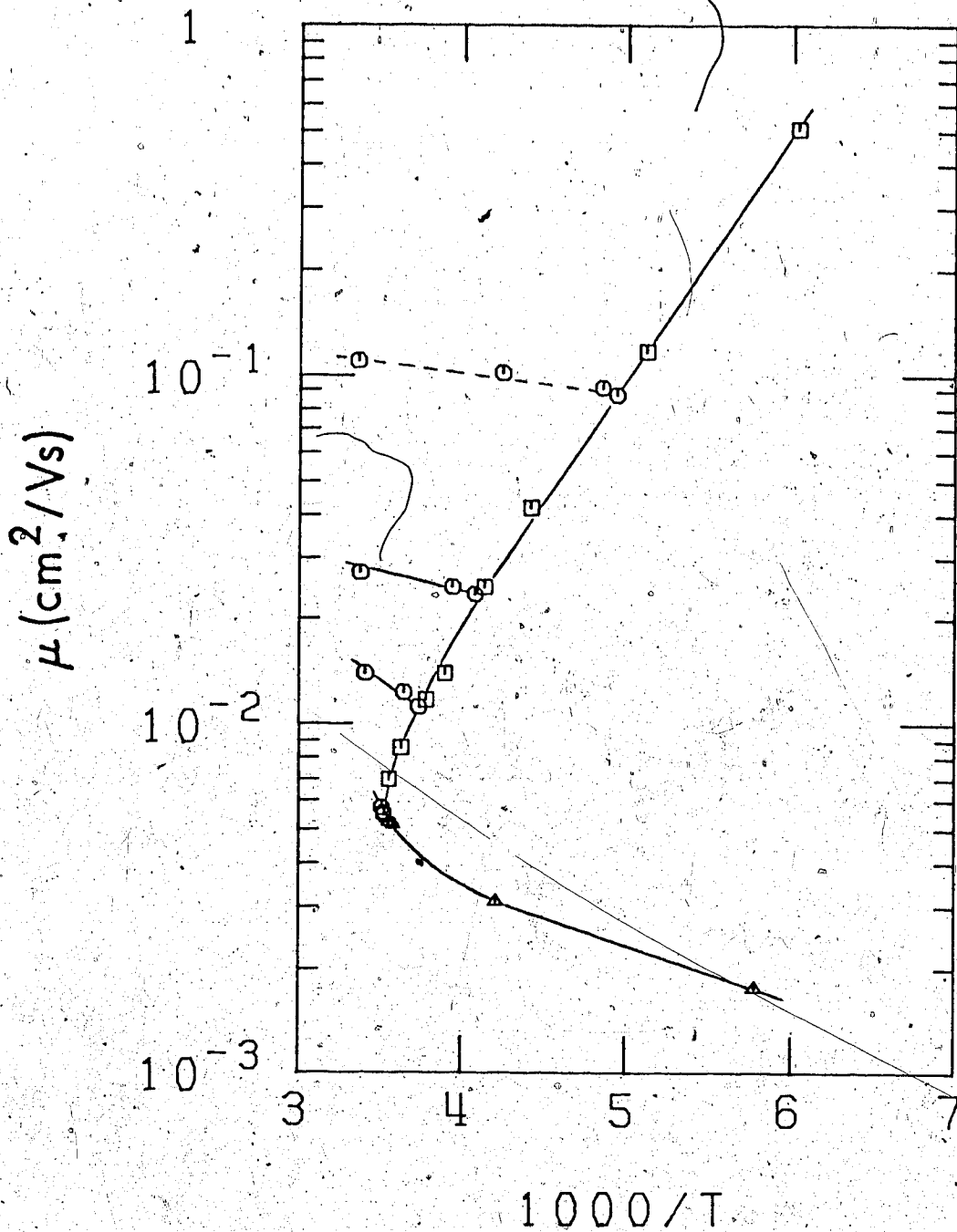


FIGURE IV-28. Arrhenius plot of the ion mobility in ethene. The data are for the co-existence curve gas (\square), co-existence curve liquid (Δ) as well as along isochores in the gas (\circ). The dashed line was calculated using equation 26.

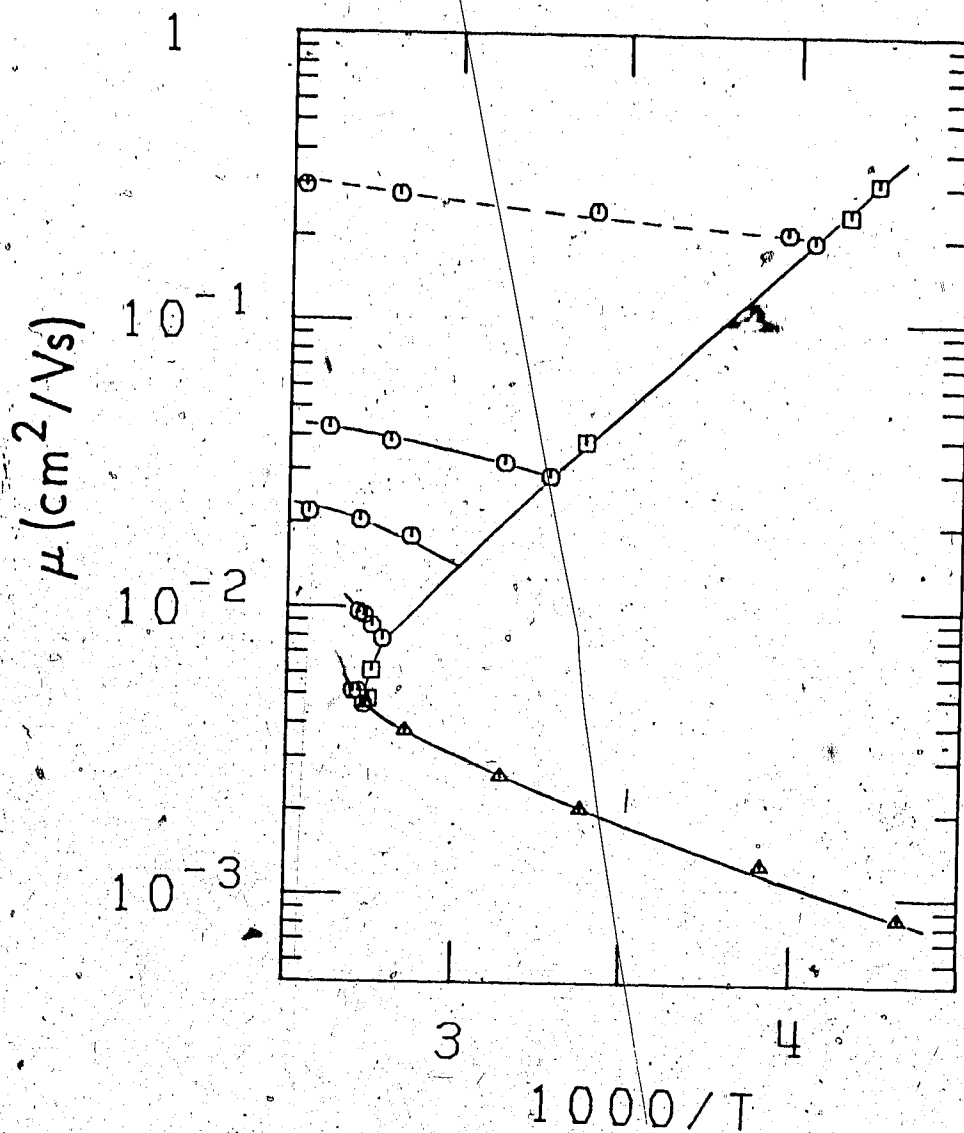


FIGURE IV-29. Arrhenius plot of the ion mobility in propene. The data are for the co-existence curve gas (\square), co-existence curve liquid (\triangle) as well as along isochores in the gas phase (\circ). The dashed line was calculated using equation 26.

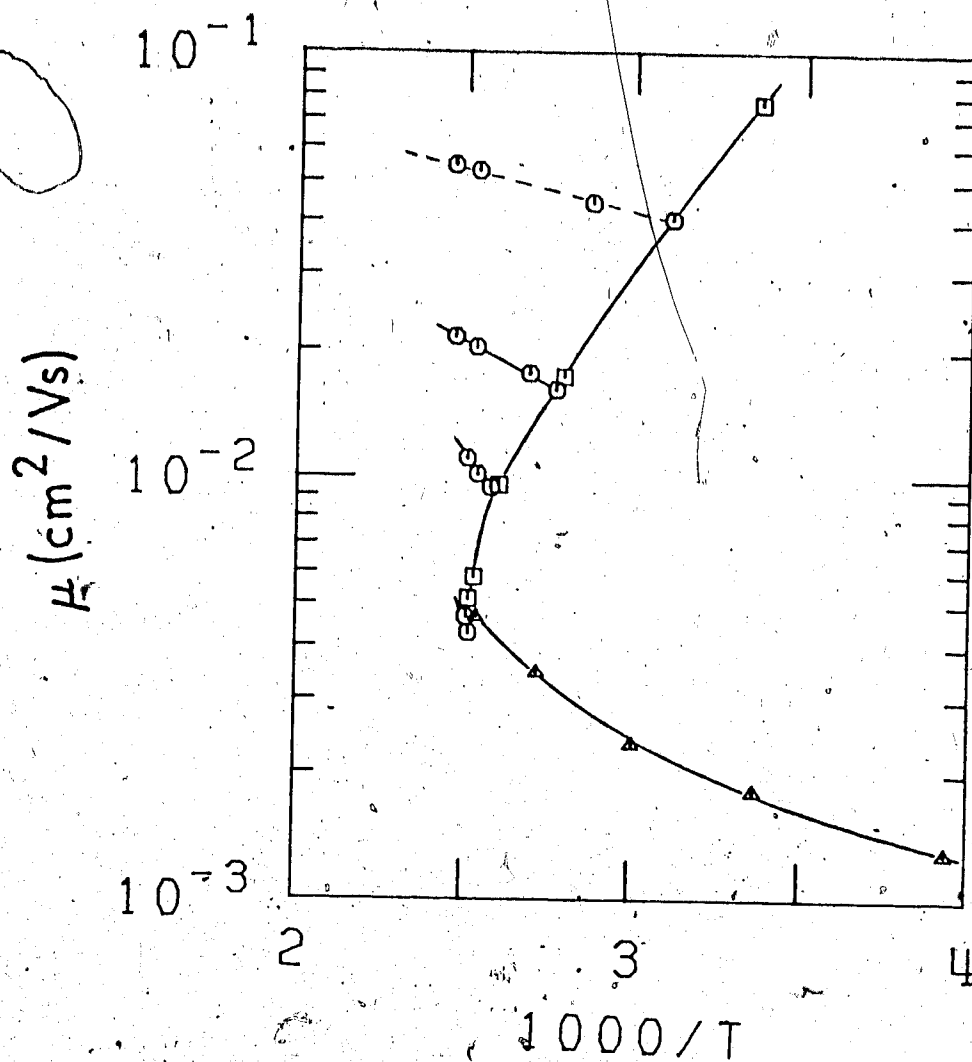


FIGURE IV-30. Arrhenius plot of the ion mobility in cyclopropane. The data are for the co-existence curve gas (□), the co-existence curve liquid (△) and along isochores in the gas (○). The dashed line was calculated using equation 26.

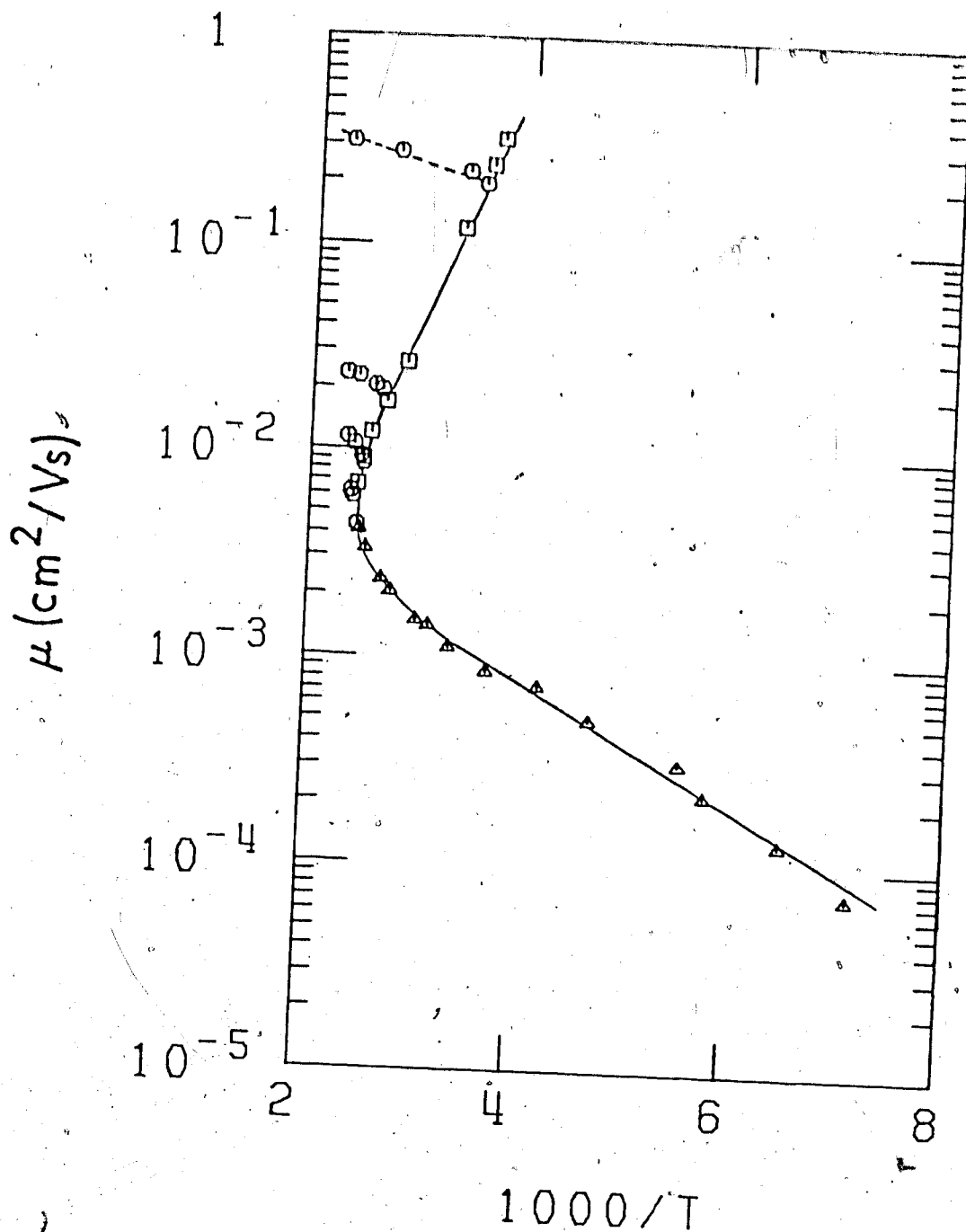


FIGURE IV-31. Arrhenius plot of the ion mobility in isobutane. Data are for the co-existence curve vapor (\square), the co-existence curve liquid (Δ) as well as along isochores in the gas (\circ). The dashed line was calculated using equation 26.

The fitting parameters and the cross-sections are tabulated in Table IV-6. Since the μ_+ n values are similar for the alkenes and their corresponding alkanes, it might be expected that the average scattering cross-sections also be similar. This is not the case at 300K, which indicates that factors other than the cross-section affect μ_+ n. These factors can be obtained by noting that combination of equations (26) and (27) gives, for 300K,

$$(\mu_+n)_{300K}(\sigma_{av})_{300K} M_r \Gamma(3-\alpha/2)\Gamma(2+\alpha/2) = \text{constant} \quad (28)$$

rather than

$$(\mu_+n)_{300K}(\sigma_{av})_{300K} = \text{constant} \quad (29)$$

Introduction of the reduced mass and the gamma functions gives a constant term, as expected from equation 28.

b. Effect of Density

As the density increases, the temperature coefficient along the isochores increases. These coefficients are not the same as those of the electron curves (section A). For example, the low density ion mobility curves for ethene and cyclopropane (Figures IV-28 and IV-30) show a clear increase with temperature whereas the electron mobility curves do not (Figures IV-17 and IV-19).

Along the co-existence curve, the variation of $\log \mu_+$ vs T^{-1} is approximately linear in both phases except near the critical region. The temperature coefficients are

TABLE IV-6

Parameters for Ion Scattering Cross-sections

	$n/10^{19}$ (molec/cm ³)	α	Λ_α		$(\sigma_{av})_{300K}$ (10^{-14} cm ²)	
			(1)	(2)	(1)	(2)
CH ₄	7.1	1.75	1.1×10^{-5}	7.2×10^{-6}	1.6	1.4
C ₂ H ₆	6.8	2.31	5.2×10^{-3}	3.3×10^{-3}	2.2	1.9
C ₃ H ₈	6.7	2.86	1.8×10^{-2}	1.2×10^{-2}	2.5	2.2
n-C ₄ H ₁₀	7.6	2.54	6.0×10^{-2}	3.6×10^{-2}	4.1	3.5
C ₂ H ₄	19	2.08	6.4×10^{-4}	4.1×10^{-4}	3.5	3.0
C ₃ H ₆ ⁻¹	6.6	2.71	4.3×10^{-1}	2.5×10^{-1}	3.1	2.7
c-C ₃ H ₆	35	3.54	4.3×10^3	2.2×10^3	2.3	2.0
i-C ₄ H ₁₀	5.9	2.99	6.0	3.4	2.8	2.4

(1) Assumed mass of ion equalled mass of molecule (monomeric ion)

(2) Assumed mass of ion equalled twice the mass of the molecule (dimeric).

given in Table IV-7. In the n-alkane series, both the temperature coefficients for the gas phase $E_{\mu}(\text{gas})$ and the liquid phase $E_{\mu}(\text{liquid})$ increase as the length of the carbon chain increases. The gas phase values are about the same in the alkene and the corresponding n-alkane. Along the co-existence curve, increasing the temperature leads to an increase both in the vapor pressure and in the gas density. Away from the critical point the pressure and density change at about the same rate. An Arrhenius plot of the vapor pressure vs T^{-1} gives an "activation energy" of ΔH_{vap} , the heat of vaporization at the normal boiling point (241). Since the density is varying approximately as the pressure, and the ion mobility varies inversely with the density, $E_{\mu}(\text{gas})$ should be about the same as ΔH_{vap} . Values of the ratio $E_{\mu}(\text{gas})/\Delta H_{\text{vap}}$ (Table IV-7) are not exactly 1.0 but are close enough that variation of $E_{\mu}(\text{gas})$ between the different systems can be taken to reflect variations in ΔH_{vap} .

The liquid phase ion mobility is most often correlated to the viscosity η (61,79,80,96,97,112,130). Stoke's Law applies for the motion of an object through a fluid if the object is large compared to the mean free path (242). If the effective radius of the sphere is constant, then the product $\mu\eta$ is constant (this is Walden's rule, ref. 243). It has been found in a number of ethers and alkanes that μ_+ varies as $\eta^{-1.2 \pm 0.1}$ (112,130). In

TABLE IV-7

Temperature Coefficients of Ion Mobilities^a


	$E_{\mu}(\text{gas})$ (kJ/mol)	E (liquid) (kJ/mol)	ΔH_{vap}^b (kJ/mol)	E_n^c (kJ/mol)	$E_{\mu}(\text{gas})$ $\frac{E_{\mu}(\text{gas})}{\Delta H_{\text{vap}}}$	$E_{\mu}(\text{liq})$ $\frac{E_{\mu}(\text{liq})}{E_n^c}$
CH ₄	8.2	2.1	8.2	1.9	1.0	1.1
C ₂ H ₆	17	3.4	15	3.3	1.1	1.0
C ₃ H ₈	19	5.2	19	3.9	1.0	1.3
n-C ₄ H ₁₀	25	5.9	22	4.9	1.1	1.2
C ₂ H ₄	15	3.0	14	3.2	1.1	0.9
C ₃ H ₆ -1	20	6.4	20	3.5	1.0	1.8
c-C ₃ H ₆	21	4.9	18	2.3	1.2	2.1
i-C ₄ H ₁₀	23	6.1	21	7.5	1.1	0.8

a. Taken from mobilities along the co-existence curve away from the critical region.

b. Heat of vaporization at normal boiling point - ref. 231.

c. Activation energy of the liquid viscosity away from the critical region - ref. 222.

general for a given compound the ion mobility should vary as the viscosity raised to a power of $(-E_{\mu}(\text{liq})/E_{\mu})$. This ratio is given in column 6 of Table IV-7 for the eight hydrocarbon systems. The values for the *n*-alkanes are similar to those reported earlier. The much larger $E_{\mu}(\text{liquid})$ for isobutane compared to *n*-butane can be attributed to the much larger E_{μ} for isobutane. The larger ratios in propene and cyclopropane, which imply that another process is nearly as important as the variation in viscosity, may be due to the $E_{\mu}(\text{liquid})$ being measured too close to the critical region.



C. Free Ion Yield

1. General

The free ion yield G_{fi}^E is defined as the number of ion pairs that escape the spur into the bulk medium for every 100 eV of absorbed dose. Application of an electric field can enhance the yield. The free ion yield at field E , G_{fi}^E can be related to the total ion yield G_{tot} by equation 31 of Chapter II which was

$$G_{fi}^E = G_{tot} \int_0^{\infty} \phi(y, E) F(y) dy$$

where $F(y)$ is the distribution of initial electron-ion separation distances y at thermalization and $\phi(y, E)$ is the likelihood that an ion pair separated by a distance of y will form a free ion pair. The curves in Chapter III, Section C are calculated using the form of $\phi(y, E)$ developed by Terlecki and Piutak (209) and a modified gaussian function for $F(y)$ (6). This form of $\phi(y, E)$ has taken into account the angle of the ion pair with respect to E and is

$$\phi(y, E) = \exp(r_c/y) \left[1 + \exp(-\beta y) \sum_{n=1}^{\infty} \frac{(\beta y)^n}{(n+1)!} \sum_{j=0}^{n-1} \frac{(n-j)(r_c/y)^{j+1}}{(j+1)!} \right] \quad (30)$$

where

$$r_c = \frac{e^2}{\epsilon kT} \quad (31)$$

and

$$\beta = \frac{eE}{300kT} \quad (32)$$

with e being the electronic charge (esu), ϵ the dielectric

constant, k Boltzmann's constant, and T the temperature.

The form of $F(y)$ used is

$$F(y) = 0.96 YG \quad y < 2.4b \quad (33)$$

$$F(y) = 0.96 \left[YG + 0.5(b^2/y^3) \right] \quad y \geq 2.4b \quad (34)$$

where

$$YG = \frac{4y^2}{\pi^{1/2}b^3} \exp(-y^2/b^2) \quad (35)$$

The 0.96 is a normalization factor and b the adjustable dispersion parameter. The value of b is also the most probable value of y and is called the thermalization range. This value is an inverse function of the electron energy loss cross-section of the molecules. The parameter usually used to approximate the ability of liquids to interact and slow down epithermal ($\epsilon > 0.1$) electrons is the density normalized thermalization range, bd , where d is in g/cm^3 (107, 141, 143, 149). The average of the positive and negative voltage values of bd from Tables III-17 to III-25 is plotted in Figures IV-32 to IV-35.

2. Low Density

For the liquid phase it has been suggested that the major portion of the thermalization length occurs when the electron has but a few tenths of an eV of energy (2). Correlation of bd curves with mobility curves over the entire liquid range, including the occurrence of maxima in bd vs T plots only when such maxima occur in μ_e vs T plots, led to the suggestion that a major part of the

range b is attained in the conduction band (3,130,132).

In the low density gas there is no conduction band. The differences in bd values as the carbon chain is increased from that of methane to that of n -butane (Figures IV-32 to IV-35) are only 12%. Differences between the other alkanes are even less. The difference between n -butane and isobutane (Figure IV-33) can be attributed to the greater flexibility of the n -butane molecule which allows a greater degree of rotational excitation.

The lesser value of bd in cyclopropane compared to that in propane (Figure IV-34) is due to the partial π electron nature of the cyclopropane bond. Ethene (Figure IV-33) though a smaller molecule than cyclopropane has full π electron character and has a smaller bd value than cyclopropane. Propene, which not only has π electron character but a permanent dipole moment, has a yet smaller bd value. These results conform to the notion of π electrons being better de-energizers of epithermal electrons than σ electrons (149).

3. Effect of Density

As noted in Section A, increasing the density from dilute gas values leads to conduction band formation at a density below n_c . The ability of a fluid to support a conduction band, that is smoothness of the potential at higher densities, can enhance the value of bd . In

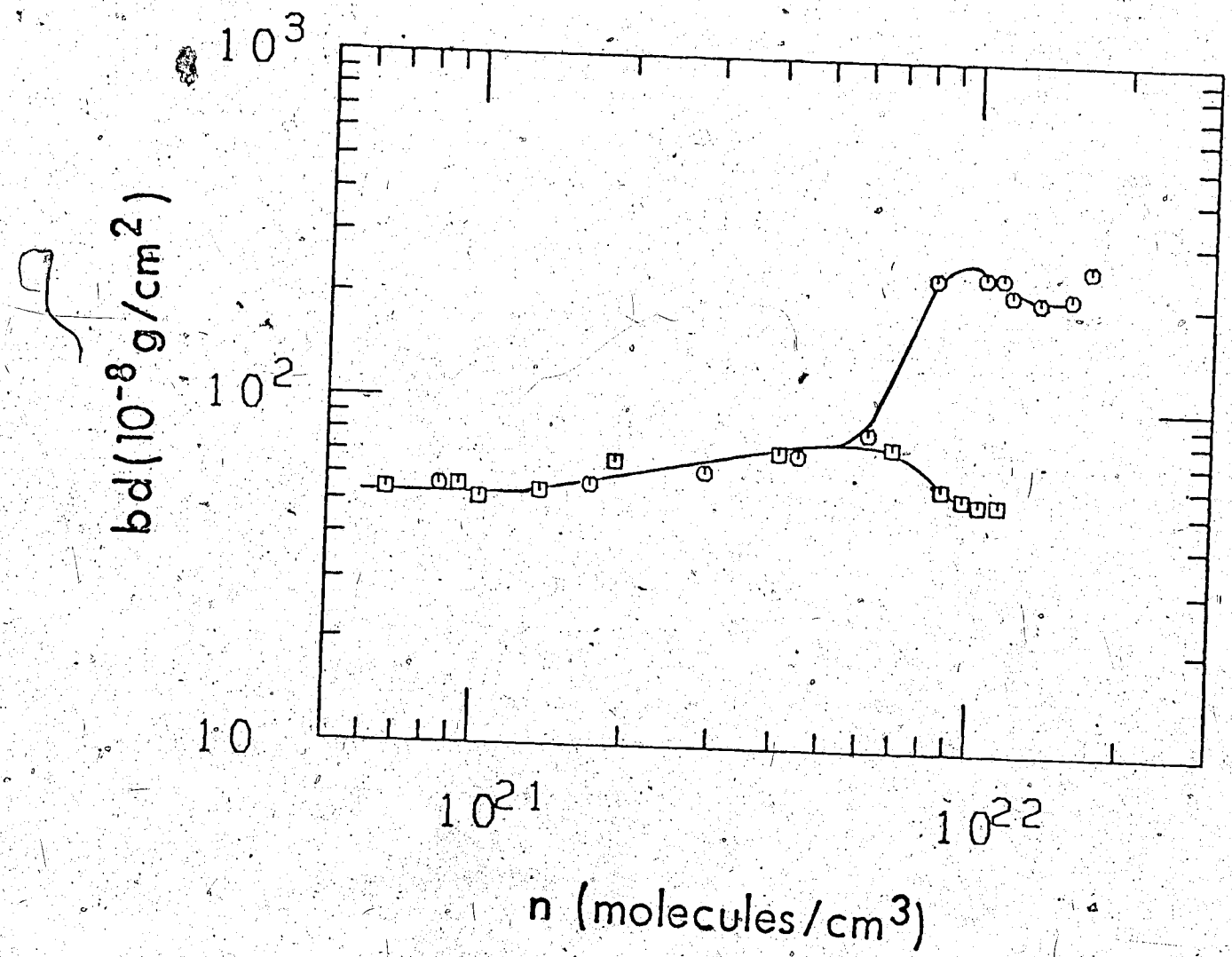


FIGURE IV-32. Density normalized thermalization range in methane (O) and in ethane (□) plotted against n.

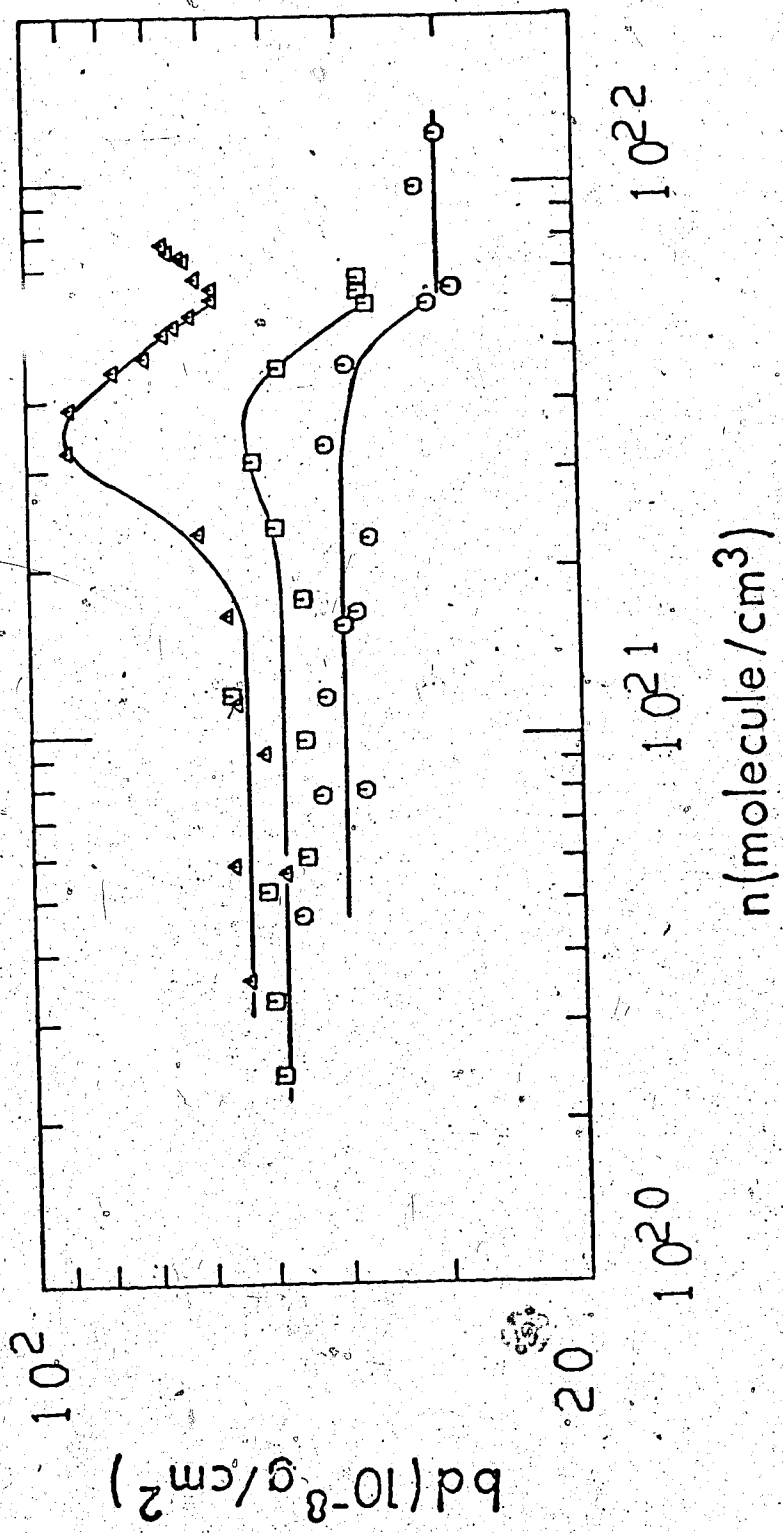


FIGURE IV-33. Density normalized thermalization range in ethene (O), n-butane (\square) and isobutane (Δ) plotted against n.

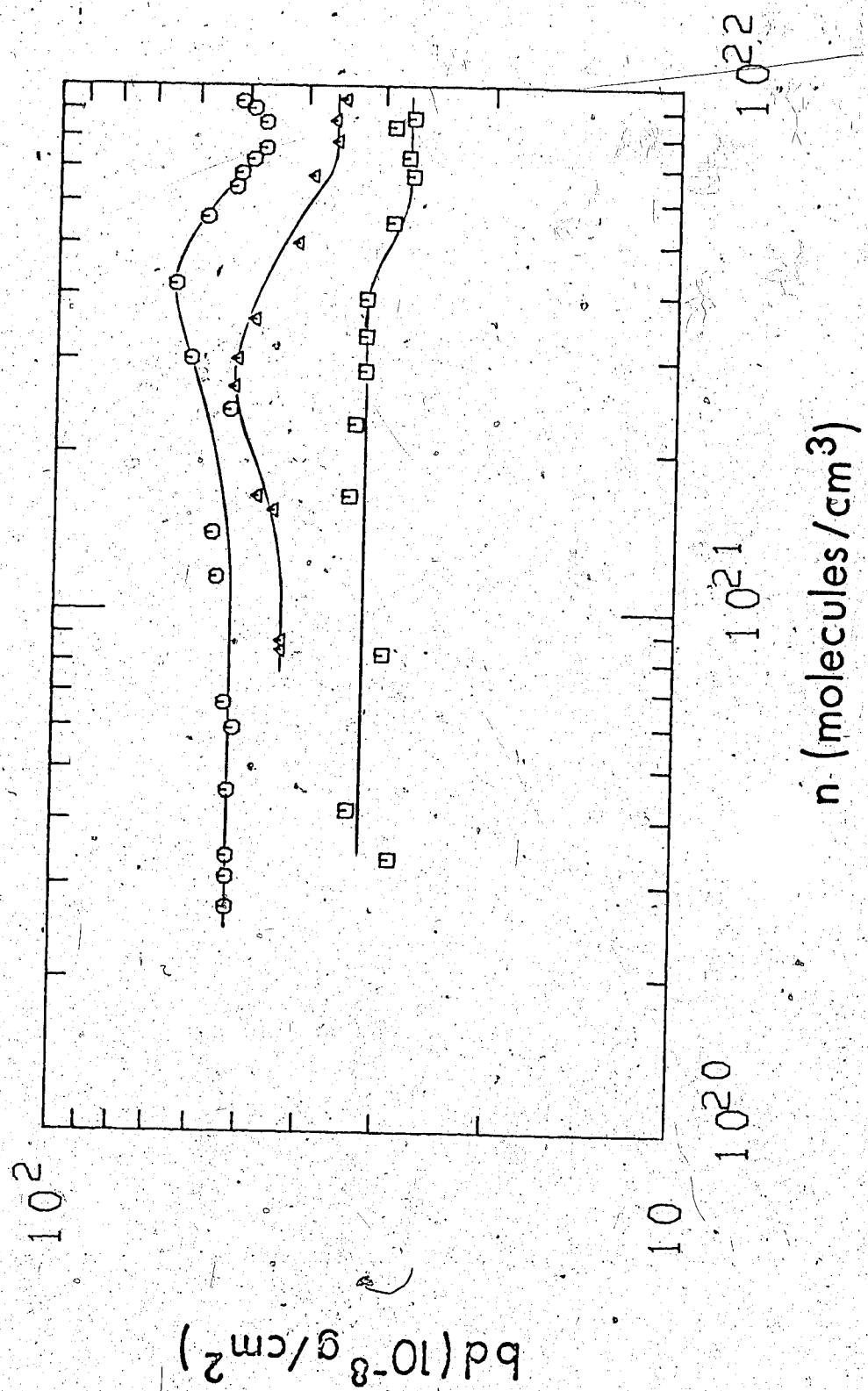


FIGURE IV-34. Density normalized thermalization range in propane (O), cyclopropane (Δ) and propene (\square) plotted against n.

methane (Figure IV-32), the greater freedom of motion of the electrons leads to a sharp separation of the bd curve from that of ethane in which the electrons are quickly localized. Propane (Figure IV-34) and n -butane (Figure IV-33) have results similar to those in ethane. There is no rise to a sharp maximum. The curves decrease slightly in the order ethane > propane > n -butane.

Isobutane, a sphere-like molecule, is usually classified as a high mobility fluid (114). It has a clear maximum in a plot of μ_e vs T . The bd curve rises to a clear maximum away from the n -butane curve, indicating the greater smoothness of the isobutane potential (Figure IV-33).

Of the remaining three compounds, only cyclopropane shows any inclination to increase in the bd curve near the critical region. The π bond compounds show a decrease in the critical region and have lower values in the liquid than in the gas.

4. Effect of Scavenger

Free ion yields were measured in mixtures of isobutane and sulfur hexafluoride, an electron scavenger. The mixtures have 0.15, 1.2, 4.9 and 9.5 mol % of SF_6 at the critical points. The bd 's are plotted against T in Figure IV-35. The effect of the SF_6 is to decrease the thermalization range. (It has been noted that if SF_6 scavenges the electrons after thermalization, the free

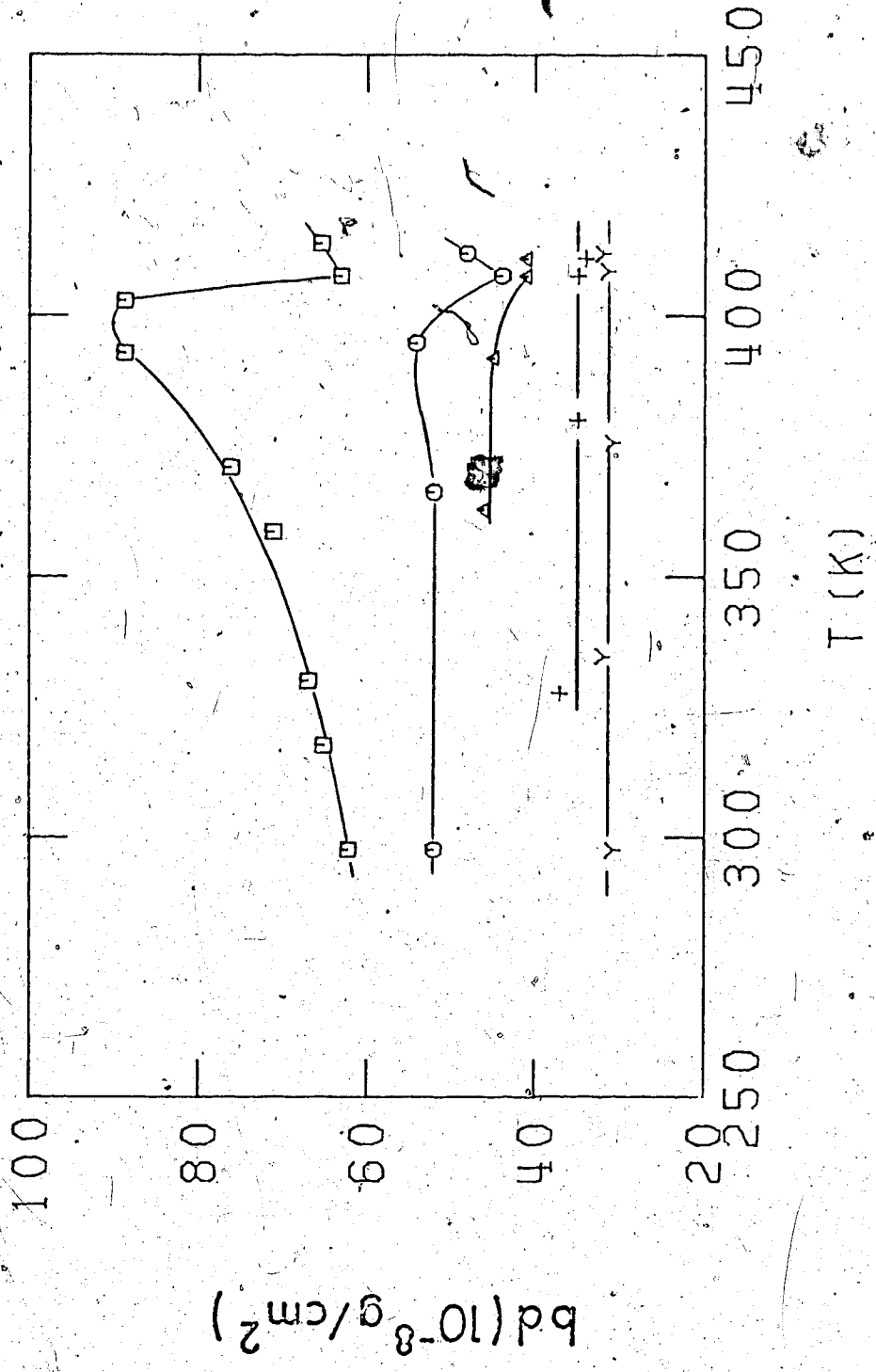


FIGURE IV-35. Density normalized thermalization range in mixture of isobutane + SF_6 plotted against T. The mol % of SF_6 are 0 (\square), 0.15 (\circ), 1.2 (\triangle), 4.9 (+) and 9.5 (Y).

ion yields and hence μ_{bd} values would not change (232). That a change occurs indicates pre-thermalization scavenging. The disappearance of the μ_{bd} maximum as the mol % of SF_6 increases may show that the amount of SF_6 is enough to block escape of the electrons through the conduction band.

D. Summary

A number of observations can be made about the interaction of electrons and ions with organic fluids.

1. Electron Mobility

The electron-molecule scattering cross-section in the low density gases depends upon the molecular structure. Properties that correlate with an increasing cross-section are an increasing size, permanent dipole moment and degree of sphericity. The density-normalized electron mobility $\mu_e n$, which is inversely proportional to the scattering cross-section, decreases at $n = 1.0 \pm 0.4 \times 10^{21}$ molec/cm³, except in the case of isobutane. As n approaches n_c , the $\mu_e n$ values tend to increase.

In the liquid, the mobility is more a function of the temperature than of the density. Away from the critical region, the electron mobility is larger and the temperature coefficient smaller if the localized state is less stable. This stability depends upon factors such as the molecular symmetry and the packing of the molecules in the liquid.

Heating the liquid towards the critical region increases the mobility and the temperature coefficient. High mobility liquids tend to have an electron mobility maximum at a temperature less than T_c .

The electron mobility shows a dependence on field strength at $E/n \gtrsim 10^{-1} \pm 1$ Td. In the gas, the region where the mobility would increase is at a lower density than the region where the mobility would decrease. The transition between these two field dependences need not occur in the gas phase. The ratio of the threshold drift velocity to the velocity of sound indicates the relative contribution of inelastic scattering processes compared to elastic processes.

2. Ion Mobility

The ion mobility is independent of applied field strength up to $E/n \approx 0.5$ Td in the liquid and $E/n \approx 2 \pm 1$ Td in the gas. Along the isochores, the ion mobility has a positive temperature coefficient which tends to be larger than that of the electron mobility at the same density. The values of $\mu_+ n$ at low gas densities depend on the molecular size. The temperature coefficient along the co-existence curve at low densities is similar to ΔH_{vap} , since μ_+ varies as n^{-1} . At higher densities the $\mu_+ n$ values increase, passing through the critical density to reach a maximum at $n > n_c$. Higher densities lead to a decrease in $\mu_+ n$ values.

In the liquid phase, the ion mobility varies inversely with the liquid viscosity although Walden's Rule does not

hold.

3. Electron Thermalization Range

The low field electron and ion mobilities reflect scattering cross-sections within a Maxwellian energy distribution for the temperature of the measurement. Thermal activation effects can be important. By contrast, the density normalized ranges bd are determined by the behavior of epithermal electrons which are affected by cross-sections at $\epsilon > 0.3$ eV. Thermal activation effects are small.

The bd values in the low density gas are decreased by increasing size, degree of unsaturation of carbon-carbon bonds and flexibility of the carbon-carbon skeleton. If a conduction band exists, the epithermal electrons can enter it. Increasing the gas density towards n_c leads to a large increase in bd in high mobility liquids. There can be a bd maximum in the same temperature range as the electron maximum. Addition of SF_6 to a high mobility liquid decreases the bd values and removes their temperature dependence. These observations are in accord with the idea that a major part of the thermalization range is attained by epithermal electrons moving along in the conduction band.

R E F E R E N C E S

1. G. R. Freeman, *Int. J. Rad. Phys. Chem.* 4, 237 (1972).
2. A. Mozumder and J. L. Magee, *J. Chem. Phys.* 47, 939 (1967).
3. J.-P. Dodelet and G. R. Freeman, *Int. J. Rad. Phys. Chem.* 7, 183 (1975).
4. G. R. Freeman, *J. Chem. Phys.* 39, 1580 (1963).
5. A. Hummel and W. F. Schmidt, *Rad. Res. Rev.* 5, 199 (1974).
6. J.-P. Dodelet, *Can. J. Chem.* 55, 2050 (1977) and references therein.
7. E. W. McDaniel, *Collision Phenomena in Ionized Gases*, J. Wiley (1964) Chapter 9.
8. Chapter 1 of ref. 7.
9. J. J. Thomson, *Nature* 55, 606 (1897).
10. H. Becquerel, *Comp. Rend.* 130, 206 (1900).
11. J. S. Townsend, *Nature* 620, 340 (1900).
12. J. S. Townsend, *Philos. Mag.* 1, 198 (1901).
13. P. Curie, *Comp. Rend.* 134, 420 (1902).
14. H. Becquerel, *Comp. Rend.* 136, 420 (1902).
15. T. E. M. Sambrook and G. R. Freeman, *Can. J. Chem.* 53, 2822 (1975).
16. C. Ramsauer, *Ann. Phys.* 66, 546 (1921).
17. C. Ramsauer and R. Kollath, *Ann. Phys.* 3, 536 (1929).
18. C. Ramsauer and R. Kollath, *Ann. Phys.* 4, 91 (1930).
19. E. Brüche, *Ann. Phys.* 4, 387 (1930).

20. E. Brüche, *Ann. Phys.* 5, 281 (1930).
21. F. Schmeider, *Z. für Elektrochemie* 36, 700 (1930).
22. R. Kollath, *Phys. Zeitschr.* 31, 985 (1930).
23. Chapter 4 of ref. 7.
24. L. B. Loeb, Basic Processes of Gaseous Electronics,
2nd ed. University of California Press, 1961.
25. A. M. Tyndall, The Mobility of Positive Ions in Gases,
Cambridge University Press, 1938.
26. J. S. Townsend and H. T. Tizard, *Proc. Roy. Soc.* A88,
336 (1913).
27. J. S. Townsend, *Philos. Mag.* 42, 873 (1921).
28. J. S. Townsend and V. A. Bailey, *Philos. Mag.* 43, 593
(1922).
29. J. S. Townsend and V. A. Bailey, *Philos. Mag.* 44, 1033
(1923).
30. J. S. Townsend and V. A. Bailey, *Philos. Mag.* 46, 657
(1923).
31. J. Bannon and H. L. Brose, *Philos. Mag.* 6, 817 (1928).
32. J. D. McGee and J. C. Jaegers, *Philos. Mag.* 6, 1107
(1928).
33. N. E. Bradbury and R. A. Nielson, *Phys. Rev.* 49, 388
(1936).
34. R. A. Nielson and N. E. Bradbury, *Phys. Rev.* 51, 69
(1937).
35. L. B. Loeb, *Phys. Rev.* 19, 24 (1922).
36. L. B. Loeb, *Phys. Rev.* 20, 397 (1922).

37. W. B. Wahlin, *Phys. Rev.* 21, 517 (1923).
38. E. W. McDaniel and E. A. Mason, *The Mobility and Diffusion of Ions in Gases*, John Wiley, 1973 and references therein.
39. L. G. H. Huxley and R. W. Crompton, *The Diffusion and Drift of Electrons in Gases*, John Wiley, 1974.
40. T. L. Cottrell and I. C. Walker, *Quarterly Rev.* XX, 153 (1966).
41. A. V. Phelps, *Rev. Mod. Phys.* 40, 399 (1968).
42. A. Gilardini, *Low Energy Electron Collisions in Gases*, Wiley-Interscience, 1972.
43. J. Dutton, *J. Phys. Chem. Ref. Data*, 4, 577 (1975).
44. W. N. English and C. C. Hanna, *Can. J. Phys.* 31, 768 (1953).
45. T. E. Bortner, G. S. Hurst and W. G. Stone, *Rev. Sci. Instr.* 28, 103 (1957).
46. J. C. Devins and R. W. Crowe, *J. Chem. Phys.* 25, 1053 (1956).
47. L. Frommhold, *Z. Phys.* 156, 144 (1959).
48. H. Tholl, *Z. Phys.* 178, 183 (1964).
49. H. Schlumbohm, *Z. Phys.* 182, 317 (1965).
50. T. L. Cottrell and I. C. Walker, *Trans. Farad. Soc.* 61, 1585 (1965).
51. E. B. Wagner, F. D. Davis and G. S. Hurst, *J. Chem. Phys.* 47, 3138 (1967).
52. C. R. Bowman and D. E. Gordon, *J. Chem. Phys.* 46, 1878 (1967).
53. W. J. Pollock, *Trans. Farad. Soc.* 64, 2919 (1968).

54. T. L. Cottrell and I. C. Walker, *Trans. Farad. Soc.* 63, 549 (1967).
55. D. R. Nelson and F. J. Davis, *J. Chem. Phys.* 51, 2322 (1969).
56. C. W. Duncan and I. C. Walker, *J.C.S. Farad.* 11 68, 1514 (1972).
57. A. H. Cookson, *Brit. J. Appl. Phys.* 17, 1069 (1967).
58. H. Lehning, *Phys. Rev. Lett.* 29A, 719 (1969).
59. N. E. Cipollini, R. A. Holroyd and M. Nishikawa, *J. Chem. Phys.* 67, 4636 (1977).
60. H. Daum, C. W. Fabjan and S. H. Pordes, *Nucl. Instr. Meth.* 152, 541 (1978).
61. I. Adamczewski, *Ionization, Conductivity and Break-down in Dielectric Liquids*, Taylor and Francis Ltd. London, 1969.
62. T. L. Cottrell, W. J. Pollock and I. C. Walker, *Trans. Farad. Soc.* 64, 2260 (1968).
63. L. G. Christophorou, M. W. Grant and D. Pittman, *Chem. Phys. Lett.* 38, 100 (1976).
64. D. L. McCorkle, L. G. Christophorou, M. V. Maxey and J. G. Carter, *J. Phys.* B11, 3067 (1978).
65. B. Huber, *Z. Naturforsch* 23A, 1228 (1958).
66. B. Huber, *Z. Naturforsch* 24A, 578 (1969).
67. D. W. Duncan and I. C. Walker, *J.C.S. Farad. II* 70, 577 (1974).
68. L. G. Christophorou, R. P. Blaustein and D. Pittman, *Chem. Phys. Lett.* 18, 509 (1973).

69. W. Roznerski and E. Gazda, Acta Phys. Polon. A49, 389 (1976).
70. I. György and G. R. Freeman (a) J. Chem. Phys. 70, April (1979); (b) Proc. 6th Int. Conf. Conduction & Breakdown in Dielectric Liquids, Editions Frontieres, Dreux, France, 1978, p.203.
71. S.S.-S. Huang and G. R. Freeman, Can. J. Chem. 56, 2388 (1978).
72. L. G. Christophorou, Atomic and Molecular Radiation Physics, Wiley-Interscience 1971.
73. S.S.-S. Huang and G. R. Freeman, J. Chem. Phys. 69, 1585 (1978).
74. J. Lekner and A.R. Bishop, Philos. Mag. 27, 297 (1973).
75. T. Kimura and G. R. Freeman, Can. J. Phys. 52, 2220 (1974).
76. B. Huber, Diplomarbeit, Institut für angewandte Physik der Universität, Hamburg, 1969. Data given in L. G. Christophorou, Int. J. Rad. Phys. Chem. 7, 205 (1975), figure 7.
77. L. W. Cochran and D. W. Forrester, Phys. Rev. 126, 1785 (1962).
78. C. W. Duncan and I. C. Walker, J.C.S. Farad. II, 68, 1800 (1972).
79. I. Adamczewski, Ann. de Phys. 8, 309 (1937).
80. I. Adamczewski, Acta Phys. Polon. 6, 432 (1937).
cited on p.192 of ref. 61.

81. O. H. LeBlanc, J. Chem. Phys. 30, 1443 (1959).
82. R. W. Crowe, J. Appl. Phys. 27, 156 (1956).
83. K. R. Atkins, Phys. Rev. 116, 1339 (1959).
84. J. Terlecki, Nature 194, 171 (1962).
85. O. Gzowski, Nature 194, 172 (1962).
86. P. Chong and Y. Inuishi, Tech. Rep. Osaka University 10, 545 (1960) data contained in Fig. 12.23 of ref. 61 (p.205).
87. A. H. Samuel, F. O. Halliday, A. K. Keast and S.I. Taimuty, Science 144, 839 (1964).
88. N. Davidson and A. E. Larsch, Phys. Rev. 74, 220 (1948).
89. G. R. Freeman, J. Chem. Phys. 39, 988 (1963).
90. G. R. Freeman and J. M. Fayadh, J. Chem. Phys. 43, 86 (1965).
91. A. Hummel and A. O. Allen, J. Chem. Phys. 44, 3426 (1966).
92. A. Hummel, A. O. Allen and F. H. Watson Jr., J. Chem. Phys. 44, 3431 (1966).
93. P. H. Tewari and G. R. Freeman, J. Chem. Phys. 49, 954 (1968).
94. P. H. Tewari and G. R. Freeman, J. Chem. Phys. 49, 4394 (1968).
95. P. H. Tewari and G. R. Freeman, J. Chem. Phys. 51, 1276 (1969).
96. G. Bakale and W. F. Schmidt, Z. Naturforsch. 28A, 511 (1973).

97. W. F. Schmidt, G. Bakale and U. Sowada, J. Chem. Phys. 61, 5275 (1975).
98. P. S. Wipokur, M. L. Roush and J. Silverman, J. Chem. Phys. 63, 3478 (1975).
99. A. O. Allen, M. P. de Haas and A. Hummel, J. Chem. Phys. 64, 2587 (1976).
100. M. S. Malkin and H. L. Schultz, Phys. Rev. 83, 1051 (1951).
101. E. E. Conrad and J. Silverman, J. Chem. Phys. 51, 450 (1969).
102. R. M. Minday, L. D. Schmidt and H. T. Davis, J. Chem. Phys. 50, 1473 (1969).
103. W. F. Schmidt and A. O. Allen, J. Chem. Phys. 50, 5037 (1969).
104. W. F. Schmidt and A. O. Allen, J. Chem. Phys. 52, 4788 (1970).
105. R. M. Minday, L. D. Schmidt and H. T. Davis, J. Chem. Phys. 54, 3112 (1971).
106. R. M. Minday, L. D. Schmidt and H. T. Davis (a) Phys. Rev. Lett. 26, 360 (1971). (b) J. Phys. Chem. 75, 442 (1972).
107. J.-P. Dodelet and G. R. Freeman, Can. J. Chem. 50, 2667 (1972).
108. J.-P. Dodelet, K. Shinsaka and G. R. Freeman, J. Chem. Phys. 59, 1293 (1973).
109. M. G. Robinson and G. R. Freeman, Can. J. Chem. 52, 440 (1974).

110. K. Shinsaka and G. R. Freeman, Can. J. Chem. 52, 3495 (1974).
111. K. Shinsaka and G. R. Freeman, Can. J. Chem. 52, 3556 (1974).
112. J.-P. Dodelet and G. R. Freeman, Can. J. Chem. 53, 1263 (1975).
113. K. Shinsaka, J.-P. Dodelet and G. R. Freeman, Can. J. Chem. 53, 2714 (1975).
114. J.-P. Dodelet, K. Shinsaka and G. R. Freeman, Can. J. Chem. 54, 744 (1976).
115. A. A. Balakin and B. S. Yakolev, High Energy Chem. 9, 22 (1975).
116. A. A. Balakin and B. S. Yakolev, High Energy Chem. 9, 69 (1975).
117. G. F. Novikov and B. S. Yakolev, Int. J. Rad. Phys. Chem. 8, 517 (1976).
118. A. A. Balakin, I. A. Boriev and B. S. Yakolev, High Energy Chem. 12, 171 (1978).
119. G. Bakale, W. Tauchert and W. F. Schmidt, J. Chem. Phys. 63, 4470 (1975).
120. G. Bakale, U. Sowada and W. F. Schmidt, 1974 Annual Report, Conf. on Electrical INSulation and Dielectric Phenomena, Nat. Acad. of Sci. p.41.
121. I. Adamczewski and J. H. Calderwood, J. Phys. D8, 1211 (1975).
122. I. Adamczewski and J. H. Calderwood, J. Phys. D9, 2479 (1976).

123. H. Schnyders, S. A. Rice and L. Meyer, Phys. Rev. 150, 127 (1966).
124. J.A. Jahnke, L. Meyer and S. A. Rice, Phys. Rev. A3, 734 (1971).
125. J. M. L. Engels and A. J. M. van Kimmenade, Chem. Phys. Lett. 42, 250 (1976).
126. J. M. L. Engels and A. J. M. van Kimmenade, Phys. Lett. 59A, 43 (1976).
127. J. M. L. Engels and A. J. M. van Kimmenade, Chem. Phys. Lett. 48, 451 (1977).
128. W. Döeldissen, G. Bakale and W. F. Schmidt, Proc. of the Vith Int. Conf. on Conductance and Breakdown in Dielectric Liquids, Edition Frontieres, Dreux, France 1978 p.203.
129. W. Döeldissen, G. Bakale and W. F. Schmidt, Chem. Phys. Lett. 56, 347 (1978).
130. J.-P. Dodelet and G. R. Freeman, Can. J. Chem. 55, 2264 (1977).
131. J.-P. Dodelet and G. R. Freeman, Can. J. Chem. 55, 2893 (1977).
132. T. G. Ryan and G. R. Freeman, J. Chem. Phys. 68, 5144 (1978).
133. N. E. Cipollini and A. O. Allen, J. Chem. Phys. 67, 131 (1977).
134. M. L. McGlashan and I. R. McKinnon, J. Chem. Thermody. 9, 1205 (1977).

135. F. L. Mohler and L. S. Taylor, J. of Res. (NBS) 13, 659 (1934).
136. A. N. Gerritsen and J. Kolhaas, Physica 10, 49 (1943).
137. C. S. Pao, Phys. Rev. 64, 60 (1943).
138. H. Ullmaier, Z. Phys. 178, 44 (1964).
139. A. H. Samuel and J. L. Magee, J. Chem. Phys. 21, 1080 (1953).
140. D. D. Hudson, U. S. AEC Report MDDC-524, 1946 cited on p.229 of ref. 5.
141. W. F. Schmidt and A. O. Allen, J. Phys. Chem. 72, 3730 (1968).
142. W. F. Schmidt, Rad. Res. 42, 73 (1970).
143. W. F. Schmidt and A. O. Allen, J. Chem. Phys. 52, 2345 (1970).
144. M. G. Robinson and G. R. Freeman, Can. J. Chem. 49, 984 (1971).
145. M. G. Robinson, P. G. Fuochi and G. R. Freeman, Can. J. Chem. 49, 3657 (1971).
146. J.-P. Dodelet, P. G. Fuochi and G. R. Freeman, Can. J. Chem. 50, 1617 (1972).
147. P. G. Fuochi and G. R. Freeman, J. Chem. Phys. 56, 2333 (1972).
148. M. G. Robinson and G. R. Freeman, Can. J. Chem. 51, 1010 (1973).
149. J.-P. Dodelet, K. Shinsaka, U. Kortsch and G. R. Freeman, J. Chem. Phys. 59, 2376 (1973).

150. S.S.-S. Huang and G. R. Freeman, Can. J. Chem. 55, 1838 (1977).
151. J. M. Warman, K.-D. Asmus and R. H. Schuler, Adv. in Chem. 82, 25 (1968).
152. G. R. Freeman and E. D. Stover, Can. J. Chem. 46, 3235 (1968).
153. K. Horacek and G. R. Freeman, J. Chem. Phys. 53, 4486 (1970).
154. G. R. Freeman and T. E. M. Sambrook, J. Phys. Chem. 78, 102 (1974).
155. M. Baba and K. Fueki, Bull. Chem. Soc. Japan 48, 3039 (1975).
156. M. Nishikawa, Y. Yamaguchi, K. Fujita, K. Kon and T. Okamoto, Can. J. Chem. 51, 3966 (1973).
157. Y. Yamaguchi and M. Nishikawa, J. Chem. Phys. 59, 1298 (1973).
158. M. Nishikawa, Y. Yamaguchi and K. Fujita, J. Chem. Phys. 61, 2356 (1974).
159. M. Nishikawa and Y. Yamaguchi, Can. J. Chem. 55, 2088 (1977).
160. G.G. Meisels, J. Chem. Phys. 41, 51 (1964).
161. P. Adler and H.-K. Bothe, Z. Naturforsch. 20a, 1700 (1965).
162. R. M. Leblanc and J. A. Herman, J. Chim. Phys. 63, 1055 (1966).
163. R. Cooper and R.-M. Mooring, Austr. J. Chem. 21, 2417 (1968).

164. T. A. Stoneheim, D. R. Ethridge and G. G. Meisels,
J. Chem. Phys. 54, 4054 (1971).
165. E. Waibel and B. Grosswendt, Rad. Res. 76, 241
(1978).
166. G. N. Whyte, Rad. Res. Rev. 18, 265 (1963) cited
on p. 4057 of ref. 164.
167. P. Langevin, Ann. de Chim. et Phys. 5, 245 (1905)
cited in Chapt. I of ref. 24, Chap. IV of ref. 25 and
in Appendix of ref. 38.
168. Reviewed in Chap. 13 of ref. 39.
169. W. P. Allis, Handbuch der Physik ed. by S. Flügge
(Springer-Verlag).
170. J. L. Pack and A. V. Phelps, Phys. Rev. 121, 798
(1961).
171. L. A. Viehland and E. A. Mason, Ann. Phys. (N.Y.)
91, 499 (1975).
172. F. W. Morrison, G. R. Akridge, H. W. Ellis, R. Y.
Pai, E. W. McDaniel, L. A. Viehland and E. A.
Mason, J. Chem. Phys. 63, 2238 (1975).
173. J. L. Pack, R. E. Voshall and A. V. Phelps, Phys.
Rev. 127, 2084 (1961).
174. S.-S. -S. Huang and G. R. Freeman, J. Chem. Phys.
70, 1538 (1979).
175. A. G. Engelhardt and A. V. Phelps, Phys. Rev. 131,
2115 (1963).
176. L. S. Frost and A. V. Phelps, Phys. Rev. 136,
A1538 (1964).

177. R. D. Hake Jr. and A. V. Phelps, Phys. Rev. 158, 70 (1967).
178. J. Lekner, Phys. Rev. 58, 130 (1967).
179. (a) H. Schnyders, S.A. Rice and L. Meyer, Phys. Rev. Lett. 15, 187 (1965). (b) D. W. Swan, Nature 196, 977 (1962). (c) D. W. Swan, Proc. Phys. Soc. (London) 83, 659 (1964).
180. M.H. Cohen and J. Lekner, Phys. Rev. 158, 305 (1967).
181. J. Lekner, Phys. Lett. A27, 341 (1968).
182. H. T. Davis, L. D. Schmidt and R. M. Minday, Phys. Rev. A3, 1027 (1971).
183. K. Fueki, Can. J. Chem. 50, 3379 (1972).
184. K. Fueki, D.-F. Feng and L. Kevan, Chem. Phys. Lett, 13, 616 (1972).
185. J.A. Jahnke, N. A. W. Holzwarth and S. A. Rice, Phys. Rev. A5, 463 (1972).
186. J. J. Thomson, Philos. Mag. 30, 321 (1915).
187. J. T. Richards and J. K. Thomas, Chem. Phys. Lett. 10, 317 (1971).
188. L. B. Magnussen, J. T. Richards and J. K. Thomas, Int. J. Rad. Phys. Chem. 3, 295 (1971).
189. H. A. Gillis, N. V. Klassen, G. G. Teather and K. H. Lokan, Chem. Phys. Lett. 10, 481 (1971).
190. J. H. Baxendale, C. Bell and P. Wardman, Chem. Phys. Lett. 12, 347 (1971).
191. L. Kevan, H. A. Gillis, K. Fueki and T. Kimura, J. Chem. Phys. 68, 5203 (1978).

192. R. Schiller, J. Chem. Phys. 57, 2222 (1972).
193. R. Schiller, Sz. Vass and J. Mandics, Int. J. Rad. Phys. Chem. 5, 491 (1973).
194. Yu. A. Berlin, L. Nyikos and R. Schiller, J. Chem. Phys. 69, 2401 (1978).
195. J.-P. Dodelet, F.-Y. Jou and G. R. Freeman, J. Phys. Chem. 79, 2876 (1975).
196. J. L. Levine and T. M. Sanders, Phys. Rev. 154, 138 (1967).
197. O. E. Mogensen, J. Chem. Phys. 60, 998 (1974).
198. J. B. Smith Jr., J. D. McGervey and A. J. Dahm, Phys. Rev. B15, 1378 (1977).
199. G. A. Kenney-Wallace, Chem. Phys. Lett. 43, 529 (1976).
200. P. R. Tremaine and R. S. Dixon, J. Phys. Chem. 82, 224 (1978).
201. N. R. Kestner and J. Jortner, J. Chem. Phys. 59, 26 (1973).
202. B. G. Bagley, Solid State Comm. 8, 345 (1970).
203. K. Funabashi and B. N. Rao, J. Chem. Phys. 64, 1561 (1976).
204. B. N. Rao, R. L. Bush and K. Funabashi, Can. J. Chem. 55, 1952 (1977).
205. U. Sowada, G. Bakale and W. F. Schmidt, High Energy Chem. 10, 290 (1976).
206. G. Jaffe, Ann. Phys. 42, 303 (1913) described in Chap. 16 of ref. 61

207. C. T. R. Wilson, Proc. Roy. Soc. A87, 277 (1912).
208. L. Onsager, Phys. Rev. 54, 554 (1938).
209. J. Terlecki and J. Fiutak, Int. J. Rad. Phys. Chem. 4, 469 (1972).
210. G. C. Abell and K. Funabashi, J. Chem. Phys. 58, 1079 (1973).
211. G. R. Freeman and J.-P. Dodelet, Int. J. Rad. Phys. Chem. 5, 371 (1973).
212. A. Mozumder, J. Chem. Phys. 60, 4305 (1974).
213. P. M. Morse, Thermal Physics, W. A. Benjamin Inc., 1969, Chap. 11.
214. J.-P. Dodelet and G. R. Freeman, J. Chem. Phys. 60, 4657 (1974).
215. R. Schiller and Sz. Vass, Int. J. Rad. Phys. Chem. 7, 193 (1975).
216. H. Sano and A. Mozumder, J. Chem. Phys. 66, 689 (1977).
217. R. A. Holroyd and M. Allen, J. Chem. Phys. 54, 5014 (1971).
218. J.-P. Dodelet, K. Shinsaka and G. R. Freeman, J. Chem. Phys. 63, 2765 (1975).
219. R. A. Holroyd and N. E. Cipollini, J. Chem. Phys. 69, 501 (1978).
220. T. Kimura and K. Fueki, J. Chem. Phys. 66, 366 (1977).
221. T. Kimura, K. Fueki, P. A. Narayana and L. Kevan, Can. J. Chem. 55, 1940 (1977).

222. R. W. Gallant, Physical Properties of Hydrocarbons, Gulf Publishing Co., Houston, Texas, 1968, Vols. 1 and 2.
223. L. N. Canjar and F. S. Manning, Thermodynamic Properties and Reduced Correlations for Gases, Gulf Publishing Co., Houston, Texas, 1967.
224. R. C. West (editor), Handbook of Chemistry and Physics, Chemical Rubber Co., Cleveland, Ohio, 1969, 50th edition.
225. R. D. Goodwin, National Bureau of Standards, Tech. Note. 653 (1974).
226. R. D. Goodwin, National Bureau of Standards. Tech. Note 684 (1976).
227. N. E. Hill, W. E. Vaughan, A. H. Price and M. Davies, Dielectric Properties and Molecular Behavior, Van Nostrand Reinhold Co., Toronto, 1969, p.23.
228. R. D. Nelson, Jr., D. R. Lide Jr., and A. A. Maryott, Selected Values of Electric Dipole Moments for Molecules in the Gas Phase, NSRDS-NBS 10, U. S. Government Printing Office, Washington, D. C. 1967.
229. J. R. Partington, An Advanced Treatise on Physical Chemistry, Vol. 5, p.349. Longmans, Green & Co. Ltd., London.
230. A. A. Maryott and E. R. Smith, Table of Dielectric Constants of Pure Liquids, NBS Circular 514, U. S. Government Printing Office, Washington, D. C., 1951.

231. R. C. Reid, J. M. Prausnitz and T. K. Sherwood, The Properties of Gases and Liquids, McGraw-Hill, 3rd edition, 1977.
232. A. Mozumder and M. Tachiya, J. Chem. Phys. 62, 979 (1975).
233. S.S.-S. Huang and G. R. Freeman, J. Chem. Phys. 68, 1355 (1978).
234. L. S. Miller, S. Howe and W. E. Spear, Phys. Rev. 166, 871 (1968) and references therein.
235. D. L. Goodstein, States of Matter, Prentice-Hall Inc. Englewood Cliffs, N.J., 1975, Chapter 4.
236. Ref. 225, p. 118; $\chi_T = [(MOL/L)(DP/DD)]^{-1}$; $S(0) = 0.082 T/(DP/DD)$.
237. S. Altschuler, Phys. Rev. 107, 114 (1957).
238. R. J. W. LeFevre, Rev. Pure and Appl. Chem., 20, 67 (1970).
239. H. Lehning, Phys. Lett. 28A, 103 (1968).
240. E. Hausmann and E. P. Slack, Physics, Van Nostrand Co., New York, 1944, p.412.
241. S. Glasstone, Textbook of Physical Chemistry, Van Nostrand, New York, 2nd ed., 1946, p.450.
242. P.12 of ref. 241.
243. P.897 of ref. 241.

A P P E N D I X

Average Deviations

The average % error was calculated for a number of sets of data in Chapter III, to illustrate their magnitudes. The results are given in Tables A-1 and A-2.

The average % error was taken to be (114):

$$\text{average \% error} = \frac{100 \sum |\text{expected} - \text{experimental}|}{\sum \text{experimental}}$$

For the mobilities, the expected value was taken to be the average mobility. For the free ion yields, the expected value was taken to be the calculated value.

TABLE A-1

Mobility Errors

<u>Figure</u>	<u>T</u> <u>K</u>	<u>n</u> <u>10²⁰ molec/cm³</u>	<u>Average</u> <u>% error</u>
a) Electron Mobility Curves *			
66	233	0.46	2.0
71	296	1.76	2.0
58	203	1.89	2.0
51	371	5.65	2.1
40	435	11.8	1.2
39	425.5	23.6	1.0
29	353	49.9	6.6
19	281	80.4	2.5
18	188	109	6.3
3	122	155	2.8
b) Ion Mobility			
83	193	0.621	3.5
99	333	1.64	2.7
75	144	4.66	4.7
89	383	7.51	1.3
97	424	16.8	2.7
106	408	23.0	3.5
117	364.6	38.6	2.1
112	282	59.7	0.1

Table A-1 (continued)

<u>Figure</u>	<u>T</u> <u>K</u>	<u>n</u> <u>10²⁰ molec/cm³</u>	<u>Average</u> <u>% error</u>
124	297	86.2	1.5
112	173	122	1.4

* Based on the field independent portion only.

TABLE A-2
Free Ion Yield Errors

Figure	T K	d gm/cm ³	Polarity of voltage	Average % error
143	149	0.680	+	2.1
138	166	0.571	+	6.6
130 B	91	0.453	+	1.5
			-	1.9
140	306	0.203	+	1.0
157A	441	0.114	+	1.0
			-	0.7
167B	398	0.107	+	1.6
			-	2.3
177	265	0.074	+	2.4
199	404	0.0611	+	0.4
			-	1.2
187	367	0.0575	+	1.8
			-	2.0